Testing alternative models of continental collision in Central Turkey by a study of the sedimentology, provenance and tectonic setting of Late Cretaceous–Early Cenozoic syn-tectonic sedimentary basins.

Steven Nairn

Thesis submitted for the degree of Doctor of Philosophy

The University of Edinburgh

2010

I declare that this thesis has been written by myself and is the result of my own research, except where contributions have been stated and duly acknowledged.

Steven Nairn 2010

Abstract

In central Anatolia, Turkey, a strand of the former northern Neotethys Ocean subducted northwards under the Eurasian (Pontide) active margin during Late Cretaceous–Early Cenozoic time. Subduction and regional plate convergence were associated with the generation and emplacement of accretionary complexes and supra-subduction zone-type ophiolites onto former passive margins of microcontinents. The resultant suture zones contain Late Cretaceous to Middle Eocene basins ("The Central Anatolian Basins") including: 1) the Kırıkkale Basin; 2) the Çankırı Basin, 3) the Tuz Gölü Basin and; 4) the Haymana - Polatlı Basin. Using stratigraphic logging, igneous geochemistry, micropalaeontology and provenance studies, this study tests two end-member models of basin evolution. In model one, the basins developed on obducted ophiolitic nappes following closure of a single northern Neotethys Ocean during the latest Cretaceous. In model two, northern Neotethys comprised two oceanic strands, the İzmir-Ankara-Erzincan Ocean to the north and the Inner Tauride Ocean to the south, separated by the Niğde-Kırşehir microcontinent, which was rifted from the Gondwana continent to the south. In this scenario, the basins developed as accretionary-type basins, associated with north-dipping subduction which persisted until the Middle Eocene when continental collision occurred.

Where exposed, the basements of the Central Anatolian Basins comprise the Ankara Mélange, a mainly Upper Cretaceous subduction-accretion complex and the western/northern margin of the Niğde-Kırşehir microcontinent. New geochemical data from the composite basement of the Kırıkkale Basin identify mid ocean-ridge basalt (MORB), here interpreted to represent relict Upper Cretaceous Neotethyan oceanic crust. During the latest Cretaceous, the Kırıkkale and Tuz Gölü Basins initiated in deep water above relict MORB crust and ophiolitic mélange, bordered by the Niğde-Kırşehir microcontinent to the east where marginal facies accumulated. Further west, the Haymana-Polatlı Basin represents an accretionary-type basin constructed on the Ankara Mélange. To the north, the Çankırı Basin developed on accretionary mélange, bounded by the Pontide active margin to the north. Palaeocene sedimentation was dominated by marginal coralgal reef facies and siliciclastic turbidites. Latest Palaeocene–middle Eocene facies include shelf-type Nummulitid limestone, shallow-marine deltaic pebbly sandstones and siliciclastic turbidites.

This thesis proposes a new model in which two north-dipping subduction zones were active during the late Mesozoic within northern Neotethys. In the south, ophiolites formed above a subduction zone consuming the Inner Tauride Ocean until the southward retreating trench collided with the northern margin of the Tauride continent emplacing ophiolites and mélange. In the north, subduction initiated outboard of the Eurasian margin triggering the genesis of supra-subduction zone ophiolites; the subduction zone rolled back southwards until it collided with the Niğde-Kırşehir microcontinent, again emplacing ophiolites during latest Cretaceous time. Neotethyan MORB still remained to the west of the Niğde-Kırşehir microcontinent forming the basement of the Kırıkkale and Tuz Gölü Basins. Latest Palaeocene–middle Eocene regional convergence culminated in crustal thickening, folding, uplift and strike-slip faulting which represent final continental collision and the geotectonic assembly of central Anatolia.

Acknowledgements

There are many people to thank who have helped me complete this project.

First, I owe Alastair Robertson an enormous debt for his enthusiasm and help. Working with Alastair, particularly in the field, was an inspiration.

Thank you to other Edinburgh-based staff, including Sue Rigby, my adviser of studies, and to the many others who have both helped and inspired me during my under- and post-graduate years including John Dixon, Simon Harley, John Underhill and Hugh Sinclair.

Thank you to my fellow Tethyan workers: Pete MacKintosh, Tim Kinnaird, Gillian McCay and Mat Booth.

My field work in Turkey would not have been possible without the help and support of Ulvi Can Ünlügenç and his family, who made me welcome in Adana and provided crucial logistical support. A special thanks to my Turkish field assistants Turgut Aksu and especially Ahmet Can Akinci, who helped me out of many tricky situations. His friendship and banana sandwiches were a great comfort during my time in Turkey.

A special thanks to Nurdan İnan and Kemal Taşlı from Mersin University, Turkey, for identifying various micro-fossils.

In Edinburgh, thanks to Nic Odling, for patiently teaching me geochemical techniques, and Mike Hall for preparing numerous thin sections.

Thank you to Christine Brouet-Menzies, Andy Witham and Steve Vincent at CASP.

Last, but by no means least, thank you to Laura Rollinson for proof reading my manuscripts and introducing page breaks to them. Mostly, however, thank you for all your love and support without which I would not be where I am today. Laura, I hope I have explained how ‘they’ know, and I hope there is not too much bunkum involved.

Final thanks go to Jack Nairn, who made his appearance into this world midway through my PhD study, and has brought so much happiness to his Mum and Dad.

Table of Contents

Chapter 1: Introduction

Chapter 2: The Kırıkkale Basin

Chapter 3: The Çankırı Basin

Chapter 4: The Tuz Gölü Basin

Chapter 5: The Haymana–Polatlı Basin

Chapter 6: Conclusions: a new model of continental collision

References

Appendices

Chapter 1: Introduction

1.1 Organisation of the thesis

This thesis is presented in a journal format as a series of chapters representing individual papers to be submitted for publication. A journal format is, by necessity, concise so the introductory chapter will: 1) assess the nature of the problem and how it is to be tackled; 2) explain why this thesis material is ideal for a journal format and; 3) set out the regional geological context of the thesis.

1.2 Rationale

Many interpretations of ancient orogens assume a simple evolution based on the Wilson cycle; i.e. rifting, followed by closure of a single oceanic basin to form a mountain belt (Wilson 1966; Burke *et al.* 1976; Gurnis 1988). However, many modern oceanic areas, such as the southwest Pacific (e.g. Charlton 2000; Milsom 2001; Hinschberger *et al.* 2005) and the Caribbean (e.g. Burke 1988; Meschede & Frisch 1998) show a more complex evolution with the interaction of microplates and the closure of several small oceanic basins. Similar scenarios may apply to ancient oceans whose presence is now only recorded by suture zones. Central Turkey lies in the Alpine-Himalayan orogen and is ideal for the study of microplate assembly leading to the incipient development of a mountain belt. In this region there are a variety of tectonic units which are well exposed, including accretionary prisms, ophiolites, magmatic arc rocks, forearc-type sedimentary basins and inferred microcontinents (Fig. 1.1). Some of the units are, geologically, quite young (Mesozoic-Cenozoic); they are also commonly well exposed at a variety of structural levels and include relevant sedimentary, igneous and metamorphic units.

The Tethyan development of Turkey includes a complex history of rifting, subduction, accretion and collision episodes. It can be divided into two partly

overlapping phases: Palaeotethyan and Neotethyan (Şengör & Yılmaz 1981). Palaeotethys was a wedge-shaped ocean basin which resulted from the rifting of Pangea (Bullard *et al.* 1965). There is vigorous debate on the geodynamic evolution of Neotethys in the Eastern Mediterranean region. There is a consensus that Neotethyan oceanic crust formed by rifting of a Gondwanan passive margin to the south during the Permian or Triassic (Fig.1.2) however, the nature and timing of rifting is debated (Robertson & Dixon 1984; Şengör *et al.* 1984b; Stampfli 2000; Stampfli & Borel 2002; Okay *et al.* 2006; Mackintosh 2008; Mackintosh & Robertson 2008). There is also disagreement on the number of rifted continental fragments, subduction zones and associated sutures during the development of Neotethys (Fig.1. 3). For some (Şengör & Yılmaz 1981; Görür *et al.* 1984; Robertson & Dixon 1984; Şengör *et al.* 1984b; Görür *et al.* 1998) Neo-Tethys consisted of up to three different oceanic strands: 1) the Intra-Pontide; 2) the northern and; 3) the southern ocean basins. In this scenario, northern Neotethys may be further subdivided into: the İzmir-Ankara-Erzincan Ocean (located between the Eurasian plate to the north and the Tauride-Antolide Platform to the south) and the Inner Tauride Ocean (Fig.1.3a and Fig.1.3b). Other authors (e.g. Ricou *et al.* 1984) proposed that Neotethys was a single ocean basin, with ophiolites being formed at spreading ridges (Dercourt *et al.* 1986) (Fig.1. 3c). A further model argues that a 'Cimmerian' continental fragment including the Tauride Platform rifted from the northern margin of Gondwana, opening Neotethys during the Late Permian-Early Triassic time. Simultaneously, Palaeotethys subducted northwards under the Eurasian active margin. An 'Anatolide block' rifted from Eurasia and collided with the Tauride Platform in the latest Triassic. Sinistral strike-slip is thought to have played a role in suturing the Gondwana-derived Tauride platform and the Eurasia-derived Anatolide block (Stampfli 2000; Stampfli & Borel 2002; Moix *et al.* 2008).

In central Turkey it is commonly accepted that northern Neotethys was subducted northwards under the Eurasian (Pontide) active margin during Late Mesozoic-Early Cenozoic time (Şengör & Yılmaz 1981; Robertson & Dixon 1984; Şengör *et al.* 1984b). Subduction was associated with the formation of accretionary prisms (Koçyiğit 1991; Görür *et al.* 1998), while intra-oceanic subduction is thought

to have generated ophiolites in a supra-subduction zone (SSZ) setting (Yaliniz *et al.* 1996; Floyd *et al.* 2000; Robertson 2002) (Fig.1. 3d).

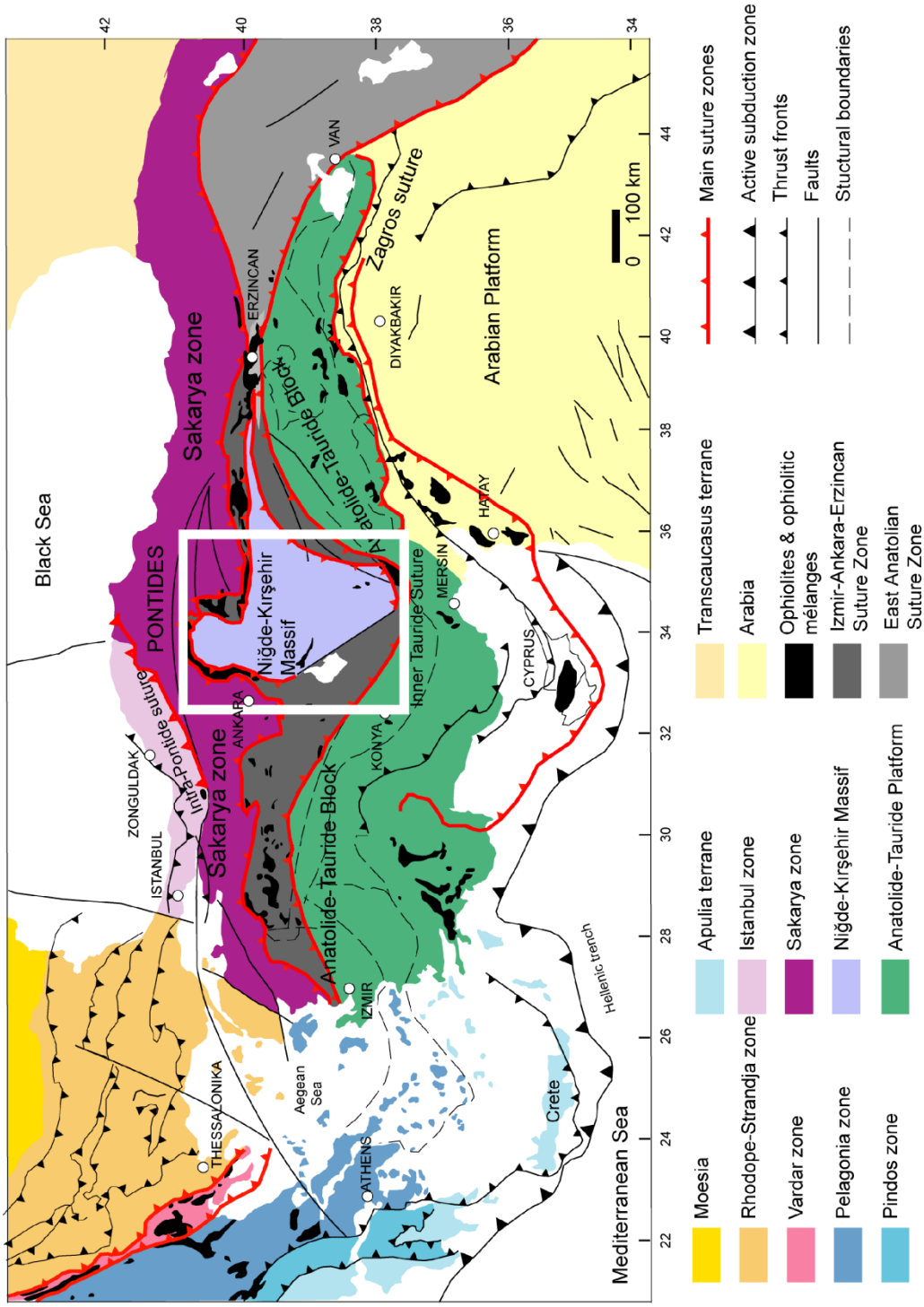

Figure 1.1 Outline tectonic map of the Eastern Mediterranean, modified after (Okay & Tüysüz 1999; Moix *et al.* 2008). The white box is the location of Fig.1.4.

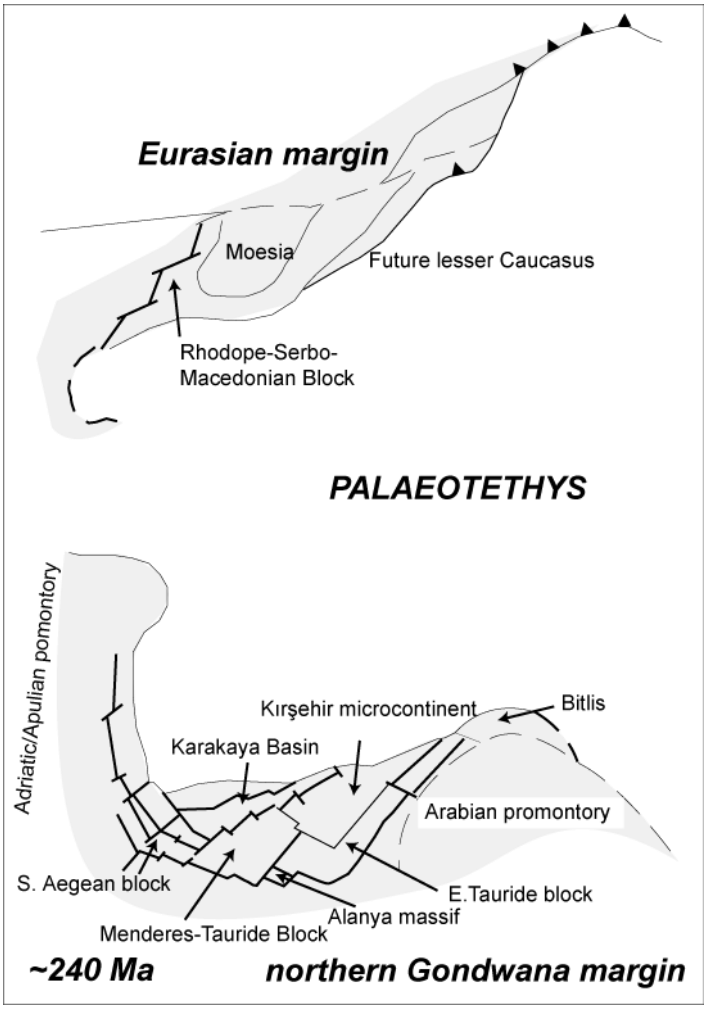

Figure 1.2 Schematic palaeotectonic map of the Eastern Mediterranean for ~240 Ma shows Triassic rifting of a Gondwana margin to the south of Palaeotethys. The continental fragments were to drift to the north and open the small ocean basins of Neotethys. After Robertson and Dixon (1984).

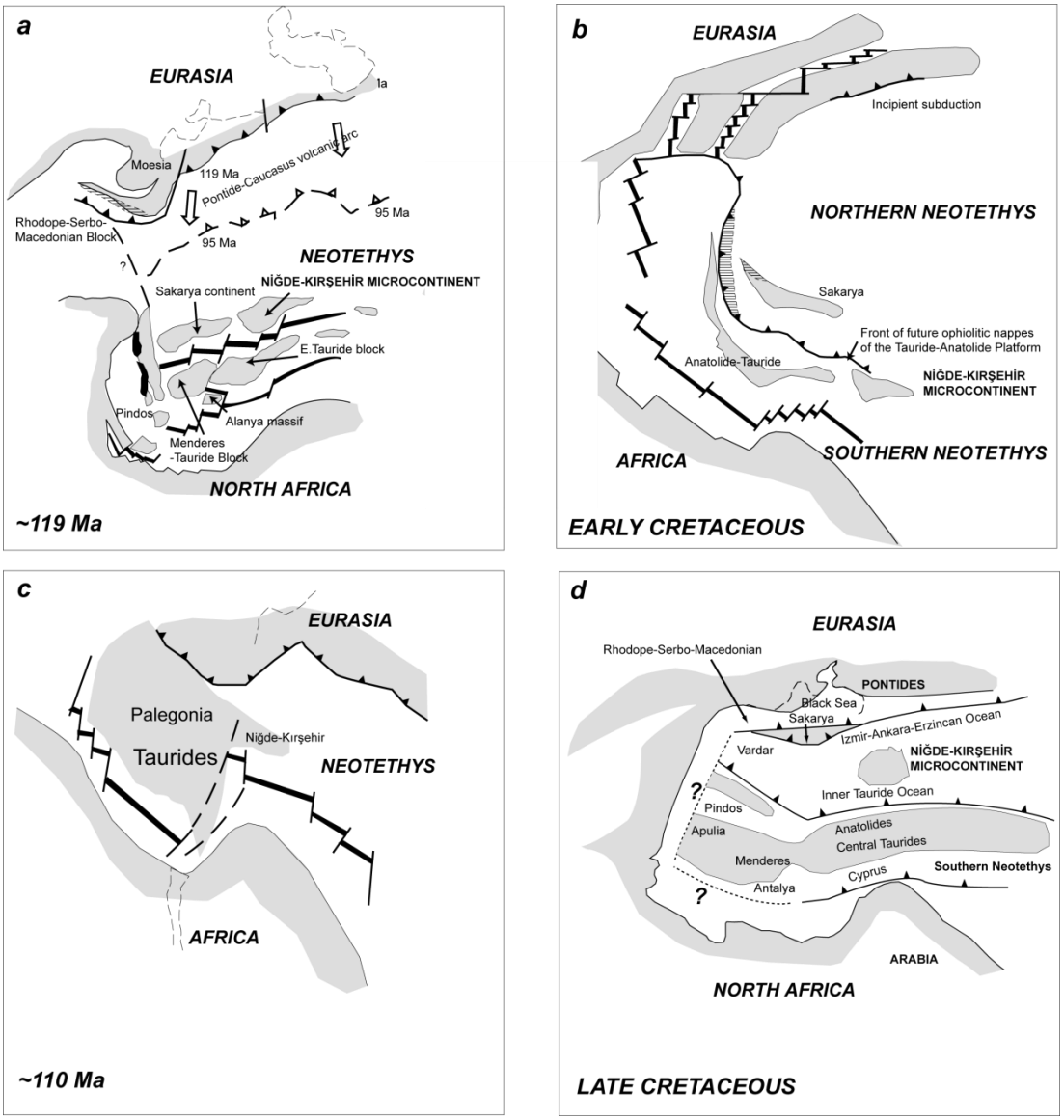

Figure 1.3 Selected palaeotectonic reconstructions of the Eastern Mediterranean during the Cretaceous. **(a)** Northward subduction of northern Neotethys beneath the Eurasian active margin and the drift of Gondwana-related continental fragments separated by small ocean basins. Ophiolites were formed above subduction zones (Robertson & Dixon 1984). **(b)** Northward drift of continental fragments (Cimmeria) towards a Eurasian passive margin (Şengör *et al.* 1984b). **(c)** One evolving Tethys Ocean in which Neotethyan ocean crust formed in a single ocean basin to the north of Gondwana where Cretaceous ophiolites were generated at spreading ridges (Dercourt *et al.* 1986). See Robertson *et al*. (1996) for further discussion. **(d)** Tectonic sketch showing the positions of the İzmir-Ankara-Erzincan Ocean and the inferred Inner Tauride Ocean (Robertson *et al.* 2009).

1.3 The central Anatolian sedimentary basins

Critical to understanding microplate assembly in central Anatolia is the role of its Upper Cretaceous-Cenozoic sedimentary basins (termed the "Central Anatolian Basins"). They are convergent-type basins and record the assembly of several tectonic elements of the region including; 1) the Ankara Mélange – an inferred subduction/accretion complex (Bailey & MacCallien 1950; Norman 1984; Rojay *et al.* 2001; Dilek & Thy 2006); 2) the Eurasian continental margin (Robinson *et al.* 1995; Okay & Şahintürk 1997; Rice *et al.* 2006); 3) the Niğde-Kırşehir Massif [also known as the Central Anatolian Massif (Erkan 1981), the Kırşehir Continent (Şengör *et al.* 1984a), the Kırşehir Complex (Lünel 1985) and the Central Anatolian Crystalline Complex (Göncüoğlu *et al.* 1991)] - an inferred microcontinent.

There are two contrasting Upper Cretaceous-Cenozoic basin types in central Anatolia. To the south and east of the Niğde-Kırşehir Massif two important localities are the Sivas Basin (Cater *et al.* 1991; Gürsoy *et al.* 1997; Dirik *et al.* 1999; Yılmaz & Yılmaz 2006) and the Ulukışla Basin (Göncüoğlu 1986; Alpaslan *et al.* 2004; Clark & Robertson 2005; Alpaslan *et al.* 2006; Kurt *et al.* 2008). These basins differ from those to the north and west of the Niğde-Kırşehir Massif (i.e. the basins featured in this study) because they are interpreted to have developed after Northern Neotethyan ophiolite emplacement over the Gondwana-derived Tauride carbonate platform and are associated with the closure of the Inner Tauride Ocean. The Maastrichtian-Neogene Sivas Basin is generally seen as post-collisional and transtensional to transpressional (Yılmaz & Yılmaz 2006). The Maastrichtian-Upper Eocene Ulukışla Basin is interpreted as being extensional or transtensional and formed after ophiolite emplacement on the Bolkar carbonate platform on the northern margin of the Tauride plate (Clark & Robertson 2002; 2005).

The subject of this thesis is a family of basins situated to the northern and western margin of the Niğde-Kırşehir Massif (Fig.1.4). They are convergent basins, show a complex evolution during the latest Cretaceous-Cenozoic time and have developed on different regional tectonic units including the Niğde-Kırşehir Massif,

the Eurasian active margin and accretionary material forming the İzmir-Ankara-Erzincan Suture Zone (Fig.1.5). They are ideal for this study because they contain well-exposed rocks, often display complete stratigraphic sequences, and have experienced little or no metamorphism. Norman *et al.* (1980) describe "a series of interconnected basins...within the 'melange belt' during Late Cretaceous-Early Tertiary times". The basins have received little attention since pioneering sedimentary and stratigraphic studies, mainly during the 1970s and 1980s. These include: the **Kırıkkale Basin** (Norman 1972; Norman 1973a; Norman 1973b); the **Sungurlu and Bayat areas of the Çankırı Basin** (Şenalp 1979; Şenalp 1981); the **Tuz Gölü Basin** (Rigo de Righi & Cortesini 1959; Arikan 1975; Dellaloğlu & Aksu 1984; Görür *et al.* 1984) and the **Haymana-Polatlı Basin** (Gökçen 1976b; Gökçen 1976a; Ünalan & Yüksel 1978; Koçyiğit 1991) (Fig.1.4). Reviews of the regional tectono-sedimentary development of these basins are provided by Norman *et al.* (1980), Görür *et al.* (1998) and Gürer & Aldanmaz (2002). Recent studies in this area have concentrated on the structural and geophysical nature of the basins (Çemen *et al.* 1999; Ateş *et al.* 2005; Aydemir & Ateş 2005; Aydemir & Ateş 2006; Aydin *et al.* 2006; Aydemir & Ateş 2008) and burial history (Tokatlı *et al.* 2006).

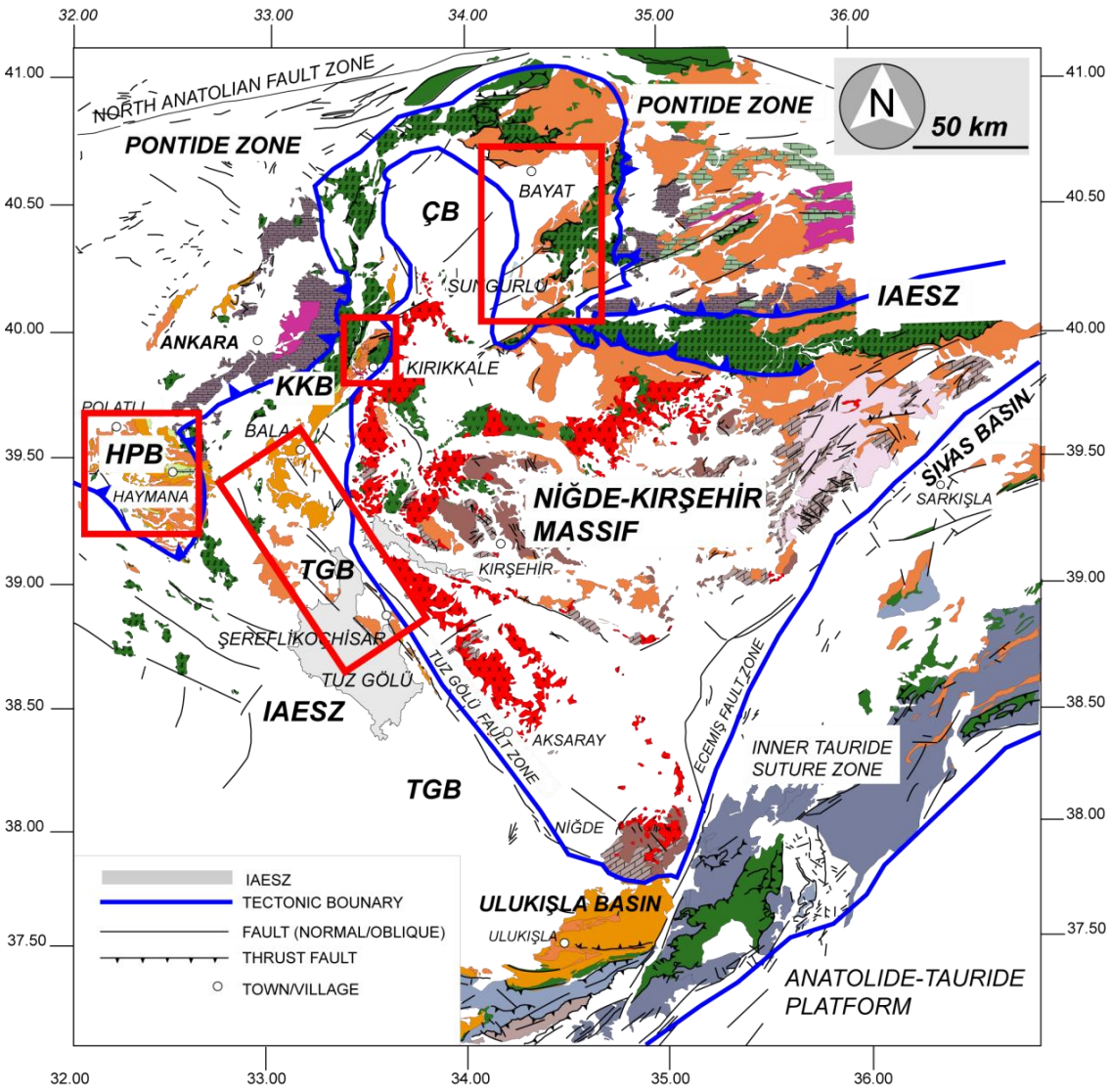

PALAEOGENE - NEOGENE COVER

- Oligocene - Neogene sediments and volcanics
- Eocene sandstones, shales, limestones, volcanics
- Palaeocene sandstones, shales, limestones

OPHIOLITES AND MELANGES

- Upper Cretaceous stratiform ophiolites
- Ophiolitic mélange containing metabasites
- Izmir-Ankara accretionary complex
- Permo-Triassic limestone block mélange
- Permo-Triassic metamorphic block mélange

METAMORPHIC BASEMENT (NİĞDE-KIRŞEHİR MASSIF)

- Upper Cretaceous granitoids
- Upper Palaeozoic marbles, cherty marbles
- Palaeozoic schists, marbles, calc-silicates
- Palaeozoic paragneisses, garnet quartzites, amphibolites

INNER TAURIDE SUTURE ZONE

- Jurassic marbles
- Palaeozoic-Mesozoic sediments

PONTIDE ZONE

- Jurassic neritic limestone

Figure 1.4 Regional geological map of the central Anatolian region surrounding the Niğde-Kırşehir Massif and the position of the four study areas signified by red boxes; i.e. the Haymana-Polatlı Basin (HPB), the Kırıkkale Basin (KKB), the Tuz Gölü (Salt Lake) Basin (TGB) and the Sungurlu and Bayat Areas in the Çankırı Basin (ÇB). Data are from MTA (2002) and field observations.

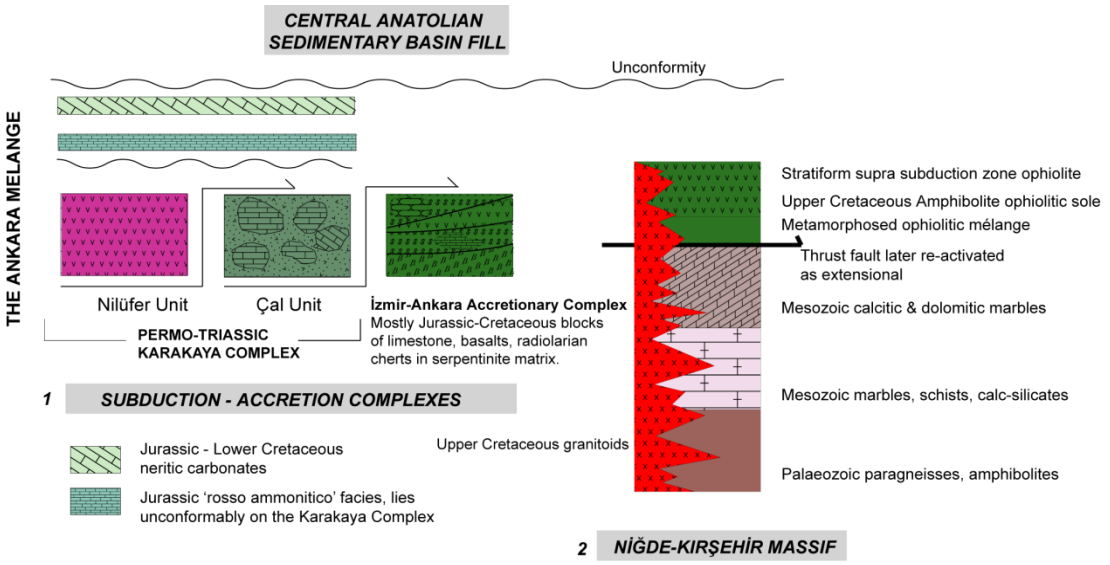

Figure 1.5 Stratigraphic cartoon showing the basement material of the central Anatolian sedimentary basins: 1) subduction/accretion complexes of the Ankara Mélange and; 2) the Niğde-Kırşehir Massif. Note the structural positions and ages of the Karakaya Complex and the İzmir-Ankara Accretionary Complex. The outline stratigraphy of the Niğde-Kırşehir Massif is adapted from Floyd *et al.* (2000). See text for further discussion.

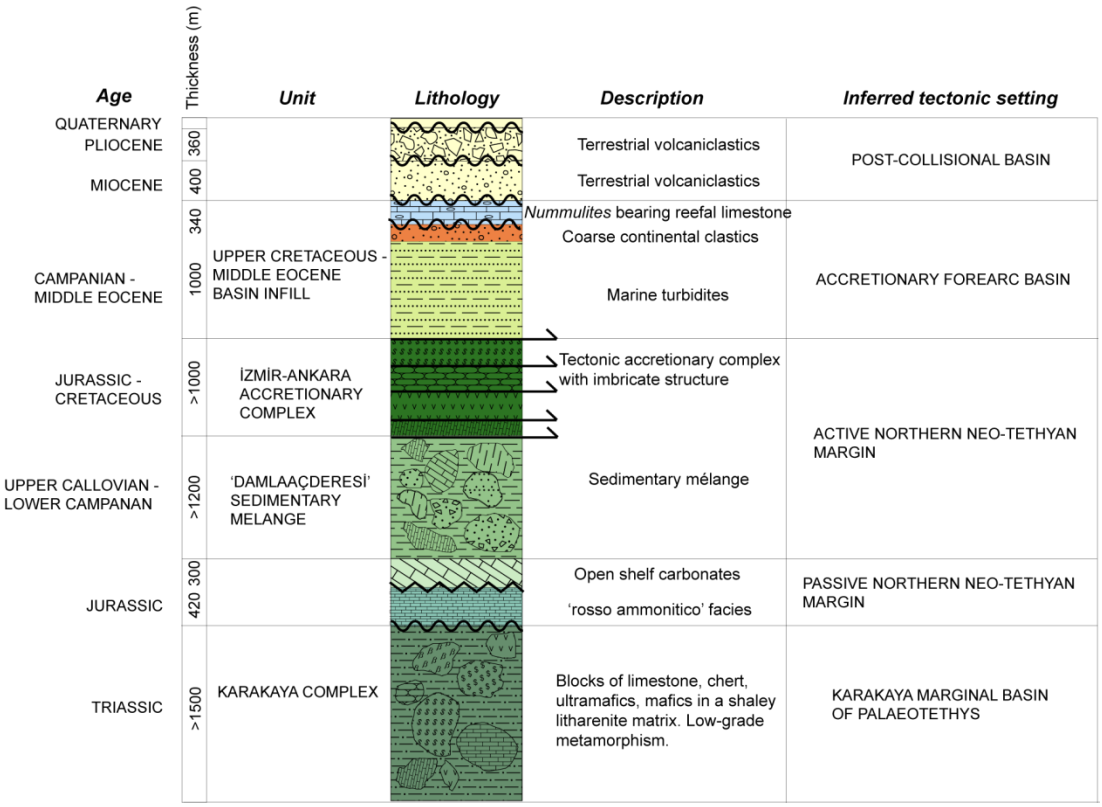

Figure 1.6 Generalised stratigraphy of the Ankara Region showing the Triassic Karakaya Complex, Jurassic sediments, the İzmir-Ankara Accretionary Complex and overlying basinal sediments. The stratigraphy and inferred tectonic settings are redrawn from Koçyiğit (1991).

1.4 Aims

The aim of this study is to test existing tectono-sedimentary models of basin evolution and place the findings in a regional geodynamic context. This will be achieved by utilising modern geological methods to provide data that remain undocumented in the literature including: 1) measured stratigraphic sections; 2) facies analysis and facies correlations between the basins; 3) fault kinematics and structural evolution; 4) provenance studies; 5) systematic palaeontological control on the stratigraphic framework; 6) palaeocurrent studies and; 7) geochemistry of igneous rocks. It is important to note that several of these studies were published before a coherent tectonic model of the evolution of central Turkey was developed (e.g. Şengör & Yılmaz 1981; Robertson & Dixon 1984). It is therefore crucial to relate the evolution of these basins to regional tectonics.

Pre-fieldwork literature surveys enabled the following areas to be targeted, all of which offer unique insights into tectono-sedimentary processes associated with regional plate convergence: 1) the Kırıkkale Basin (Chapter 2) provides an excellent opportunity to investigate basin evolution on an inferred subduction-accretion complex (the Ankara Mélange) and a microcontinent (the Niğde-Kırşehir Massif); 2) The Sungurlu and Bayat areas of the Çankırı Basin (Chapter 3), this northerly basin is proximal to the Pontide magmatic arc; 3) the Tuz Gölü Basin (Chapter 4) is critical to understanding sedimentary processes on the margin of a microcontinent and; 4) the Haymana-Polatlı Basin (Chapter 5) was targeted for study because it was constructed on the Ankara Mélange and is located in a unique position to the west of the Niğde-Kırşehir Massif. The basins are geographically varied, however, this is a process-based study therefore geological processes in operation at each locality will be examined, compared and contrasted. Chapter 6 integrates the evolution of the Central Anatolian basins into a new regional tectonic model of basin evolution.

1.5 Geophysical data

Limited gravity, magnetic and seismic data suggest that the basins are connected at depth (Aydemir & Ateş 2005; Aydemir & Ateş 2006). Figure 1.7 shows regional gravity and magnetic anomaly maps for western central Anatolia. The gravity anomaly map (Fig. 1.7a) shows that there are no separating structures and/or gravity anomalies separating the Tuz Gölü, Haymana-Polatlı and Kırıkkale Basins. The Tuz Gölü and Haymana-Polatlı are linked by a small channel-shaped basin called the Terkasan Basin (Aydemir & Ateş 2006).

The magnetic anomaly map (Fig. 1.7b) shows the central Anatolian basins bound by a northwest-southeast trending positive anomaly. This is interpreted to be Neogene volcanics associated with a fault zone (Aydemir & Ateş 2006). A branch of older volcanics extends north-eastwards to the east of Haymana, through Bala and towards Kırıkkale. There are two possibilities to explain this branch: 1) the basin-fill may be composed of volcaniclastic sediments; 2) volcanic lava flows may be inter-bedded with basin sediments. Other positive anomalies to the north of Kırşehir are probably representative of granitoid plutons.

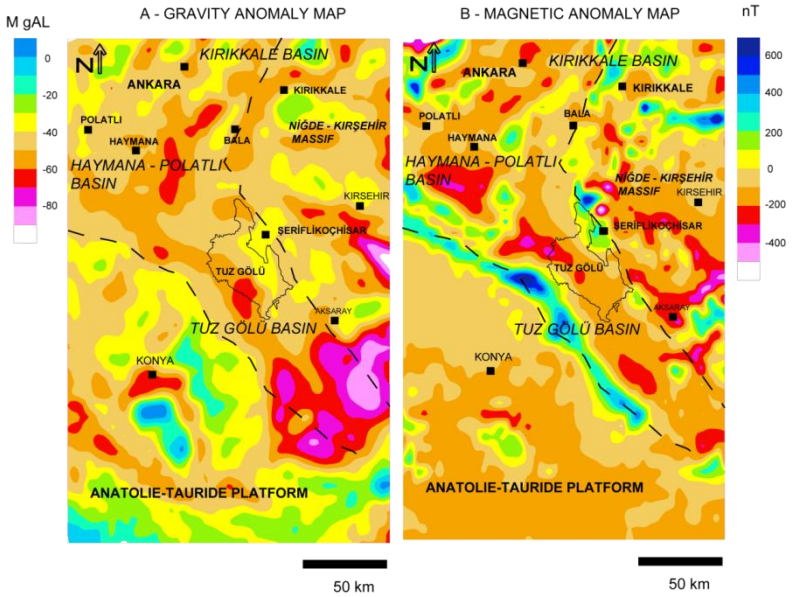

Figure 1.7 A – Gravity anomaly map (in mGal) and B-Magnetic anomaly map (in nT) of western central Anatolia. The maps are redrawn from Aydemir & Ateş (2005).

The Tuz Gölü and Haymana-Polatlı Basins have been the subject of several hydrocarbon exploration projects, mostly conducted by the Turkish Petroleum Corporation (TPAO), thus seismic data has been published in the literature for these areas (Arikan 1975; Ünalan & Yüksel 1978; Ergün & Sari 1982; Turgay & Kurtuluş 1985; Çemen *et al.* 1999; Aydemir & Ateş 2006; Aydemir & Ateş 2008) but they are absent for the Kırıkkale and Çankırı Basins. Seismic evidence suggests that the deepest part of the Haymana-Polatlı Basin is located to the east of Haymana and reaches ~6 to ~7 km in depth and 3-D modelling gives depths of the Tuz Gölü Basin sediments at ~7 to ~13 km (Aydemir & Ateş 2006). Deep structures are commonly interpreted as extensional. In the Haymana-Polatlı Basin Ünalan & Yüksel (1978) report a north-west to south-east aligned graben and Turgay & Kurtuluş (1985) describe folding cut by north-west to south-east trending fault zones. The Tuz Gölü Basin is thought to have been controlled by northwest-striking extensional faulting during its initial development during the Late Cretaceous (Çemen *et al.* 1999).

1.6 Previous Work

1.6.1 The Kırıkkale Basin

Pioneering work in the Kırıkkale Basin was conducted on its stratigraphy (Norman 1972), sedimentology (Norman 1973a) and post-Eocene tectonic development (Norman 1973b). A brief review of this work is as follows: the stratigraphy of the basin is characterised by a continuous Upper Cretaceous–Lower Cenozoic sedimentary sequence including submarine slumps, olistostromes and turbidity currents. To the west of the basin, this sequence reached ~3200 m in thickness. On the eastern margin of the basin, a Palaeocene granitic pluton was emplaced into a sequence of oceanic lavas and tuffaceous rocks. In the Late Eocene, a marine regression led to the deposition of red continental clastics, gypsum and lagoonal limestones (Norman 1972). The post-Eocene (mainly Oligocene) tectonic development produced asymmetric folds overturned eastwards; this was followed by thrust faulting then right-lateral strike-slip faulting. (Norman 1973b). A later report

(Akyürek *et al.* 2001) was based on the western margin of the basin and updated lithological descriptions and renamed selected formation names (see Chapter 2).

Recent work (Dönmez *et al.* 2008) subdivided rocks belonging to the İzmir-Ankara-Erzincan Suture Zone and the Niğde-Kırşehir Massif. In this interpretation, rocks associated with the İzmir-Ankara Accretionary Complex and its cover of Upper Cretaceous volcaniclastic sandstones, shales and limestones were thrust south-eastwards over Upper Cretaceous granitoids and lavas associated with the Niğde-Kırşehir Massif. The Middle Eocene saw deposition of continental conglomerates and shallow marine limestone on an uplifted erosion surface. The submarine lavas and tuffaceous rocks are correlated to the Çiçekdağ Ophiolite which overthrusts the Niğde-Kırşehir Massif and is interpreted to have formed in a supra-subduction zone-type tectonic setting (Yılmaz & Boztuğ 1998; Yalınız *et al.* 2000).

In this basin, this thesis will discuss new data which are currently missing from the literature. The need here is for stratigraphic, palaeontological, structural and whole rock igneous geochemical data.

1.6.2 The Çankırı Basin (Sungurlu and Bayat Areas)

The Sungurlu and Bayat areas are located on the north-eastern margin of the Çankırı Basin. Previous studies from the Sungurlu locality are restricted to two works in the late 1970s to early 1980s (Şenalp 1979; Şenalp 1981) and a brief review by Norman *et al.* (1980). This locality is very well-exposed and displays complete stratigraphic sequences of Eocene sediments and lavas. In the Bayat locality, the stratigraphy of Eocene sedimentary and volcanic rocks have been published in just one recent study (Kaymakcı 2000). The need here is to carefully document stratigraphy, sedimentology, palaeontology and igneous geochemistry.

1.6.3 The Tuz Gölü Basin

The Tuz Gölü Basin has been of interest to both academia and industry since early hydrocarbon exploration in 1959 (Aydemir & Ateş 2008). Early published work concentrated on the stratigraphy, sedimentology and tectonic setting of the basin (Arikan 1975; Görür *et al.* 1984; MTA 1989; Görür *et al.* 1998; Çemen *et al.* 1999) and recent work on the geophysical nature and hydrocarbon potential (e.g. Aydemir & Ateş 2006; Ayyıldız 2006; Tekin *et al.* 2007; Aydemir 2008; Aydemir & Ateş 2008). For some authors (Görür *et al.* 1984; Koçyiğit *et al.* 1988; Koçyiğit 1991; Görür *et al.* 1998) the Tuz Gölü and Haymana-Polatlı Basins are related as they developed coevally as accretionary forearc basins associated with the Eurasian active margin and Neotethyan subduction-accretion complexes. The requirements for this area are measured stratigraphic sections, palaeontology, sedimentology and structural data.

1.6.4 The Haymana-Polatlı Basin

Early work in the Haymana-Polatlı Basin established a stratigraphic framework for the Upper Cretaceous-Middle Eocene sequences (Erünal 1942; Uysal 1959). In the 1970s and 1980s the basin received further attention through stratigraphic and sedimentary reports (Sîrel 1975; Gökçen 1976a; Gökçen 1976b; Ünalan *et al.* 1976; Gökçen 1978; Meriç & Görür 1979; Görür *et al.* 1984; Çetin *et al.* 1986) seismic studies (Ünalan & Yüksel 1978; Ergün & Sari 1982; Turgay & Kurtuluş 1985) and micro-palaeontology (Duru & Gökçen 1985; Duru & Gökçen 1990). Recent work has focused on geophysical data (Aydemir & Ateş 2006), further sedimentology (Çiner *et al.* 1996a; Çiner *et al.* 1996b) and macro-palaeontology (Okan & Hoşgör 2008). In order to test existing models of basin evolution, the data needed in this area are sedimentary, structural, and palaeontological.

1.7 Contrasting tectonic models of basin development

A number of contrasting tectonic hypotheses have been proposed to explain basin development in the context of regional convergent tectonics. This thesis aims to test two end-member models. In one model (Gürer & Aldanmaz 2002) northern Neo-Tethyan supra-subduction zone-type ophiolites were emplaced southwards onto the northern margin of the Gondwana-related Tauride platform during continental collision in the latest Cretaceous. This was followed by 'piggy-back' post-collisional basin development on the underlying ophiolitic nappe. In this model, all the basins are post-collisional, have a common origin and follow a *"similar evolutionary model to one another"*(Gürer & Aldanmaz 2002). The Cenozoic is characterised by suture tightening and local thrusting of ophiolitic nappes (Figure 1.8-Model 1).

In the second model, northern Neotethys was palaeogeographically complex and included a microcontinent (the Niğde-Kırşehir Massif) which was rifted from the Tauride continent to the south. The ophiolites derived from this ocean formed in supra-subduction zone settings and were emplaced when subduction trenches collided with continental margins (Robertson 2002; Robertson 2004; Robertson *et al.* 2009). The subduction was associated with the development of an intra-oceanic magmatic arc and accretionary forearc-type basins as well as an active Eurasian continental margin arc further north (Görür *et al.* 1984; Koçyiğit 1991; Görür *et al.* 1998). In this model (Figure 1.8 – Model 2) northern Neotethys involved two oceanic strands, the İzmir-Ankara-Erzincan Ocean to the north and the Inner Tauride Ocean to the south, separated by the Niğde-Kırşehir Massif microcontinent. Basins developed as convergent, accretionary-type basins associated with north-dipping subduction which persisted until the Middle Eocene.

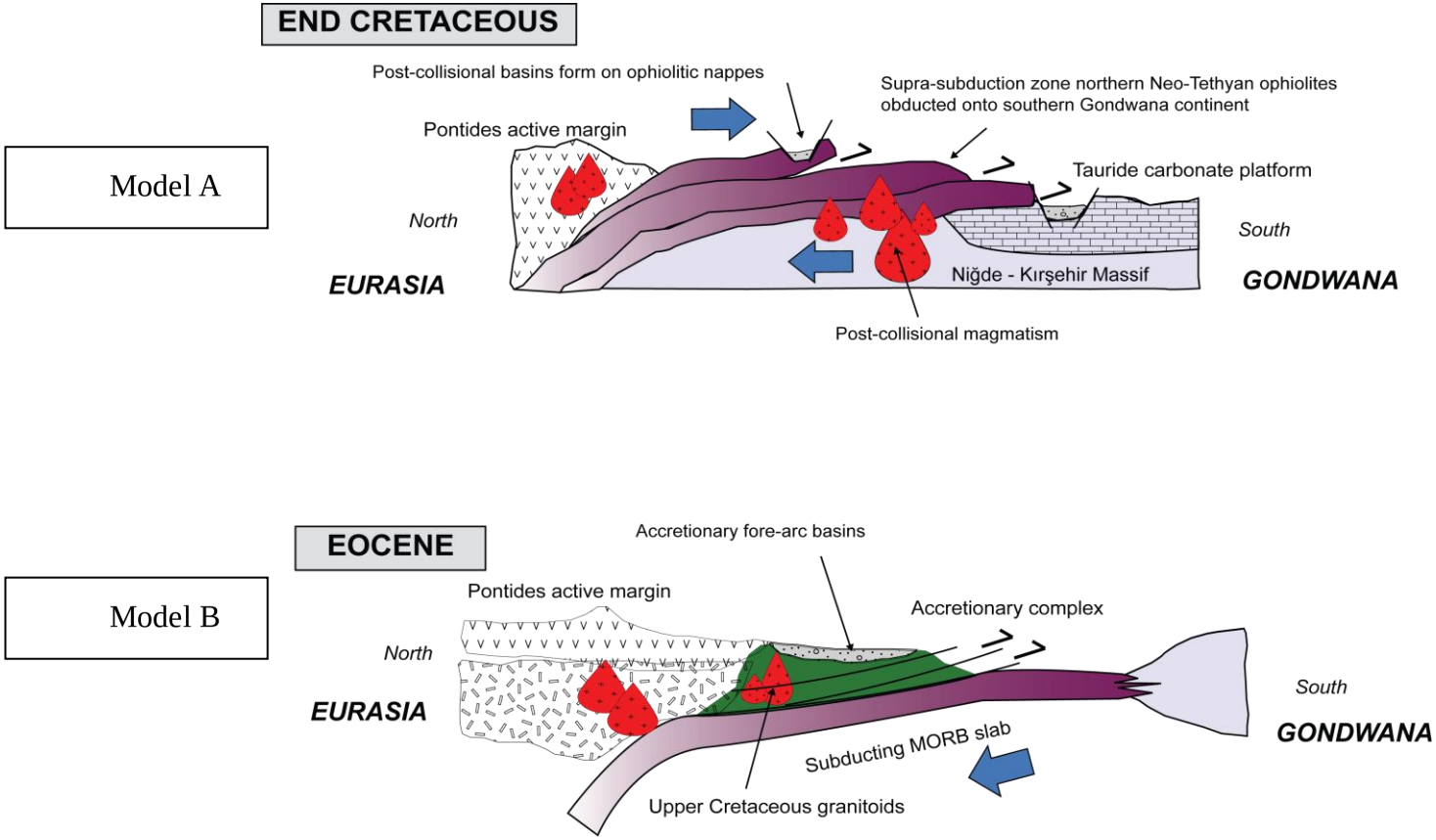

Figure 1.8 Alternative models of basin evolution in central Anatolia. In model A, ophiolites were emplaced southwards onto the Niğde-Kırşehir massif followed by a post-collisional basin evolution on the underlying ophiolite nappes (Gürer & Aldanmaz 2002). In model (B) Neotethyan subduction continues until the Eocene. Accretionary forearc basins were formed on subduction/accretion complexes (Koçyiğit 1991).

1.8 Regional geological units

1.8.1 The Ankara Mélange (specifically the İzmir-Ankara Accretionary Complex)

It is important to summarise the regional geological units associated with Upper Cretaceous-Middle Eocene basin development. This thesis uses the definition of a mélange as - blocks of heterogeneous lithologies set in an incompetent matrix, commonly pelitic or serpentinitic. The area to the south and east of Ankara is one of the world's finest examples of a mélange. The Ankara Mélange was first described by Bailey and McCallien (1950) who interpreted it as a component of the Tauride mountains to the south beneath a south-verging thrust nappe. The nappe comprised the Pontides to the north and the crystalline basement of the Niğde-Kırşehir Massif. In this initial interpretation, Turkey was essentially divided into three units with the Pontides on top, the Ankara Mélange in the middle and the Taurides at the base. This model, however, was later disproved by Ketin (1966) who described evidence of the Ankara Mélange lying *on* the crystalline basement of the Niğde-Kırşehir Massif, in contrast to the hypothesis of Bailey and McCallien (Şengör 2003).

The Ankara Mélange trends east-west over several hundred kilometres and measures ~80 km north-south (Norman 1984) It is not a rectilinear feature but is segmented and forms several loops along its length. The Ankara Mélange marks the position of part of the İzmir-Ankara-Erzincan suture zone and is best exposed to the south and east of Ankara. Modern interpretations recognise three distinct tectonic units, from structurally high to low: 1) an Upper Triassic-Lower Jurassic metamorphic mélange, composed of metasedimentary and metamorphosed mafic/ultramafic rocks in a greywacke matrix, thought to correspond to the Nilüfer Unit of the Karakaya Complex (Pickett & Robertson 1996; Okay & Tüysüz 1999; Okay & Göncüoğlu 2004); 2) a Permo-Triassic limestone block mélange consisting of neritic limestone, conglomerate, agglomerate, dolerite and turbidites in a shaley volcaniclastic matrix, corresponding to the Çal Unit of the Karakaya Complex

(Pickett & Robertson 1996; Okay & Tüysüz 1999); 3) a mainly Upper Cretaceous ophiolitic mélange which carries kilometre-scale thrust sheets and blocks of serpentinised upper mantle peridotites, gabbros, dykes, massive lava flows, radiolarian chert, sandstone and limestone in a serpentinite matrix (Norman 1984; Koçyiğit 1991; Dilek & Thy 2006). Studies of radiolarian cherts and biomicritic carbonates within the ophiolitic mélange (Bragin & Tekin 1996; Rojay *et al.* 2001) have revealed biostratigraphic ages of Late Triassic (Norian) to Mid Cretaceous (Albian/Turonian). The ophiolitic unit of the Ankara mélange represents dismembered thrust sheets accreted to a forearc platform during the Cretaceous - Cenozoic closure of the İzmir-Ankara-Erzincan Ocean. The complex includes remnants of Neo-Tethyan oceanic lithosphere and pelagic sediments carried on a northward-trending subducting slab. Tankut *et al.* (1998) recognised three chemically different types of volcanic rocks: 1) sub-alkaline N-MORBs; 2) island-arc tholeiites; 3) within-plate oceanic island-type alkaline basalts. U/Pb zircon dating gives Early Jurassic crystallisation dates (~179±15 Ma) for a plagiogranite dyke cutting upper mantle material (Dilek & Thy 2006). The term 'Ankara Mélange' covers multiple geological units, ages and accretionary events. This study prefers the term 'the İzmir-Ankara Accretionary Complex' (Okay *et al.* 2006) to refer to the lower and youngest ophiolitic unit of the Ankara Mélange. Study of the Ankara Mélange is still in its infancy, and many questions remain unresolved. For this reason, the Ankara Mélange beneath the Upper Cretaceous-Middle Eocene basins was included within this study.

1.8.2 The Pontide active margin

The Pontide (Eurasian) active margin can be divided into the western, central and eastern Pontides. The Pontides include the Sakarya Zone which forms a ~1500 km-long by ~200 km-wide Mesozoic rifted continental fragment which incorporates the Sakarya 'continent' of Şengör and Yılmaz (1981). The zone is bounded to the south by the İzmir-Ankara-Erzincan Suture Zone and to the northwest by the

Istanbul Zone. The Central and Eastern Pontides contain well-developed magmatic arc rocks (Akıncı 1984; Robinson *et al.* 1995; Rice *et al.* 2009). Biostratigraphic ages and radiometric dating of plutonic rocks indicate that calc-alkaline magmatism was active from the Turonian to the end of the Maastrichtian in the Eastern Pontides (Okay & Şahintürk 1997; Okay *et al.* 2001). The Sakarya zone is underlain by Permo-Triassic subduction-accretion complexes of the Karakaya Complex, which are in turn unconformably overlain by a Lower Jurassic to Eocene sedimentary sequence (Koçyiğit 1991; Pickett & Robertson 1996; Okay & Tüysüz 1999). The Permo-Triassic subduction-accretion complexes can be subdivided into a lower and an upper unit. The lower part of the Karakaya Complex is a highly deformed and sheared sequence of metabasites intercalated with phyllite and marble and corresponds to the Nilüfer unit (Pickett & Robertson 1996; Pickett & Robertson 2004). The upper Karakaya Complex is composed of several tectonostratigraphic units including: 1) arkosic sandstone; 2) greywacke with exotic limestone blocks; 3) basalts and olistostromes with Upper Permian limestone clasts (Çal unit) and; 4) black shales (Pickett & Robertson 1996; Okay & Göncüoğlu 2004; Sayıt & Göncüoğlu 2009). Interpretations of the Karakaya Complex (Pickett & Robertson 1996; 2004) suggest a Triassic subduction-accretion complex related to the collision of oceanic seamounts, mid-ocean ridge type oceanic crust, pelagic sediments and continental fragments to the Eurasian active margin during the closure of Palaeotethys.

1.8.3 The Niğde-Kırşehir massif

The Niğde-Kırşehir massif is a ~300 km x ~200 km roughly triangular-shaped tectonostratigraphic unit, bounded by the Tuz Gölü and Ecemiş fault zones and composed of metamorphic, ophiolitic and intrusive granitoid rocks. The Palaeozoic-Mesozoic metamorphic basement consists of platform metasediments (marbles, calc-silicates, mica-schists) amphibolites and garnet gneisses (Seymen 1981). Peak Low-*P*-high-*T* (>700 °C) Barrovian metamorphism has been dated as

Late Cretaceous (84.1 ± 0.8 Ma) (Whitney & Hamilton 2004) when the massif was buried to a depth of 16 - 20 km (Whitney & Dilek 1997). The northern margin of the massif has been overthrust from the north by fragmented Upper Cretaceous supra-subduction zone ophiolites (Yaliniz *et al.* 1996; Floyd *et al.* 2000; Yalınız *et al.* 2000). This assemblage was subsequently intruded by Upper Cretaceous granitoid plutons. The Niğde-Kırşehir Massif comprises four different tectonic blocks, characterised by different P-T-t paths. At ~40 Ma the southern Niğde massif remained at mid-crustal levels whilst the more northerly Kırşehir and Akdağ massifs were at, or near, the Earth's surface (Whitney *et al.* 2001). There is presently considerable debate on the Mesozoic tectonic setting and evolution of the Niğde-Kırşehir Massif. It is seen as a promontory of the Tauride-Antolide Platform (Yaliniz *et al.* 1996; Floyd *et al.* 2000; Göncüoğlu *et al.* 2006), as a microcontinent of the Northern Neotethys (Görür *et al.* 1984; Robertson & Dixon 1984; Whitney *et al.* 2001; Robertson *et al.* 2009), as a part of the Eurasian margin (Kazmin & Tikhonova 2006) or as an allochthonous terrane translated laterally along the orogen to near its present position during Triassic time (Stampfli *et al.* 2001).

1.8.4 Intrusive rocks of the Niğde-Kırşehir Massif

Granitoid plutonic associations of the Niğde-Kırşehir Massif have been studied in detail in recent years in terms of their petrogenesis, mineralogy, petrology and tectonic setting. They may be subdivided into the following broad classifications: 1) Calc-alkaline: metaluminous/peraluminous I- to S-type plutons ranging from monzodiorite to granite; 2) Sub-alkaline: metaluminous I-type plutons ranging from monzonite to granite; 3) Alkaline: metaluminous to peralkaline plutons, predominantly A-type, ranging from monzosyenite to granite (e.g. Ilbeyli *et al.* 2004; Köksal *et al.* 2004; Ilbeyli 2005; Tatar & Boztuğ 2005; Boztuğ *et al.* 2007; Köksal *et al.* 2008). Dated intrusive rocks show U/Pb SHRIMP ages of 85-92 Ma (Whitney *et al.* 2003), U/Pb titanite ages of 74.0±2.8 and 74.1±0.7 Ma (Köksal *et al.* 2004). U/Pb SHRIMP dating of zircon rims of country rock sillimanite schist gives

crustal melting at 91.0 ± 2.0 Ma (Whitney *et al.* 2003). K/Ar cooling ages of hornblende and biotite give dates of 66.6±1.1 Ma to 79.5±1.7 Ma (Ilbeyli *et al.* 2004). $^{40}Ar/^{39}Ar$ biotite cooling ages are 77.6±0.3 Ma (Kadıoğlu *et al.* 2003). Many authors believe that the plutonic associations were generated in a syn- to post-collisional tectonic setting, following the closure of northern Neotethys (e.g. Göncüoğlu & Türeli 1994; Boztuğ 1998; Kenan M. Yaliniz *et al.* 1999; Boztuğ 2000; Köksal *et al.* 2001; Kuşcu *et al.* 2002; Ilbeyli *et al.* 2004). Another model (Kadıoğlu *et al.* 2003; Kadıoğlu *et al.* 2006) points to an Andean-type subduction related genesis of the Ağaçoren Intrusive Suite on the western margin of the Niğde-Kırşehir Massif. The nature of the intrusive associations will be discussed in further detail in Chapter Two.

1.9 Methodology

Fifteen weeks over three separate field seasons (September 2006, May/June 2007 and May/June 2008) were spent in central Turkey, which allowed a large amount of data to be gathered, and over two hundred rock samples to be collected. Fieldwork included rock sample collection, fossil collection, photographing and sketching key features, detailed stratigraphic logging, and gathering structural and palaeocurrent data. Field mapping was restricted to crucial areas.

Collection of primary data was backed up by laboratory-based work including:

1) Whole rock X-Ray Fluorescence (XRF) studies of igneous rocks were achieved using the method of Fitton (1998). See Appendix 1 for further methodology and data;

2) Petrographic analysis using a Nikon Eclipse e2000 petrological microscope with a Nikon Coolpix camera. Point counting was done on a Leica

microscope using the Gazzi-Dickinson method (Gazzi 1966; Dickinson 1970). See Appendix 2 for further discussion and data;

3) Reconstruction of palaeocurrents using palaeocurrent indicators including flute marks, groove marks and imbricated gravels. See Appendix 3 for further discussion and data.

4) Fault analysis using TectonicsFP software (Ortner *et al.* 2002). See Appendix 4 for fault data and a discussion of methods employed in data analysis;

5) Fossils were analysed initially at the University of Edinburgh then a detailed investigation was conducted by Prof. N İnan and Dr. K Tasli of Mersin University, Turkey. The ages provided were incorporated into the stratigraphic model presented in this thesis. The timescale used is that of Gradstein *et al.* (2004).

Presently, there is an array of local formation names assigned by previous studies in the Central Anatolian Basins. In order to integrate and cross-correlate the individual basins in the Central Anatolian, it is necessary to change several local formation names. For example, a Palaeocene succession of in-situ coralgal reefs and collapsed limestone blocks is variously referred to as the Dizilitaşlar Formation in the Kırıkkale Basin and the Çankırı Basin (Norman 1972), the Yeşilyurt Formation (Ünalan *et al.* 1976) or the Çaldağ Formation (Görür *et al.* 1984) in the Haymana-Polatlı Basin. While recognising and acknowledging the value of previous studies, unified formation names permit a focused and coherent view of basin development throughout central Anatolia. Therefore, several formation names are changed, and previous stratigraphic models are redefined in this thesis; the reader's attention will be drawn to such changes.

Stratigraphic descriptions and interpretations are accompanied by sedimentary descriptions of lithofacies, which are defined by lithology, textures, sedimentary structures, bounding surfaces and bed thicknesses, fossils content and

inferred depositional processes. Detailed interpretations of sedimentary transport and depositional processes are beyond the remit of this thesis.

The individual chapters contain descriptions and interpretations of stratigraphic, sedimentary, geochemical and structural data. Short summaries are provided which highlight the role of new data gathered during this study. In particular, where new data has added to, confirmed or redefined existing geological models.

1.10 Turkish pronunciation

Listed below are some of the common pronunciations of Turkish letters used in this thesis with the accompanying sounds.

Letters:

c/C: pronounced ‘j’ as in Jack

ç/Ç: pronounced ‘ch’ as in church

ğ/Ğ: a silent ‘g’ and lengthens the sound of the preceding vowel

ı/I: pronounced ‘i’ as in cousin

i/İ: pronounced ‘ee’ as in see

ö/Ö: pronounced ‘e’ as in Bert

ş/Ş: pronounced ‘sh’ as in sugar

ü/Ü: pronounced ‘oe’ as in shoe

Towns / key words: (*letters in **bold** should be stressed)*

Kırıkkale: pronounced *Ki-**ri**-kaleh* (town name, translates as ‘broken castle’).

Sungurlu: pronounced *Soon-**goor**-loo* (town name).

Bayat: pronounced ***Bay**-at* (town name. Turkish ‘a’ is always short as in ‘hat’, never long as in ‘day’).

Tuz Gölü: pronounced *Tooz **Guhl**-ooh* (translates as ‘Salt Lake’).

Şereflikoçhisar: pronounced *Sher-ef-lee-**koch**-heesar* (town name: originally named

after Koçhisar Castle, Şerefli translates as ‘honorable’ and was added to commemorate the many men from the town lost in Gallipoli during the Great War).

Haymana: pronounced ***Hay****-ma-na* (town name: named after *Hayme Ana* the mother of the father of Osman I the founder of the Ottoman Empire).

Polatlı: pronounced *Pohl-**at**-lih* (town name).

dere: pronounced ***der****-eh* (translates as ‘river/stream’)

tepe: pronounced ***tep****-eh* (translates as ‘hill’)

köy: pronounced *keuy* (translates as ‘village’)

taş: pronounced *tash* (translates as ‘stone’)

Chapter 2: The Kırıkkale Basin

2.1 Introduction

Central Turkey lies in the Alpine-Himalayan orogen and is ideal for the study of micro-plate assembly leading to the incipient development of a mountain belt. In this region there is a collage of tectonic units including magmatic arcs, subduction-accretion complexes and inferred micro-continents. Within central Anatolia, the Mesozoic Neotethys ocean crust formed by rifting of a Gondwana passive margin in the Permian or Triassic, the nature and timing of rifting is debated (Şengör & Yılmaz 1981; Robertson & Dixon 1984; Stampfli 2000; Stampfli & Borel 2002; Okay *et al.* 2006; Mackintosh & Robertson 2008).

It is commonly accepted that Neotethys existed as several oceanic strands separated by microcontinents. The largest oceanic strand was northern Neotethys, which according to some authors (Şengör & Yılmaz 1981; Görür *et al.* 1984; Robertson & Dixon 1984; Şengör *et al.* 1984b; Görür *et al.* 1998), was further divided into two strands: 1) the İzmir-Ankara-Erzincan Ocean to the north and; 2) the Inner Tauride Ocean to the south. The strands were separated by an inferred microcontinent, here termed the Niğde-Kırşehir Massif. Other workers, however, argue that northern Neotethys existed as one single ocean basin (e.g. Göncüoğlu 1986b).

The İzmir-Ankara-Erzincan Ocean was subducted northwards under the Eurasian active margin during the Late Mesozoic-Early Cenozoic (Şengör & Yılmaz 1981; Robertson & Dixon 1984; Şengör *et al.* 1984a; Okay *et al.* 2001; Robertson *et al.* 2009). Subduction generated accretionary prisms, supra-subduction zone-type ophiolites (Yaliniz *et al.* 1996; Floyd *et al.* 2000; Robertson 2002) and was associated with the formation of several large Late Mesozoic-Early Cenozoic sedimentary basins. The basins play a critical role in the understanding of tectono-sedimentary processes involved in the assembly of several key tectonic units in the region including: 1) the Ankara Mélange (Bailey & MacCallien 1950), an inferred

subduction-accretion complex (Norman 1984; Rojay *et al.* 2001; Dilek & Thy 2006); 2) the Eurasian active continental margin (Robinson *et al.* 1995; Rice *et al.* 2006) and; 3) the Niğde-Kırşehir Massif (Robertson *et al.* 2009), also known as the Central Anatolian Crystalline Complex (e.g. Akıman *et al.* 1993) the Kırşehir Continent (Şengör *et al.* 1984a), the Kırşehir Complex (Lünel 1985) and the Kırşehir Block (Robertson & Dixon 1984).

Within central Anatolia, there are two contrasting types of sedimentary basins bordering the Niğde-Kırşehir Massif: 1) to the south and east, the Maastrichtian-Eocene Ulukışla Basin (Göncüoğlu 1986a; Clark & Robertson 2002; Alpaslan *et al.* 2004; Alpaslan *et al.* 2006; Kurt *et al.* 2008) and the Maastrichtian-Neogene Sivas Basin (Cater *et al.* 1991; Gürsoy *et al.* 1997; Dirik *et al.* 1999; Yılmaz & Yılmaz 2006) are both transtensional basins, interpreted to have formed after Neotethyan ophiolite emplacement over the Gondwana-derived Anatolide-Tauride Platform. They probably relate to the closure of the Inner Tauride Ocean; 2) to the north and west of the Niğde-Kırşehir Massif (Fig. 2.1 and Fig.2.2) there is a family of Upper Cretaceous-Middle Eocene convergent basins considered, in the light of geophysical evidence (Aydemir & Ateş 2005) to be interconnected (Norman *et al.* 1980; Koçyiğit *et al.* 1988; Koçyiğit 1991; Görür *et al.* 1998). These basins include the Haymana-Polatlı Basin (e.g. Sîrel 1975; Gökçen 1976b; Gökçen 1976a; Ünalan *et al.* 1976; Gökçen 1978; Ünalan & Yüksel 1978; Çiner *et al.* 1996a; Çiner *et al.* 1996c), the Tuz Gölü Basin (Arikan 1975; Görür *et al.* 1984; Çemen *et al.* 1999), the Çankırı Basin (Birgili *et al.* 1975; Erdoğan *et al.* 1996; Kaymakcı *et al.* 2009) and the subject of this chapter, the Kırıkkale Basin (Norman 1972; Norman 1973a; Norman 1973b; Akyürek *et al.* 1984; Akyürek *et al.* 2001; Delibaş & Genç 2004; Dönmez *et al.* 2008) (Fig.2.2).

The basins have received little attention, in terms of sedimentology and tectono-stratigraphy, since pioneering work in the 1970s and 1980s. Recent work has focused on the geophysical nature of these basins (Ateş *et al.* 2005; Aydemir & Ateş 2005; Aydemir & Ateş 2006; Aydin *et al.* 2006; Aydemir & Ateş 2008) and burial history (Tokatlı *et al.* 2006).

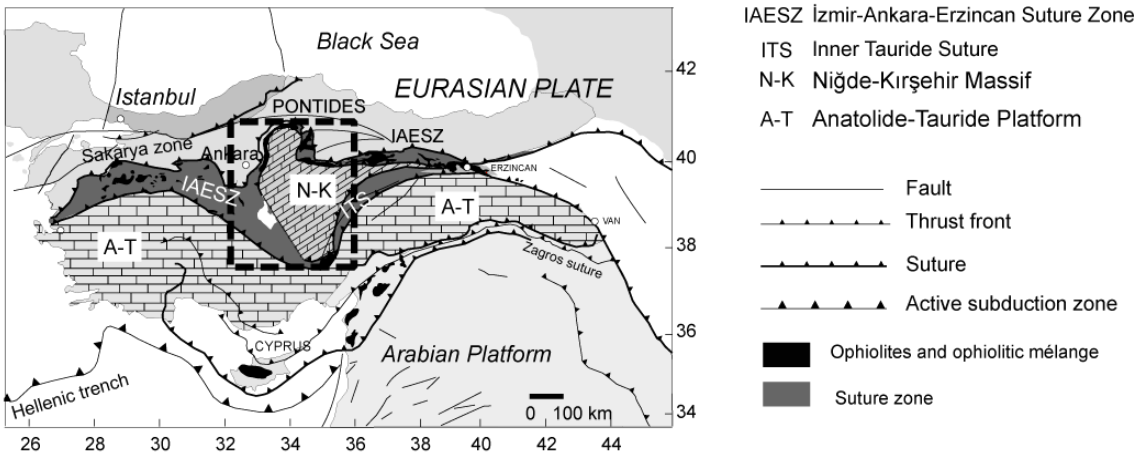

Figure 2.1 Outline tectonic map of Turkey. Regional map (Figure 2.2) is indicated by the dashed black box.

2.2 Aims

The Kırıkkale Basin provides an ideal opportunity to study a wide variety of geological processes involved in suturing northern Neotethys. The basin was chosen for study because it contains the following units which are either absent or not exposed in the other Central Anatolian basins: 1) a subduction-accretion complex and its sedimentary cover which comprises Upper Cretaceous volcaniclastic rocks and calciturbidites that are only exposed in the Kırıkkale area; 2) the Kırıkkale Massif, a magmatic complex which consists of Upper Cretaceous pillow basalts, silicic volcanics and granitoid plutons; 3) a basement of massive basalt and metalliferous sediments.

This chapter focuses on the tectonostratigraphic evolution of the basin. The objective here is to provide modern data that are absent from the literature. Provided here, for the first time are: 1) accurate, measured stratigraphic sections; 2) detailed sedimentary and lithofacies analysis; 3) new palaeontological studies; 4) provenance of sedimentary rocks; 5) geochemical data of igneous rocks; 6) palaeostress data and the structural evolution of the Kırıkkale Basin. A further aim is to use this new understanding of the basin to test existing models of basin development in central

Anatolia and to shed light on the nature and timing of continental collision in central Turkey.

2.3 Regional Geology

2.3.1 The İzmir-Ankara Accretionary Complex

The Kırıkkale Basin straddles two important tectonic units of central Anatolia, the İzmir-Ankara Accretionary Complex and the Niğde-Kırşehir Massif (Fig. 2.1). The İzmir-Ankara Accretionary Complex (Okay *et al.* 2006) is the structurally lowest unit of the classic Ankara Mélange (Bailey & MacCallien 1950; Norman 1984) which is a Mesozoic ophiolitic mélange. It represents dismembered thrust sheets of deep-marine sediments, oceanic crust and sea mounts related to the Late Cretaceous-Early Cenozoic closure of the İzmir-Ankara Ocean. Studies of radiolarian cherts and biomicritic carbonates within the ophiolitic mélange (Bragin & Tekin 1996; Rojay *et al.* 2001) have revealed biostratigraphic ages of Late Triassic (Norian) to Mid Cretaceous (Albian/Turonian). The complex includes remnants of Neotethyan oceanic lithosphere and pelagic sediments carried on a northward-trending subducting slab. Tankut *et al.* (1998) recognise three chemically different types of volcanic rocks: 1) sub-alkaline N-MORBs; 2) island-arc tholeiites; 3) within-plate oceanic island-type alkaline basalts. U/Pb zircon dating gives Early Jurassic crystallisation dates (~179 ± 15 Ma) for a plagiogranite dyke (Dilek & Thy 2006) intruding ultramafic upper mantle ophiolitic material, which suggests part of the accretionary complex could be even older.

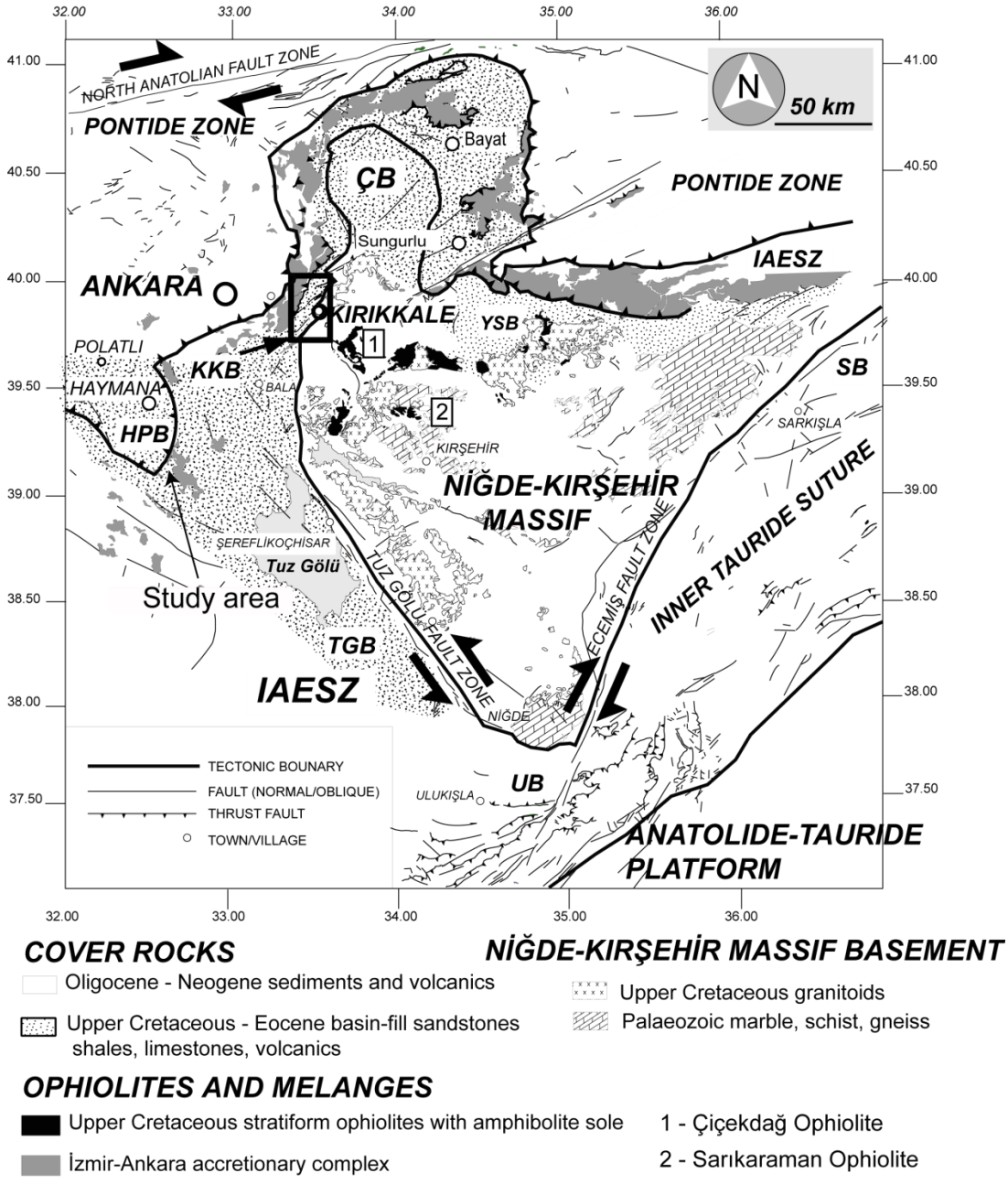

Figure 2.2 Regional map of central Anatolia indicating major basin areas and tectonic units. İzmir-Ankara-Erzincan Suture Zone (IAESZ), Tuz Gölü (Salt Lake) Basin (TGB), Ulukışla Basin (UB), Sivas Basin (SB), Yozgat-Sorgun Basin (YSB), Çankırı Basin (ÇB), Haymana-Polatlı Basin (HPB) and Kırıkkale Basin (KKB). The area of study is indicated by the black box. Note the locations of the Çiçekdağ and the Sarıkaraman ophiolites. Modified after (Clark & Robertson 2002; MTA 2002).

2.3.2 The Niğde-Kırşehir Massif

The Niğde-Kırşehir Massif is a triangular-shaped continental tectono-stratigraphic unit bound to the west by the Tuz Gölü fault zone (e.g. Çemen *et al.* 1999) and to the east by the Ecemiş fault zone (Jaffey & Robertson 2001) (Fig.2.1). It is composed of the Niğde Massif to the south and the Kırşehir Massif to the north. Its basement comprises platform marbles, calc-silicates, amphibolites, schists and garnet-gneisses of inferred Mesozoic to Palaeozoic age (Seymen 1981; Floyd *et al.* 2000). Metamorphic grades range from upper amphibolite to lower amphibolite/greenschist (Whitney & Dilek 2001). There is considerable debate on the Mesozoic tectonic setting and evolution of the Niğde-Kırşehir Massif. It is seen as a promontory of the Tauride-Antolide Platform (Yaliniz *et al.* 1996; Floyd *et al.* 2000; Göncüoğlu *et al.* 2006) as a microcontinent of the northern Neotethys, rifted from a larger Tauride continent to the south (Görür *et al.* 1984; Robertson & Dixon 1984; Whitney *et al.* 2001; Robertson *et al.* 2009) or as a part of the Eurasian margin (Kazmin & Tikhonova 2006).

Overlying the continental metamorphic basement is a meta-olistostromal sequence mostly containing blocks of MORB (Floyd *et al.* 1998a; Yalınız *et al.* 2000a) which is generally interpreted to represent the southward obduction of MORB oceanic crust onto the Niğde-Kırşehir Massif in the Turonian (Yalınız *et al.* 2000a; Yalınız *et al.* 2000b). Above are fragmented Upper Cretaceous supra-subduction zone-type stratiform ophiolites, including the Çiçekdağ Ophiolite (Yılmaz & Boztuğ 1998; Yalınız *et al.* 2000a) and the Sarıkaraman Ophiolite (Yaliniz *et al.* 1996). The ophiolites were obducted onto the Niğde-Kırşehir Massif from the north (Yalınız & Göncüoğlu 1998; Floyd *et al.* 2000; Yalınız *et al.* 2000b). This assemblage was then intruded by a series of I-, A- and S-Type Upper Cretaceous granitoid plutons (Boztuğ 2000; Köksal *et al.* 2001; Kadıoğlu *et al.* 2003; Ilbeyli *et al.* 2004). The geodynamic setting of pluton intrusion is variously interpreted as syn- to post-collisional associated with crustal thickening and the closure of northern Neotethys (e.g. Göncüoğlu & Türeli 1994; Erler & Göncüoğlu

1996; Boztuğ 2000; Düzgören-Aydin *et al.* 2001; Ilbeyli 2005) or an Andean-type subduction setting associated with Inner Tauride subduction (Kadıoğlu *et al.* 2006).

2.4 Tectonic models of continental collision in central Anatolia

The nature and timing of continental collision in central Turkey is controversial such that a number of tectonic hypotheses have been proposed to describe basin development. In one hypothesis (Gürer & Aldanmaz 2002) northern Neotethyan supra-subduction zone-type ophiolites were emplaced southwards onto the Gondwana margin during continental collision in the latest Cretaceous. This was followed by 'piggy-back' post-collisional basin formation on the underlying ophiolitic nappe. The Cenozoic was characterised by suture tightening and local thrusting of ophiolitic nappes. A second hypothesis is that northern Neotethys was palaeogeographically complex and included a rifted microcontinent, the Niğde-Kırşehir Massif. The ophiolites derived from this ocean formed in supra-subduction zone settings and were emplaced when subduction trenches collided with continental margins (Robertson 2004; Robertson *et al.* 2009). Subduction was associated with the development of an intra-oceanic magmatic arc and forearc-type basins as well as an active Eurasian continental margin arc further north.

Several studies (Görür *et al.* 1984; Koçyiğit 1991; Çiner *et al.* 1996b; Görür *et al.* 1998) place the Haymana-Polatlı and Tuz Gölü Basins in an evolving forearc/accretionary forearc tectonic setting, with final continental collision delayed until the Middle Eocene time associated with uplift, deformation, continental sedimentation and erosion (Görür *et al.* 1984; Görür *et al.* 1998). According to Görür *et al.* (1988) the Kırıkkale Basin evolved in an intra-arc tectonic setting. In another hypothesis (Okay & Tüysüz 1999; Okay *et al.* 2001) continental collision occurred diachronously during Early to latest Palaeocene.

2.5 Previous work

Early work on the Kırıkkale Basin was based on stratigraphy (Norman 1972) (Fig. 2.3a), sedimentology (Norman 1973a) and inferred post-Eocene structural development (Norman 1973b). These works confirmed the stratigraphy of the basin as including a Campanian-Middle Eocene sedimentary sequence. The basement of the western part of the basin was interpreted as an ophiolitic mélange, whereas igneous rocks of the basement of the eastern part of the basin were named the Kırıkkale Massif and were interpreted to be related to the Niğde-Kırşehir Massif. The Late Palaeocene to Middle Eocene interval was interpreted to have been a time of basin subsidence associated with a marine transgression during which volcaniclastic turbidites were deposited. After this time, regional uplift triggered a marine regression that allowed the deposition of red conglomerates, marls and lacustrine limestones.

Structurally, the basin was considered to be affected by post-depositional east-verging overturned folds then dissected by large-scale, E- to SE-verging thrust faulting (Norman 1973b). This interpretation was continued in later works, which included regional stratigraphic studies (Akyürek *et al.* 1984) (Fig. 2.3b) and local maps and reports by the General Directorate of Mineral Research and Exploration of Turkey (MTA) (Dönmez *et al.* 2008) (Fig. 2.3c).

Dönmez *et al.* (2008) divided the basin units into those associated with the İzmir-Ankara-Erzincan Suture Zone to the west and those belonging to the Niğde-Kırşehir Massif to the east. In this interpretation the western margin of the basin has been thrust southeastwards over the eastern margin. The lavas and tuffaceous rocks at the eastern margin was named the Çiçekdağ Formation and correlated with the Çiçekdağ Ophiolite, situated to the NW of the Niğde-Kırşehir Massif

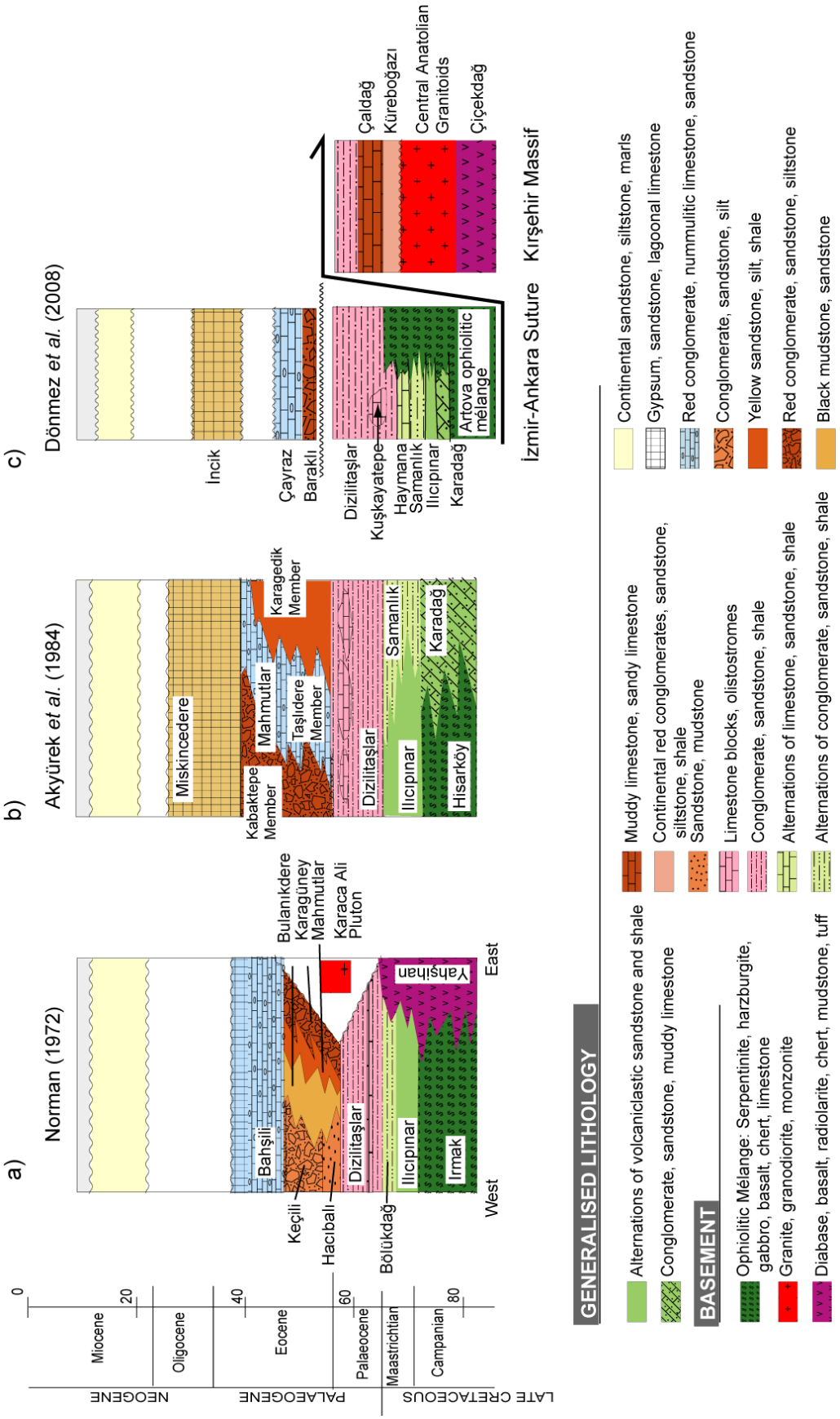

Figure 2.3 Previous stratigraphic schemes (with formation names) of the Upper Cretaceous-Middle Eocene Kırıkkale Basin, **(a)** the pioneering work of Norman (1972), **(b)** the proposed scheme of Akyürek *et al.* (1984) which covered the western margin of the Kırıkkale Basin and the Ankara Mélange, **(c)** stratigraphy of the MTA Map from Kırıkkale to Ankara (Dönmez *et al.* 2008). See text for further discussion.

(Yılmaz & Boztuğ 1998; Yalınız *et al.* 2000a). Locally, the igneous rocks to the east of the basin margin have been studied, in terms of mineralisation processes, by Gelibaş & Genç (2004).

The area under investigation forms a ~20 km x ~25 km rectangle around the town of Kırıkkale. During this study, the 1:100,000-scale maps of both Norman (1972) and MTA (2008) were tested using new sedimentary, geochemical, palaeontological and structural data. Measured stratigraphic logs were measured at the localities described by Norman (1972). Detailed mapping was carried out in several key areas. The resulting new geological map is presented in Fig. 2.4 and Fig. 2.5. A new stratigraphic model, based on this study, is featured in Fig. 2.6. The time scale used is that of Gradstein *et al.* (2004). Each section ends with an interpretation of new data gathered during this study and examines the role of new data in adding to, confirming or changing previous interpretations. This chapter now discusses the basement geology of the Kırıkkale Basin which features new stratigraphic, palaeontological and geochemical data.

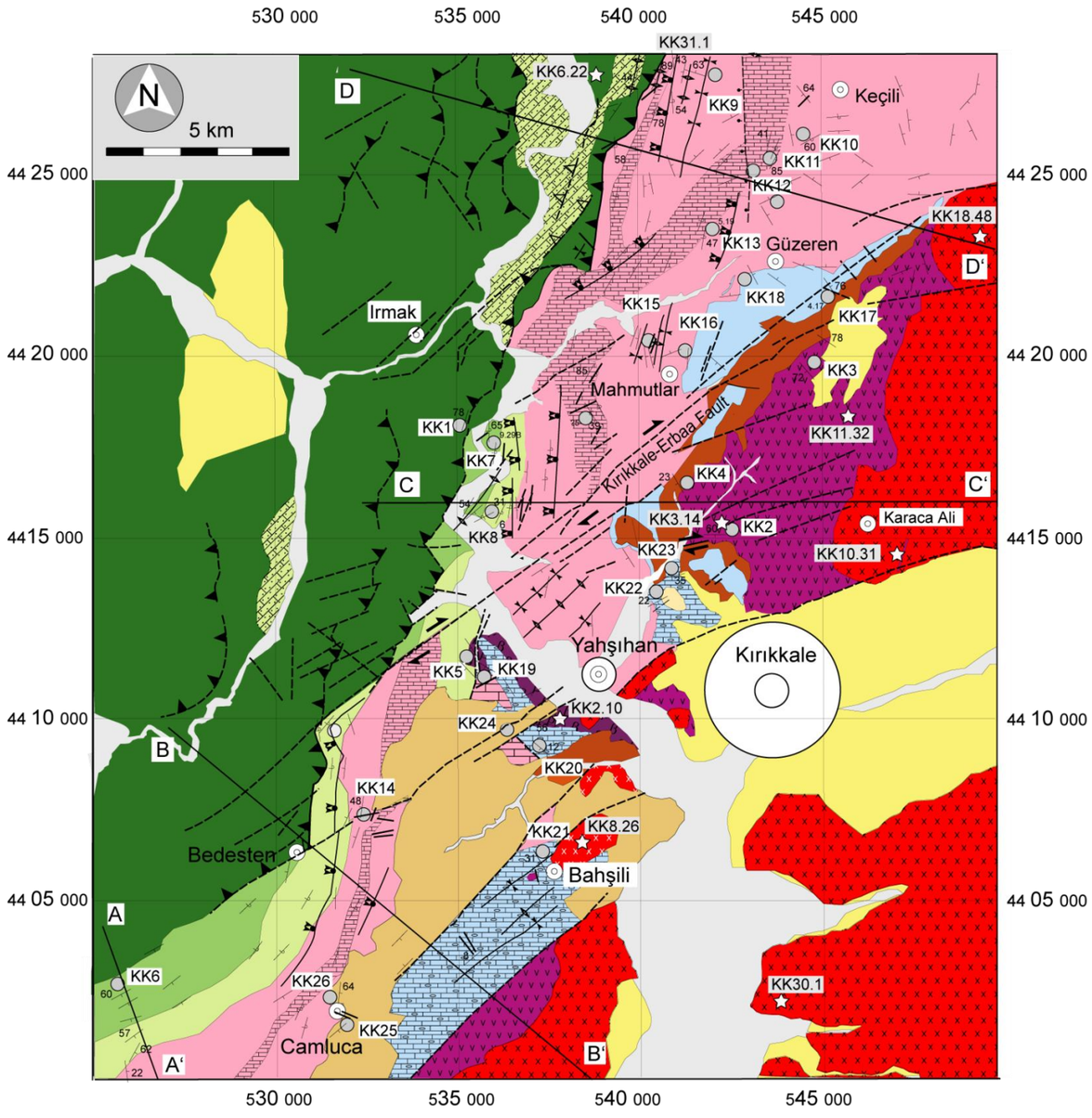

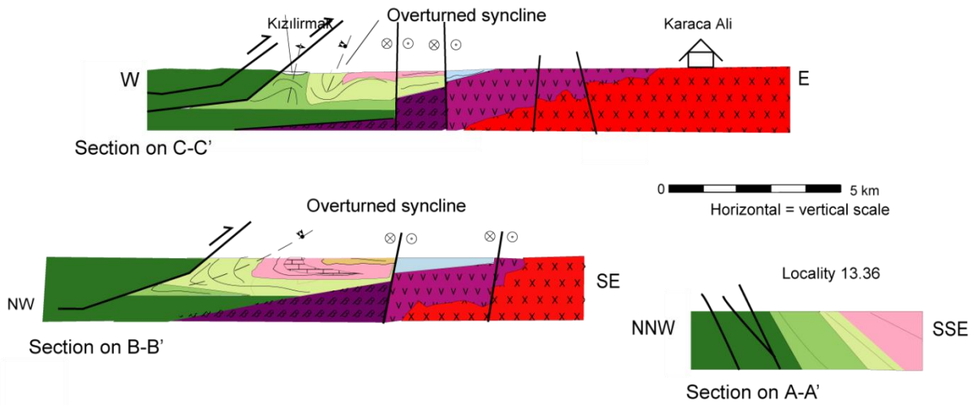

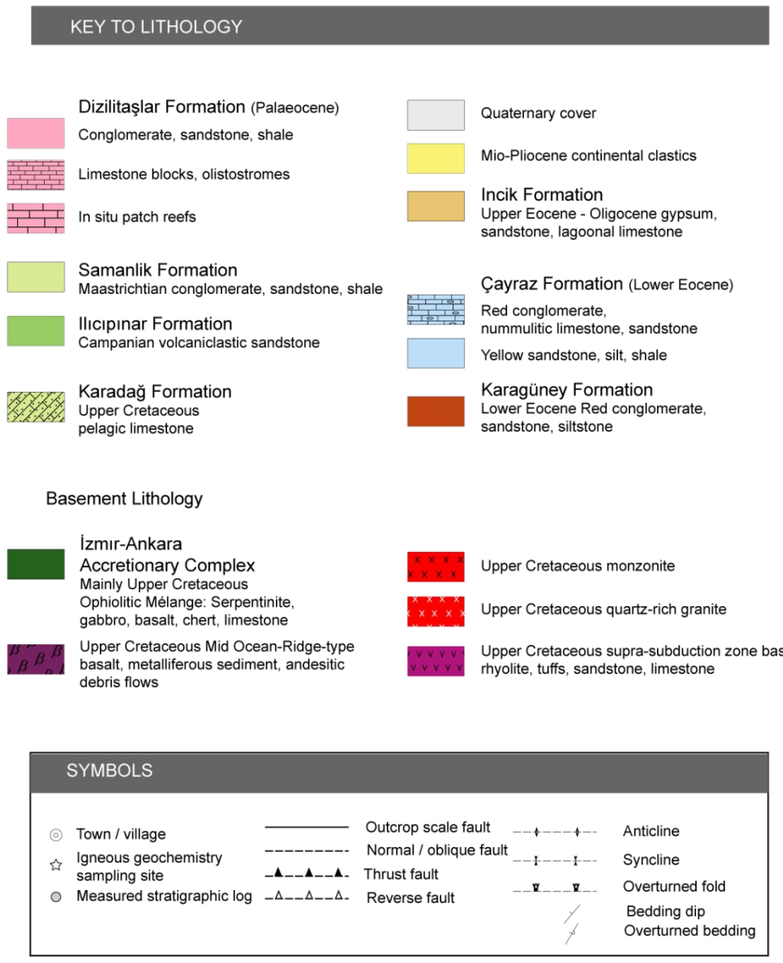

Figure 2.4 New geological map of the Kırıkkale Basin, partly based on Norman (1972) and Dönmez *et al*.(2008), mostly base on this study. The grid system is UTM Grid Zone 36.

Figure 2.5 Key to lithology and symbols of the new geological map (Fig. 2.4) and stratigraphic diagram (Fig. 2.6)

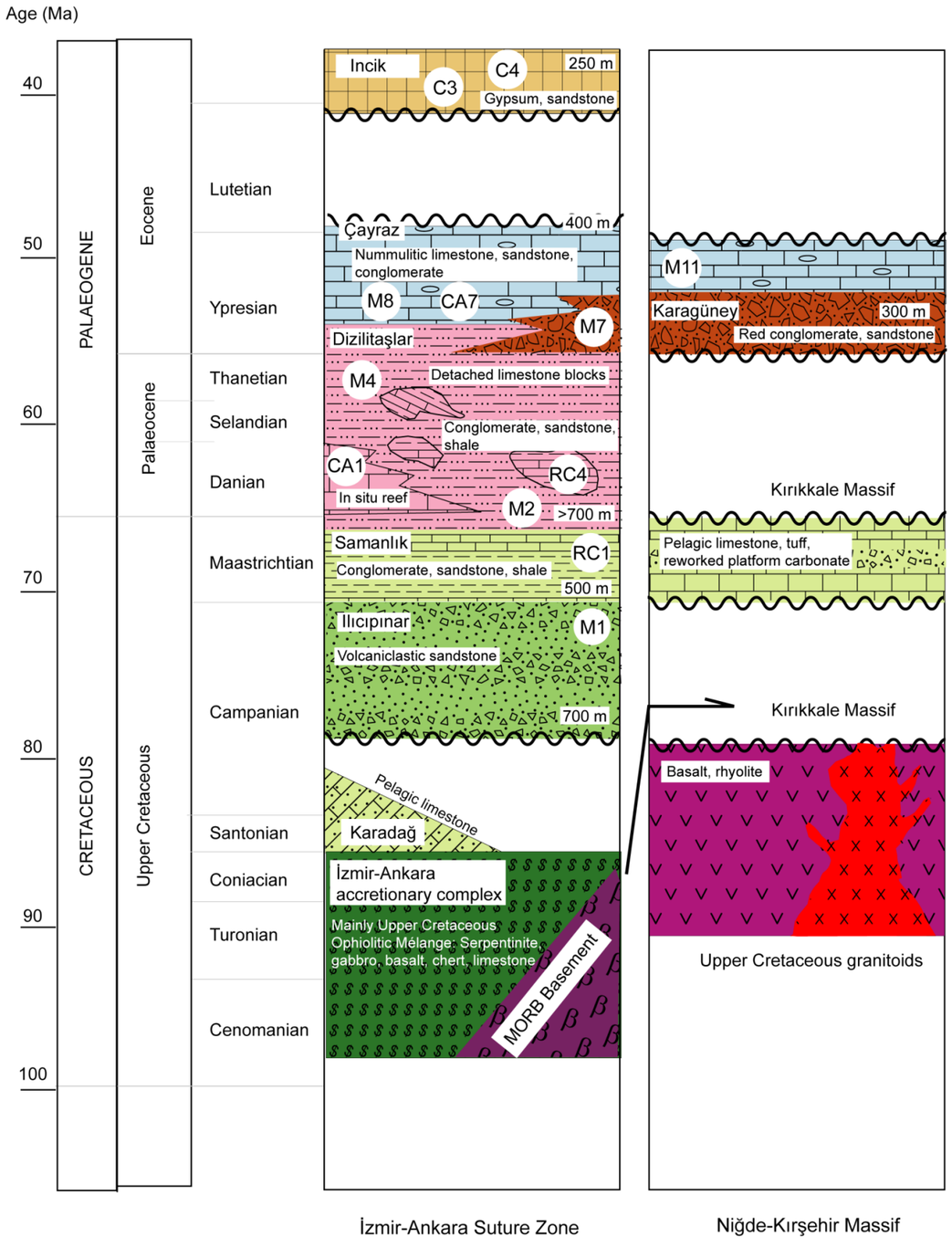

Figure 2.6 New stratigraphic scheme proposed by this study, based on field observations and microfossil dating. All palaeontological data are from N. İnan & K. Taslı (pers. comm. 2009). The white circles contain lithofacies codes.

2.6 Basement geology of the Kırıkkale Basin

The basement of the Kırıkkale Basin comprises three separate tectonostratigraphic units which give valuable insights into tectonic and sedimentary processes during the closure of northern Neotethys. The units are: 1) the İzmir-Ankara Accretionary Complex to the west; 2) a structurally intact fragment of massive basaltic and andesitic lavas and sedimentary cover which are exposed in the basin centre, and; 3) a massif at the eastern basin margin consisting of pillow basalts and massive silicic volcanics which have been intruded by granitoid plutons.

The stratigraphy, petrology and geochemistry of basement rocks helps to infer the tectono-magmatic history of the basin. Presently, no geochemical studies of igneous rocks of the basin have been conducted.

2.6.1 The Izmir-Ankara Accretionary Complex (western basement)

Also known as the Irmak Formation (Norman 1972) and the Hisarköy Formation (Akyürek *et al.* 1984; Akyürek *et al.* 2001), the İzmir-Ankara Accretionary Complex is exposed to the west of the Kırıkkale Basin and forms its basement on the western margin. The accretionary complex is characterised by east- to southeast-verging thrust sheets and blocks of serpentinite (Fig.2.7a), basic igneous rocks, limestone, radiolarian chert (Fig.2.7c) and sandstone (Fig.2.7c). The ~170 m-thick measured section Log KK1 (Fig. 2.8) exhibits a range of lithologies and depositional settings. Its base is strongly sheared serpentinite, above which come micaceous sandstone and mudstone alternations, pelagic muddy limestone and metre-scale blocks of red radiolarian chert. Towards the top of the section is a chaotic, matrix-supported debris flow conglomerate that shows a shear fabric dipping to the west. Clasts are composed of sandstone, radiolarian chert, and pelagic limestone. Above come alternations of thinly-bedded pelagic limestone and marl. Elsewhere, (e.g. 39304:26435) the complex features blocks of basaltic and feldspar-phyric andesitic debris flows, containing cobble, to boulder, sized clasts. This

locality was previously mapped as being a component of the Campanian-Maastrichtian Ilıcıpınar Formation (Norman 1972). However, they form part of a sheared zone of blocky outcrops close to the western basin margin belonging to the İzmir-Ankara Accretionary Complex. The İzmir-Ankara Accretionary Complex is overlain by a structurally coherent succession of bedded pelagic muddy limestones (Fig.2.7d) containing poorly preserved radiolaria. These deposits were termed the Karadağ Formation (Akyürek *et al.* 1984; Akyürek *et al.* 2001; Dönmez *et al.* 2008) and assigned a Santonian to Campanian age on the basis of planktonic and benthic foraminifera (Akyürek *et al.* 1984).

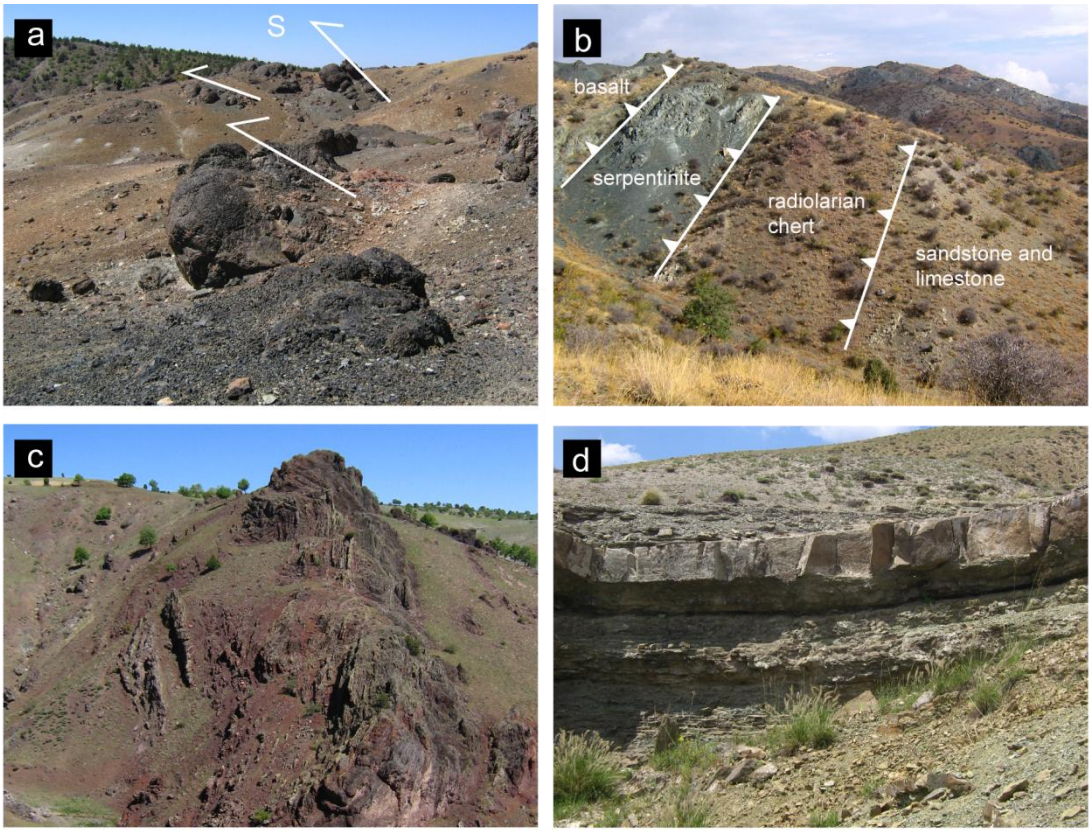

Figure 2.7 Field photographs of the İzmir-Ankara Accretionary Complex, **(a)** field photograph (looking south) of blocks of serpentinised basalts (1 to 2 m in height) in a muddy matrix, white arrows indicate thrust fault planes and inferred thrust direction to the east, **(b)** view, looking north, of serpentinite, red radiolarian chert, and sandstones separated by steeply dipping shear zones, **(c)** Folded block of red radiolarian chert, west of Bedesten Village, the block is ~ 40 m in height, **(d)** well-bedded pelagic limestone in the Karadağ Formation, which overlies the İzmir-Ankara Accretionary Complex, the thick bed in the centre of the photograph is ~ 50 cm in thickness.

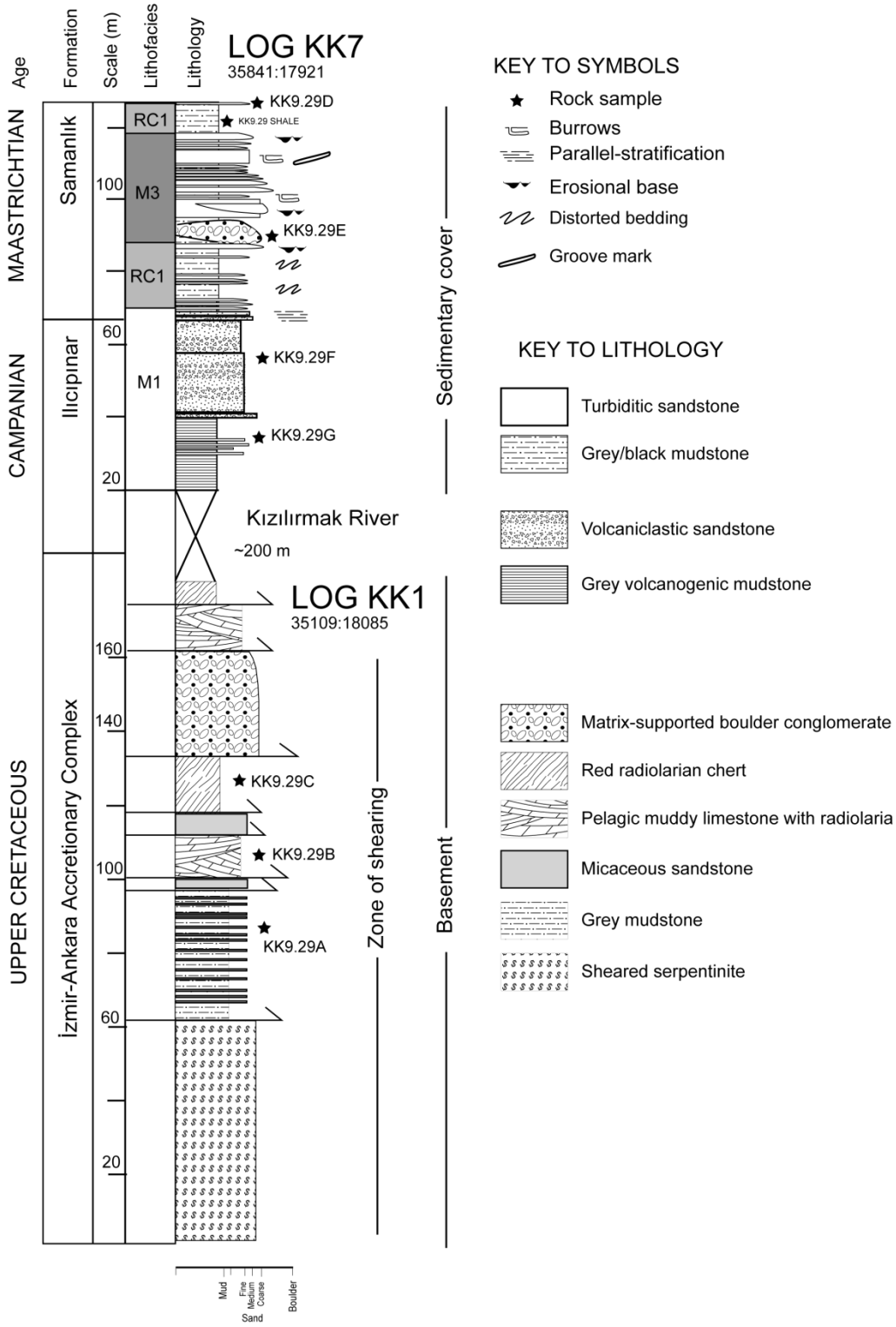

Figure 2.8 Measured stratigraphic log of the İzmir-Ankara Accretionary Complex at the western basin margin. See Fig. 2.2 for locations. The sedimentary cover is discussed in sections 2.71 and 2.72. All sedimentary data are from this study.

2.6.2 Oceanic crust (central basement)

New mapping as part of this study has reinterpreted small basement outcrops south of the Kızılırmak River which were previously mapped as Palaeocene sediments (Norman 1972; Dönmez *et al.* 2008) (Fig. 2.1). This part of the basement comprises structurally coherent massive basaltic and andesitic lavas overlain by metalliferous sediments, tuffaceous pelagic limestone, andesitic conglomerates (Fig.2.9a), and rudist-bearing sandstone. At locality KK2.10 (37217:09696) (Fig. 2.9b) massive basaltic lavas are intercalated with tuffaceous limestone and 2 m-thick beds of metalliferous sediments. In places (e.g. log KK5; Fig. 2.10) andesite lava flows up to ~20 m thick are interbedded with pelagic silty mudstones. New palaeontological evidence indicates that the mudstone contains the pelagic foraminifera *Calcisphaerulidae*, *Globotruncanidae* and *Hastigerinelloides sp.* (N. İnan & K. Taslı pers. comm. 2009), giving a Late Cretaceous deposition age (~100 to 65 Ma).

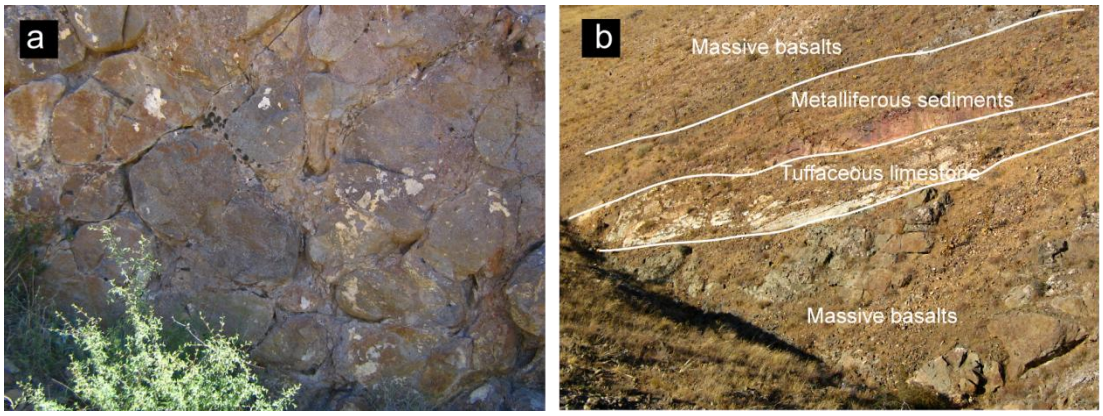

Figure 2.9 (a) Field photograph of andesite conglomerate, the outcrop is ~2 m-high, **(b)** photograph of tuffaceous limestone and metalliferous sediment overlying massive basalt.

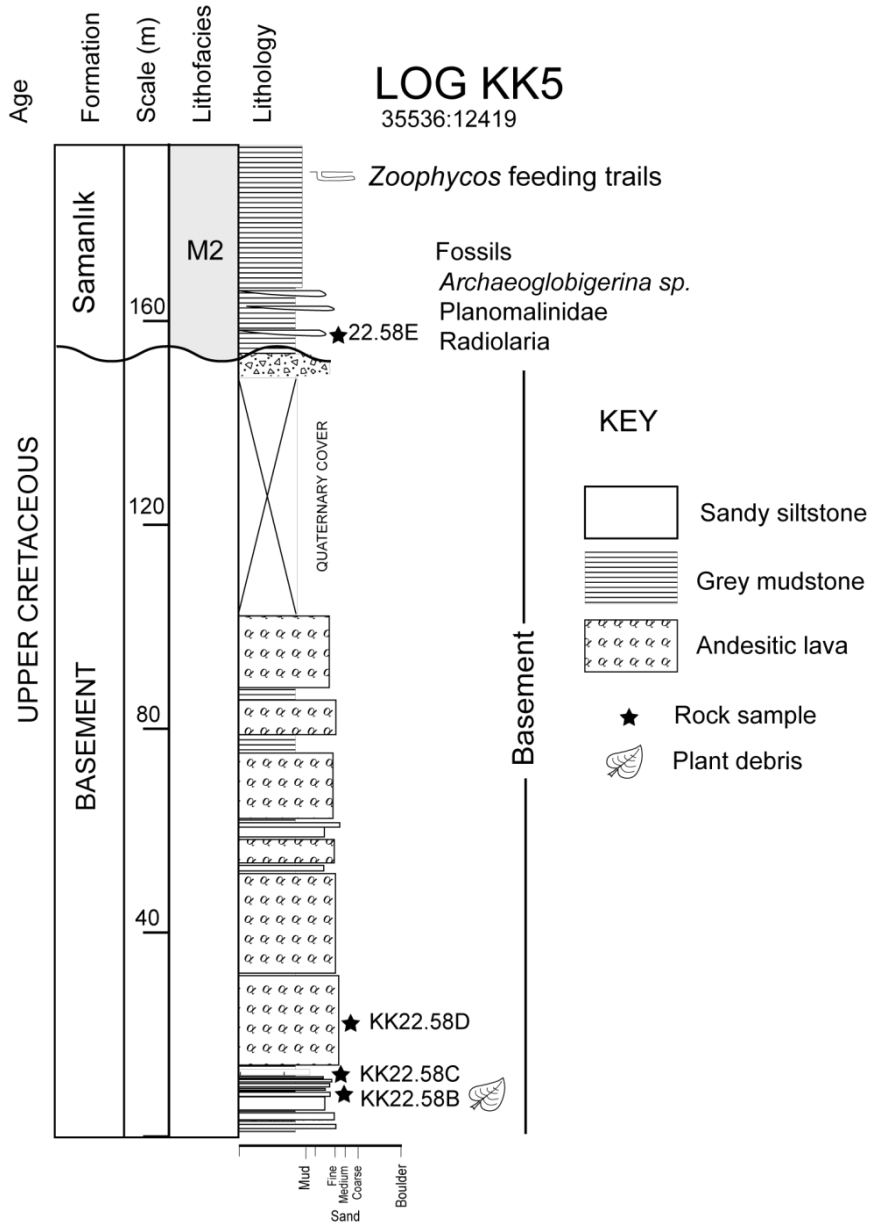

Figure 2.10 Measured stratigraphic log of Upper Cretaceous andesitic lava flows covered by pelagic mudstone and siltstone. Sedimentary data are from this study, fossil data are from N. İnan & K. Taslı (pers. comm.. 2009).

2.6.3 The Kırıkkale Massif (eastern basement)

At the eastern basin margin, the Kırıkkale Massif (Norman 1972) comprises a volcanic complex including rhyolitic, tuffaceous, basaltic and andesitic rocks, all of which were intruded by a series of granitoid plutons, which were consequently locally cut by basic dykes. The sedimentary cover includes pelagic limestones, conglomerates and sandstones. Alternative names of the Kırıkkale Massif are the Yahşıhan Formation (Norman 1972) the Çiçekdağ Formation (Dönmez *et al.* 2008) and the Karacaali (Kırıkkale) Magmatic Complex (Delibaş & Genç 2004). Other workers (e.g. Kaymakcı 2000) have interpreted this sequence as a part of an ophiolitic mélange, however, it is structurally coherent and does not contain many of the lithologies (e.g. serpentinite, radiolarian chert) present in the İzmir-Ankara Accretionary Complex. In contrast, some authors (e.g. Dönmez *et al.* 2008; Kaymakcı *et al.* 2009) consider this sequence to be a supra-subduction zone-type ophiolite which was obducted onto the Niğde-Kırşehir Massif. The Kırıkkale Massif has previously been studied in terms of its iron mineralisation of basaltic rocks and copper-molybdenum and lead mineralisation of granitoid rocks (Delibaş & Genç 2004).

Based on four new measured stratigraphic logs, the Kırıkkale Massif is at least 200 m thick but its base is not exposed in the study area. Basaltic lavas locally form pillows measuring up to 1 m in height (e.g. Locality KK3.14, 42257:15059; Fig. 2.11a) in sequences up to 60 m thick and can also form massive ponds up to ~30 m thick showing columnar jointing (e.g. 45211:18905). Rhyolitic flows (Fig.2.11b) are typically up 4 m thick and laterally continuous for ~30 to ~40 m; however, near the top of stratigraphic log KK4 (Fig.2.13) individual flows amalgamate into a sequence of ~100 m in thickness. At its western margin, between Kırıkkale and Mahmutlar (see Fig. 2.4), the Kırıkkale Massif is unconformably overlain by red sandstones and conglomerates of the lower Eocene Karagüney Formation (Fig. 2.11c). Granitoid plutons intrude the extrusive igneous rocks of the Kırıkkale Massif and are themselves locally cut by basic dykes (Fig.2.11d).

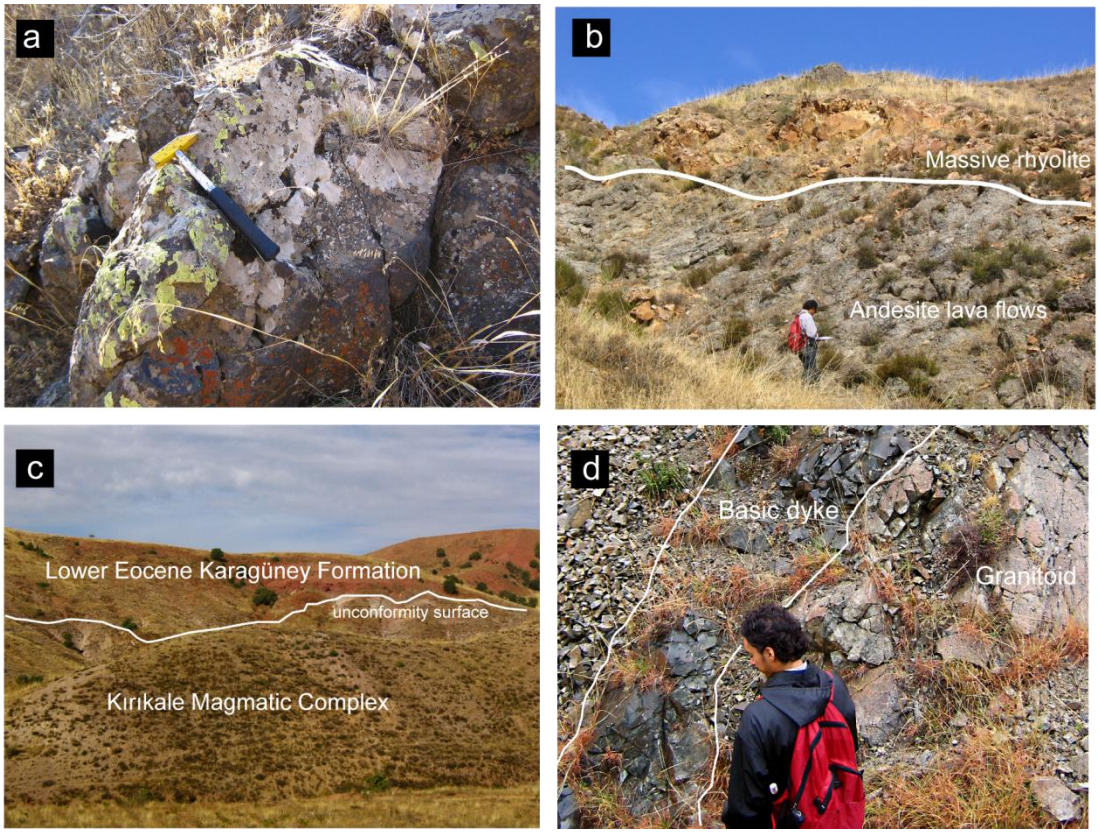

Figure 2.11 Representative field photographs of the Upper Cretaceous Kırıkkale Massif, **(a)** basaltic pillow lava (Locality KK3.14), **(b)** view of bedded andesitic lava flows capped by massive rhyolite, **(c)** view looking west of rhyolite lavas unconformably overlain by Lower Eocene red conglomerates and sandstones of the Karagüney Formation, **(d)** a basic dyke (shown by white lines) intruding a granitoid pluton.

Thin section study showed that the rhyolites are composed of quartz and altered sanidine phenocrysts set in a microgranular quartz groundmass (Fig. 2.12a). For ~1 km from the granitoid intrusion contact zone, rhyolites were extensively altered. The micro-granular quartz groundmass has been chloritised and locally shows flow banding around clusters of sanidine phenocrysts. Larger quartz phenocrysts are heavily altered, strained and show a preferred alignment. Rare 1 mm-wide veinlets of relatively unstrained and fresh quartz indicate secondary crystallisation. Another thin section (KK11.32A) shows an equigranular quartz groundmass including rare sanidine and clusters of epidote (Fig.2.12b).

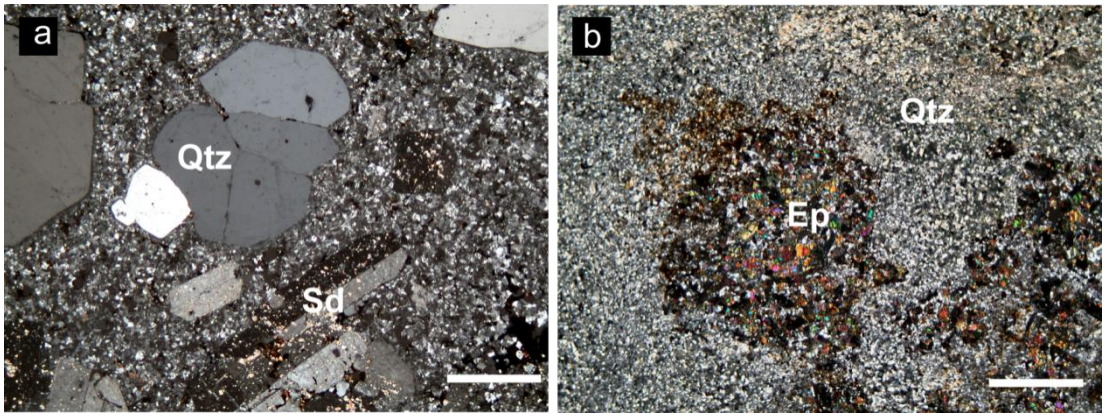

Figure 2.12 Photomicrographs of Upper Cretaceous rhyolitic rocks from the Kırıkkale Massif, **(a)** rhyolite with volcanic quartz (Qtz) and twinned sanidine (Sd) phenocrysts, **(b)** a rhyolite sample (KK11.32A) from the granitoid intrusion zone showing mottled epidote (Ep) and a quartz (Qtz) groundmass. Scale bars = 1 mm.

2.6.3.1 Upper Cretaceous sedimentary cover of the Kırıkkale Massif

The sedimentary cover of the Kırıkkale Massif varies in thickness from ~120 m to ~20 m. It generally consists of pelagic muddy limestones, redeposited shelf carbonates and fine-grained sandstones interbedded with intermediate to silicic volcanics. One measured stratigraphic section, Log KK3 (45296:20590) (Fig.2.13) is ~50m-thick and features andesites and rhyolites, both topped by 1 to 2 m-thick tuffaceous horizons that are composed of a micro-granular quartzo-feldspathic groundmass. Interbedded with these extrusive rocks are ~4 m-thick massive beds of silty limestone. Another section, measured ~1 km to the southeast (Log KK3a) contains: 1) green ribbon cherts with poorly preserved radiolarians (Fig. 9e); 2) redeposited carbonate platform material containing the large benthic foraminifera *Siderolites calcitrapoides* Lamarck and *Anomalina* sp. (N. İnan & K. Taslı pers. comm. 2009) and; 3) a thick (~100 m) uniform sequence of medium-bedded sandstones. Fossil evidence indicates a Maastrichtian age (N. İnan & K. Taslı pers. comm. 2009) which provides a minimum age for the underlying Kırıkkale Massif.

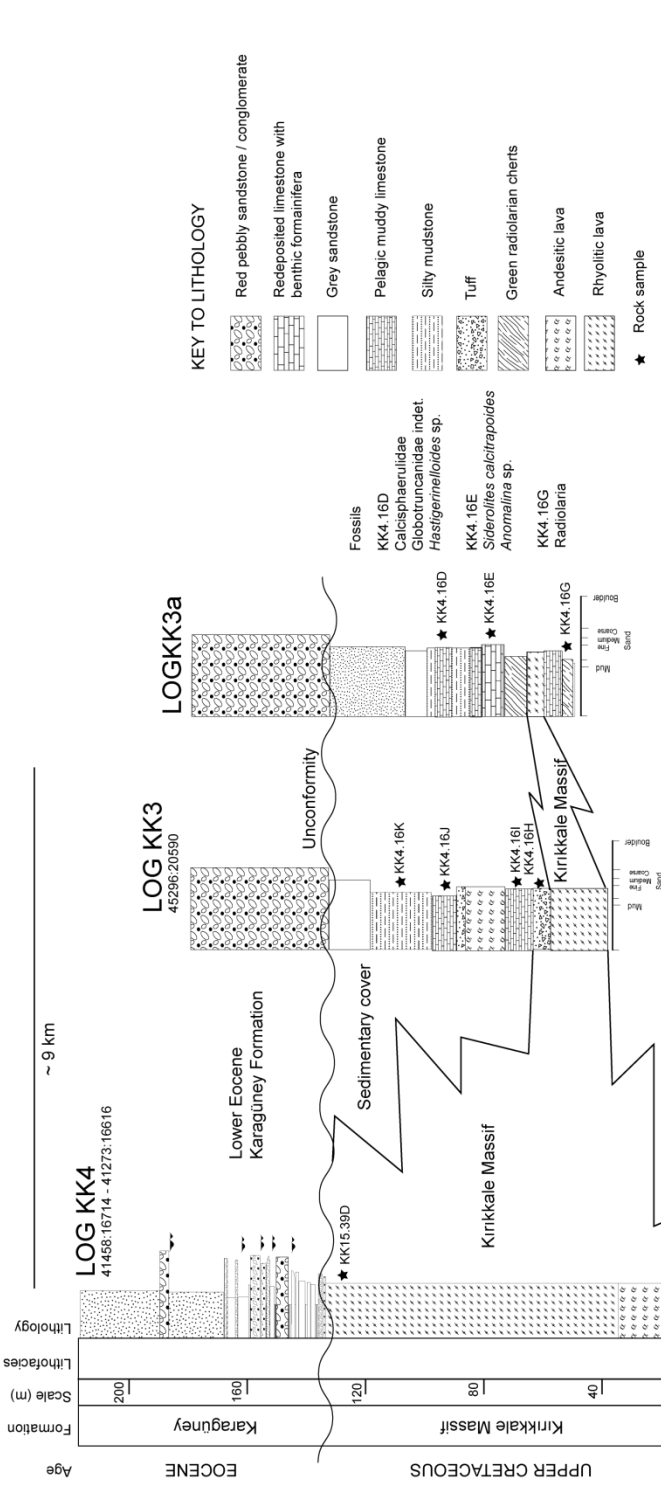

Figure 2.13 Three measured stratigraphic logs showing the igneous rocks of the Kırıkkale Massif, its Maastrichtian sedimentary cover, and lower Eocene sandstone and conglomerate of the Karagüney Formation lying on an unconformity. All sedimentary data are from this study, fossil data are from N. İnan & K. Taslı (pers. comm.. 2009).

2.6.4 Geochemistry of basic basement rocks

No geochemical studies of the igneous rocks of the Kırıkkale Basin exist in the literature. Previous works (e.g. Dönmez *et al.* 2008) related the basic igneous rocks of the Kırıkkale Massif to the Çiçekdağ Ophiolite, inferring a geochemical affinity. The Çiçekdağ Ophiolite is one of a number of allocthonous bodies that lie on the meta-sedimentary basement of the Niğde-Kırşehir Massif that are interpreted to represent Neotethyan ocean crust (Yaliniz *et al.* 1996; Floyd *et al.* 1998b; Yalınız & Göncüoğlu 1998; Yılmaz & Boztuğ 1998; Floyd *et al.* 2000; Yalınız *et al.* 2000a). The Çiçekdağ Ophiolite retains a magmatic stratigraphy as follows: 1) layered gabbro; 2) isotropic gabbro; 3) plagiogranite; 4) a dolerite dike complex; 5) basaltic volcanics and; 6) a Turonian to Santonian sedimentary cover (Yalınız *et al.* 2000a). It lies ~50 km to the SE of the Kırıkkale Basin, is Upper Cretaceous in age and is considered to have formed in a supra-subduction zone (SSZ)-type tectonic setting (Floyd *et al.* 2000; Yalınız *et al.* 2000a). Clearly, an investigation of the basic igneous rocks of the Kırıkkale Basin is crucial in testing the thesis of Dönmez *et al.* (2008) and in shedding light on the basin's tectono-magmatic evolution.

A data set consisting of twenty two basic rock samples was collected for analysis by X-Ray Fluorescence (XRF) using the method of Fitton *et al.* (1998) in order to determine major oxides and trace element abundances. Analyses were performed at the School of GeoSciences, University of Edinburgh on a Panalytical PW2404 wavelength-dispersive sequential X-ray spectrometer, for the methodology and tabulated data see Appendix 1.

Two sets of samples represent the İzmir-Ankara Accretionary Complex: 1) a set of four basalts from locality KK6.22 (see Figs. 2.4 and 2.5 for localities) and; 2) five from locality KK31.1. Four samples represent the central basin basement (locality KK2.10) and eight samples were collected from pillow basalts in the Kırıkkale Massif (locality KK3.14). One sample represents a dyke cutting a granitoid pluton (locality KK10.31).

2.6.4.1 Petrology

Thin section study revealed that the majority of the samples are aphyric to weakly porphyritic with plagioclase as the phenocrysts phase (Fig. 2.14a). One sample set from the İzmir-Ankara Accretionary Complex (locality KK31.1) features clinopyroxene as the dominant phenocrysts phase (Fig. 2.14b). The groundmass commonly comprises feldspar laths and opaque oxides in a glassy matrix. Chloritisation affects the glassy groundmass and sericite commonly replaces plagioclase.

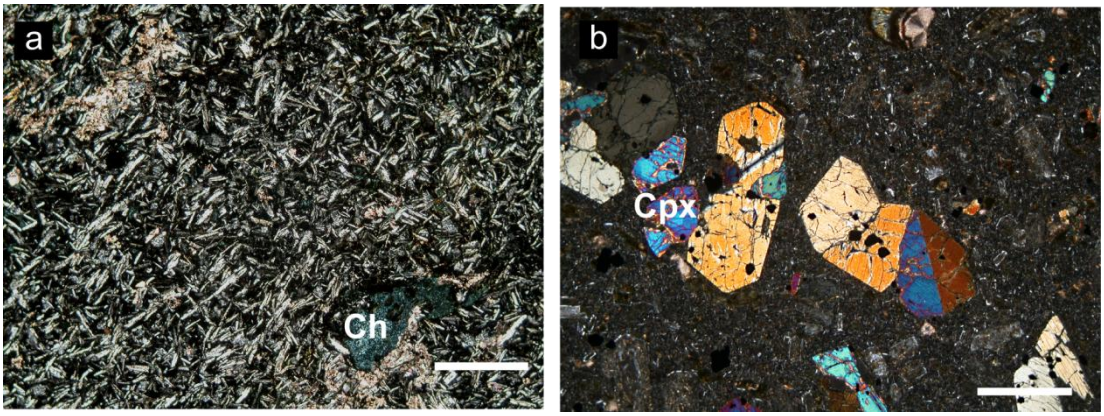

Figure 2.14 (a) Photomicrograph of altered aphyric basalt (sample KK3.14), note the patch of chlorite (Ch) and sericite replacing plagioclase (top left corner), **(b)** photomicrograph of relatively unaltered basalt from the İzmir-Ankara Accretionary Complex (sample KK31.1), Cpx = clinopyroxene. Images are in crossed-polars, scale bars = 1 mm.

2.6.4.2 Alteration

The samples show some degree of secondary alteration and can be expected to have experienced selected element mobility, particularly involving large-ion-lithophile (LIL) elements (Thompson 1991). LIL element (e.g. K, Na, Rb, Ba) abundances are commonly variable and are thus unreliable indicators of petrogenesis. Loss-on-ignition (LOI) values provide a crude measure of the degree of alteration and the abundance of secondary hydrated and carbonate phases. LOI values are relatively modest in samples from the İzmir-Ankara Accretionary Complex (3.32 -

6.49 wt. %), lower in the central basin basement (3.15–3.71 wt. %) and higher in the Kırıkkale Massif (4.66–6.35 wt. %).

2.6.4.3 Geochemistry of basic rocks from the İzmir-Ankara Accretionary Complex

The basic rocks from the İzmir-Ankara Accretionary Complex comprise two distinct types representing two distinct eruptive settings. Samples from locality KK6.22 are tholeiitic according to the AFM diagram of Irvine & Baragar (1971) (Fig.2.15a) and plot on the basaltic trachy-andesite field of the Total-Alkali-Silica (TAS) diagram (Le Bas *et al.* 1986) (Fig. 2.15b) and the basalt-andesite field of the Zr/TiO_2 vs. Nb/Y diagram (Winchester & Floyd 1977) (Fig.2.15c).

Trace element patterns (Fig.2.16a) are depleted in LIL elements Sr, K, Rb and Ba relative to the mid-ocean ridge basalt (MORB) standard of Pearce (1982). In contrast, HFS elements exhibit little deviation from MORB. High-Field-Strength (HFS) elements are typically utilised in tectonic discrimination diagrams because they are interpreted to be immobile during alteration (e.g. Pearce & Cann 1973). The samples plot in the MORB field of the Zr/Y vs. Zr tectonic discrimination diagram (Pearce & Norry 1979) (Fig.2.16b). This figure contains the results of previous studies in the İzmir-Ankara Accretionary Complex for comparison. The data are from pillow basalts in the Ankara region, to the W and N of the Kırıkkale Basin, near Haymana (Rojay *et al.* 2001), Orhaniye and Kılıçlar (Gökten & Floyd 2007) and the Kaleçik Ophiolitic Massif (Tankut *et al.* 1998). Data representing dolerite dykes from the Kaleçik Ophiolitic Massif (Tankut *et al.* 1998) are also present.

In contrast, basalts from locality KK31.1 are calc-alkaline (Fig.2.15a), and plot in the basanite field of the TAS diagram (SiO_2=45.07–45.81wt. %) (Fig.2.15b) and the basalt-andesite field of the Zr/TiO_2 vs. Nb/Y diagram (Fig.2.15c). The trace element pattern (Fig.2.16a) is enriched in LIL elements and somewhat depleted in HFS elements, especially Zr, Ti and Sc. The large Nb depletion (5.4–5.8 ppm) is suggestive of a melt source which has been chemically modified by subduction fluids

(Pearce & Cann 1973; Pearce *et al.* 1984b). In terms of the Zr/Y vs. Zr diagram, these rocks plot in the field where MORB and island arc basalt (IAB) overlap (Fig.2.16b).

2.6.4.4 Geochemistry of basic rocks from the basin basement

Samples from locality KK2.10 are tholeiitic (Fig.2.15a) and plot on the basalt field of the TAS diagram (SiO_2=48.61–49.74 wt. %) (Fig. 2.15b) and the andesite/basalt field of the Zr/TiO_2 vs. Nb/Y diagram (Fig.2.15c). The trace element pattern (Fig. 2.16a) exhibits a generally smooth trend with slight enrichment of Nb, Ba and Rb and depletion in La and Cr relative to the MORB standard. These samples plot on the MORB field of the Zr/Y vs. Zr diagram (Fig. 2.16b).

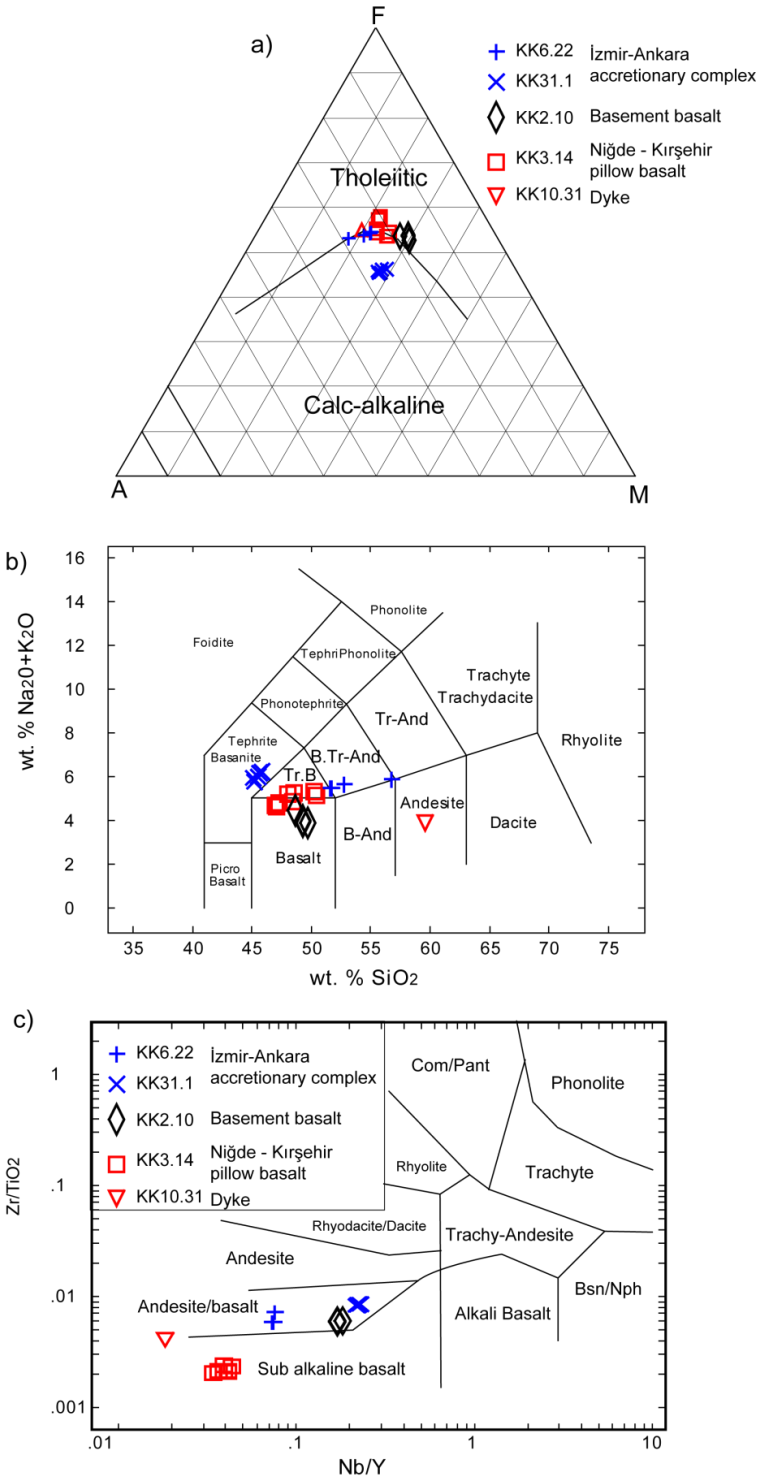

Figure 2.15 (a) AFM diagram after Irvine & Baragar (1971), **(b)** Total Alkali Silica (TAS) diagram after Le Bas *et al.* (1986), Tr.B – Trachy basalt, Tr-And – Trachy andesite, B-And – Basaltic andesite,**(c)** Zr/TiO2 vs. Nb/Y discrimination diagram after Winchester & Floyd (1977).

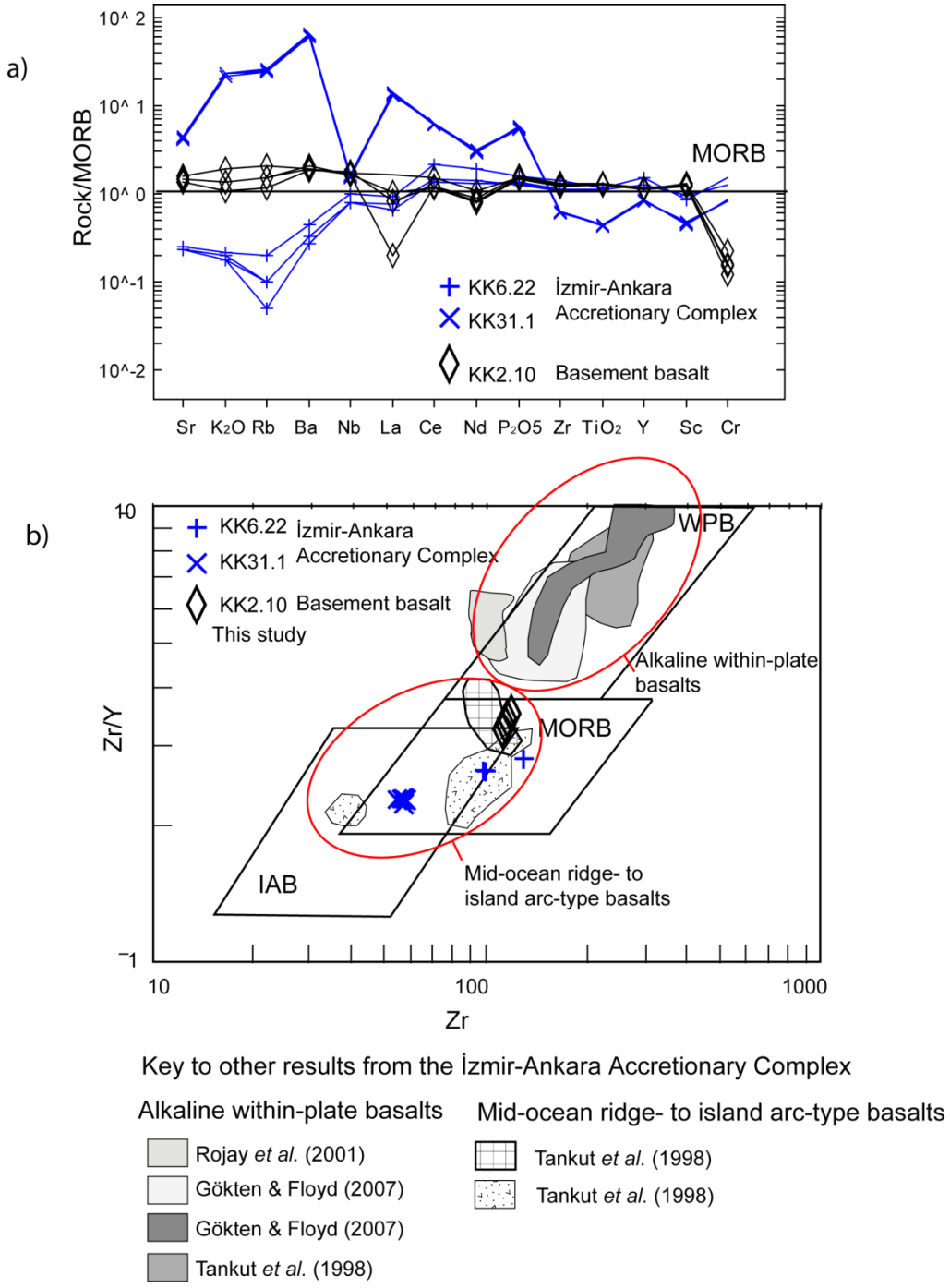

Figure 2.16 (a) multi element patterns of basalts from the İzmir-Ankara Accretionary Complex and the basin basement, normalised to Mid-Ocean Ridge Basalt (MORB) (Pearce 1982), **(b)** Zr/Y vs. Zr discrimination diagram (Pearce & Norry 1979). Values of basalts from the Kırıkkale Basin are shown in comparison to other basalts and dolerites in the İzmir-Ankara Accretionary Complex.

2.6.4.5 Geochemistry of basic rocks from the Kırıkkale Massif

Samples from the Kırıkkale Massif were collected from pillow basalts at locality KK3.14. They are tholeiitic (Fig.2.15a) and plot at the boundary of the basalt and trachy-basalt field on the TAS diagram (SiO_2=46.98–50.44 wt. %) (Fig. 2.15b) and the sub-alkaline basalt field of the Zr/TiO_2 vs. Nb/Y diagram (Fig. 2.15c). The trace element pattern (Fig. 2.17a) shows a general depletion in LIL elements with the exception (in some samples) of Ba, presumably caused by secondary alteration. However, LIL elements are not considered to be indicators of petrogenesis. Light rare earth (LRE) elements (La, Ce, Nd) show moderate depletions. Of the HFS elements, Zr and Y are depleted, Sc is marginally enriched. TiO_2 and P_2O_5 values are slightly enriched.

Figure 2.17a shows the MORB-normalised trace element pattern in comparison to pillow basalt samples from two ophiolitic sequences that lie on the metamorphic basement of the Niğde-Kırşehir Massif, the Çiçekdağ Ophiolite (Yalınız *et al.* 2000a) and the Sarıkaraman Ophiolite (Yaliniz *et al.* 1996). The ophiolites are chemically characterised by high LIL/HFS element ratios and overall low HFS values (<1) and are interpreted as SSZ-type ophiolites (Yaliniz *et al.* 1996; Yalınız & Göncüoğlu 1998; Yalınız & Göncüoğlu 1999; Floyd *et al.* 2000; Yalınız *et al.* 2000a; Yalınız *et al.* 2000b). Chemically, pillow basalts from the ophiolites are broadly comparable to those from the Kırıkkale Massif. Differences include lower Rb and higher P_2O_5 and TiO_2 abundances in the Kırıkkale Massif. Figure 2.17b is a Zr/TiO2 vs. Nb/Y diagram showing that pillow basalts from the Kırıkkale Massif are similar to those from the Çiçekdağ Ophiolite and plot on the Island Arc Basalt (IAB) field.

One sample (KK10.31) represents a dyke (Fig. 2.11d) which intrudes a granitoid pluton in the Kırıkkale Massif. The sample is tholeiitic and plots in the andesite field of the TAS diagram (Fig. 2.15b) and the basalt-andesite field of the Zr/TiO2 vs. Nb/Y diagram (Fig.2.15c). Its multi element pattern (Fig.2.17c) shows a relative enrichment in Sr, K, Rb and Ba and a lack of enrichment in others, notably

Nb and La, and also the HFS elements Zr, Ti and Y. This feature suggests a modification by a mantle source by aqueous and siliceous fluids derived from an underlying subduction zone. On the Zr/TiO2 vs. Nb/Y diagram (Fig.2.17b) the sample plots in the Island Arc Basalt field.

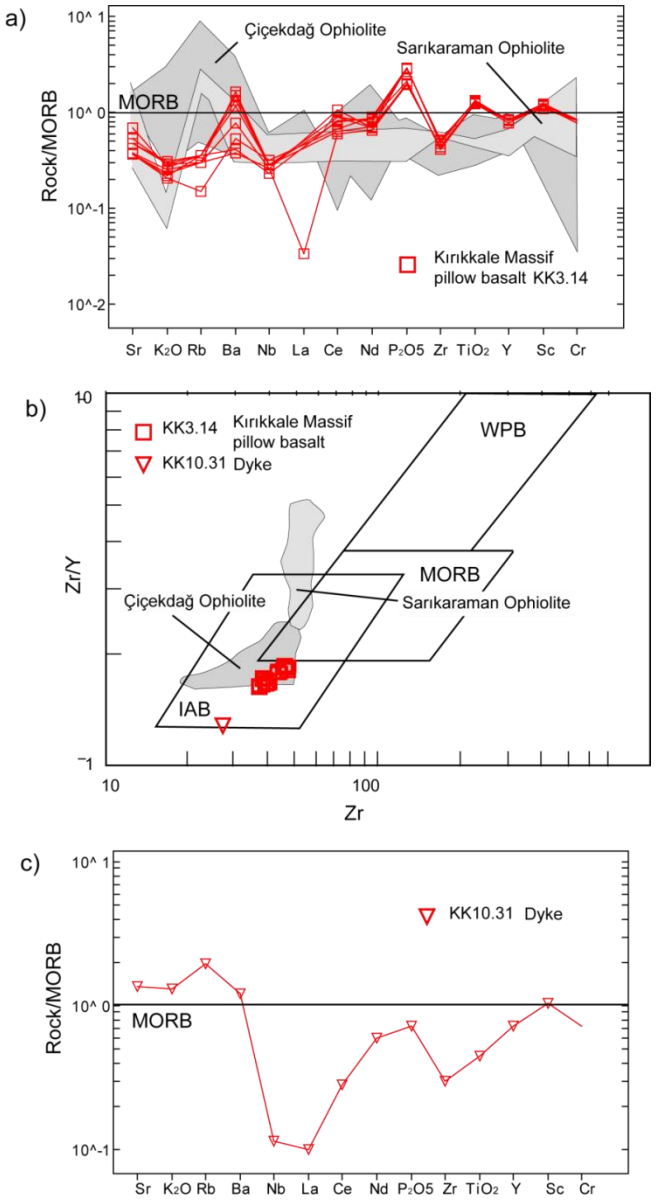

Figure 2.17 (a) Multi element patterns of Upper Cretaceous basalts from the Kırıkkale Massif, normalised to MORB values of Pearce (1982) and shown with pillow basalts from the Çiçekdağ Ophiolite (Yalınız *et al.* 2000a) and the Sarıkaraman Ophiolite (Yaliniz *et al.* 1996), **(b)** Zr/Y vs. Zr discrimination diagram (Pearce & Norry 1979), values of basalts from the Kırıkkale Massif are shown in comparison to basalts from the Çiçekdağ and Sarıkaraman ophiolites, **(c)** multi element pattern of a dyke that intrudes a granitoid (sample KK10.31).

2.6.4.6 Interpretation of Geochemical results

New geochemical data presented in this chapter shed light on the tectono-magmatic development of the Kırıkkale Basin basement. The Izmir-Ankara Accretionary Complex contains tholeiitic MORB (locality KK6.22) and calc-alkaline IAB (locality KK31.1) which is a new finding. Previously, most pillow basalts in the İzmir – Ankara Accretionary Complex in central Anatolia have been interpreted as ocean island-type alkali basalts (Tankut *et al.* 1998; Rojay *et al.* 2001; Gökten & Floyd 2007) representing Upper Cretaceous seamount-type volcanism on the floor of the Izmir-Ankara-Erzincan Ocean. However, this study provides evidence that the İzmir-Ankara Accretionary Complex contains basalts related to mid-ocean ridge and subduction-type volcanism. This evidence confirms previous studies (Tankut 1984; Tankut 1990; Tankut *et al.* 1998) that related doleritic dykes and ultramafic material to mid-ocean ridge and subduction-type volcanism. Moreover, the multi element patterns of the calc-alkaline IAB samples are consistent with those of SSZ-type basalts (e.g. Pearce *et al.* 1984b) which are thought to represent the initial stages of intra-oceanic subduction.

The basement tholeiitic MORBs from locality KK2.10 clearly represent mid-ocean ridge-type volcanism. This small outcrop is structurally intact and is a separate entity to the İzmir-Ankara Accretionary Complex. This is a new finding and is here interpreted a fragment of the Izmir-Ankara-Erzincan Ocean floor.

Pillow basalts from the Kırıkkale Massif are tholeiitic IABs. Their multi element trace patterns and Zr/Y ratios and absolute Zr values suggest a chemical affinity to the Upper Cretaceous Çiçekdağ Ophiolite, as suggested by the MTA map of Dönmez *et al.* (2008) (Fig. 2.17a and 2.17b). It therefore seems likely that pillow basalts and silicic volcanics of the Kırıkkale Massif are part of an upper ophiolitic sequence, possibly related to the Çiçekdağ Ophiolite (Fig. 2.18).

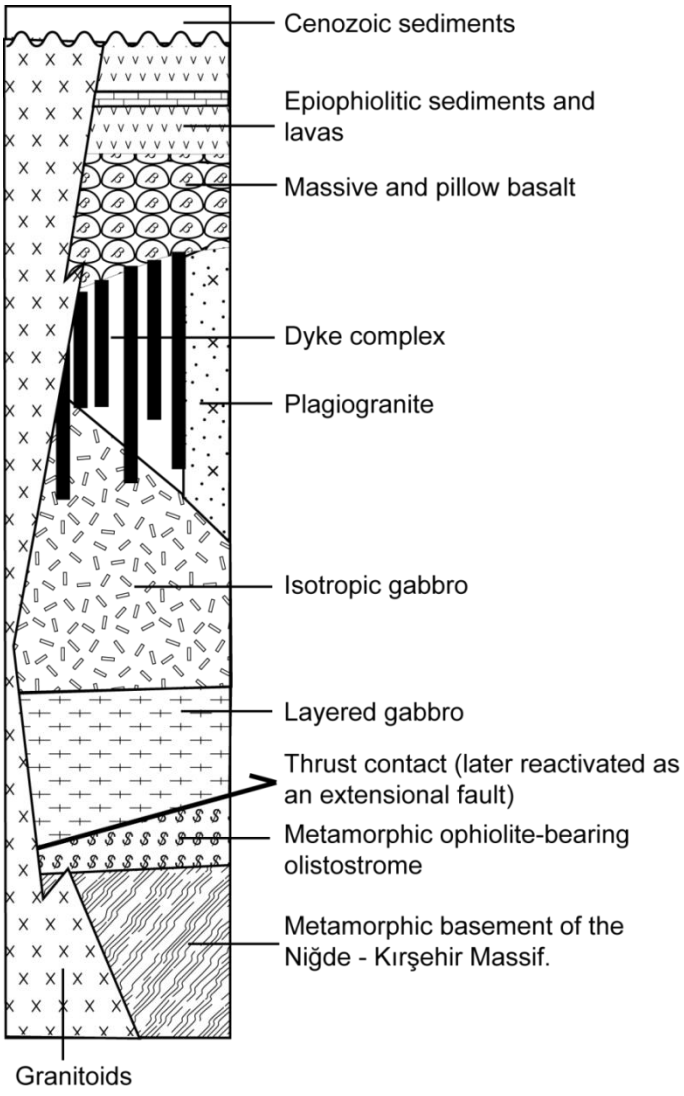

Figure 2.18 Schematic stratigraphy of the Upper Cretaceous Çiçekdağ Ophiolite, redrawn from Yalınız *et al.* (2000a), not to scale.

Moreover, based on the relative enrichment in most LIL elements, and the lack of enrichment in HFS elements, the Çiçekdağ Ophiolite has been interpreted as a SSZ-type ophiolite with chemical similarities with the Izu-Bonin Arc (Yılmaz & Boztuğ 1998; Yalınız *et al.* 2000a). Additionally, the upper parts of the Çiçekdağ and Sarıkaraman ophiolites contain an epi-ophiolitic cover of pelagic sediments, reworked carbonate platform material, tuffs and rhyolites. The sedimentary cover of the Kırıkkale Massif exhibits similarities (Section 2.6.3.1) and possibly represents an

ophiolitic cover. Pelagic foraminifera from the Sarıkaraman Ophiolite indicate a Middle Turonian to Early Santonian age for the cover (Yalınız *et al*. 2000b). However, the Maastrichtian deposition date in the Kırıkkale Basin inferred by this study is younger.

2.6.5 Granitoid basement rocks

Granitoid plutons intrude the southern and eastern margins of the Kırıkkale Basin (Fig. 2.4), and are considered to be chemically and tectonically related to the granitoids of the Niğde-Kırşehir Massif (Dönmez *et al.* 2008). This study is the first to discuss geochemical data from the granitoids of the Kırıkkale Basin. Four samples were collected from Locality KK8.26, north of Bahşili, four samples were collected from Locality KK18.48, and three from Locality KK30.1 (see Fig.2.4).

2.6.5.1 Petrology

Thin section revealed that the granitoids from Locality KK8.26 are coarse-grained and rich in hornblende, plagioclase and quartz with minor biotite (Fig.2.19a). Samples from Localities KK18.48 and KK30.1 are petrographically similar and contain quartz, K-Feldspar and plagioclase with minor hornblende and titanite (Figs. 2.19b and 2.19c).

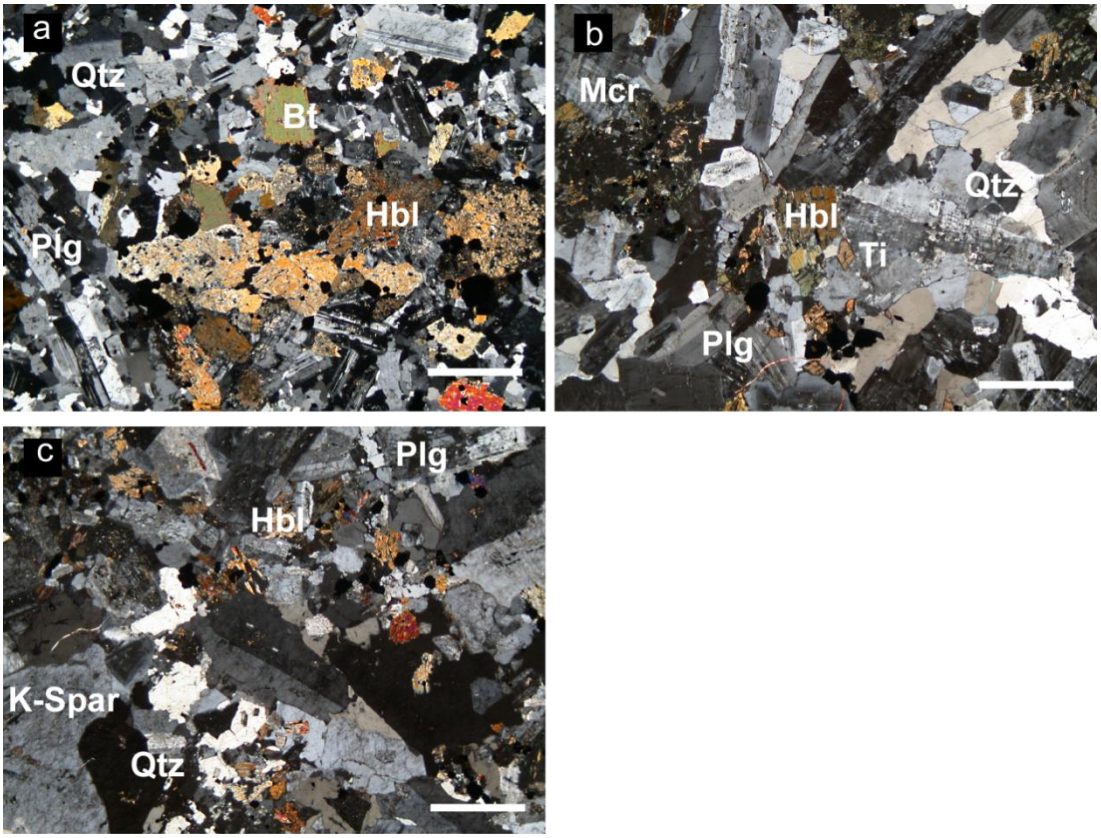

Figure 2.19 Photomicrographs (in crossed polars) of representative granitoid samples from the Kırıkkale Basin, **(a)** granitoid from Locality KK8.26, **(b)** granitoid from Locality KK18.48, **(c)** granitoid sample from Locality KK30.1. All scale bars = 1 mm. Qtz – quartz, Bt – biotite, Hbl – hornblende, Plg – plagioclase, Mcr – microcline, K-Spar – K-Feldspar, Ti – titanite.

2.6.5.2 Granitoid geochemistry and classification

The samples were prepared for XRF analysis as described in Appendix 1, which presents tabulated data. Classification was achieved by using the plutonic Total-Alkali-Silica (TAS) diagram of Middlemost (1994). Rocks from Locality KK8.26 are quartz-rich (~75 wt. % SiO_2) alkali-poor (~3.7 wt. % $Na_2O + K_2O$), and are thus classified as granites. In contrast, granitoids from Localities KK18.48 and KK30.1 are less quartz-rich (63.81–65.5 wt. % SiO_2) and richer in alkalis (7.86–9.45 wt. % $Na_2O + K_2O$). They are thus classified as quartz monzonites (Fig. 2.20a).

On the Total-Alkali-Silica diagram (Fig. 2.20b), where the alkaline-subalkaline division is from Irvine & Baragar (1971), all the rocks are subalkaline.

The granites from Locality KK8.26 are tholeiitic, quartz monzonites from Locality KK31.1 show compositions typical of high-K calc-alkaline series and quartz monzonites from Locality KK18.46 show compositions typical of shoshonitic series (Peccerillo & Taylor 1976) (Fig. 2.21a). The Aluminium Saturation Index (ASI) is one of the key factors to discriminate I (igneous)-type granites and S (sedimentary)-type granitoids (Chappell & White 1974; Chappell 1984; Chappell 1999) (Table 2.1). Figure 2.21b indicates that all the granitoids are I-type. Granites are peraluminous and quartz monzonites are metaluminous (Shand 1951).

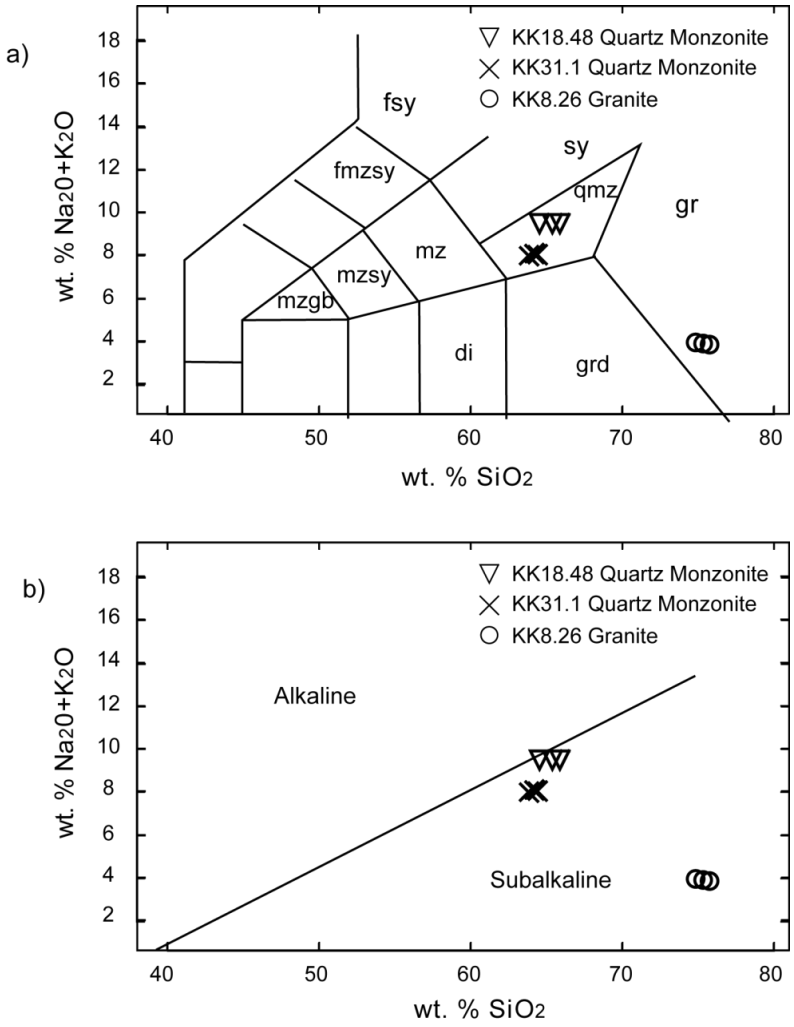

Figure 2.20 (a) Total-Alkali-Silica (TAS) plutonic diagram (Middlemost 1994) showing rock classification, gr – granite, grd – granodiorite, di – diorite, qmz – quartz monzonite, mz – monzonite, mzgb – monzo-gabbro, fmsy – foid monzosyenite, fsy – foid syenite, sy – syenite, **(b)** TAS diagram, Alkaline-subalkaline division is from Irvine & Baragar (1971).

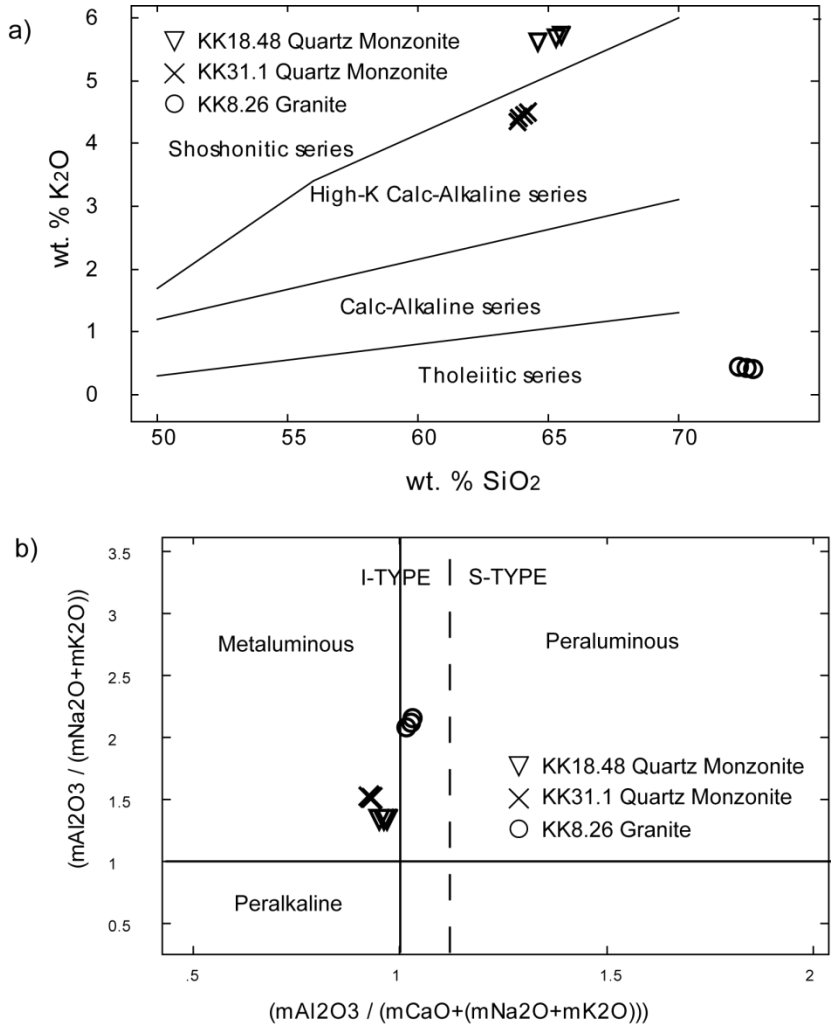

Figure 2.21(a) K_2O vs. SiO_2 diagram for magmatic rocks, the divisions are from Peccerillo & Taylor (1976), **(b)** rock classification using the Aluminium Saturation Index (ASI, expressed as molar Al_2O_3 / molar CaO + (molar Na_2O + molar K_2O)) (Shand 1951) (Chappell & White 1974; Chappell 1984).

Table 2.1 Summary of the main features of granitoids in the I-, S- and A-Type classification scheme (Chappell & White 1974; Chappell 1984).

I-Type	S-Type	A-Type
Relatively high sodium, Na_2O normally >3.2% in felsic varieties, decreasing to >2.2% in more mafic types	Relatively low sodium, Na_2O normally < 3.2% in rocks with approximately 5% K_2O,decreasing to < 2.2% in rocks with approximately 2% K_2O	From partial melting of dry granultitc residue remaining in the lower crust after extraction of orogenic (I- and S-Type) granites.
Mol. $Al_2O_3/(Na_2O+K_2O+ CaO) < 1.1$	Mol. $Al_2O_3/(Na_2O+K_2O+ CaO)>1.1$	High $Fe_{total}/(Fe_{total} + Mg)$
Broad spectrum of compositions from felsic to mafic	Relatively restricted in composition to high SiO_2 types	Strongly alkaline to sub-alkaline transition. High SiO_2 and ($Na_2O + K_2O$). Low Sr and CaO
Initial 87Sr/86Sr ratios between 0.704 and 0.706		

Figure 2.22 shows multi-element patterns normalised to ocean ridge granite (ORG) (Pearce *et al.* 1984a). In general, all the samples exhibit enrichment in LIL elements and depletions in HFS elements relative to ORG. Quartz monzonites show relatively more enrichment in LIL elements and most HFS elements, except for Y, compared to the granites. Nb depletions suggest a source melt which has been modified by subduction-related fluids.

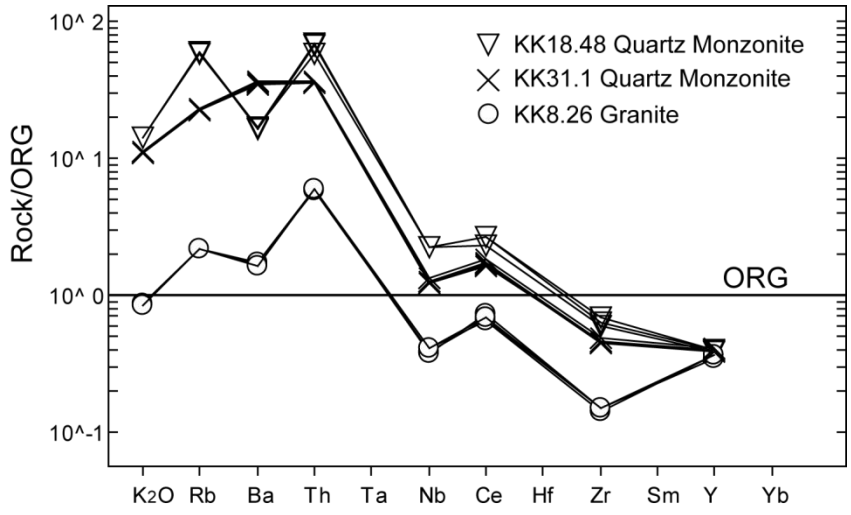

Figure 2.22 Ocean ridge granite (ORG)-normalised trace element patterns for the granitoid samples from the Kırıkkale Basin. The ORG normalisation values are from Pearce *et al.* (1984).

2.6.5.3 Interpretation of granitoid geochemistry and comparison to other Upper Cretaceous granitoids from the Niğde-Kırşehir Massif.

In order to place the new geochemical results for granitoids from the Kırıkkale Basin into a regional context, this section compares them to other mainly Upper Cretaceous granitoids which intrude the Niğde-Kırşehir Massif. A large data set, which consists of 285 major oxide and trace element measurements, was generated for this study by an extensive literature survey. The data set is larger than any other review in the literature (e.g. Düzgören-Aydin *et al.* 2001). Radiometric and isotopic data, where present, were also surveyed. The granitoid data are representative of; 1) the Ağaçören Intrusive Suite (location-Aksaray); 2) the Çelebi

Pluton (Kırşehir-Kaman); 3) the Yozgat, Kerkenez, Gelingüllü and Sivritepe plutons of the Yozgat Batholith (Yozgat); 4) the Çamsarı, Durmuşlu, Bayındır, Hamit and Baranadağ Plutons of the Baranadağ-Kortundağ Complex (Kırşehir-Kaman); 5) the Danacıobası Pluton of the Behrekdağ Batholith (Kırıkkale); 6) the Ekekcıdağ Pluton (Aksaray); 7) the Terlemez Pluton (Nevşehir); 8) the İdışdağı Pluton (Nevşehir); 9) the Çefalıkdağ Pluton (Kırşehir-Kaman) and; 10) the Atdere Pluton (Nevşehir). The main features of the plutons are summarised in Table 2.2.

Table 2.2 Summary of the granitoids of central Anatolia.

PLUTON	*GRANITOID TYPE*	*PRINCIPAL ROCK TYPES*	*PRIMARY MINERAL ASSEMBLAGE*	*WALL ROCK*	*REFERENCES AND DATA SOURCES*
İDIŞDAĞI	ALKALINE A-TYPE	Foidmonzosyenites/syenites/Foidsyenites. Cut by feldspathoid dykes.	K-feldspar, quartz, plagioclase, amphibole.	Metamorphic basement + Late Cretaceous calcalkaline granites.	(Düzgören-Aydin *et al.* 2001; Kadıoğlu *et al.* 2006)
DURMUŞLU	ALKALINE A-TYPE	Foidsyenites	K-Feldspar, nosean, plagioclase, nepheline, riebeckite, aegerine, melanite, biotite	Metamorphic basement + Hamit Pluton	(Otlu & Boztuğ 1998)
BAYINDIR	ALKALINE A-TYPE	Syenites, foidsyenites, monzonites.	K-Feldspar, nepheline, cancrinite, riebeckite, aegirine, melanite and biotite	Metamorphic basement + Hamit Pluton + Çamsari unit.	Kadıoğlu *et al.* 2006; Otlu & Boztuğ 1998
HAMIT	CALCALKALINE/ ALKALINE A-TYPE	Quartzmonzonites, syenites.	K-Feldspar, plagioclase, quartz, hastingite, biotite, augite	Metamorphic basement	(Otlu & Boztuğ 1998; Ilbeyli *et al.* 2004)
ATDERE	ALKALINE A-TYPE	Foidsyenites	K-Feldspar, nepheline, sodalite, cancrinite, melanite, aegerine, augite.	?	Düzgören-Aydin *et al.* 2001
BARANADAĞ	ALKALINE/ CALCALKALINE A-TYPE	Monzonites, quartzmonzonites, syenites. Features mafic microgranular enclaves and cross-cutting by aplitic dykes.	K-Feldspar, plagioclase, quartz, hastingsite, augite, biotite, hornblende. K-feldspar megacrysts.	Metamorphic basement	(Otlu & Boztuğ 1998; Aydin & Önen 1999; Köksal *et al.* 2004)
DANACIOBASI Behrekdağ batholith	S-TYPE CALCALKALINE	Granite	Quartz, K-Feldspar, plagioclase, with variable amounts of biotite	Metamorphic basement +Central Anatolian ophiolites	(Tatar & Boztuğ 2005)
ÇELEBİ	I-TYPE CALCALKALINE	Granite, monzonites, quartzmonzonites. Cut by aplitic dykes.	Plagioclase, biotite, K-Feldspar, hornblende, pyroxene ± quartz.	Metamorphic basement + Central Anatolian ophiolites.	(Kuşcu *et al.* 2002)

Table 2.2 (continued) Summary of the granitoids of central Anatolia.

PLUTON	*GRANITOID TYPE*	*PRINCIPAL ROCK TYPES*	*PRIMARY MINERAL ASSEMBLAGE*	*WALL ROCK*	*REFERENCES AND DATA SOURCES*
AĞAÇÖREN INTRUSIVE SUITE	I-TO S-TYPE CALCALKALINE	Granites, granodiorites Mafic microgranular enclaves (quartz diorite, diorite)	Quartz, K-Feldspar, plagioclase, amphibole, biotite	Metamorphic basement	(Kadıoğlu *et al.* 2003; Kadıoğlu *et al.* 2006)
EKECIKDAĞ	CALCALKALINE I-TYPE	Granites, granodiorites. Mafic enclaves.	Quartz, plagioclase, biotite, amphibole: K-Feldspar megacrysts	Metamorphic basement + Central Anatolian ophiolites.	(Düzgören-Aydin *et al.* 2001)
TERLEMEZ	CALCALKALINE/ALKALINE I-TYPE	Quartzmonzonites, syenites	Quartz, plagioclase, amphibole, biotite, pyroxene, K-Feldspar. K-feldspar megacrysts.	Central Anatolian ophiolites	(Yalınız *et al.* 1999)
ÇAMSARI	I-TO S-TYPE CALCALKALINE/ALKALINE	Granites, quartzmonzonites, syenites	K-Feldspar, plagioclase, quartz, hastingsite, biotite, fluorite	Metamorphic basement + Central Anatolian ophiolites	(Otlu & Boztuğ 1998)
ÇEFALIKDAĞ	I-TYPE CALCALKALINE/ALKALINE	Monzonites, quartzmonzonites, syenites Intruded by aplitic–pegmatitic dykes K-Feldspar megacrysts	Quartz, plagioclase, K-Feldspar, amphibole, biotite, Cpx.	Metamorphic basement + Central Anatolian ophiolites	(Düzgören-Aydin *et al.* 2001; Ilbeyli 2005; Kadıoğlu *et al.* 2006)
YOZGAT	I-TO S-TYPE CALCALKALINE/ALKALINE	Leucogranites, granites, granodiorites. Cut by K-Feldspar granite and diorite dykes	Quartz, plagioclase, K-Feldspar ± hornblende, biotite.	Metamorphic basement + Central Anatolian ophiolites	(Erler & Göncüoğlu 1996; Düzgören-Aydin *et al.* 2001; Kadıoğlu *et al.* 2006)
KERKENEZ (Yozgat)	CALC-ALKALINE I-TYPE	Quartzmonzonites K-Feldspar megacrysts	Quartz, K-Feldspar, Plagioclase, hornblende, biotite, muscovite	Metamorphic basement + Yozgat Batholtih	(Erler & Göncüoğlu 1996)
GELINGÜLLÜ (Yozgat)	CALC-ALKALINE I-TYPE	Granites, quartzmonzonites Cut by aplitic and syenitic dykes,	Quartz, K-Feldspar, plagioclase, hornblende, biotite, muscovite	Metamorphic basement + Yozgat Batholtih	(Erler & Göncüoğlu 1996)
SIVRITEPE (Yozgat)	CALC-ALKALINE I-TYPE	Granites, quartzmonzonites	Quartz, K-Feldspar, plagioclase, hornblende.	Metamorphic basement + Yozgat Batholtih	(Erler & Göncüoğlu 1996)

The granitoids intrude both the Palaeozoic-Mesozoic metamorphic basement of the Niğde-Kırşehir Massif and the inferred Upper Cretaceous Supra-Subduction Zone ophiolites. On the basis of the TAS classification diagram of Middlemost (1984) the granitoids can broadly be subdivided into three major suites; granites, monzonites and syenites (Fig.2.23). In terms of SiO_2 there is a decrease from the granite suite (78–65 wt. %) to the monzonite suite (68–60 wt. %) and the syenite suite (65–51 wt. %). $Na_2O + K_2O$ shows the opposite trend from the granite suite (6 – 8.5 wt. %) the monzonite suite (8–10 wt. %) and the syenite suite (10–17 wt. %).

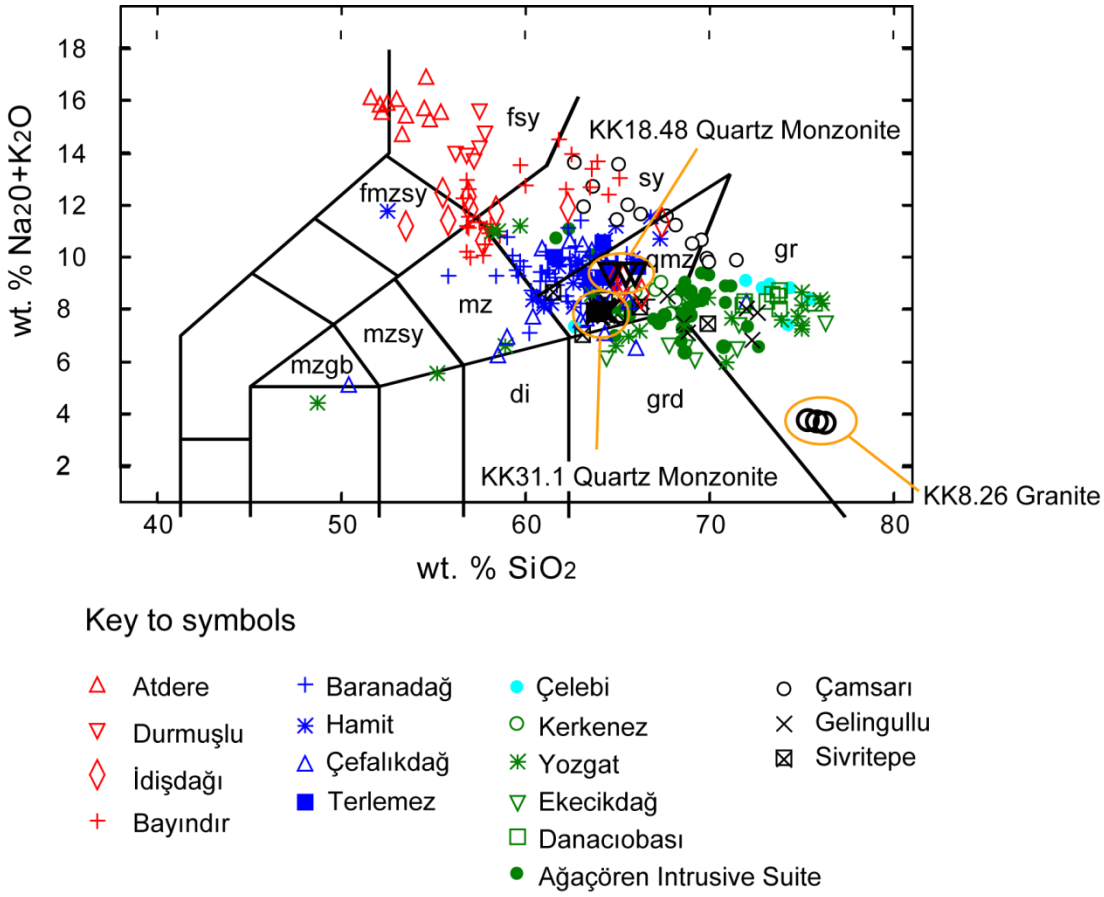

Figure 2.23 TAS diagram (Middlemost 1984) showing the dataset of Upper Cretaceous granitoid samples intruding the Niğde-Kırşehir Massif taken from a literature survey. Symbols in red are from mostly syenitic plutons, symbols in blue from monzonitic plutons, and those in green are from granitic plutons. Black symbols are from plutons that exhibit a wide compositional variety. Samples from the Kırıkkale Basin are highlighted with an orange circle.

The granite suite is represented by samples of the Ağaçören Intrusive Suite, the Çelebi, Yozgat, Kerkenez, Gelingüllü and Sivritepe, the Danacıobası and Ekekcıdağ Plutons. These granitoids outcrop in a curvilinear pattern along the north/western margin of the Niğde-Kırşehir Massif. They are composed of biotite/amphibole granites and granodiorites. Minerals are plagioclase, quartz, biotite, amphiboles with minor pyroxenes. Microcline granites, biotite/K-Feldspar granites exist as cross-cutting dykes. Common features are the presence of mafic microgranular enclaves, and K-Feldspar megacrysts.

The monzonite suite appears in the north and is represented by the Baranadağ, Terlemez, Çefalıkdağ, Hamit and Kerkenz Plutons; it is composed of monzonite and quartzmonzonite rocks. The plutons are locally cut by quartzmonzonite porphyry and granite porphyry dykes and feature K-Feldspar megacrysts. Principal minerals are Quartz, K-Feldspar, Plagioclase, hornblende, biotite and muscovite.

The syenite suite is made up of the Durmuşlu, Bayındır, Hamit, Atdere, İdışdağı, most samples of the Çamsarı, and samples from the Baranadağ Plutons. These granitoids crop out towards the centre of the Niğde-Kırşehir Massif and often intrude granitic plutons. The suite features syenite, foid-syenite and foid-monzosyenite rocks. Typical mineral assemblages are K-Feldspar, nepheline, cancrinite, riebeckite, aegirine, melanite and biotite (see Table 2.2 for references).

The Fe_2O_3 + MgO vs. SiO_2 plot (Fig.2.24a) shows a broadly linear trend with increasing Fe_2O_3 + MgO as SiO_2 decreases through the granite, monzonite and syenite suite. This pattern is consistent with the early fractionation of ferromagnesian minerals from parental melts. Two syenitic plutons (Durmuşlu and Bayındır) lie off the linear trend; both have low Fe_2O_3 + MgO. On the TiO_2 (Fig.2.24b), P_2O_5 (Fig.2.24c) and CaO (Fig.2.25a) vs. SiO_2 Harker variation plots, the granite and monzonite suites show a negative correlation. However, most samples from the syenite suite are depleted in TiO_2, P_2O_5 and CaO. The depletion in TiO_2 is probably due to the early fractionation of Ti-oxides.

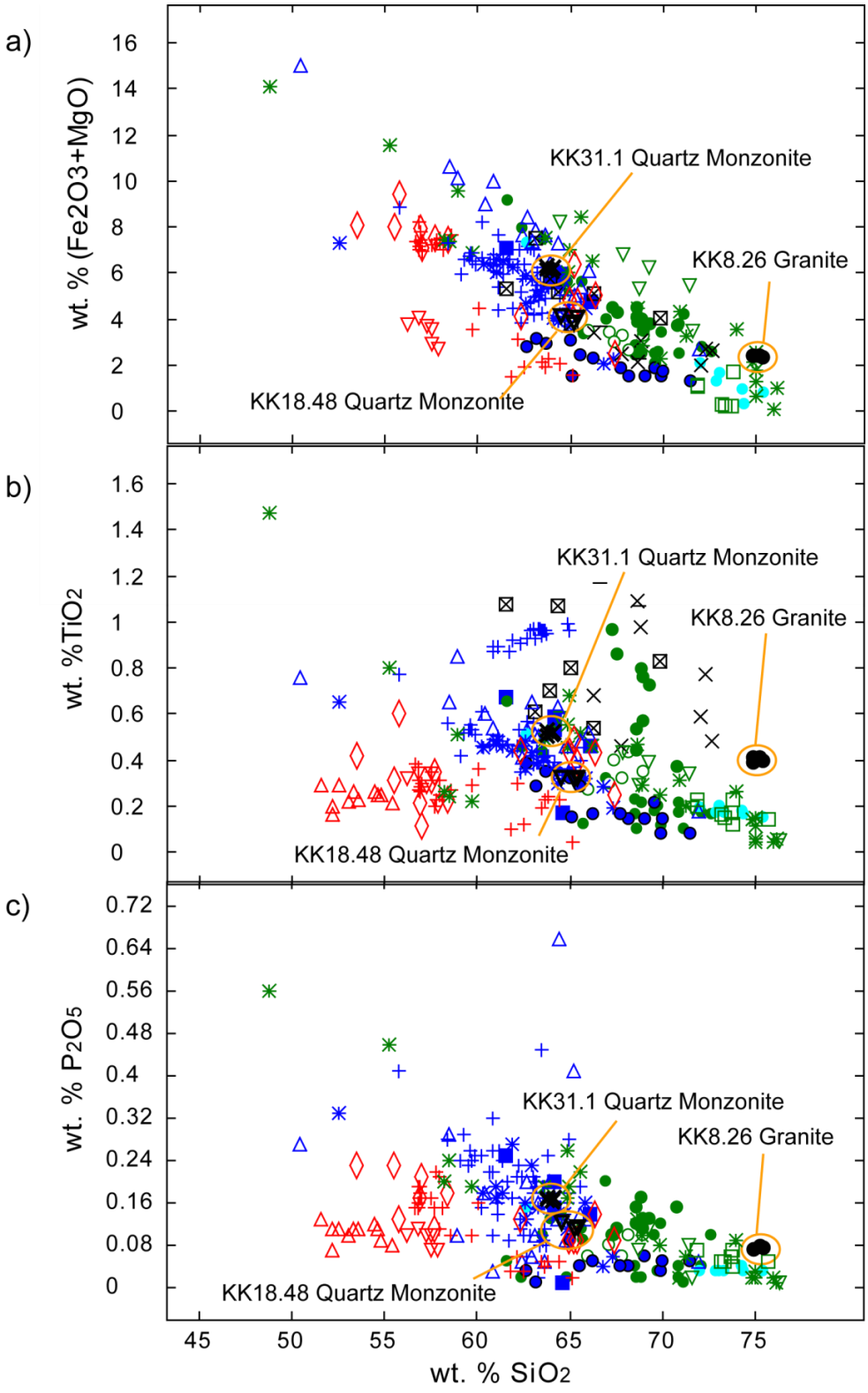

Figure 2.24 Harker variations diagrams, **(a)** Fe_2O_3 vs. SiO_2, **(b)** TiO_2 vs. SiO_2, **(c)** P_2O_5 vs. SiO_2 showing the relationship between the granite (green symbols), monzonite (blue symbols) and syenite (red symbols) suites. See Figure 2.23 for symbols. Data for the Kırıkkale Basin (highlighted in orange) are from this study. See Table 2.2 for other data sources.

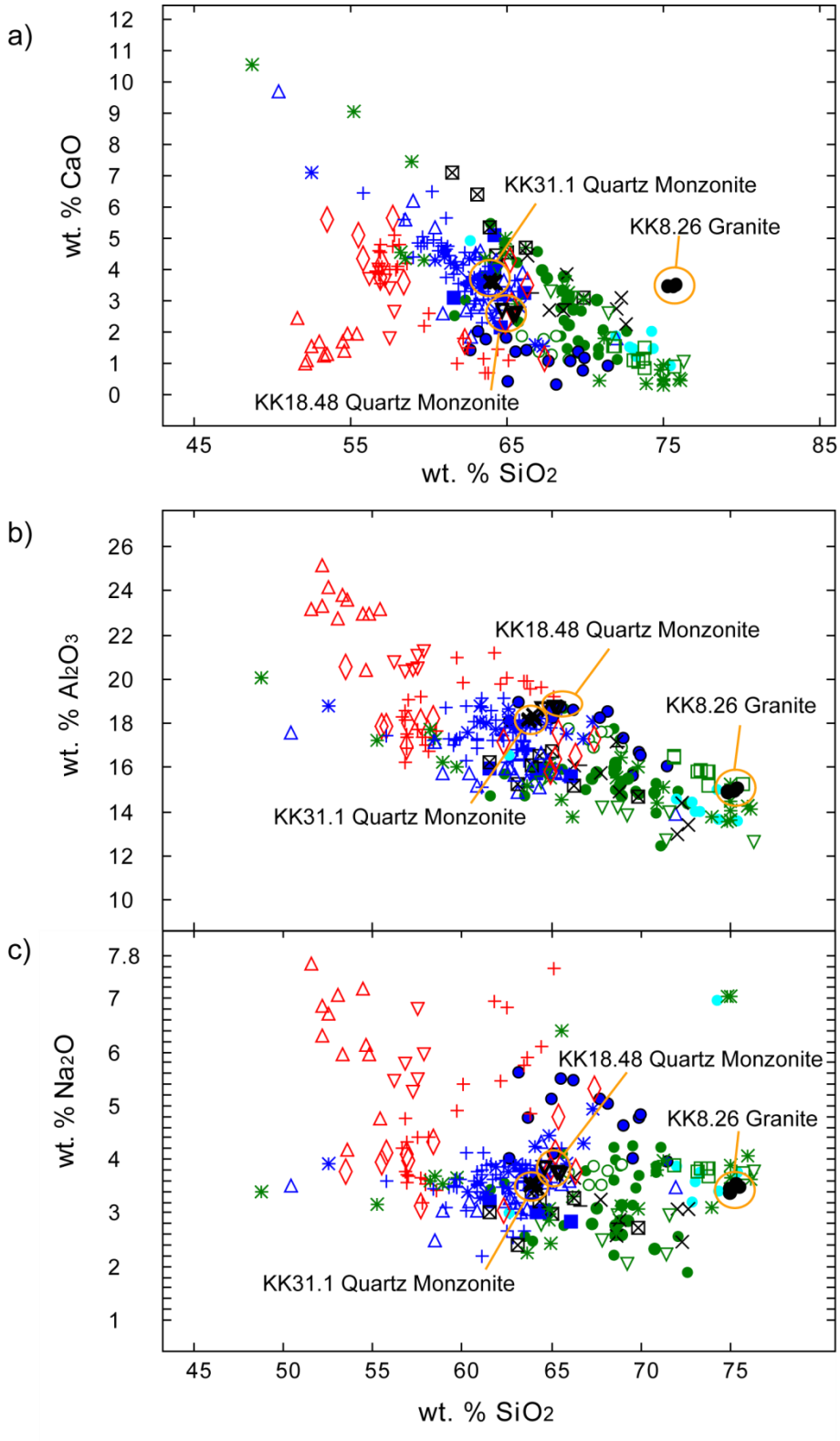

Figure 2.25 Harker variations diagrams, **(a)** CaO vs. SiO_2, **(b)** Al_2O_3 vs. SiO_2, **(c)** Na_2O vs. SiO_2 showing the relationship between the granite (green symbols), monzonite (blue symbols) and syenite (red symbols) suites. See Figure 2.23 for symbols. Data for the Kırıkkale Basin (highlighted in orange) are from this study. See Table 2.2 for other data sources.

Figure 2.25b shows a negative correlation between Al_2O_3 and SiO_3, while the correlation between Na_2O and SiO_2 (Fig.2.25c) is less clear. The granite suite is predominantly I-Type (i.e. K-Poor and Mol. Al_2O_3/ (Na_2O+CaO+K_2O) <1.1, Na_2O ranges from 2.1 wt. % to 4.3 wt. %) with the Danacıobası Pluton being S-Type (i.e. Mol. Al_2O_3/ (Na_2O+CaO+K_2O) >1.1 but with high Na_2O of 3.8 wt. %). The monzonite suite is I-Type (Mol. Al_2O_3/ (Na_2O+CaO+K_2O) <1.1; Na_2O > 3.1 wt. %) and the syenite suite is A-Type (highly alkaline) (Fig.2.26). The syenite suite is mostly alkaline in character, the monzonite suite is high-K shoshonitic, and the granite suite is mostly high-K calc-alkaline (Fig.2.27).

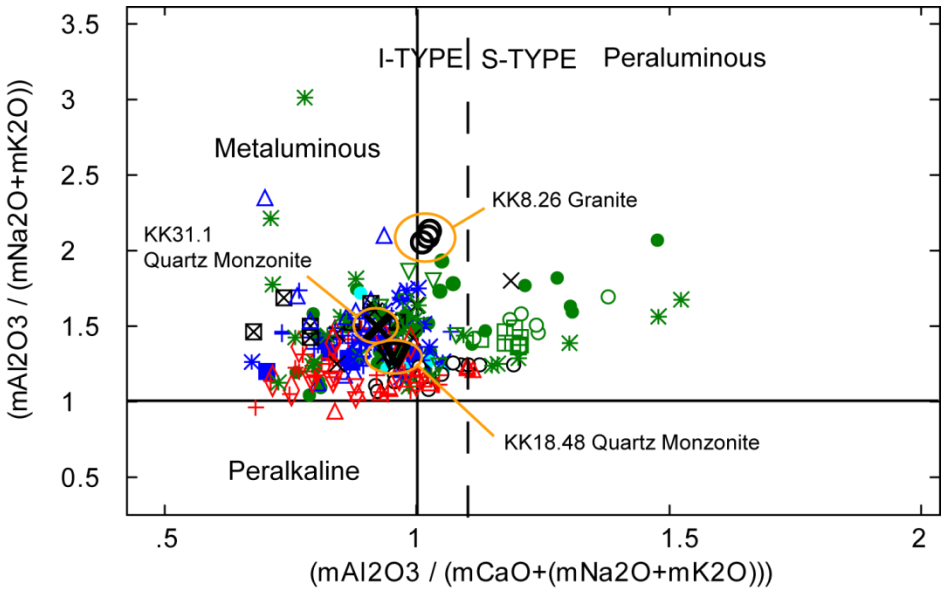

Figure 2.26 Rock classification using the Aluminium Saturation Index (ASI, expressed as molar Al_2O_3 / molar CaO + (molar Na_2O + molar K_2O)) (Shand 1951). Data from the Kırıkkale Basin (highlighted in orange) are from this study.

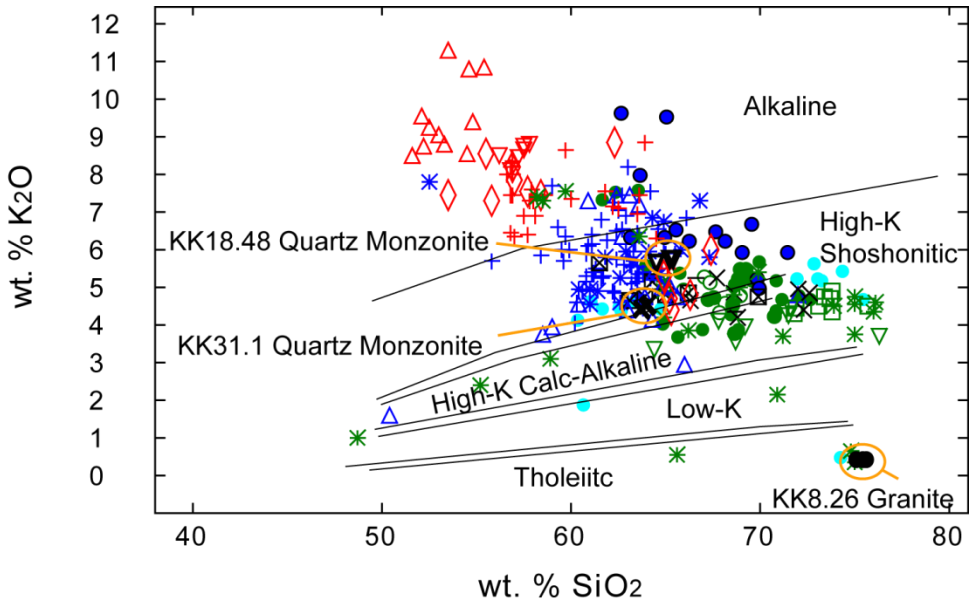

Figure 2.27 K2O vs. SiO2 diagram showing the relationships between the granite suite (green symbols) the monzonite suite (blue symbols) and the syenite suite (red symbols). Divisions are from Peccerillo & Taylor (1976). Data from the Kırıkkale Basin (highlighted in orange) are from this study. See Figure 2.23 for a key to the symbols.

2.6.5.3.1 Trace element patterns

In general the syenite suite is relatively more enriched than are the monzonite and granite suites, similar to the pattern shown in Fig. 2.22. Normalised to Ocean Ridge Granite, there is an enrichment of LIL elements and depletion in HFS elements. All the suites show particularly strong enrichment in Rb and Th and marked depletion in Zr, Y and Yb. Nb depletion is present in the granite suite and partially in the monzonite suite, but wholly absent in the syenite suite. This indicates a trend of a subduction-modified source from the granite and monzonite suites to a syenite source that has been less modified by subduction. If the assumption is made that immobile elements are indicative of parental melts, there is evidence of the syenite suite being unrelated to both the granite and monzonite suites. The enrichment in fluid-mobile elements and LIL elements (e.g. Ba, Th, K) suggests a close association with arc magmatism and metasomatised mantle. The granite suite is most closely associated with arc characteristics (e.g. Nb, Ta and Ti depletion) and this signature is progressively reduced through the monzonite and syenite suite.

Granite and monzonite suites samples have Ba/Nb > 30 (Gill 1981) and high Ba/Zr. Depletions in P and Ti suggests that fractionation processes have occurred.

Oxygen isotopic work is severely limited in this region and comprises two studies (Boztug & Arehart 2007; Ilbelyi *et al*. 2009). Oxygen isotopes are powerful tracers of source melt composition and/or crustal contaminants since fractional crystallisation has little effect on $\delta^{18}O$ ‰ values. Mantle-derived rocks have $\delta^{18}O$ values of ~5.7‰, weathered sediments generally exhibit $\delta^{18}O$ ‰ values of 12‰ to 25‰ (Wei *et al.* 2000). Boztuğ & Arehart (2007) presented oxygen isotope data which displayed a wide range of values from 7.4‰ to 13.7‰. A-, S- and I-Type granitoids generally have high data on values of >10‰, which suggests a significant crustal contribution to parental magma. Ilbeyli *et al.* (2009) published $\delta^{18}O$ values between 6.5‰ and 14.8‰ in samples from the Behrekdağ, Cefalıkdağ and Celebi intrusions. The granitoid suite exhibited higher $\delta^{18}O$ values than alkaline samples (the syenite suite) which infers that the granite suite is more enriched in sedimentary crustal components.

2.6.5.3.2 Tectonic discrimination diagrams

There are presently a wide range of chemical discrimination diagrams that attempt to characterise granitoids in terms of their tectonic setting at the time of intrusion. There are, however, a range of difficulties in using granitoids as tectonic indicators; principally because it is often difficult to sample granitoids of a known tectonic setting. In addition, granitoids show a complex petrogenetic history often involving fractionation, crustal assimilation and the mixing of elements by volatile fluxing.

The most common discrimination diagrams are that of Pearce *et al.* (1984). This scheme proposes that groups of granitoids with known tectonic settings have distinctive trace element characteristics. Discriminations are most effective using Y-Nb, Yb-Ta, Rb - (Y + Nb) and Rb – (Yb + Ta). It is important to emphasise that

discriminatory fields reflect source regions rather than tectonic setting. SiO2 variation diagrams for Y, Nb and Rb were plotted which provides information on the sensitivity of these elements to fractional crystallisation. The Y vs. SiO_2 diagram (Fig.2.28a) is used to discriminate between (volcanic arc and collisional) sources and (within-plate and 'normal' ocean ridge, i.e. not supra-subduction) settings. The syenite suite plots in the within-plate and 'normal' ocean ridge field, as does the transitional Çamsarı Pluton. The granite suite and most of the monzonite (including all samples from the Kırıkkale Basin) suite plot in the volcanic arc and collisional fields. Nb is generally more enriched in within-plate granites, and this is reflected in the Nb vs. SiO_2 diagram (Fig.2.28b) which displays similar results to that of Fig.2.28a. Rb is thought to discriminate between volcanic arc and syn-collisional settings. The Rb vs. SiO_2 diagram (Fig. 2.28c) shows that most samples plot in the volcanic arc field. However, the entire Çamsarı Pluton, some samples from the Yozgat and Çelebi plutons, and quartz monzonite from locality KK18.48 plot in the syn-collisional field. This diagram, however, is acknowledged by Pearce *et al.* (1984) to contain an overlap of post-orogenic granitoids. Thus, within-plate granitoids cannot be determined by Rb vs. SiO_2 diagrams.

The plots of Nb vs. Y (Fig.2.29a) and Rb vs. (Y + Nb) (Fig. 2.29b) show that: 1) most of the granite suite (including the granite from locality KK8.26) belongs to the volcanic arc fields; 2) the monzonite suite is transitional between the volcanic arc and within-plate fields (quartz monzonites from KK31.1 plots in the volcanic arc field, those from KK18.48 plot in the within-plate field) and; 3) the syenite suite plots in the within-plate field.

To interpret the results in terms of central Turkey, it is necessary to consider the source geochemical data used by Pearce *et al.* (1984) to obtain the discriminatory fields. The volcanic arc data (corresponding to the granite/monzonite suites of this study) were from: 1) oceanic, tholeiitic arcs (Little Port Complex, Newfoundland, Canyon Mountain, Oregon and the late Intrusive complex, Oman); 2) oceanic calc-alkaline arcs (Jamaica, SW Pacific, Aleutians) and; 3) active continental margins (Antarctic Peninsula, central Chile and the Tuolumne Batholith, Sierra Nevada). Given the tectonic evolution of the Niğde-Kırşehir Massif an oceanic arc source can

be ruled out. Thus the granite and monzonite suites, in terms of trace elements, are similar to granitoids sourced from an active continental margin setting.

The within-plate analyses (generally corresponding to the syenite suite of this study) were from a variety of settings including: 1) intra-continental ring complexes (Nigeria, Sabaloka complex, Sudan and the Oslo graben); 2) attenuated continental crust (Skaergaard, Greenland and Mull, Scotland) and; 3) oceanic islands (Ascension Islands and Reunion). The syenite suite is not sourced from an oceanic island setting, so is therefore similar to 1) and/or 2).

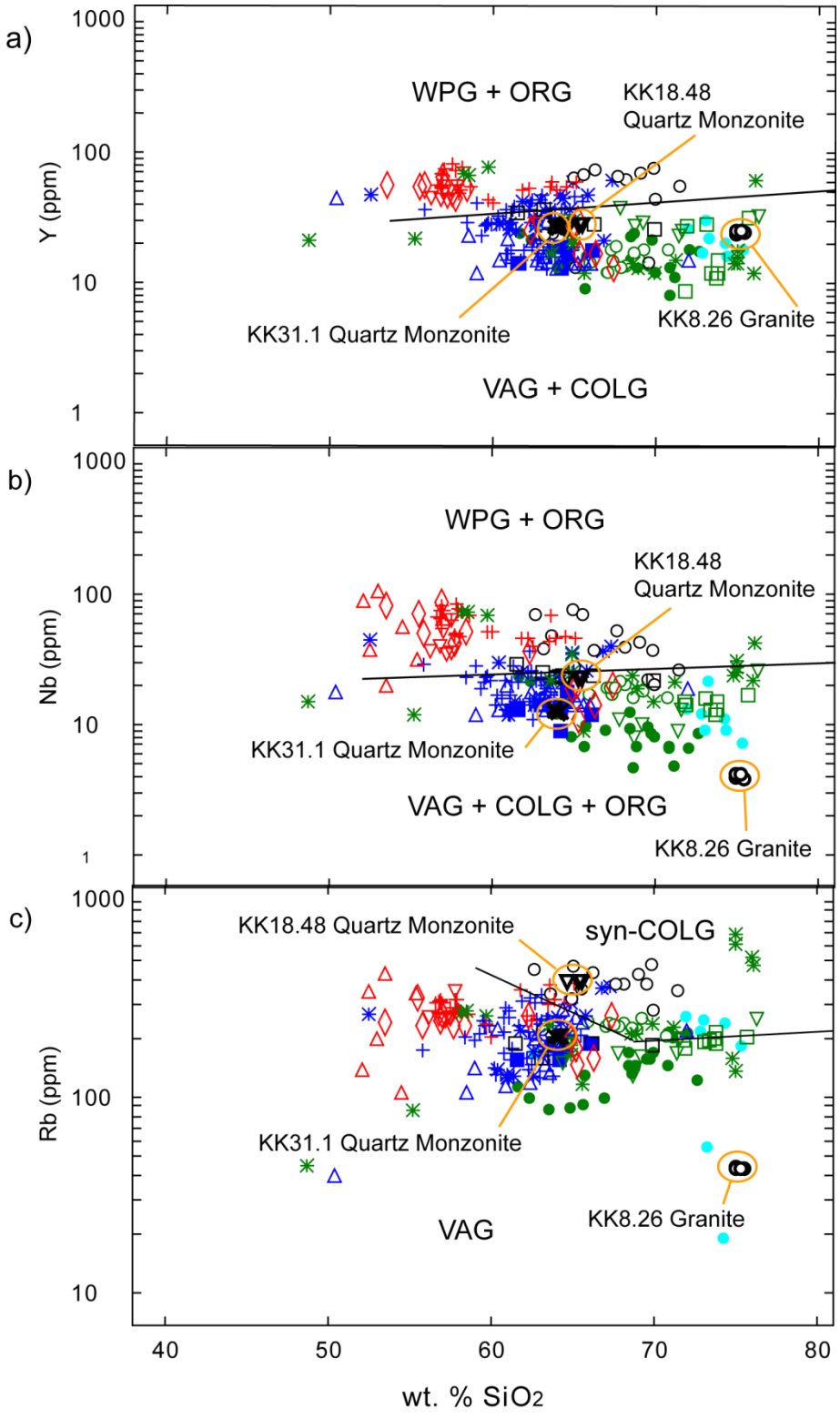

Figure 2.28 (a) Y vs. SiO_2 **(b)** Nb vs. SiO_2 **(c)** Rb vs. SiO_2 tectonic discrimination diagrams for granitoids rocks (Pearce *et al.* 1984) showing the relationships between the granite (green symbols), monzonite (blue symbols) and syenite (red symbols) suites. See Figure 2.23 for a list of symbols. Granitoids from the Kırıkkale Basin (outlined in orange) are from this study. See Table 2.2 for other data sources. WPG – within-plate granite, ORG – ocean-ridge granite, VAG – volcanic arc granite.

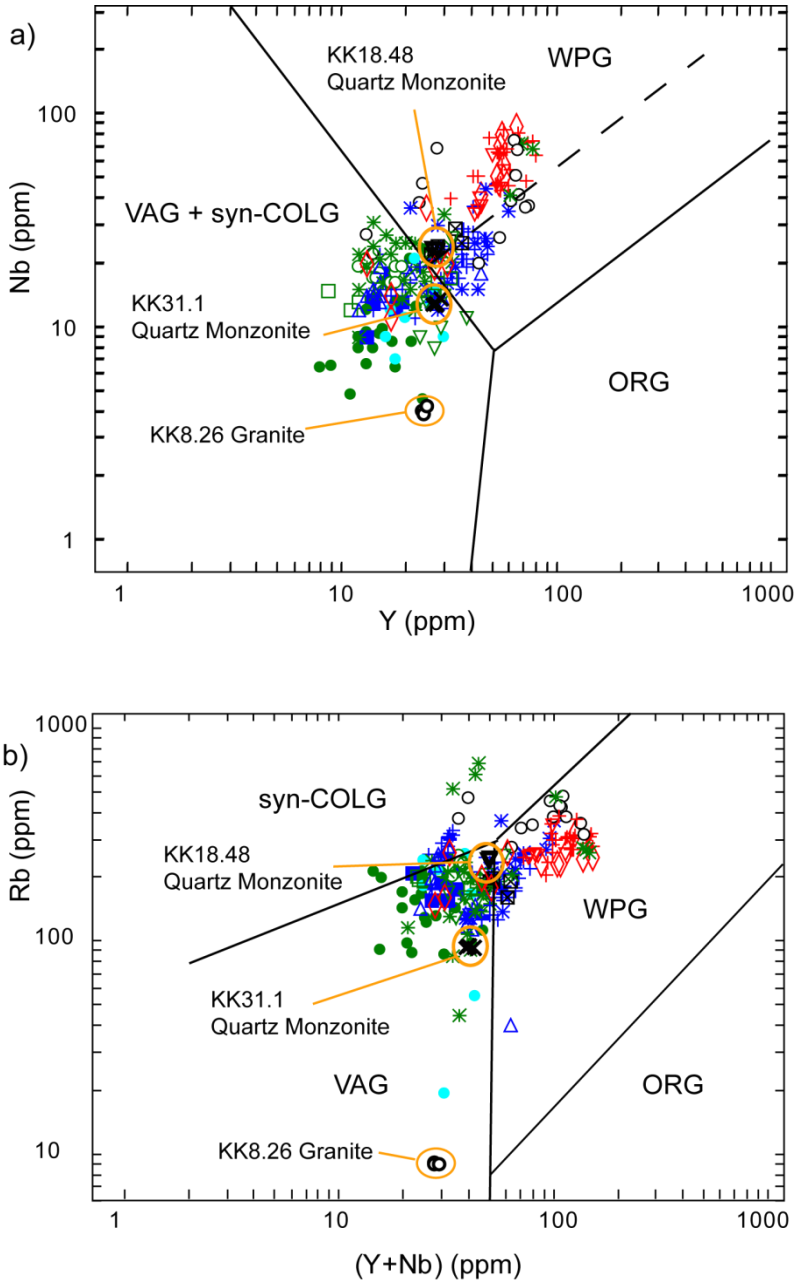

Figure 2.29 (a) Nb vs. Y, **(b)** Rb vs. (Y+Nb) tectonic discrimination diagrams for granitoids rocks (Pearce *et al.* 1984) showing the relationships between the granite (green symbols), monzonite (blue symbols) and syenite (red symbols) suites. See Figure 2.23 for a list of symbols. Granitoids from the Kırıkkale Basin (outlined in orange) are from this study. See Table 2.2 for other data sources. WPG – within-plate granite, ORG – ocean-ridge granite, VAG – volcanic arc granite, syn-COLG – syn-collisional granite.

2.6.5.3.3 Geochronology

Table 2.3 is a summary of the geochronological results for intrusion (U-Pb and $^{207}Pb/^{206}Pb$) and cooling (K-Ar and $^{40}Ar/^{39}Ar$) ages for selected plutons intruding the Niğde-Kırşehir Massif. In general, the granitoids are Campanian to Santonian in age, while several exhibit Maastrichtian ages, and one sample from the Çamsarı syenitic pluton yielded a $^{207}Pb/^{206}Pb$ single zircon age of 94.9 ± 3.4 Ma (Cenomanian).There is no apparent regional trend of radiometric dates between the different rock suites or plutons. In contrast, Kadıoğlu *et al* (2006) used three K/Ar cooling dates to infer that the granite suite is the oldest, followed by the monzonite suite and syenite suite. Locally, however, the age relationships of Kadıoğlu *et al* (2006) appear to hold true. An example is the relationships within the Kortundağ and Baranadağ Plutons in the Kaman-Kırşehir region (Otlu & Boztuğ 1998). Here, the Baranadağ quartz monzonite and the Hamit quartz syenite plutons intrude into the metasedimentary basement of the Niğde-Kırşehir Massif but themselves are interpreted to be cut by the syenitic Durmuşlu, Bayındır and Çamsarı Plutons.

Table 2.3 Existing radiometric dates for granitoids intruding the Niğde-Kırşehir Massif. K-Ar and $^{40}Ar/^{39}Ar$ dates are generally interpreted as cooling ages, U-Pb and $^{207}Pb–^{206}Pb$ are interpreted as intrusion dates.

PLUTON	ROCKTYPES	METHOD	AGE	REFERENCE
ÜÇKAPILI	Granite	Rb-Sr (whole rock, biotite, muscovite)	95 ± 11 Ma	(Göncüoğlu 1986b)
	Granodiorite	U-Pb monazite	13.7–20 Ma	(Whitney & Dilek 1997)
	Granodiorite	U-Pb SHRIMP (Zircon)	85–92 Ma	(Whitney *et al.* 2003)
	Granodiorite	$^{40}Ar/^{39}Ar$ (Biotite)	79 Ma	(Whitney *et al.* 2003)
ÇEFALIKDAĞ	Granite, granodiorite	Rb-Sr (whole rock, biotite)	71 ± 1.1	(Ataman 1972)
TERLEMEZ	Quartzmonzonite	K-Ar (K-Feldspar) K-Ar (Amphibole)	67.1 ± 1.3 Ma - 70.1 ± 1.5 Ma 81.5 ± 1.9 Ma	(Yalınız *et al.* 1999)

Table 2.3 (contd.) Existing radiometric dates for granitoids intruding the Niğde-Kırşehir Massif. K-Ar and $^{40}Ar/^{39}Ar$ dates are generally interpreted as cooling ages, U-Pb and $^{207}Pb–^{206}Pb$ are interpreted as intrusion dates.

PLUTON	ROCKTYPES	METHOD	AGE	REFERENCE
AĞAÇÖREN INTRUSIVE SUITE	Granites Gabbro	$^{40}Ar/^{39}Ar$ (Amphibole)	77.6 ±0.3 Ma 78.6 ± 0.3 Ma	(Kadıoğlu *et al.* 2003)
BAYINDIR	Syenite	$^{40}Ar/^{39}Ar$ (Amphibole)	69.8 ± 0.3 Ma	(Kadıoğlu *et al.* 2006)
DANACIOBASI	Leucogranite	K/Ar (Biotite) $^{207}Pb–^{206}Pb$ single-zircon	69.1±1.42 Ma - 71.5±1.45 Ma 85.5 ± 5.5 Ma	(Tatar & Boztuğ 2005) (Boztuğ *et al.* 2007)
BARANADAĞ	Monzonite, Quartzmonzonite	U-Pb titanite K-Ar (hornblende) $^{207}Pb–^{206}Pb$ single-zircon	74.0±2.8 Ma 76.4 ± 1.3 Ma 74.9 ± 3.4 Ma	(Köksal *et al.* 2004) (Ilbeyli *et al.* 2004) (Boztuğ *et al.* 2007)
ÇEFALIKDAĞ	Monzonite	K-Ar (biotite) $^{40}Ar/^{39}Ar$ (Amphibole)	66.6 ± 1.2 Ma 70.0 ± 1.0 Ma	(Ilbeyli *et al.* 2004) (Kadıoğlu *et al.* 2006)
ÇAMSARI	Syenite	U-Pb titanite $^{207}Pb–^{206}Pb$ single-zircon	74.1±0.7 Ma 94.9 ± 3.4 Ma	(Köksal *et al.* 2004) (Boztuğ *et al.* 2007)
CANKILI – YOZGAT	Monzodiorite	K-Ar (Hornblende + Biotite) K-Ar (Biotite)	58.7 ±0.6 Ma 71.1 ±1.9 Ma	(Boztuğ *et al.* 2009)
AKÇAKOYUNLU – YOZGAT	Quartzdiorite	K-Ar (Hornblende) K-Ar (Hornblende)	77.6 ± 0.2 Ma 79.3 ± 1.5 Ma	(Boztuğ *et al.* 2009)
KARAKAYA – YOZGAT	Monzogranite	K-Ar (Hornblende + Biotite)	71.3 ± 0.9 Ma 77.0 ± 0.0 Ma	(Boztuğ *et al.* 2009)
YASSIAĞIL – YOZGAT	Monzogranite	K-Ar (Hornblende + Biotite)	79.8 ± 0.1 Ma 69.9 ± 2.0 Ma	(Boztuğ *et al.* 2009)
ADATEPE – YOZGAT	Quartzmonzonite	K-Ar (Hornblende + Biotite) K-Ar (Hornblende)	48.9 ± 0.5 Ma 68.0 ± 0.3 Ma	(Boztuğ *et al.* 2009)
KERKENEZ (YOZGAT)	Quartzmonzonite Granite	$^{40}Ar/^{39}Ar$ (Amphibole) $^{40}Ar/^{39}Ar$ (Amphibole)	81.2 ± 0.5 Ma [1] 72.6 ± 0.2 Ma	(Isik *et al.* 2008)
KERKENEZ shear zone	Shear zone	$^{40}Ar/^{39}Ar$ (Amphibole) $^{40}Ar/^{39}Ar$ (K-Feldspar)	71.6 ± 0.3 Ma 71.7 ± 0.2 Ma	(Isik *et al.* 2008)
BEHREKDAĞ	Leucogranite Quartzmonzonite	K-Ar (biotite) K-Ar (hornblende)	69.1 ± 1.42–71.5 ± 1.45 Ma 68.8 ± 1.43–81.2 ± 3.36 Ma	(Tatar *et al.* 2003)

2.6.5.3.4 Magma source composition

Ratios of certain HFS elements such as Nb and Zr can be used to infer magma source composition (e.g. Davidson 1996). Nb and Zr are depleted in subduction zone magmas and are assumed to be derived from the mantle. They are relatively immobile and are strongly fractionated only during melting processes. Nb/Zr ratios are unaffected by fractional crystallisation and are mostly immune to crustal contamination. Different Nb/Zr ratios are usually interpreted as evidence of variations in source composition and/or changes in degree of partial melting of the mantle (Seghedia *et al.* 2004). The Nb/Zr vs. Nb diagram (Fig.2.30) shows that Nb and Nb/Zr increase from the granite suite through the monzonite suite to the syenite suite. The granite and monzonite suites (including all the samples from the Kırıkkale Basin) are closer to a mid-ocean ridge-like source and the syenite suite is closer to an ocean island basalt-like source.

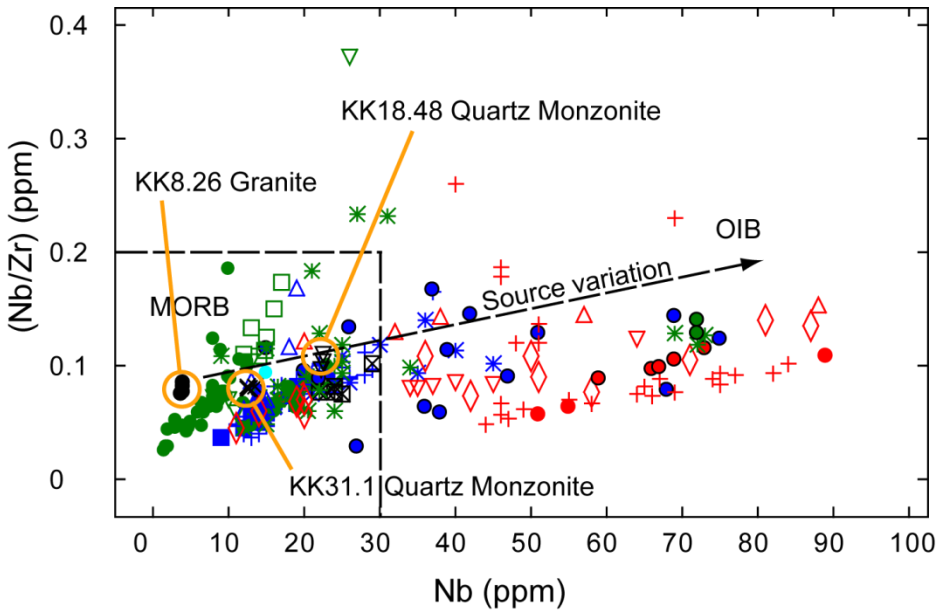

Figure 2.30 Nb/Zr vs. Nb diagram after Seghedia et al. (2004) showing the relationships between the granite suite (green symbols), the monzonite suite (blue symbols) and the syenite suite (red symbols). Data from the Kırıkkale Basin (highlighted with orange circles) are from this study, all others from a literature survey.

2.6.5.3.5 Summary and discussion

A review of published petrological, geochemical and isotopic data from granitoids of the Niğde-Kırşehir Massif can be used to summarise the present understanding of their parental melt sources, magmatic evolution and tectonic emplacement setting. The plutons can be effectively sub-divided into three suites based on their $Na_2O + K_2O$ vs. SiO_2 content: a granite, a monzonite, and a syenite suite. The granite suite comprises silica rich, low-K to high-K calc-alkaline I- to S-Type peraluminous to metaluminous plutons. They are enriched in LIL elements and depleted in HFS elements relative to ocean ridge granite, and show Nb and Ta depletions, which suggest the parental magma source inherited a subduction signature from fluids driven off a subducting slab. High $\delta^{18}O$ values suggest a significant crustal component to many of the S-Type granitic rocks, which indicates that crustal assimilation occurred. According to tectonic discrimination diagrams, they are related to volcanic arc-type granites. New data from this study indicate that granite samples from the Kırıkkale Basin (Locality KK8.26) are among the most silica-rich (~75 wt. % SiO_2) and alkali-poor (~3.7 wt. % $Na_2O + K_2O$) of the Niğde-Kırşehir Massif granitoids.

Rocks of the monzonite suite consist of less silica rich, high-K shoshonitic I-Type metaluminous plutons. They are also enriched in LIL elements and depleted in HFS elements relative to ocean ridge granite (Fig. 2.22). Nb and Ta depletions are less than those of the granite suite. On tectonic discrimination diagrams, they plot on the volcanic arc and within-plate granitoid fields. New data indicate that the granitoids (Localities KK18.48 and KK31.1) intruding the Kırşehir Massif situated at the eastern and southeastern margins of the Kırıkkale Basin belong to this group.

The syenite suite comprises the most silica-poor (65 – 51 wt. % SiO_2) and alkali-rich (10 – 17 wt. % $Na_2O + K_2O$) plutons. They are alkaline, mostly A-Type and metaluminous. The syenite suite is mildly enriched in LIL elements and depleted in HFS elements. However, Nb and Ta depletions are absent, suggesting that parental melt was not as strongly associated with a subducting slab as were the granite and monzonite suites. Harker variations diagrams suggest that parental melt underwent

extensive fractionation. Different HFS element abundances suggest a different melt to that of the granite and monzonite suites. In particular, Nb/Zr ratios infer that the parental melt of the granite and monzonite suite is a MORB-type melt, and the parental melt of the syenite suite was an OIB-type melt. Generally low $\delta^{18}O$ values imply lower crustal assimilation than that of the monzonite an granite suites. On tectonic discrimination diagrams, most syenite samples plot in the within-plate granitoid field.

Temporal associations between the three different granitoid suites are evident at local level, where syenitic plutons cut more silica-rich plutons. However, at a regional scale, such evidence is lacking. Moreover, recent radiometric dating indicates that some of the oldest plutons (94.9 ± 3.4 Ma) are syenitic.

2.6.5.3.6 Tectonic implications

Any geotectonic model of Late Mesozoic-Early Cenozoic collision in northern Neotethys must take into account the source melt, magmatic evolution and emplacement setting of the Niğde-Kırşehir granitoids. The granite suite and some samples of the monzonite suite show geochemical evidence of having a parental melt which was enriched in fluid mobile elements and LILEs relative to HFSEs. The timing and location of the subducting slab is critical and requires careful evaluation in the context of regional geotectonics. The basement of the Niğde-Kırşehir Massif is partially covered by ophiolitic rocks which represent dismembered remnants of the İzmir-Ankara-Erzincan Ocean. These ophiolites were thrust southwards when an oceanic trench collided with the northern margin of the Niğde-Kırşehir Massif. This subduction zone featured a north-dipping slab beneath the Pontide margin (i.e. away from the Niğde-Kırşehir Massif) that could not have influenced the source melt of the granitoids. Instead, one possibility is that a north-dipping subduction slab was situated to the south of the Niğde-Kırşehir Massif, and was associated with a subduction zone that consumed the Inner Tauride Ocean (Görür *et al.* 1984;

Kadıoğlu *et al.* 2006; Robertson *et al.* 2009). The heterogeneity of the source melt beneath the Niğde-Kırşehir Massif has been interpreted as a geochemical signal of a slab break-off event (Kadıoğlu *et al.* 2006; Boztuğ *et al.* 2009; Ilbeyli *et al.* 2009). In this scenario, the granite suite was associated with Andean-type magmatism. Subsequently, slab break-off resulted in asthenospheric upwelling and melting in the lithospheric mantle which produced the parental melts of the monzonite and syenite suites. Magmatism weakened the overlying Niğde-Kırşehir crust and resulted in tectonic extension.

In contrast, another model suggests that the granitoids are a result of Late Cretaceous collision between the Pontides to the north and the Taurides to the south (Boztuğ 2000). In this scenario, the granite suite is collision-related and the monzonite and syenite suites are post-collisional. The granite suite was formed from crustal melting associated with metamorphism induced by Late Cretaceous continental collision. The monzonite and syenite suites were formed by mixing processes between mantle-derived underplated mafic magmas and crustal-derived felsic melts. Mafic magmas were interpreted to be the result of decompression melting during mantle upwelling following crustal thickening. Following crustal thickening, further uplift was presumed to have caused further decompressional melting which produced the syenite suite. This model does not take into account the presence of an Inner Tauride subduction zone.

A rigorous test of these models is beyond the remit of this study, however, Late Cretaceous magmatism in the Niğde-Kırşehir Massif was a critical process. A further discussion of the tectonic implications is developed in Chapter 6.

2.7 Stratigraphy and sedimentology of the basin-fill sediments

This section describes and interprets the Upper Cretaceous-Middle Eocene sediments of the Kırıkkale Basin. The aim here is to interpret the nature of these deposits and reconstruct the sedimentary processes responsible for their deposition in space and time. This approach allows a series of palaeogeographic maps of the Kırıkkale Basin to be constructed which combine lithofacies interpretation, palaeocurrent analysis and provenance data. The basin-fill formations and their constituent lithofacies associations are described below. Lithofacies are interpreted in terms of lithology, sedimentary structures, bed thickness and bounding surfaces, fossil content and inferred depositional processes and environment.

2.7.1 The Ilıcıpınar Formation (Upper Cretaceous)

The Ilıcıpınar Formation, first named by Norman (1972), is exposed in the southwest margin of the basin and unconformably overlies the İzmir-Ankara Accretionary Complex. At its thickest, southwest of the village of Bedesten, (25684:02631 to 26099:01396) the formation is ~740 m thick (Fig 2.31), significantly thinner than the ~1250 m reported by Norman (1972). The contact between basin sediments and the basin basement dips at 77/171(dip angle/dip azimuth). At its base is a ~200 m-thick zone of exotic blocks derived from the underlying İzmir-Ankara Accretionary Complex. The upper ~540 m consists of medium- to coarse-grained grey/green volcaniclastic sediment gravity deposits interbedded with grey mudstone (Lithofacies M1).

The zone of exotic blocks is set in a matrix of massive grey mudstone. The blocks are 10 cm to 2 m in size and include grey pelagic muddy limestones containing radiolarians, sandstones, siltstones and feldspar-phyric basalts. The distribution of the exotic blocks is chaotic and patchy, making the nature of their deposition difficult to determine, but they were probably deposited by mass flow processes.

2.7.1.1 Lithofacies association M1: volcaniclastic sediments

The upper part of the Ilıcıpınar Formation is composed of lithofacies M1, which is characterised by thin (0.1 m) to medium (0.6 m) beds of medium- to coarse-grained grey/green volcaniclastic sandstone. Sandstones are rich in plagioclase, accessory minerals (opaque oxides, hornblende, biotite and clinopyroxene) and microlitic volcanic lithoclasts (see section 2.77 for provenance data). The matrix, where present, is heavily altered devitrified glassy material. Locally (e.g. 35289:15639) 9 m-thick tuffaceous flows contain shattered plagioclase and biotite crystals embedded in a groundmass of volcanic glass fragments showing well developed flow banding around large biotite crystals. Sedimentary features are mostly absent with beds being typically massive. Individual beds are laterally persistent with non-erosive bases and sharp tops grading into grey mudstone. Spheroidal weathering is well developed in the volcaniclastic sandstone. Carbonate concretions occur within the mudstone. The coarse-grained, massive deposits suggest deposition by high density turbidity currents (Lowe 1982) where high concentrations of sediments are deposited simultaneously as a poorly-sorted mixture. The massive nature of the grey mudstone suggests deposition from hemipelagic fallout.

Locally, this lithofacies features thickly-bedded (up to ~2 m) amalgamations of volcaniclastic sediments producing thickening-upwards packages up to ~20 m thick. Individual beds are occasionally separated by thin (<0.1 m) structureless grey mudstone, bases are sharp and non-erosional. Sedimentary features include sub-cm scale continuous parallel laminations (Bouma Division B), suggesting deposition in the upper flow regime (Fig.2.32a). Packages are laterally continuous for 100s of metres and are frequently lens-shaped (Fig.2.32b); slump folding is present locally.

2.7.1.2 Interpretation of the Ilıcıpınar Formation

The Ilıcıpınar Formation in the Kırıkkale Basin is probably the lateral equivalent to the volcano-sedimentary Yaylaçayı Formation, which is exposed north

of Kırıkkale along the western margin of the Çankırı Basin (Kaymakcı *et al.* 2009). The Yaylaçayı Formation comprises three lithostratigraphic associations. From bottom to top these are: 1) red marl, pelagic limestone, volcanogenic sandstone and tuff; 2) pelagic limestone and green shales intercalated with tuff and spilitic olistostromes, and; 3) turbiditic sandstone and shale alternations with tuff and agglomerate which grade up into beige argillaceous sandstone, limestone and marl (Kaymakcı *et al.* 2009). The Ilıcıpınar Formation in the Kırıkkale Basin therefore represents the lower part of the uppermost lithostratigraphic association of the Yaylaçayı Formation. Given its association with the İzmir-Ankara Accretionary Complex, and volcaniclastic petrology, the Ilıcıpınar Formation has been interpreted as deposition in a fore-arc setting (Norman 1972; Rojay & Süzen 1997a). However, the absence of terrigenous material suggests an intra-oceanic arc-type setting (Tüysüz *et al.* 1995; Kaymakcı *et al.* 2009). Comparable depositional environments include volcaniclastic turbidites of the Oligocene Izu-Bonin intraoceanic forearc basin (Hiscott *et al.* 1993).

No fossils were observed during this study, however Tüysüz *et al.* (1995) infer a Campanian to Maastrichtian deposition date on the basis of pelagic foraminifera observed to the north of the Kırıkkale basin.

To the north, the Yaylaçayı Formation was dissected by south-verging thrust faulting of an underlying ophiolitic mélange, indicating syn-sedimentary imbrication (Tüysüz *et al.* 1995). In contrast, the Ilıcıpınar Formation in the Kırıkkale Basin has not been tectonically dissected by the İzmir-Ankara Accretionary Complex. This suggests that thrust imbrication of the İzmir-Ankara Accretionary Complex in the Kırıkkale Basin was complete by the Campanian to Maastrichtian interval.

In summary, new data from this study confirms previous interpretations of Upper Cretaceous volcaniclastic sediments and correlates the deposits to thicker sediments exposed to the north of Kırıkkale.

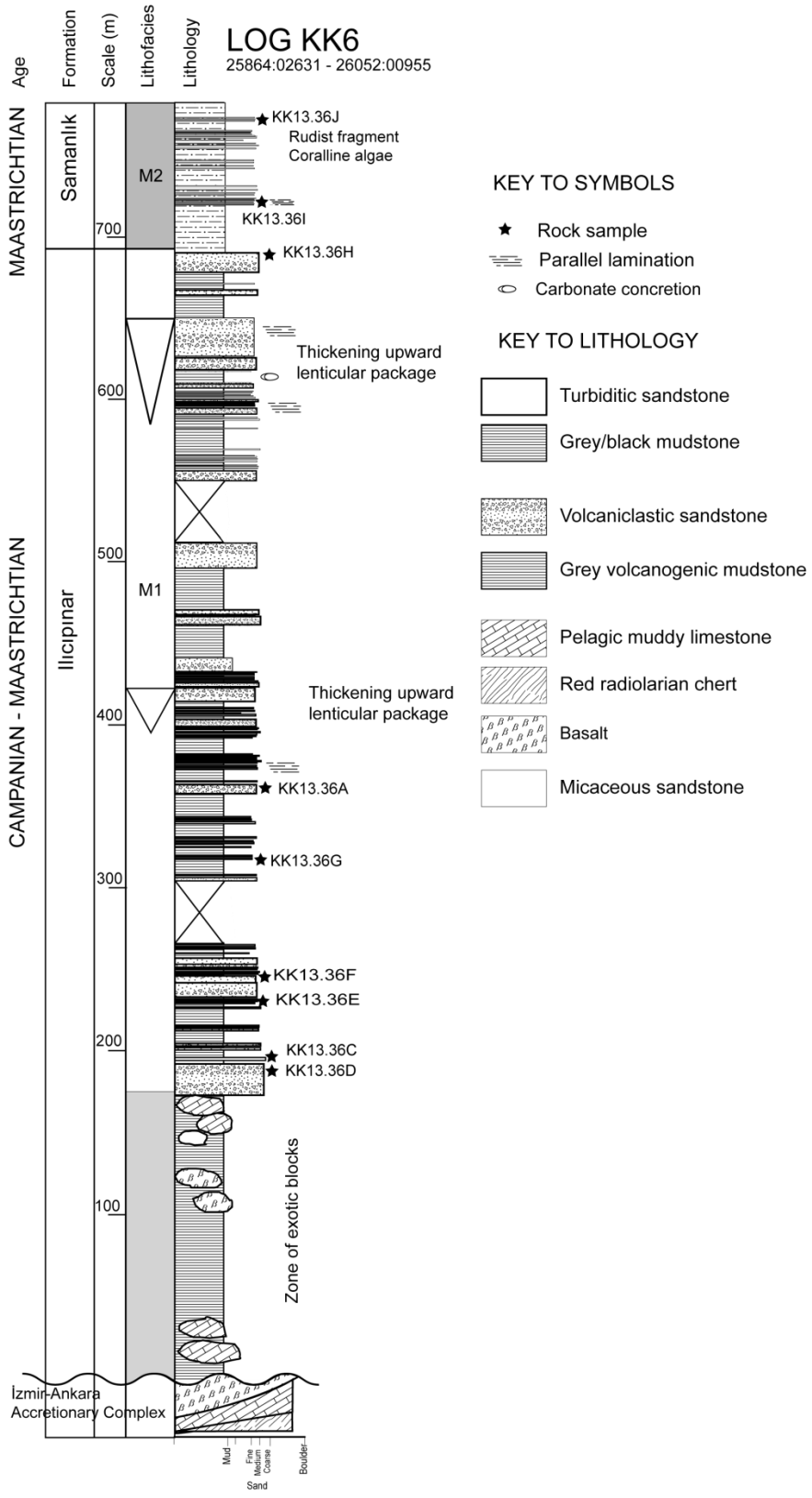

Figure 2.31 Measured stratigraphic log through the Campanian-Maastrichtian Ilıcıpınar Formation. See Figure 2.4 for location. All data are from this study.

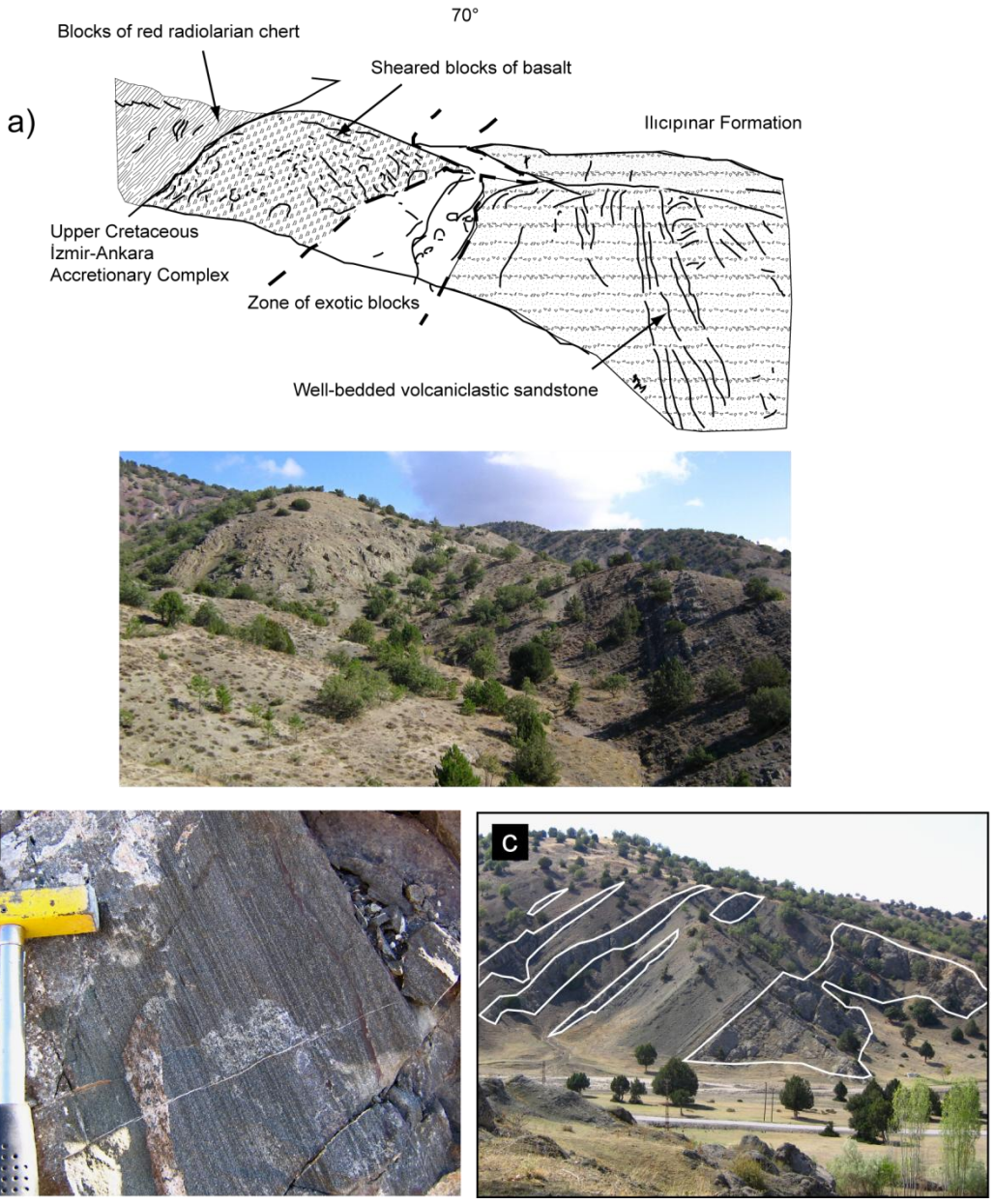

Figure 2.32 (a) Field sketch (above) and photograph (below), looking ~70° at the contact between the İzmir-Ankara Accretionary Complex and the overlying Campanian-Maastrichtian Ilıcıpınar Formation, **(b)** field photograph of well developed parallel lamination in a medium-grained volcaniclastic sandstone bed, **(c)** field photograph of the Ilıcıpınar Formation with lenticular sediment packages highlighted.

2.7.2 The Samanlık Formation (Maastrichtian)

The Samanlık Formation was originally termed the Bölükdağ Formation by Norman (1972) but its present name came into use after the work of Akyürek *et al.* (1984). It lies conformably on the Ilıcıpınar Formation and is exposed along the western basin margin (Fig.2.4). Its type section (Log KK8; 36231:15693 to 35289:15781) was originally described by Norman (1972) and lies to the NW of Kırıkkale near the eastern bank of the Kızılırmak River, and is ~500 m thick (Fig.2.33). The Samanlık Formation comprises yellow/beige graded sandstone beds and channel deposits (Figs. 2.34a and 2.34b) with abundant groove and flute marks (Lithofacies association RC1).

2.7.2.1 Lithofacies association RC1: yellow/beige sandstone

The Samanlık Formation consists of thin (0.1 m) to medium (<0.8 m) beds of graded bioclast-and volcanic lithoclast-rich sandstone deposits intercalated with grey mudstone and marl (Lithofacies M2). Beds are laterally continuous with sharp tops and bases frequently arranged in thinning upwards packages of ~1 m in size (Fig. 2.34a). This lithofacies association is notable for abundant sedimentary structures including groove and flute marks (Fig. 2.34c), parallel laminations, rip-up clasts, wave-formed ripple marks, bioturbation, horizontal burrowing (Fig. 2.34d), *Zoophycos* feeding trails (Fig. 2.34e) and convolute laminae (Fig. 2.34f). Compositionally, the sandstone is dominated by microlitic volcanic clasts, bioclasts, calcite grains and minor angular quartz.

Also present are lenticular deposits up to ~20 m thick and ~50 m wide that form topographic ridges. These deposits are often composed of conglomerates, coarse sandstone and siltstone. Internally massive conglomerates are common towards the base of the formation and are moderately sorted and matrix-supported. Clasts are ~90% igneous, typically sub-rounded feldspar-phyric andesites. Sandstone units show normal grading with erosive granulestone bases and are up to ~2.5 m

thick. Siltstones and mudstones are massive, dark grey and fissile. Sedimentary features observed are slump folding, erosive bases, sand volcanoes and local cross-stratification.

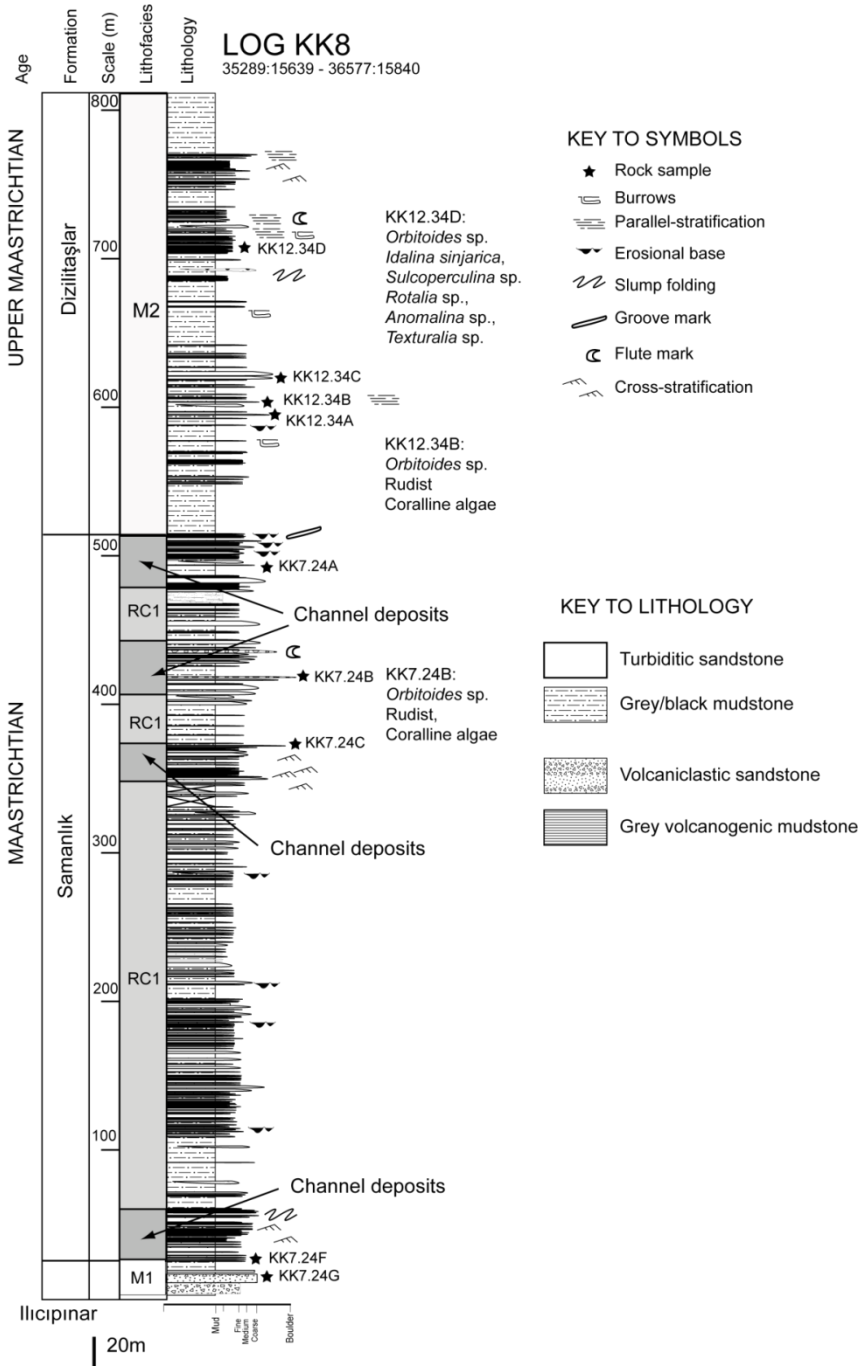

Figure 2.33 Measured stratigraphic log KK8, All sedimentary data are from this study. Palaeontological data are from N. İnan & K. Taslı (pers. comm. 2009).

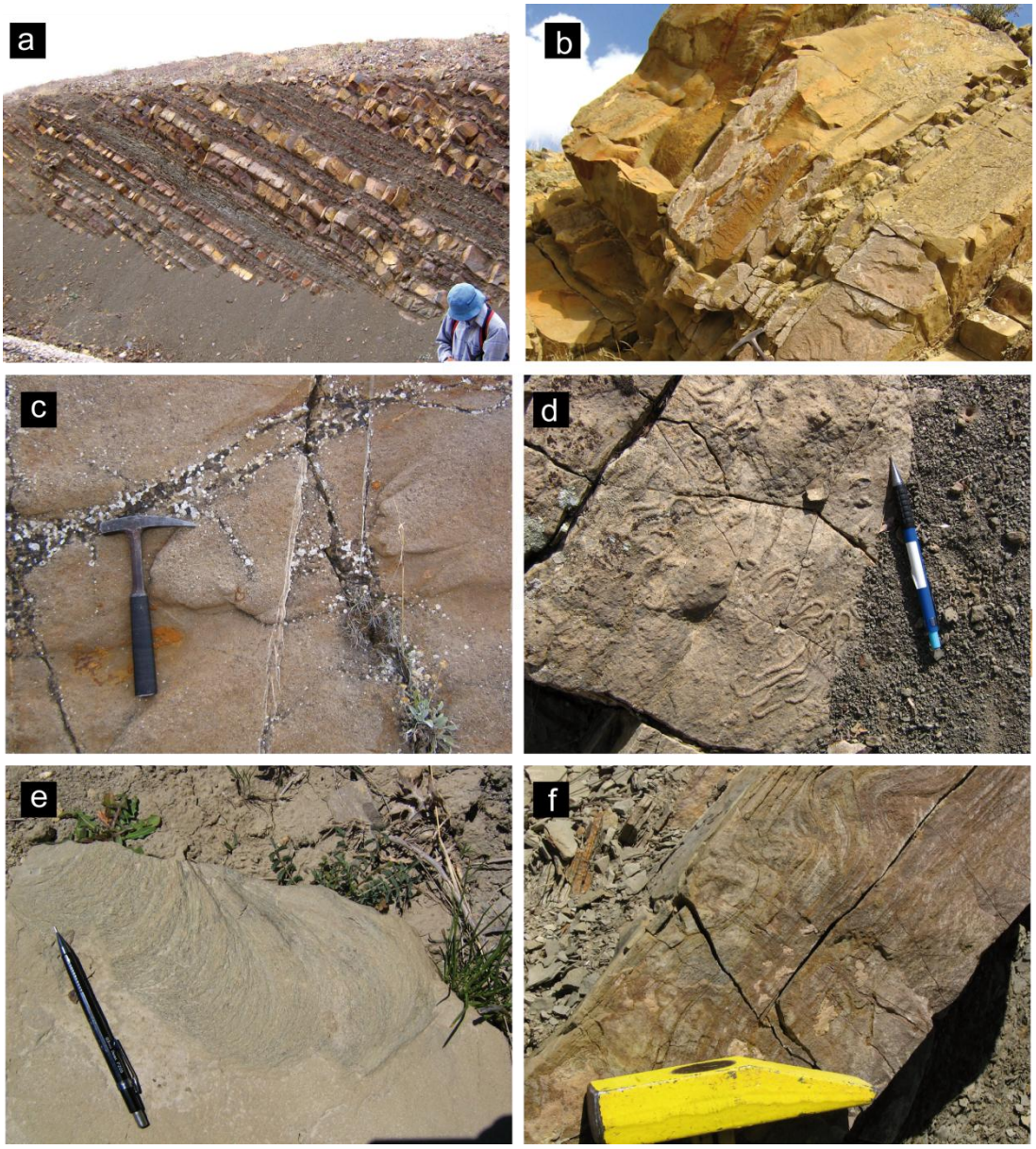

Figure 2.34 Representative field photographs of lithofacies RC1 in the Upper Cretaceous Samanlık Formation, **(a)** thinning upwards packages of yellow sandstone deposits – note that these beds are overturned, **(b)** medium-bedded yellow sandstone, **(c)** flute marks on the base of a turbidity deposit, **(d)** horizontal burrowing, **(e)** *Zoophycos* feeding pattern, **(f)** convolute laminae in turbiditic sandstone.

Based on ten flute measurements gathered during this study, the dominant palaeoflow was to the south and southwest. These results are broadly similar to that of Norman (1973a), who published a south-verging palaeoflow in the Samanlık Formation (See Appendix 3 for tabulated palaeocurrent data and methods). Fossils are typically the large benthic foraminifera *Orbitoides* sp., as well as rudist bivalve fragments, coralline algae and bryozoa (sample KK7.24B; Log KK8). The presence

of *Orbitoides* sp. infers an Upper Cretaceous deposition age (N. İnan & K. Taslı pers. comm. 2009). This date is in agreement with that of Norman (1972) who inferred a Maastrichtian date on the basis of sparse large benthic foraminifera.

2.7.2.2 Interpretation of lithofacies RC1

The abundant sedimentary structures described above on the sandstone beds suggest deposition by turbidity current in a slope-type setting. There is little evidence of classic Bouma division turbiditic structures; probably as a result of extensive bioturbation. This, in turn, infers a low sedimentation rate (Wetzel 1984; Bockelie 1991). The lenticular deposits are best interpreted as channel-fill material. Matrix supported debris flows suggest cohesive laminar flows, where deposition occurred by sediment freezing (Mulder & Alexander 2001). Sand volcanoes are associated with liquefied flows which can be associated with strongly cohesive debris flows (Marr *et al.* 2001).

Turbidity currents, channel-fill material and slump folding suggests deposition on an unstable slope. The abundance of volcanic lithoclasts in the sandstone beds suggests that the source of lithofacies RC1 is a volcanic arc. The abundant large benthic foraminifera and rudist bivalve fragments provide evidence of a shallow-water carbonate build-up associated with the arc. Carbonate detritus was subsequently redeposited in a basinal slope-type setting. Carbonate reworking in an arc environment is commonly attributed to volcanic eruptions and/or uplift within the arc and fragmentation of carbonate build-ups (Soja 1996).

2.7.3 The Dizilitaşlar Formation (mainly Palaeocene)

The Dizilitaşlar Formation was first named by Norman (1972) who also mapped the Keçili and Hacıbalı formations as part of a Palaeocene-Lower Eocene turbiditic basin-fill sequence. However, based on stratigraphic logging and lithofacies interpretation, this study interprets the Keçili and Hacıbalı formations as debris flow deposits within the Dizilitaşlar Formation. The formation lies conformably on the Maastrichtian Samanlık Formation and unconformably on basement igneous rocks. Thicknesses are variable, ranging from ~500 m in the northeast, to >700 m in the central and southwestern localities.

The Dizilitaşlar Formation consists of four lithofacies associations: 1) thin grey sandstones and black mudstone (M2); 2) thin greywacke turbidites, siliciclastic debris flows and grey mudstone (M4); 3) carbonate debris flows and blocks (RC4) and; 4) *In situ* coralgal reefs (CA4).

2.7.3.1 Lithofacies association M2: thin grey sandstone and black mudstone

Lithofacies association M2 lies at the base of the Dizilitaşlar Formation and overlies conformably the Maastrichtian Samanlık Formation. It is exposed at the western basin margin where outcrops are typically intensely folded, especially at the northwestern margin. As a result, total thickness difficult to determine, however, the total thickness is at least 200 m (Fig. 2.35). The lithofacies association is represented by thinly bedded (<0.4 m) litho- and bioclastic-rich sandstones, commonly normally graded and laterally continuous (Fig. 2.37a). Sandstone bed bases are erosive and very coarse-grained (Bouma division A). Bed tops are sharp and exhibit parallel laminations (Bouma division B) (Fig.2.37b) and local cross-stratification (Bouma division C). Bioturbation, horizontal burrowing, slump folding, flute and groove marks are other sedimentary features. Individual beds are separated by black

mudstone, usually massive with hackly conchoidal fractures. Sandstone is rich in volcanic lithoclasts and bioclasts.

Fossil assemblages are dominated by large benthic foraminifera, along with rudist bivalve fragments and coralline algae. The following fossil assemblages were identified: one sample, KK12.34D, (Log KK8; Fig.2.33) yielded the large benthic foraminifera *Orbitoides* sp., *Idalina sinjarica* Grimsdale, *Sulcoperculina* sp., *Rotalia* sp., *Anomalina* sp., *Texturalia* sp. and rudist, bryozoa and coralline algae, giving a Maastrichtian age (N. İnan & K. Taslı pers. comm. 2009) (Fig. 2.38a). Another sample (KK14.38C; Log KK9; Fig. 2.35) contained large benthic foraminifera *Orbitoides* sp., *Sirtina orbitoidiformis* Brönnimann and Wirtz, *Hellenocyclina beotica* Reichel, *Siderolites calcitrapoides* Lamarck, *Gypsina* sp., *Smoutina cruysi* Drooger, and the coral *Litharaeopsis subepithecata* (Oppenheim), giving an Upper Maastrichtian age (N. İnan & K. Taslı pers. comm. 2009).

2.7.3.2 Interpretation of lithofacies association M2

Normal grading, sharp bases and Bouma divisions A, B and C are typical of deposits from low- to medium-density turbidity currents (Lowe 1982; Mulder & Alexander 2001; Mattern 2005). The contact relationship with the underlying Samanlık Formation (lithofacies association RC1) is abrupt, which led to previous authors interpreting the contact as a thrust fault (Norman 1972; Akyürek *et al.* 1984; Akyürek *et al.* 2001; Dönmez *et al.* 2008). However, there is no structural evidence of faulting, instead the contact is depositional. Based on pelagic and benthic foraminifera, the Dizilitaşlar Formation was previously considered to be Palaeocene-Lower Eocene (Norman 1972; Norman 1973a; Norman *et al.* 1980; Akyürek *et al.* 1984; Akyürek *et al.* 2001; Dönmez *et al.* 2008). However, new palaeontological data discussed above extend the base of the Dizilitaşlar Formation to latest Maastrichtian time.

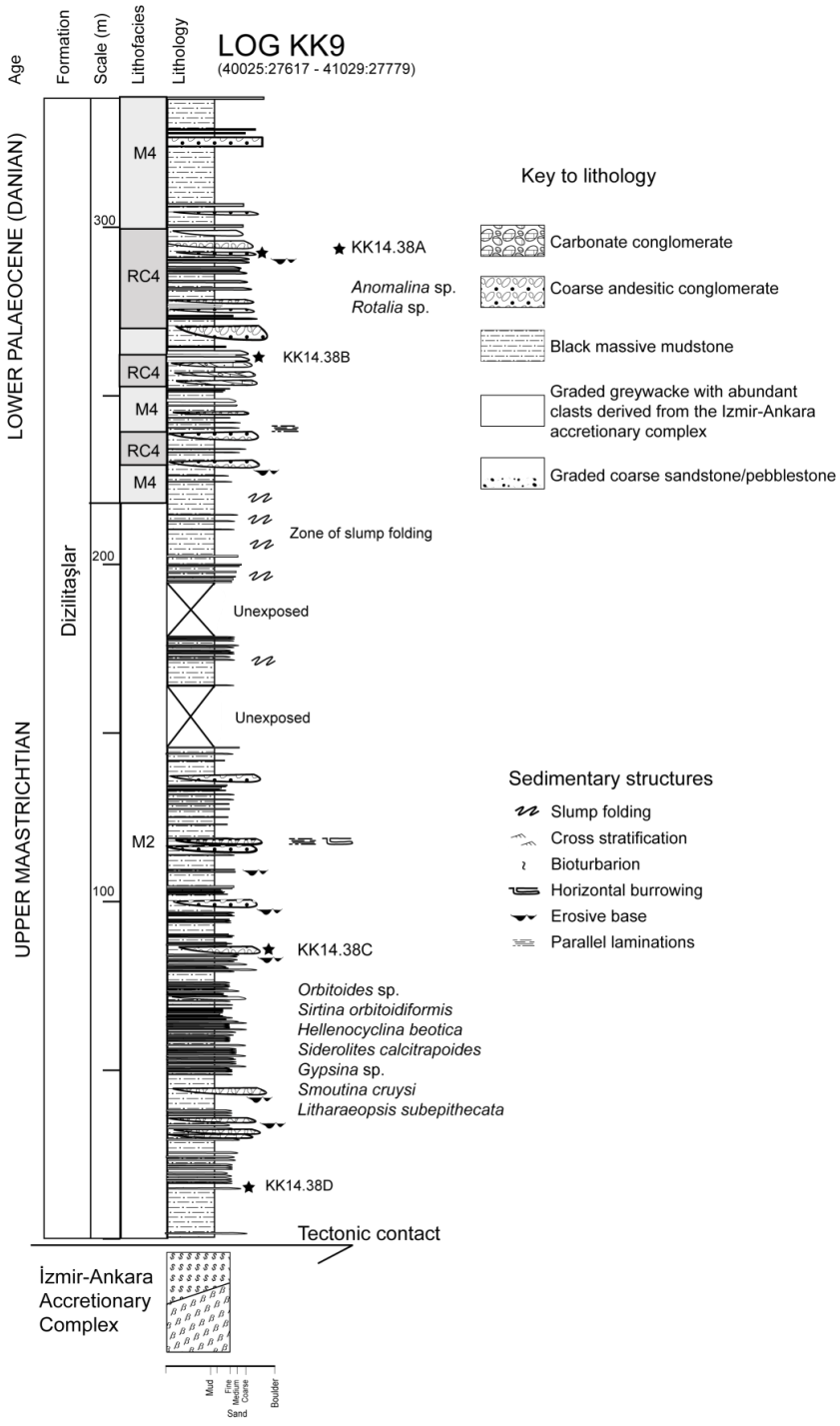

Figure 2.35 Measured log of the Upper Maastrichtian-Lower Palaeocene section of the Dizilitaşlar Formation. See Figure 2.4 for location; note that the beds are overturned. All sedimentary data are from this study. Palaeontological data are from N. İnan & K. Taslı (pers. comm. 2009).

2.7.3.3 Lithofacies association M4: thin greywacke turbidites, siliciclastic debris flows and grey mudstone

Above lithofacies association M2 comes a succession of thin, mostly greywacke, deposits intercalated with black mudstone, and siliciclastic conglomerates (lithofacies association M4). This association is particularly well exposed in the north of the basin (Fig. 2.37c). Greywacke beds are <0.4 m in thickness and are characterised by normal grading with sharp tops and bases. Parallel laminations (Bouma division B) are locally present. Mudstones are featureless and hackly with conchoidal fractures. The greywacke is composed of chloritised microlitic volcanic lithoclasts, serpentinite, microgranular quartzo-feldspathic groundmass, mudstone and quartz. These clasts may represent detritus from the İzmir-Ankara Accretionary Complex. Based on measured logs (Figs. 2.35 and 2.36) the thickness of lithofacies association M4 is at least 300 m.

The depositional age is considered to be Palaeocene to lowest Eocene (Norman 1972; Akyürek *et al.* 2001; Dönmez *et al.* 2008) based on benthic and rare pelagic foraminifera.

Siliciclastic conglomerates are best exposed to the southwest of Keçili village (44584:26032) and were considered by Norman (1972) to be a distinct formation, i.e. the Keçili Formation. They consist of medium-bedded (~0.5 m) laterally discontinuous coarse sandstones and micro-conglomerates. Bed bases are frequently erosive with gradational sandy tops showing parallel lamination. The units are commonly amalgamated into packages up to ~3 m thick. Micro-conglomerates are well-sorted, matrix- and clast-supported, and are composed of well-rounded andesite, basalt, serpentinite and red radiolarian chert pebbles (Fig. 2.37d), locally exhibiting a preferred orientation. Imbricated pebbles indicate a palaeoflow from the northeast.

Other clastic debris flows are dominated by limestone, silicic volcanic, granitoid and basalt clasts. This composition infers a source from the Niğde-Kırşehir Massif to the southeast.

2.7.3.4 Interpretation of lithofacies association M4

Normal grading and parallel laminations suggest that the greywacke beds represent deposits from low-density turbiditic flows (e.g. Postma 1986). The clastic conglomerates are interpreted as channel-fill debris flows which scoured into the soft sediments of the mudstone/greywacke succession in a slope-type setting.

A notable feature, inferred by clast composition, is that these deposits represent a shift from older volcaniclastic- and bioclastic-rich sediments to those dominated by detritus derived from the İzmir-Ankara Accretionary Complex and the Niğde-Kırşehir Massif. This event possibly coincides with uplift, and subaerial exposure, of the İzmir-Ankara Accretionary Complex and the Niğde-Kırşehir Massif adjacent to the Kırıkkale Basin.

2.7.3.5 Lithofacies association RC4: carbonate debris flows and blocks

Carbonate debris flows and detached blocks scour into lithofacies association M4 and are exposed in a north-northwest – south-southeast trending zone in the western part of the Kırıkkale Basin. These deposits represent lithofacies association RC4, which is ~50 m thick and is dominantly Lower Palaeocene (Danian) and Upper Palaeocene (Thanetian) in age.

A striking example of a carbonate debris flow is exposed northwest of Camluca village in the southwest of the basin (31189:02371). This outcrop features laterally discontinuous debris flows scouring into lithofacies association M4 and deforming underlying soft sediments. The thickly-bedded (up to 5 m) debris flows are mostly chaotic, very poorly sorted and contain a range of clast sizes, from pebble to boulder. Clasts display a range of angularities and are mostly composed of andesite and limestone with minor felsic volcanics and sandstone. Mudstone rip-up clasts are common at the base of each conglomerate bed.The matrix, where present,

is typically composed of rounded carbonate clasts up to 3cm; however mudstone matrices are also present. The individual conglomerate horizons are amalgamated into multi-flow features ~20 m thick. Other examples are located in the northwest of the basin (Fig. 2.37e). Debris flows are commonly associated with deposits of detached limestone blocks.

Limestone blocks are mostly exposed in the north of the basin, southwest of Keçili (see Fig. 2.4) (see Log KK11 and Log KK12; Fig. 2.36). This association features 'blocks' of limestone reaching sizes of tens of metres, lying in a fissile mudstone matrix (lithofacies association M4) (Fig. 2.37f). Previous work has described these structures as olistoliths (e.g. Norman *et al*. 1980), but close inspection reveals a variety of depositional settings and lithologies including: 1) debris flows composed of poorly-sorted sub-angular clasts (<5 cm) of limestone and feldspar-phyric andesite; 2) lithified blocks of neritic packstone (<5 m); 3) sequences of bedded (<0.15 m) packstone and grainstone intercalated with thin (<0.1 m) horizons of muddy limestone. Individual blocks grade into a sandy facies towards their margins where they are extensively faulted, however internal deformation is negligible.

The limestones are classified as packstones and grainstone. They are grain-supported with a muddy matrix (where present) and calcite spar cement. Bioclasts are mostly large benthic foraminifera, skeletal calcareous algae and coral fragments reaching up to 4mm in size. Subordinate siliciclastic clasts are fresh angular monocrystalline quartz, plagioclase and muscovite. The presence of miliolid benthic foraminifera (e.g. *Idalina sinjaric*, see below) indicates that the depositional environment was a low-energy shallow carbonate platform/lagoon-type facies (Sartorio & Venturini 1988; Taheri *et al.* 2008).

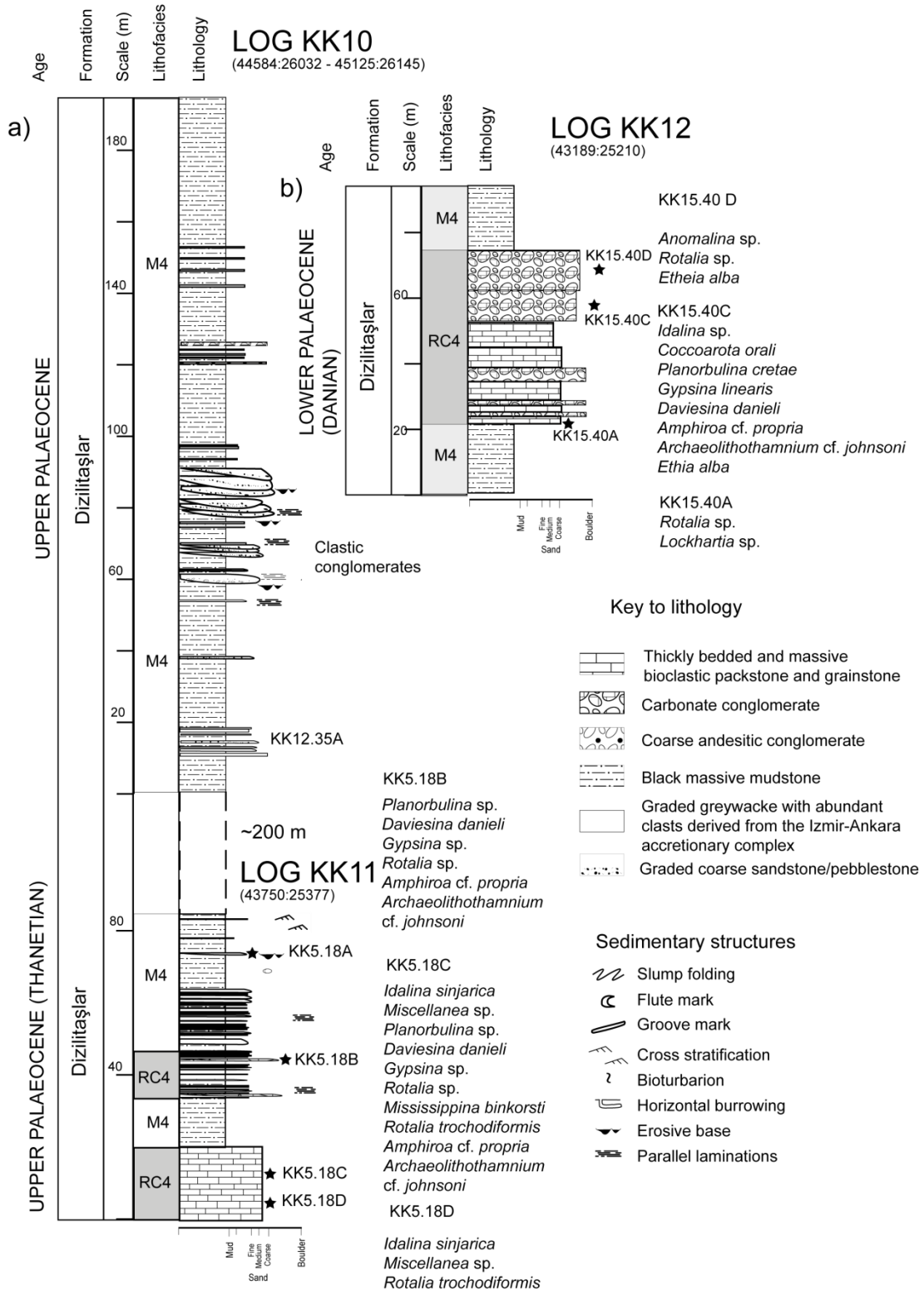

Figure 2.36 Measured logs of the mainly Palaeocene Dizilitaşlar Formation, **(a)** composite log comprising Logs KK11 and KK10 through the Upper Palaeocene part, **(b)** Log KK12 through a limestone "block" of lithofacies association RC4. All sedimentary data are from this study, palaeontological data are from N. İnan & K. Taslı (pers. comm. 2009).

Norman (1972), Norman *et al.* (1980) and Dönmez *et al.* (2008) reported the rudist bivalves, *Hippuritella cornucopiae* (Defrance) and *Pironaea polystyla siavonica* (Hilber), the coral *Phyllocoenia corollaries* (Reuss) and the large benthic foraminifera *Siderolites* cf. *calcitropoides* (Lamarck) and *Orbitoides media* (d'Arch.) which indicates a Maastrichtian age. During this study, rudist bivalves were observed (40974:28315) which may confirm a Maastrichtian age. Log KK12 (43189:25210) documents a limestone 'block' that contains the following benthic foraminifera: *Anomalina* sp., *Rotalia* sp., *Idalina* sp., *Coccoarota orali* İnan, *Planorbulina create* (Marsson), *Gypsina linearis* (Hanzawa), *Daviesina danieli* Smout, *Lockhartia* sp. and the calcareous algae *Etheia alba* Pfender and *Amphiroa* cf. *propria*, *Archaeolithothamnium* cf. *Johnsoni* (samples KK15.40D, KK15.40C and KK15.40A; Fig. 2.38c). This assemblage infers an Early Palaeocene (Danian) age (N. İnan & K. Taslı pers. comm. 2009).

Log KK11 (43750:25377) features a ~20 m-thick block of well-lithified limestone, above which comes black mudstone intercalated with siliciclastic and carbonate turbidites. The benthic foraminifera *Planorbulina* sp., *Daviesina danieli* Smout, *Gypsina* sp., *Rotalia* sp., *Idalina sinjarica*, Grimsdale, *Miscellanea* sp., *Mississippina binkorsti* Reuss, *Rotalia trochodiformis* Lamarck, and the coralline algae *Amphiroa* cf. *propria* and *Archaeolithothamnium* cf. *Johnsoni* (samples KK5.18C and KK5.18D) indicate a Late Palaeocene (Thanetian) age (N. İnan & K. Taslı pers. comm. 2009).

2.7.3.6 Interpretation of lithofacies association RC4

Microfossil assemblages in lithofacies association RC4 indicate that primary carbonate deposition occurred in a shallow marine, platform-type environment from Late Cretaceous to Late Palaeocene time. Limestone blocks and debris flows represent the transfer of carbonate debris into a siliciclastic basin margin slope/upper slope setting (lithofacies association M4) by episodic mass wasting events (e.g. sliding and slumping), which can transport material for up to tens of kilometres

basinward (Spence & Tucker 1997). The mechanism of limestone block deposition is commonly thought to be the catastrophic failure of a steep slope (Cook *et al.* 1972) or seismic failure, which can occur on steep and shallow slopes. Many limestone block and debris flow deposits are interpreted to have formed during relative sea-level lowstands (Spence & Tucker 1997).

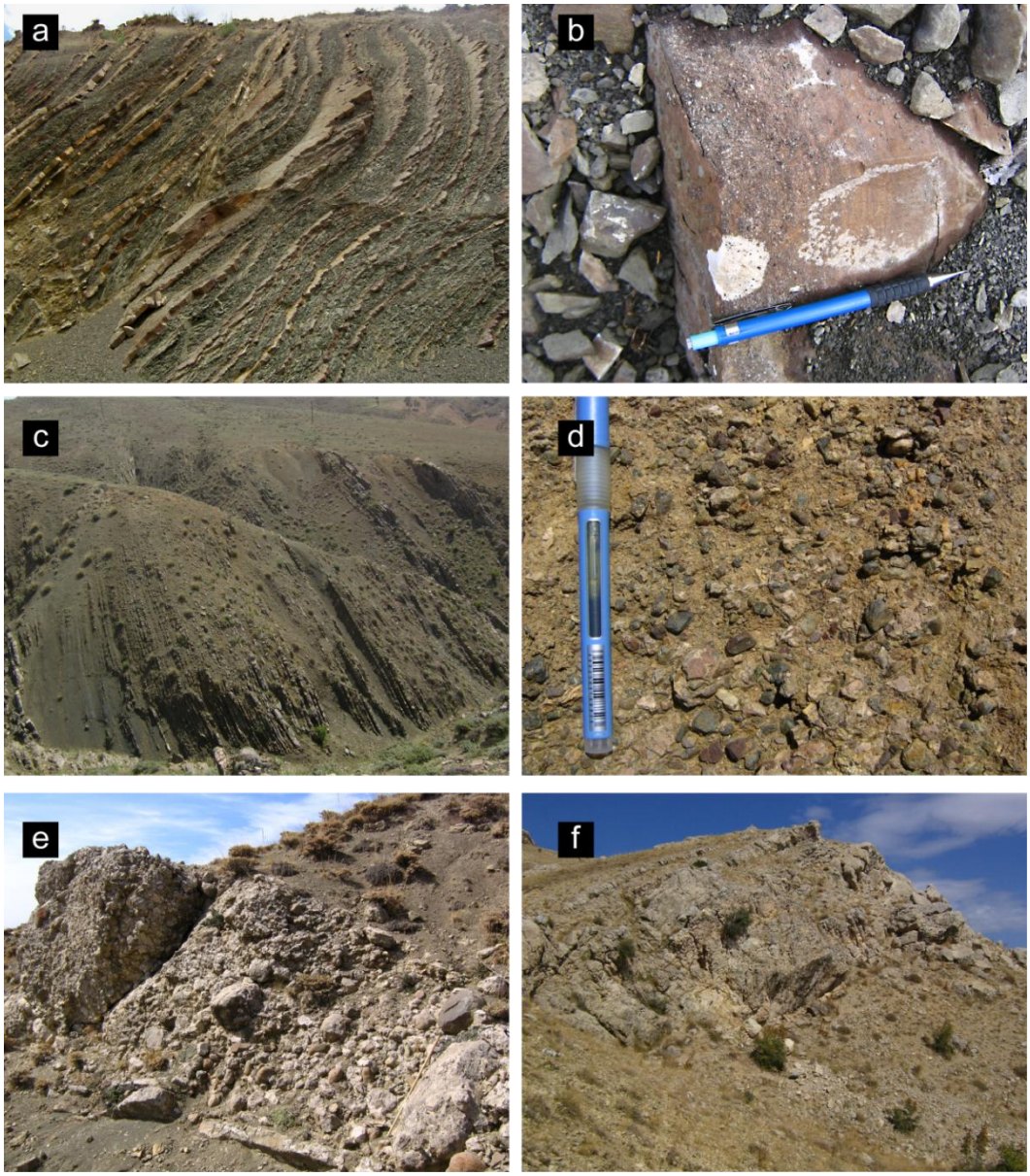

Figure 2.37 Representative field photographs of the mainly Palaeocene Dizilitaşlar Formation, **(a)** turbidites of lithofacies association M2 (the outcrop is ~5 m high), **(b)** detail of a graded turbiditic deposit (M2) exhibiting coarse base (left) and parallel lamination **(c)** stacked turbidites in the north of the basin (M4), **(d)** clastic debris flow containing basic volcanic clasts, serpentinite and red radiolarian chert (M4), **(e)** carbonate debris flows, note the metre-stick to the right, **(f)** detached limestone "block" (see Log KK12).

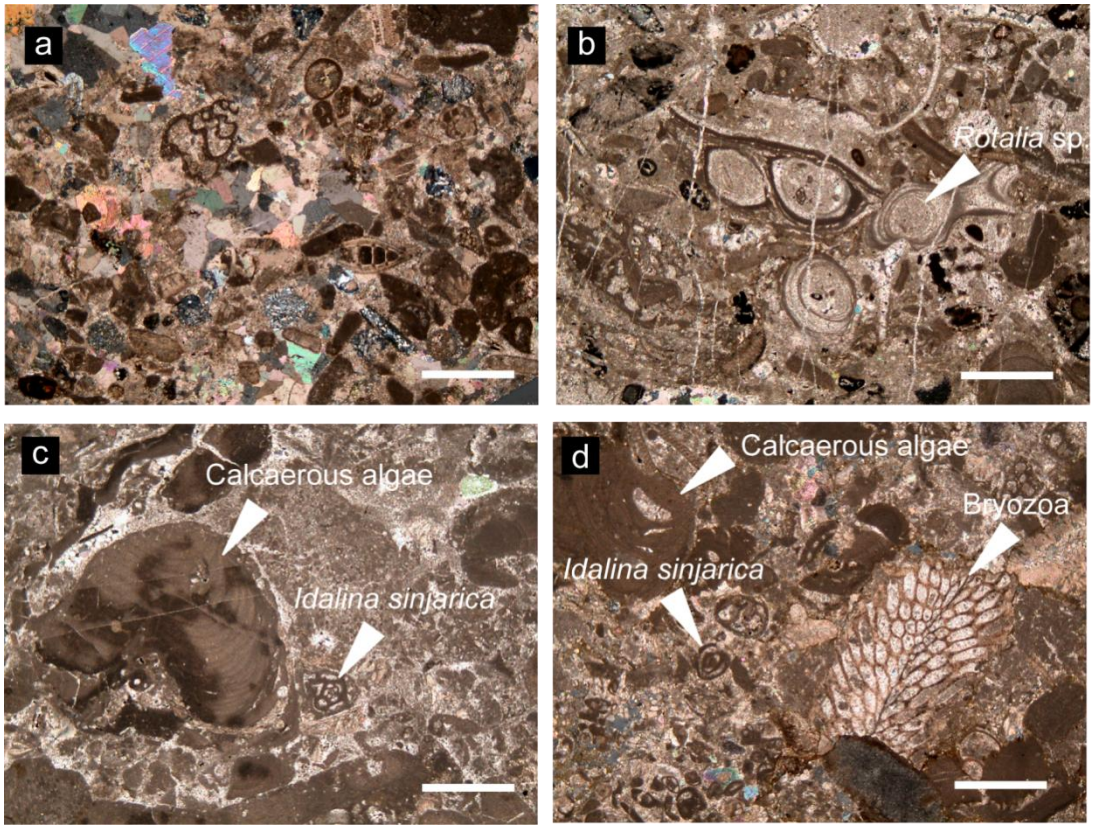

Figure 2.38 Photomicrographs of samples from the Dizilitaşlar Formation, (a) Upper Maastrichtian bioclast- and volcanic lithoclast-rich sandstone (sample KK12.34D), (b) *Rotalia* sp. benthic foraminifera from Palaeocene (Danian?) packstone (sample KK14.38A) (c) Lower Palaeocene (Danian) packstone from a debris flow containing abundant calcareous algae and *Idalina sinjarica* Grimsdale benthic foraminifera, (sample KK15.40C), (d) Upper Palaeocene (Thanetian) debris flow packstone containing *Idalina sinjarica* Grimsdale, skeletal algae and bryozoan (sample KK5.18E). All scale bars = 1mm, images are in plane polarised light. Palaeontological data are from N. İnan & K. Taslı (pers. comm. 2009).

2.7.3.7 Lithofacies association CA1: In situ reefs

The Dizilitaşlar Formation also contains *in situ* coral-rich carbonates (lithofacies association CA1). This lithofacies association is best exposed in a small abandoned quarry, south of the Kızılırmak River, at 36341:09376 (Fig. 2.39a). The total thickness is ~10 m and is composed of reef boundstone (Fig. 2.39b) in life position. The limestone has undergone secondary alteration and is stained red with hematite alteration infilling joints. Fossils are the benthic foraminifera *Idalina* sp., and the corals *Actinacis cognata* Oppenheim, *Goniopora elegans* (Leymerie) and

Litharaeopsis subepithecata (Oppenheim), indicating a Palaeocene (possibly Danian) age (N. İnan & K. Taslı pers. comm. 2009) (Fig. 2.39d).

Another locality Log KK19 (Fig. 2.40) features *in situ* algal patch reefs, probably of Palaeocene age. A ~200 m succession of basal conglomerates lies unconformably on an erosion surface of the igneous basin basement. The dominant feature of this section is conglomerates composed of rounded andesite clasts from pebble-, to boulder-size, which are arranged in packages varying in thickness from 1 to 25 m thick. Bases are erosional and tops grade into coarse sandstone; otherwise individual packages lack internal structure. Clasts are supported in a coarse sandstone matrix, are poorly to moderately sorted and randomly orientated. Other lithologies present in this association are coarse grey sandstones containing "floating" volcanic pebbles and occasional 3 mm-sized flecks of plant remains.

The upper 50 m of Log KK19 features lens-shaped in situ patch reef boundstone. The reefs are 8 to 10 m thick and ~80 m in lateral extent. They contain abundant corals, *Cympolia elongata* (Defrance) calcareous algae and the benthic foraminifera *Idalina sinjarica* Grimsdale (N. İnan & K. Taslı pers. comm. 2009) (Fig. 2.39c). Sealing the patch reefs are boulder-sized conglomerates featuring randomly orientated clasts of algal debris, sandstone and andesite. In turn this debris is sealed by coarse, flaggy-bedded bioclastic, algal rich sandstone. Above are 0.5 to 2 m beds coarse-grained bioclastic sandstones and ~1 m beds of pebbly conglomerates composed of bioclastic sandstone pebbles in a dark grey muddy limestone matrix.

2.7.3.8 Interpretation of lithofacies association CA1

This study is the first to describe and interpret patch reefs in the Dizilitaşlar Formation. The age of the patch reefs at this locality is rather poorly constrained by fossil evidence and is either Palaeocene or Eocene (N. İnan & K. Taslı pers. comm. 2009). However, coralgal reefs containing *Idalina* foraminifera are typical of the Palaeocene (e.g. Scheibner & Speijer 2008). In contrast, reefs from the Eocene are commonly characterised by large benthic foraminifera including *Nummulites,*

Assilina and *Alveolina* (Scheibner & Speijer 2008). Therefore a tentative interpretation is that the reefs are Palaeocene.

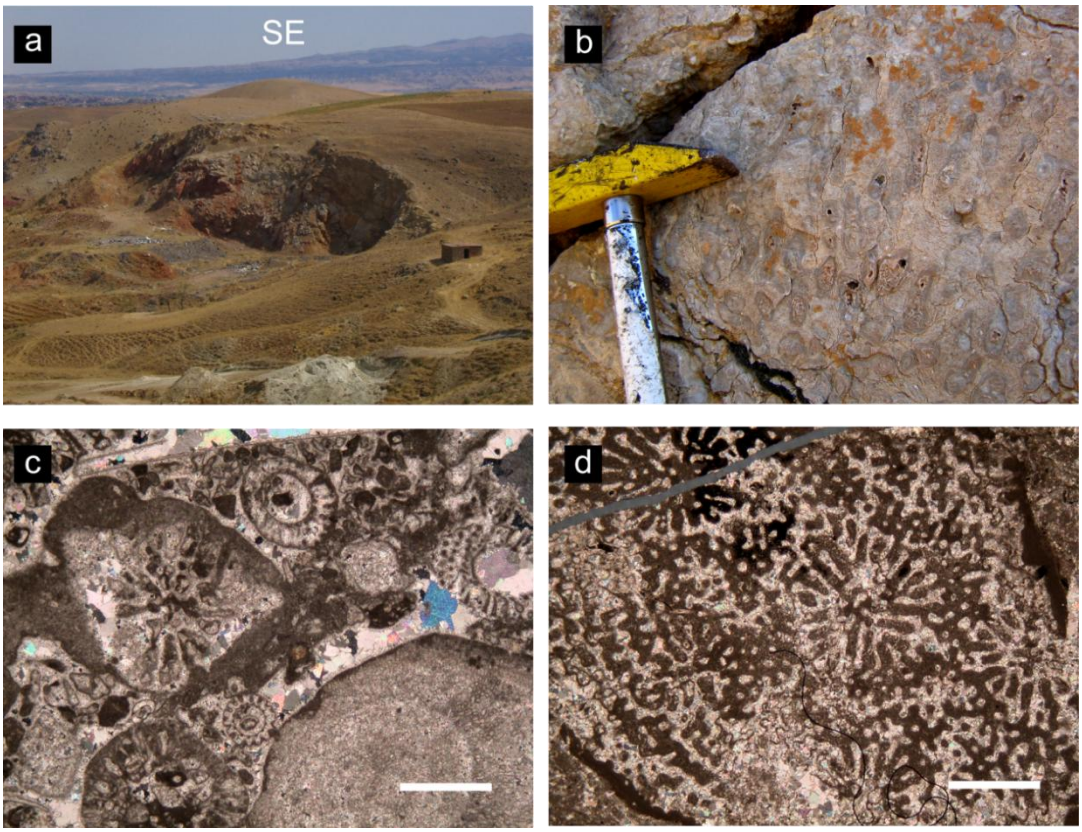

Figure 2.39 (a) Field photograph (looking ~southeast) of small quarry composed of lithofacies association CA1, **(b)** photograph of coral boundstone, **(c)** photomicrograph of *Cympolia elongata* (Defrance) algae in reef limestone (sample KK22.58I; see Log KK19; Fig. 2.40), **(d)** in situ coral from Palaeocene reef limestone (sample KK 2.8A). Scale bars on thin section images = 1 mm, images photographed in plane polarised light. Palaeontological data are from N. İnan & K. Taslı (pers. comm. 2009).

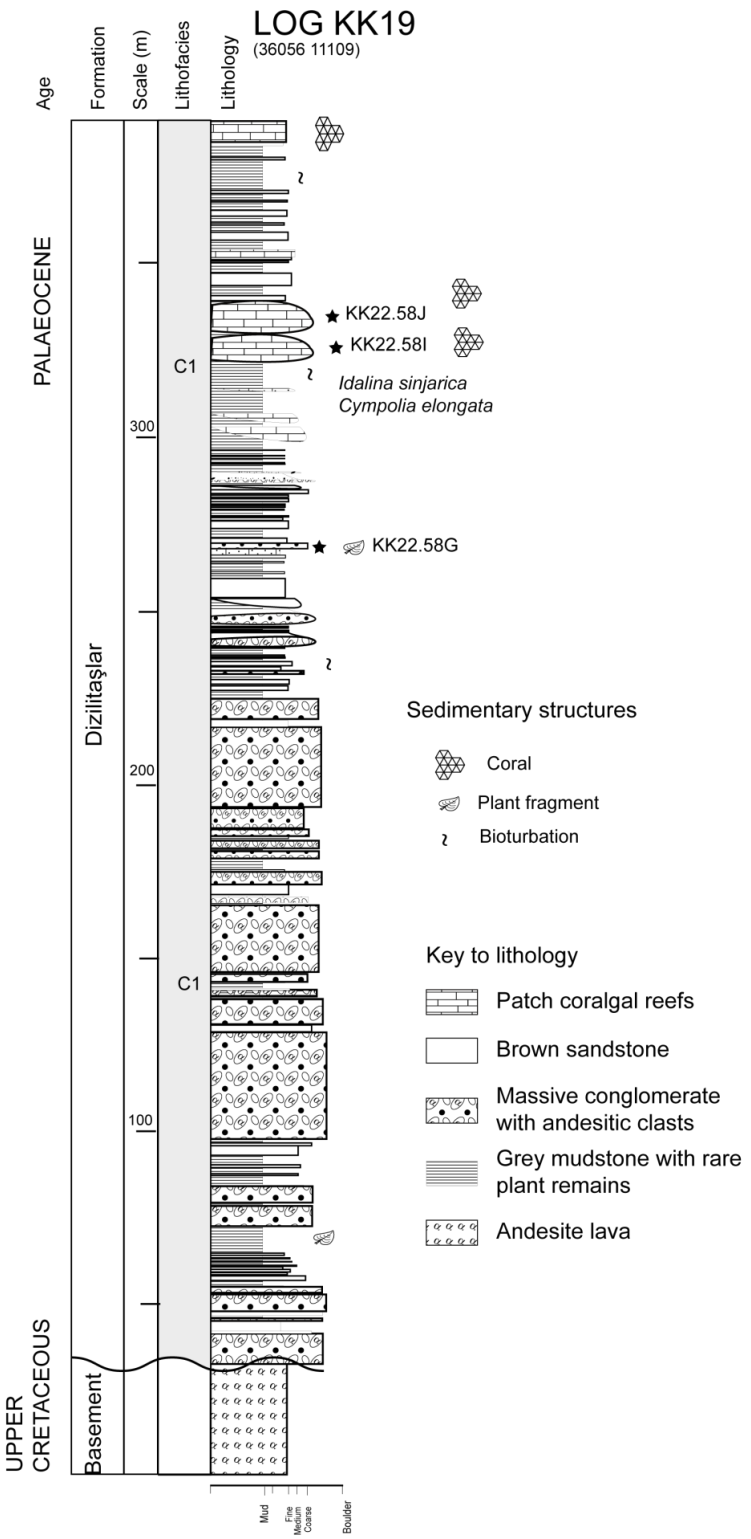

Figure 2.40 Measured stratigraphic log KK19 showing lithofacies association C1. All sedimentary data are from this study, palaeontological data are from N. İnan & K. Taslı (pers. comm. 2009).

2.7.4 The Karagüney Formation: red conglomerates and coarse sandstones (Lower Eocene).

The Karagüney Formation was first named by Norman (1972) and was described as a ~300 m-thick succession of red and green conglomerates. Some authors (e.g. Kaymakcı 2000; Kaymakcı *et al.* 2009) retain the name Karagüney. However the formation has also variously been called the Kabaktepe Member (Akyürek et al. 1984) and the Baraklı Formation (Dönmez et al. 2008). It was studied during this project to the southeast of Mahmutlar (Fig. 2.4). The conglomerates, red sandstones and siltstones are often loosely consolidated and poorly exposed. The Karagüney Formation typically lies trangressively on the Kırıkkale Massif (Figs. 2.41and 2.42a), however, local outcrops indicate a strike-slip faulted contact (42113:14814). It is overlain by the Middle Eocene Çayraz Formation (Fig.2.42b) and is >200 m thick.

The Karagüney Formation consists of lithofacies association M7 which is dominated by deposits of conglomerate sheets. At one locality (44943:21470) conglomerates consist of poorly-sorted, rounded to sub-angular, pebble- to cobble-size clasts of andesite, rhyolite, basalt and granite in a coarse matrix of red sandstone. Beds are up to 3 m thick, lack stratification, and exhibit erosive bases and tops that grade into coarse sandstone. Grading, where present, is normal and occasionally inverse.

2.7.4.1 Interpretation of lithofacies association M7

No fossils were recovered during this study; however Dönmez *et al*. (2008) documented the gastropods *Melanatria* cf. *dufresnei* (Deshayes), *Melanatria* cf. *Cuvieri* (Deshayes), *Velates schmideli* (Chemnitz), and the oyster *Ostrea* sp.. This faunal assemblage implies a shallow marine shelf-type depositional setting of Early Eocene age. Limited outcrop makes the Karagüney Formation a challenge to interpret. The poor sorting, matrix support and lack of stratification suggest

deposition was by cohesive mass flow (Johnson 1984; Nemec & Steel 1984) graded sandy tops indicate dilution of the top of the coarse cohesive mass flow (Nemec & Steel 1984). Rounded clasts of basalt, granite, rhyolite and andesite suggest a sediment supply from the Kırıkkale Massif.

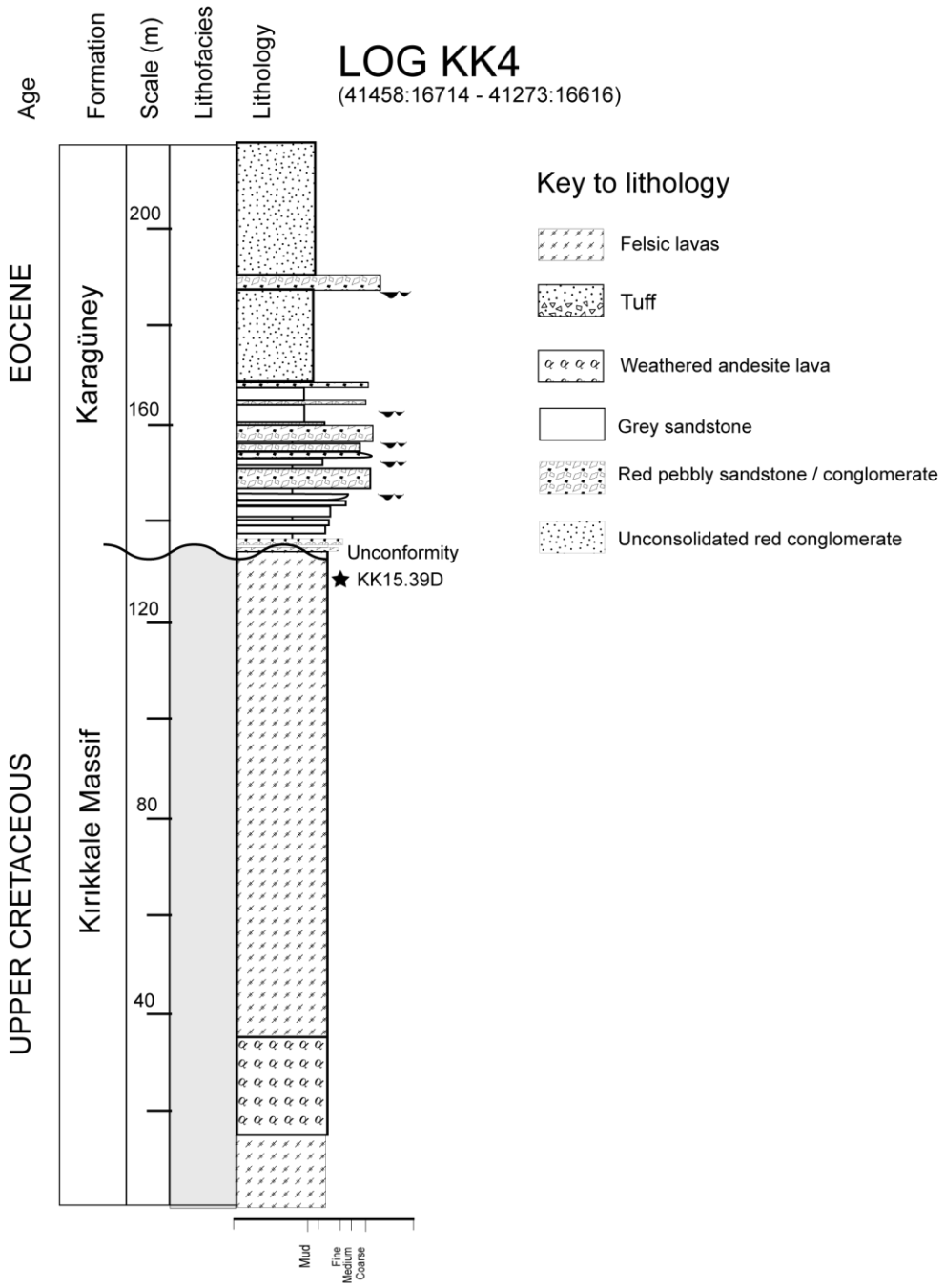

Figure 2.41 Measured stratigraphic log showing the unconformable relationship between the Lower Eocene Karagüney Formation and the magmatic rocks of the Upper Cretaceous Kırıkkale Massif.

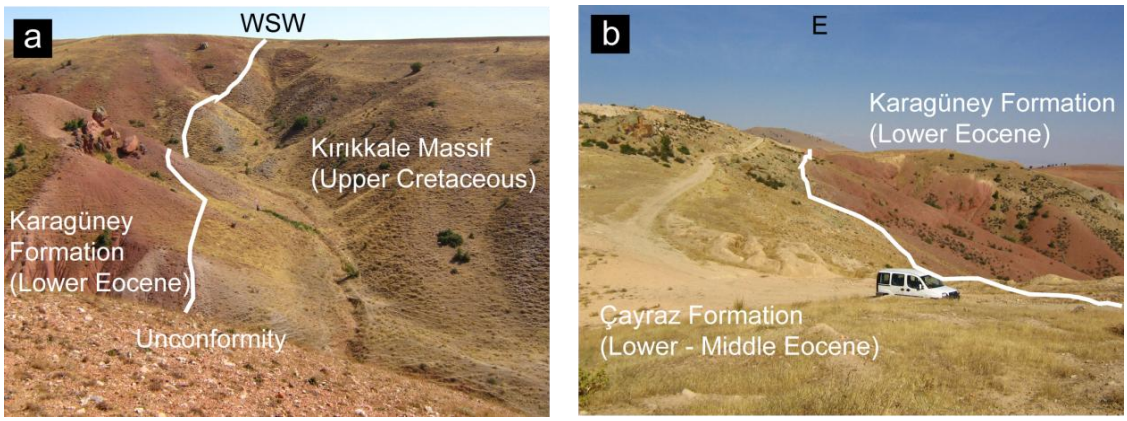

Figure 2.42 Field photographs of the Lower Eocene Karagüney Formation, (a) view, looking ~WSW of the Karagüney Formation overlying the Upper Cretaceous Kırıkkale Massif, (b) view, looking ~E, of the Lower-Middle Eocene Çayraz Formation overlying the Karagüney Formation.

2.7.5 The Çayraz Formation: Lower Eocene carbonates, sandstones and conglomerates.

The Çayraz Formation is composed of Lower Eocene (Ypresian) carbonates, sandstones and conglomerates. In the south of the basin, it lies unconformably on igneous basement rocks, and represent a marine transgression. In the northeast of the basin, to the east of Mahmutlar, the formation lies on the Lower Eocene Karagüney Formation and interfingers with the Upper Maastrichtian-Lower Eocene Dizilitaşlar Formation. In total, the formation is ~400 m in thickness. The formation was termed the Bahşili Formation by Norman (1972), the Taşlidere Member by Akyürek *et al.* (1984) and the Çayraz Formation in recent MTA reports and maps (Akyürek *et al.* 2001; Dönmez *et al.* 2008).

The Çayraz Formation can be subdivided into three lithofacies association: 1) yellow sandstone and mudstone (lithofacies association M11); 2) red/orange conglomerates and coarse sandstone (lithofacies association M8) which intercalates with; 3) sandy limestone containing large benthic foraminifera (lithofacies association CA7).

2.7.5.1 Lithofacies association M11: yellow sandstone and mudstone

Lithofacies association M11 is well exposed to the northeast of Mahmutlar (Fig. 2.4). It lies on the Karagüney Formation and lithofacies association M4 of the Dizilitaşlar Formation (see Log KK16 and Log KK17; Fig. 2.43a and 2.43b). Locally, it interfingers with the Dizilitaşlar Formation. The lower part is represented by a ~100 m-thick sequence of ~1 m-thick low-angle tabular-bedded quartz-rich yellow sandstone (Fig. 2.44a) exhibiting subtle normal grading, separated by ~1cm mudstone beds. These individual units are amalgamated to form units from ~2 to ~40 m thick, and often contain "floating" pebbles and stringers, 1 to 2 cm thick. The sandstone is medium- to coarse-grained and well sorted; bases are weakly erosive and tops are sharp to gradational. The interbedded mudstone contains iron-oxide concretions. Sedimentary structures include symmetrical ripple marks (Fig. 2.44b) and horizontal burrowing. The upper part of lithofacies association M11 exhibits medium-bedded (0.2 to 0.9 m in thickness) fine-grained sandstone beds alternating with up to 2 m of mudstone. Sandstone units are mostly ungraded with sharp tops and bases which combine to form thickening-upwards sequences < 4 m thick.

2.7.5.2 Interpretation of lithofacies association M11

Tabular cross-bedding typically occurs in fluvial, aeolian and shallow marine deposits (Collinson & Thompson 1989). The presence of burrowing and ripple marks suggests the depositional environment in this area was marine. Sedimentary structures tabular cross-bedding, ripple marks and burrowing are consistent with those from a marine delta front environment (Rasmussen 2000).

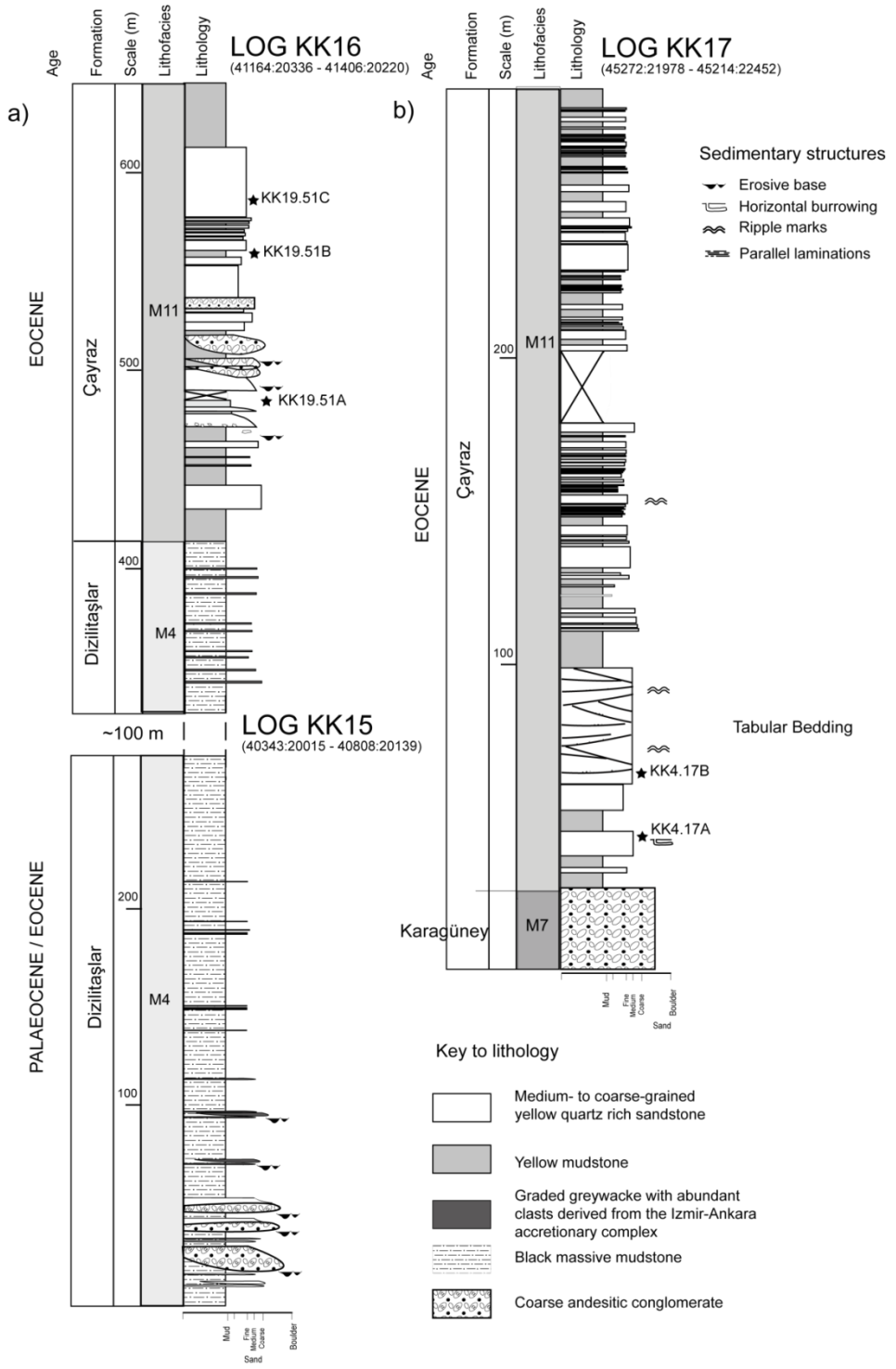

Figure 2.43 (a) measured composite log comprising logs KK15 and KK16 through the Dizilitaşlar Formation and lithofacies association M11 of the Çayraz Formation, **(b)** measured log through lithofacies association M11 **of** the Çayraz Formation. All data are from this study.

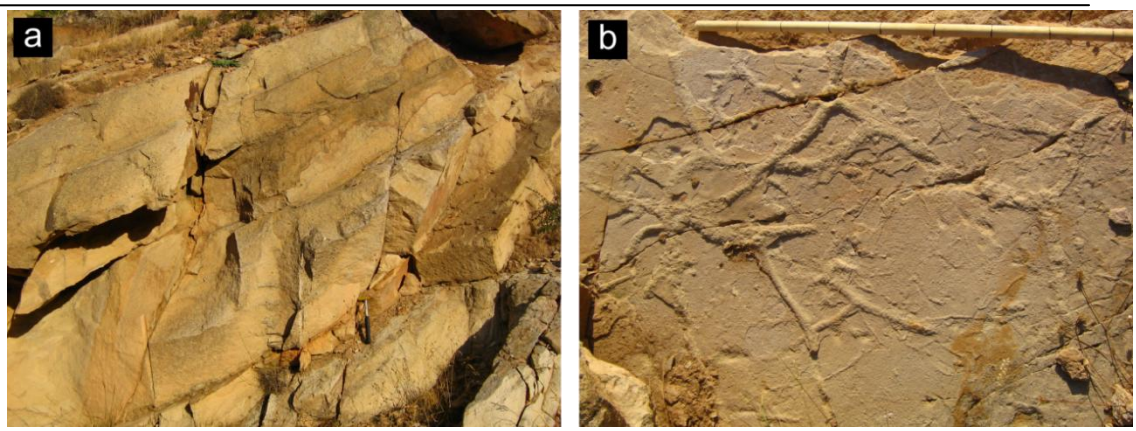

Figure 2.44 (a) Tabular bedding in lithofacies association M11, (b) horizontal burrowing (the staff at the top of the picture is ~90 cm long).

2.7.5.3 Lithofacies association M8: red/orange conglomerates and coarse sandstone

Lithofacies association M8 is exposed to the northeast of Yahşıhan (Log KK22 and Log KK23; Fig. 2.47) and to the southwest of Bahşili (Log KK2; Fig. 2.45). It consists of red/orange conglomerates, medium- to coarse-grained red/yellow sandstones and pebbly sandstones, all of which were deposited unconformably on igneous basement rocks.

Conglomerates are matrix supported and contain rhyolitic and andesitic clasts up to boulder size. The clasts display a range of angularities, are poorly sorted and are arranged in sheets < 8 m thick. Bases are irregular to sharp and tops grade into medium- to coarse-grained sandstone. Rare conglomerate lenses are present, representing channel-fills, which range in thickness from 3 to 10 m and are frequently inversely graded.

Sandstones are medium-, to coarse-grained and often contain <2 cm-sized rounded andesite and rhyolite pebbles and stringers of ~20 cm-sized rounded volcanic clasts. Sandstones are typically intercalated with grey massive mudstone exhibiting varying degrees of bioturbation. The sandstones are typically thickly (<12 m) bedded and massive with sharp tops and scoured bases. Pebbly sandstone beds show strong grading and fine upwards to medium sandstone with scattered pebbles. Sandstone lenses are thin (0.2 m) and exhibit cross lamination. Pebblestones are

poorly sorted, massive, typically unconsolidated and thickly (<8 m) bedded. Clasts are 2 - 3 cm in size, medium- to well-rounded and mainly compose of silicic volcanics. Sandstone composition is dominated by microgranular quartz litholcasts and volcanic quartz grains. The clay matrix features Fe-oxide alteration, which gives the sandstones their characteristic reddish colour.

2.7.5.4 Lithofacies association CA7: sandy limestone containing large benthic foraminifera.

Lithofacies association CA7 intercalates with the red/orange sandstones and conglomerates of lithofacies association M8 (Log KK21 and Log KK22). The lithofacies association is characterised by well bedded bioclastic limestone and mudstone with varying amounts of siliciclastic material. The bioclasts are typically large benthic foraminifera, including *Nummulites*, with minor amounts of bivalve shell fragments. Beds are typically graded from a coarse, sandy base to a muddy top which suggests sediment reworking.

The following benthic foraminifera were present in a sample of sandy packstone (sample KK8.26A; Log KK21) *Ranikothalia nuttali* (Davies), *Nummulites globulus* Leymerie, *Nummulites minervensis* (Schaub), *Assilina prisca* (Schaub), *Nummulites* cf. *pengaronensis*, *Miscellanea miscella* (d'Archiac and Haime), *Medocia blayensis* Parvati, *Orbitclypeus* sp. and *Rotaliconus persicus* Hottinger. Another sample (KK3.11C; Log KK22) yielded *Anomalina* sp., *Asterigerina rotula* (Kaufmann), *Glomalveolina lepidula* Schwager, *Nummulites* sp., *Nummulites globulus* Leymerie, *Lacazina* cf. *Blumenthali* and *Alveolina minervensis* Hottinger. A third sample (KK2.10F; 37217:09696) contained *Idalina sinjarica* Grimsdale, *Glomalveolina lepidula* Schwager, Orbitolites sp., *Nummulites* sp. and *Alveolina* sp. (N. İnan & K. Taslı pers. comm. 2009).

Sample KK3.11F (Log KK22) was selected from a horizon of algal mats which contained the benthic foraminifera *Gypsina linearis* (Hanzawa) (N. İnan & K.

Taslı pers. comm. 2009) which typically is an encrusting foraminifera (e.g. Bosellini 1998).

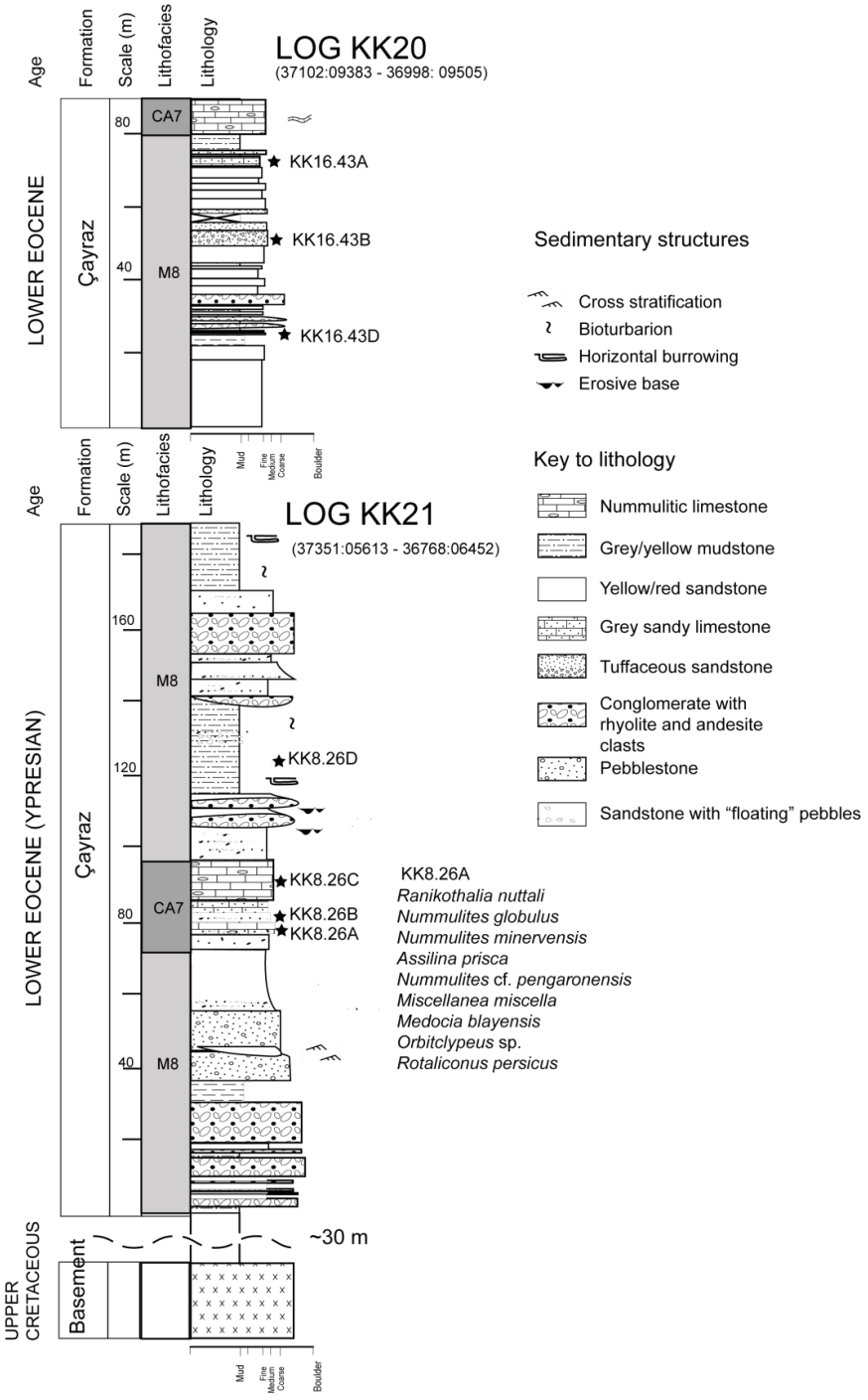

Figure 2.45 Measured stratigraphic logs KK20 (top) and KK21 (bottom), from north of Bahşili, showing the red conglomerates and sandstones of lithofacies association M8. All sedimentary data are from this study, palaeontological data are from N. İnan & K. Taslı (pers. comm. 2009).

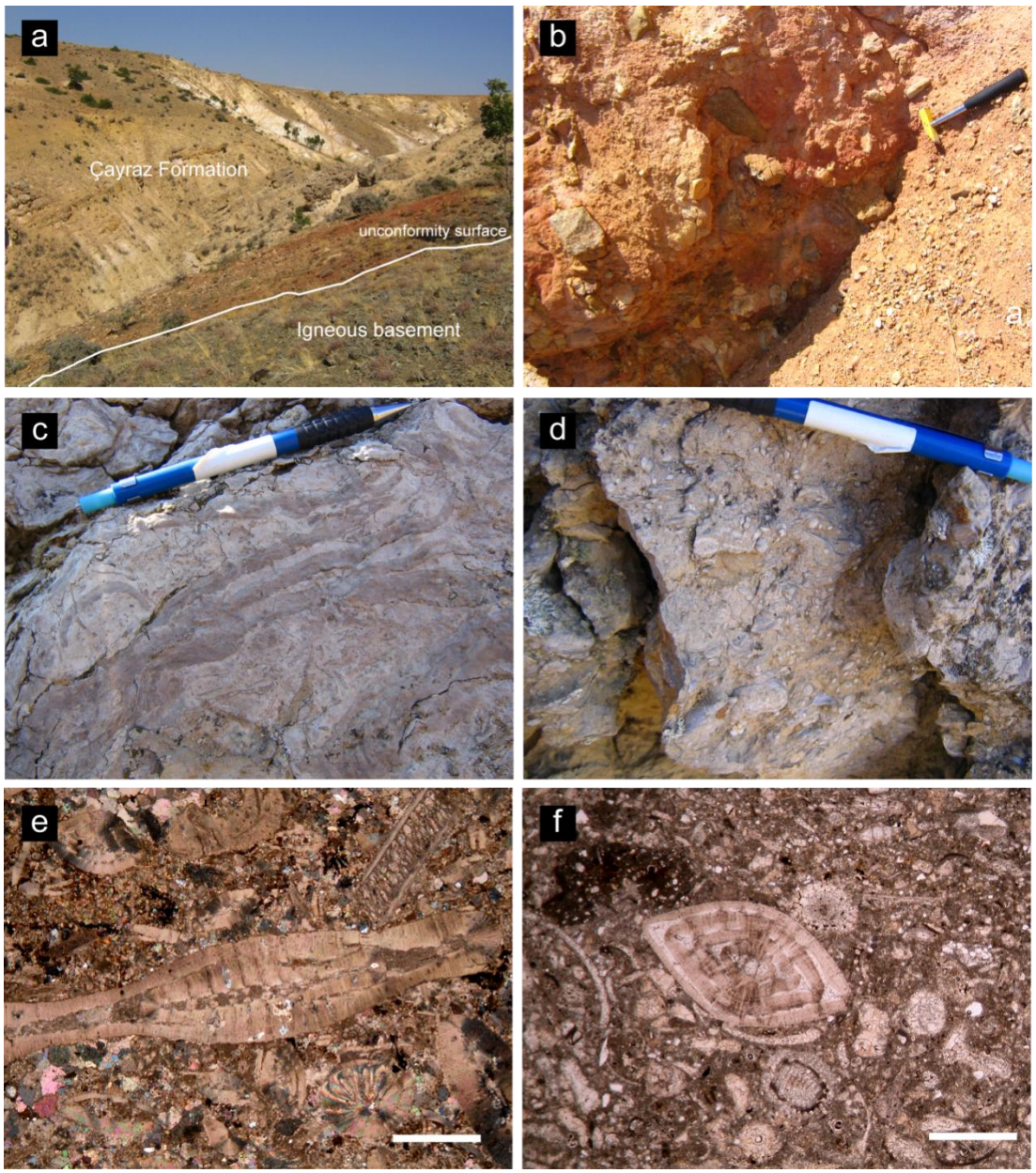

Figure 2.46 (a) field photograph (37022:05830), looking ~north, of the deltaic sands of lithofacies association M8 lying unconformably on igneous basement rocks, **(b)** view of red pebbly sandstone, **(c)** algal mats in lithofacies association C7, **(d)** large benthic foraminifera, **(e)** photomicrograph of *Assilina* sp. benthic foraminifera (sample KK8.26A) from Bahşili area (Log KK21), **(f)** photomicrograph of *Nummulites* sp. benthic foraminifera, (sample KK3.11C), both photomicrographs in plane polarised light, scale bars= 1 mm.

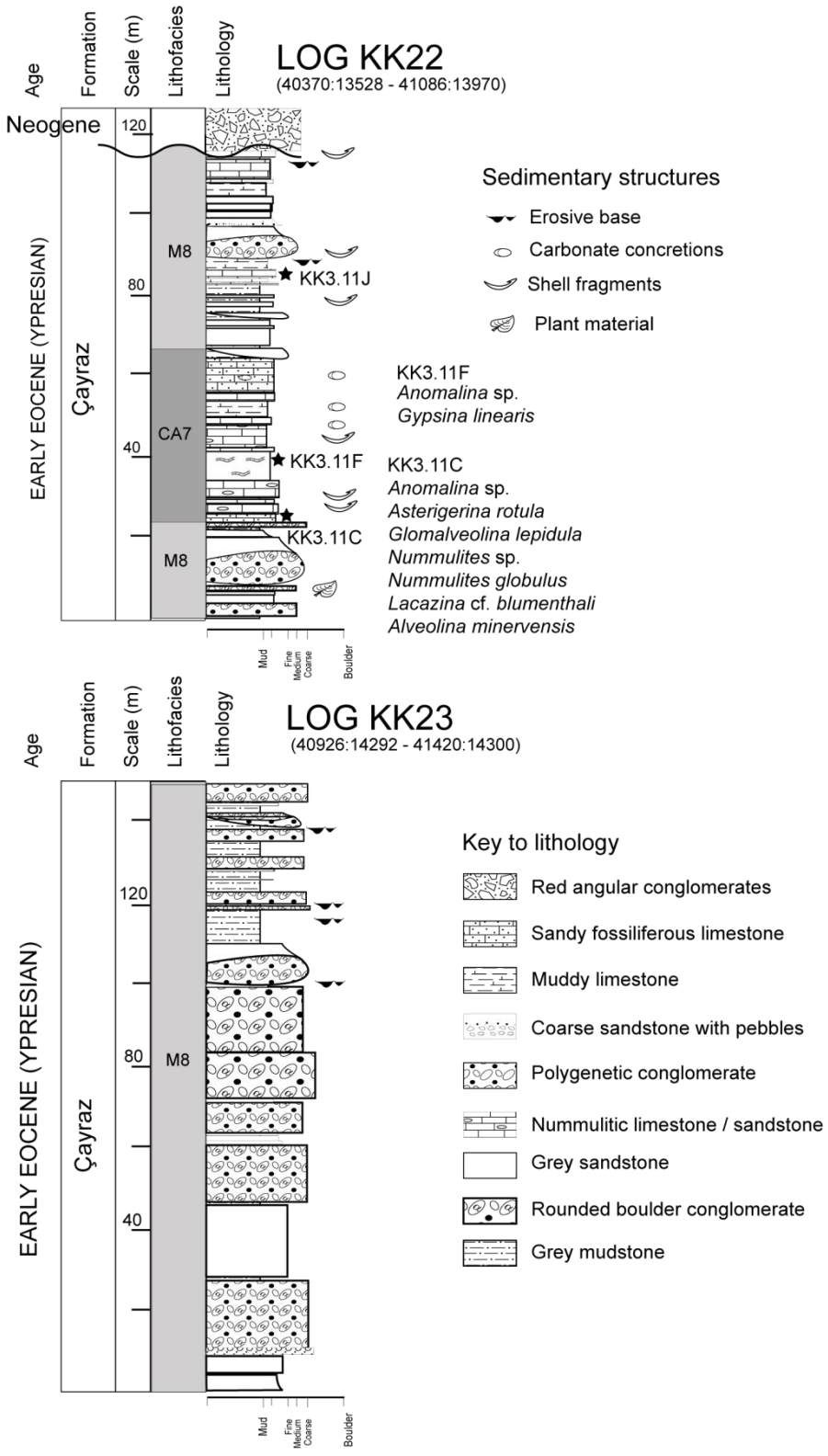

Figure 2.47 Measured logs KK22 (top) and KK23 (bottom) through lithofacies associations M8 and CA7 to the northeast of Yahşıhan, all sedimentary data are from this study, palaeontological data are from N. İnan & K. Taslı (pers. comm. 2009).

2.7.5.5 Interpretation of the Çayraz Formation

Lithofacies associations M8, M11 and CA7 represent the final marine deposits of the Kırıkkale Basin. The Çayraz Formation is possibly the lateral equivalent of the Hacıhalil Formation which is mainly exposed to the north of Kırıkkale at the northern margin of the Çankırı Basin (Ocakoğlu & Çiner 1997; Kaymakcı *et al.* 2009). This formation is characterised by 30 m-thick matrix-supported conglomerate sheets, locally graded 2 m-thick sandstone beds, and burrowed mudstones. The Hacıhalil Formation was interpreted to represent 6 different facies. They are, from north to south: proximal alluvial fan, braided river, meandering river, fan delta and near shore to prodelta/open marine facies (Ocakoğlu & Çiner 1997).

The Çayraz Formation in the Kırıkkale Basin possibly represents fan delta margin to pro-delta-type facies. Fan deltas produce small (tens of kilometres) wedge-shaped sediment bodies featuring abrupt facies changes. Their sedimentary deposits are typically coarse-grained, poorly sorted and matrix rich (McPherson *et al.* 1987). The conglomerates of the Çayraz Formation lack internal stratification, which is typical of Gilbert-type deltas; they are poorly sorted, matrix-supported and exhibit normal and inverse grading. These characteristics may represent deposition by subaqueous debris flow (Johnson 1984). In a fan delta setting, poorly sorted, subaqueous massive debris flow conglomerates are commonly deposited on a steep slope (Deynoux *et al.* 2005). The interbedded laterally continuous sandstones and bioturbated mudstones probably represent pro-delta deposits.

Carbonate sedimentation (lithofacies association CA7) represents periods of low siliciclastic influx. *Nummulites* are common in the Palaeogene Neotethyan realm and are present in foreland basins of the French Alps (e.g. Sinclair *et al.* 1998), the Spanish Pyrenees (e.g. Monstad 2000) and elsewhere in Turkey, e.g. the Sivas Basin (Atabey 1996) and the Ulukışla Basin (Clark & Robertson 2005). The presence of *Nummulites* benthic foraminifera suggests a shallow marine shelf-type depositional environment. *Nummulites* typically form shoals and banks of metre-scale thickness

and tens- to hundreds-metre scale lateral extent that were common in open shelf-type environments in the Tethyan realm (Schaub 1981; Racey 1995; Racey 2001). Patch reefs in fan deltas are reported in the Miocene Köprüçay Basin, Isparta Angle, Turkey (Deynoux *et al.* 2005).

2.7.6 The Incik Formation (Upper Eocene-Oligocene)

The Incik Formation is well exposed in the south of the basin near Camluca and comprises terrigenous coarse sandstones, conglomerates and gypsum. Other names for the Incik Formation are the Bahşili Formation (Norman 1972; Norman *et al.* 1980) and the Miskincedere Formation (Akyürek *et al.* 1984; Akyürek *et al.* 2000). It is mostly exposed south of the Kızılırmak River; in the south of the basin, at Camluca it lies unconformably on the Upper Maastrichtian-Lower Eocene Dizilitaşlar Formation (Fig. 2.48a). However the base of the formation is not exposed further north.

Two lithofacies association are present: 1) a ~100 m succession of evaporite blocks and coarse sandstone (Logs KK23 and KK24; Fig. 2.49) (lithofacies association C3) and; 2) a ~150 m sequence of pebbly sandstone and imbricated conglomerates (Log KK26: Fig. 2.49) (lithofacies association C4).

2.7.6.1 Lithofacies association C3: evaporite blocks

The distinguishing feature of lithofacies association C3 is the presence of angular boulders of gypsum, up to 90 cm in size, arranged as debris flow sheets up to 20 m thick. Boulders are typically sheared and cut by veins of secondary selenite which dip at 53/155 and define a shear fabric (Fig. 2.48b). Other lithologies are pebbly conglomerates, composed of radiolarian chert, limestone and well-rounded volcanic clasts in a coarse sandy matrix and grey/brown marl.

The top of log KK24 (Fig. 2.49) features rounded boulders of fossiliferous packstone in a coarse unconsolidated pebbly sandstone. The packstones contain Bryozoa and shell fragments along with pelagic foraminifera *Globigerina* sp., and the benthic foraminifera *Rotalia* sp., *Asterigerina rotula* (Kaufmann), *Idalina sinjarica* Grimsdale and *Miscellanea* sp. These taxa indicate a Palaeocene age (N. İnan & K. Taslı pers. comm. 2009) and have been reworked from the underlying Dizilitaşlar Formation.

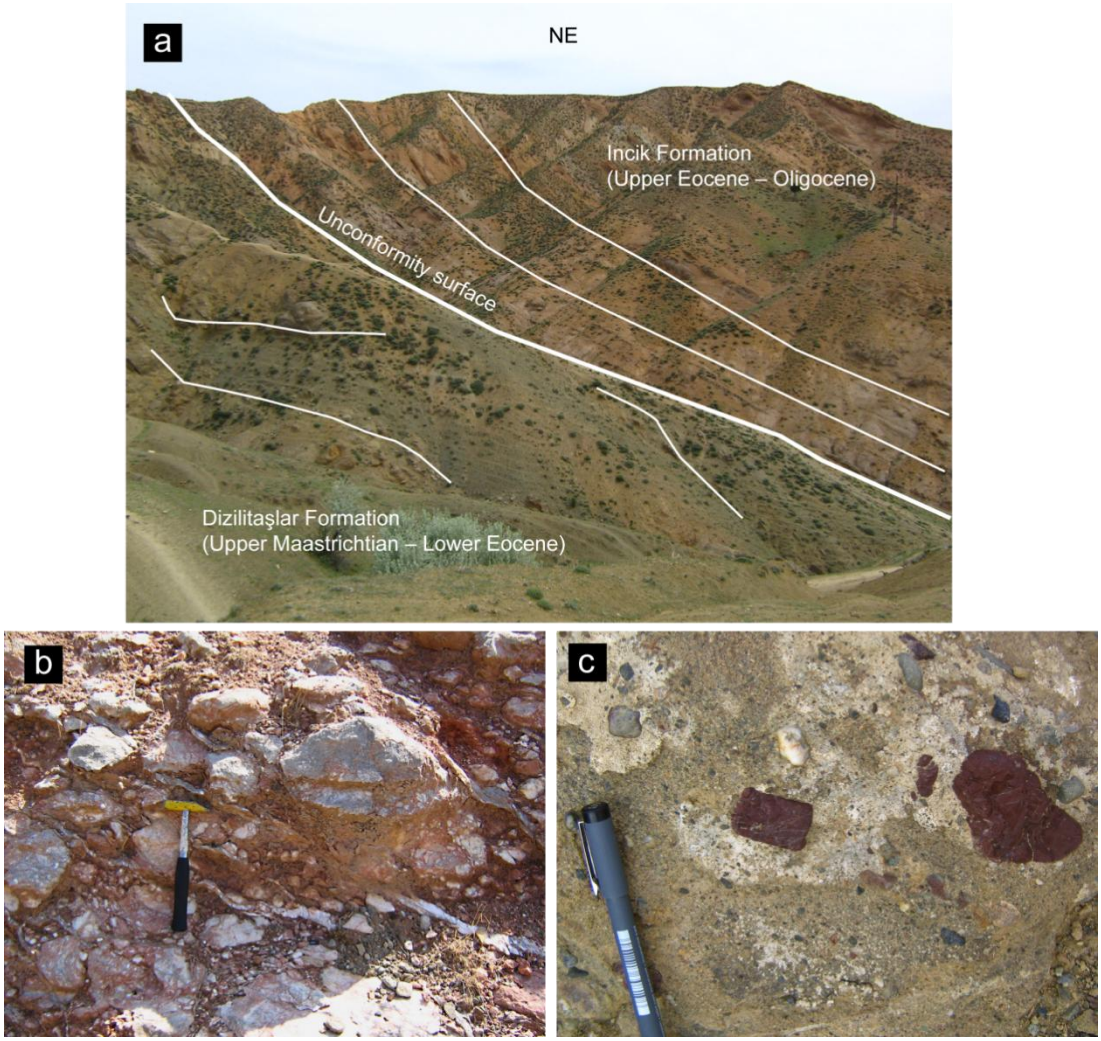

Figure 2.48 (a) Field photograph (looking NE) showing the angular unconformity between red sandstones Upper Eocene-Oligocene Incik Formation and grey mudstone and turbidites of the Upper Maastrichtian-Middle Eocene Dizilitaşlar Formation, **(b)** sheared blocks of gypsum, **(c)** angular red radiolarite clasts in coarse sandstone.

2.7.6.2 Lithofacies association C4: pebbly sandstone and imbricated conglomerates

Based on one stratigraphic log (Log KK25) and local mapping, lithofacies association C4 lies unconformably on the Dizilitaşlar Formation. Its base consists of medium bedded (0.4 to 1.6 m), flaggy bedded coarse-grained sandstones with scattered pebbles and pebbly conglomerates. Angular pebble clasts reach 4 cm in size, are moderately sorted, supported in a coarse sandy matrix and chiefly composed of limestone and red radiolarian chert (fig. 2.48c) derived from the İzmir-Ankara Accretionary Complex and granite derived from the Kırıkkale Massif. This passes into clast-supported cobble conglomerates. Clasts are angular, up to 7 cm in size and show a preferred orientation, indicating unidirectional flow to the east (n=4 measurements). Above lies matrix-supported conglomerate sheets of rounded radiolarian chert, limestone and sandstone cobbles, frequently poorly consolidated.

2.7.6.3 Interpretation of the Incik Formation

The Incik Formation represents a period of non-marine sedimentation. The dating of the Incik Formation is problematic given the absence of autochthonous fossil evidence. It is, however, present in the Çankırı Basin to the north of the Niğde-Kırşehir Massif which has been dated as Late Eocene to Oligocene using freshwater gastropods (Kaymakcı 2000; Kaymakcı *et al.* 2009).

This is consistent with the evidence in the Kırıkkale Basin given that there is an unconformity between the underlying Dizilitaşlar Formation and the Incik Formation (Log KK25).

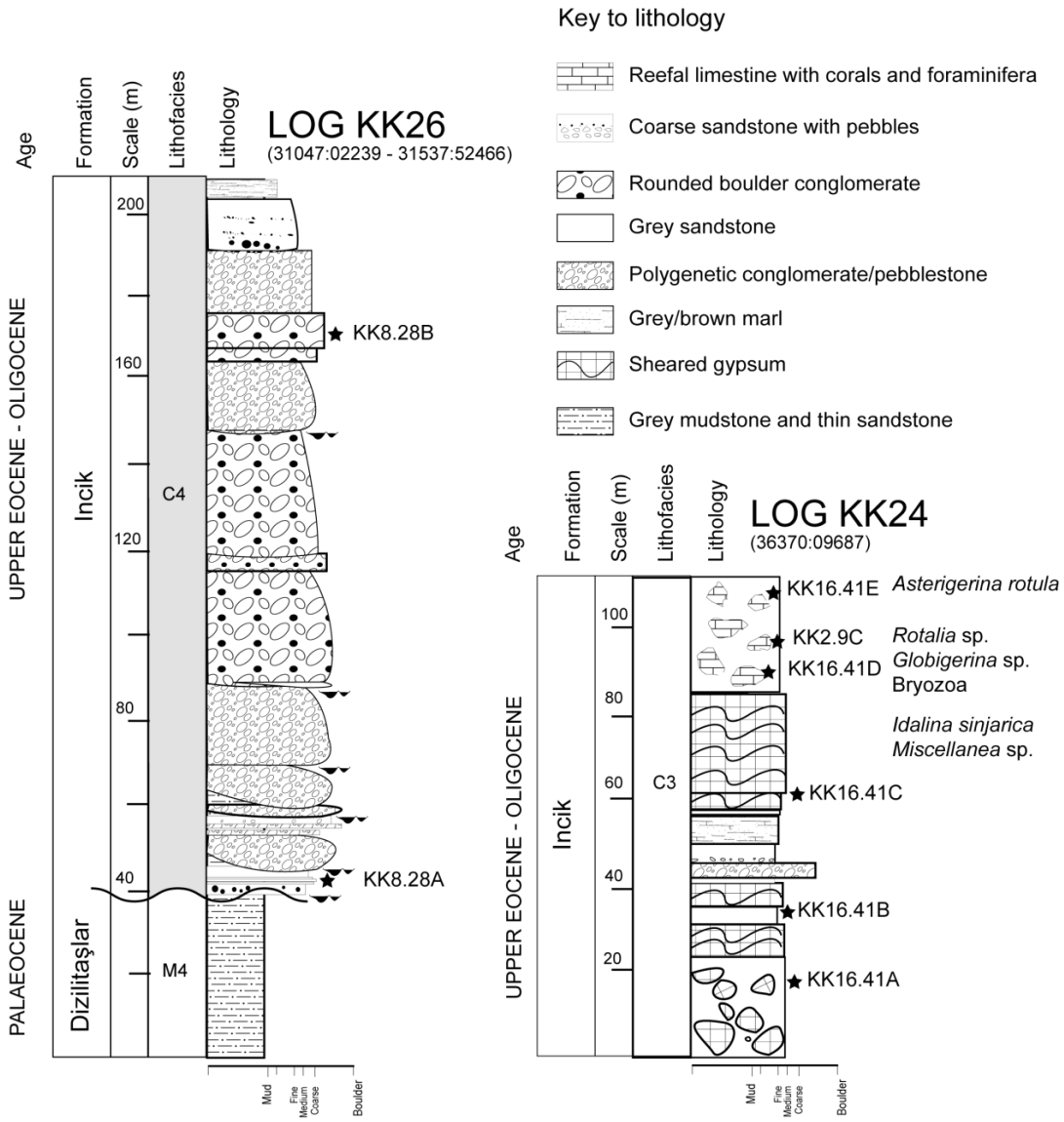

Figure 2.49 Measured stratigraphic logs KK26 (lithofacies association C4) and KK24 (lithofacies association C3), all sedimentary data are from this study, palaeontological data are from N. İnan & K. Taslı (pers. comm. 2009).

2.7.7 Provenance

This section discusses sandstone petrography and palaeocurrent data with the aim of inferring the provenance of basin-fill sediments. This study utilised the Gazzi-Dickinson point counting technique (Gazzi 1966; Dickinson 1970) to count 300 points per slide. See Appendix 2 for a full discussion on methodology and tabulated data. Fig. 2.51 is a ternary Qt:F:Lt-c diagram (where Qt= Total quartz, F= Feldspars, Lt-c = Total non-carbonate lithoclasts) which presents point-counting results graphically.

Palaeocurrents were measured in the field from a variety of indicators including unidirectional data (flute marks and clast imbrication) and bidirectional data (groove marks). Data from a previous study (Norman 1973) are discussed for comparison. See Appendix 3 for tabulated data and a discussion of data treatment.

2.7.7.1 The Campanian Ilıcıpınar Formation

Seven samples were examined to determine the petrology and provenance of the volcaniclastic sediments of the Ilıcıpınar Formation. In general, grains are angular, to subangular, with a grain-supported fabric. One sample shows a slight preferred orientation. The samples are moderately- to poorly-sorted and are compositionally and texturally immature. The most abundant mineral is angular plagioclase (26 – 55%) commonly affected by sericite alteration (Fig. 2.50a). Accessory minerals (opaque oxides, biotite, clinopyroxene and hornblende) are also common and account for 12 – 43% of the total grains counted. Monocrystalline quartz (5 – 11%) grains are angular and fresh. Microlitic volcanic clasts (11 – 45%) are subrounded and sedimentary clasts of shale and sandstone are less common (1 – 6%). Qt:F:Lt-c ratios are 13:30:57 (Sample No. KK13.36C), 10:53:27 (KK13.36G), 9:63:29 (KK13.36A), 6:69:25(KK13.36H), 14:67:19 (KK9.29G), 14:67:18 (KK7.24F), 14:70:16 (KK7.24G) (See Fig. 2.51).

No palaeocurrent indicators were observed during this study. However, Norman (1973a) published palaeoflow directions from the east and north-northwest (Fig. 2.52a).

2.7.7.2 The Maastrichtian Samanlık Formation

Petrological examination of two samples indicated that clasts are fine- to medium-grained, sub-rounded, moderately sorted, and grain-supported with calcite spar cement. The samples are dominated by microlitic volcanic clasts, bioclasts, calcite grains and fresh, angular quartz (Fig. 2.50b). Diagenesis includes calcite veining. Calculated Qt:F:Lt-c ratios are 9:10:81 (KK13.36J) and 6:10:84 (KK7.24B).

Palaeocurrent indicators (n= 10; flute marks) indicate a flow broadly from the north, which is in agreement with those of Norman (1973) (Fig. 2.52b).

2.7.7.3 The Upper Maastrichtian-Lower Eocene Dizilitaşlar Formation

In the lower Dizilitaşlar Formation, sandstone is compositionally similar to that of the underlying Samanlık Formation. It is coarse- to medium-grained and cemented by calcite spar. Sorting is poor and the dominant grains are sub-rounded, to rounded, volcanic clasts up to 3 mm in size. One sample (KK12.34C) is moderately sorted, grain supported with sub-rounded volcanic clasts (~43%) calcite (~ 34%), monocrystalline quartz (~12%), sedimentary clasts (~6%), large (>2mm) polycrystalline quartz (~3%) and plagioclase and accessories (~2%). This assemblage is probably sourced from an intra-oceanic arc. Calculated Qt:F:Lt-c ratios are 23:3:74 (KK7.24C) and 17:9:74 (KK7.25A). Higher in the stratigraphy of the Dizilitaşlar Formation, sandstones are represented by sample KK6.21A (Fig. 2.50c) which contains ~40% carbonate mud matrix. Clasts are microlitic volcanic,

serpentinite and a microgranular quartzo-feldspathic volcanic groundmass (69%), mudstone (~18%), fresh angular monocrystalline quartz (~9%) with rare augite, serpentinite, micaceous sandstone, plagioclase and calcite. This mineral assemblage is typical of detritus from the İzmir-Ankara Accretionary Complex. The Qt:F:Lt-c ratio is 10:2:88 (KK6.21A) (See Fig. 2.51).

Palaeoflow was generally from the northeast, based on measurements of flute marks (n= 2) and groove marks (n= 3). These data confirm those of Norman (1973a) who inferred a palaeoflow from the north-northeast (n= 19). Clast imbrication (n= 4) indicates a unidirectional subaqueous flow from the north-northwest (Fig. 2.52c).

2.7.7.4 The Lower Eocene Çayraz Formation

Sandstones of the Lower-Middle Eocene Çayraz Formation are more quartz-rich than older Upper Cretaceous and Palaeocene sandstones. Three samples were examined in thin section, two from northeast of Mahmutlar (samples KK4.17A and KK4.17B; Log KK17) and another from Bahşili (KK8.26D; Log KK21). The samples from Mahmutlar are dominated by sub-rounded < 3mm volcanic lithoclasts of microgranular quartz (46–47%). Other grains are fresh, angular volcanic quartz with resorbed edges (27–32%) and polycrystalline plutonic quartz (18–24%) (Fig. 2.50d). Qt:F:Lt-c ratios are 51:2:48 and 52:2:46 respectively (Fig.2 .51). A likely source is the rhyolite flows and granitoids of the Niğde-Kırşehir Massif to the east.

Another sample (KK8.26D) (Fig. 2.50e) is quartz rich (71% monocrystalline quartz grains) and is less abundant in silicic volcanic lithoclasts; the Qt:F:Lt-c ratio is 71:3:26 (Fig. 2.51).

2.7.7.5 The Upper Eocene-Oligocene Incik Formation

One representative sample from the terrigenous Incik Formation is rich in sedimentary clasts (~44%), monocrystalline quartz (28%) and silicic volcanic lithoclasts (17%) other clasts are angular monocrystalline quartz and large subangular polycrystalline quartz (Fig. 2.50f). Minor clasts include plagioclase, calcite and opaque oxides, the Qt:F:Lt-c ratio is 36:2:6 (Fig. 2.51).

Palaeocurrent indicators in the Çayraz Formation are absent. Imbricated clasts in the Incik Formations showed a palaeocurrent from northeast. However, given that the sandstones are composed of quartz-rich clasts representing detritus from the Niğde-Kırşehir Massif, it is probable that their source was to the south and east.

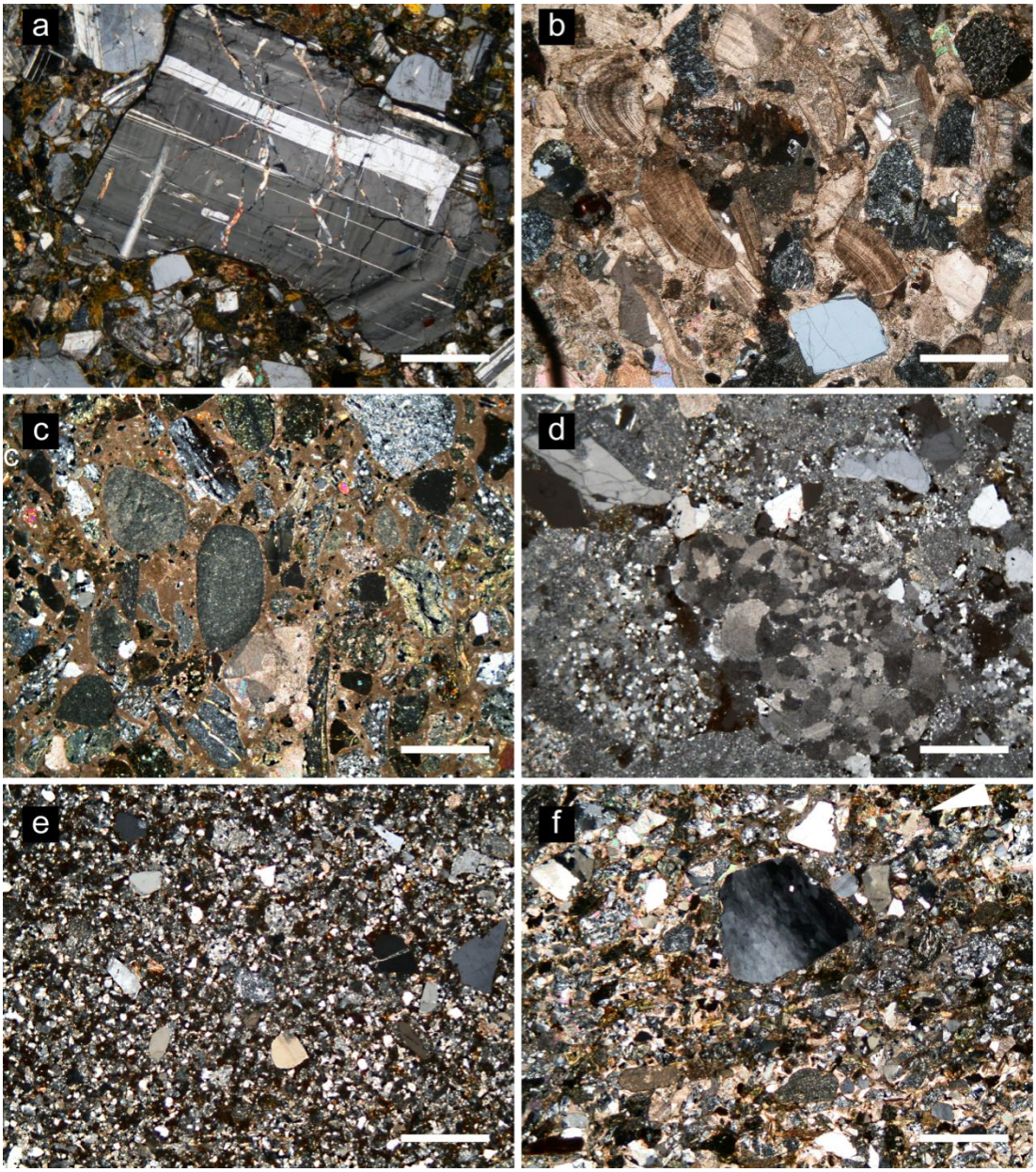

Figure 2.50 Photomicrographs of representative sandstones used in the provenance study, **(a)** volcaniclastic sandstone from the Campanian Ilıcıpınar Formation (sample KK13.36H), **(b)** bioclastic sandstone, rich in volcanic lithoclasts from the Maastrichtian Samanlık Formation (sample KK12.34B), **(c)** greywacke with clasts of volcanic lithoclasts and serpentinite from the mainly Palaeocene Dizilitaşlar Formation (sample KK6.21A), **(d)** coarse-grained quartz-rich sandstone from the Lower Eocene Çayraz Formation (sample KK 4.17A), **(e)** fine-grained quartz-rich sandstone from the Lower Eocene Çayraz Formation (sample KK8.26A), **(f)** poorly sorted sandstone from the Upper Eocene – Oligocene Incik Formation (sample KK8.28A).

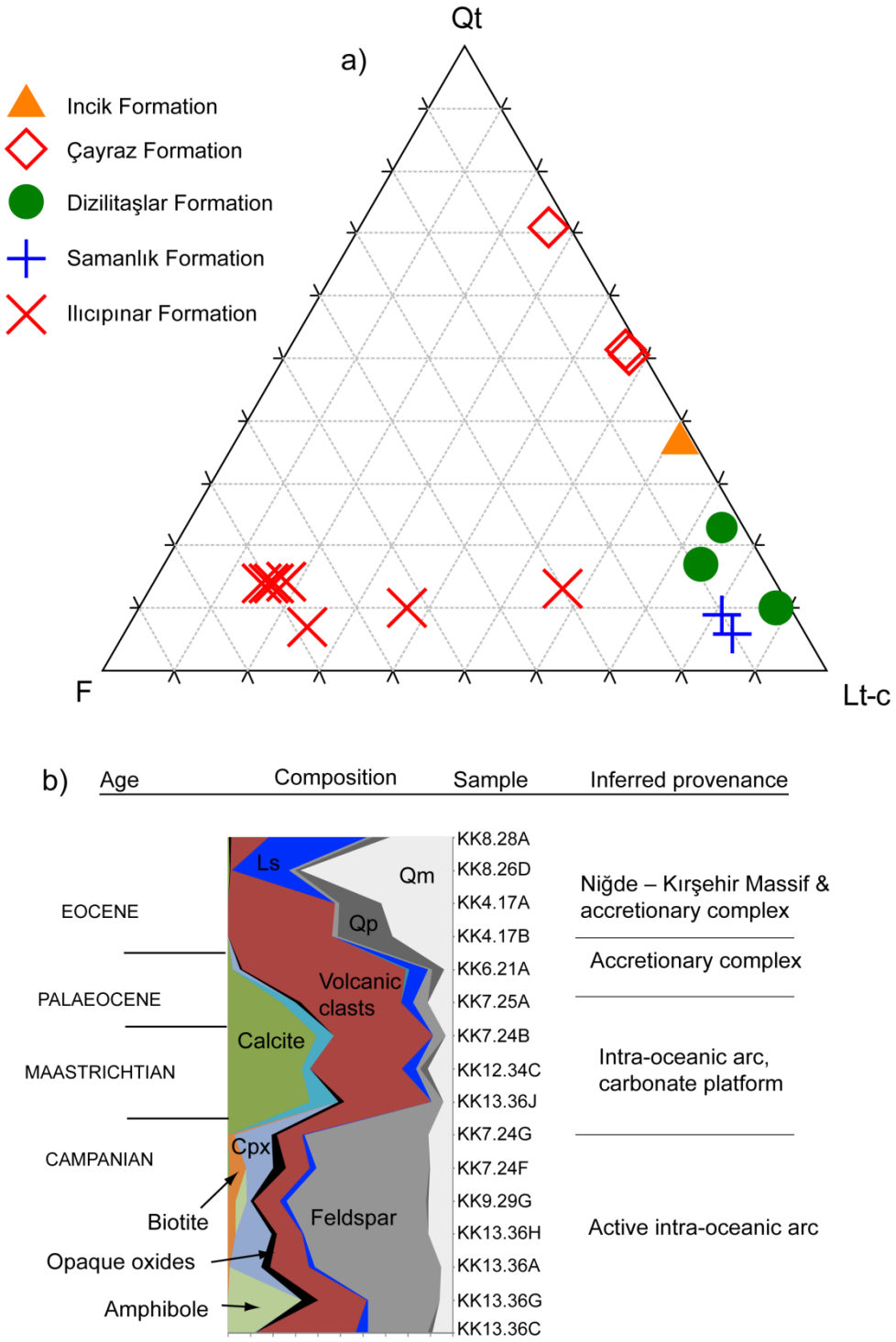

Figure 2.51 (a) Qt-F-Lt-c ternary diagram of the sandstones used in the provenance study, Qt – total quartz, F – feldspar, Lt-c – total lithic clasts (excluding carbonate clasts), **(b)** stratigraphic diagram of point-counting results, showing sample numbers and inferred provenance, Qm – monocrystalline quartz, Qp – polycrystalline quartz, Ls – sedimentary clats, Cpx – clinopyroxene.

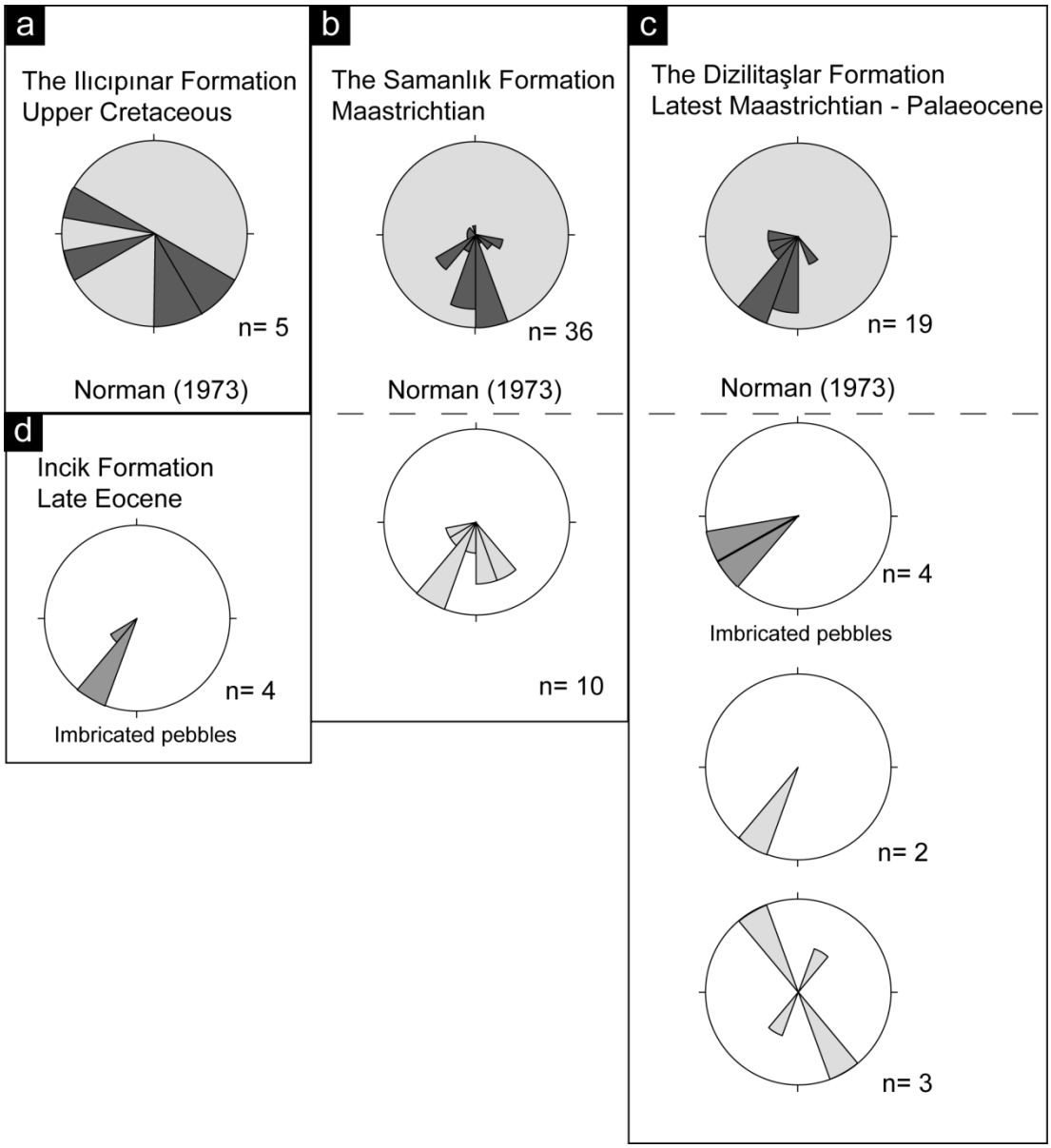

Figure 2.52 Palaeocurrent rose diagrams from **(a)** the Campanian Ilıcıpınar Formation, **(b)** the Maastrichtian Samanlık Formation, **(c)** the mainly Palaeocene Dizilitaşlar Formation, **(d)** the Upper Eocene-Oligocene Incik Formation, the rose diagrams with dark grey circles are from Norman (1973a), those with white circles are from this study, grey indicators are from imbricated pebbles, light grey indicators are from flute and groove marks.

2.7.8 New stratigraphic and sedimentary results

In summary, the following results are new and are the result of this study:

- The Campanian **Ilıcıpınar Formation** was sourced from an active intra-oceanic arc setting to the north. It is probably the lateral equivalent of the Yaylaçayı Formation, which is exposed in the Çankırı Basin to the north, and is less thick than was previously described (Norman 1972).
- The Maastrichtian **Samanlık Formation** was mostly deposited by turbidity current from an intra-oceanic arc setting; however, classic Bouma-type turbiditic structures are absent. The high abundance of shallow-marine fossils implies that a carbonate platform-type environment was associated with the arc.
- The Upper Maastrichtian-Palaeocene **Dizilitaşlar Formation** contains a number of lithofacies association association. The lower part of the formation lies depositionally on the Samanlık Formation, in contrast to previous studies that interpret the contact as structural. Based on large benthic foraminifera, the base of the Dizilitaşlar Formation is Upper Maastrichtian, which is older than was previously thought.
- Sandstones of the lower part of the formation are dominated by basic/intermediate volcanic lithoclasts. Those from the upper part are composed of detritus from the İzmir-Ankara Accretionary Complex.
- Limestone blocks and debris flows are Early and Late Palaeocene in age, rather than the Maastrichtian date which had previously been published.
- *In situ* coralgal reefs of probable Palaeocene age lie on an erosional surface on the basin basement.
- Palaeocurrent indicators from this study confirm those of Norman (1973).
- The Eocene **Çayraz Formation** is probably the result of deposition in a marine fan delta/pro-delta type of setting. This interpretation is based on the presence of tabular bedding in sandstone, pebbly sandstones, debris flow conglomerates, burrowed mudstones and reworked sandy limestone beds containing Nummulites

fossils. Sediment provenance was probably from the Niğde-Kırşehir Massif to the south and east of the basin.

- Large benthic foraminifera are dated in this study as Ypresian, older than the Lutetian date which was previously published.
- The Upper Eocene-Oligocene **Incik Formation** is the oldest non-marine formation in the Kırıkkale Basin. In the south of the basin it lies unconformably on the mainly Palaeocene Dizilitaşlar Formation. The Incik Formation contains reworked boulders of Palaeocene-aged coralgal limestone.

A correlation diagram of lithofacies associations is presented in Fig. 2.53, which represents an approximate north northwest-south southeast section parallel to most palaeocurrent directions.

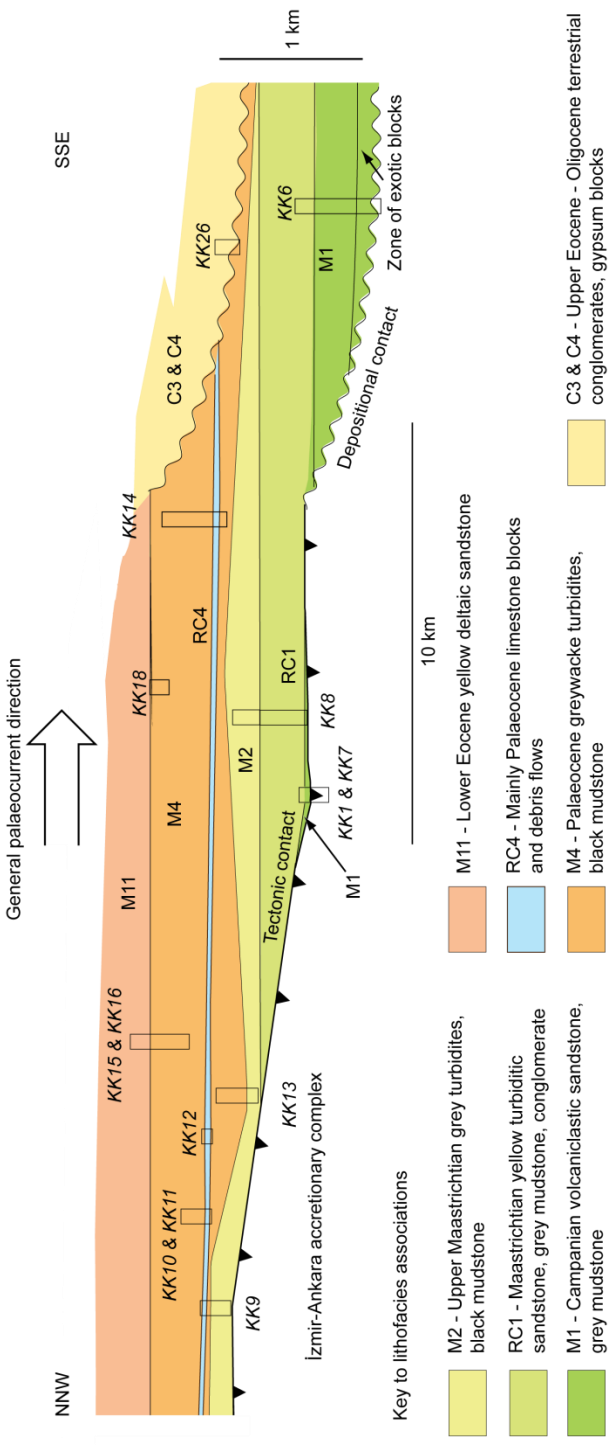

Figure 2.53 Correlation diagram of lithofacies associations based on measured logs from this study. The diagram trends approximately north-northwest to south-southeast parallel to the basin axis and most palaeocurrent directions.

2.8 Structural development of the Kırıkkale Basin

Previous work on the structural development of the Kırıkkale Basin is limited. Norman (1973b) reported post-Eocene east-verging overturned folding followed by thrust faulting and right-lateral strike-slip faulting. Kaymakcı *et al.*(2003) reported three phases of deformation in this region: 1) Palaeogene (Late Palaeocene–pre-Burdigalian) transpression; 2) Early Miocene oblique extension and; 3) regional strike-slip deformation associated with the development of the Miocene to recent North Anatolian Fault Zone (e.g. Şengör 1979).

In order to test these results, fault planes, slickenside indicators (where present) and fold axes were measured in the field and processed using TectonicsFP software (Ortner *et al.* 2002). The aim is to reconstruct palaeostress fields which can be related, with care, to regional tectonics. Determination of palaeostress was achieved by processing fault data in terms of P-, B- and T-axes (Turner 1953). Concentrations of P (pressure)- and the T (tension)-axes are interpreted as the orientation of $\sigma 1$ and $\sigma 3$, respectively and thus represent an approximation of palaeostress stress axes (Sperner *et al.* 1993). Importantly, TectonicsFP software contains a function which calculates the probability that a given set of faults were formed in a similar palaeostress field. Appendix 4 contains tabulated fault data and a full discussion of data treatment and processing.

Thirty fault planes were measured, of which sixteen had reliable slickenside indicators which were recorded in terms of the plunge and azimuth of movement of the hanging wall. Most faults strike SW–NE, a smaller subset strikes N-S (Fig. 2.54a). On an Angelier plot (Angelier 1979), which shows faults planes a great circles and movement of the hangingwall as arrows, the sixteen faults with slickenside indicators comprise a heterogeneous fault population (Fig. 2.54b). The heterogeneity is confirmed by the P- and T-axes diagram (Fig. 2.54c) which exhibits low probability (R) values on every axis that the fault set comprises a single fault population produced in the same palaeostress field (P- 44%, B- 46%, T -14%). The faults were filtered by dip angle and strike azimuth which produced homogenous

fault sets with significantly higher R values. The fault sets are characterised by compressional, extensional and strike-slip deformation.

2.8.1 Compressional deformation

2.8.1.1 Faults

The first set comprises four low dipping thrust faults in the southern region of the İzmir-Ankara Accretionary Complex (R >94%). The P-axis dips at 277/08, B-axis at 187/01 and the T-axis at 093/82. This set indicates a deformation phase associated with a sub-horizontal σ1, aligned WNW, and a sub-vertical σ3 where hangingwall movement was to the ESE (Fig. 2.54d; these figures combine a P-T axes diagram with an Angelier plot).

2.8.1.2 Folds

Compressional deformation was probably associated with a set of basin-scale overturned folds which deform Palaeocene and older sediments at the western basin margin. Folding is most intense towards the northern basin margin, where the underlying accretionary basement has been reverse-faulted against the basin margin (Fig. 2.57). In contrast to previous reports (e.g. Norman 1972; Norman 1973b; Dönmez *et al.* 2008) the relationship between the basin sediments and the accretionary basement is not exclusively a faulted contact. To the southeast of the basin, the volcaniclastic sediments of the Upper Cretaceous Ilıcıpınar Formation lie depositionally on the accretionary basement.

Fold axes (i.e. π-axes) near the western basin margin generally plunge gently and trend parallel to the basin/accretionary complex basement fault contact. Three map-scale folds have their π-axes orientated (plunge/trend) 31/349, 17/007 and

41/299 (Fig. 2.56a). Geometrically, the folds are situated in the footwall of the thrust faults and have an overturned limb verging in the direction of fault propagation i.e. mostly eastwards. The folds have an inferred wavelength of ~1.5 km, high bedding dips (>40°) and are often associated with parasitic open synclines. Fig. 2.56b displays three synclines which mostly trend parallel to the basin margin at (plunge/trend of fold axis) 21/227, 08/020 and 06/187.

Classic models of fault propagation folds (e.g. Suppe 1985) do not account for footwall deformation. Instead the folds are probably detachment folds (e.g. McNaught & Mitra 1993) where deformation of the mud-rich basin sediments occurs ahead of the propagating thrust fault tip. If the thrust cuts up through the core of the detachment fold it will leave behind the forelimb of the detachment fold as a footwall syncline. Overturned footwall synclines are common in thrust regions and have been recognised in the Neogene Southern Apennines (Piedilato & Prosser 2005) , the Cenozoic High Atlas Mountains (Teixell *et al.* 2003) and the Cenozoic of Greece (Underhill 1989).

2.8.2 Extensional deformation

The second fault set comprises three transtensional faults which cut the Palaeocene Dizilitaşlar Formation in the Mahmutlar area. The P-axis is orientated at 069/64 (R= 97%), the B-axis at a77/12 (R= 87%) and the T-axis at 273/22 (R= 86%). Deformation was therefore associated with sub-vertical σ1 and sub-horizontal σ3, hangingwall movement was to the east (Fig. 2.54e).

2.8.3 Strike-slip deformation

Two subsets of high angle strike-slip faults are recognised, which formed in different palaeostress regimes. The first subset (n= 4) comprises west-southwest – east-northeast striking right-lateral faults, three of which cut sediments of the

Dizilitaşlar Formation. Another fault forms a boundary between the Lower Eocene Karagüney Formation and the Upper Cretaceous Kırıkkale Massif. The P-axis is orientated at 280/15 (R= 99%), the B-axis at 109/75 (R= 99%) and the T-axis at 010/02 (R= 98%). This deformation phase was associated with approximately east-west compression (Fig. 2.54f).

A second subset (n=2) is composed of SSW - NNE striking high-angle right-lateral faults, which cut the Dizilitaşlar Formation in the north of the basin. This phase featured northeast –southwest compression (Fig. 2.55a).

2.8.3.1 Outcrop-scale folds

Outcrop-scale folds have amplitudes of ~1 m so that their fold axes can be measured directly. Fig. 2.56c is a lower hemisphere stereonet plot of great circles and poles to fold axes (n= 6). Five of the axes dip to the northeast and strike northwest to southeast, suggesting a southwest to northeast compressive event, possibly relating the folds to the second strike-slip phase.

Three other strike faults were measured, 2 high-angle right-lateral strike-slip faults and on high-angle extensional fault (Figs. 2.55b,c and d).

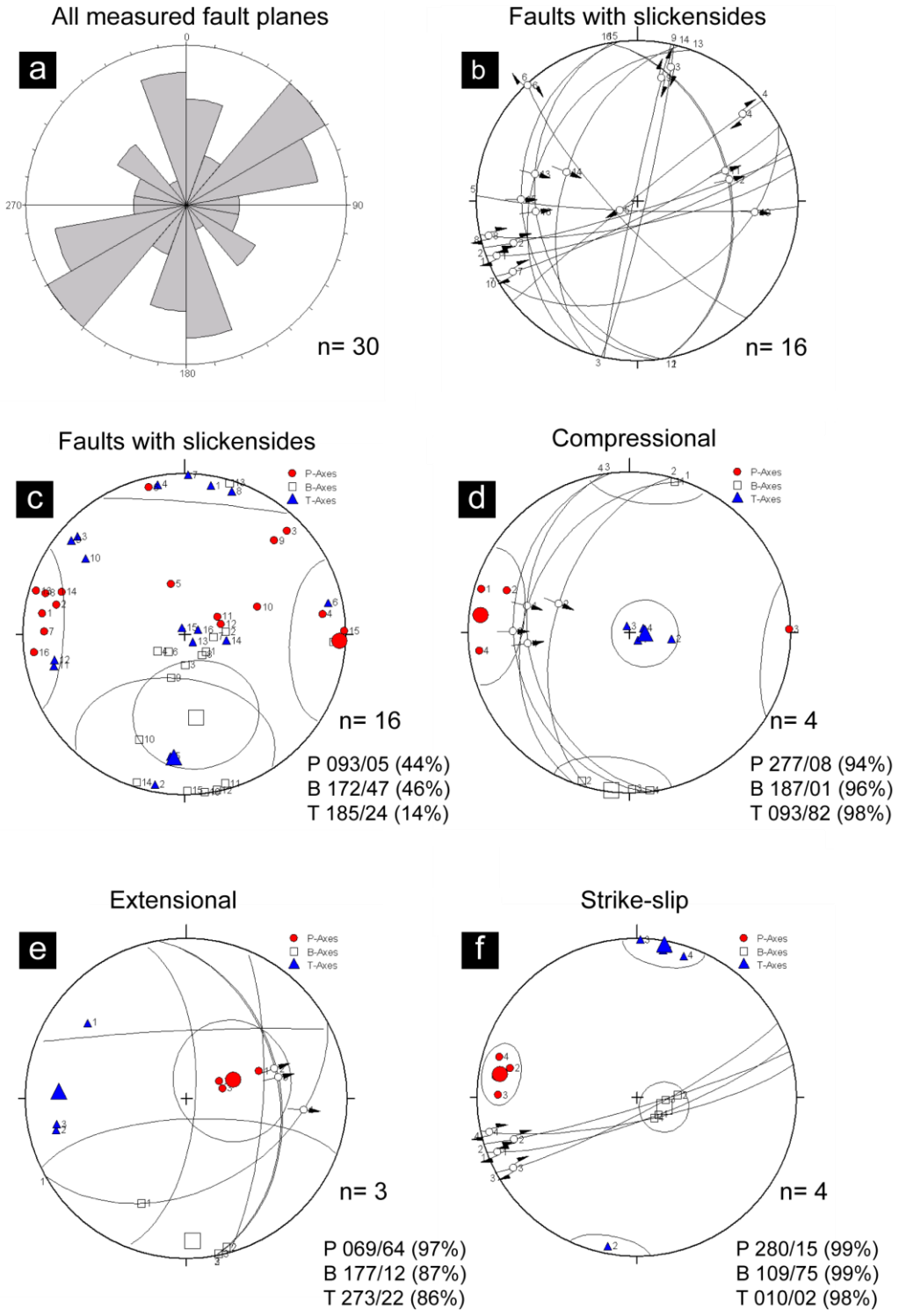

Figure 2.54 (a) Rose diagram of all measured fault planes, **(b)** Angelier lower hemisphere plot of all fault planes which contained slickensides, **(c)** P-T axes plot of all faults with measured slickensides. Combined P-T axes and Angelier plot of compressional faults **(d)** extensional faults **(e)** and strike-slip faults **(f).**

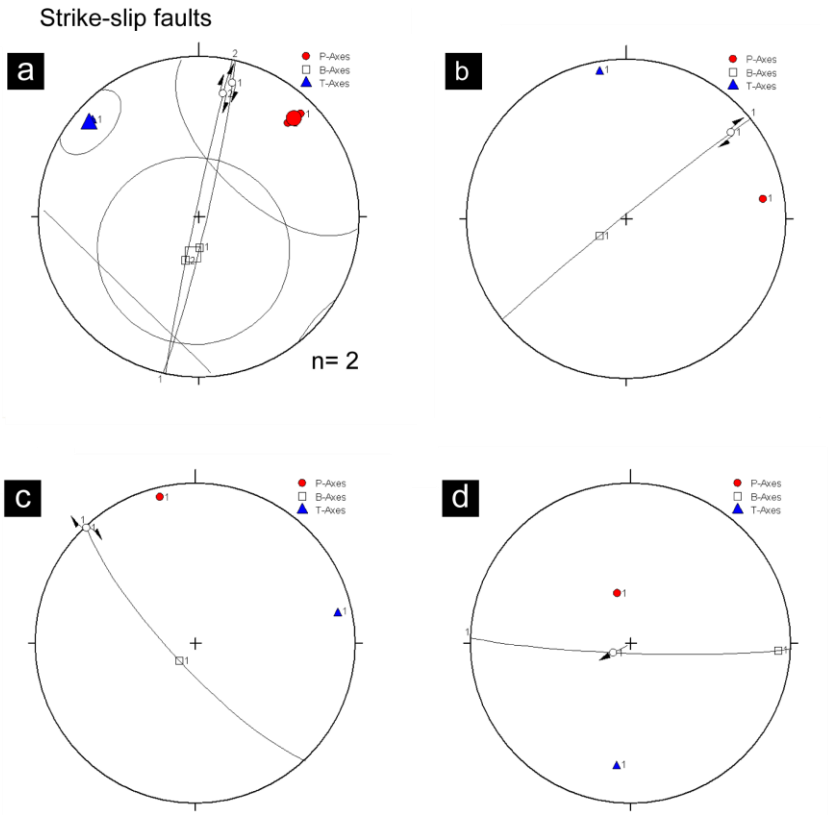

Figure 2.55 Combined P-T-axes diagram and Angelier plots of **(a)** a strike-slip fault set, **(b)-(d)** individual high-angle faults.

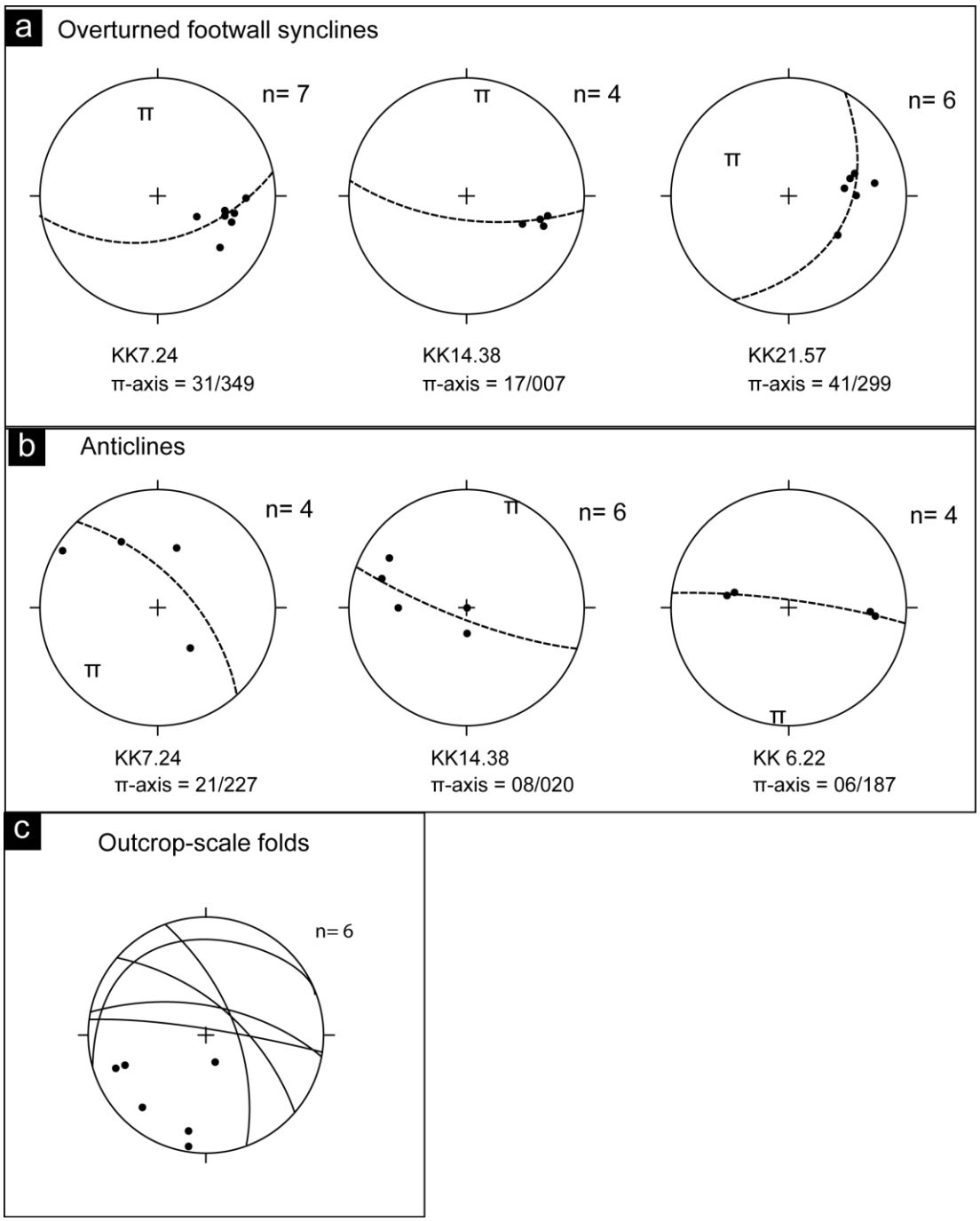

Figure 2.56 (a) Lower hemisphere best-fit girdles (dashed lines) and Π-axes for overturned footwall synclines at the western basin margin, **(b)** lower hemisphere best-fit girdles (dashed lines) and Π-axes for anticlines at the western basin margin, **(c)** measured outcrop-scale folds, the great circles represent fold axes, the black dots represent poles to fold axes.

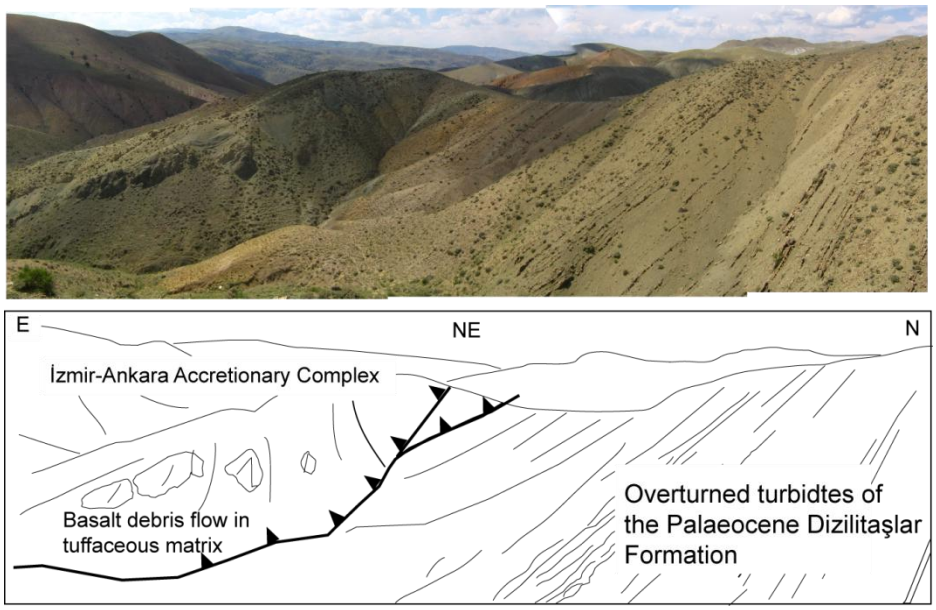

Figure 2.57 Photomosaic (above) and interpretive field sketch (below) of the western basin margin, looking NE.

2.8.4 Interpretation of structural results

Establishing the timing of the deformation phases described above is not straightforward. The Palaeocene Dizilitaşlar Formation and older sediments are typically intensely deformed by overturned folding, particularly in the northwest. However, younger sediments are relatively undeformed, implying that thrust faulting and folding occurred in the Late Palaeocene, earlier than the post-Middle Eocene deformation date of Norman (1973b). Previous studies (Norman 1973b; Akyürek *et al.* 1984; Akyürek *et al.* 2001; Dönmez *et al.* 2008) interpreted the basin-fill sediments to be affected by brittle thrust faulting. However, there is no structural or stratigraphic evidence (e.g. repeating stratigraphic units) for thrust faulting in the basin. Instead, there are unconformities, debris flows, collapsed limestone blocks and abrupt facies changes, all of which have previously been interpreted as thrust faults. Cross-sections can be used to infer shortening, here, the cross-section on D-D' (Fig. 2.58) has been line-length balanced to an undeformed section representing a possible structural state in the Early Palaeocene. Bed lengths in relation to a pin-line indicate a shortening of ~40 %.

Cross-cutting relationships infer that strike-slip faulting occurred after thrust faulting and folding. This is exemplified by a major basin-scale right-lateral fault zone which strikes southwest – northeast and cuts basin-margin folds and thrust faults with an estimated displacement of ~5 km. This strike-slip fault zone is generally considered to be a segment of the Kırıkkale-Erbaa Fault Zone (Piper *et al.* 1997; Aydemir 2009) a right-lateral splay of the Mio-Pliocene to present North-Anatolian Fault Zone (e.g. Şengör 1979). The trace of the Kırıkkale-Erbaa marks the contact between the İzmir-Ankara Accretionary Complex and its sedimentary cover to the west and the Niğde-Kırşehir Massif and cover to the east. The contact is marked by a steep topographic break. The Kırıkkale-Erbaa Fault strikes northeast through Kırıkkale, Sungurlu and Erbaa. It is therefore conceivable that the fault zone is likely to be Miocene and younger in age and represents the post-collisional reorganisation of the central Anatolian tectonic collage. However, this is speculative and needs testing by further study.

The phase of extensional faulting and the other phases of strike-slip faulting display no cross-cutting relationships, meaning that their ages are presently unresolved.

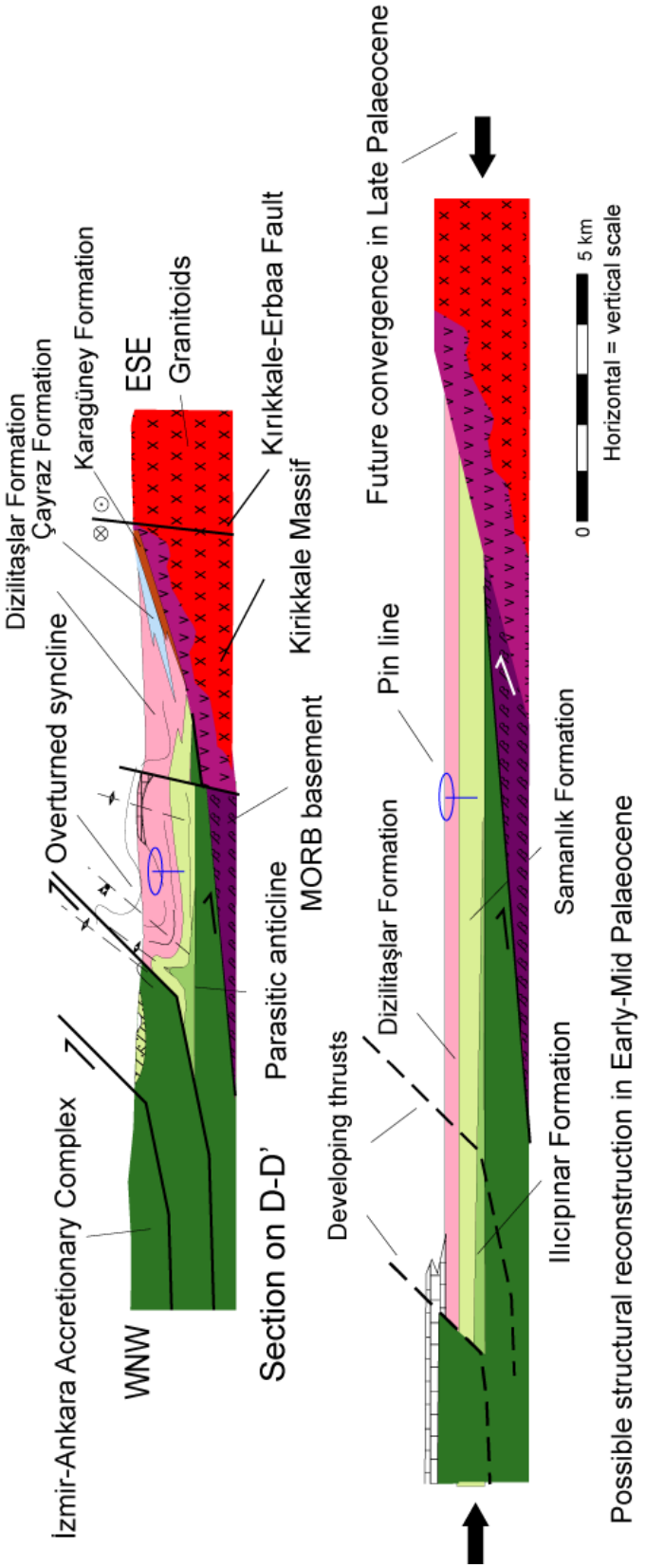

Figure 2.58 Structural cross-section on D-D' (above), balanced cross-section indicating a possible reconstruction before Late Palaeocene compression (below), see Fig. 2.4 for location of section lines.

2.9 Discussion: Evolution of the Kırıkkale Basin

New geochemical, sedimentary, stratigraphic and structural data permit a reconstruction of the Kırıkkale Basin which can be integrated into regional context.

2.9.1 Pre-Maastrichtian events

The northward subduction of the İzmir-Ankara Ocean under the Pontide active margin began in the Turonian. Subduction also drove the development of the mainly Cretaceous İzmir-Ankara Accretionary Complex, an accretionary prism composed of deep sea sediments, oceanic crustal fragments and seamounts. In the Eastern Pontides, Upper Cretaceous magmatism persisted from the Turonian to the Late Maastrichtian/Danian (Robinson *et al.* 1995). In the Western and Central Pontides, magmatism lasted from the Coniacian to the Campanian (Okay & Tüysüz 1999). It is possible that subduction was oblique to the Pontide margin, with magmatism concentrated inboard in the Eastern Pontides and outboard of the Western Pontides, which could explain the relative lack of arc-related rocks in the Central and Western Pontides (Rice *et al.* 2006).

Subduction initiated outboard of the Central Pontide margin triggering the genesis of SSZ-type ophiolites in an extensional backarc setting to the north of an intra-oceanic arc. Floyd *et al.* (2000) used faunal evidence to date ophiolite generation at 90-85 Ma (Turonian–Coniacian) while Göncüoğlu *et al.* (2006) proposed a younger, Santonian, date. In the Turonian, ophiolitic mélange, including blocks of MORB-type ocean crust, obducted onto the northern margin of the Niğde-Kırşehir Massif (Yalınız *et al.* 2000a). The arc retreated seaward (south), probably driven by subduction rollback, until it collided with the northern margin of the Niğde-Kırşehir Massif, emplacing SSZ-type ophiolites as far south as Kırşehir. The time of emplacement is considered to be ~80 Ma (Campanian) (Floyd *et al.* 2000). To the north of the Niğde-Kırşehir Massif, remaining MORB-type oceanic crust was

consumed prior to the emplacement of SSZ ophiolites. However, the presence of MORB basement (see Section 2.6.4.4) in the Kırıkkale Basin, situated at the northwestern margin of the Niğde-Kırşehir Massif, indicates that an embayment of MORB oceanic crust persisted to the west (Fig. 2.59). The Campanian emplacement of ophiolites onto the Niğde-Kırşehir Massif either represents an incipient 'soft' collision in a palaeogeographically complex northern Neotethyan region, where continental collision was delayed until the Early Cenozoic (Görür *et al.* 1984; Görür *et al.* 1998; Kaymakcı *et al.* 2009; Robertson *et al.* 2009) or terminal continental collision associated with the collision of the Pontides to the north and the Tauride – Anatolide Platform to the south (e.g. Floyd *et al.* 2000; Gürer & Aldanmaz 2002).

The evolution of the Kırıkkale Basin began in Santonian to Campanian time on the İzmir-Ankara Accretionary Complex and remnant MORB oceanic crust, to the south of an intra-oceanic arc. Campanian volcaniclastic sandstones of the Ilıcıpınar Formation lie on the İzmir-Ankara Accretionary Complex, deposited by high-density turbiditic flow on a slope-type setting. The Santonian to Campanian Karadağ Formation is exposed in the far northwest of the Kırıkkale Basin and, based on its radiolarian content, was deposited in a deep marine setting. However, exposure of the Karadağ Formation is patchy and its relationship with the Ilıcıpınar Formation to the south of the basin is unclear. To the east of the basin, granite and monzonite plutons were emplaced into the continental crust of the Niğde-Kırşehir Massif and its SSZ-type ophiolitic cover. Emplacement and cooling ages have not been determined radiometrically; however, the plutons in the Kırıkkale basin share chemical affinities with many granitoid plutons in the Niğde-Kırşehir Massif whose timing of emplacement and cooling is well constrained.

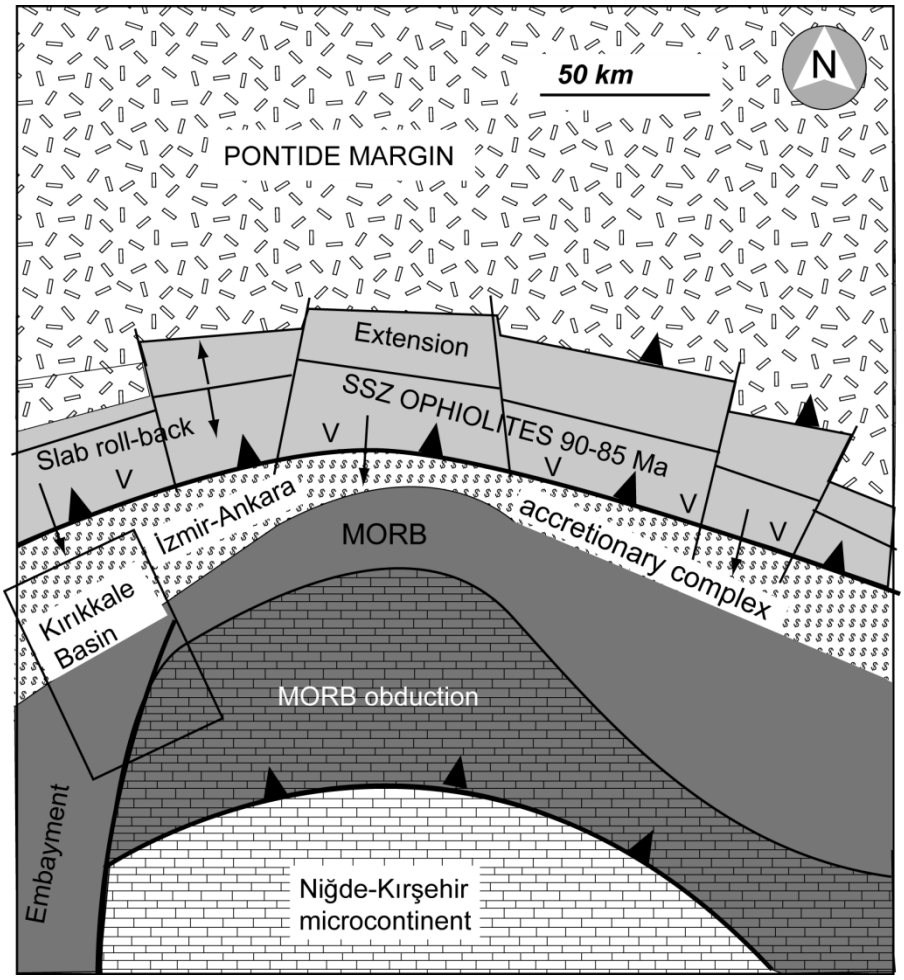

Figure 2.59 Schematic palaeogeographic scenario in the Turonian, based on *Kaymakcı et al.* (2009).

2.9.2 Maastrichtian events

In the Maastrichtian, yellow bioclastic-rich sandstones of the Samanlık Formation were deposited conformably on the Ilıcıpınar Formation. Sedimentary structures including groove marks and flute marks indicate a deposition from turbidity currents on a lower slope setting. Abundant volcanic lithoclasts suggest a source from an intra-oceanic arc, however, an increase in the abundance of terrigenous sediments imply that arc magmatism ceased by Maastrichtian time. This timing is consistent with evidence from volcanic arc rocks in the Central Pontides to

the north. (Okay & Şahintürk 1997; Rice *et al.* 2009). Sandstone also contains abundant shallow-marine bioclasts, suggesting the development of a carbonate platform adjacent to the arc. New palaeontological dating from this study indicates that the black mudstone and grey sandstone, which represent the base of the Dizilitaşlar Formation were deposited during this time.

To the south of the accretionary complex, MORB oceanic crust persisted. Its sedimentary cover included metalliferous sediments, pelagic foraminifera-bearing silts and limestone, which pass upward into sandstone and rudist-bearing conglomerates (Section 2.6.3).

In the east, Maastrichtian sedimentary deposition continued on the SSZ-type ophiolite of the Kırıkkale Massif (Section 2.6.3.1). Sediments consist of green ribbon chert, pelagic limestone, sandstone and redeposited shallow marine carbonates. There is no evidence of convergence at this time, which would be expected in the Late Cretaceous, continental collision model.

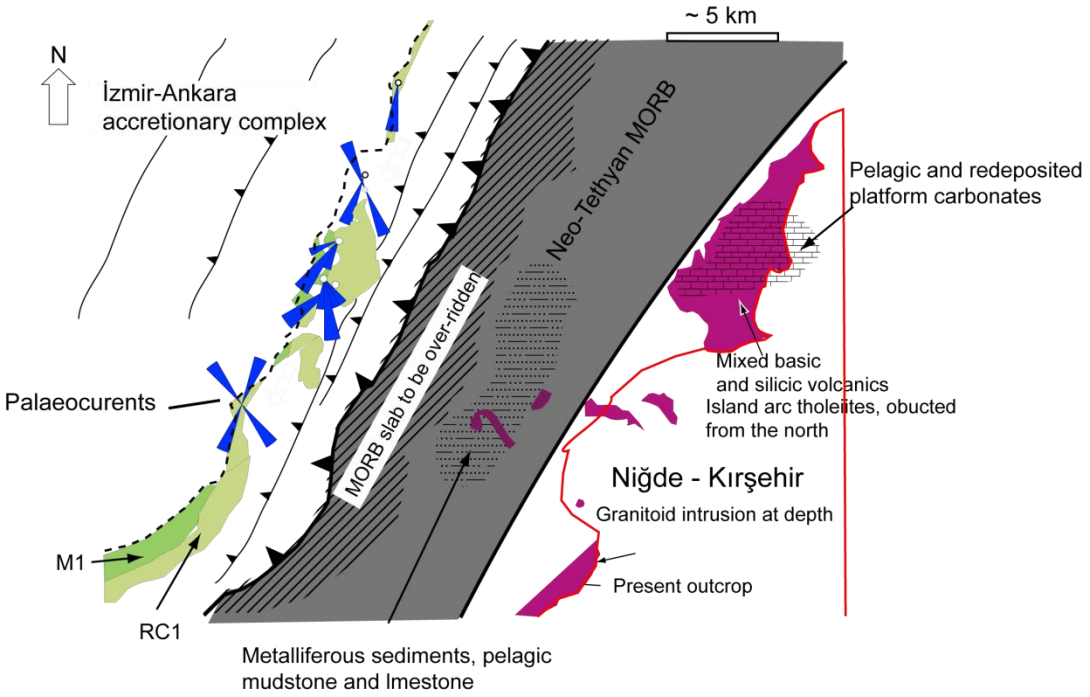

Figure 2.60 Non-palinspastic schematic palaeogeographic map of the Kirikkale Basin in the Maastrichtian

2.9.3 Palaeocene events

The Palaeocene is dominated by deep marine mudstone, siltstone and sandstone of the Dizilitaşlar Formation. The lower, Maastrichtian parts of the Dizilitaşlar Formation are dominated by volcanic lithoclasts and bioclasts; however sandstone composition switches to a composition dominated by detritus from the İzmir-Ankara Accretionary Complex and the Niğde-Kırşehir Massif. Detached blocks of coralgal limestone suggest a shallow-marine carbonate build up, probably to the north of the basin associated with uplifted blocks of the İzmir-Ankara Accretionary Complex (e.g. Rojay & Süzen 1997b).

During the Late Palaeocene, thrusting and associated folding deformed Palaeocene and older sediments, particularly at the western basin margin (Section 2.8.1). Kaymakcı *et al.* (2003) related this compressive event to the collision of the Niğde-Kırşehir Massif and the Pontide Margin.

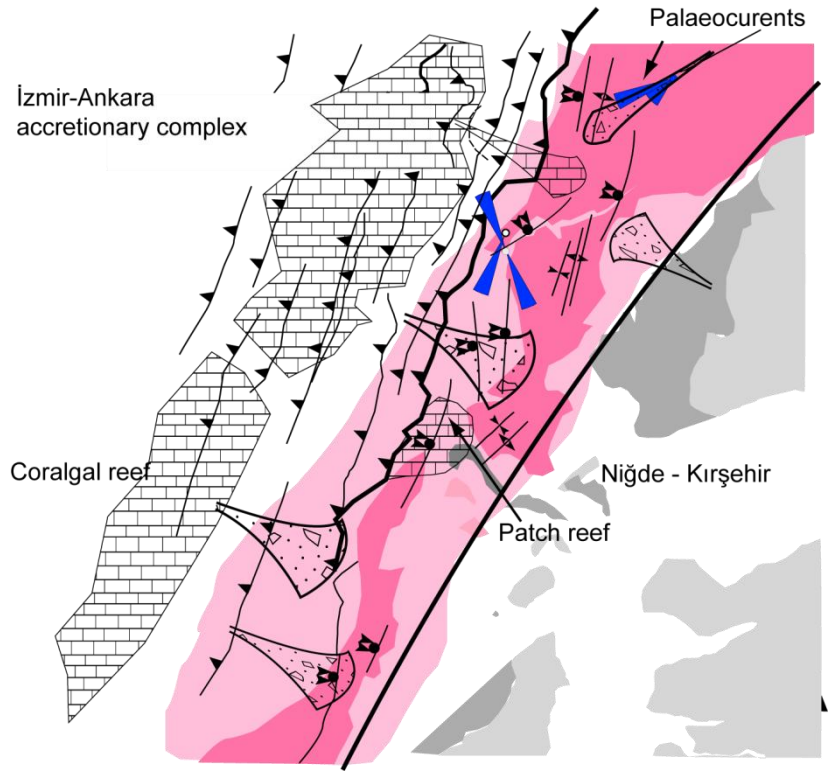

Figure 2.61 Non-palinspastic schematic palaeogeographic map of the Kirikkale Basin in the Palaeocene. Note that dark pink represents present outcrop of Palaeocene sediments, lighter pink is the inferred extent in the Palaeocene.

2.9.4 Eocene events

The Early Eocene is characterised by shallow marine sedimentation which is represented by the Karagüney and Çayraz formations. The dominant sedimentary source was the Niğde-Kırşehir Massif to the south and east, which was deposited as conglomerate mass flows, and pebbly sandstone in a delta margin setting. Deposition was mostly unconformable on basement rocks and was associated with a marine transgression. Episodic periods of low siliciclastic input were dominated by shelf-type carbonates containing large benthic foraminifera. New palaeontological dating from this study indicates an Ypresian age, older than the Lutetian age which was previously proposed.

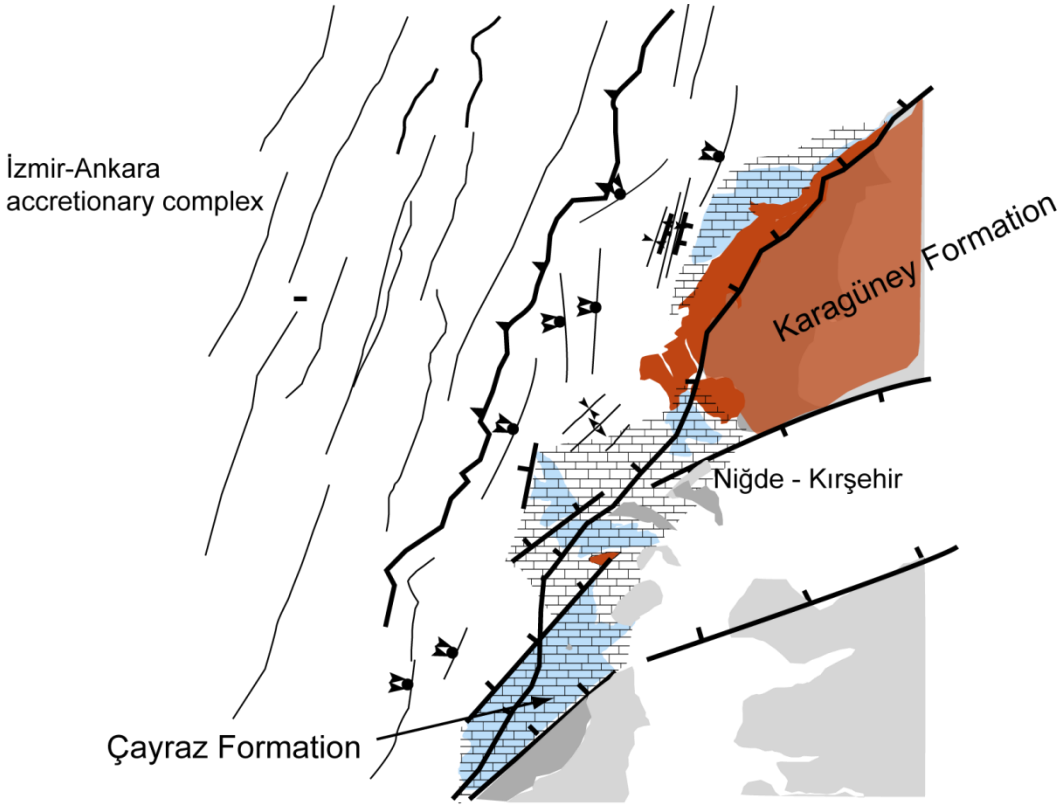

Figure 2.62 Non-palinspastic schematic palaeogeographic map of the Kirikkale Basin in the Middle Eocene.

2.9.5 Post-Eocene events

The basin was emergent during this time as terrestrial sandstone and gypsum were deposited (the Upper Eocene-Oligocene Incik Formation). Post-Oligocene preservation is restricted to isolated outcrops of Mio-Pliocene red, continental clastic sediments. This period was characterised by Neotectonic extensional and strike-slip faulting. Strike-slip faulting cut across previous thrust faults and produced right-lateral displacements of ~ 5 km. However, fault data from the Kırıkkale basin is currently insufficient to establish the timing of brittle deformation in this time.

2.10 Conclusions and summary of new data from Chapter 2

- The Upper Cretaceous-Eocene Kırıkkale Basin offers unique insights into tectono-sedimentary processes associated with collisional processes. This area was studied because; 1) well-exposed basement rocks associated with the Mainly Upper Cretaceous İzmir-Ankara Accretionary Complex and the Niğde-Kırşehir Massif; 2) Campanian volcaniclastic sandstone (the Ilıcıpınar Formation) is unique to this basin among the basins studied.
- Geochemical data from the basin basement has not been studied before. This study indicates that a variety of basic volcanic rocks are present including: 1) MORB and IAT of probable Upper Cretaceous age from in the İzmir-Ankara Accretionary Complex; 2) a fragment of MORB in the centre of the basin and; 3) SSZ-type IAT in the Kırıkkale Massif which, geochemically, can be correlated to the Çiçekdağ Ophiolite, which lies on the Niğde-Kırşehir Massif to the southeast. Analysis of granitoid plutons indicates the presence of a silica-rich, K-Poor granite pluton in the south and monzonite plutons in the east.
- Basin-fill sediments have been analysed in terms of lithofacies associations and depositional environments. Localised mapping and stratigraphic logging has re-interpreted and improved several previous interpretations. See Section 2.7.8 for a summary of new sedimentary and stratigraphic data.
- New structural data provide insights into the development of the basin, including a period of Late Palaeocene compression and Neo-Tectonic strike-slip and extensional faulting.
- A new model of the tectonic setting of the basin has been described (Section 2.9) which is consistent with new data gathered during this study and a wider literature review. The evolution of the Kırıkkale Basin lends support to a model of Late Cretaceous incipient collision followed by Cenozoic continental collision.

Chapter 3: The Çankırı Basin

3.1 Introduction

The Çankırı Basin is a composite basin of pre- and post-Middle Eocene rocks which record two separate tectonic settings. Pre-Middle Eocene rocks are pre- to syn-collisional, post-Middle Eocene lithologies represent a post-collisional setting and as such were disregarded during this study. The Çankırı Basin was chosen for study because it is the most northerly of the Central Anatolian basins, and is therefore proximal to the Pontide margin. Much of the centre of the basin is covered by Neogene sediments, however, the basin margins contain well exposed Palaeocene-Eocene sediments and lavas which provide unique insights, and provide time constraints, on collisional processes. This chapter focuses on two parts of the Çankırı Basin: 1) Sungurlu and 2) Bayat, which are exposed at the eastern and northern margins of the basin, respectively.

The Çankırı Basin occupies an area of ~22 500 km^2 and is one of Turkey's largest Upper Mesozoic-Cenozoic basins (Tokatlı *et al.* 2006). It is situated between the Pontide margin (see Chapter 1) to the north and the Niğde-Kırşehir Massif to the south (see Chapter 1). The basin forms a Ω-shape and contains a ~4 km thick Late Cretaceous to Neogene sedimentary infill (Kaymakcı 2000). It is also referred to as the Çankırı-Çorum Basin (e.g. Şenalp 1981). The basin is situated in the İzmir-Ankara-Erzincan Suture Zone (Ketin 1966) which marks the partial remnants of the İzmir-Ankara-Erzincan Ocean (Şengör & Yılmaz 1981; Robertson & Dixon 1984). Its northern, eastern and western margins are delimited by ophiolitic mélange representing the İzmir-Ankara Accretionary Complex (Okay *et al.* 2006), the structurally lowest unit of the classic Ankara Mélange (Bailey & MacCallien 1950; Norman 1984). The İzmir-Ankara Accretionary Complex represents dismembered thrust sheets and blocks of Neotethyan oceanic lithosphere, seamounts, pelagic sediments and terrigenous clastic sediment which were accreted to the over-riding plate during the Late Cretaceous-Middle Eocene closure of the İzmir-Ankara-Erzincan Ocean. The İzmir-Ankara Accretionary Complex forms the basement of the

basin, as encountered in an exploration well (Topuzsaray-1) at a depth of 3566 m in the centre of the basin (Tokatlı *et al.* 2006; Kaymakcı *et al.* 2009).

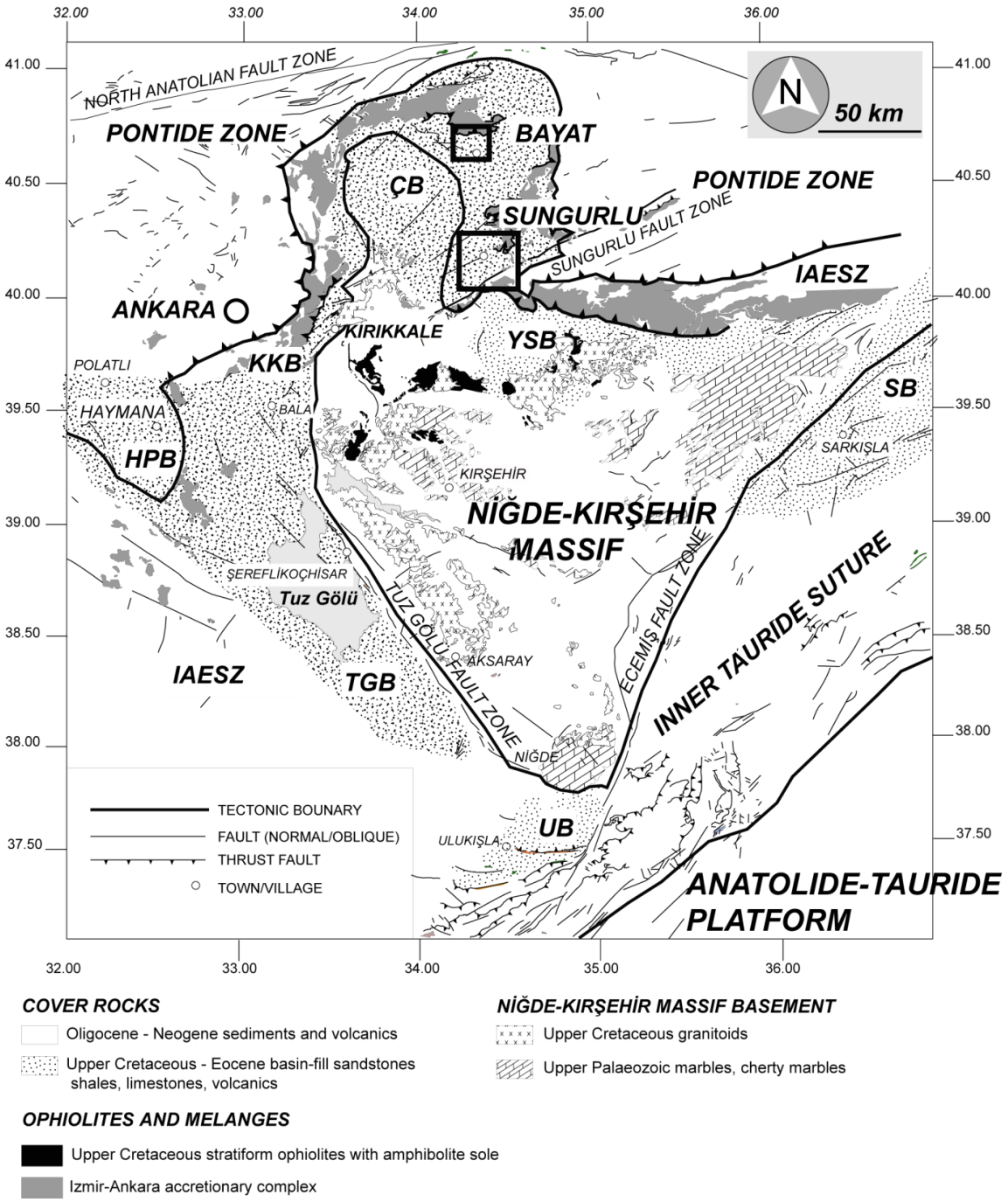

Figure 3.1.Regional map of Central Anatolia indicating major basin areas and tectonic units. İzmir-Ankara-Erzincan Suture Zone (IAESZ), Tuz Gölü (Salt Lake) Basin (TGB), Ulukışla Basin (UB), Sivas Basin (SB), Yozgat-Sorgun Basin (YSB) Haymana-Polatlı Basin (HPB), Kırıkkale Basin (KKB) and the Çankırı Basin (ÇB). The areas discussed in this chapter are indicated by the black boxes. Modified after Clark & Robertson (2002) and MTA (2002).

3.2 Aims

The objective of this chapter is to discuss new sedimentary, stratigraphic, geochemical, palaeontological and structural data gathered during this study. Detailed stratigraphic and sedimentary data are largely lacking in the literature, therefore new data is used to test existing stratigraphic models (Şenalp 1979; Norman *et al.* 1980; Şenalp 1981; Erdoğan *et al.* 1996; Kaymakcı 2000). Key areas were re-mapped using the 1:500 000 scale maps of the General Directorate of Mineral Research and Exploration (MTA) (2002). The resulting new geological maps are presented in Figs. 3.3 and 3.16.

The region also contains Eocene lavas which are unique to the Central Anatolian basins. Sungurlu and Bayat are located in the Middle Eocene volcano-sedimentary belt, a Lutetian magmatic zone that spans almost the entire length of Turkey and trends parallel to the İzmir-Ankara-Erzincan suture zone (Keskin *et al.* 2008). The origin, tectonic setting, and magmatic development of the lavas are presently unresolved. Geochemical data from Sungurlu and Bayat are poorly represented the literature, this study is the first to discuss new data, and their implications from these key localities.

3.3 Previous work

Previous work on the Çankırı Basin includes studies of structure and stratigraphy (Norman 1975b; Tüysüz & Dellaloğlu 1992; Kaymakcı 2000; Karadenizli *et al.* 2003; Kaymakcı *et al.* 2009), palaeocurrents (Norman 1975a), biostratigraphy (Kazancı *et al.* 1999; Akgün *et al.* 2002; Okan & Hoşgör 2009) and regional tectonics (e.g. Koçyiğit *et al.* 1995; Erdoğan *et al.* 1996; Görür *et al.* 1998; Gürer & Aldanmaz 2002). The pre-Middle Eocene history of the basin has been interpreted as a collision-related basin (Erdoğan *et al.* 1996) and as a series of

foreland piggy-back basins (e.g. Koçyiğit *et al.* 1995; Gürer & Aldanmaz 2002; Kaymakcı *et al.* 2009) formed on south-verging ophiolitic thrust sheets. Studies of petroleum potential began in the 1960s (Akkuş 1962) and include recent organic geochemical studies (Altunsoy *et al.* 2004) and burial history and thermal maturity assessments (Tokatlı *et al.* 2006).

The Sungurlu area has previously been described in terms of stratigraphy and sedimentology (Şenalp 1979; Norman *et al.* 1980; Şenalp 1981). The Bayat locality has been studied in unpublished reports conducted by the Turkish Petroleum Corporation (TPAO) (e.g. Ayan 1969; Birgili *et al.* 1975). Kaymakcı *et al.*(2003) provide a structural and stratigraphic interpretation of the two areas. The stratigraphy of Erdoğan *et al.* (1996) is presented in Fig. 3.2.

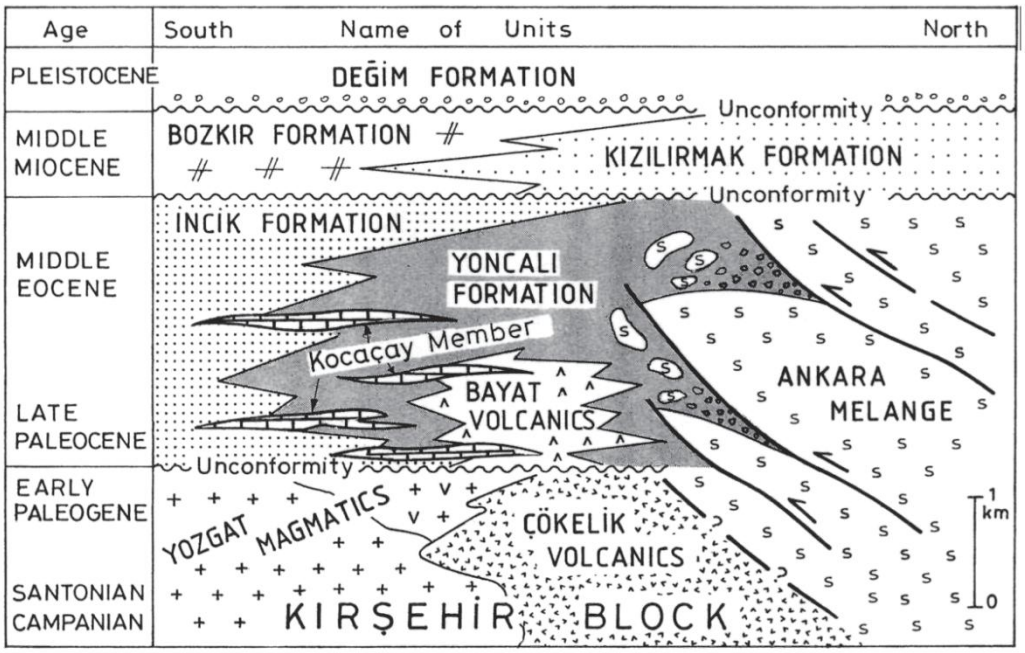

Figure 3.2 Generalised stratigraphic column of the Çankırı Basin, scanned from Erdoğan *et al.* (1996).

3.4 Stratigraphy and sedimentology

In this section, new stratigraphic and sedimentary data are presented based on measured stratigraphic logs, new field-mapping and the petrologic and palaeontological study of rock samples collected in the field. Lithofacies analysis is, to date, absent from the literature. Lithofacies are defined in terms of grain size, bed thickness, sedimentary structures and lithology.

3.4.1 Sungurlu

Based on this study, the following diagrams are presented: 1) a new geological map (Fig. 3.3); 2) a new stratigraphic interpretation (Fig. 3.4) and; 3) a schematic stratigraphic section showing correlations between measured sections. This diagram introduces newly-defined lithofacies (Fig. 3.5)

3.4.1.1 The İzmir-Ankara Accretionary Complex

The İzmir-Ankara Accretionary Complex is exposed to the east of the study area and is unconformably overlain by Neogene continental sediments (MTA 2002) and lavas of inferred Eocene age (see Section 3.7). It is dissected by the Sungurlu Fault Zone (Fig.3.3) which is interpreted as a dextral strike-slip splay fault (e.g. Kaymakcı *et al.* 2000) of the Mio-Pliocene to present North Anatolian Fault Zone (Şengör 1979). During this study, the complex was studied and mapped in detail between the villages of Cevherı and Kırankışla, because this area is well exposed and allows the contact between the complex and basin sediments to be examined in detail. It consists of S- to SE-verging thrust sheets and blocks of serpentinised ultra mafic material, radiolarian chert, gabbro and limestone. In contrast to the Kırıkkale Basin (Chapter 2) where the matrix is commonly volcaniclastic, the matrix of the İzmir-Ankara Accretionary Complex in the Sungurlu region is commonly poorly-lithified mudrock. The matrix is grey to brown and contains angular to rounded

cobble to boulder-sized clasts of limestone, basalt, radiolarian chert and serpentinite. Based on observations during this study, the complex has a faulted contact with Eocene conglomeratic basin-fill deposits.

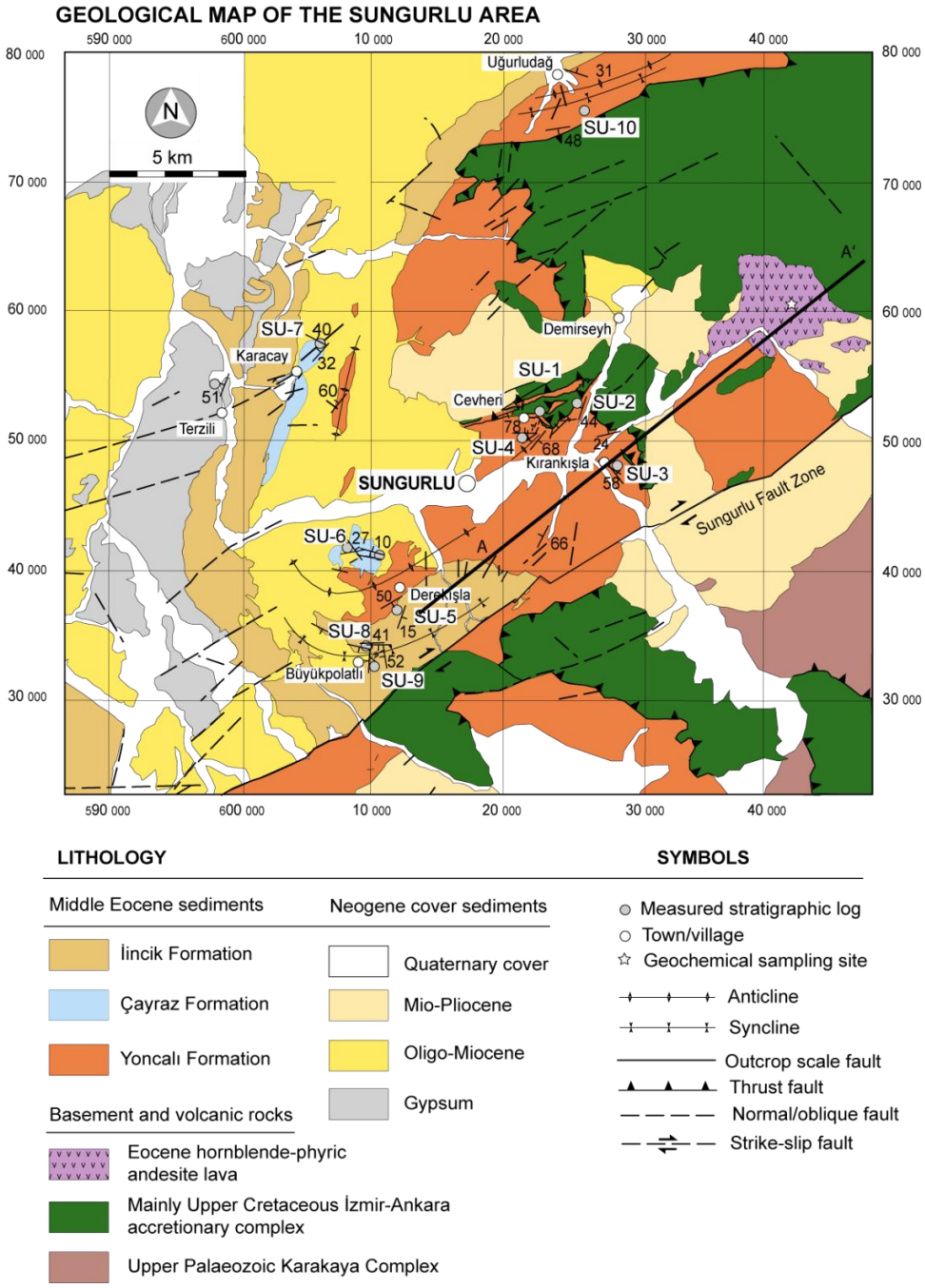

Figure 3.3 New geological map of the Sungurlu study area mostly based on field observations during this study, partly modified after MTA (2002) and Kaymakcı (2000). The grid system is UTM Zone 36.

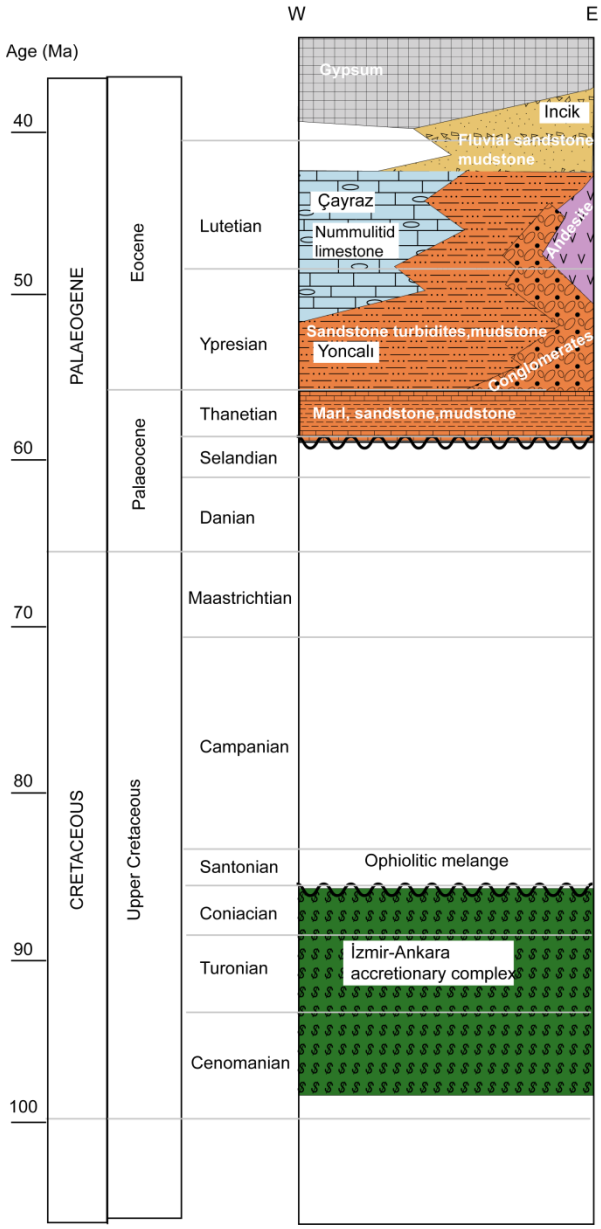

Figure 3.4 New stratigraphic scheme of the Upper Cretaceous-Oligocene interval proposed by this study, based on field observations and microfossil dating. All palaeontological data are from N. İnan & K. Taslı (pers. comm. 2009).

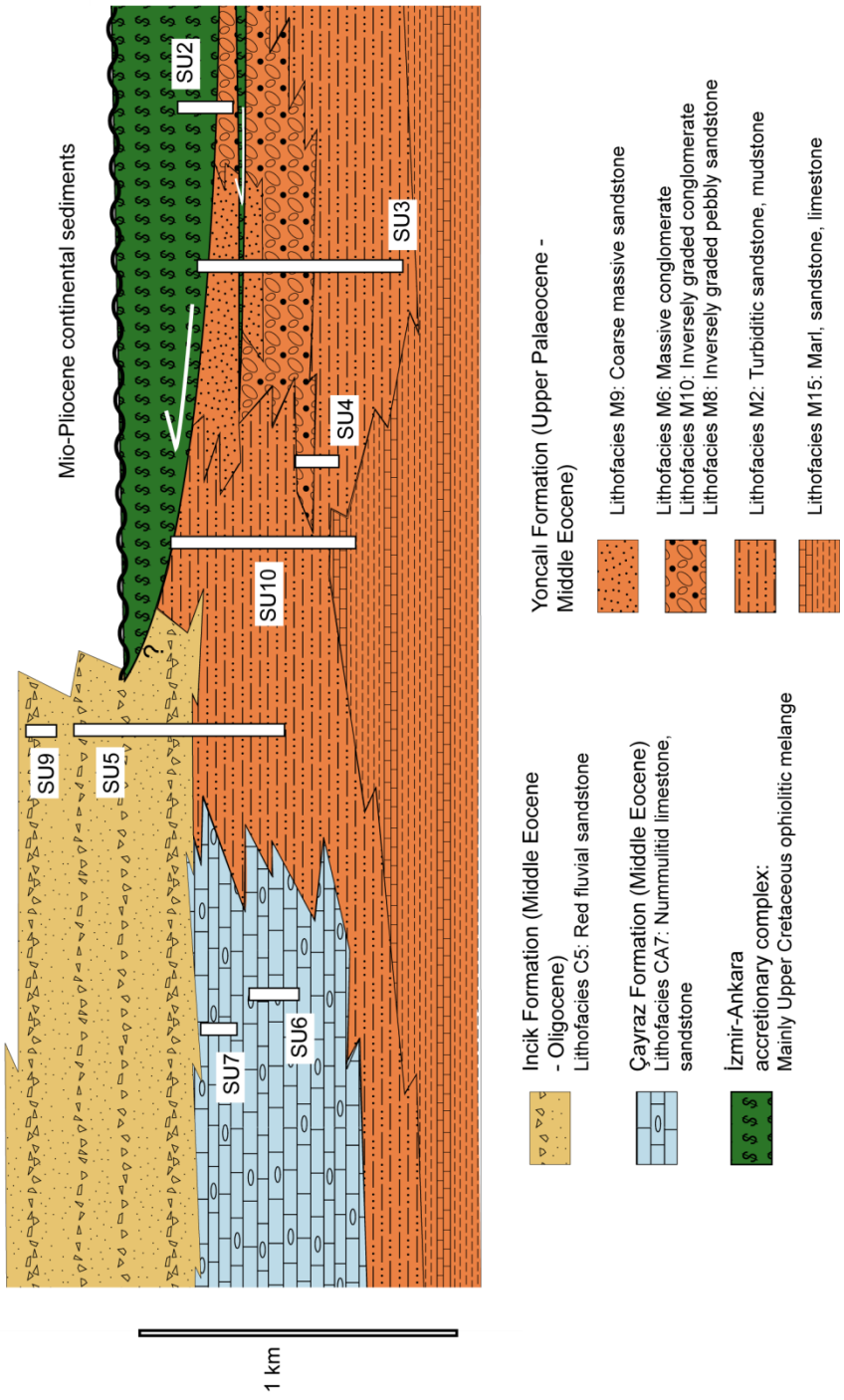

Figure 3.5 Stratigraphic section showing correlations between measured logs

3.4.1.2 The Yoncalı Formation: Late Palaeocene-Middle Eocene siliciclastic turbidites, marls, conglomerates.

The shallow-marine Yoncalı Formation was first named by Birgili *et al.* (1975) and is also referred to as the Cevherli Formation (Şenalp 1979; Norman *et al.* 1980). It has a lateral faulted contact with the İzmir-Ankara Accretionary Complex. The base of the formation is not exposed in the Sungurlu or Bayat areas. According to Şenalp (1979) the formation is 1427 m thick, but based on new measured logs in the Sungurlu locality, it is ~600 m thick. Şenalp (1979) reported pelagic foraminifera which were interpreted to indicate an Ypresian deposition age. The Yoncalı Formation is composed of a diverse array of lithofacies which are listed, with their assigned codes, below:

1) Massive conglomerates (M6)
2) Inversely graded conglomerates (M10)
3) Inversely graded pebbly sand (M8)
4) Sand-mud couplets (M2)
5) Massive sandstone beds (M9)
6) Marl, sandstone, calcarenite (M15)

The lithofacies are described and interpreted below.

3.4.1.2.1 Lithofacies (M6): massive conglomerates

Conglomerates and pebbly sands are typically exposed at the tectonic contact with the İzmir-Ankara Accretionary Complex in the eastern margin of the basin (Figs. 3.3, 3.6 and 3.7a). Lithofacies M6 is characterised by lens-shaped beds of up to ~2 m thick. Beds are generally flat based with irregular tops and regularly feature amalgamated depositional surfaces (Fig. 3.7b). Clasts are poorly sorted and range from pebble to boulder size. Clast composition is dominated by recrystallised limestone, basic volcanics and red radiolarian chert. Locally, boulder-sized clasts of

algal-rich grainstone contain the benthic foraminifera *Orosenia* sp. of Palaeocene? age (N. İnan & K. Taslı pers. comm. 2009).

3.4.1.2.2 Interpretation of lithofacies M6

Sediment transport was by debris flow and deposition by *en-masse* frictional freezing (Nemec *et al.* 1980). Clast composition indicates a source from the İzmir-Ankara Accretionary Complex.

3.4.1.2.3 Lithofacies M10: inversely graded conglomerate

Inversely graded conglomerates are exposed at locality SU2 (25921:52748) (Fig. 3.5) below the faulted contact with the İzmir-Ankara Accretionary Complex. They are arranged in matrix-supported beds 0.6 to 4 m thick, with erosive bases and poorly sorted clasts which range in size from pebble to boulder. The matrix is coarse sandstone containing basic volcanic granules. Individual beds commonly feature an abrupt transition from the underlying pebbles to the overlying coarser clasts (Fig. 3.7c). Clast imbrication is locally well developed and indicates a unidirectional subaqueous flow from NE to SW (see Section 3.5 for palaeocurrent data).

3.4.1.2.4 Interpretation of lithofacies M10

Sediment transport was probably by sandy debris flow, and the deposition by *en-masse* sediment freezing (Lowe 1982). The origin of inverse grading in debris flows is debated (Legros 2002) and is likely to be caused by shearing at the base of the flow (e.g. Nichols 1999) or kinetic sieving (Middleton 1970).

3.4.1.2.5 Lithofacies M8: inversely graded pebbly sand

Inversely graded gravels (lithofacies M10) pass upwards into inversely graded pebbly sand (lithofacies M8). This lithofacies features beds of 0.7-2 m thickness, locally amalgamated into units containing up to five depositional surfaces. The sandstone is very coarse and dark grey; clasts are up to pebble size and are composed of basic volcanics, limestone and radiolarian chert. Pebbles are arranged in ~10 cm-thick zones near the top of individual beds. Clast imbrication (Fig. 3.7d) indicates a unidirectional flow from north-northeast to south-southwest.

3.4.1.2.6 Interpretation of lithofacies M8

Transport is interpreted as being by high concentration turbidity current while deposition was by frictional freezing of a traction carpet at the base of the flow (Lowe 1982).

These conglomeratic deposits (lithofacies M6, M10 and 8) have not been described in detail before. An Upper Palaeocene 2 to 5 m-thick basal conglomerate sequence was described by Erdoğan *et al.* (1996) in the south of the basin, but is probably derived from underlying magmatic rocks. In contrast, the coarse clastic deposits from the Sungurlu area were deposited in debris flows and high density turbidity flows ahead of an advancing thrust front represented by the İzmir-Ankara Accretionary Complex.

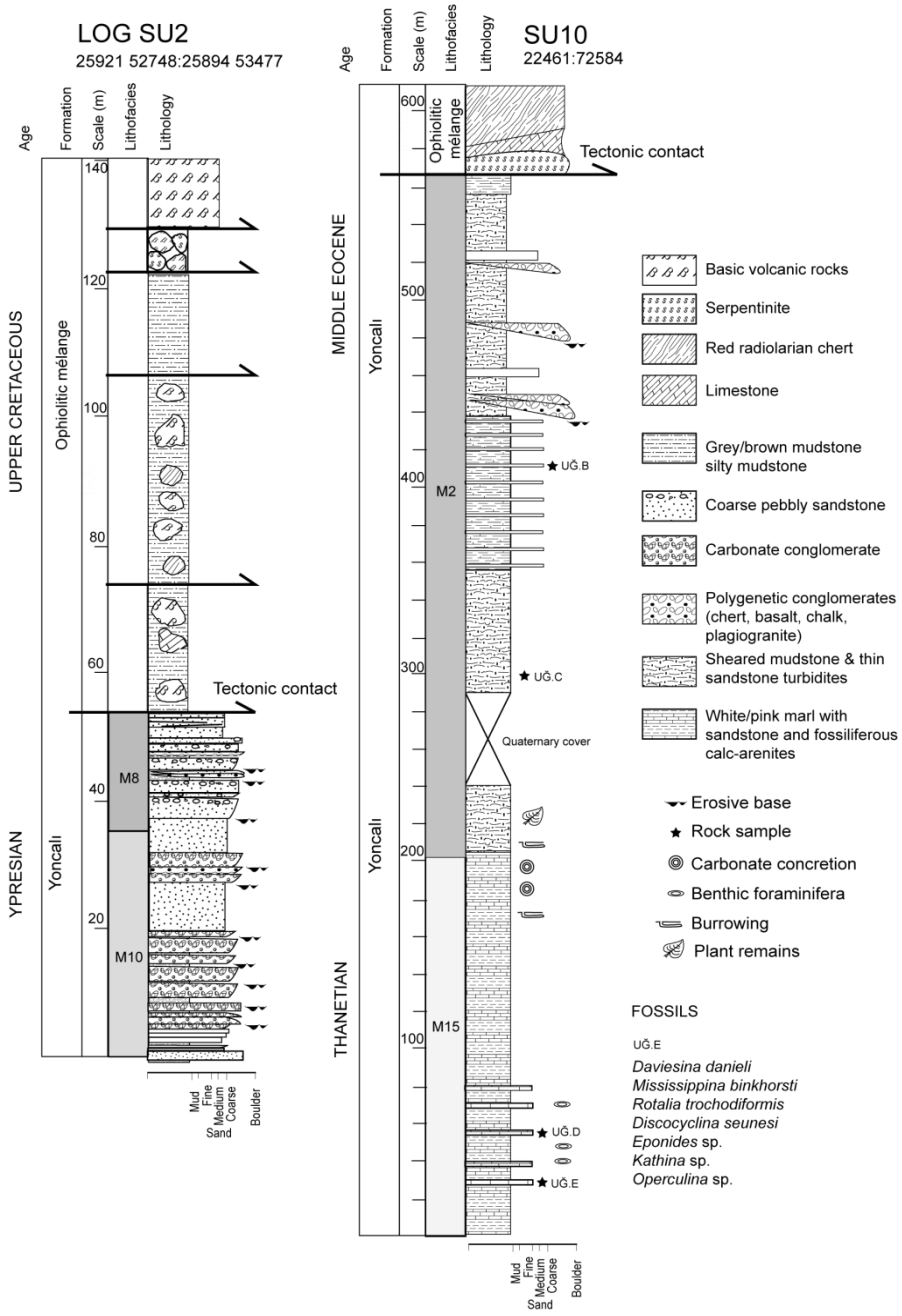

Figure 3.6 Measured logs SU2 (left) and SU10 (right), of the İzmir-Ankara Accretionary Complex that is thrust onto the Upper Palaeocene-Middle Eocene Yoncalı Formation, all sedimentary data are after this study, all palaeontological data are from N. İnan & K. Taslı (pers. comm. 2009).

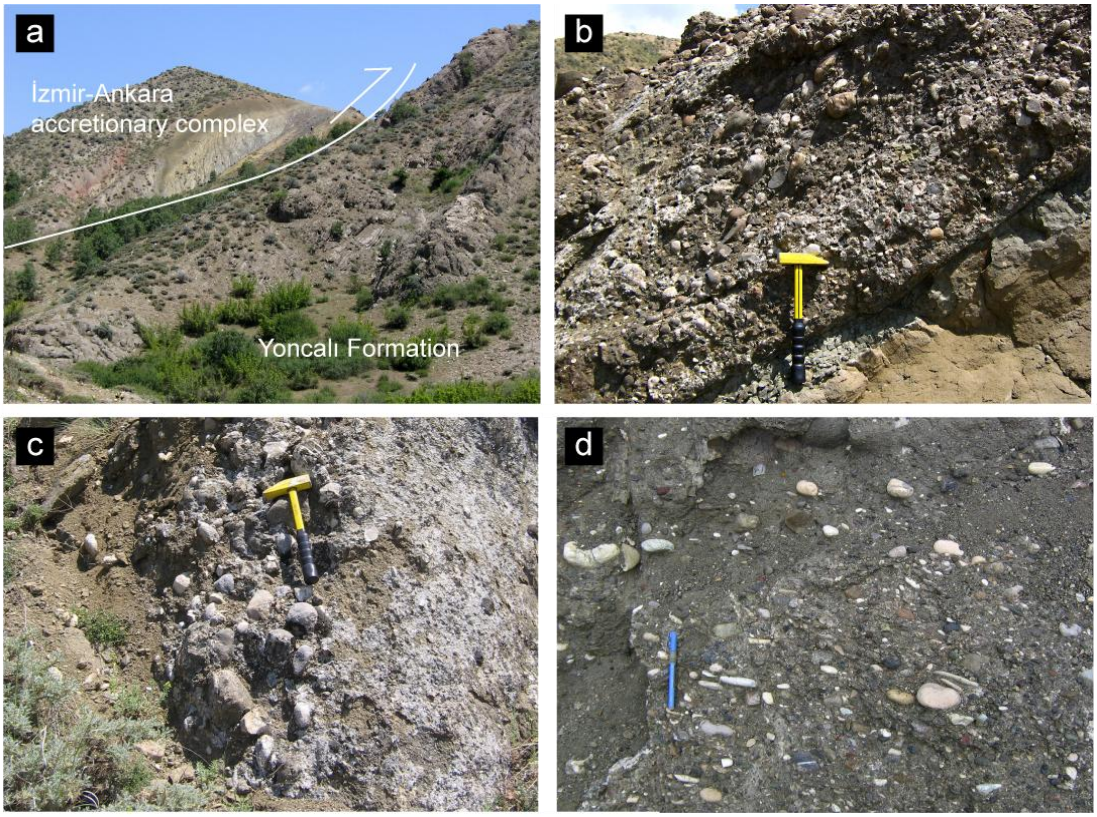

Figure 3.7 Representative field photographs of **(a)** the İzmir-Ankara Accretionary Complex thrusting over the Upper Palaeocene-Middle Eocene Yoncalı Formation (looking ~north), **(b)** massive conglomerate (lithofacies M6), **(c)** inversely graded conglomerate (lithofacies M10), **(d)** pebbly grey sandstone (lithofacies M8), note the well developed clast imbrication.

3.4.1.2.7 Lithofacies M2: Eocene turbiditic sand-mud couplets

Lithofacies M2 is represented by Eocene turbiditic sand-mud couplets and is the most widespread lithofacies of the Yoncalı Formation. It is represented by grey to yellow mudstones, siltstones, mostly coarse-grained sandstones and minor conglomerates. A representative section was measured southeast of Derıkişla village (Log SU5) (11875:38225). Sandstone beds are ~0.1 to 0.4 m thick with planar tops and bases, scoured bases are rare. Beds tend to show weakly-developed normal grading. Sedimentary structures are otherwise rare, but locally include plane parallel laminae (Bouma Division T_b), horizontal burrowing and ripple marks. Sandstones are typically composed of detritus from the İzmir-Ankara Accretionary Complex; locally, however, sandstones contain reworked large benthic foraminifera. One sample (SU2.4A; Log SU5; Fig 3.9) contained *Nummulites globulus* Leymerie,

Nummulites ataticus Leymerie, *Assilina prisca* Drobne, *Assilina* cf. *placentula, Nummulites* cf. *pengaronensis, Orbitoclypeus* cf. *ramaraoi, Gypsina marianensis* Hanzawa, which suggests an Ypresian age assigned (N. İnan & K. Taslı pers. comm. 2009).

3.4.1.2.8 Interpretation of lithofacies M2

Normal grading and horizontal lamination suggest that the sandstone deposits of lithofacies M2 were probably deposited from turbidity currents. The presence of benthic foraminifera indicates that turbidites reworked Ypresian shallow-marine self-type deposits into the basin depo-centre, possibly on an upper slope- to slope-type setting.

3.4.1.2.9 Lithofacies M9: massive sandstone beds

Toward the eastern basin margin, close to the İzmir-Ankara Accretionary Complex, sandstone deposits increase in bed thickness and grain size. These deposits represent lithofacies M9. Thick- to medium-bedded, disorganised dark grey sands are common toward the top of Log SU3 (Fig. 3.9) north-east of Karınkışla village. Sandstones are litharenites according to the classification scheme of Pettijohn *et al.* (1987). Beds are between 0.4 to 2.7 m thick and mostly structureless, but locally display crude normal grading with pebbly bases. They are typically lenticular and laterally extensive for up to ~50 m. They are intercalated with thin (<0.5 m) beds of siltstone and mudstone. Angular clasts of "floating" limestone up to cobble size are abundant throughout this lithofacies, spheroidal weathering is widespread.

3.4.1.2.10 Interpretation of lithofacies M9

Pebbly bases and crude normal grading are suggestive of S_1 and S_2 Lowe-type high density turbiditic deposits. However, "floating" clasts are typical of sandy debris flows (Shanmugam 2000). The deposits, however, are interpreted to represent proximal deposits, deposited in channels, close to active thrust faulting. The top of the Karınkışla sequence (Log SU3; Fig. 3.9) is characterised by imbricated thrust contacts with the İzmir-Ankara Accretionary Complex. These observations confirm those of Erdoğan *et al.* (1996), who described this lithofacies as an "intra-nappe flysch facies".

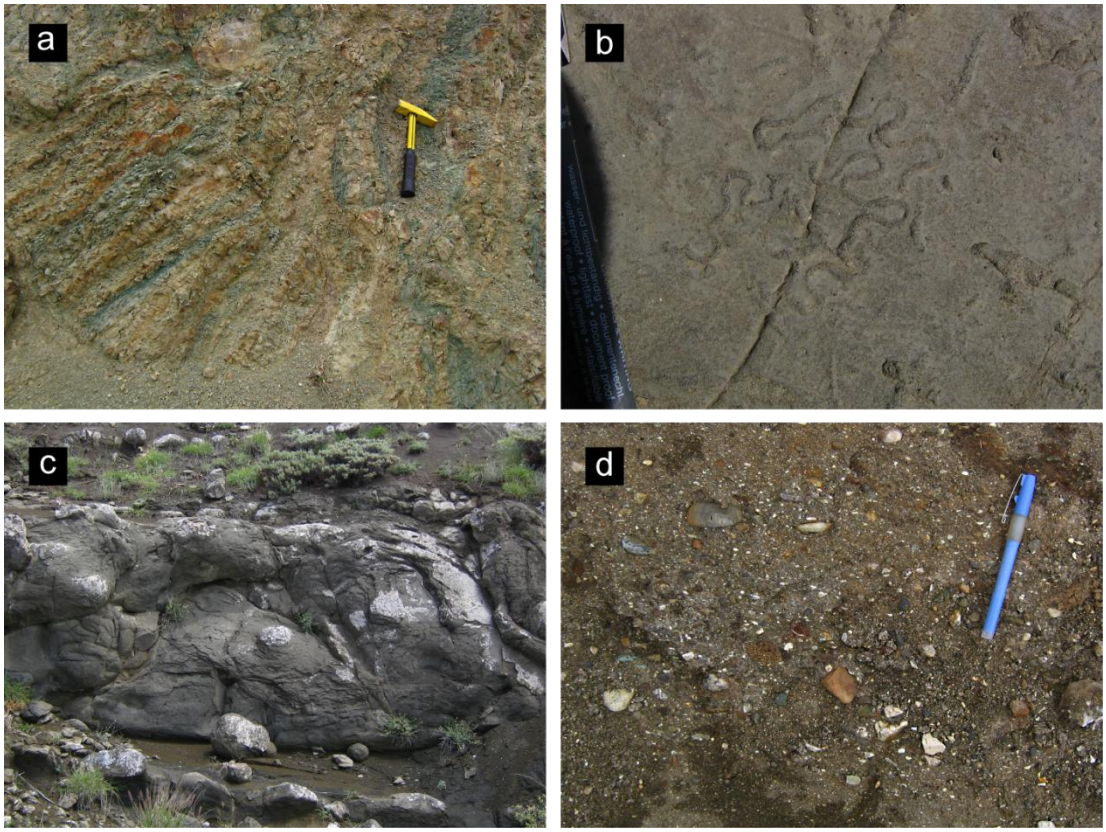

Figure 3.8 Field photographs of the Upper Palaeocene-Middle Eocene Yoncalı Formation, **(a)** sheared sandstone-mudstone couplets of lithofacies M2, **(b)** horizontal burrows on the base of a sandstone bed in lithofacies M2, **(c)** grey sandstone of lithofacies M9, the bed is ~1 m thick, (d) sub-angular pebbles associated with lithofacies M9.

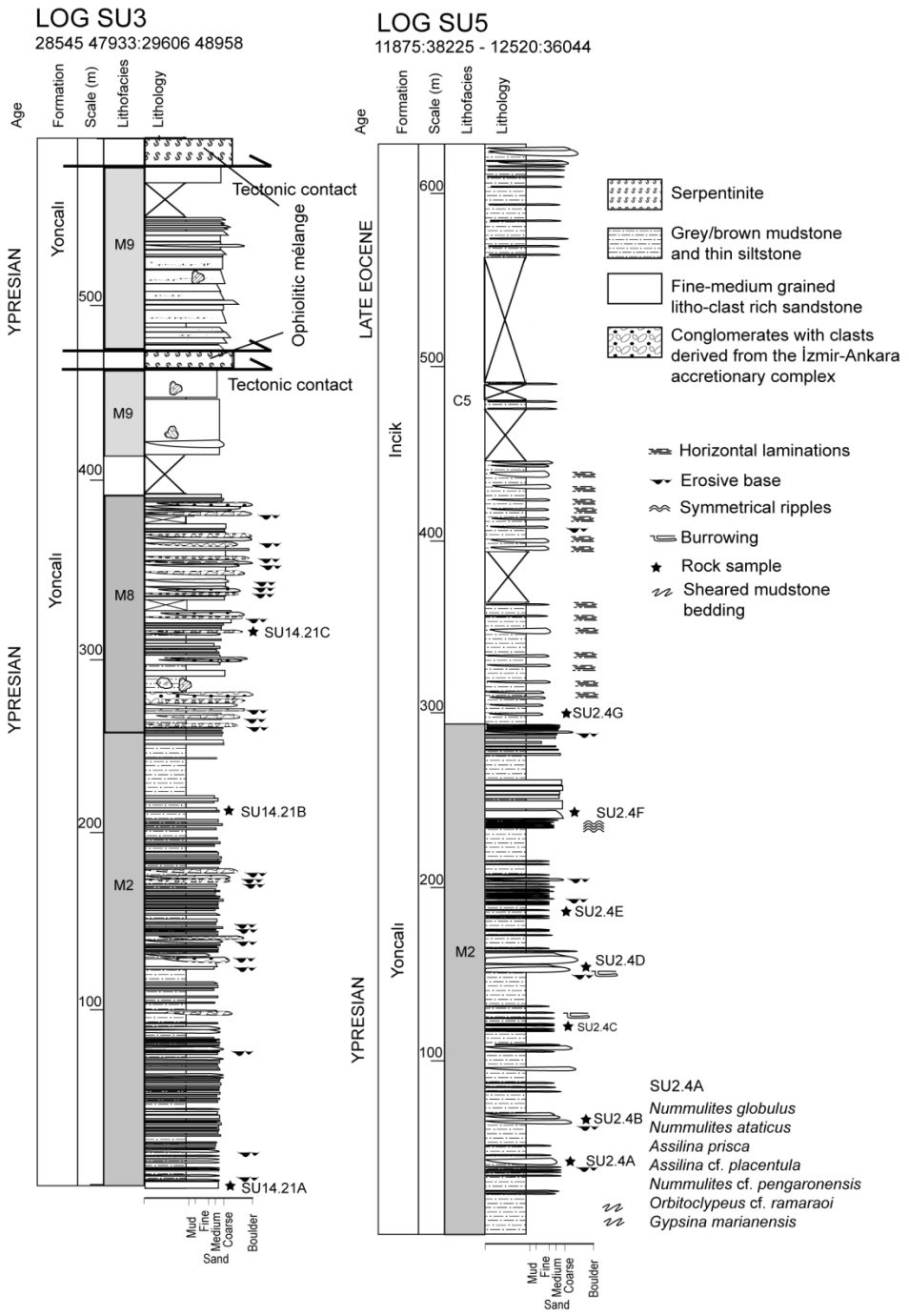

Figure 3.9 Measured logs **SU3** and **SU5**. SU3 shows the tectonic contact with the İzmir-Ankara Accretionary Complex. SU5 shows the Ypresian Yoncalı Formation grading vertically into the post-Middle Eocene İncik Formation. All sedimentary data are from this study, all palaeontological data are from N. İnan & K. Taslı (pers. comm. 2009).

3.4.1.2.11 Lithofacies M15: Upper Palaeocene marl, sandstone, calcarenite

Lithofacies M15 is exposed to the south of Uğurludağ (Log SU10; Fig. 3.6) and consists of ~200 m of thin, burrowed, white/pink marls interbedded with thin sandstones and bioclastic algal calc-arenites. Based on the presence of the large benthic foraminifera *Daviesina danieli* Smout, *Mississippina binkhorsti* Reuss, *Rotalia trochodiformis* Lamarck, *Discocyclina seunesi* Douville, *Eponides* sp., *Kathina* sp. and *Operculina* sp., a latest Palaeocene (Thanetian) age is assigned (N. İnan & K. Taslı pers. comm. 2009). These new data are give a deposition date which is in agreement with a recent study (Kaymakcı *et al.* 2009).

3.4.1.2.12 Interpretation of lithofacies M15

These deposits have not been described previously, and represent shallow marine shelf-type deposits which lie stratigraphically at the base of the Yoncalı Formation (Erdoğan *et al.* 1996).

3.4.1.2.13 Summary and interpretation of the Yoncalı Formation.

Deposits of the Yoncalı Formation discussed above indicate a lateral transition from coarse, proximal clastic conglomerates and pebbly sands to distal clastic thinly-bedded clastic turbidites. At the base of the formation is a sequence of marl and sandstone containing benthic foraminifera. Based on microfossil content, the age of the Yoncalı Formation is Upper Palaeocene to Ypresian, possibly Lutetian. This is in agreement with previously described dates, and, because deposition was syn-tectonic, constrains the age of thrust faulting at the basin margin.

3.4.1.3 The Çayraz Formation (Ypresian-Lutetian)

The Çayraz Formation has a limited exposure in the Sungurlu study area. It consists of two outcrops situated ~5 km to the southwest of Sungurlu (at Kepir Tepe) and at Karaçay village, to the northwest of Sungurlu. Other names given to this formation are the Kepir Tepe Formation (Şenalp 1979; Norman *et al.* 1980) the Kocaçay Formation (Kaymakcı *et al.* 2009) and the Kocaçay Member (Erdoğan *et al.* 1996). The Çayraz Formation is represented by lithofacies CA7. In this study area, the Çayraz Formation lacks the coarse red deltaic sandstones observed in the Kırıkkale area, and consists of grey and red mudstones (Fig. 3.10a) passing up into limestones containing large benthic foraminifera (Fig. 3.10b). A description of the sedimentary succession from two localities: 1) Kepir Tepe and; 2) Karaçay follows below.

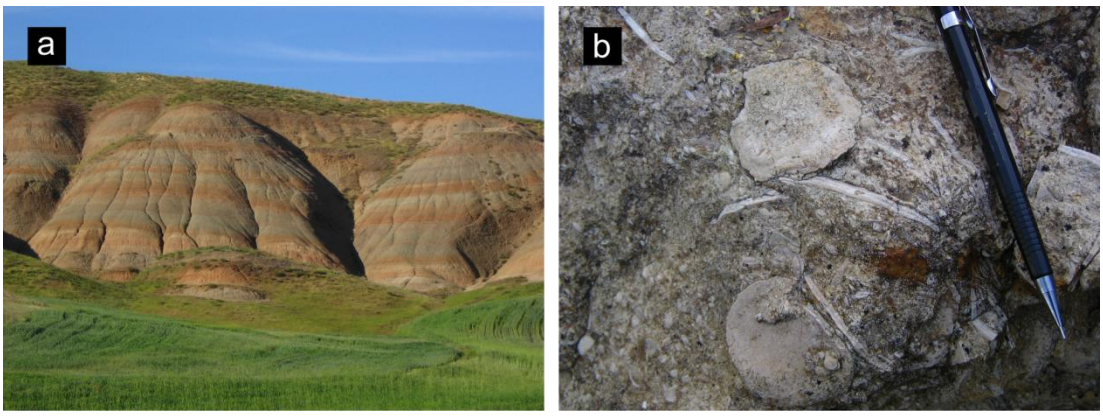

Figure 3.10 Field photographs of **(a)** alternating red and grey mudstone in the Middle Eocene Çayraz Formation (Karacay locality), the outcrop is ~40 m thick, **(b)** large Nummulites in Çayraz Formation limestone.

3.4.1.3.1 Lithofacies CA7: shelf-type carbonates, mudstone and sandstone

i) Kepir Tepe

The outcrop at Kepir Tepe (Log SU6; Fig. 3.12a), ~100 m thick, consists of a ~25 m sequence of thick (<7 m) massive benthic foraminiferal grainstone beds

intercalated with siltstones and marls. A full list of benthic foraminifera is given below:

Sample SU5.7

Daviesina danieli Smout, *Asterigerina rotula* (Kaufmann), *Smoutina* sp., *Nummulites globulus* Leymerie, *Nummulites formosus* De La Harpe, *Assilina prisca Assilina* cf. *placentula*, *Nummulites* cf. *pengaronensis*, *Coccoarota orali* İnan, *Sphaerogypsina globulus* (Reuss), *Lockhartia* cf. *haimei*, *Lockhartia diversa* Smout

Sample SU5.7A

Anomalina sp., *Smoutina* sp., *Nummulites globulus* Leymerie, *Nummulites ataticus* Leymerie, *Alveolina* cf. *pisella*, *Assilina* cf. *placentula*, *Nummulites* cf. *pengaronensis*, *Austrotrillina* cf. *eocenica*, *Medocia blayensis* Parvati, *Gypsina marianensis* Hanzawa.

Both of these assemblages indicate an Ypresian deposition date (N. İnan & K. Taslı pers. comm. 2009) which is in agreement with previous studies (Şenalp 1979; Erdoğan *et al.* 1996; Kaymakcı *et al.* 2009). This lithofacies is interpreted to occur in banks, shoals and channels in a restricted carbonate platform setting (e.g. Flügel 2004). The grainstones pass upwards into brown, poorly lithified mudstones containing abundant basaltic cobbles and also conglomerates composed of sub-angular cobble-sized clasts of serpentinites, feldspar-phyric basalt and radiolarian chert. The upper 70 m of the succession features brown mudstones, thin planar-bedded marls and thinly bedded sandstone (Log SU6; Fig, 3.12a).

ii) Karaçay

The succession to the northeast of Karaçay, ~150 m thick, consists of red and grey mudstones. They pass up into foraminiferal packstones and grainstones and sandy limestones yielding echinoids and gastropods. Beds are 0.4 - 1.4 m thick and normally graded, which suggests sediment reworking.

Thin section study reveals that the benthic foraminiferal limestones. Fauna present in sample SU12.17 (Fig. 3.11b) are *Asterigerina rotula* (Kaufmann), *Assilina* sp., *Nummulites* cf. *pengaronensis, Orbitoclypeus* cf. *ramaraoi* and *Discocyclina scalaris* (Schlumberger) (Fig. 3.10b) giving a Lutetian date (İnan & Taslı pers. comm.). This date confirms previous interpretations (e.g. Erdoğan *et al.* 1996). A weakly defined bioclast alignment suggests reworking in a low-energy environment. Debris flow conglomerates within channels are made up of pebble-sized clasts of basalt, radiolarian chert, sandstone and serpentinite and scour into underlying mudstones.

3.4.1.3.2 Interpretation of lithofacies CA7

The Çayraz Formation in the Sungurlu area represents shelf-type carbonate sedimentation, probably in banks and shoals, intercalated with periods of siliciclastic influx. This occurred contemporaneously with deeper-water siliciclastic deposition which characterises lithofacies M2 of the Yoncalı Formation, and episodically transported carbonate material into a slope-type setting. The Ypresian – Lutetian deposition date is younger than the deltaic sequences in the Kırıkkale Basin (see Chapter 2).

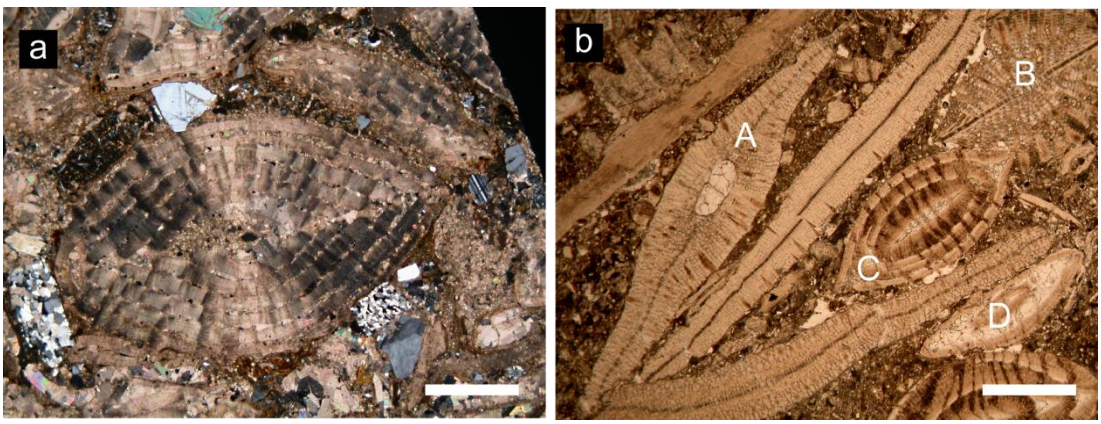

Figure 3.11 Photomicrographs of **(a)** Ypresian Nummulitid in a turbidite of the Yoncalı Formation; note the sub-angular quartz and plagioclase grains, **(b)** Foraminiferal packstone (sample SU12.17) from the Karaçay section of the Çayraz Formation, A - *Discocyclina scalaris* (Schlumberger) B - *Orbitoclypeus* c.f. *ramaraoi* C – *Nummulites sp.* D – *Assilina sp.*, scale bars = 1 mm. Data are from N. İnan & K. Taslı (pers. comm. 2009).

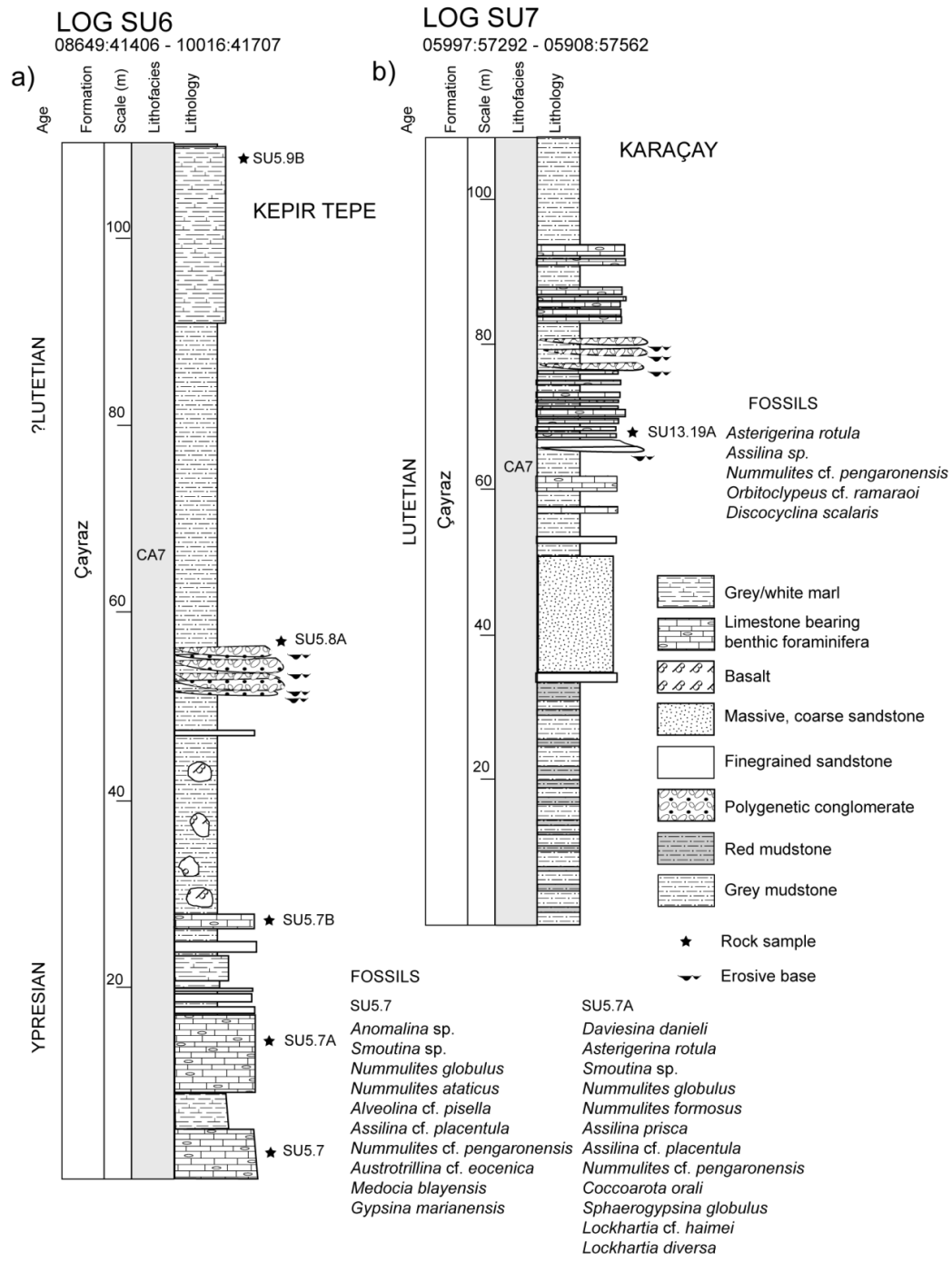

Figure 3.12 Measured logs through the Middle Eocene Çayraz Formation, **(a)** the Ypresian Kepir Tepe sequence, **(b)** the Lutetian Karaçay sequence. Sedimentary data are from this study, all palaeontological data are from N. İnan & K. Taslı (pers. comm. 2009).

3.4.1.3.3 The Incik Formation (?Middle-Late Eocene to Oligocene)

In the measured Log SU5 (Fig. 3.9), the Lower to Middle Eocene Yoncalı Formation shallows upwards and grades vertically into the Incik Formation. This formation was first named in an unpublished TPAO report (Azız 1975) and is also known as the Büyük Polatlı Formation (Şenalp 1979; Norman *et al.* 1980; Şenalp 1981). It is represented by continental red clastics and is one of the most abundant and thickest (~2000 m) in the Çankırı Basin (Kaymakcı *et al.* 2009). Its age is not well-constrained owing to a lack of fossils, but must be younger than Ypresian. Based on stratigraphic relationships, most authors cite a Middle Eocene to Oligocene age (e.g. Şenalp 1979; Kaymakcı *et al.* 2009). Previous interpretations suggested that the Incik Formation represents a meandering river depositional environment (Şenalp 1979; Norman *et al.* 1980; Erdoğan *et al.* 1996).

3.4.1.3.4 Lithofacies C5: red terrigenous sandstone

The Incik Formation is represented by lithofacies C5, which is characterised by red sandstone, mudstone and conglomerates. The base of lithofacies C5, as seen in Log SU5 (Fig. 3.9) is represented by red sandstone, in beds 0.8 to 3.5 m thick. Beds are lenticular with scoured bases. Angular, pebble-sized clasts derived from the İzmir-Ankara Accretionary Complex are abundant at the base of some beds (Fig. 3.13a). Normal grading and parallel lamination are common (Fig. 3.13b). The sandstones are intercalated with thick packages of red/purple mudstones. Further up, the sequence, near the village of Büyük Polatlı (10011:34731; Fig. 3.14), the İncik Formation is characterised by of coarse red sandstone channel-fill deposits. Beds range in thickness from 0.6 - 2.5 m and are laterally extensive for up to ~30 m. Bed bases are commonly erosive and contain angular clasts of limestone. The beds commonly fine up into medium- to coarse-grained sandstone.

The İncik Formation is also exposed in the west of study area near Karacay village where it is faulted against deformed Neogene gypsum. Sandstones are purple, and frequently show parallel lamition, cross-bedding and wavy flaser bedding.

3.4.1.3.5 Interpretation of lithofacies C5

The red/purple colour and absence of marine fossils suggest that the İncik Formation was probably deposited in a non-marine setting. The coarse sandstone deposits are most likely to represent meandering channel-fill deposits, with the angular lag clasts at the base, material that a river can only move at peak flood time (Walker & Cant 1986). Some features of classic meandering river system models are, however, lacking, including lateral accretion surfaces on point bars and trough cross-bedding. However, Walker & Cant (1986) speculated that a lack of trough cross-bedding and the development of horizontal lamination could result from high flow velocities, shallow-water depths or fine grain sizes. Mudstone and thin sandstone intercalations possibly represent a flood-plain environment. During this study, however, no further features of fluvial flood plains (e.g. caliche nodules, root traces, desiccation cracks) (Walker & Cant 1986) were observed. Desiccation cracks have been reported at the southern margin of the basin (Erdoğan *et al.* 1996).

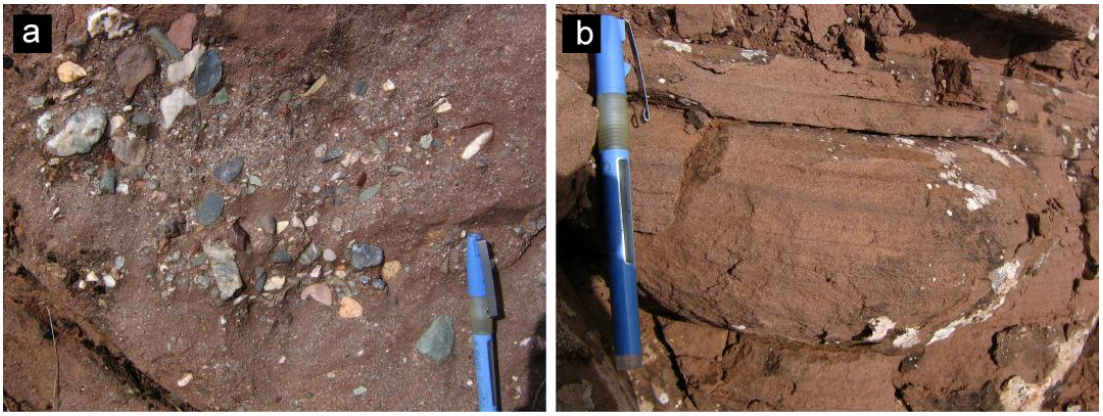

Figure 3.13 Field photographs of **(a)** angular clasts derived from the İzmir-Ankara Accretionary Complex, **(b)** horizontal laminations in coarse red sandstones of the Upper Eocene-Oligocene İncik Formation.

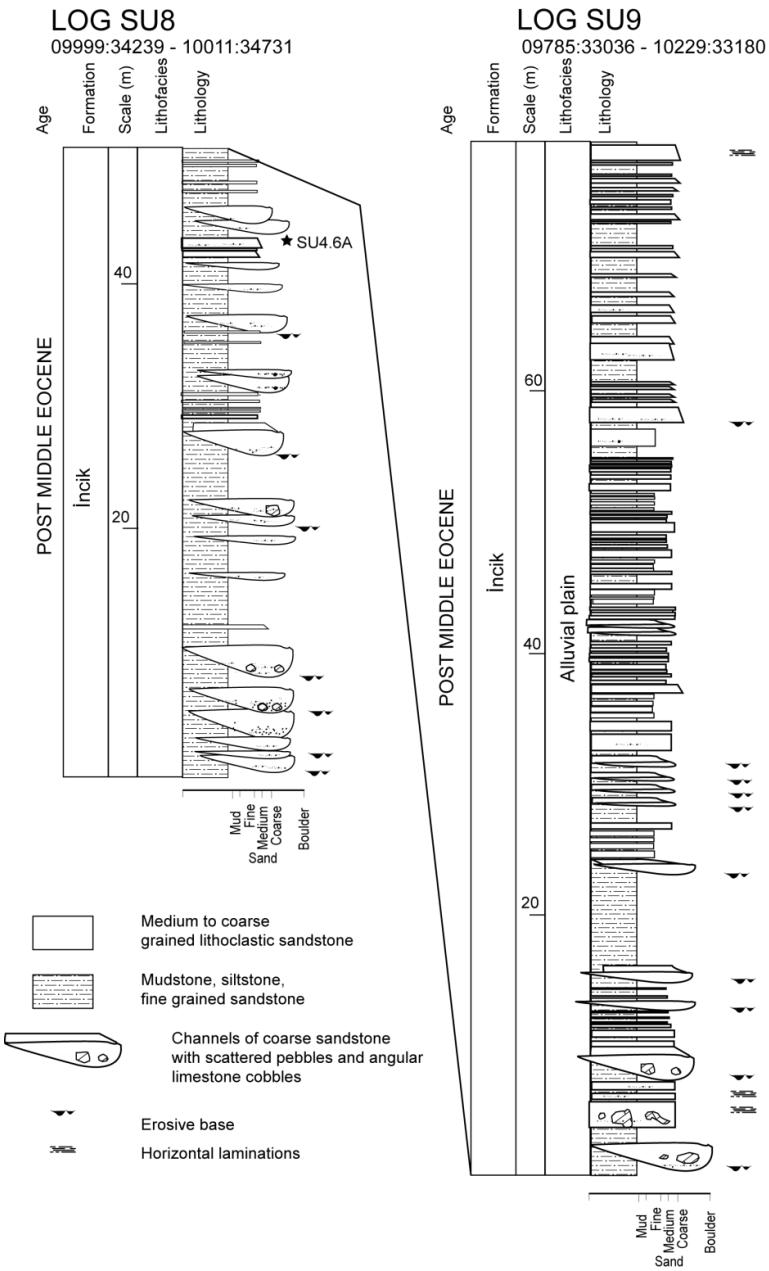

Figure 3.14 Measured logs SU8 and SU9 through lithofacies 5 of the ?Middle Eocene-Oligocene Incik Formation, sedimentary data are from this study.

3.4.2 Bayat

This section discusses new stratigraphic and sedimentary data from the Bayat study area. Based on this study, the following diagrams are presented: 1) a new geological map (Fig. 3.15); 2) a new stratigraphic interpretation (Fig. 3.16).

3.4.2.1 The İzmir-Ankara Accretionary Complex

The İzmir-Ankara Accretionary Complex is exposed to the north of the Bayat study area (Fig. 3.15). The complex, as seen near Kunduzlu (02724:11498), consists of thrust sheets and blocks of radiolarian chert, grey shale, sheared pebbly sandstone, serpentinite and recrystallised limestone. The complex has a tectonic contact with the Upper Palaeocene-Middle Eocene Yoncalı Formation.

3.4.2.2 The Yoncalı Formation (Upper Palaeocene-Middle Eocene)

The Yoncalı Formation in the Bayat area is ~700 m thick and grades laterally and vertically into the Middle Eocene Bayat and Karabalçık formations (see Section 3.4.2.5). It is overthrust by the İzmir-Ankara Accretionary Complex near Kunduzlu village (Log BAY1; Fig. 3.18). In contrast to the Sungurlu area, the conglomerates and pebbly sandstones of lithofacies M6, M10 and M8 are absent. Instead, the Yoncalı Formation in the Bayat area is represented by two lithofacies: 1) the dominant lithofacies of the lowermost deposits are silt-grade sediments (lithofacies M13), whereas the uppermost part of the formation is represented by thinly-bedded sandstone-mudstone couplets (lithofacies M2) and thin conglomerate beds.

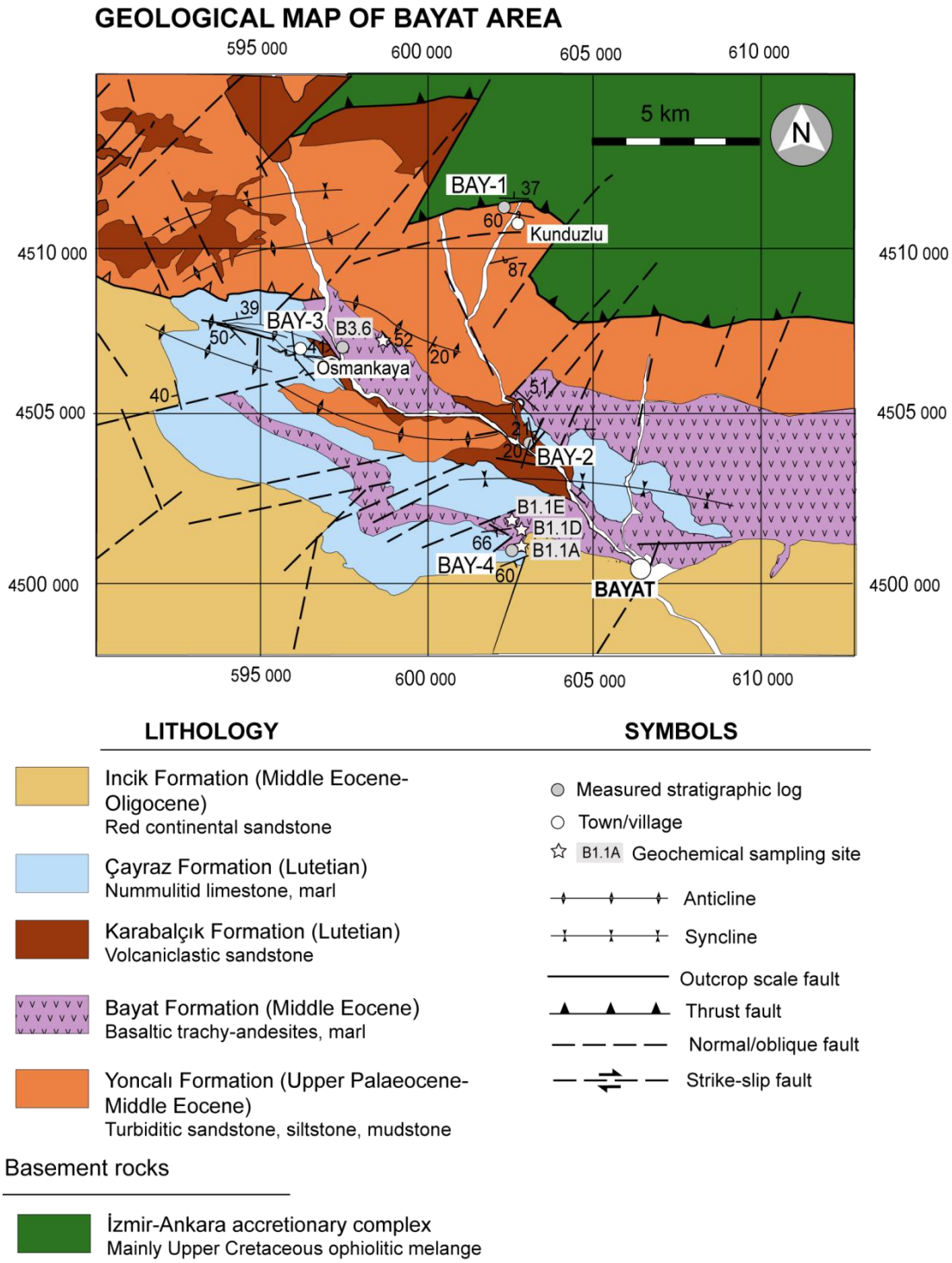

Figure 3.15 Geological map of the Bayat study area, partly modified after Kaymakcı (2000). The grid system is UTM Zone 36.

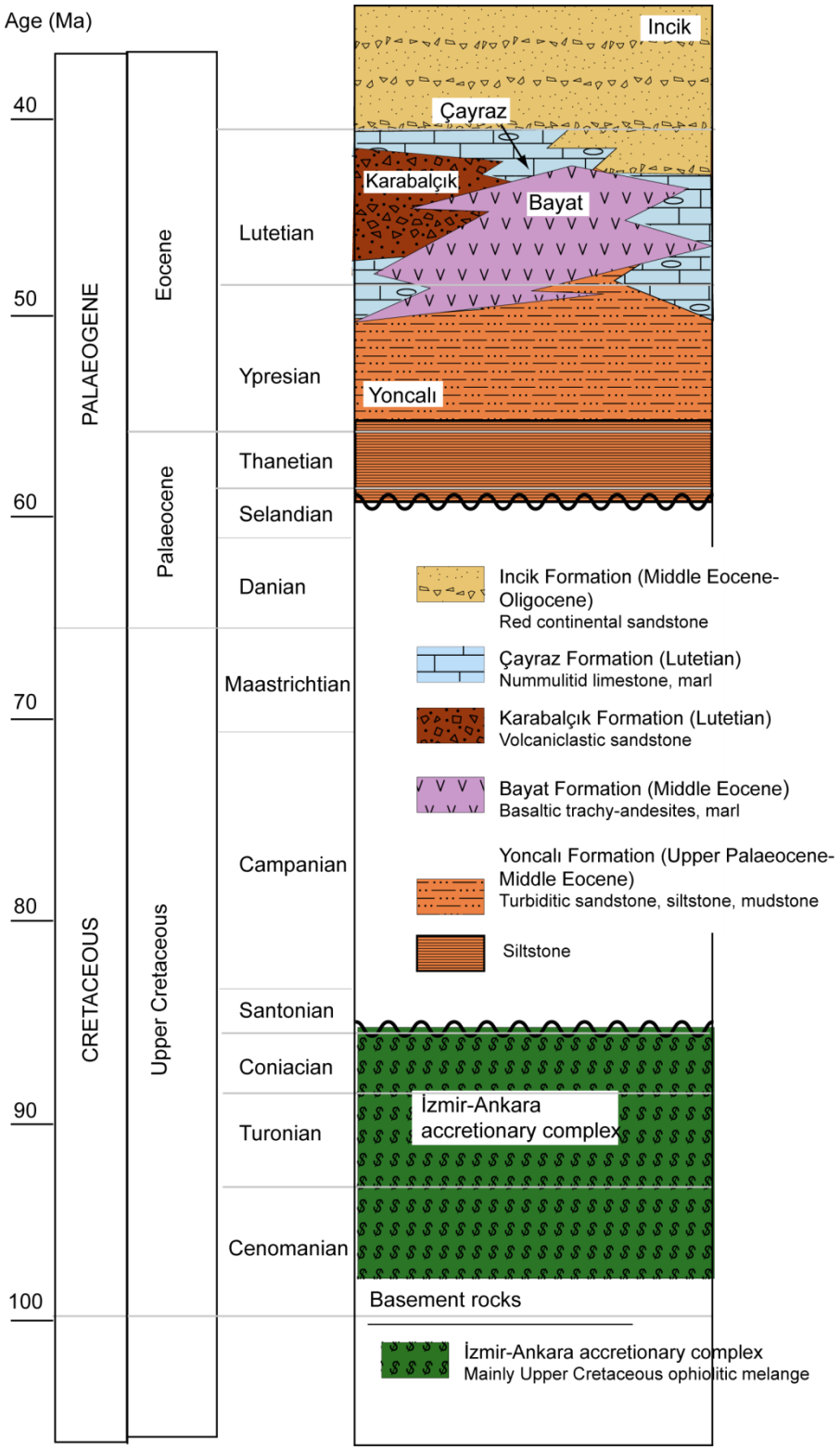

Figure 3.16 Stratigraphic scheme proposed by this study, based on field observations and microfossil dating. All palaeontological data are from N. İnan & K. Taslı (pers. comm. 2009).

3.4.2.2.1 Lithofacies M13: graded, stratified siltstone

Siltstone beds comprise a ~100 m-thick sequence, which is well developed to the north of the study area near Kunduzlu. Beds are overturned and sheared near the tectonic contact with the İzmir-Ankara Accretionary Complex. Beds are commonly ~10 cm thick and exhibit scoured bases and gradational tops (Fig. 3.17a). Normal grading, convolute and horizontal laminae are commonly developed, vertical burrowing is locally present.

3.4.2.2.2 Interpretation of lithofacies M13

The sediment transport was probably by dilute, low concentration turbidity currents and deposition was grain-by-grain from suspension, followed by traction transport to produce lamination (Pickering *et al.* 1989).

3.4.2.2.3 Lithofacies M2: sandstone-mudstone couplets

The upper part of the Yoncalı Formation consists of alternations of grey sandstone and dark grey fissile mudstone (Fig. 3.17b). Sandstone beds range in thickness from 0.4 – 1.0 m and are mostly massive. Parallel laminae were observed locally and probably represent Bouma division T_b. Bed bases are sharp while tops are sharp, to gradational.

3.4.2.2.4 Interpretation of lithofacies M2

Sediment transport was by turbidity current and deposition was from suspension followed by traction transport as bedload (Pickering *et al.* 1989).

3.4.2.2.5 Summary and interpretation of the Yoncalı Formation in the Bayat area.

No fossils were observed during this study, however, Kaymakcı *et al*. (2009) inferred an Upper Palaeocene to Middle Eocene date on the basis of pelagic foraminifera. Deposition of the Yoncalı Formation was therefore contemporaneous in the Sungurlu and Bayat localities. However, thrust imbrication of the İzmir-Ankara Accretionary Complex produced overturned folding in siltstone beds at Bayat, in contrast to the imbricated conglomerates at Sungurlu.

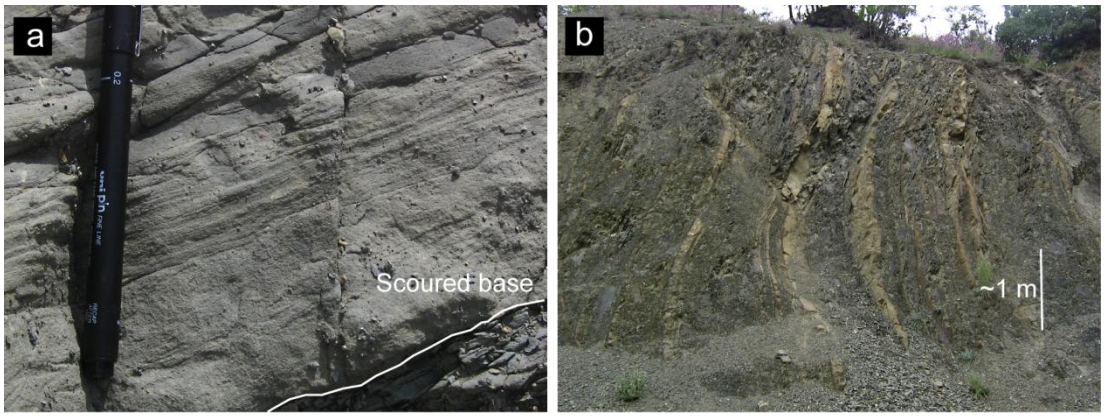

Figure 3.17 Field photographs from the Upper Palaeocene-Middle Eocene Yoncalı Formation in the Bayat area, **(a)** laminated grey siltstone, **(b)** turbiditic sandstone-mudstone couplets.

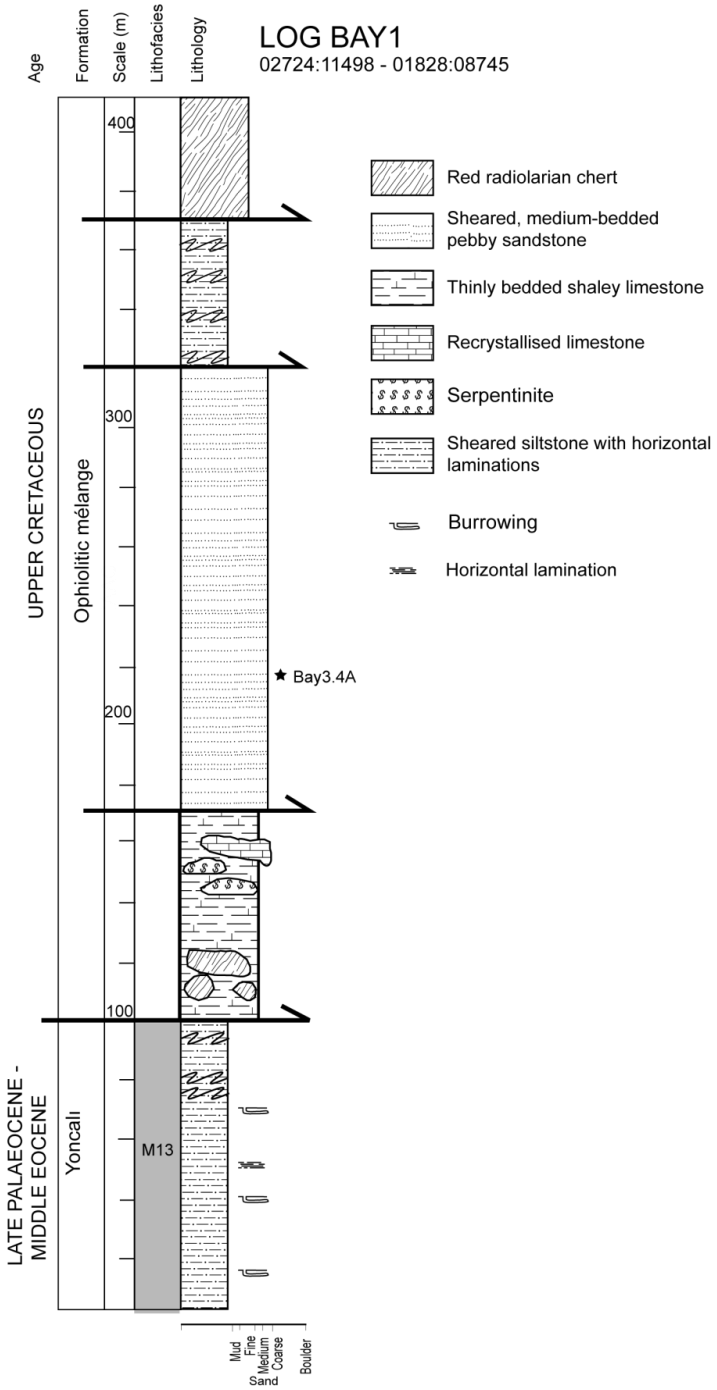

Figure 3.18 Measured log BAY1 of the İzmir-Ankara Accretionary Complex thrust onto the Upper Palaeocene-Middle Eocene Yoncalı Formation at as seen at Kunduzlu Village in the Bayat Study area. See Figure 3.15 for location.

3.4.2.3 The Çayraz Formation

The Çayraz Formation, represented by lithofacies CA7, is well developed in the Bayat area and consists mostly of white/buff marl (Fig. 3.19a) and red/grey shales locally intercalated with thin (<0.5 m) beds of Nummulites-bearing limestone, together with fossiliferous sandstones yielding bivalves and gastropods. The formation overlies the Upper Palaeocene-Middle Eocene Yoncalı Formation and grades laterally into the Middle Eocene Bayat Formation (See section 3.4.2.4); its maximum thickness is >300 m. The formation has a Lutetian age based on the large benthic foraminifera in sample Bay1.2A, *Asterigerina rotula* (Kaufmann), *Smoutina* sp., *Nummulites globulus* Leymerie, *Nummulites* cf. *pengaronensis, Lockhartia conditi* (Nuttall) (N. İnan & K. Taslı pers. comm. 2009).

The Çayraz Formation contains a sequence of conglomerates which are well exposed near the village of Osmankahya (Fig. 3.19b). The sequence there is ~70 m thick and is a ~3 km-wide channel shape, grading laterally and vertically into Nummulites-bearing marls and limestones. Conglomerate beds are ~2 m thick and massive, with local normal grading. Clast imbrication is frequently well developed and indicates a unidirectional flow from NNW to SSE. Clasts are composed of sub-rounded, medium-sorted, cobble-sized basalt, radiolarian chert, serpentinite, sandstone and recrystallised limestone. The beds are intercalated with ~10 m-thick packages of alternating red and grey mudstones, which can be correlated to the Lutetian Karaçay sequence in the Sungurlu area (Section 3.4.1.3.1).

The uppermost ~45 m of the Çayraz Formation consists of a succession of thickly bedded (0.7 – 5 m) conglomerates. Clasts are angular to sub-rounded, poorly sorted and range from pebble to boulder size. They are variably altered, feldspar-phyric, vesicular basic volcanic rocks derived from the underlying Middle Eocene Bayat Formation (Section 3.4.2.4). Beds are mostly massive with crude normal grading being observed locally. Clast imbrication is locally developed and indicates a palaeoflow from northeast to southwest.

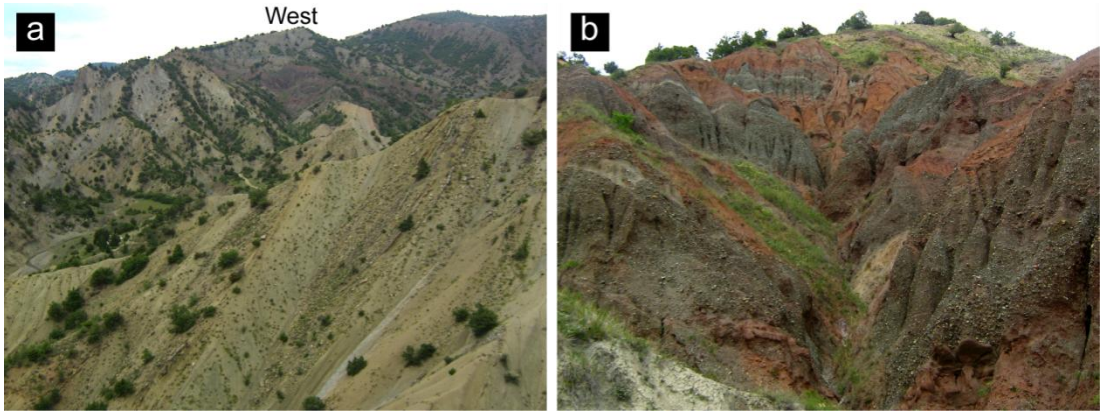

Figure 3.19 Field photographs of the Middle Eocene Çayraz Formation **(a)** view, looking west, of buff marls, **(b)** intercalated grey conglomerates and red mudstone.

3.4.2.3.1 Interpretation of the Çayraz Formation

The Çayraz Formation in the Bayat area can be laterally correlated to Lutetian carbonate deposits at Sungurlu. It shares a similar depositional setting (shallow-marine, shelf-type deposits) but contains a higher concentration of siliciclastic influx, represented by cobble-sized clasts shed from the İzmir-Ankara Accretionary Complex.

3.4.2.4 The Bayat Formation (Middle Eocene)

The Bayat Formation, first named by Ayan (1969), is ~300 m thick and composed of mildly alkaline plagioclase- and pyroxene-phyric trachy-basalts and basaltic trachy-andesites (see Section **3.7** for new geochemical data and interpretation) interbedded with *Nummulites*-bearing marls, sandstones, tuffs and volcanic breccia. The formation is best exposed at locality BAY4 (02476:00576 – 02014:01591) to the west of Bayat town (Figs.3.20 and 3.21). The Bayat Formation grades laterally into the Middle Eocene Yoncalı Formation and the Middle Eocene Çayraz Formation. It is conformably overlain by the Middle Eocene Karabalçık Formation (see below).

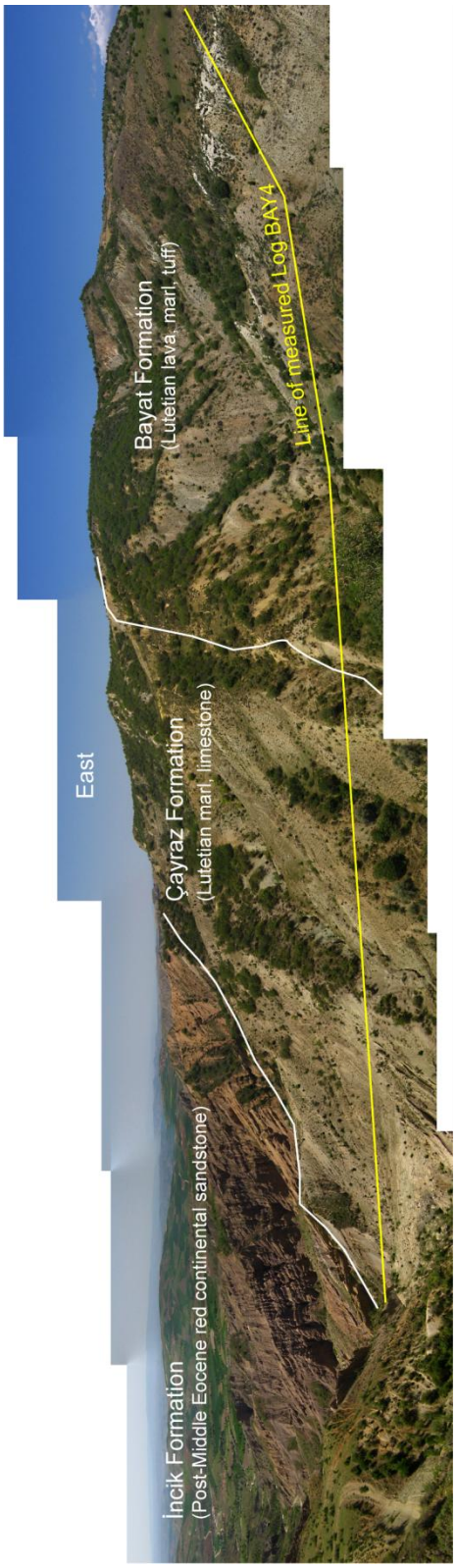

Figure 3.20 Photo-mosaic, looking east, of the relationships and inferred boundaries of the Lutetian Bayat and Çayraz formations, and the post-Middle Eocene Incik Formation. The yellow line marks the approximate trace of measured Log BAY4 (see Fig. 3.21)

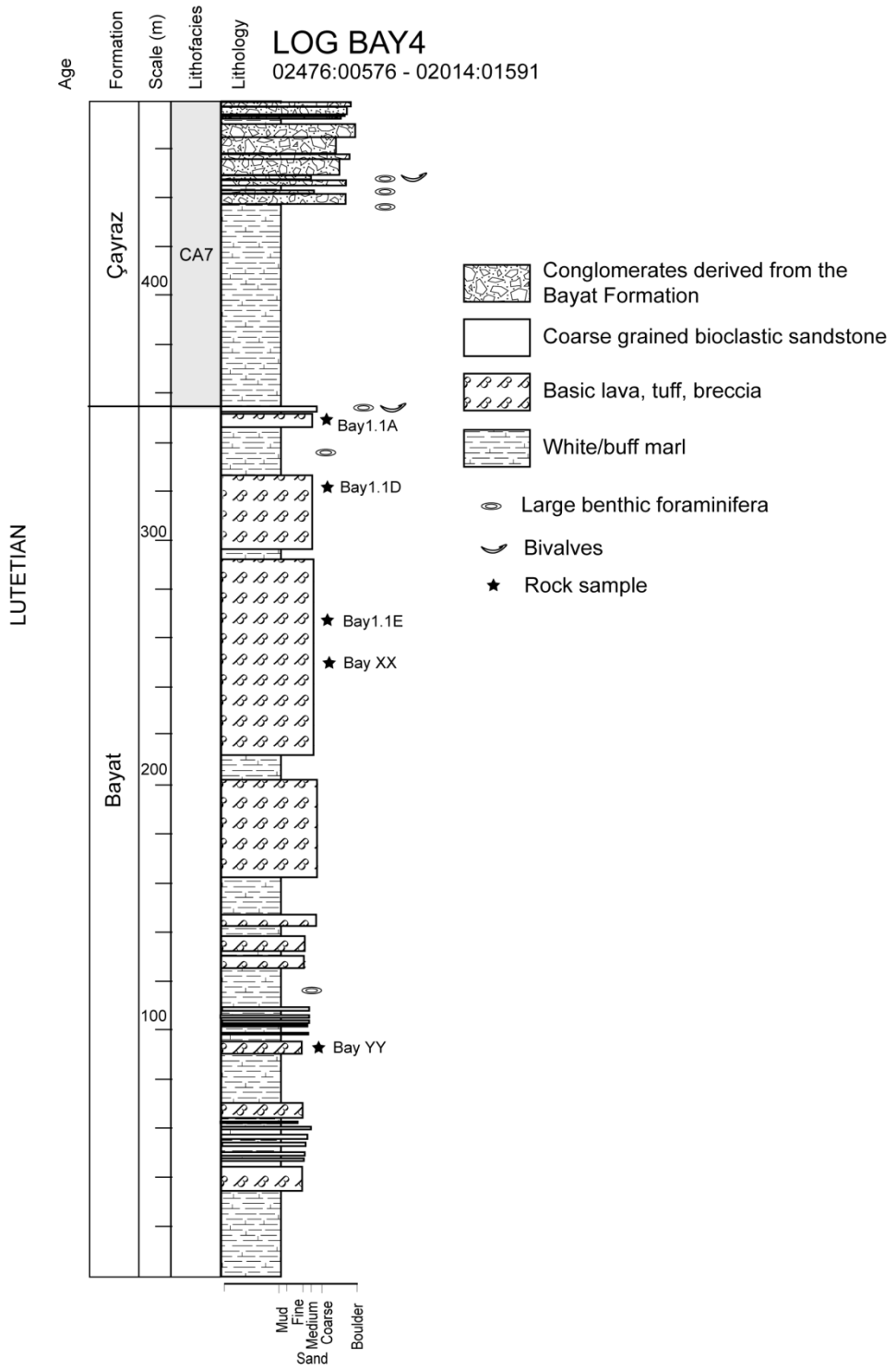

Figure 3.21 Measured log BAY4 showing the Middle Eocene Bayat Formation passing upwards into marls of the Middle Eocene Çayraz Formation, see Figure3.15 for location, all data are from this study.

3.4.2.5 The Karabalçık Formation (Middle Eocene)

The Karabalçık Formation, first named by Dellaloğlu *et al.* (1992), is well developed to the northeast of Bayat but is absent from the Sungurlu area. It lies conformably on the Middle Eocene Bayat Formation and the Upper Palaeocene – Middle Eocene Yoncalı Formation although local unconformities are present. The formation consists of well-bedded, coarse, fossiliferous volcaniclastic sandstones and conglomerates, intercalated with quartz-rich, grey sandstone. The formation is up to ~120 m thick. The following benthic foraminifera in two rock samples collected during this study assign the formation as Lutetian: Sample Bay2.9A - *Smoutina* sp., *Assilina* sp., *Fabiania cassis* Oppenheim. Sample Bay3.10B - *Nummulites* sp., *Nummulites* cf. *laevigatus*, *Assilina* cf. *tenuimarginata* (N. İnan & K. Taslı pers. comm. 2009). This age agrees with previous reports (Kaymakcı *et al.* 2009).

There are two lithofacies present in the Karabalçık Formation including debris flow conglomerates (lithofacies M6), and coarse sandstones exhibiting parallel- and cross-stratification (lithofacies M17).

3.4.2.5.1 Lithofacies M6: debris flow conglomerates

This facies is present in logs BAY2 and BAY3 (Fig. 3.22). Conglomerates form beds up to 2 m thick, consisting of very poorly sorted, rounded clasts, from pebble to boulder size (Fig. 3.23a). Clasts display a range of angularities, composed, almost exclusively, of variably altered feldspar-phyric lavas with minor limestone and radiolarian chert. Clast sources are inferred from both the underlying Middle Eocene Bayat Formation and the İzmir-Ankara Accretionary Complex. Bed bases and tops are irregular, with no sedimentary structures or grading. Transport was presumably by debris flow, while deposition was probably by *en-masse* frictional freezing (e.g. Nemec *et al.* 1980).

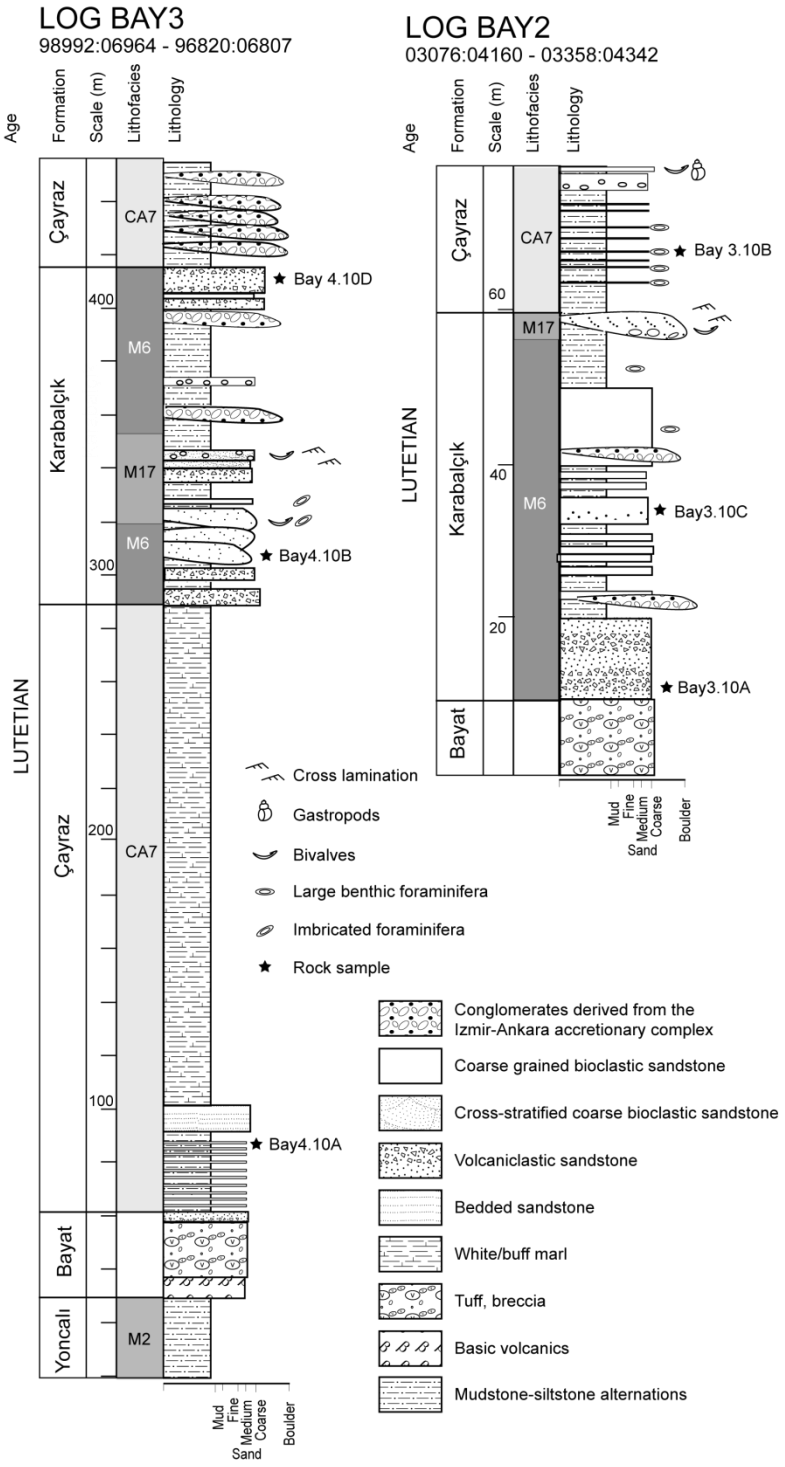

Figure 3.22 Measured logs BAY2 and BAY3 showing the Lutetian Karabalçık and Çayraz formations, all data are from this study.

3.4.2.5.2 Lithofacies M17: stratified sandstone

i) Cross-stratified sands

Coarse-grained, to granular dark brown sandstone forms irregular beds, ~40 cm thick with locally erosive bases and sharp tops. The foresets (Fig. 3.23b) are characterised by granule/pebble layers with the coarsest material often being near the toe of each foreset. Sediment transport was possibly as bed load beneath low-density turbidity currents, while deposition was by grain flow and/or suspension fall out (Pickering *et al.* 1989). Sparse plant remains are present locally; coal seams have been reported in previous studies (Erdoğan *et al.* 1996; Kaymakcı *et al.* 2009).

ii) Parallel-stratified sands

Parallel-stratified sands are well developed to the northeast of Bayat (02726:05339). Bed thickness is from 5-50 cm. Bed bases are commonly erosional (Fig. 3.23d) and tops are sharp or grade into silt grade material. Beds show overall crude normal grading but inverse grading is evident between each stratified band. Sandstones often feature bivalve fragments and 5-10 cm horizons of reworked and imbricated Nummulites and Alveolina fossils (Fig. 3.23c). Transport is interpreted to be by high-concentration turbidity current while deposition was by freezing of successively generated traction carpets at the base of the flow (Pickering *et al.* 1989).

3.4.2.5.3 Interpretation of the Karabalçık Formation

The presence of large benthic foraminifera, coal seams and plant remains suggest a very shallow marine depositional environment for the Middle Eocene Karabalçık Formation. Cross- and parallel-stratification along with poorly sorted, coarse conglomerate debris flows are consistent with a south-facing deltaic environment. The formation intercalates with the Middle Eocene Çayraz Formation (Log BAY3; Fig. 3.22), which is suggestive of episodic deposition in a shallow-marine shelf-type setting.

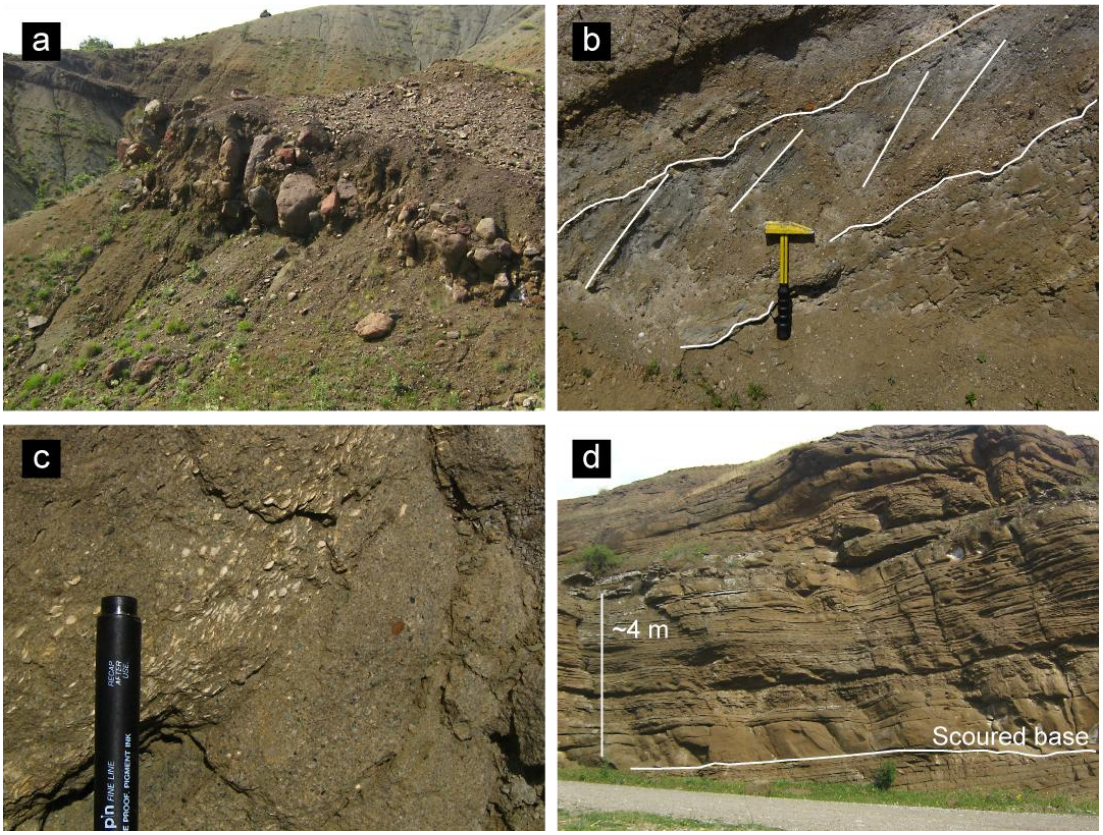

Figure 3.23 Representative field photographs of the Lutetian Karabalçık Formation (a) coarse, poorly-sorted boulder debris flow (lithofacies M6) ~2 m thick in this photograph, (b) cross-stratified brown sandstone (lithofacies M17), (c) imbricated large benthic foraminifera (lithofacies M17), (d) parallel stratification (lithofacies M17).

3.5 Sandstone provenance

This section discusses sandstone petrology and inferred provenance. This involves petrological descriptions, point-counting and palaeocurrent analysis. The aim is to identify sandstone provenance which aids in reconstructing depositional and palaeogeographic settings. Provenance has largely been ignored in previous studies; one exception is Norman (1975b) who published palaeocurrent data from the Çankırı Basin.

Standard thin sections of twelve representative sandstone samples were analysed using an optical microscope. Three hundred grains per sample were counted

using the Gazzi-Dickinson method which helps to reduce the effect of grain size differences on provenance data (See Appendix 2 for a full discussion on point-counting techniques and tabulated data). The sandstone samples were collected from the Sungurlu and Bayat areas and represent the Upper Palaeocene-Middle Eocene Yoncalı Formation, the Middle Eocene Çayraz Formation and the Lutetian Bayat and Karabalçık formations. Point-counting results were plotted on a Qt:F:Lt-c ternary diagram (Fig. 3.24) (where Qt= Total quartz, F= Feldspars, Lt-c = Total non-carbonate lithoclasts) which presents point-counting results graphically.

Palaeocurrents were measured from imbricated clasts in conglomerates, and flute casts and groove marks on sandstone beds (See Appendix 3 for a discussion data collection, data processing and tabulated data).

3.5.1 The Upper Palaeocene-Middle Eocene Yoncalı Formation

Litharenites (Pettijohn *et al.* 1987) in the Yoncalı Formation is usually fine- to coarse-grained and moderately- to well-sorted; grains are usually sub-rounded. Compositionally, the samples are feldspar-poor and rich in sedimentary lithoclasts including terrigenous mudstone, micrite and radiolarian chert. Volcanic lithoclasts, including variably altered basic microlitic and metamorphosed silicic grains, are less abundant. Quartz is present as outsized polycrystalline and strained monocrystalline grains, minor grains include serpentinite and biotite (Figs. 3.24a and 3.24b). Litharentites from the Yoncalı Formation form a tight cluster on the Qt:F:Lt-c ternary diagram (Fig. 3.25).

Palaeocurrents at Sungurlu (n= 1 flute mark; n=12 imbrication) and Bayat (n= 4 flute marks; n= 2 imbrication) are consistently from north-northwest to south-southeast. One set of measurements taken in the north of the Sungurlu area, near Uğurludağ, are orientated from south-southeast to north-northwest (n=1 imbrication) and from east to west (n= 3 flute marks). Groove marks (n= 3) indicate an east-west orientated palaeoflow (Fig.3.26a).

3.5.2 The Middle Eocene Çayraz Formation

One sample from the Middle Eocene Çayraz Formation (Sample SU5.8B) represents the most quartz-rich sandstone (Fig. 3.25). Grains are composed of unstrained quartz and plagioclase, while lithoclasts are mostly composed of a microgranular quartz matrix. Two populations of quartz grains are present; one is rounded with silica overgrowths, the other is angular. Two set of imbricated pebbles were measured from the Bayat area; one set (n= 3) indicates a flow from south-southeast to north-northwest, the other (n=4) from W to E (Fig. 3.26b).

3.5.3 The Lutetian Bayat Formation

Sandstone from the Lutetian Bayat Formation is fine- to coarse-grained, and predictably rich in plagioclase and volcanic lithoclasts (e.g. Sample BAY.YY; Fig. 24c and Fig. 3.25). Grains are sub-angular and composed of basic volcanic lithoclasts, plagioclase, oxides, biotite and augite. Quartz is a minor component and exhibits undoluse extinction where present. No palaeocurrent indicators were observed.

3.5.4 The Lutetian Karabalçık Formation

The Lutetian Karabalçık Formation contains sandstone that is invariably rich in plagioclase and basic volcanic lithoclasts, as exemplified by Sample BAY 3.10A (Fig. 3.24d; Fig. 3.25). This sandstone, an arkosic arenite, is coarse-grained and poorly sorted. Grains are mostly sub-angular and consist of plagioclase, biotite, fragmental clinopyroxene, basic volcanic lithoclasts and rare polycrystalline quartz. On sample (4.10B), a lithic arenite, is plagioclase-poor and dominated by foliated polycrystalline quartz clasts. Other grains present are mudstone, siliceous chert, red radiolarian chert, elongate grains of quartz groundmass and microlitic volcanic grains. Minor components comprise detrital mica.

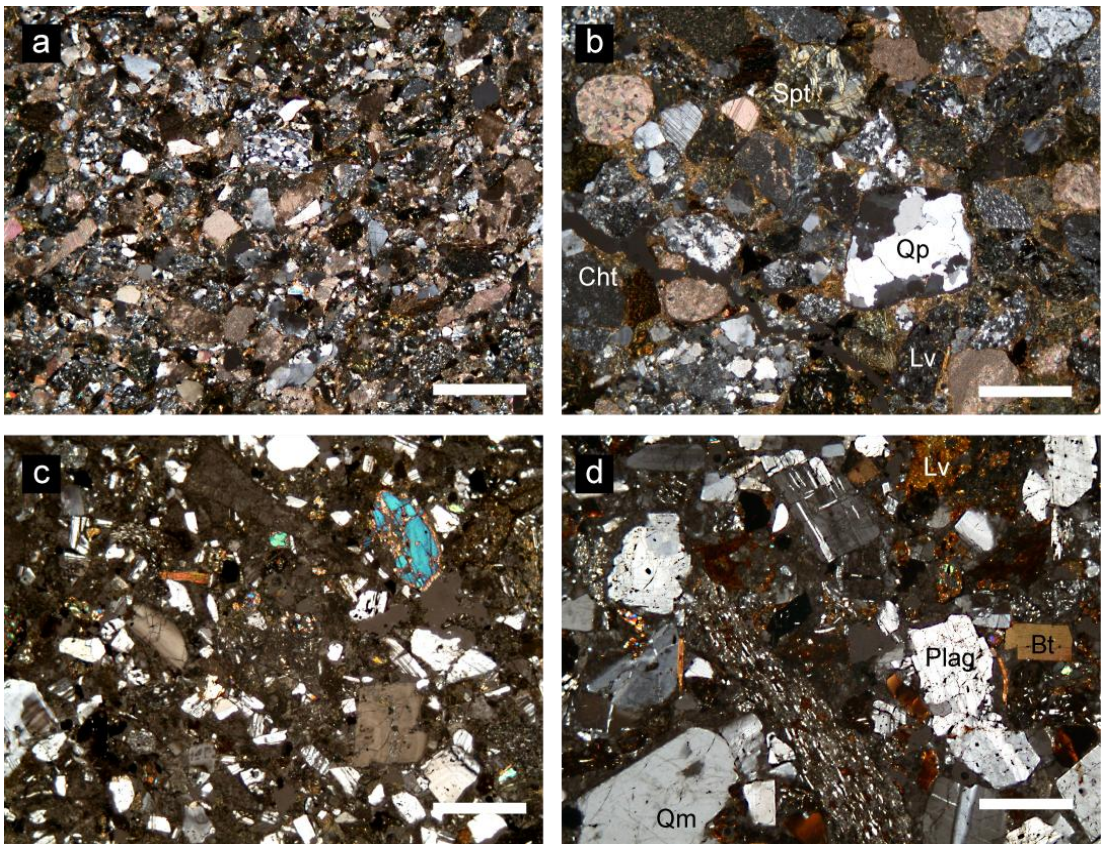

Figure 3.24 Photomicrographs of selected sandstone samples, **(a)** a well-sorted medium-grained clast-rich litharenite from the Upper Palaeocene-Middle Eocene Yoncalı Formation (Sample SU14.21), **(b)** a coarse-grained clast-rich litharenite with chert, polycrystalline quartz and volcanic lithoclasts from the Upper Palaeocene-Middle Eocene Yoncalı Formation (Sample SU1.1B), **(c)** medium-grained litharenite rich in basic volcanic lithoclasts from the Lutetian Bayat Formation (Sample BAY.YY), **(d)** a coarse feldspar-rich arkosic arenite from the Lutetian Karabalçık Formation (Sample BAY3.10A). All images in crossed polars, all scale bars = 1mm. Spt – serpentinite, Cht – chert, Qp – polycrystalline quartz, Lv – volcanic lithoclast, Qm – monocrystalline quartz, plag – plagioclase, Bt – biotite.

3.5.5 Summary and interpretation of provenance results

On the basis of new provenance data discussed above, the following conclusions may be drawn. Turbiditic sandstone from the Upper Palaeocene-Middle Eocene Yoncalı Formation is suggestive of detritus shed from the İzmir-Ankara Accretionary Complex. Coarser grained sediments are interpreted to be locally-derived syn-tectonic deposits, associated with active thrusting of the İzmir-Ankara Accretionary Complex. Conglomerates are frequently observed ahead of propagating

thrust fronts; a notable example is the presence of Oligo-Miocene conglomerates at the Pyrenean thrust front in Spain (Lloyd *et al.* 1998). Palaeoflow is aligned from north-northeast to south-southwest and from east to west which probably represents a flow from the basin margin to the basin depocentre. The shallow-marine, Lutetian Bayat and Karabalçık formations comprise abundant volcanic detritus which constrains the age of volcanic activity.

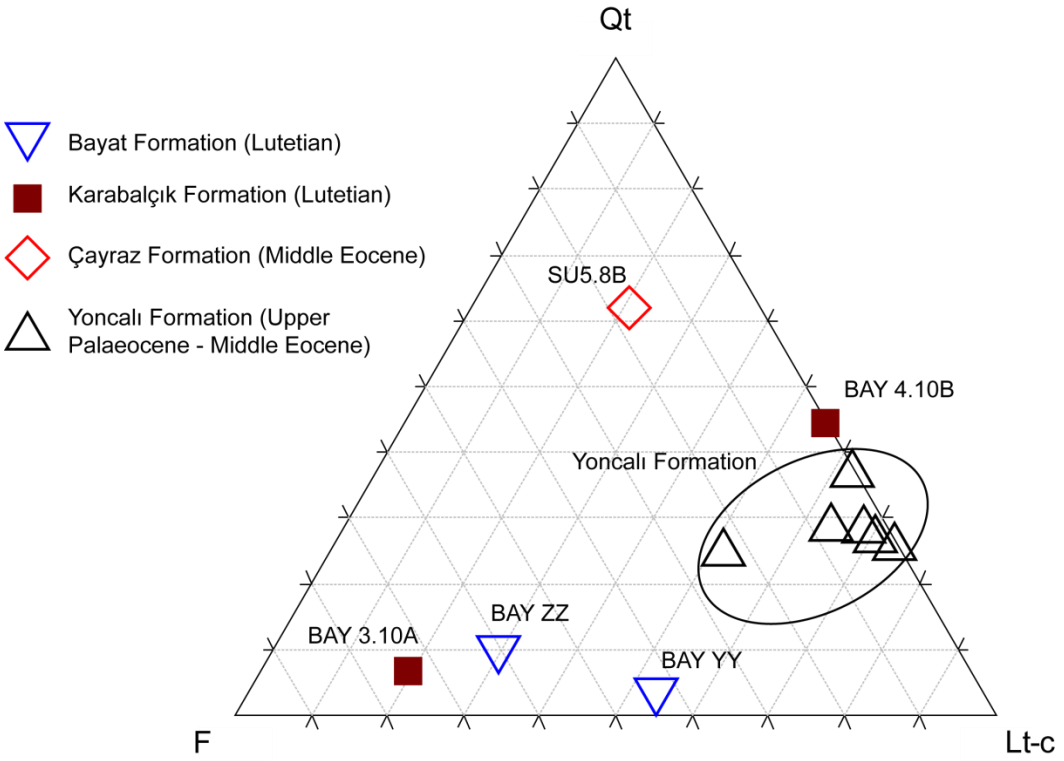

Figure 3.25 Ternary diagram of sandstone compositions counted using the Gazzi-Dickinson point counting method. Qt = total quartz, F = Feldspar, Lt-c = total lithic grains excluding carbonates.

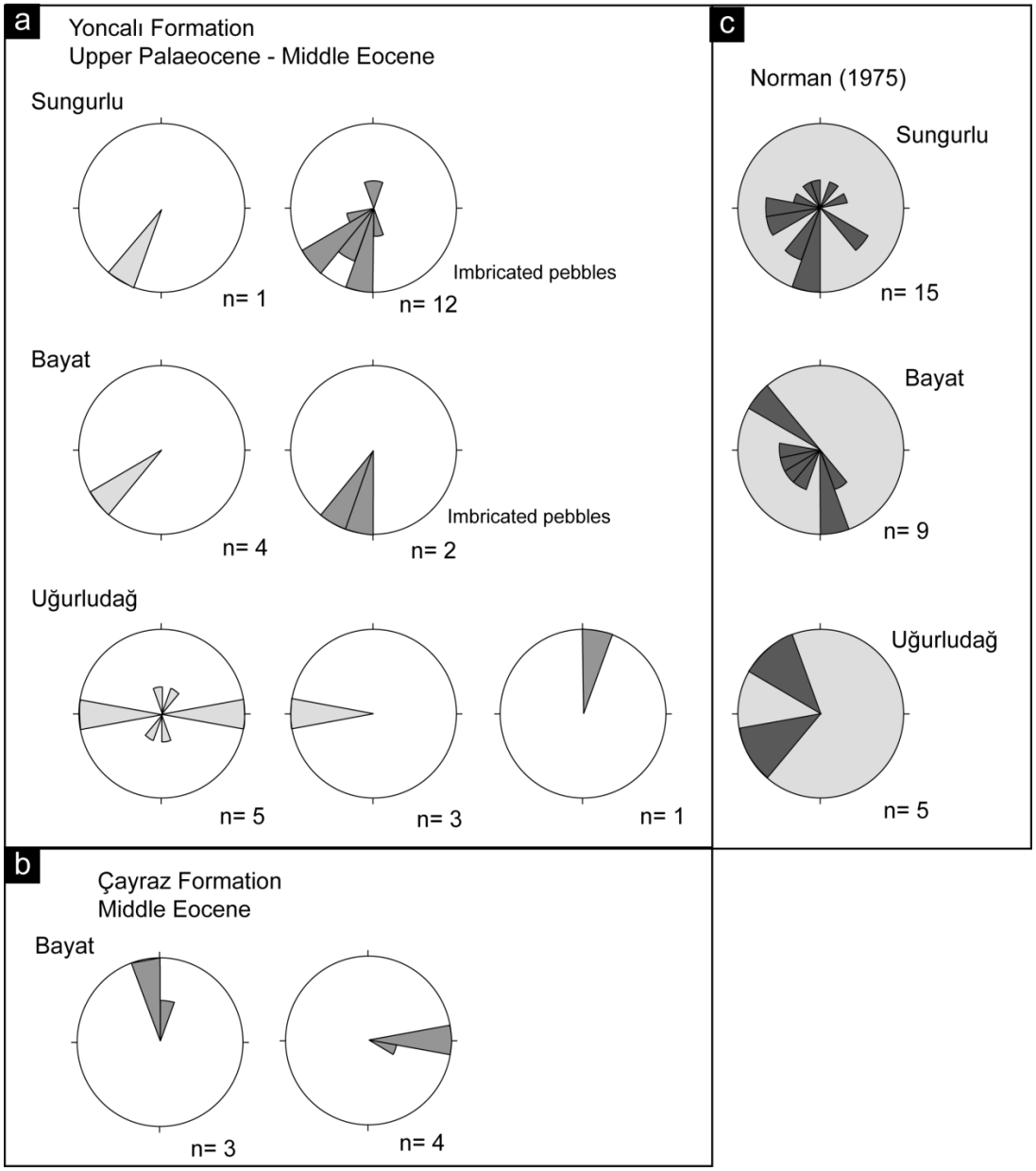

Figure 3.26 Palaeocurrent rose diagrams of formations in the Sungurlu-Bayat area. **(a)** and **(b)** are from this study, Light grey unidirectional diagrams represent flute marks, light grey bi-directional diagrams represent groove marks. Dark grey diagrams represent imbricated clasts, **(c)** diagrams were drawn using data from Norman (1975).

3.6 New stratigraphic and sedimentary results

The following data are new stratigraphic and sedimentary results:

- Upper Palaeocene to Middle Eocene sediments of the Çankırı Basin have been systematically interpreted in terms of lithofacies, which has provided new insights into depositional environments and processes.
- Sedimentary deposition ages, based on large benthic foraminifera, largely confirm previous studies.
- The Upper Palaeocene-Middle Eocene **Yoncalı Formation** is composed of detritus shed from the Upper Cretaceous İzmir-Ankara Accretionary Complex. Conglomerates and pebbly sands observed at the Sungurlu area are tectonically overlain by thrust slices of the İzmir-Ankara Accretionary Complex. They are thus interpreted to represent syn-tectonic detritus which was deposited, by debris flow, ahead of a propagating thrust zone. Locally, sandstone turbidites contain Ypresian benthic foraminifera, suggesting that shallow-marine, shelf-type carbonates were reworked to a slope setting.
- The Ypresian-Lutetian **Çayraz Formation** represents the generation of Nummulitid shoals and banks in a shelf-type environment. Clastic material, derived from the İzmir-Ankara Accretionary Complex forms channelised deposits.
- Sediments of the Lutetian **Bayat Formation** are mostly volcaniclastic deposits, which have not been described in terms of sandstone petrology before.
- Similarly, the Lutetian **Karabalçık Formation** mostly comprises volcaniclastic sandstone. Large benthic foraminifera have not been described from these deposits before.

3.7 Middle Eocene lava geochemistry

This section presents geochemical data from the Sungurlu and Bayat localities in the context of existing geodynamic models of Middle Eocene magmatism in central Turkey. The Sungurlu and Bayat areas are located within a Middle Eocene volcano-sedimentary belt that spans almost the entire length of Turkey, parallel to the İzmir-Ankara-Erzincan and Intra-Pontide suture zones (Keskin *et al.* 2008) (Fig. 3.27). The belt mostly overlies deformed, imbricated Palaeocene or older units associated with these two suture zones (Okay & Tüysüz 1999). Another magmatic belt consisting of Eocene granitoid plutons is located in northwest Turkey and intrudes a blueschist belt (the Tavşanlı Zone) which has a Cretaceous metamorphic age (Okay & Satir 2006; Altunkaynak 2007; Ustaömer *et al.* 2009). The geodynamic setting of extrusive igneous rocks from the Middle Eocene volcano-sedimentary belt has been studied in several localities in Turkey, including : 1) from the Gümüşhane-Aluera-Şebinkarahisar-Gölköy and Kastamonu localities in northern Anatolia (Peccerillo & Taylor 1976; Tokel 1977); 2) near Yozgat, ~60 km southeast of Sungurlu (Erdoğan *et al.* 1996), and; 3) in the eastern Anatolian region, mostly near İskilip and Çorum (Keskin *et al.* 2008) (Fig. 3.27). To date, there are no geochemical data from Sungurlu and Bayat present in the literature.

The origin of the Middle Eocene volcano-sedimentary belt is controversial. The extrusive igneous lavas span a range of compositions from basalts to rhyolites, with andesites being the most common. They are calc-alkaline in character except for alkaline lavas near the top of the sequence; all exhibit a chemical subduction signature (Keskin *et al.* 2008). There are several models for the geodynamic evolution of the belt. For some (e.g. Altunkaynak 2007; Keskin *et al.* 2008) the magmatic belt is a product of a post-collisional slab break-off event; others envisage the belt as the result of an active continental arc (Peccerillo & Taylor 1976; Tokel 1977), or as a result of syn-collisional extension caused by basin subsidence which was related to the emplacement of ophiolitic mélange at the northern margin of the Çankırı Basin (Erdoğan *et al.* 1996).

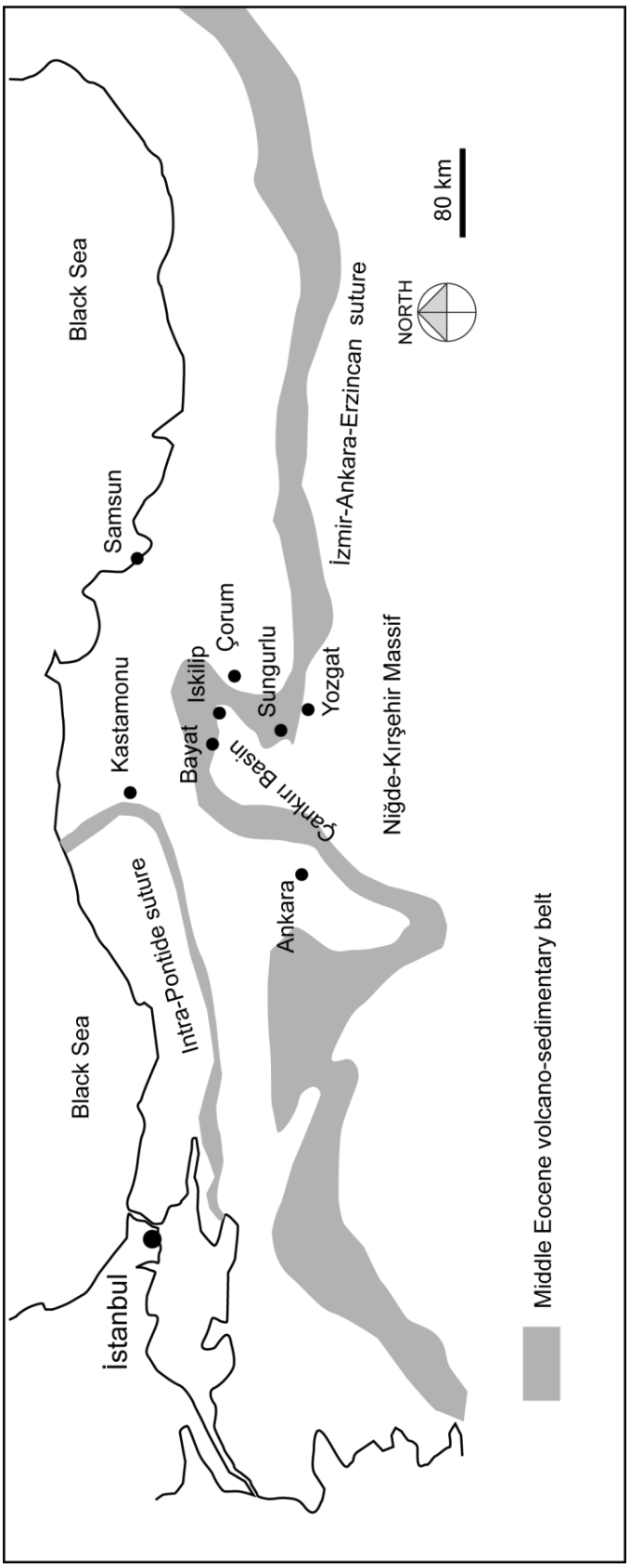

Figure 3.27 Sketch map of Turkey showing the distribution of the Middle Eocene volcano-sedimentary belt. Modified after Keskin *et al.* (2008).

The Sungurlu locality includes a ~3 x ~2 km outcrop of massive lava that cuts the İzmir-Ankara Accretionary Complex, although the contact relationships are covered by Neogene sediments. The lava is well exposed on the roadside ~10 km northeast of Sungurlu and has been mapped as being of Eocene age (MTA 2002). To the north-west of Bayat, a ~300 m succession of extrusive volcanic rocks and tuffs in the Bayat Formation are intercalated with marls containing Lutetian Nummulites. This implies shallow (tens of m) subaqueous lava eruption. Three samples were collected from Sungurlu and fourteen from Bayat for analysis by X-Ray Fluorescence (XRF) to determine major element oxides and trace elements using the method outlined in Fitton *et al.* (1998). Analyses were performed at the School of GeoSciences, University of Edinburgh on a Panalytical PW2404 wavelength-dispersive sequential X-ray spectrometer.

3.7.1 Petrology

The lavas from Sungurlu contain phenocrysts of plagioclase, green euhedral amphibole and rare biotite in a grey glassy microlitic groundmass (Fig. 3.28a). The plagioclase phenocrysts commonly display absorption/reaction rims and zoning. The Bayat lavas contain plagioclase and clinopyroxene phenocrysts, commonly twinned, and set in a black glassy microlitic groundmass (Fig. 3.28b). Accessory minerals are opaque oxides (magnetite) and rutile.

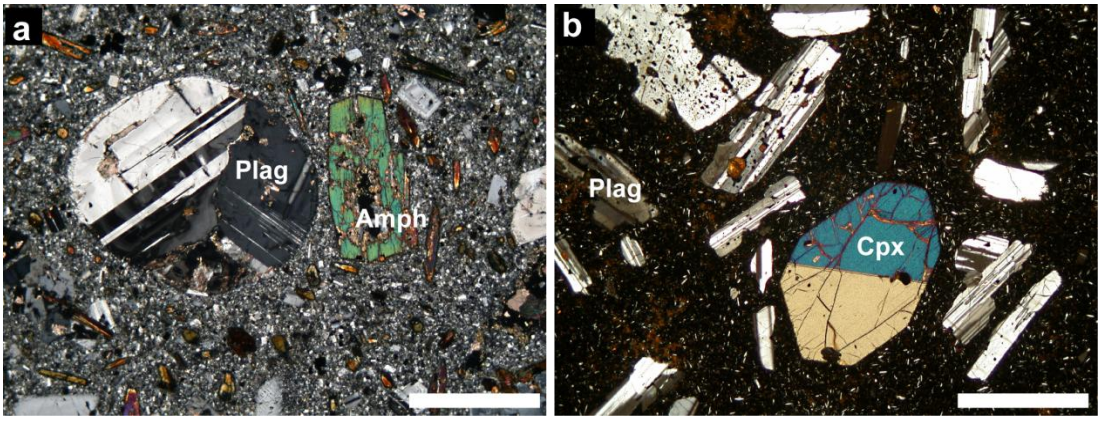

Figure 3.28. Photomicrographs of **(a)** –andesite from Sungurlu and **(b)** – basaltic trachy-andesite from Bayat. Plag – plagioclase, Amph – amphibole, Cpx – clinopyroxene. Scale bars = 1mm, images in cross-polarised light.

3.7.2 Results

The geochemical results of lavas from Sungurlu and Bayat can be usefully compared to the works of Keskin *et al.* (2008), Erdoğan *et al.* (1996) and Peccerillo & Taylor (1976). In terms of major oxides the Sungurlu samples range from 60.41 to 61.08 wt % SiO_2 and from 5.7 to 5.8 wt % Na_2O + K_2O. They thus plot in the andesite field of the Total Alkali Silica (TAS) diagram of Le Bas *et al.*(1986) (Fig. 3.29a). The Bayat samples range from 50.67 to 55.57 wt % SiO_2 and from 5.16 to 7.75 wt % Na_2O + K_2O and plot in the trachy-basalt and basaltic trachy-andesite field field of the TAS diagram. Using the alkaline/sub-alkaline division line of Kuno (1966), the Sungurlu andesites are sub-alkaline and the Bayat trachy-basalts and basaltic trachy-andesites are alkaline. The Sungurlu andesite is calc-alkaline and the Bayat samples are shoshonitic according to the K_2O vs. SiO_2 diagram of Peccerillo & Taylor (1976) (Fig. 3.29b) The Sungurlu andesites plot on the calc-alkaline field of the AFM diagram (Irvine & Baragar 1971) (Fig. 3.30).

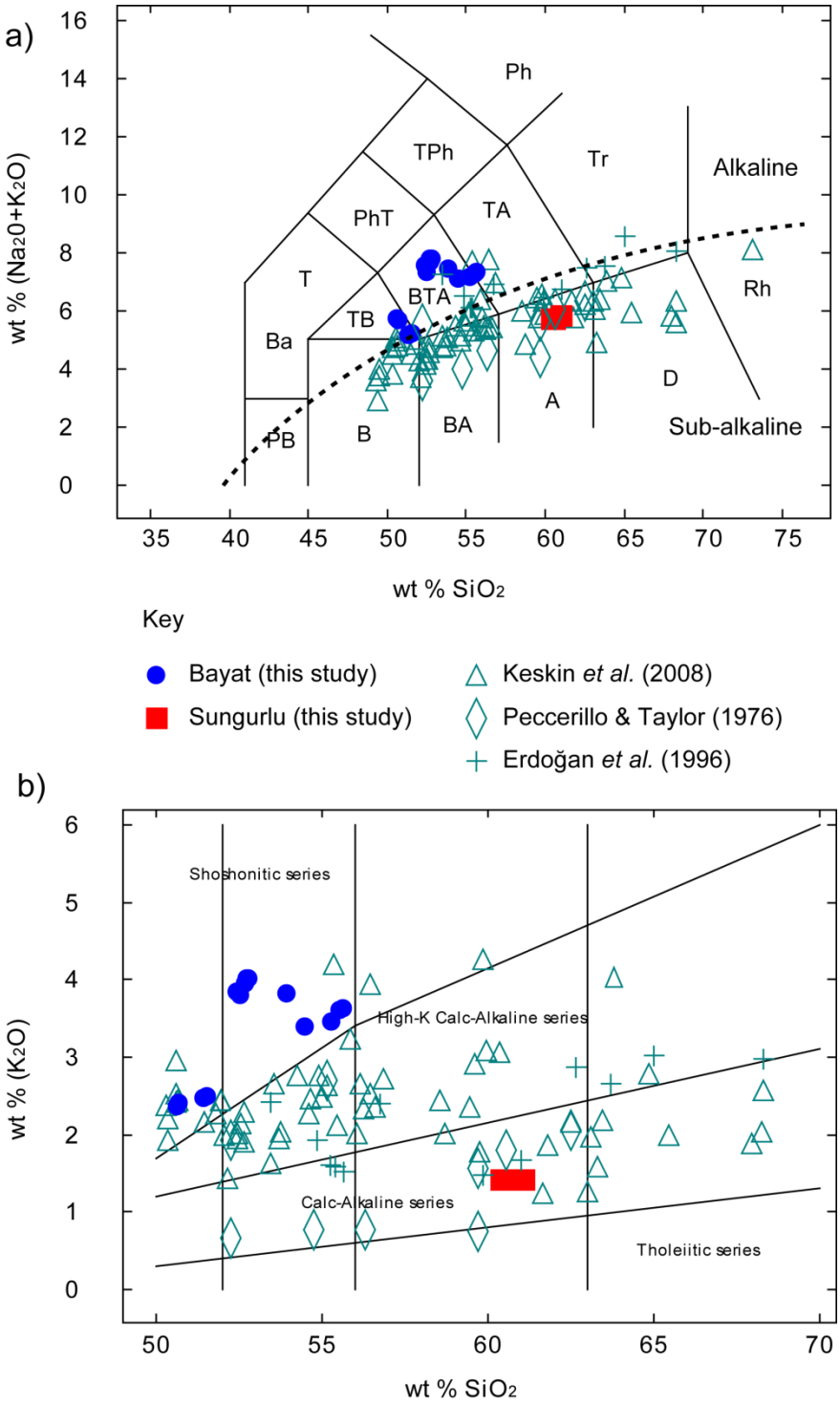

Figure 3.29 (a) Total Alkali Silica (TAS) diagram for samples from Bayat (in blue) and Sungurlu (in red) after Le Bas *et al.* (1986). Abbreviations: PB – picrobasalt, B – basalt, BA – basaltic andesite, A – andesite, D – dacite, Rh – rhyolite, TB – trachy-basalt, BTA – basaltic trachy-basalt, TA – trachy-andesite, Tr – trachyte, T – tephrite, Ba – basanite, PhT – phonotephrite, TPh – tephriphonolite, Ph – phonolite, **(b)** K_2O vs. SiO_2 diagram (Peccerillo & Taylor 1976).

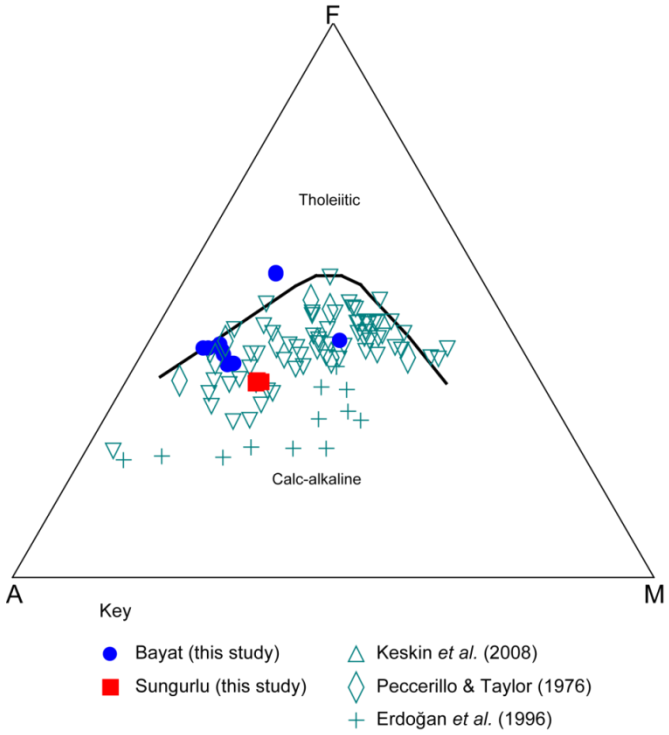

Figure 3.30 AFM diagram for sub-alkaline basalts after Irvine & Baragar (1971).

3.7.2.1 Multi element 'spider' diagrams

Selected element concentrations were plotted on a multi-element diagram normalised to the normal mid-ocean-ridge basalt (N-MORB) values (Pearce (1982). The diagram (Fig. 3.31) shows that most samples display enrichment in Large Ion Lithophile Elements (LILEs) (Sr, K, Rb, Ba) and, to a lesser extent, in Light Rare Earth Elements (LREEs) (La, Ce, Nd) relative to N-MORB. Nb shows a depleted pattern relative to LILEs and LREEs, but is mostly >1. High Field Strength Elements (HFSEs) (Ti, Y, Sc, Cr) generally show a depleted pattern relative to N-MORB. The patterns from this study are broadly comparable to those Keskin *et al.* (2008), Erdoğan *et al.* (1996) and Peccerillo & Taylor (1976). Nb depletions suggest a

magma source that has been chemically affected by subduction-related fluids (Pearce & Cann 1973b; Pearce *et al.* 1984).

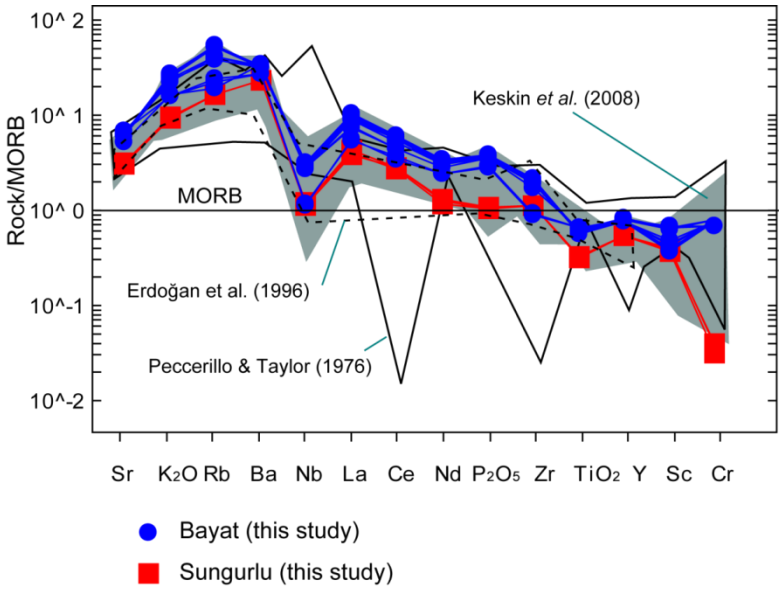

Figure 3.31 Multi element 'spider diagrams' normalised to the mid-ocean ridge values of Pearce (1982). Bayat lavas (blue circles) and Sungurlu andesites (red squares) are compared to the results of Keskin *et al.* (2008), Erdoğan *et al.* (1996) and Peccerillo & Taylor (1976).

3.7.2.2 Tectonic discrimination diagrams

Tectonic discrimination diagrams can be used to infer the tectonic setting of igneous source melt. Results, however, must be used with caution and always with a consideration of field-based observations. During this study it was found that several discrimination diagrams (e.g. the Ti/Y vs. Nb/Y diagram of Pearce (1982) cannot adequately discriminate in this complex tectonic setting invloving calc-alkaline to shoshonitic moderately evolved (i.e. 50.67 to 55.57 wt % SiO_2) trachy-basalts and basaltic trachy-andesites. Çankırı Basin

One potentially useful scheme is the Nb-Zr-Y diagram of Meschede (1986) which shows that the Bayat basaltic trachy-andesites plot in the within-plate alkali basalt field (Fig.3.32a), whereas the Bayat trachy-basalts and the Sungurlu andesites plot in the volcanic arc/ MORB field.. These fields must be treated with caution because volcanic arc basalts plot in both of these fields (Meschede 1986). A further tectonic discrimination scheme is shown on the Zr/Y vs. Zr diagram of Pearce &

Norry (1979). Fig. 3.32b shows that most samples plot in the within-plate basalt field.

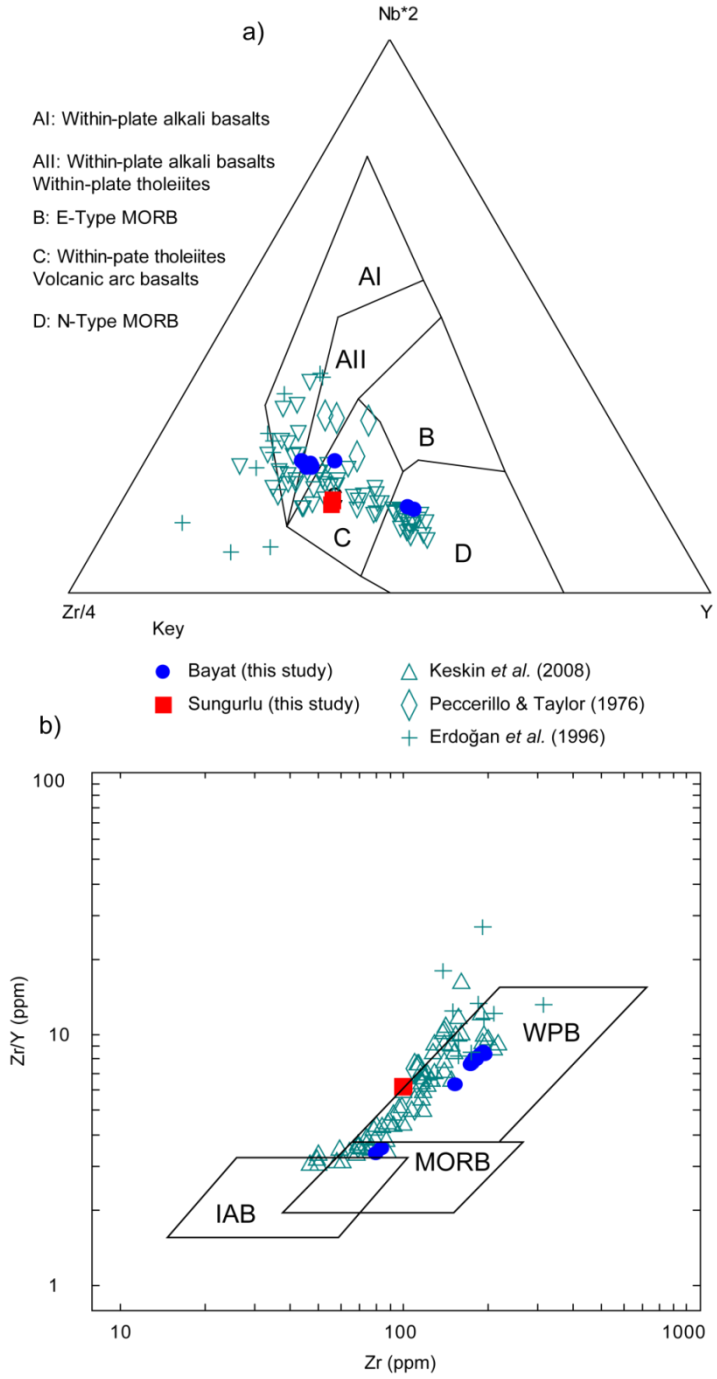

Figure 3.32 (a) the Nb-Zr-Y diagram of Meschede (1986), (b) the Zr/Y vs. Zr discrimination diagram of Pearce & Norry (1979)

3.7.3 Tectonic implications

Any geodynamic model of plate convergence in central Turkey should account for the generation of the Middle Eocene volcano-sedimentary belt. The cause of the Lutetian volcanism is presently not well understood. A Tibetan-type post-collisional magmatic event, triggered by crustal thickening seems unlikely, because the Lutetian magmatism was, in the Çankırı Basin at least, wholly submarine. This would suggest that the Lutetian was characterised by extensional tectonics.

The tectonic model of Keskin *et al.* (2008) (Fig. 3.33) proposed a slab break-off event to explain the origin of the Lutetian magmatism. This is partly based on an inferred chemical evolution of the lavas within the Middle Eocene volcano-sedimentary belt. Lavas at the base of the belt are calc-alkaline in character, whereas those at the top are more alkaline. Their source is interpreted as mixture of: 1) lithospheric mantle influenced by subduction-modified fluids and; 2) upwelling, hot, more enriched, asthenospheric mantle following slab break-off.

A full test of this model is beyond the scope of this chapter, but the following trends are observed from the geochemical affinities of lavas in Bayat. In the Bayat area, basaltic trachy-andesites are more alkaline, more evolved and more enriched in Nb than trachy-basalts. The alkali basaltic trachy-andesites are nearer the top of the Bayat Formation than the less alkali trachy-basalts. The geochemical trends are, therefore, broadly consistent with the inferred chemical evolution of the slab break-off model. However, a chemical trend of increasing alkalinity is not evidence of a slab break-off. After the termination of subduction, relaxation of the compressive regime often results in extension which triggers the generation of alkaline magmatism (Fitton & Upton 1987).

Furthermore, there are inconsistencies in the slab break-off model with the local stratigraphy observed in the field. Keskin et al. (2008) proposed that lower levels of Middle Eocene sediments are clastic and deposited in shallow marine, to

sub-aerial environments whereas those at higher levels were exclusively sub-aerial volcanic units. Keskin *et al.* (2008) infer a sudden uplift of the İzmir-Ankara-Erzincan suture zone prior to Lutetian volcanism, triggered by slab break-off. This, however, is at odds with the observations from Bayat and Sungurlu, where the sedimentary succession is exclusively shallow marine and includes Nummulite-rich marls. Only above the Bayat Formation (i.e. post-Lutetian) is there evidence of uplift as shown by the deposition of the terrestrial red sandstone of the İncik Formation (see Section 3.4.1.3.3) (Kaymakcı *et al.* 2009).

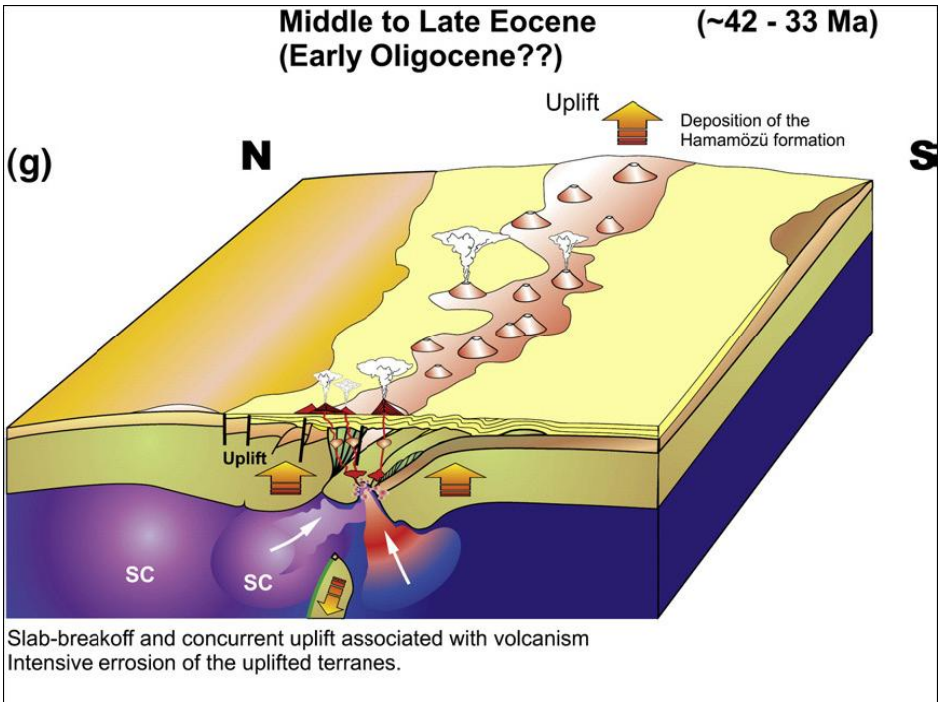

Figure 3.33 Block diagram showing slab break-off in the Lutetian, note that, in this model, a major uplift occurs prior to volcanism, copied from Keskin *et al.* (2008).

An active island-arc setting was envisaged by Peccerillo & Taylor (1976). In this scenario, Middle Eocene calc-alkaline volcanic rocks were erupted onto the Pontide active margin above a north-dipping island-arc subduction zone. However, further details and a plausible tectonic model were not developed. Erdoğan *et al.* (1996) inferred an extensional setting for the development of the Middle Eocene volcanics, which they referred to as the "Bayat Volcanics" (Fig. 3.34). In this model, post-collisional extension was inferred to have developed locally after thrust imbrication of ophiolitic melange at the northern margin of the Çankırı Basin during Late Palaeocene-Early Eocene time.

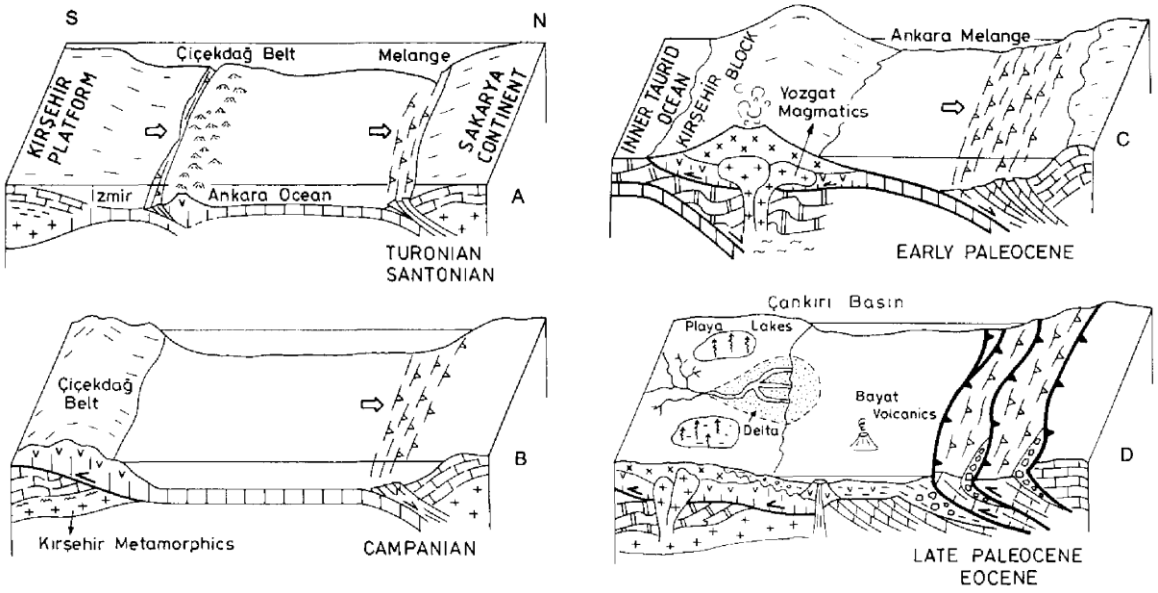

Figure 3.34 Block diagrams showing the evolution of central Anatolia between Late Cretaceous and Middle Eocene time, **(a)** Turonian – Santonian, **(b)** Campanian, **(c)** Early Palaeocene, **(d)** Middle Eocene, copied from Erdoğan *et al.* (1996).

The presence of mildly negative Nb anomalies, enriched LIL elements, depleted HFS elements and hydrous phases indicate that source magma was derived from hydrous melting above a subducting slab. However, high Zr/Y ratios and wt % $Na_2O + K_2O$ values suggest that most of the samples from the Bayat locality are mildly alkaline, and erupted in a within-plate-type setting (e.g. Pearce & Cann

1973a). These chemical characteristics are typical of a post-collisional extensional setting where magmas typically exhibit a transition from "orogenic" calc-alkaline andesites to mildy alkaline trachy-basalts and trachy-andesites. This transition has been documented elsewhere in northwestern Turkey and is interpreted to occur after continental collision (Güleç 1991; Harris *et al.* 1994), this model is preferred by this study.

3.8 Structural development

Previous work related to the structural evolution of the Çankırı Basin is limited and includes a remote-sensing study by Norman (1975b) and more recent kinematic and palaeostress studies (Kaymakcı *et al.* 2000; Seyitoğlu *et al.* 2000; Kaymakcı *et al.* 2003). Work on the structural evolution of the İzmir-Ankara suture zone is still in its infancy and many problems remain unsolved, namely: 1) the nature and duration of post-collisional Palaeotectonic regimes; 2) the nature and timing of Neotectonic deformation (see Koçyiğit & Deveci 2008).

The works of Kaymakcı *et al.* (2000; 2003) modelled three deformation phases: 1) a Late Palaeocene to Early Miocene transpressional phase, related to continental collision; 2) an Early to Middle Miocene extensional phase, possibly related to post-orogenic relaxation and; 3) a recent (Neotectonic) transcurrent phase related to the post-collisional reorganisation of central Anatolia influenced by the North Anatolian fault zone.

Structural data from this study are presented below at two different scales: map-scale and outcrop-scale. See Chapter 2 (Section 2.8) and Appendix 4 for discussions on data gathering and processing.

3.8.1 Map-scale structures

Thrust faulting along the basin margin occurs in each of the study areas and gives rise to a variety of structural features. In the Sungurlu area, the presence of mélange blocks in the Upper Palaeocene-Middle Eocene Yoncalı Formation was previously attributed to olistolith emplacement by submarine sliding (Şenalp 1979; Norman *et al.* 1980). During this study, however, the contact with the İzmir-Ankara Accretionary Complex and the Yoncalı Formation was carefully mapped and the structure was found to be an imbricated thrust zone. Loading of the thrust stack onto the basin sediments produced downward flexure of sedimentary bedding which dips towards the fault at angles up to 60°.

In the Bayat area, compression folded Late Palaeocene to Middle Eocene sediments. Fold axes are orientated approximately west-east and have a wavelength of ~4 km.

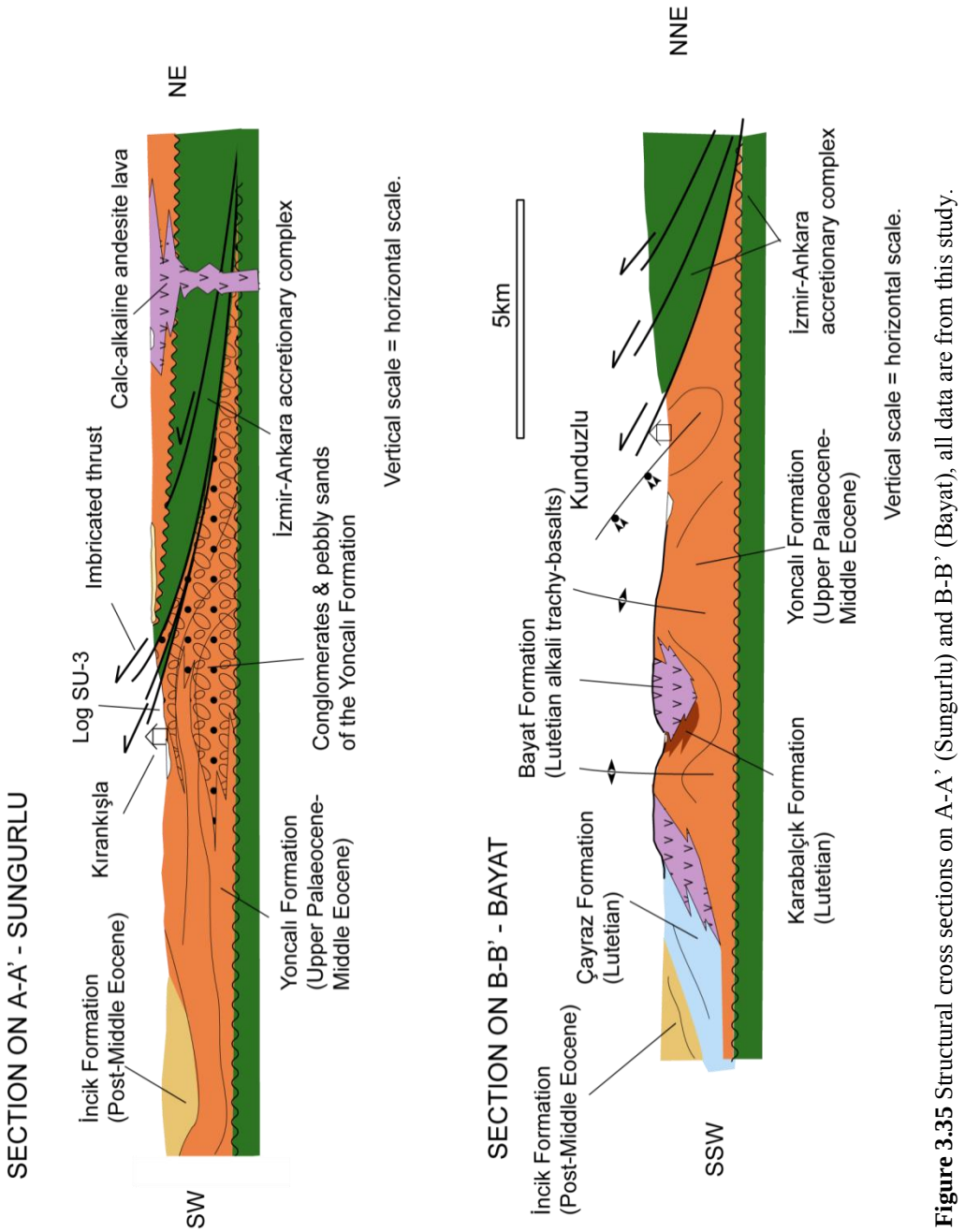

Figure 3.35 Structural cross sections on A-A' (Sungurlu) and B-B' (Bayat), all data are from this study.

3.8.2 Outcrop-scale structures

Outcrop-scale fault plane and fold axis orientation data were collected in the field with the aim of identifying palaeostress phases and relating them to regional tectonics. Forty fault planes were measured of which twenty-three had reliable kinematic indicators. The strike pattern of all forty faults is displayed in Fig.3.36a and shows a polymodal pattern with two dominant strike directions W-E and NNE-SSW. Faults with slickenside indicators comprise a heterogeneous dataset (Fig. 3.36b) and, with some exceptions, exhibit steeply dipping fault planes with sub-horizontal P- and T-axes (Fig. 3.36c).

The faults, where possible, were arranged into groups that yielded high probability (R) values. One fault indicates N-S orientated compression, and is a low-angle thrust fault (Fig. 3.36d). One group (n= 5) comprises a conjugate set of strike-slip faults striking N-S and NNW-SSE respectively (Fig. 3.36e), R values for all three axes are >92, compression was orientated N-S. Another group (n= 5) (Fig. 3.36f) is also made up of conjugate strike-slip faults (R> 93), that strike NNW-SSE and W-E, indicating NW-SE compression. A further group (Fig. 3.37a) are mostly W-E-striking oblique-slip faults, with marginally lower R values (P – 84%, B – 80%, T – 90%). This group broadly indicates WSW-ENE compression. Three other oblique faults (Figs. 3.37b, c and d) indicate a non-Andersonian stress regime, and cannot be correlated to the other fault groups.

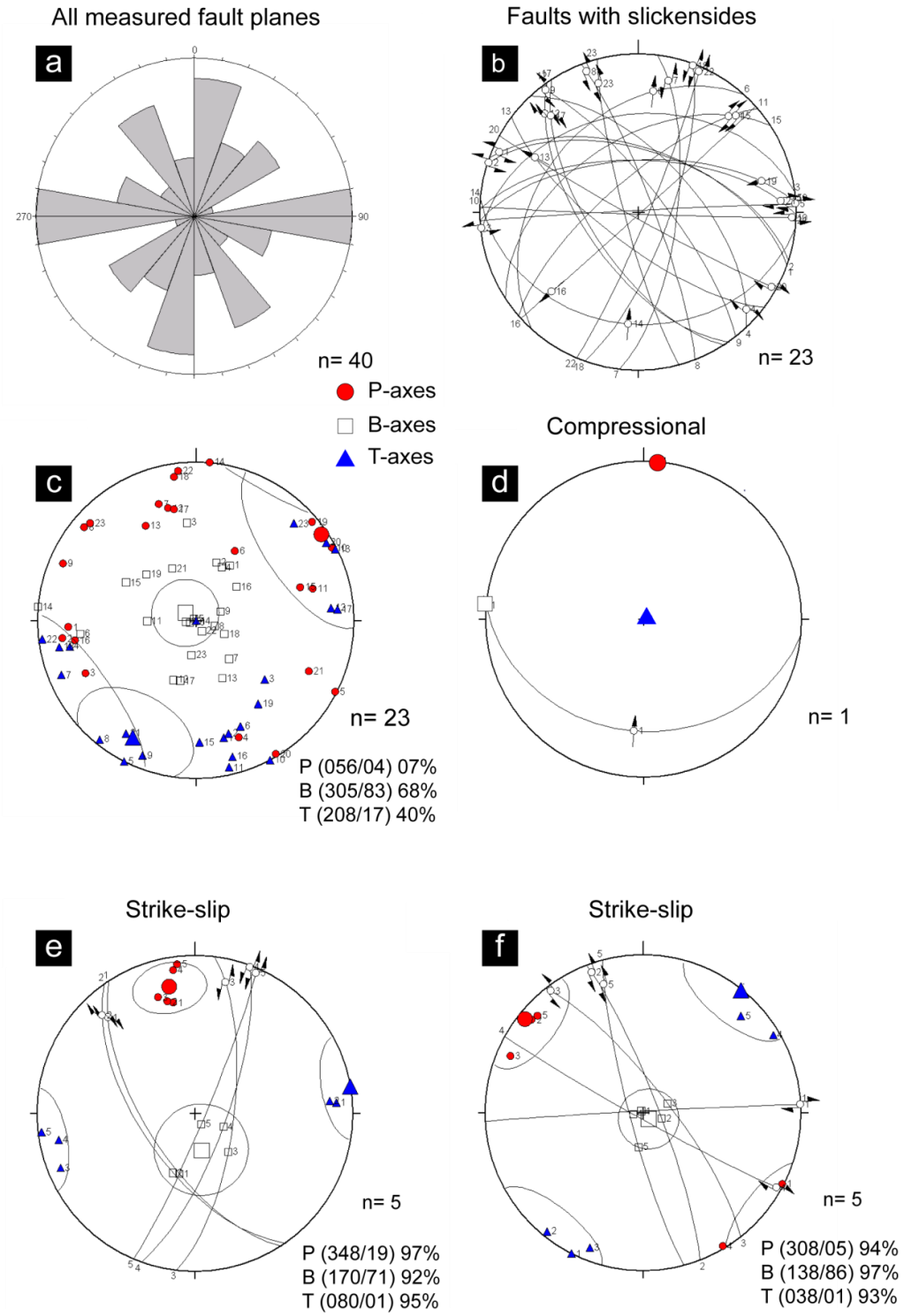

Figure 3.36 (a) rose diagram of all faults in the Sungurlu and Bayat areas, **(b)** Angelier plot of faults with kinematic indicators, **(c)** P-T axes plot of all faults with measured slickensides. Combined P-T axes and Angelier plot of a compressional fault **(d)** and strike-slip faults **(e-f).**

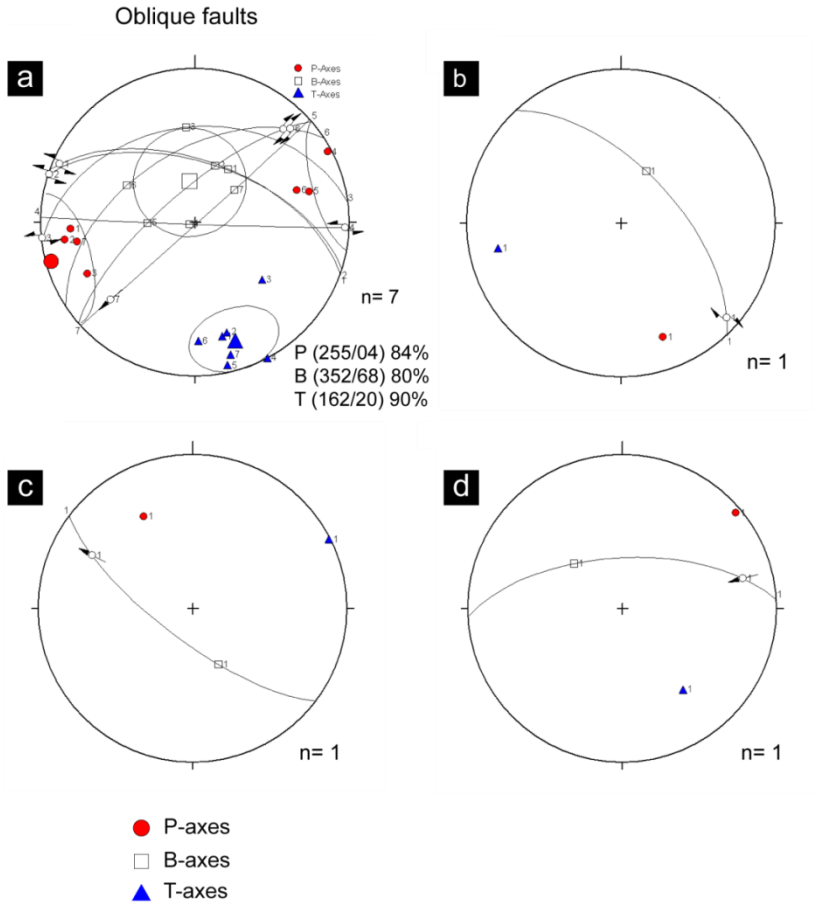

Figure 3.37 Combined P-T axes and Angelier plots of (a) a group of oblique-slip faults, (b-d) individual oblique-slip faults.

The axes of eight outcrop-scale folds, deforming Middle Eocene sediments were measured and plotted as great circles on a stereonet (Figure 3.38). There are two strike directions of the fold axes indicating N-S and E-W compressional events.

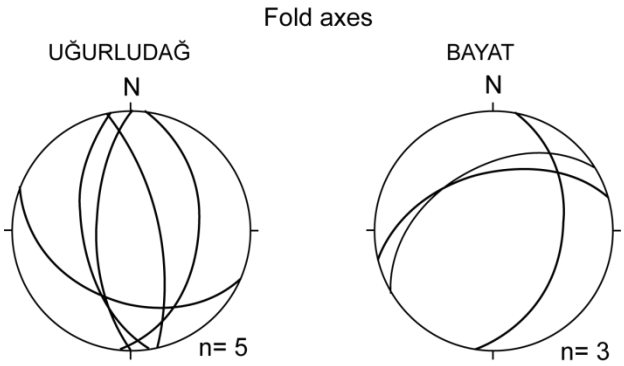

Figure 3.38 Lower hemisphere stereoplot of outcrop-scale folds in Uğurludağ (Sungurlu study area) and the Bayat study area

3.8.3 Structural interpretation

Compressional tectonics produced basin-scale thrust faulting in the Sungurlu area and East-West-orientated basin- and outcrop-scale folding in the Bayat area. Stratigraphic evidence in the Sungurlu area, notably the presence of Palaeocene-Ypresian fine-grained sediments and conglomerates, derived from the İzmir-Ankara Accretionary Complex, beneath thrust contacts suggest that a major compressional phase occurred in Late Palaeocene to Middle Eocene time.

Outcrop-scale faults are dominated by high-angle strike-slip faults, and feature another group of oblique-slip faults. There are, however, problems with inferring the timing of these faults. First, the faults cut units of all ages, so must be younger than Middle Eocene. Second, there are no cross-cutting relationships with which to infer a sequence of events. It is likely that the strike-slip faults are Neotectonic, and therefore relate to the Neotectonic phase of the deformation model of Kaymakcı *et al.* (2000; 2003).

3.9 Evolution of the Sungurlu and Bayat areas

This section aims to integrate the sedimentary, stratigraphic, geochemical, palaeocurrent and structural data discussed in this chapter in the form of basin-scale palaeogeographic maps (Fig. 3.39). First, the inferred depositional environments are summarised and their relationships to regional tectonics. Second, tectonic implications, in the context of continental collision in central Anatolia, are considered. The latest Palaeocene to Middle Eocene evolution of the northeastern margin of the Çankırı Basin is characterised by rapid lateral and vertical facies changes. The basin infill is dominated by detritus derived from the İzmir-Ankara Accretionary Complex, which acted as the primary erosional source area. The Ypresian to Lutetian development shows evidence of a compressional tectonic regime, probably related to the collision of the Pontides to the north and the Niğde-Kırşehir Massif to the south.

3.9.1 Late Palaeocene (Thanetian: 58-55 Ma)

The earliest sedimentation is represented by Late Palaeocene (Thanetian) marls, rich in benthic foraminifera, as seen in the Uğurludağ locality of the Sungurlu study area.

3.9.2 Early Eocene (Ypresian: 55-49 Ma)

The Ypresian saw the deposition of shelf carbonates and slope/basinal clastics. Clastic sedimentary basin infill was mostly derived from the İzmir-Ankara Accretionary Complex. Local development of Nummulitic banks (Lithofacies CA7) at Kepir Tepe in the Çayraz Formation in the Sungurlu study area indicates shallow-marine shelf-type conditions. Carbonate deposition was contemporaneous with sandstone and silt turbidite deposition (Lithofacies M2 and M13), characteristic of the Upper Palaeocene-Middle Eocene Yoncalı Formation.

Turbidity currents reworked sediments comprising bioclastic material from the local carbonate banks, and lithoclastic material from the İzmir-Ankara Accretionary Complex, from the basin margin into a basin/slope setting. The turbidites are thin- to medium-bedded and medium- to coarse-grained. A lack of three-dimensional exposure, however, hinders an architectural analysis of the turbidite system. Conglomerates and pebbly sands of the Yoncalı Formation contain clasts sourced from the İzmir-Ankara Accretionary Complex (i.e. limestone, basalt, red radiolarian chert, serpentinite) and occur below the tectonic contact with the İzmir-Ankara Accretionary Complex (see logs SU-2 and SU-3). This suggests that the clastic sediments were deposited in debris flows and high density turbidity flows ahead of a propagating thrust front, represented by tectonic slices of the İzmir-Ankara Accretionary Complex, were emplaced onto the basin margin. Palaeocurrents indicate a perpendicular flow from the basin margin towards the depocentre.

3.9.3 Middle Eocene (Lutetian: 49-41 Ma)

A shallowing-upwards sequence occurred during the Lutetian, probably related to the thickening and uplift of the İzmir-Ankara Accretionary Complex. Carbonate shelf-type deposition became widespread as a result. Deposition of the Çayraz Formation continued in the Sungurlu area and initiated in the Bayat area. Both areas feature large benthic foraminiferal, and, locally, bivalve, gastropod and echinoid fauna, indicating a shallow marine (tens of metres) depositional environment. Clastic deposition shallowed in the Sungurlu area.

Clastic sedimentation in the Bayat area was dominated by turbidites of the Upper Palaeocene-Middle Eocene Yoncalı Formation, and the deltaic, volcaniclastic sandstones of the Lutetian Karabalçık Formation. The shallow marine clastics and carbonates of the Bayat area interfinger and overlie the Lutetian volcanic Bayat Formation.

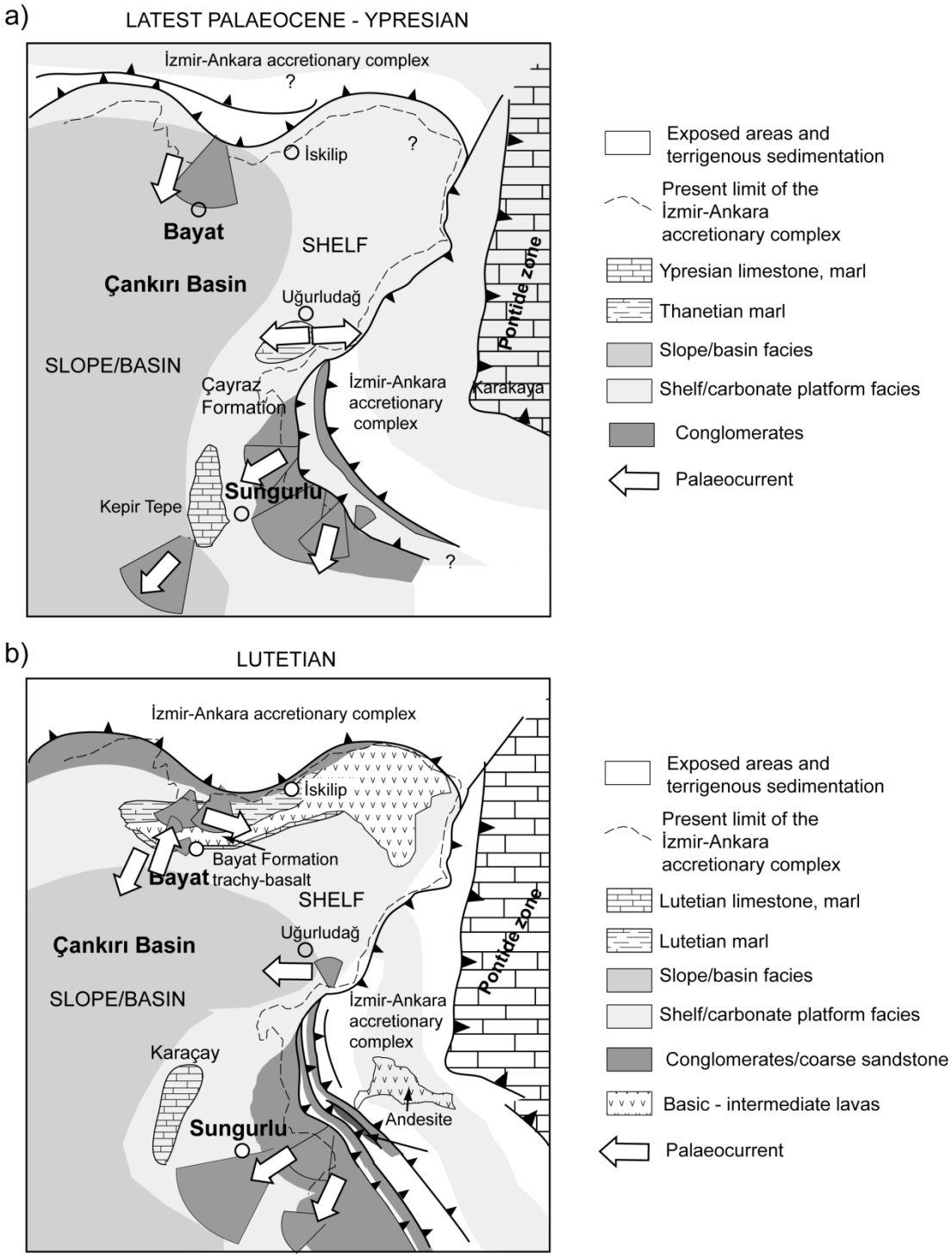

Figure 3.39 Schematic palaeogeographic reconstructions of the north-eastern margin of the Çankırı Basin, based on this study, **(a)** latest Palaeocene-Ypresian, **(b)** Lutetian. The maps show outline structural elements, inferred depositional environments and palaeocurrent trends. The reconstructions assume no palaeotectonic rotation.

3.9.4 Post-Middle Eocene

Post-Middle Eocene time was characterised by a cessation of marine deposition. A major regression occurred, probably due to continuing tectonic uplift. Depositional environments are represented by the continental İncik Formation, probably deposited in a flood plain fluvial environment. Strike-slip and oblique-slip faulting occurred as a result of north-south, northwest-southeast and west southwest-east northeast compression; however the data are insufficient to infer the relative and absolute timing of this brittle deformation.

3.9.5 Tectonic setting

The latest Palaeocene-Middle Eocene development of the northeastern margin of the Çankırı Basin records critical events in the geological history of central Anatolia. The development of the Çankırı Basin occurred ahead of a syn-orogenic fold-thrust belt that comprised the Izmir-Ankara Accretionary Complex and the Pontide margin (represented by the Karakaya Complex). In terms of competing tectonic hypotheses of collision, the following evidence is consistent with a model of a Middle Eocene collision event: 1) major, Middle Eocene compressional deformation is evident in both the Sungurlu and Bayat areas; 2) sediments generally exhibit a shallowing-upwards depositional environment and; 3) lava geochemistry suggests a transition from a calc-alkaline nature to a mildly alkaline character, possibly erupted in an extensional, post-collisional setting.

3.10 Conclusions and summary of new data from Chapter 3

- This chapter has presented new sedimentary, stratigraphic, palaeontological, geochemical, and structural data which shed new light on the latest Palaeocene –

Middle Eocene evolution of the north-eastern margin of the Upper Cretaceous-recent Çankırı Basin.

- The Çankırı Basin developed in a suture zone between the Pontide active margin to the north and the northern passive margin of the Niğde-Kırşehir Massif to the south. The northeastern margin of the basin is delimited by south/south-easterly verging thrust sheets of the İzmir-Ankara Accretionary Complex, which also forms the basin basement.

- New stratigraphy, sedimentology and palaeontology show that latest Palaeocene-Middle Eocene sediments record a regional shallowing-upwards sequence from marine to continental environments. Deposition started in the Late Palaeocene (Thanetian) with previously undocumented fossiliferous marls. Clastic sedimentation transported detritus from the İzmir-Ankara Accretionary Complex to shelf and slope environments by turbidity currents and debris flows.

- New geochemical data confirm a subduction-related source melt for Middle Eocene calc-alkaline to mildly alkaline extrusive lavas. Geochemically, the lavas correlate with a belt of Middle Eocene volcanic rocks which, in one interpretation, is thought to have been generated by a slab break-off event in a post-collisional setting. However, evidence is lacking of an abrupt pre-Lutetian regional uplift as proposed by the slab break-off model. Instead, the parental magmas were probably generated in a collisional arc-type to an extensional, post-collisional-type setting.

- New structural data confirm that the study areas are cut by thrust and transcurrent faults. Thrust faults are related to Middle Eocene compression, whereas transcurrent faults are probably associated with Neotectonic events involving the post-collisional reorganisation of central Anatolia.

- New data imply a collision event in the Middle Eocene, in contrast to regional tectonic models of Late Cretaceous continental collision in central Anatolia.

Chapter 4: The Tuz Gölü Basin

4.1 Introduction

It is generally accepted that central Anatolia is composed of accreted micro-continental units and associated suture zones (Şengör & Yılmaz 1981; Robertson & Dixon 1984). In this region, a strand of the former northern Neo-Tethys Ocean (the İzmir-Ankara-Erzincan Ocean) was subducted northwards under the Eurasian (Pontide) active margin during the Cretaceous-Early Cenozoic time. Subduction was associated with the genesis and emplacement of accretionary prisms, ophiolites and deep-water margin units onto the former passive margins of micro-continents. The suture zone is associated with several large Late Cretaceous-Early Cenozoic sedimentary basins (the "Central Anatolian Basin Complex"). The basins hold a critical record of the tectono-sedimentary processes related to the assembly of central Anatolian tectonic units.

Many modern interpretations recognise two contrasting types of basins in central Anatolia which border the Niğde-Kırşehir Massif [also known as the Central Anatolian Crystalline Complex (e.g. Akıman *et al.* 1993), the Kırşehir Continent (Şengör *et al.* 1984), the Kırşehir Complex (Lünel 1985) and the Kırşehir Block (Robertson & Dixon 1984)] an inferred micro-continental block (e.g. Görür *et al.* 1984; Robertson *et al.* 2009). To the south and east of the Niğde-Kırşehir Massif, two important localities are the Sivas Basin (Kavak et al. 1997; Cater *et al.* 1991; Gürsoy *et al.* 1997; Dirik *et al.* 1999; Yılmaz & Yılmaz 2006) and the Ulukışla Basin (Göncüoğlu 1986; Clark & Robertson 2002; Alpaslan *et al.* 2004; Clark & Robertson 2005; Alpaslan *et al.* 2006; Kurt *et al.* 2008) (Fig.4.1). These two basins are interpreted to have developed on northern Neotethyan ophiolites as the ophiolites were emplaced onto the Gondwana-derived Tauride carbonate platform.

At the northern and western margin of the Niğde-Kırşehir Massif, several basins developed during regional plate convergence in the Upper Cretaceous-Middle Eocene time. These include the Çankırı Basin (Ayan 1969; Birgili *et al.* 1975; Tüysüz & Dellaloğlu 1992; Erdoğan *et al.* 1996; Kaymakcı *et al.* 2009), the Haymana-Polatlı Basin (Gökçen 1976; Ünalan *et al.* 1976; Gökçen 1978; Görür *et al.* 1984), the Kırıkkale Basin (Norman 1972; Norman 1973a; Norman 1973b; Akyürek

et al. 1984; Akyürek *et al.* 2001) and the Tuz Gölü (Salt Lake) Basin (Rigo de Righi & Cortesini 1959; Arikan 1975; Uğurtaş 1975; Dellaloğlu & Aksu 1984b; Görür *et al.* 1984; Çemen *et al.* 1999; Derman *et al.* 2000) (Fig.1). The tectono-sedimentary development of the Central Anatolian Basin Complex is still not fully understood.

Presently, there are two competing end-member tectonic models of basin formation. In one interpretation, plate convergence continued until the Middle Eocene, generating magmatic arcs and associated accretionary fore-arc basins (Görür *et al.* 1984; Koçyiğit 1991; Görür *et al.* 1998). In this scenario, the northern Neotethys comprised two oceanic strands: 1) the İzmir-Ankara-Erzincan Ocean to the north and; 2) the Inner Tauride Ocean to the south. Separating the oceanic strands was the Niğde-Kırşehir Massif, a microcontinent rifted from the larger Tauride continent to the south. In contrast, other interpretations propose that northern Neotethys existed as a single oceanic basin that sutured in the Late Cretaceous, implying that the Central Anatolian basins are post-collisional (Göncüoğlu *et al.* 1995; Boztuğ 1998; Gürer & Aldanmaz 2002).

The Tuz Gölü Basin was chosen for study because it provides a unique opportunity to study sedimentation on the margin of the Niğde-Kırşehir microcontinent during the destruction of the Neotethyan Ocean. Study of the Late Cretaceous-Middle Eocene history of the basin is hampered by a post-Middle Eocene to recent sedimentary cover of continental clastics, evaporites and lacustrine limestone (Görür *et al.* 1984). Furthermore, exposures of Upper Cretaceous-Middle Eocene rocks are mostly restricted to a semi-continuous ~15 km long strip on the eastern basin margin between the towns of Şereflikoçhisar and Hanobası (Fig. 4.3a). However, the basin contains Upper Cretaceous-Middle Eocene marginal facies that are not found in other central Anatolian basins (e.g. the Upper Cretaceous non-marine Kartal Formation) and an opportunity to examine a major bounding fault zone (termed the "Tuz Gölü Fault Zone"). Previous studies (see below) have not presented detailed sedimentological, palaeontological, sandstone provenance, palaeocurrent or palaeostress data. Using data gathered in the field, and a wider literature survey, the purpose of this chapter is to present and integrate these data into a coherent model of tectono-sedimentary processes involved in the development of

the Tuz Gölü Basin. A further aim is to test two existing end-member models of basin formation in central Anatolia, outlined above, and, if necessary, develop a new one.

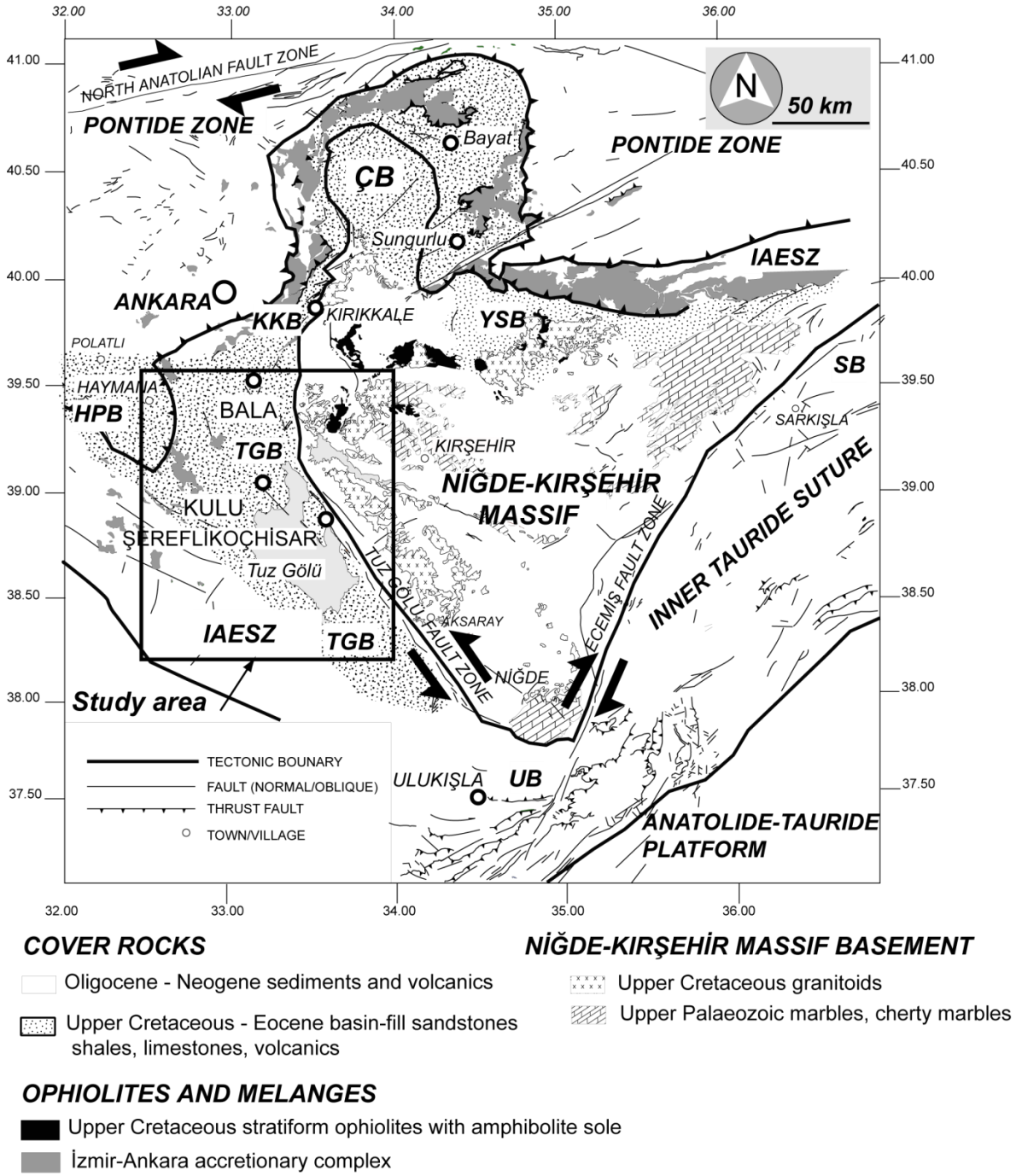

Figure 4.1 Regional map of central Anatolia indicating major basin areas and tectonic units. İzmir – Ankara – Erzincan Suture Zone (IAESZ), Tuz Gölü Basin (TGB), Kırıkkale Basin (KB), Çankırı Basin (ÇB), Ulukışla Basin (UB), Sivas Basin (SB). The area discussed in this chapter is indicated by the black box. Modified after Clark & Robertson (2002); MTA (2002).

4.2 Regional Geology

The basin is situated on the western margin of the Niğde-Kırşehir Massif and is bound to the south by the Ulukışla Basin, to the west by the Yeniceoba and Cihanbeyli fault zones (Özsayin & Dirik 2007), to the east by the Tuz Gölü fault zone and to the north by the İzmir-Ankara accretionary complex south of the Haymana – Polatlı Basin (i.e. the Samsam High of Görür *et al.* 1984). To the southwest lie blueschists associated with the Anatolide Unit, interpreted as part of the Inner Tauride suture (Okay 1984). It should be noted that several studies (e.g. Görür *et al.* 1984; Çemen *et al.* 1999) consider the 'Tuz Gölü Basin complex' to comprise of two sub-basins, the Haymana-Polatlı Sub-Basin and the Tuz Gölü Sub-Basin. This chapter is concerned with the Tuz Gölü Sub-Basin only. Most interpretations (e.g. Dellaloğlu & Aksu 1984a; Görür *et al.* 1984) suggest that the basin developed on a composite basement of the İzmir-Ankara accretionary complex and the Niğde-Kırşehir microcontinent.

The İzmir-Ankara accretionary complex (Okay *et al.* 2006) is the youngest and structurally highest unit of the classic Ankara Mélange (Bailey & MacCallien 1950; Norman 1984; Dilek & Thy 2006). The İzmir-Ankara accretionary complex is an ophiolitic mélange which represents dismembered blocks and thrust sheets of Neotethyan oceanic lithosphere, ocean island-type seamounts and pelagic sediments. Tankut *et al.* (1998) recognise three chemically different types of volcanic rocks: 1) sub-alkaline N-MORBs; 2) island-arc tholeiites; 3) within-plate oceanic island-type alkaline basalts. Biostratigraphic ages range from Late Triassic (Norian) to Mid Cretaceous (Albian / Turonian) (Bragin & Tekin 1996; Rojay *et al.* 2001). U/Pb zircon dating yields Early Jurassic dates for a plagiogranite dyke intruding serpentinised upper mantle peridotite (Dilek & Thy 2006).

The Niğde-Kırşehir microcontinent is composed of a metamorphic basement, overlying ophiolitic fragments and intrusive granitoids. The metamorphic rocks are inferred to be Mesozoic/Palaeozoic in age and consist of platform marbles, calc-silicates, schists and gneisses (Seymen 1981; Floyd *et al.* 2000). Metamorphic grades

range from upper amphibolite to lower amphibolite/greenschist (Whitney & Dilek 2001). There is presently considerable debate on the Mesozoic tectonic setting and evolution of the Niğde-Kırşehir Massif. It is interpreted as a promontory of the Tauride-Antolide Platform (Yaliniz *et al.* 1996; Floyd *et al.* 2000; Göncüoğlu *et al.* 2006), as a microcontinent of the Northern Neotethys Ocean (Görür *et al.* 1984; Robertson & Dixon 1984; Robertson *et al.* 2009), as part of the Eurasian margin (Kazmin & Tikhonova 2006), or as an allochthonous terrane moved laterally to its present position during the Triassic (Stampfli *et al.* 2001).

The northern and western margins of the massif have been overthrust from the north by fragmented Upper Cretaceous supra-subduction zone Neotethyan ophiolites (Yalınız & Göncüoğlu 1998; Floyd *et al.* 2000; Yalınız *et al.* 2000b), including the Sarıkaraman Ophiolite (Yaliniz *et al.* 1996) and the Çiçekdağ Ophiolite (Yılmaz & Boztuğ 1998; Yalınız *et al.* 2000a). The metamorphic basement and ophiolites have been intruded by a series of granitic plutons of I-, A- and S-Type (e.g. Boztuğ 2000; Köksal *et al.* 2001; Köksal *et al.* 2004; Tatar & Boztuğ 2005; Boztuğ *et al.* 2007). Dated intrusive rocks show U/Pb SHRIMP ages of 85-92 Ma (Whitney *et al.* 2003), U/Pb titanite ages of 74.0±2.8 and 74.1±0.7 Ma (Köksal *et al.* 2004). K/Ar cooling ages of hornblende and biotite give dates of 66.6±1.1 Ma to 79.5±1.7 Ma (Ilbeyli *et al.* 2004). $^{40}Ar/^{39}Ar$ biotite cooling ages are 77.6±0.3 Ma (Kadıoğlu *et al.* 2003). The geodynamic setting of the granitoid source melt is variously interpreted as syn- to post-collisional associated with the closure of northern Neotethys (e.g. Göncüoğlu & Türeli 1994; Boztuğ 1998; Düzgören-Aydin *et al.* 2001; Köksal *et al.* 2001; Ilbeyli *et al.* 2004; Köksal *et al.* 2004) or an Andean-type subduction setting associated with the closure of Inner Tauride Ocean (Kadıoğlu *et al.* 2006).

4.3 Previous work

The Tuz Gölü Basin has been the subject of several studies, and has been of interest to both academia and industry since the 1960s. Work up to the 1970s focused on developing a stratigraphic framework and included early seismic studies (Rigo de

Righi & Cortesini 1959; Arikan 1975; Uğurtaş 1975) (Fig. 4.2a). During the 1980s and 1990s, the basin was interpreted in the context of regional convergent tectonics (Dellaloğlu & Aksu 1984a; Dellaloğlu & Aksu 1984b) (Fig. 4.2b). According to Görür *et al.* (1984), the Late Cretaceous-Middle Eocene history of the basin developed as a fore-arc basin associated with a northeast-dipping subduction zone that consumed the oceanic lithosphere of the Inner Tauride Ocean (Fig. 4.2c). Alternatively, Çemen *et al.* (1999) interpret the basin as a tensional/trans-tensional basin that developed on the margin of the Niğde-Kırşehir / Kütahya-Bolkardağı unit of the Taurides during the Late Maastrichtian-Eocene (Fig. 4.2d). Recent work includes geophysical and geochemical interpretations in relation to petroleum potential (Ayyıldız 2006; Tekin *et al.* 2007; Aydemir 2008; Aydemir & Ateş 2008).

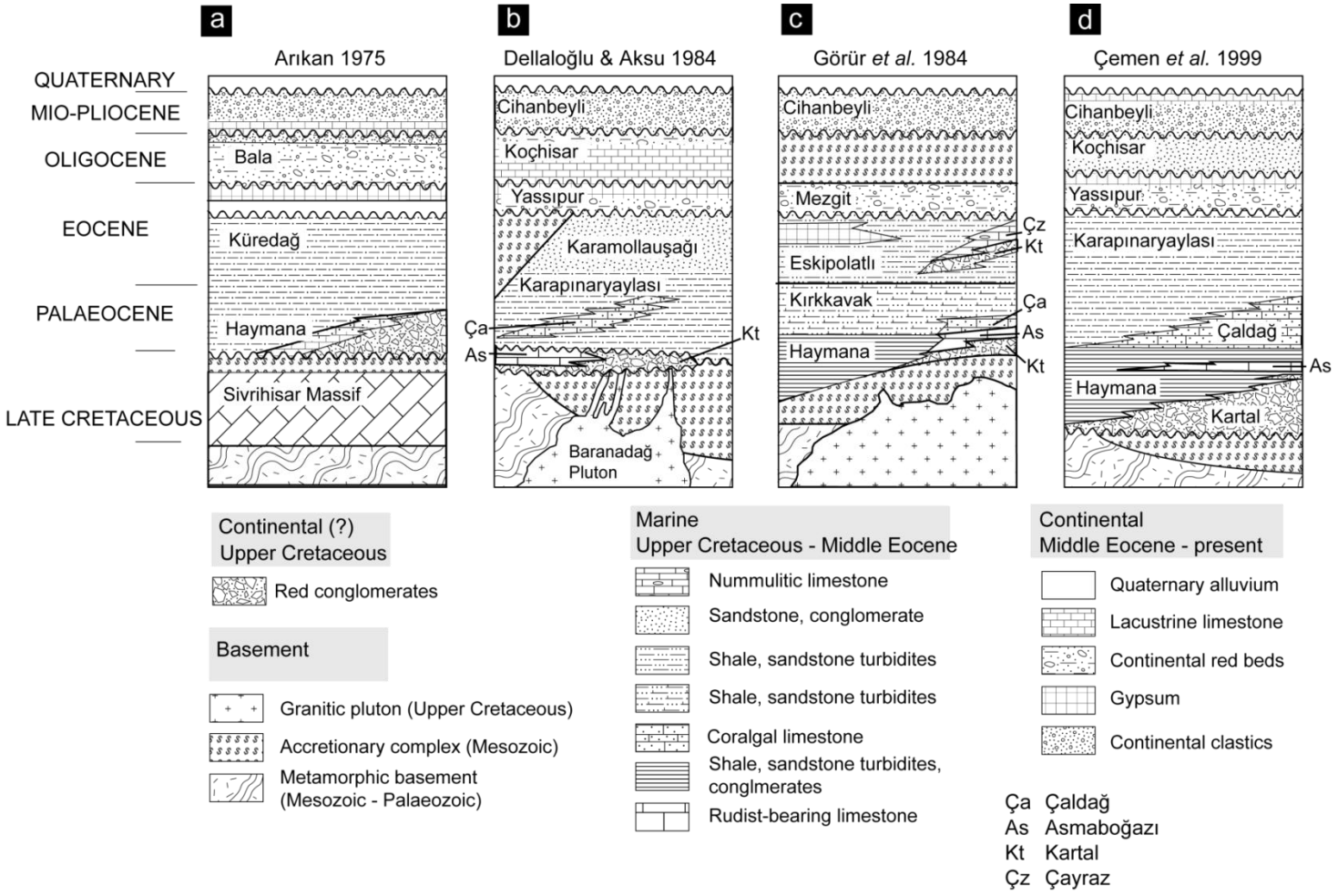

Figure 4.2 Previous stratigraphic schemes (with formation names) of the Tuz Gölü Basin (a) an early stratigraphic interpretation (Arıkan 1975) (b) the stratigraphy of Dellaloğlu & Aksu (1984a) (c) the stratigraphy of Görür *et al.* (1984) in which the basin developed in a forearc-type setting (d) the stratigraphic model of Çemen *et al.* (1999) who favoured a post-collisional setting.

4.4 Stratigraphy and sedimentology

Gravity anomaly studies suggest that the total sedimentary thickness of the Tuz Gölü Basin is ~4 km, with isolated depocentres reaching up to ~8 km (Aydemir & Ateş 2006). Based on wildcat wells, Çemen *et al.* (1999) suggest a sediment thickness of ~2.5 km near the basin margins. Study of the Late Cretaceous-Middle Eocene history of the Tuz Gölü Basin is hampered by erosion and a post-Middle Eocene to recent post-collisional sedimentary cover. Exposures of Upper Cretaceous-Middle Eocene rocks are mostly restricted to a semi-continuous ~15 km long strip on the eastern basin margin between the towns of Şereflikoçhisar and Hanobası (Figs. 4.3, 4.4, 4.5 and 4.6). The strip represents the footwall of the Tuz Gölü fault zone which forms the study area of the eastern basin margin. In the basin depocentre, exposure of Upper Cretaceous-Middle Eocene rocks is severely limited and consists of small, metre-scale outcrops in roadside and quarry cuttings near the town of Kulu (Fig. 4.3). This study also discusses data from the northernmost outcrops of the Tuz Gölü Basin near the town of Bala (Fig. 4.3). This area allows useful comparisons to be made with the southern area around Şereflikoçhisar.

On the basis of their inferred depositional environments, the lithofacies of the Tuz Gölü Basin have been divided into three groups:

1) Continental lithofacies (prefixed with ‘C’) (Table 1)

2) Shallow marine reefal carbonate lithofacies (prefixed with ‘R’) (Table 2) and

3) Deeper marine slope lithofacies consisting of siliciclastic (prefixed with ‘M’) (Table 4) and reworked carbonate deposits (prefixed with ‘RW’) (Table 3).

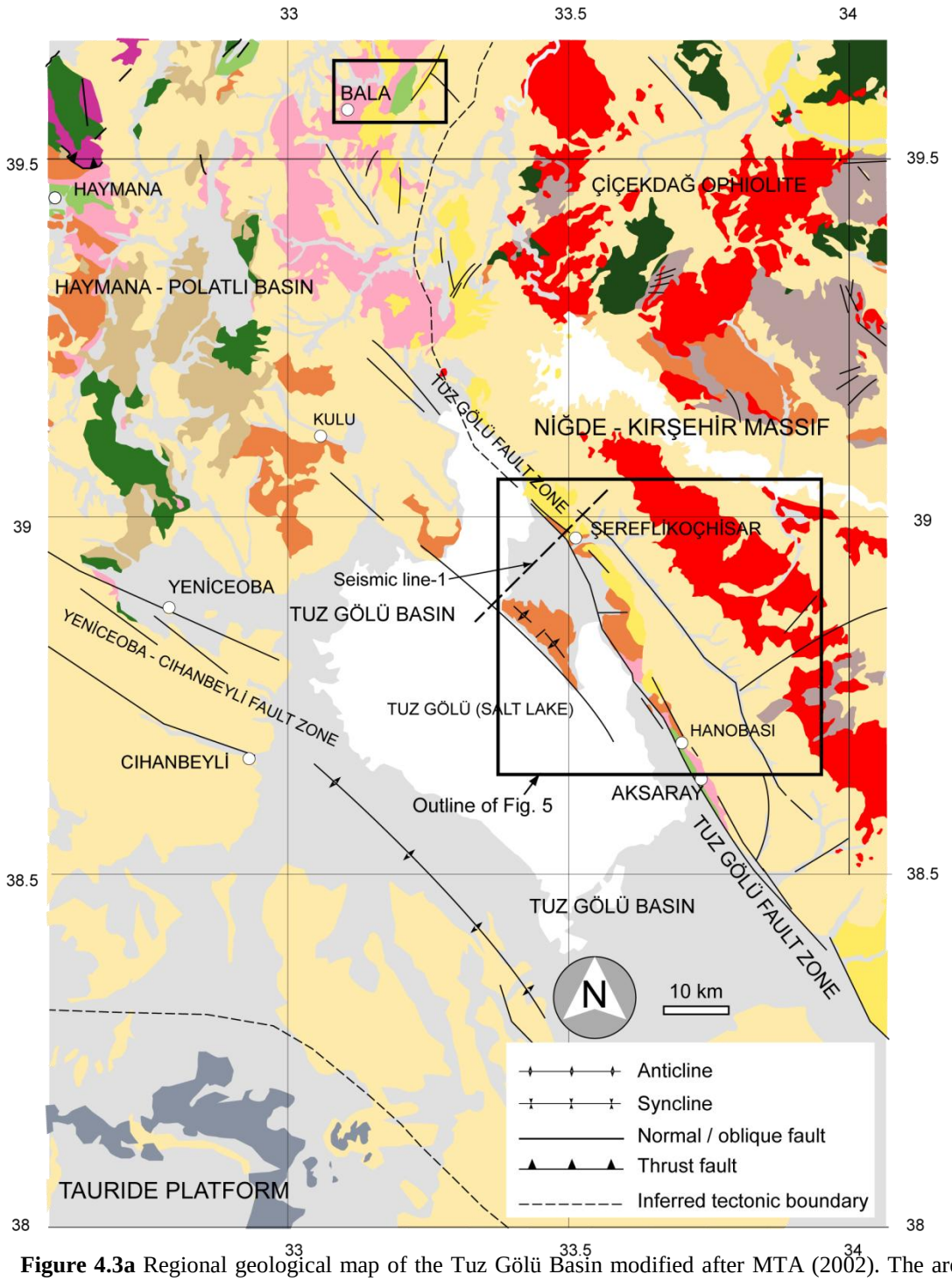

Figure 4.3a Regional geological map of the Tuz Gölü Basin modified after MTA (2002). The areas under discussion in this chapter are the area between Şereflikoçhisar and Hanobası (indicated by the black box), Kulu to the northwest and Bala to the north. See Figure 4.4 for key.

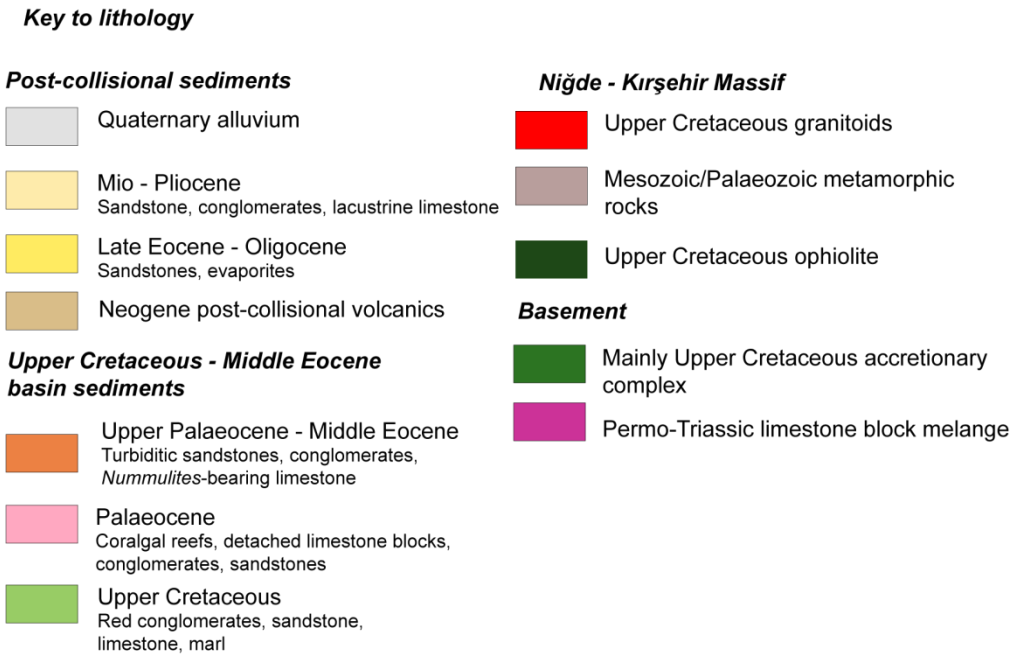

Figure 4.3b Lithological key to the regional map of Figure 4.3a. The sediments under discussion in this chapter are Upper Cretaceous-Middle Eocene. Post Middle Eocene rocks are of post-collision origin.

This study is the first to attempt a detailed lithofacies analysis and aims to increase the understanding of sedimentation in the Tuz Gölü Basin. Below is a discussion of the sedimentary formations and associated lithofacies of the Tuz Gölü Basin. Summaries of lithofacies are provided in Tables 1 to 4. The role of new data gathered during this study will be highlighted, and comparisons made with existing work. Particular attention will be paid to where new data confirm, add to or change existing studies.

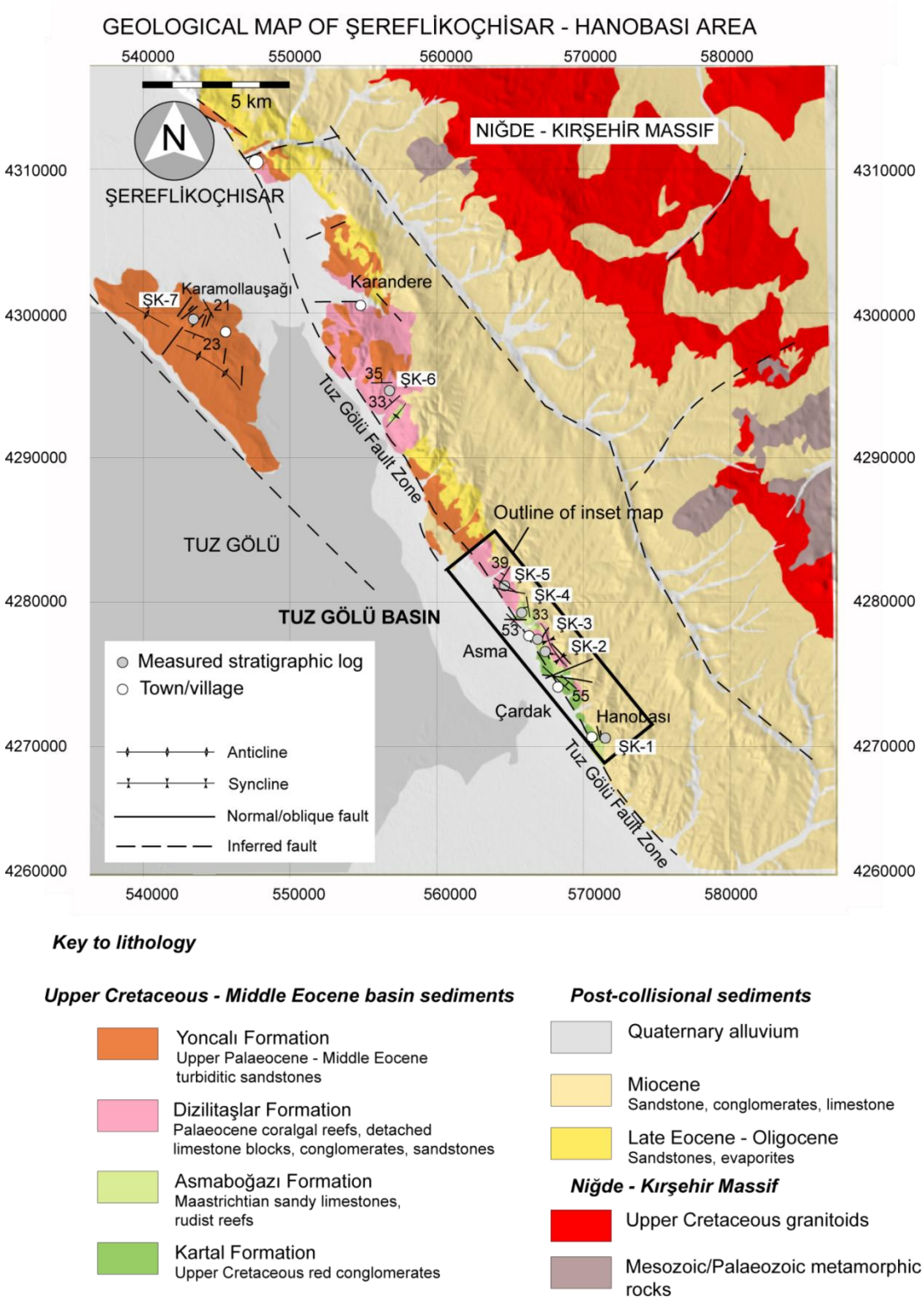

Figure 4.4 Geological map of the eastern margin of the Tuz Gölü Basin, redrawn from MTA (1989)

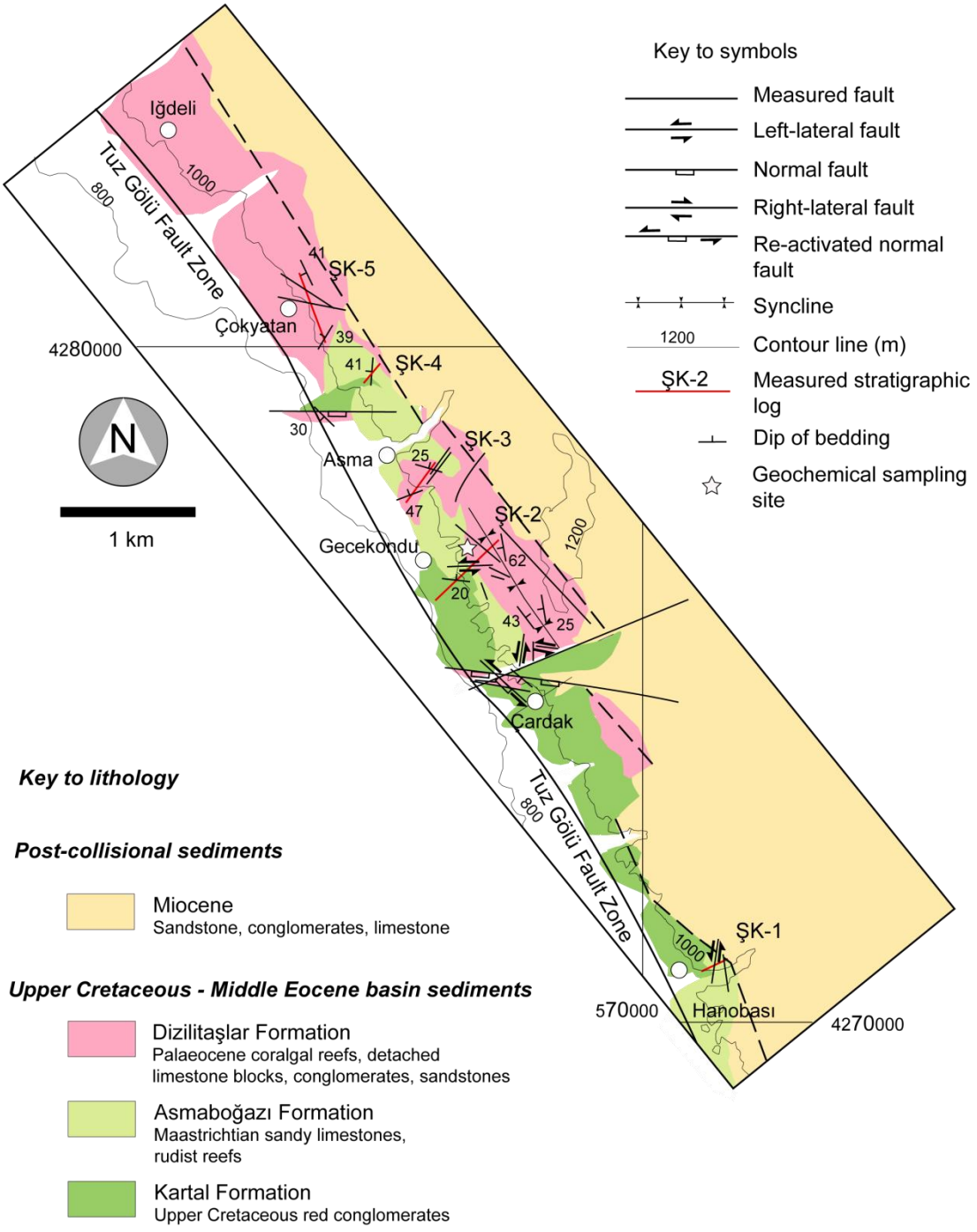

Figure 4.5 Geological map of the Şereflikoçhisar – Hanobası area of the eastern margin of the Tuz Gölü Basin. Data are based on this study.

Table 1 Summary of continental lithofacies in the Tuz Gölü Basin

Facies	Lithology	Textures	Sedimentary structures	Bounding surfaces & Bed thicknesses	Fossils and outsized clasts	Inferred depositional process
C1	Clast-rich pebble - boulder conglomerate . Coarse red sandstone.	Very poorly sorted. Range of clast angularities from sub- to well-rounded. Local textural inversion in Bala area.	Mostly absent. Local normal grading.	Erosive bases and irregular tops. Beds < 6 m thick	None	Mass flow deposits in alluvial fan setting.

Table 2 Summary of shallow marine shelf-type carbonate lithofacies

R1	Grey/yellow rudist limestone	Interstitial pebble-grade limestone conglomerate	Preferential alignment of rudist fossils	Irregular beds up to ~8 m thick.	Rudists	Lightly reworked fore-reef facies
R2	Algal- and benthic foraminifera-rich limestone	Aggregates of algal-rich wackestone and foraminifera-rich packstone	Absent	In-situ lenses <2.5 m-thick. Continuous for ~20 m laterally. In Bala area, ~100 m thick.	Skeletal algae, benthic foraminifera	Low energy restricted inner shallow platform. Reworked in higher energy environment.
R3	Orange sandy limestone	Poorly sorted packstone with terrigenous grains (<10%)	Absent	Sharp bases and tops. Beds <0.5 m-thick.	Skeletal algae, large benthic foraminifera Angular quartz grains	Mixing of a range of carbonate shelf settings in high energy environment

Table 3 Summary of reworked carbonate lithofacies

RW1	Sandy limestone	Moderately well-sorted	Normal grading	Erosive bases, sharp tops	Benthic foraminifera Volcanic pebbles, bivalves.	Coarse-grained turbidites
RW2	Carbonate conglomerates	Well-sorted, angular clasts, <12 cm.	Absent	Lenticular beds with irregular bases and tops. 0.3 – 2 m thick.	Abundant benthic foraminifera	Debris flow
RW3	Detached blocks of coralgal limestone.	Benthic foraminifera- and coral-rich packstone/ wackestone	Absent	Blocks < 3 m-thick. Commonly showing faulted margins	Benthic foraminifera,coral, algae, rare gastropods and bivalve shells	Mass transport on a steep slope

Table 4 Summary of terrigenous lithofacies

Facies	Lithology	Textures	Sedimentary structures	Bounding surfa ces & Bed thicknesses	Fossils and outsized clasts	Inferred depositional process
M1	Sandstone / Sandy limestone	Moderately well-sorted, sub-angular grains	Normal grading, local plane-parallel lamination.	Erosive bases, gradational tops. Beds typically <0.5 m thick	Rare benthic foraminifera	Bouma-type medium grained turbidite.
M2	Extra-formational clastic conglomerates	Poorly sorted clasts with range of angularities, <10 cm. Local clast imbrication.	Absent	Irregular, erosive bases, sandy tops. <0.6 m-thick	Angular limestone blocks <80 cm.	Debris flow
M3	Lithoclast-rich sandstone	Fine- to coarse-grained, range of grain angularities and sorting.	Packages of up to four depositional surfaces	Sharp tops and bases. Beds <5 m-thick.	Basic volcanic lithoclasts and alerted plagioclase.	High density turbidity currents
M4	Pebbly sand and shale intercalations	Coarse-grained, poorly sorted sandstone. Pebbly bases.	Normal grading from pebbly bases to coarse / medium sand.	Erosive bases, irregular and diffuse tops. Beds <2.3 m-thick.	Pebbles of limestone, basalt, sandstone, radiolarian chert. Rare benthic foraminifera	High density turbidites
M5	Massive, brown, clast-rich sandstone and mudstone couplets	Moderately well-sorted grains. Abundant volcanic lithoclasts and plagioclase.	Flute marks, burrowing. Grading and lamination are commonly absent.	Sharp bases and tops. Beds <0.4 m-thick.	None	Turbidity currents followed by bioturbation.
M6	Limestone and black chert conglomerates	Very poorly sorted clasts, pebble- to cobble-size. Matrix supported.	Inverse grading at base.	Sharp bases with protruding clasts	Floating rafts of sandstone	Debris flow

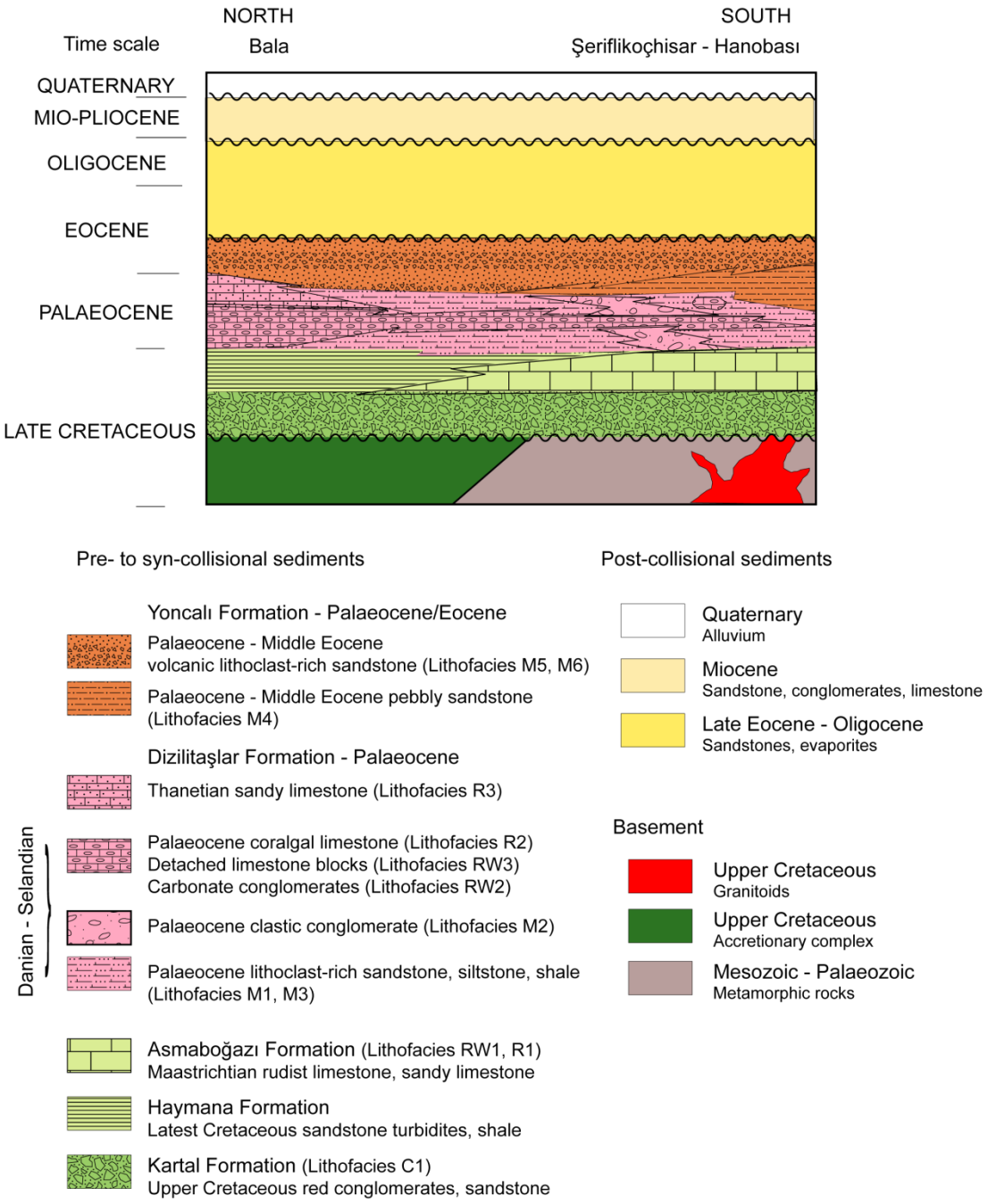

Figure 4.6 New stratigraphic scheme proposed by this study. Data and lithofacies interpretations in Upper Cretaceous – Middle Eocene sediments are based on this study. The Basement and post-Middle Eocene geology is based on Dellaloğlu & Aksu (1984) and Görür *et al.* b1984). Palaeontological data are from N. İnan & K. Taslı (pers. comm. 2009).

4.4.1 The Şereflikoçhisar-Hanobası area.

4.4.1.1 The Kartal Formation (Upper Cretaceous)

The oldest sedimentary unit of the Tuz Gölü Basin is the Kartal Formation, first named by Turkish Gulf Oil (1961). Until now, the Kartal Formation has not been described in terms of sedimentary and depositional processes. The exposed thickness of the Kartal Formation in this area is ~200 m, however based on subsurface seismic evidence its inferred maximum thickness is 1080 m (Aydemir & Ateş 2006). The Kartal Formation is represented by lithofacies C1, which is well exposed between Asma and Hanobası (Fig. 4.6) where it consists of a very poorly sorted, matrix-supported, red conglomerate intercalated with coarse red sandstone and mudstone. Sandstone is medium- to coarse-grained and locally parallel stratified.

Conglomerates contain rounded pebble- to boulder-sized randomly orientated clasts. Beds reach a maximum thickness of ~6 m and feature erosive bases and irregular tops. Sedimentary structures are rare; however, grading is locally normal and disrupted by ~0.5 m-thick layers of outsized clasts (Fig. 4.8a). Clast abundance is dominated by basalt and andesite (~80%) followed, in abundance, by gabbro (~10%), sandstone (~5%) with minor amounts of granite, dacite, metamorphic rocks and serpentinite. One notable trend is an increase in serpentinite clasts from very rare near Asma, to ~20 % of total clast abundance near Hanobası to the south. The matrix is red mudstone and coarse red sandstone.

4.4.1.1.1 Interpretation of the Kartal Formation

The lack of internal structure and imbrication within the conglomerates suggests they were the product of high-viscosity mass flows (e.g. Collinson 1986). In addition, red sandstones intercalated with conglomerates are here interpreted as the product of waning flood stages (e.g. Steel 1974). The Kartal Formation has been

interpreted as basin margin alluvial fan deposits possibly associated with basin-margin parallel extensional faulting (e.g. Çemen *et al.* 1999). This implies the source area of the conglomerates, presumably the Niğde-Kırşehir Massif and ophiolitic mélange, were at least partially sub-aerially exposed and formed highland areas adjacent to the eastern basin margin. Presently, there is no fossil evidence with which to date the Kartal Formation, however, most studies suggest a Late Cretaceous age (Dellaloğlu & Aksu 1984a; Görür *et al.* 1984; MTA 1989; Çemen *et al.* 1999). Given that the Kartal Formation is overlain by the Maastrichtian Asmaboğazı Formation, a Late Cretaceous age is probably correct.

4.4.1.2 The Asmaboğazı Formation (Maastrichtian)

The Kartal Formation grades vertically into the Asmaboğazı Formation (Figs. 4.8b, 4.9a, 4.9c). This formation was first named by Rigo de Righi & Cortesini (1959) and crops out near Asma and Çardak (Fig. 4.6). The Asmaboğazı Formation reaches a maximum thickness of ~40 m and is divided into two distinctive parts, lower reworked sandy limestone (lithofacies RW1; Table 3) and upper Rudist reef (lithofacies R1; Table 2).

4.4.1.2.1 Lithofacies RW1: sandy limestone

The lower part consists of lithofacies RW1 and is composed of yellow/brown bioclastic sandy limestone beds, up to 0.8 m thick, interbedded with laminated yellow/brown mudstone and siltstone. Individual beds are frequently graded with erosive bases. The average grain size fines upwards from granule/pebble to medium-grained. Out-sized cobble-sized clasts include well-rounded pebbles of basic volcanic rocks and also bivalves in varying states of disarticulation (Figs. 4.8c, 4.8d).

4.4.1.2.2 Interpretation of lithofacies RW1

These deposits are indicative of an influx of resedimented carbonate facies with a clastic component. These beds are interpreted as coarse-grained calciturbidites (e.g. Lowe 1982) that include a coarse, pebbly layer (R_2 layer in the classic coarse-grained turbidite model) that was the result of grain-flow deposits. In thin section, the sandy grainstone is composed of large benthic foraminifera (showing preferential alignment), sub-angular, poorly-sorted quartz grains and rare bivalve fragments now composed of drusy sparite. A Late Maastrichtian age is given by the presence of the benthic foraminifera *Omphalocyclus macroporus* Lamarck, *Orbitoides medius* d'Archiac, *Lepidorbitoides* sp. (Sample ŞK8.9A) and *Lepidorbitoides minor* Schlumberger, and *Orbitoides apiculatus* Schlumberger (Sample 8.9B) (N. İnan & K. Taslı pers. comm. 2009) (Fig. 4.8e). This date is in agreement with previous studies (e.g. Dellaloğlu & Aksu 1984a; Görür *et al.* 1984). Given the sedimentary structures observed and the presence of abundant large benthic foraminifera, these deposits probably represent sediment reworking from a carbonate platform edge/upper slope environment (Sartorio & Venturini 1988), probably on the western margin of the Niğde-Kırşehir Massif.

4.4.1.2.3 Lithofacies R1: rudist limestone

The lower part of the Asmaboğazı Formation shallows upwards into grey/yellow rudist-bearing limestone (lithofacies R1) containing *Hippurites* sp. and *Pironaea* sp. (Özer 1988) which are particularly well exposed in log ŞK4 (Fig. 4.9b) north of Asma (65912:79609). Rudists in log ŞK4 are preferentially orientated and feature interstitial angular carbonate clasts which suggests slight current reworking (Fig. 8f). Beds are <2 m thick at the base of the sequence and thin upwards. The rudist deposits form mounds, ~8 m in height that are covered by coarse clastic conglomerates of the Dizilitaşlar Formation (see below).

4.4.1.2.4 Interpretation of lithofacies R1

The rudist carbonates are interpreted as fore-reef facies (e.g. Wilson 1975; Aqrawi *et al.* 1998; Flügel 2004). Many Cretaceous carbonate platforms in the Neotethyan realm were characterised by rudist bivalves (e.g. Stössel & Bernoulli 2000; Sarı & Özer 2009) and indicate shallow-water deposition and low siliciclastic input. The Asmaboğazı Formation is here interpreted as recording a Maastrichtian marine transgression permitting the development of a carbonate platform. The platform is now eroded and/or covered by younger sediments but its likely position was to the east/northeast, fringing the basin margin along the western margin of the Niğde-Kırşehir microcontinent.

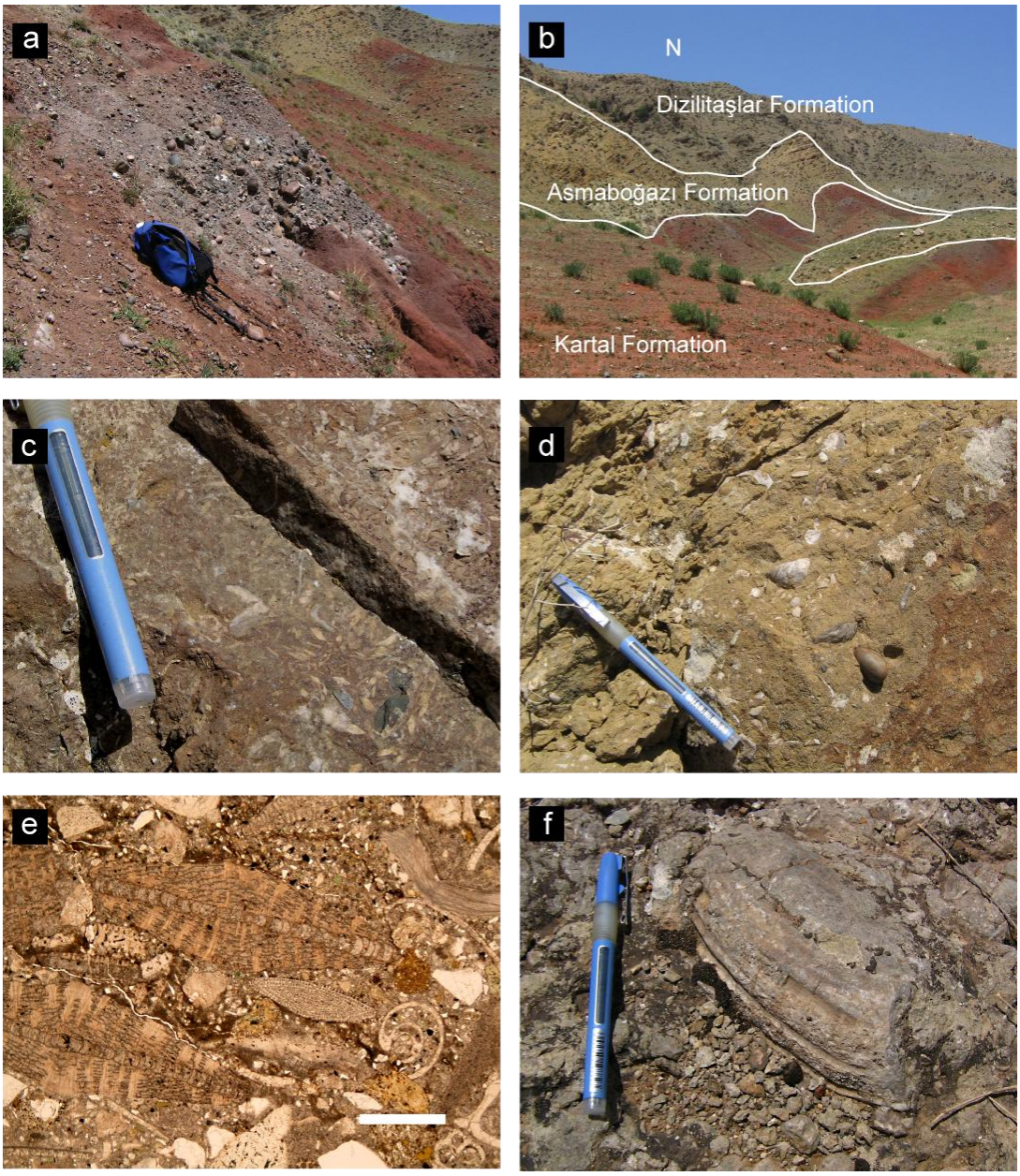

Figure 4.7 (a) Detail (looking north) of Upper Cretaceous conglomerates in the Kartal Formation, **(b)** view, looking approximately north, of the area measured in stratigraphic log ŞK-4. Foreground is the Kartal Formation; above comes the Maastrichtian Asmaboğazı Formation which is sealed by Palaeocene clastic conglomerates of the Dizilitaşlar Formation, **(c)** – **(d)** details of Maastrichtian sandy limestones (Lithofacies RW1) of the Asmaboğazı Formation. Note the outsized clasts of pebbles and bivalve shells, **(e)** photomicrograph (in plane-polarised light) of sample ŞK8.9B showing large benthic foraminifera *Orbitoides apiculatus* Schlumberger. Scale bar = 1mm, **(f)** field photograph of a rudist specimen in Lithofacies R1.

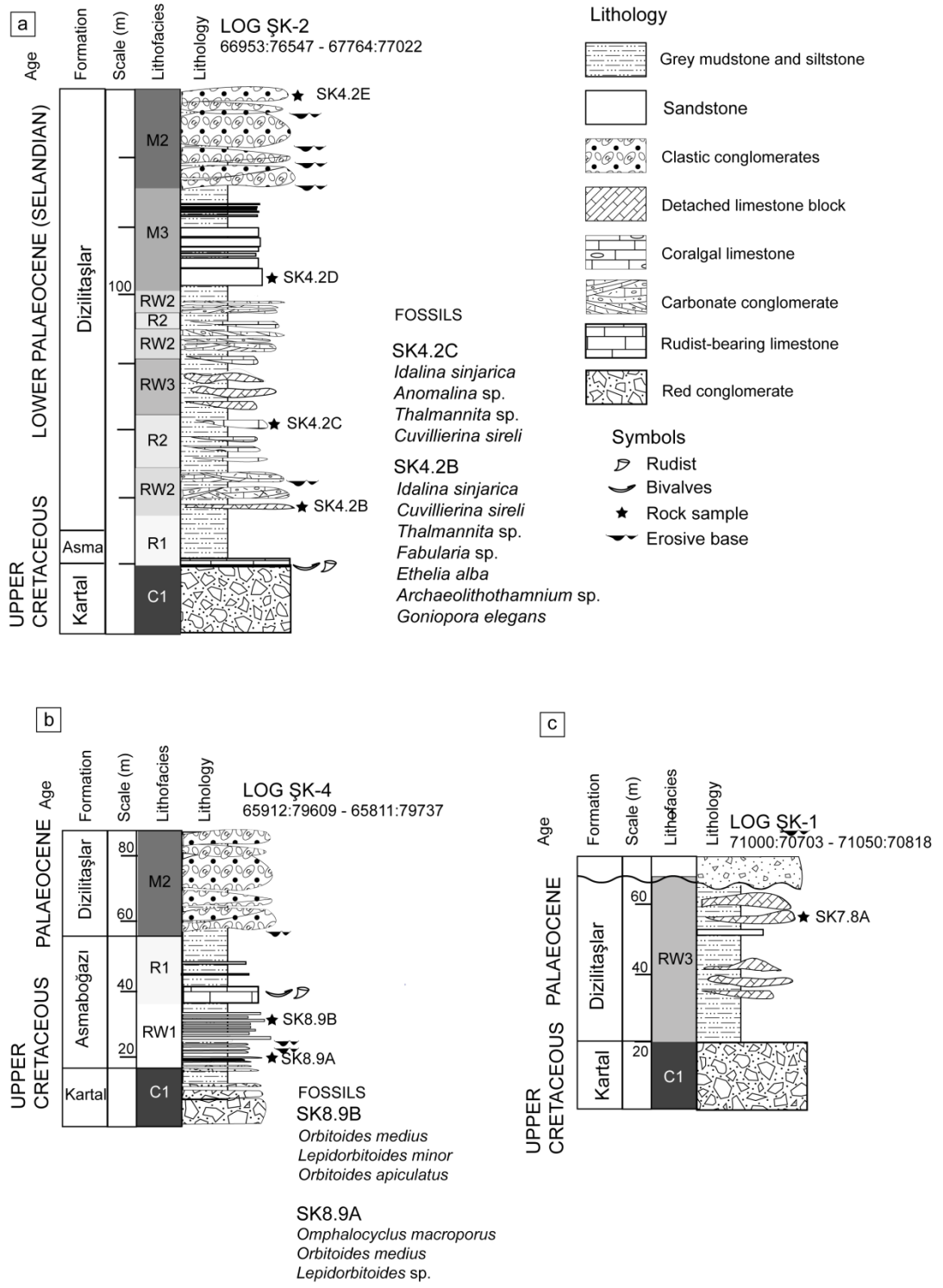

Figure 4.8 Stratigraphic logs showing the transition from Upper Cretaceous to Palaeocene sediments on the eastern margin of the Tuz Gölü Basin. All sedimentary data are based on this study. Palaeontological data are from N. İnan & K. Taslı (pers. comm. 2009).

4.4.1.3 The Dizilitaşlar Formation (Palaeocene)

The Maastrichtian Asmaboğazı Formation passes upwards into the Dizilitaşlar Formation which represents a transition to deeper-water terrigenous and reworked carbonate sedimentation. The Dizilitaşlar Formation was first named by Norman (1972) and reaches a thickness of >500 m on the eastern margin of the Tuz Gölü Basin. Other names for this formation are the Çaldağ Formation and the Kırkkavak Formation (Rigo de Righi & Cortesini 1959; TGO 1961; MTA 1989; Çemen *et al.* 1999; Derman *et al.* 2000; Aydemir 2008). A complete Palaeocene succession is observed South of Karandere village to the west of Karamollauşağı village. However, part of the succession is missing near the villages of Asma and Çardak. The Dizilitaşlar Formation includes a wide range of lithofacies ranging from medium-grained clastic turbidites (Lithofacies M1), carbonate conglomerates (Lithofacies RW2), clastic conglomerates (Lithofacies M2), algal and benthic foraminiferal limestone (Lithofacies R2), detached blocks of coralgal reefs (Lithofacies RW2) and Thickly-bedded high density turbidites (Lithofacies M3).

4.4.1.3.1 Lithofacies M1- Medium-grained turbidites

The lower part (Lithofacies M1) of the Dizilitaslar Formation crops out in a measured section south of Karandere (Log ŞK6; Fig. 4.11). The base of the section contains sand – mud couplets of thin sandstone and sandy limestone beds (<0.5 m) intercalated with laminated black siltstone and mudstone (Fig. 4.10a). The sandstone beds are frequently graded, typically with micro-conglomeratic, erosive bases fining upwards to medium/fine sand. Plane-parallel lamination is present locally; sedimentary structures are otherwise absent. Based on measured stratigraphic logs, the sand:mud ratio is 0.13:1. An Early to Middle Palaeocene (Danian to Selandian) date is suggested for Lithofacies M1 by the occurrence of the following benthic foraminifera present in two samples of sandy limestone: *Idalina sinjarica* Grimsdale,

Quinqueloculina sp., *Kathina* sp. and *Smoutina* sp. (sample ŞK6.6B) and *Idalina sinjarica* Grimsdale, *Kayseriella* cf. *decastroi Planorbulina* sp. *Cuvillierina sireli* İnan (Sample ŞK7.7D; Fig. 4.10d) (N. İnan & K. Taslı pers. comm. 2009). This date confirms previous studies (Rigo de Righi & Cortesini 1959; MTA 1989).

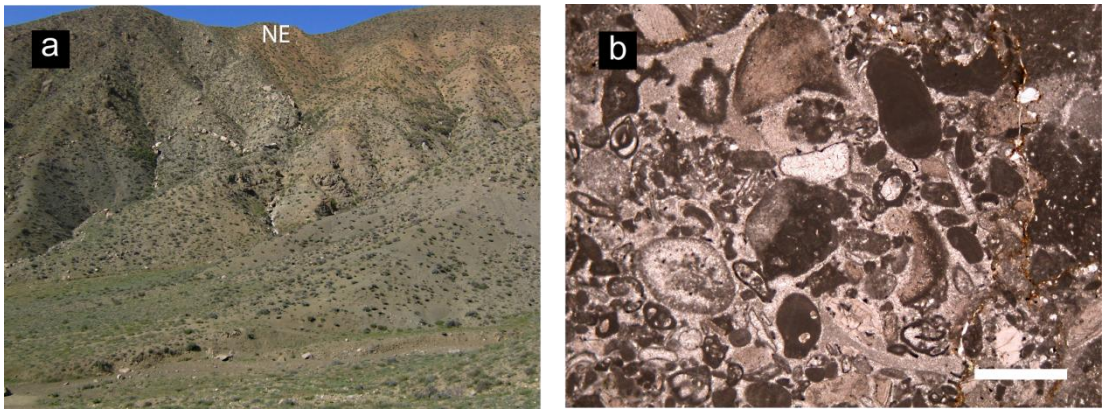

Figure 4.9 **(a)** Field photograph, (looking ~ northeast), of Danian-Selandian sandstone / shale couplets representing Lithofacies M1 of the Dizilitaşlar Formation, **(b)** Photomicrograph (in plane-polarised light) of Selandian algal- and foraminifera-rich sandy limestone (sample ŞK7.7D). Scale bars = 1mm.

4.4.1.3.2 Interpretation of lithofacies M1

The deposits are interpreted as medium-grained turbidites (Bouma 1962) showing Bouma Divisions Ta (erosive, graded base) Tb (plane-parallel lamination) and Td (massive mud).

4.4.1.3.3 Lithofacies RW2: carbonate conglomerates

Carbonate conglomerates scour into sand-mud couplets of Lithofacies M1 (see above). They form laterally discontinuous lenticular beds, 0.3 – 2.5 m-thick. Clasts are generally angular, <12 cm in size and composed of algal- and benthic

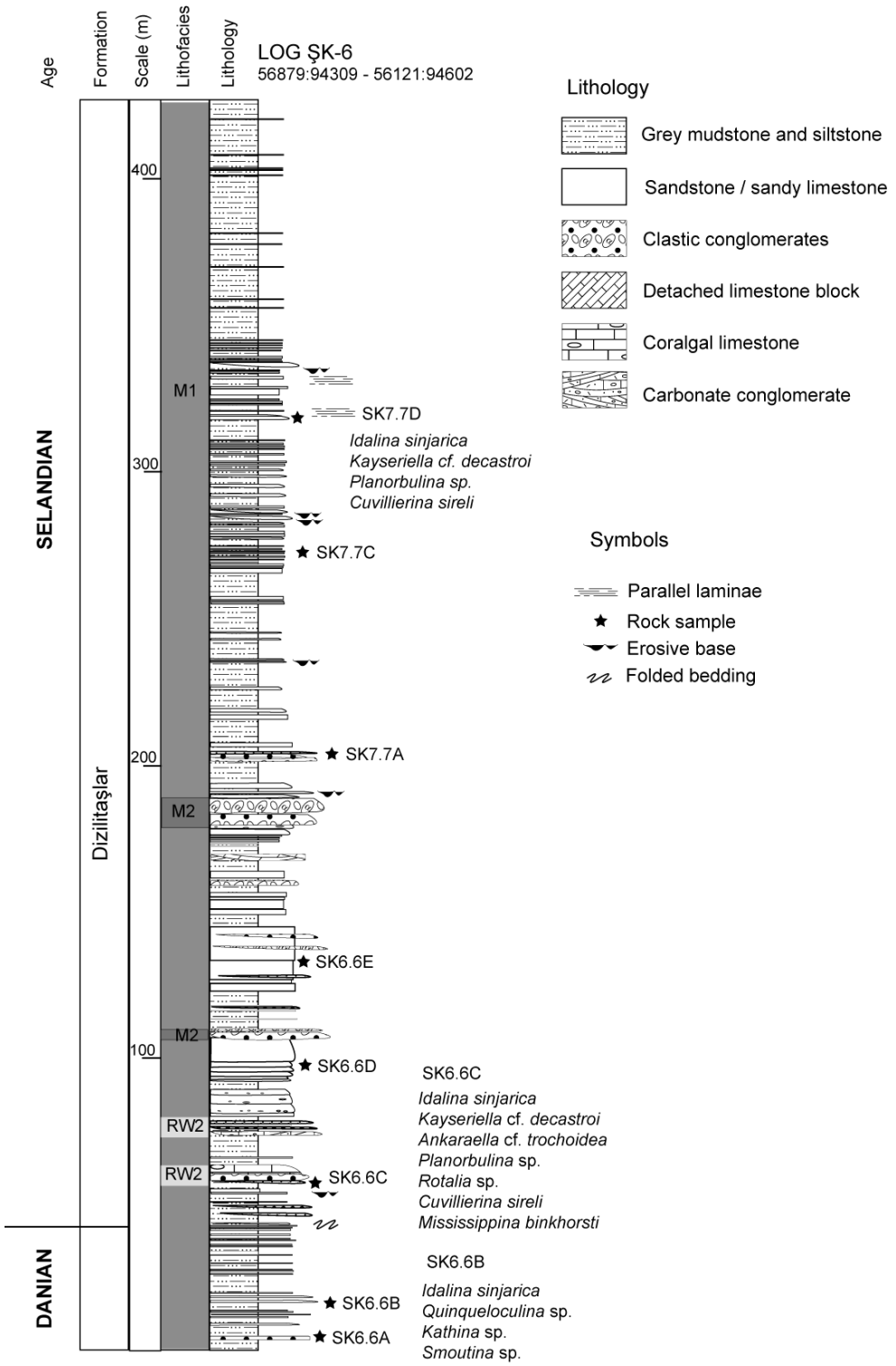

Figure 4.10 Measured stratigraphic log ŞK-6, located south of Karandere (see Fig. 4.5), showing Lithofacies M1, medium-grained turbidites, of the Palaeocene Dizilitaşlar Formation. All stratigraphic data are from this study, palaeontological data are from N. İnan & K. Taslı (pers. comm. 2009).

foraminifera-rich packstone containing abundant angular quartz grains.. In thin section, packstone is medium- to coarse-grained, poorly sorted and comprises milliolid foraminifera and fractured and abraded skeletal algal fragments in a fine-grained matrix of calcite, algal fragments and angular quartz grains (Fig. 4.12b). A Middle Palaeocene (Selandian) date is inferred (sample ŞK6.6C) by the presence of the following benthic foraminifera: *Idalina sinjarica* Grimsdale, *Kayseriella* cf. *decastroi*, *Ankaraella* cf. *trochoidea*, *Planorbulina* sp., *Rotalia* sp., *Cuvillierina sireli* İnan and *Mississippina binkhorsti* Reuss (N. İnan & K. Taslı pers. comm. 2009), confirming previous studies (Rigo de Righi & Cortesini 1959; MTA 1989).

4.4.1.3.4 Interpretation of lithofacies RW2

The conglomerates lack any grading or other sedimentary structures and are interpreted in as debris flow deposits (e.g. Hiscott & James 1985) (Fig. 4.12a). The deposits clearly indicate reworking of reefal carbonates on a slope setting and provide evidence of algal-rich reefs during Early Palaeocene time.

4.4.1.3.5 Lithofacies M2: clastic conglomerates

This lithofacies contains scoured channels of clastic, matrix-supported conglomerates containing pebbles/cobbles of andesite, limestone and granite set in a carbonate or coarse sandstone matrix (Fig. 4.12c). Clasts are <10 cm in size and display a range of angularities. Angular blocks of limestone <80 cm in size are present locally. Beds are lenticular in shape with erosive bases and coarse sandy tops. Bed thicknesses are variable but are <6 m thick with irregular, internal erosional contacts commonly amalgamating into multi-depositional surfaces. Individual beds are locally intercalated with thin sandstone layers.

4.4.1.3.6 Interpretation of lithofacies M2

The conglomerates are very poorly sorted, structureless and are interpreted as debris flows (Stow 1986). Clasts are locally imbricated and show palaeocurrents to the southwest and to the southeast. (See Appendix 3 for palaeocurrent data and methods). Given the clast lithology (i.e. andesite and granite), it is likely that the source area is the granitic plutons and volcanic rocks of Niğde-Kırşehir Massif to the west/northwest.

4.4.1.3.7 Lithofacies R2: benthic foraminiferal limestone

Lithofacies R2 comprises a ~25 m zone of *in situ* limestone lenses which crop out in log ŞK-2 (66953:76547 - 67764:77022) northwest of Çardak (Figs. 4.6, 4.9a). The lenses are up to 2.5 m thick, laterally continuous for ~20 m, and commonly capped by carbonate conglomerates. Individual units are drowned by 2 – 3 m-thick deposits of grey calcareous mudstone. In thin section (e.g. sample ŞK4.2C) limestones comprise aggregates of wackestone containing chaotically orientated skeletal algae and packstone fragments composed large benthic foraminifera. A Selandian age is indicated by large benthic foraminifera *Idalina sinjarica,* Grimsdale, *Anomalina* sp., *Thalmannita* sp. and *Cuvillierina sireli* İnan (N. İnan & K. Taslı pers. comm. 2009), which confirms previous work (Rigo de Righi & Cortesini 1959; MTA 1989).

4.4.1.3.8 Interpretation of lithofacies R2

The presence of miliolid foraminifera (e.g. *Idalina sinjarica*) suggests that the depositional environment was a restricted low energy inner shallow

platform/lagoonal facies, rich in large benthic foraminifera (e.g. Sartorio & Venturini 1988; Taheri *et al.* 2008).

4.4.1.3.9 Lithofacies RW3: detached blocks of Coralgal Reefs

Lithofacies RW3 is represented by a 40 m-thick zone of detached reefal limestone blocks up to which was measured in logs ŞK-2 (66953:76547 - 67764:77022) (Fig. 4.9a) and ŞK-3 (66595:77703 - 66848:78205) (Fig. 4.13b) near Gecekondu village. Blocks show faulted margins and are up to 3 m thick. They are composed of well lithified limestone, commonly overlying poorly sorted, rounded volcanic pebbles. Thin section study reveals that the reefal limestone is algal-rich packstone/wackestone with abundant benthic foraminifera and less common coral fragments, bivalve shells and gastropods. A Selandian date is given by the following fauna (Sample ŞK4.2B): benthic foraminifera *Idalina sinjarica* Grimsdale, *Cuvillierina sireli* İnan, *Thalmannita* sp., *Fabularia* sp., *Anomalina* sp., *Thalmannita* sp., *Kayseriella* cf. *decastroi* and *Planorbulina* sp., coral *Goniopora elegans* (Leymerie) and algae *Ethelia alba* Pfender and *Archaeolithothamnium* sp. (N. İnan & K. Taslı pers. comm. 2009).

4.4.1.3.10 Interpretation of lithofacies RW3

Slope/upper slope facies rich in re-deposited carbonate material are abundant in the Palaeocene Dizilitaşlar Formation in the Kırıkkale Basin (Chapter 2) and the Haymana-Polatlı Basin (see Chapter 5). One interpretation is that the carbonate accumulated as a result of mass-transport processes on a slope. Comparable facies are found in a Palaeocene-Eocene foreland basin in Euboea, Eastern Greece (Robertson 1990).

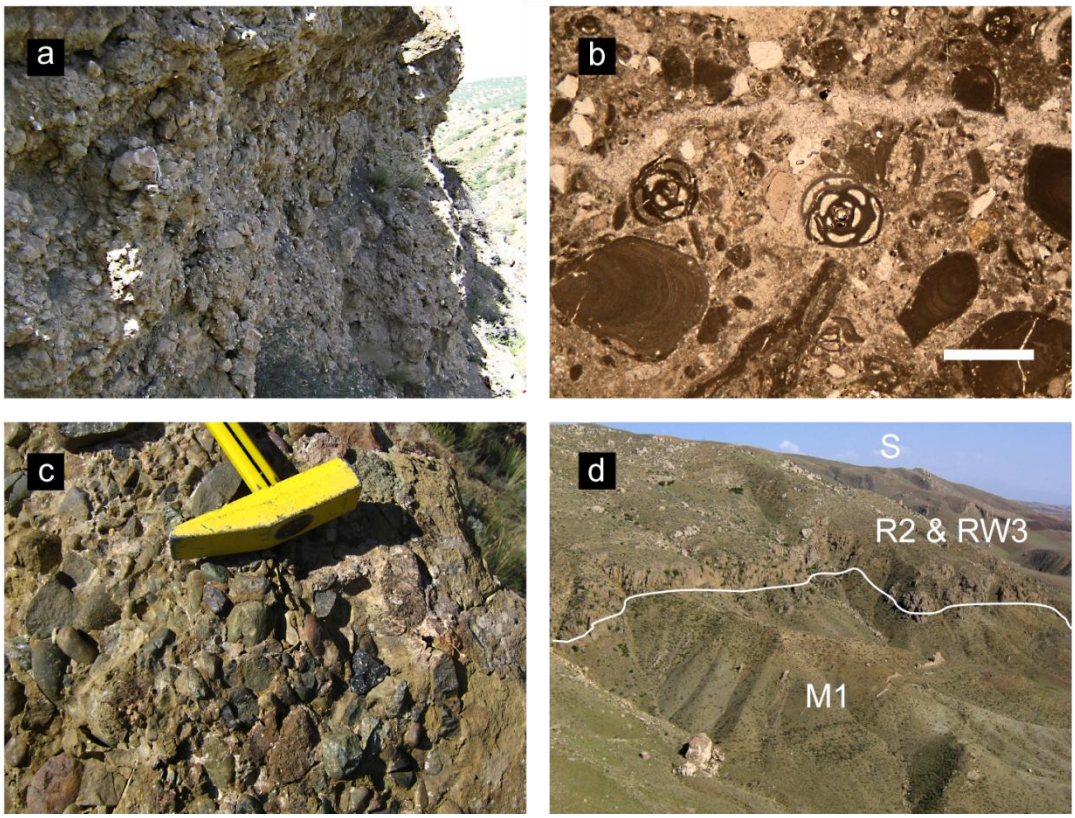

Figure 4.12 (a) Field photograph of a Palaeocene carbonate debris flow (Lithofacies RW2) in the Dizilitaşlar Formation; the exposure is ~3 m-high **(b)** Photomicrograph (in plane-polarised light) of a carbonate clast (sample ŞK6.6C) from the debris flow showing fractured grains of skeletal algae (bottom) and Milliolid foraminifera (centre). Scale bar = 1mm **(c)** field photograph of andesitic conglomerate (Lithofacies M2) in log ŞK-2 **(d)** Field photograph (looking approximately south) of Danian-Selandian sediments comprising Lithofacies M1 (sand-mud couplets) and, above, Lithofacies R2 (in situ lenticular reefs) and RW3 (detached limestone blocks).

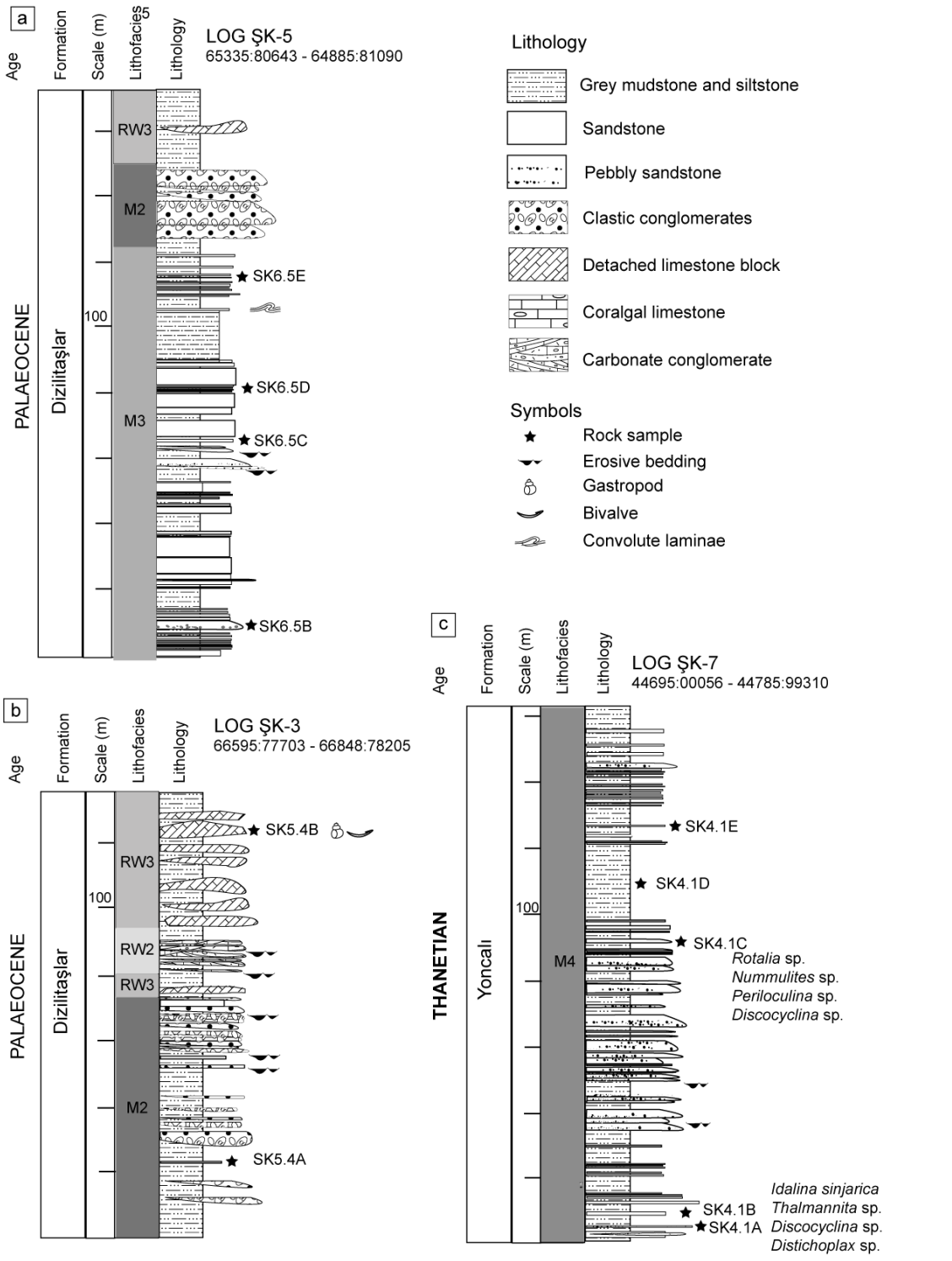

Figure 4.13 Measured stratigraphic logs of Palaeocene sediments of the Dizilitaşlar and Yoncalı Formations from the eastern margin of the Tuz Gölü Basin. All sedimentary data are from this study, fossil data are from N. İnan & K. Taslı (pers. comm. 2009).

4.4.1.3.11 Lithofacies M3: high density turbidites

Lithofacies M3 comprises distinctive thick-bedded massive sandstone (Figs. 4.14a, 4.14b). This lithofacies is particularly well-exposed in log ŞK-2 (66953:76547 - 67764:77022) (Fig. 4.9a) northwest of Çardak, where it represents the drowning of the underlying carbonate lithofacies by a rapid influx of siliciclastic sediments. Beds are up to 5 m thick and composed of grey/yellow, medium-grained, moderately well-sorted lithoclast-rich sandstone. Sedimentary structures are absent and beds locally form packages of up to four depositional surfaces.

In terms of depositional processes, one interpretation is that they represent incomplete medium-grained turbidite deposits (Bouma 1962) lacking in Bouma Divisions Tb, Tc, Td and Te, but instead contain Ta (i.e. massive or graded basal sand). Alternatively, they could be classified as structureless deposits from high concentration turbidity currents (e.g. Lowe 1982); however, they lack dish structures and fluid escape pipes associated with these deposits (see Pickering *et al.* 1989). However, the sandstone is best interpreted as mass-flow deposits.

.

Figure 4.14 (a) Field photograph of Palaeocene thickly-bedded high-density turbidites (Lithofacies M3) in log ŞK-2 **(b)** Field photograph of Lithofacies M3 (looking northeast) in log ŞK-5

4.4.1.3.12 Summary of new data from the Palaeocene Dizilitaşlar Formation

New data discussed above have: 1) confirmed the depositional age of the Dizilitaşlar Formation as Palaeocene, in agreement with previous studies (Rigo de Righi & Cortesini 1959; Arikan 1975; Görür & Derman 1978; Dellaloğlu & Aksu 1984a; MTA 1989; Çemen *et al.* 1999); 2) for the first time, permitted a discussion of the formation in terms of lithofacies and depositional environments; 3) provided detailed sedimentary descriptions and; 4) correlated the deposits to the Palaeocene deposits in the Kırıkkale Basin to the north (See Chapter 2).

4.4.1.4 The Yoncalı Formation (Upper Palaeocene-Middle Eocene)

Rocks of the Yoncalı Formation were characterised in a measured section (LOG ŞK-7, 44695:00056 - 44785:99310) to the southwest of Şereflikoçhisar on a peninsula west of Karamollauşağı village (Fig.14c). The Yoncalı Formation is also known as the Karapınaryaylası Formation (Dellaloğlu & Aksu 1984a; Çemen *et al.* 1999), the Boyalı Formation (MTA 1989), and the Eskipolatlı Formation (Görür *et al.* 1984). Previous dates given to the Yoncalı Formation are Lutetian (MTA 1989), Middle Eocene (Görür *et al.* 1984) and Palaeocene-Middle Eocene (Dellaloğlu & Aksu 1984a). The Yoncalı Formation is made up of two lithofacies: pebbly sand (Lithofacies M4) and massive turbidites (M5).

4.4.1.4.1 Lithofacies M4: pebbly sand

The lower part of the section consists of coarse grey/yellow sandstone, interbedded with grey mudstone and siltstone. The measured sand:mud ratio is

0.67:1. Sandstone beds are lenticular and up to 2.3 m thick (Fig. 4.15a), frequently amalgamate into multiple depositional surfaces, leading to irregular, diffuse bed contacts. Beds commonly show erosive bases and show an overall fining up from pebble/cobble bases to coarse/medium sand tops; however, ~10 cm layers of coarser clasts are locally repeated throughout the beds. Pebbles, up to 12 cm in size, display a range of angularities, composed of limestone, altered basalt, sandstone and rare radiolarian chert (Fig. 4.15b). Small (<1 m) exotic "olistoliths" (detached blocks) of bioclastic limestone are locally present. A single groove mark was observed and indicated a palaeocurrent trend to or from SSW.

The section fines and thins upwards into medium-grained thinly-bedded sandstone, intercalated with grey and red mudstone in a sand:mud ratio of 0.35:1. Sandstone beds in the upper part are mostly <0.5 m thick and laterally continuous. Erosive bed bases occasionally contain rounded pebbles (<2 cm) and normal grading from coarse- to medium/fine-grained sand was observed. One groove mark indicated a palaeocurrent to or from SSE.

4.4.1.4.2 Interpretation of lithofacies M4

These deposits are interpreted as proximal high concentration lenticular turbidites (Walker 1978; Lowe 1982) and display R2, S1 (stratified) and S2 (graded-stratified) sequences of the classic Lowe (1982) model. The age of this sequence was previously given as Middle Eocene (Lutetian) (MTA 1989) based on the following gastropods: *Lucina carbarica* Leymeria, *Turitella trempina* Carez, *Ampullin* cf. *Brevispira* Leymeria; and the benthic foraminifera *Assilina spira* da Raissy, *Assilina exponens* Sowerby, *Nummulites* sp., *Orbitolites* sp., *Asterigina* sp., *Discocycilna* sp., *Lockhartia* sp. and *Gypsina* sp. The presence of gastropods was not confirmed during this study.

In contrast, however, based on the presence of *Rotalia* sp., *Nummulites* sp., *Periloculina* sp. *and Discocyclina* sp. in sample ŞK4.1C, a Late Palaeocene (possibly

Thanetian) age is assigned by this study (N. İnan & K. Taslı pers. comm. 2009). This agrees with the date of Dellaloğlu & Aksu (1984).

Above the measured section is a sequence of detached limestone blocks interbedded with turbiditic sandstones and shales, commonly dated as Middle Eocene (Lutetian) (e.g. MTA 1989). This outcrop, however, was inaccessible during this study; therefore this date should re-assessed in future work.

4.4.1.4.3 Lithofacies M5: massive turbidites

To the northwest of Şereflikoçhisar, outcrops of the Yoncalı Formation are limited to metre-scale roadside and small quarry exposures south of Kulu (00626:12799) (Fig. 4.3). However, the Yoncalı Formation in this locality is represented by mdiem- to coarse-grained volcaniclastic sandstone beds and laminated shale (lithofacies M5). Beds are up to 0.4 m-thick and mostly devoid of sedimentary structures (Fig. 4.15c). Locally, the beds are intensely folded (Fig. 4.15d).

4.4.1.4.4 Interpretation of lithofacies M5

In terms of sediment transport, one possible interpretation is that the deposits represent turbidites. The unexpected absence of parallel- or cross-lamination could be the result of post-depositional reworking or bioturbation (e.g. Baas 2004). Unconformably overlying the Yoncalı Formation are continental and lacustrine sediments of Late Eocene, Oligo-Miocene, Mio-Pliocene and Quaternary ages. These sediments developed after continental collision and were, therefore, not included in this study.

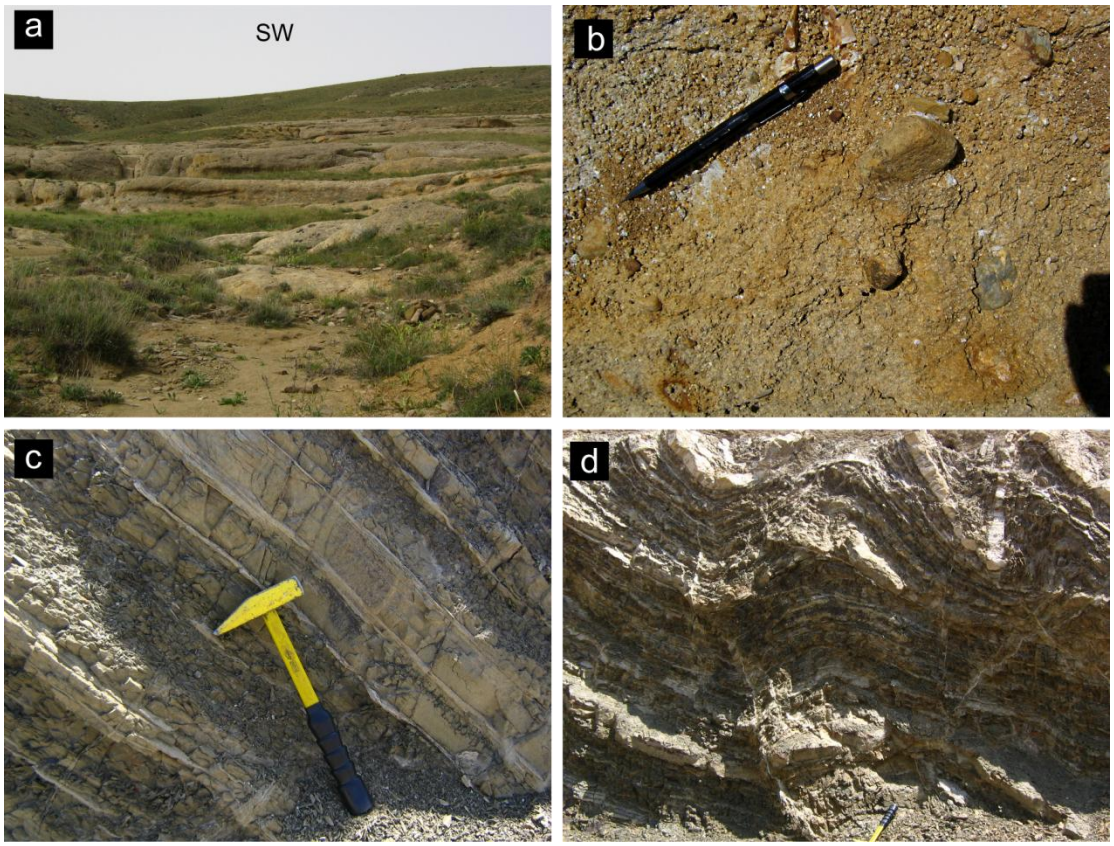

Figure 4.15 (a) Field photograph, looking ~southwest, of coarse-grained, clast-rich pebbly sandstone of deposits (Lithofacies M4). Image taken in log SK-7, south of Şereflikoçhisar, **(b)** detail of pebbles in the coarse sandstone, **(c)** field photograph of thinly-bedded massive turbidites in the Kulu locality (Lithofacies M5), **(d)** folding in turbidites of Lithofacies M5.

4.4.2 The Bala area

The most northerly outcrop of the Tuz Gölü Basin is situated near the town of Bala, on the northwest margin of the Niğde-Kırşehir Massif (Fig.3). This area contains Upper Cretaceous-Palaeocene (possibly Eocene) sediments which are broadly comparable to those south of Şereflikoçhisar. To date, there are no sedimentary, stratigraphic, palaeontological or structural data from this area in the literature. This section will discuss these data with the aim of comparing and contrasting the Bala area with the more southerly outcrops in the Tuz Gölü Basin.

4.4.2.1 The Kartal Formation (Upper Cretaceous)

The Kartal Formation (lithofacies C1) is moderately well exposed and is composed of conglomerates containing pebble- to cobble-sized clasts of granite, sandstone, silicic volcanics and radiolarian chert set in an oxidised red sandstone matrix. The clasts display textural inversion; i.e. rounded clasts have been fractured to produce angular clasts, suggestive of reworking possibly during the Neogene time (Fig.4.16a). Sedimentary structures are absent, hampering depositional interpretation. The Maastrichtian rudist-bearing limestone (lithofacies R1) and large benthic foraminiferal sandy limestone (lithofacies RW1) of the Asmaboğazı Formation is absent in the Bala area. Instead, the Kartal Formation grades vertically into a poorly exposed ~200-m thick succession of grey shales intercalated with thin siltstone (Fig. 4.16b). Sedimentary data associated with the Haymana Formation are discussed in Chapter 5.

4.4.2.2 The Dizilitaşlar Formation (Palaeocene)

4.4.2.2.1 Lithofacies R2: algal- and benthic foraminifera-rich limestone

Above the shales of the Haymana Formation lies a thick (~100 m) outcrop of algal- and foraminifera-rich limestone (Fig. 4.16c), which is well exposed in a working quarry to the northeast of Üçem (18979:80829). The limestone is generally massive with no evidence of primary bedding. Petrographic study reveals that the limestones can be classified as packstones with large benthic foraminifera and calcareous algae which are commonly fragmented and abraded. Where present, the matrix is composed of micrite and benthic foraminiferal fragments. The presence of calcareous algae suggests deposition in the photic zone, while miliolid foraminifera suggest an original depositional environment in an open-marine, lagoonal setting. The fragmented nature of the fauna indicates high energy reworking, possibly by storms in an environment open to marine circulation. The fauna present in two

samples indicate a Lower (Danian) to Middle (Selandian) Palaeocene age. Sample BAL1.3B contains the benthic foraminifera *Anomalina* sp. and the algae *Amphiroa* cf. *propria, Lithophyllum mengaudi* var. *carpathica,* and *Archaeolithothamnium* cf. *johnsoni* giving a Danian age (N. İnan & K. Taslı pers. comm. 2009). Sample BAL1.3C contains abundant algae and the benthic foraminifera *Idalina sinjarica* Grimsdale and *Cuvillierina sireli* İnan, indicating a Selandian age (N. İnan & K. Taslı pers. comm. 2009). This outcrop is comparable to lithofacies R2 from the southern area, but represents a thicker more laterally extensive equivalent.

4.4.2.2.2 Lithofacies R3: orange sandy limestone

The carbonates of lithofacies R2 are abruptly covered by a unit of orange-weathered sandy limestone, >180 m thick (Lithofacies R3) (Fig. 4.16c). Near the base, there is a ~20 m-thick succession of intercalated limestone and thin sandy limestone beds. Locally, this unit unconformably overlies the Upper Cretaceous Kartal formation (Fig. 4.16b). The limestone beds are ~0.5 m thick and are dominated by skeletal algae with large benthic foraminifera. Terrigenous material comprises <10% of the total rock and consists mostly of angular volcanic lithoclasts with minor monocrystalline quartz.

Benthic foraminifera are typically well preserved with little evidence of fracturing or abrasion; in contrast, algae are frequently fractured suggestive of reworking in a relatively high-energy environment. One sample (BAL1.2C) contains the benthic foraminifera: *Idalina sinjaric* Grimsdale, *Coccoarota orali* İnan, *Miscellanea* sp., *Alveolina (Glomalveolina)* sp., *Fabularia donatae liburnica* Drobne, *Periloculina slovenica* Drobne, *Nummulites* sp., *Smoutina* sp., *Austrotrillina* cf. *eocenica, Lacazina* cf. *blumenthali, Medocia blayensis* Parvati, *Ranikothalia nuttali (Davies), Assilina azilensis* (Tambareau) and the algae: *Amphiroa* cf. *propria, Lithophyllum mengaudi* var. *carpathica, Distichoplax* cf. *baykali, Distichoplax biserialis* (Dietrich), *Archaeolithothamnium* cf. *johnsoni, Etheia alba*

Pfender algae. This faunal assemblage indicates a Late Palaeocene (Thanetian) age (N. İnan & K. Taslı pers. comm. 2009).

4.4.2.2.3 Interpretation of lithofacies R3

This lithofacies represents a diverse range of fauna and is here interpreted as deposits in high energy environment possibly near a carbonate platform edge. It contains the first influx of siliciclastic material which was associated with carbonate platform drowning in the latest Palaeocene. These deposits are unique to the Bala study area.

4.4.2.2.4 Lithofacies M2: clastic conglomerates

The carbonates of Lithofacies R3 pass into a deepening upwards, terrigenous succession comprising grey/orange shales intercalated with clastic and carbonate conglomerates. Clastic conglomerates form lenticular deposits <4 m thick and comprise matrix-supported, well-rounded clasts ranging from pebble- to boulder-size; beds are massive, both bed bases and tops are irregular. Clasts include feldspar-phyric lava, radiolarian chert, granite, sandstone and limestone, presumably sourced from the Niğde-Kırşehir Massif, although the presence of radiolarian chert suggests a source from an oceanic setting. Clasts are locally imbricated and indicate a uni-directional flow from W to E (n= 2 measurements). The mostly chaotic nature of the clasts, lenticular bed shape and lack of sedimentary structures are evidence of these deposits being debris flows. They thus correlate with lithofacies M2 in the southern area.

4.4.2.2.5 Lithofacies RW2: carbonate conglomerates

Carbonate conglomerates are lenticular and up to 3 m thick; bed bases and tops are irregular and sedimentary structures are absent. These deposits are comparable to lithofacies RW2 and comprise well-sorted limestone clasts. In thin section, the clasts are algal-rich wackestones with a minor (<5 %) clastic input. Skeletal algae and benthic foraminifera are set in a micritic matrix; angular mudstone intraclasts contain algal fragments in a matrix of micrite and fossil fragments, suggesting a low-energy lagoonal setting. The benthic foraminifera: *Anomalina* sp. and *Planorbulina create* (Marsson) indicate a Danian age (N. İnan & K. Taslı pers. comm. 2009). These carbonates correlate to lithofacies R2 and indicate that Danian lagoonal carbonates were reworked and transported down-slope in debris flows during Late Palaeocene time.

4.4.2.3 The Yoncalı Formation (Palaeocene-Middle Eocene)

The Yoncalı Formation is best exposed in a roadside cutting to the west of Bala (08816:81304) (Fig. 16d) and, in this study area, represents the transition from the underlying carbonates, to the east of Bala, to deeper-marine clastic sedimentation. In this area, the Yoncalı Formation comprises massive turbidites (lithofacies M5) and inverse-graded debris flows (lithofacies M6).

4.4.2.3.1 Lithofacies M5 – Massive turbidites

Lithofacies M5 is represented by planar grey/brown coarse-grained sandstone beds (<0.4 m thick), intercalated with grey fissile shale. Sandstone beds lack grading and have sharp tops and bases (Fig. 4.16e). Sedimentary structures include horizontal

burrowing and flute marks indicating a current from northwest to southeast (n= 6). The sandstone is made up of volcanic lithoclasts, quartz, serpentinite and cherts (see Section 4.X for comprehensive data). The age of the Yoncalı Formation in this area is given as Palaeocene (MTA 2002); however, this date is untested due to an absence of fossils. Sandstone composition is broadly similar to that of the turbidites near Kulu (Fig. 16f), although plagioclase is much less abundant.

4.4.2.3.2 Lithofacies M6: iInverse-graded debris flows

Incising into the sand-shale couplets are channelised deposits of chaotic conglomerates. Beds are up to ~1 m thick, with sharp bases. with protruding clasts and overlie chaotically folded shale (Fig. 4.16f). Clasts are pebble- to cobble-sized, poorly sorted and primarily composed of limestone and black chert with rare "floating" rafts of sandstone. Beds frequently display inverse grading at the base and form fining- and thinning-upward amalgamations. These observations are suggestive of deposits from sub-aqueous debris flows (e.g. Johnson 1984).

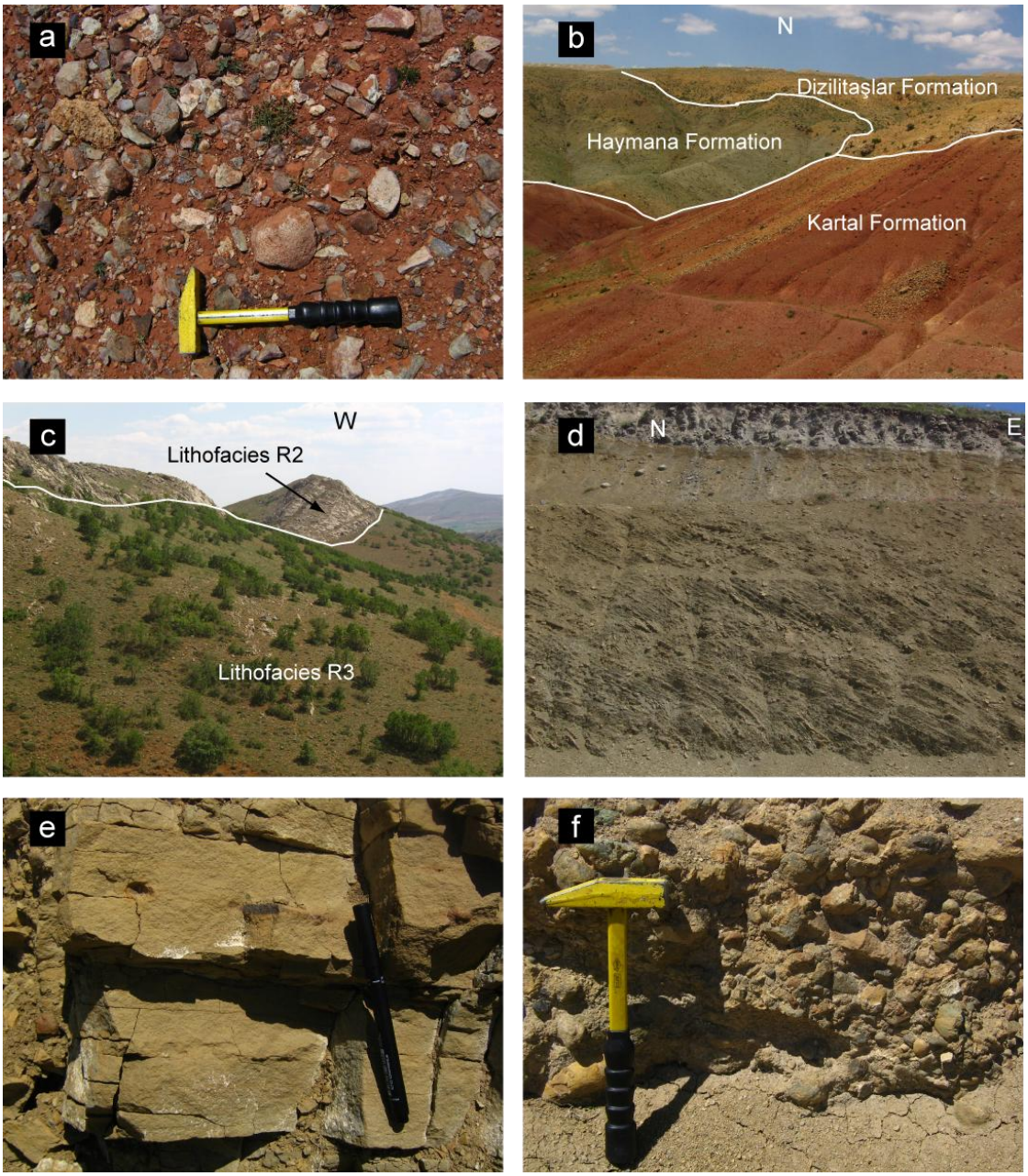

Figure 4.16 (a) Textural inversion of clasts in the Upper Cretaceous Kartal Formation **(b)** view, looking north, of the Kartal Formation grading into grey shales of the Upper Cretaceous Haymana Formation to the left. To the right, Thanetian sandy limestones of the Palaeocene Dizilitaşlar Formation overlie the Kartal Formation and the Haymana Formation unconformably **(c)** view, looking west, of Lithofacies R2 (Danian - Selandian algal limestone) and Lithofacies R3 (Thanetian orange sandy limestone) **(d)** thin volcaniclastic turbidites of Lithofacies M5 west of Bala. Beds are dipping to the east **(e)** massive turbidite of Lithofacies M5 **(f)** Inverse-graded conglomerate debris flow (Lithofacies M6).

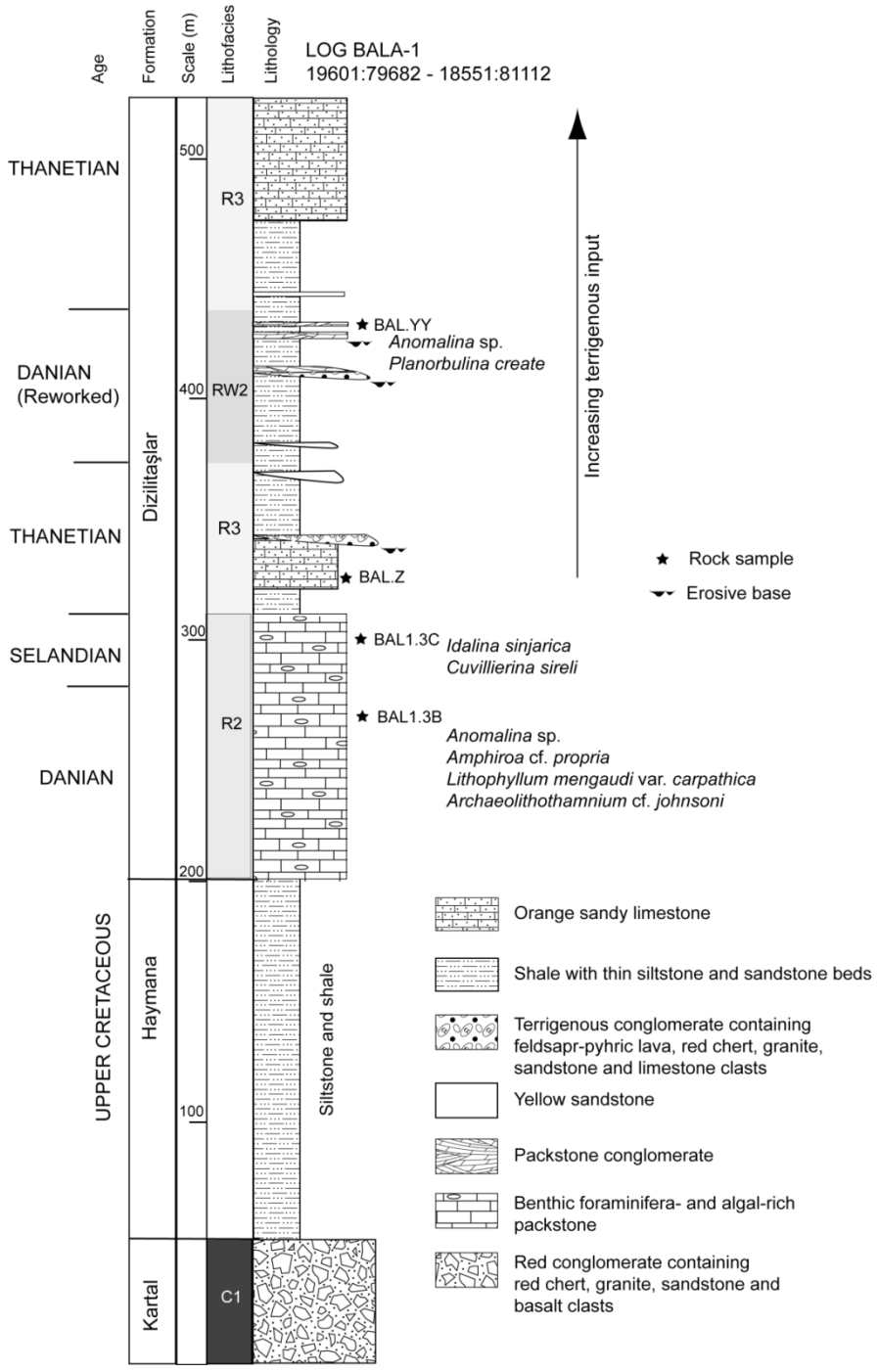

Figure 4.17 Measured stratigraphic logs of Upper Cretaceous - Palaeocene sediments of the northern Bala study area. All sedimentary data are from this study, fossil data are from N. İnan & K. Taslı (pers. comm. 2009).

4.4.3 Sandstone provenance

This section discusses new sandstone petrography and palaeocurrent data with the aim of inferring the provenance of basin-fill sediments. This project utilised the Gazzi-Dickinson point counting technique (Gazzi 1966; Dickinson 1970) to count 300 points per slide. See Appendix 2 for a full discussion on methodology and tabulated data. Fig. 4.18 is a ternary Qt:F:Lt-c diagram (where Qt= Total quartz, F= Feldspars, Lt-c = Total non-carbonate lithoclasts) which presents point-counting results graphically.

Palaeocurrents were measured in the field from a variety of indicators including unidirectional data (flute marks and clast imbrication) and bidirectional data (groove marks). See Appendix 3 for tabulated data and a discussion of data treatment.

Ten representative sandstone samples from the Palaeocene Dizilitaşlar Formation and the Upper Palaeocene – Middle Eocene Yoncalı Formation were analysed.

4.4.3.1 Dizilitaşlar Formation (Palaeocene)

Sandstone from Lithofacies M1 the Dizilitaşlar Formation is fine- to medium-grained, exhibits a range of grain angularities, and is mostly well sorted. However, one sample from Lithofacies M1 is poorly-sorted and contains out-sized volcanic lithoclasts (Fig. 4.19a). Compositionally, the sandstone is dominated by lithoclasts and quartz, whereas feldspar grains are rare (<4 %) (Fig. 4.18). Lithoclasts are composed of, in order of abundance: silicic volcanic, and altered, basic volcanic material and minor sedimentary lithoclasts (micrite, siliceous chert, mudstone). Quartz is mostly angular and monocrystalline; polycrystalline quartz is rare. Accessory minerals are extremely rare; one exception, however, is Sample ŞK5.4A

which contains opaque oxides, and detrital clinopyroxene (Fig. 4.19b). Grains are set in a matrix, where present, that is composed of calcite. In comparison to the Dizilitaşlar Formation exposed in the Kırıkkale Basin, sandstone in the Tuz Gölü Basin is richer in quartz and poorer in lithoclasts.

Few palaeocurrent indicators were observed; however imbricated conglomeratic clasts indicate a general trend from N to S (Fig. 4.20a).

4.4.3.2 Yoncalı Formation (Late Palaeocene – Middle Eocene)

In terms of grain composition, most sandstone from the Yoncalı Formation is similar to that of the Dizilitaşlar Formation (Fig. 4.18). However, sorting tends to be poorer and grain size slightly larger (e.g. Sample Şk4.1A; Fig. 4.19c). One exception is a sample from the Kulu area (Sample KULU15.2D; Fig. 4.18; Fig. 4. 19d), which exhibits a Qt:F:Lt-c ratio of 13:32:55. This sample is quartz-poor and contains small, fractured plagioclase grains. Sandstone in the Yoncalı Formation in the Tuz Gölü Basin is marginally more quartz-rich than sandstone in the Çankırı Basin to the north (see Chapter 3).

One palaeocurrent indicator to the south of Şereflikoçhisar inferred a flow to or from northwest (Fig. 4.20b). All other indicators were measured in the Bala area andshow a trend from northwest to southeast (n= 5 flutes), from west to east (n= 2 imbricated clasts) and to or from west (1 groove) (Fig. 4.20c).

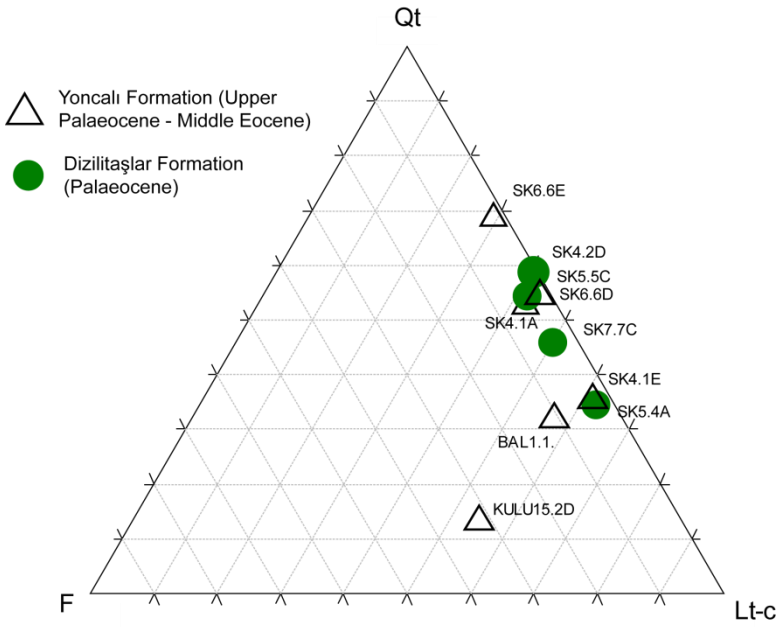

Figure 4.18 Qt-F-Lt-c ternary diagram of the sandstones used in the provenance study, Qt – total quartz, F – feldspar, Lt-c – total lithic clasts (excluding carbonate clasts).

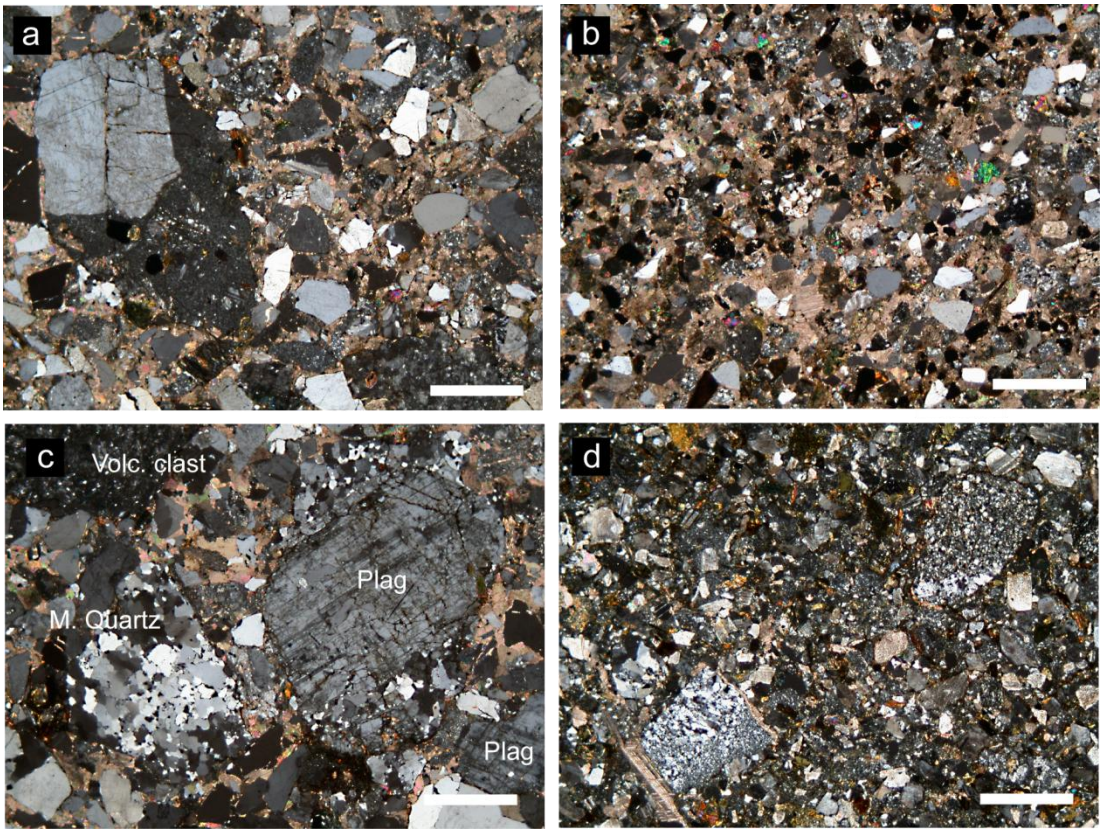

Figure 4.19 Photomicrographs of representative sandstones, **(a)** sample ŞK7.7C from Lithofacies M1 of the Palaeocene Dizilitaşlar Formation, **(b)** sample ŞK5.4A 7C from Lithofacies M1 of the Palaeocene Dizilitaşlar Formation, **(c)** sample ŞK4.1A from the Upper Palaeocene – Middle Eocene Yoncalı Formation, Volc. Clast – Volcanic Clast, Plag. – Palgioclase, M.Quartz – Monocrystalline quartz, **(d)** sample KULU15.2D. All images in crossed polars; scale bars = 1 mm.

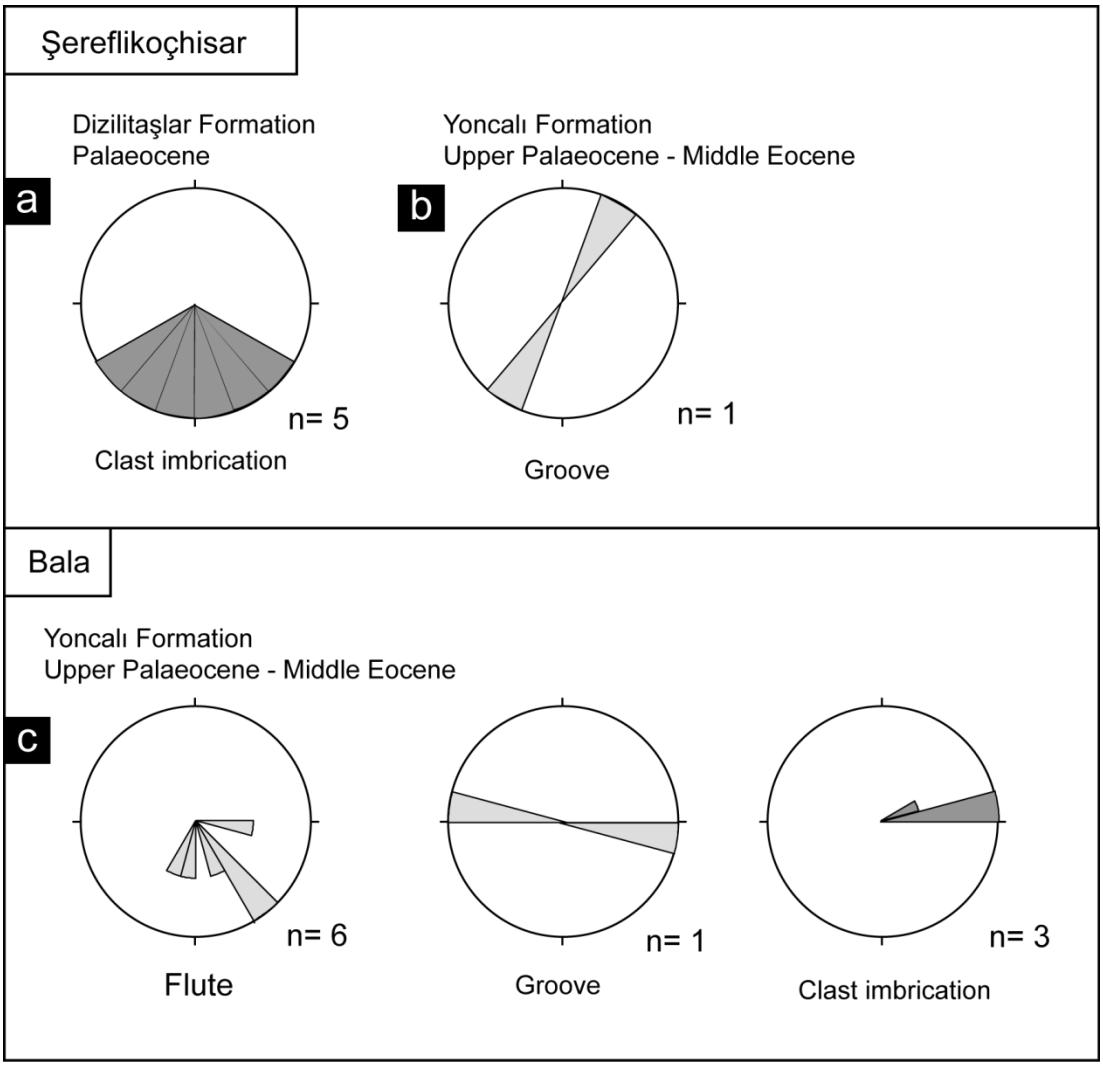

Figure 4.20 Palaeocurrent rose diagrams **(a)** from the Palaeocene Dizilitaşlar Formation, **(b)** the Upper Palaeocene – Middle Eocene Yoncalı Formation in the SŞereflikoçhisar area, **(c)** the Yoncalı Formation in the Bala area.

4.4.3.3 Interpretation of Provenance results

Based on palaeocurrent indicators, the likely source of sediments in the Şereflikoçhisar area is the Niğde-Kırşehir Massif to the E/NE. Clasts in the Upper Cretaceous Kartal Formation (basalt, andesite, gabbro, sandstone, granite, dacite, metamorphic rocks and serpentinite) probably result from the regional unroofing of the northern Neotethyan ophiolites, granitoid plutons and metamorphic basement of

the Niğde-Kırşehir Massif. The abundant volcanic lithoclastic detritus observed in Palaeocene – Middle Eocene sandstone are derived from the same source.

In contrast, Upper Palaeocene – Middle Eocene sandstone from the Kulu and Bala localities are quartz-poor and richer in plagioclase. Palaeocurrents from Bala indicate a general trend from northwest to southeast, implying that the source was to the northwest of the Tuz Gölü Basin. Sandstone composition is typical of an arc-derived provenance; exemplified by the sample from Kulu, which is compositionally similar to the Campanian volcaniclastics of the Ilıcıpınar Formation in the Kırıkkale Basin. It is therefore likely that these sediments are derived from arc volcanics to the northwest of the Tuz Gölü Basin.

4.5 Structural development of the Tuz Gölü Basin

The Tuz Gölü Basin provides an excellent opportunity to study one of the major fault zones in central Turkey. Central Anatolia is a region where Neotectonic intra-plate crust deformed internally, which resulted in the generation of new structures and the reactivation of old ones. The region is currently under approximately N-S and NNE-SSW shortening as a consequence of collision processes between the Anatolian and Arabian plates (Bozkurt 2001). The Tuz Gölü fault zone, also known as the Şereflikoçhisar – Aksaray fault zone (Görür *et al.* 1984; Derman *et al.* 2000; Aydemir & Ateş 2006) trends northwest-southeast along the eastern basin margin, from Şereflikoçhisar in the north to Aksaray in the south. To the east of the fault zone, Palaeozoic to Mesozoic basement rocks of the Niğde-Kırşehir Massif are exposed; whereas to the west of the fault zone, Upper Cretaceous to Middle Eocene basin-fill sediments are exposed.

This section presents kinematic and palaeostress data (previously missing from the literature) and integrates these data into the basin's regional tectonic development.

The initiation of the Tuz Gölü fault zone is generally considered to have occurred in the Late Cretaceous (Görür *et al.* 1984; Dırık & Göncüoğlu 1996; Çemen *et al.* 1999), based on the Upper Cretaceous age of the Kartal Formation which contains clasts of basement rocks that were presumably derived from the footwall of the extensional (or transtensional) fault zone (Fig. 4.21). In addition, an extensional shear zone on the western margin of the Niğde – Kırşehir Massif (the Emizözü shear zone) has been correlated with the Tuz Gölü fault zone. Based on cross-cutting relationships of radiometrically dated granitoid plutons, a date of 78 – 71 Ma was suggested (Isik 2009). Görür *et al.* (1984) suggest a fault downthrow of ~6.5 km as the basin subsided while the western margin of the Niğde – Kırşehir Massif was emergent or at shallow water depths.

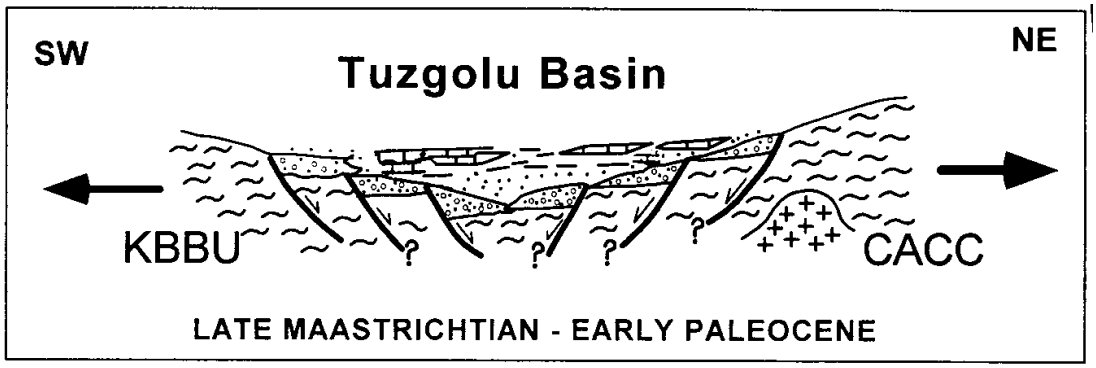

Figure 4.21 Schematic diagram of the fault-controlled structural evolution of the Tuz Gölü Basin in the Late Maastrichtian – Palaeocene time according to Çemen *et al.* (1999). CACC = Central Anatolian Crystalline Complex; KBBU = Kütahya-Bolkardağı belt units. The diagram was copied from Çemen *et al.* (1999).

In contrast, one recent interpretation of the Tuz Gölü fault zone favours an east-dipping reverse fault (Coskun 2004). However, this model is apparently contradicted by seismic profiles indicating that the fault zone dips to the west – southwest and can be interpreted as a low-angle extensional detachment surface at

depth below the basin depocentre but as a high angle fault along its surface trace on the eastern basin margin (e.g. Aydemir 2009) (Fig. 4.22).

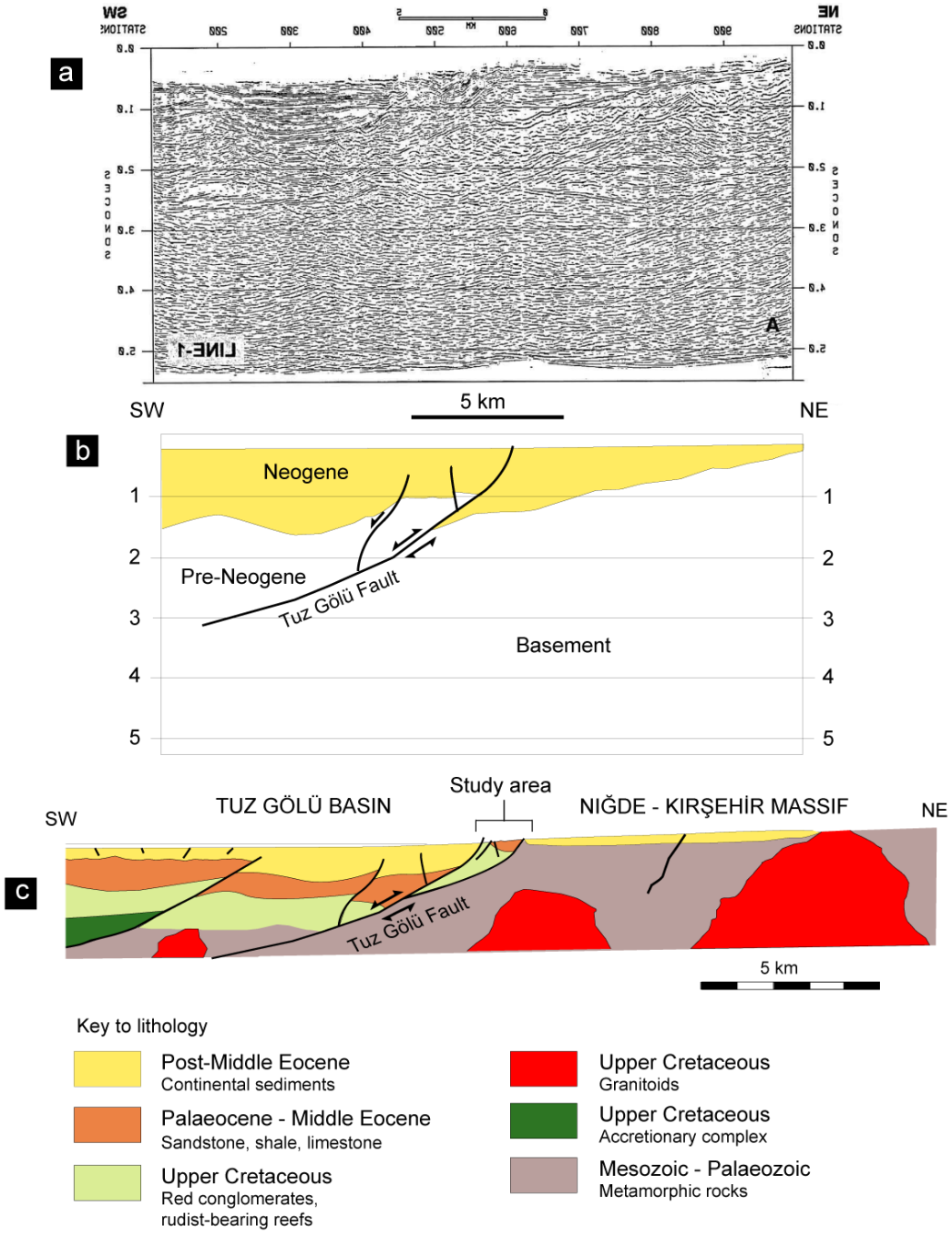

Figure 4.22 (a) An uninterpreted and **(b)** interpreted seismic profile along the eastern margin of the Tuz Gölü Basin. See Figure 4.3a for the approximate position of the seismic line. The uninterpreted image was taken from Aydemir (2009); the interpreted image was redrawn after Aydemir (2009). Vertical axes represent two-way travel time, **(c)** highly simplified geological cross-section along section line A (see Figure 4.3). Note that most of the basin is covered by largely undeformed Neogene-Quaternary continental sediments.

During the Maastrichtian, extensional tectonics were dominant in the Niğde-Kırşehir Massif, which was the upper plate during subduction processes that consumed the Inner Tauride Ocean to the south (e.g. Robertson *et al.* 2009). Extension was probably related to thermal weakening of the crust during the emplacement of granitoid plutons, mostly in Santonian to Campanian time (e.g. Kadıoğlu *et al.* 2006; see Chapter 2). Crustal extension facilitated the exhumation of the Niğde Massif to the southeast (Whitney & Dilek 1997; Whitney *et al.* 2003; Whitney & Hamilton 2004; Fayon & Whitney 2007; Whitney *et al.* 2008; Fig. 4.23) and the Kırşehir Massif to the east and northeast of the basin (Genç & Yürür 2010).

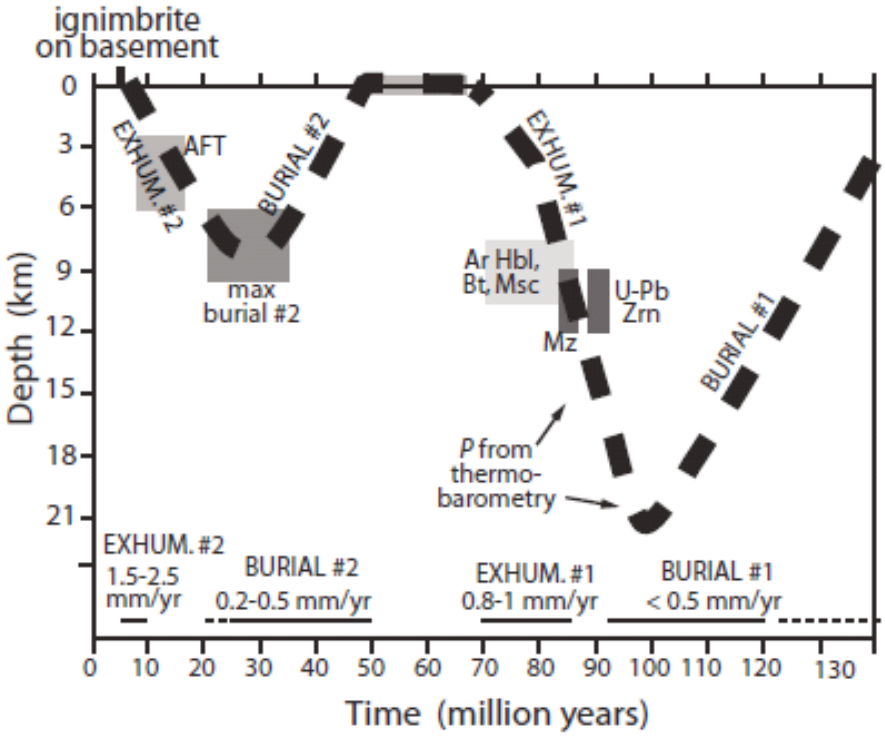

Figure 4.23 Depth-time path and rates for the Niğde Massif, note the Late Cretaceous exhumation. Copied from Fayon *et al.* (2008).

The Tuz Gölü Fault Zone was reactivated as a strike-silp fault during the post-collisional Neogene time (Çemen *et al.* 1999). The sense of strike-slip movement is still debated; many studies favour right-lateral movement (e.g. Görür *et al.* 1984; Çemen *et al.* 1999; Aydemir & Ateş 2006). Dırık & Göncüoğlu (1996)

inferred a right-lateral movement by the alignment of alluvial fans on the downthrown western block, the clockwise bending of streams and right-lateral offset of Neogene lava flows further south. However, these geographic data could not be confirmed during this study, both in the field and by studying satellite images. In contrast, later studies suggest left-lateral motion (Derman *et al.* 2000; Derman & Engin 2007).

4.5.1 New structural data

During this study, 28 fault plane orientations were measured, of which 21 had reliable slickenside indicators. Fault data are from the Upper Maastrichtian Asmaboğazı Formation and the Palaeocene Dizilitaşlar Formation, giving a maximum age of faulting. Most faults strike northwest-southeast, with a small sub-set striking southwest- northeast (Fig. 4.24a). In terms of P-, B- and T-axes (Figs. 4.24b and 4.24c) the faults comprise a heterogeneous data set. Faults were arranged, where possible, into groups with similar P-, B- and T-Axis vectors (see Appendix 4 for fault data and methodology). There are three broad groups of faults: extensional, strike-slip and oblique. Field observations constrain the relative timing of the fault groups; some fault surfaces exhibit down-dip slickensides which were overprinted by left-lateral strike-slip slickensides (Fig. 4.25). Some fault surfaces exhibit left-lateral slickensides which have been overprinted by oblique-slip ones.

4.5.1.1 Extensional faults

Extensional faults are represented by two groups; the first group (n= 2) strikes northwest- southeast whereas the second group (n= 4) strikes WSW-ENE (Figs. 4.26a, 4.26d). Confidence (R) values give an indication of the probability, of each axis, that the faults were formed in the same palaeostress field. R values for the

second group are P- 90%, B – 93%, T – 84%. P-axes are vertical, while B- and T-axes are horizontal. Careful stratigraphic study shows that these faults cut Palaeocene sediments of the Dizilitaşlar Formation, indicating that extensional deformation phase was younger than the Palaeocene.

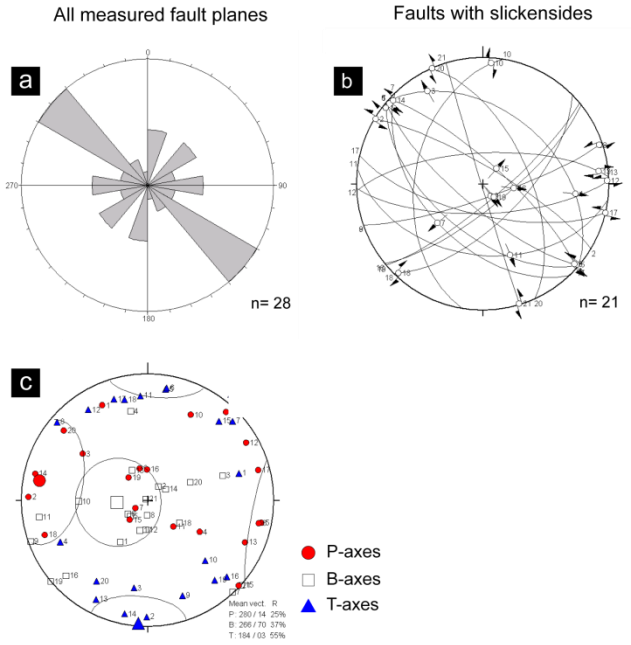

Figure 4.24 (a) rose diagram of all measured fault planes, **(b)** lower hemisphere 'Angelier' plot of faults with slickensides, **(c)** P-, B-, T-Axes figure of measured fault planes with slickensides. All data are from this study.

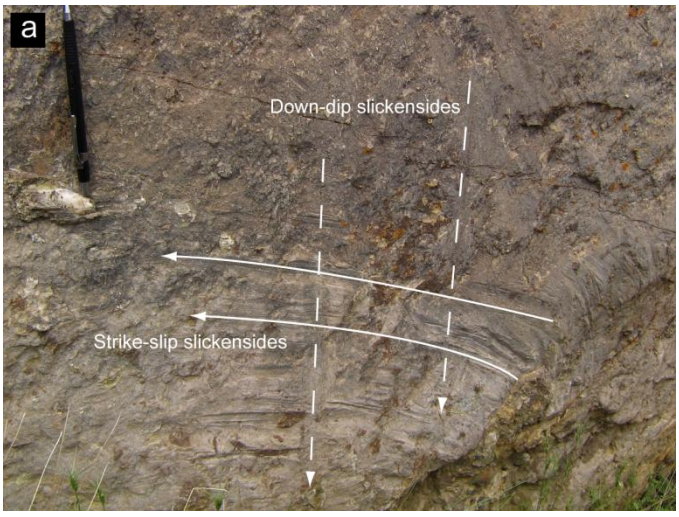

Figure 4.25 Field photograph of a fault plane showing down-dip slickensides overprinted by left-lateral strike-slip slickensides.

4.5.1.2 Strike-slip faults

A second phase of brittle deformation reactivated pre-existing faults and is characterised by strike-slip movement showing sub-horizontal P- and T-axes and sub-vertical B-axes. One group (Fig. 4.26b) comprises left-lateral, northwest-southeast striking faults (n= 4). R values are: P – 89%, B – 91% and T – 94%. The other group (n= 4) of strike-slip faults strikes ~west-east and are left-lateral. R values are P – 86%, B – 96% and T – 86%. The timing of strike-slip faulting cannot be constrained by the available data. However, it has been interpreted as a result post-Late Eocene compression by previous studies (Dırık & Göncüoğlu 1996; Çemen *et al.* 1999) based on repeating pre-Late Eocene stratigraphy in wildcat well data (which are not available in the public domain).

4.5.1.3 Oblique-slip faults

A third deformation phase is characterised by oblique-slip faults (n= 4) with a normal and right-lateral strike-slip component (Figs. 4.26c and 4.26f). Again, absolute timing cannot be constrained; however, oblique slip slickensides overprint strike-slip slickensides inferring that this phase was relatively later than left-lateral strike-slip deformation. This is broadly consistent with the structural model of Çemen *et al.* (1999) who inferred a deformation phase characterised by both right-lateral and down-to-the-SW extensional movement in the Neogene time. This is based on geographic data (e.g. bending of stream courses) and evidence from seismic profiles, trending normal to the Tuz Gölü Fault Zone, that show Neogene sediments onlapping onto a roll-over anticline which was formed during this period of normal-transcurrent faulting phase (Fig. 4.27).

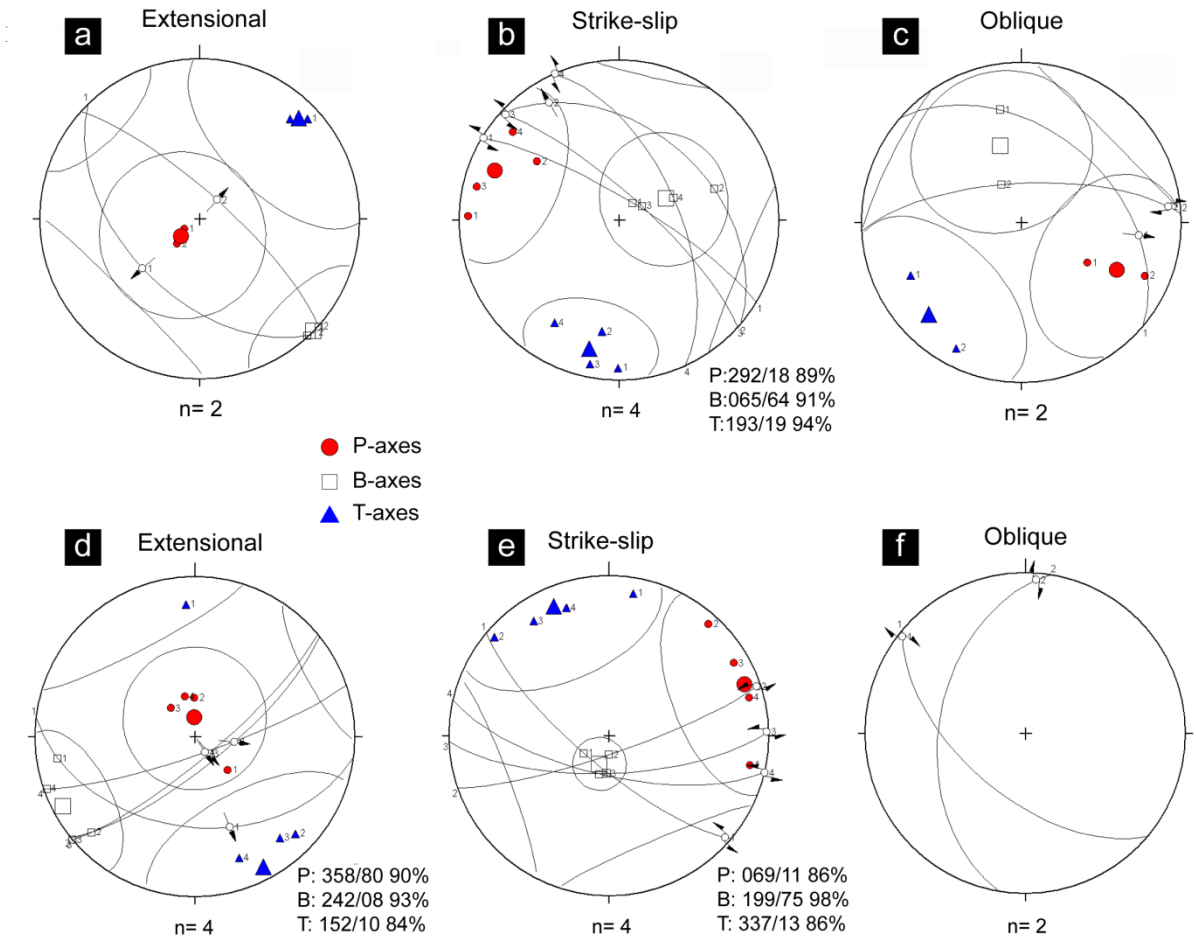

Figure 4.26 Combined P-, B- and T-axes and Angelier lower hemisphere plots of fault groups associated with the Tuz Gölü Fault Zone, **(a)** northwest-southeast-striking extensional faults, **(b)** northwest-southeast-striking left-lateral strike-slip faults, **(c)** ~northwest-southeast-striking oblique-slip faults, **(d)** west-southwest-east-northeast-striking extensional faults, **(e)** ~west-east-striking left-lateral strike-slip faults, **(f)** oblique faults.

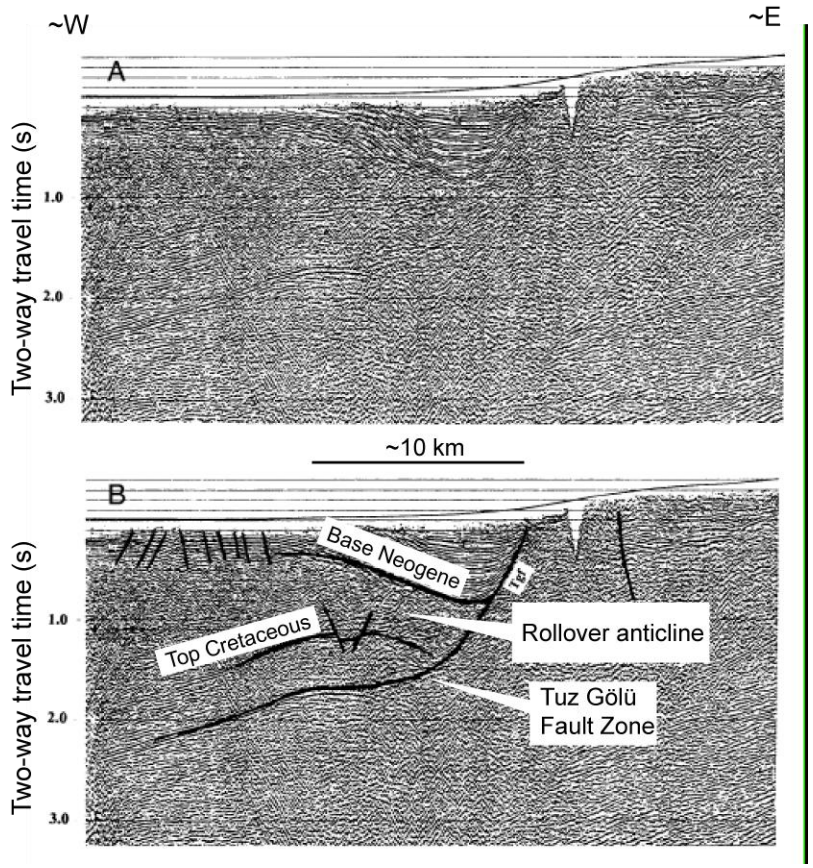

Figure 4.27 Seismic profile, normal to the Tuz Gölü Fault Zone, showing the rollover anticline covered by base of the Neogene deposits. A-Uninterpreted, B – Interpreted. Image copied from Çemen *et al.* (1999).

Basin-scale folding of Palaeocene sediments is aligned parallel to the basin margins and is interpreted to have formed during the Late Eocene – pre-Miocene time (Görür *et al.* 1984). On the eastern basin margin, folds are aligned at a low angle to the fault zone. Figure 4.28 shows the orientation of one syncline (68529:75220) determined by 18 bedding plane measurements. The π-axis of the fold trends to the north-northeast and plunges at 37°.

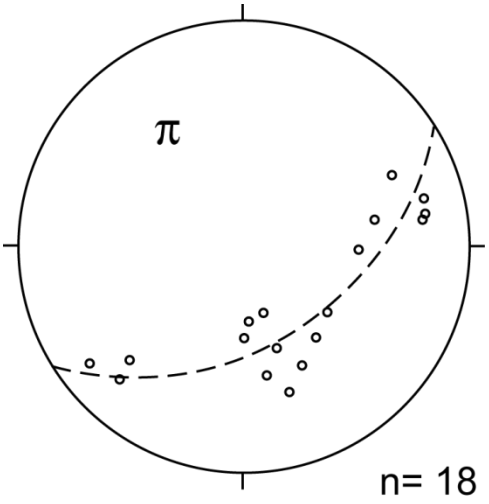

Figure 4.28 Lower hemisphere stereonet of poles to bedding planes in a basin margin syncline (68529:75220), the dashed line represents the best-fit girdle.

4.5.1.4 Interpretation of structural data

The structural interpretation of the Tuz Gölü Basin is hampered by an undeformed cover of Neogene – Quaternary sediments. However, new data offer the following insights: 1) the oldest faults are extensional, and are possibly related to the exhumation of the Niğde-Kırşehir Massif to the east. This phase of faulting persisted until post-Palaeocene time. In this scenario, the Tuz Gölü Fault Zone acted as a detachment fault; 2) the next phase reactivated pre-existing faults as left-lateral strike-slip faults. Çemen *et al.* (1999) related this phase to regional compression in post-Late Eocene time. New data indicate that compression was aligned west-northwest – east-southeast and west-southwest – east-northeast, and; 3) oblique-slip faulting probably acted on pre-existing structures and involved right-lateral and extensional movement. This phase may have been responsible for the formation of a roll-over anticline at the eastern basin margin (Fig. 4.27).

While new data cannot constrain the absolute timing of brittle deformation, they do imply the relative order of faulting phases which are, tentatively, in agreement with the model proposed by Çemen *et al.* (1999).

4.6 Evolution of the Tuz Gölü Basin

New sedimentary, stratigraphic, provenance and structural data permit a reconstruction of the Late Cretaceous – Middle Eocene development of the Tuz Gölü Basin. The basin evolved on the western margin of the Niğde-Kırşehir microcontinent during regional plate convergence. To the northeast of the basin, Turonian SSZ-type ophiolites, derived from the İzmir – Ankara – Erzincan Ocean to the north, were emplaced onto the Niğde – Kırşehir Massif prior to granitoid magmatism mostly in the Santonian to Campanian time.

4.6.1 Late Cretaceous

New palaeostress and sedimentary data presented in this chapter indicate that the extensional deformation phase persisted from the Late Cretaceous to at least the Palaeocene. Extensional deformation was probably a result of thermal weakening of the crust related to the intrusion of Santonian to Campanian granitoid plutons. It is possible that the Tuz Gölü Fault Zone, a major fault that demarcates the basin to the east evolved as a low-angle detachment fault, along which mid-crustal rocks of the Niğde-Kırşehir Massif were exhumed (Whitney & Dilek 1997; Çemen *et al.* 1999; Genç & Yürür 2010). In this respect, this tectonic development is analogous to a basin and range-type setting, a good example of which is seen in the formation of core complexes in the western United States (e.g. Thatcher *et al.* 1999).

The extensional phase led to the deposition of unroofed material, from the Niğde-Kırşehir Massif, as conglomerates of the Upper Cretaceous Kartal Formation in an alluvial setting at the basin margin. By the Maastrichtian time (Fig. 4.29), a marine transgression had occurred allowing the deposition of the sandy calciturbidites (lithofacies RW1) and rudist reefs (lithofacies R1) of the Asmaboğazı Formation in a shelf/upper slope setting on the eastern basin margin. Sub-surface

borehole data indicate that sedimentation in the deeper water basin depocentre was dominated by Maastrichtian turbidites of the Haymana Formation (Görür *et al.* 1984) (see Chapter 5). Study of the Kırıkkale Basin (see Chapter 2), to the north, indicates that the SSZ-type ophiolite was covered by Maastrichtian sediments including pelagic marls and redeposited carbonate platform material containing benthic foraminifera.

In the Bala area, the Asmaboğazı Formation is absent; instead, the Kartal Formation is covered by deeper-water turbidites of the Haymana Formation. In summary, during the Maastrichtian, the basin deepened to the north, with reefs building on palaeotopographic highs near the eastern margin south of Şereflikoçhisar. A further marine transgression, in the earliest Palaeocene drowned the marginal Maastrichtian carbonates with terrigenous sediments deposited from turbidity currents and debris flows.

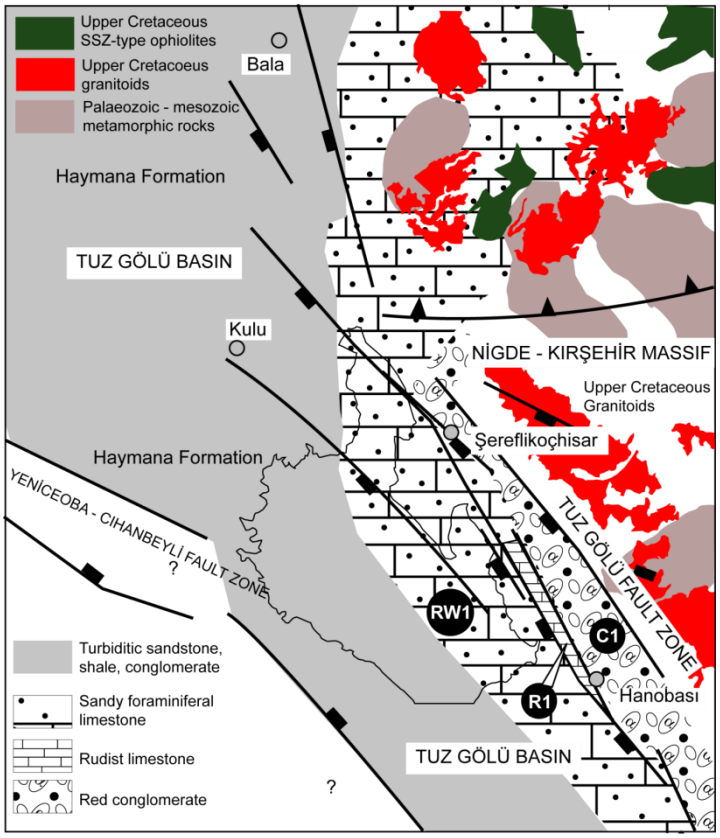

Figure 4.29 Non palinspastic palaeogeographic reconstruction of the Tuz Gölü Basin during the Maastrichtian, which formed on the western margin of the Niğde – Kırşehir Massif. During this time, a marine transgression triggered the deposition of shelf-type rudist-bearing carbonates (lithofacies R1) and foraminiferal sandy limestone (lithofacies RW1) on the eastern basin. Sedimentation in the basin depo-centre and to the north was dominated by slope/lower slope thin clastic turbidites of the Haymana Formation.

4.6.2 Palaeocene

The Early to Middle Palaeocene (Danian to Selandian) time saw the development of coralgal and foraminiferal reefs of the Dizilitaşlar Formation (Lithofacies R2) along the basin margin, and appears to correspond to a transgression triggered by elevated eustatic sea level (Miller *et al.* 2005). The reefs formed on palaeotopogaphic highs while the extra-formational conglomeratic debris flows of lithofacies M2 filled palaeotopographic lows (Fig. 4.30). Continuing tectonism

generated mass flow events that transported reefal debris into basin slope environments represented by detached limestone blocks and carbonate debris flows (Lithofacies RW2).

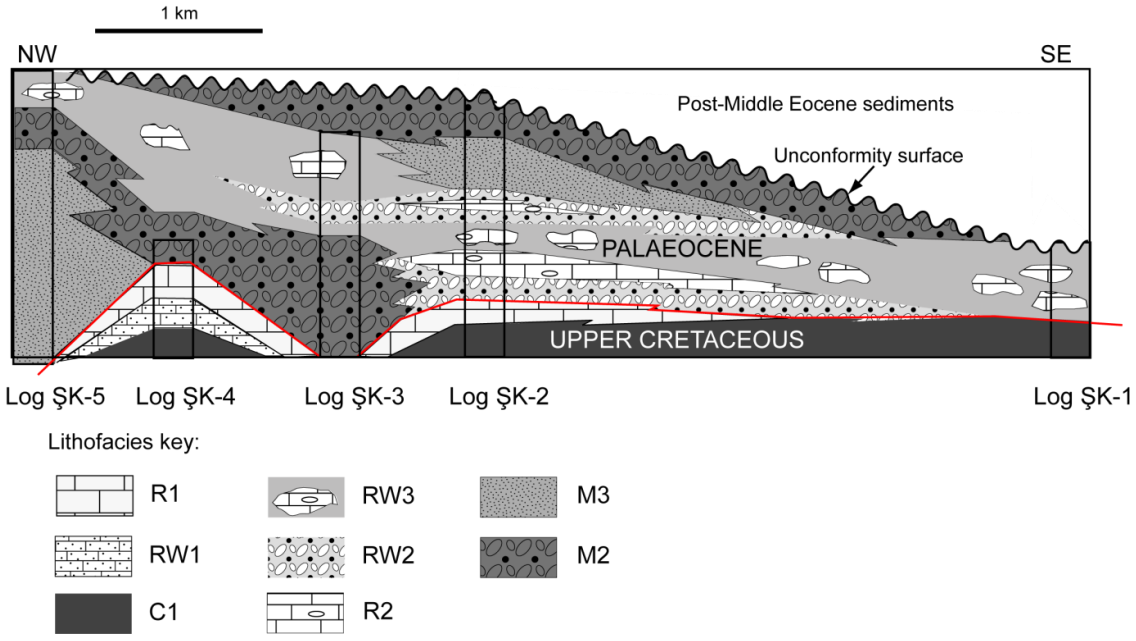

Figure 4.30 Stratigraphic correlation panel of Upper Cretaceous–Palaeocene sediments in part of the Şereflikoçhisar – Hanobası area based on data discussed in this study. Lithofacies key: C1 – Pebble- to boulder-sized red Upper Cretaceous conglomerate, RW1 – Maastrichtian sandy limestones containing large benthic foraminifera, R1 – Maastrichtian rudist-bearing limestone, R2 – Palaeocene foraminiferal and coralgal in situ reefal limestone, RW2 Palaeocene carbonate conglomerates, RW3 – Detached blocks of Palaeocene lithofacies R2, M2 – clastic conglomerates, M3 – Lithoclast-rich, high-density sandstone turbidites. Vertical scale = horizontal scale.

4.6.3 Late Palaeocene-Early Eocene

During the Late Palaeocene-Early Eocene time (Fig. 4.31), sedimentation was dominated by shelf-type clastic turbidites of the Yoncalı formation. Lithofacies M1 (Danian siliciclastic sandstone and shale) was deposited in the southern part of the basin, and lithofacies M5 (turbiditic sandstone rich in volcanic lithoclasts) and M6 (inverse-graded conglomerates) in the northern part near Kulu and Bala.

Palaeocurrent indicators at Bala indicate a flow direction from the northwest, which infers the source of the volcaniclastic sandstone was in that direction.

Lithofacies M4 (Thenatian pebbly sandstone) is well exposed on to the southwest of Şereflikoçhisar on a peninsula west of Karamollauşağı Village. Clearly, the Yoncalı Formation represents further deepening of the basin, possibly influenced by high eustatic sea level during the Palaeocene-Eocene thermal maximum (e.g. Kennett & Stott 1991). In contrast to other basins of the Central Anatolian Basin Complex, Nummulites-bearing shelf-type carbonates are not preserved in the Tuz Gölü Basin, implying deeper water depths and/or a higher terrigenous input.

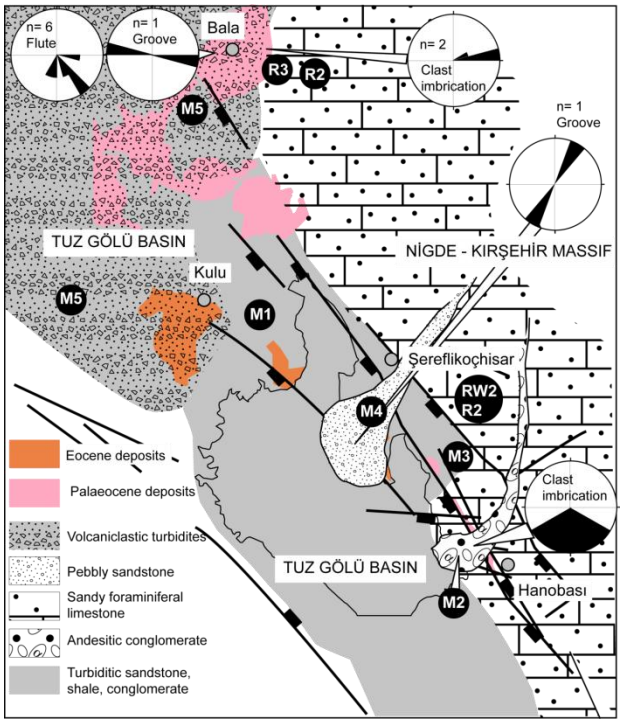

Figure 4.31 Non palinspastic palaeogeographic reconstruction, of the Tuz Gölü Basin during the Palaeocene – Early Eocene time, based on this study. Shelf-type coralgal and foraminiferal carbonates (lithofacies R2, R3, RW2 and RW3) developed on palaeotopographic highs on the eastern margin of the basin. Clastic debris flows (lithofacies M2) filled the palaeotopographic lows. Above this sequence, Pebbly sandstones (lithofacies M4) were deposited. To the north, olcaniclastic sediments (lithofacies M5) were deposited (Kulu and Bala areas) to the north. Rose diagrams indicate palaeocurrent directions.

4.6.4 Post-Middle Eocene-Neogene

Post-Middle Eocene to Neogene time (Fig. 4.32) saw a shift in the basin's tectonics and depositional regime. Palaeostress data presented in this chapter indicate a change from east-west oriented extension to approximately east-west oriented compression. This change in palaeostress is in agreement with borehole data discussed by Çemen *et al.* (1999) who infer structurally repeated Palaeocene-Eocene sediments in the basin depocentre, interpreted as compressional imbrication of basin basement rocks and pre-Middle Eocene sediments. Extensional faults along the eastern basin margin were reactivated as left-lateral strike-slip faults and basin margin-parallel folds formed. This, in turn, lead to uplift and a change in sedimentation from deep-water turbidites of the Upper Palaeocene-Middle Eocene Yoncalı Formation to evaporites and continental clastics of the post-Middle Eocene time. The tectonic uplift occurred coevally with a global sea level fall and led to end of the pre- to syn-collisional history of the Tuz Gölü Basin. Further convergence led to imbrication of the Izmir-Ankara accretionary complex which over-rid the northwest basin margin, and formed a boundary between the Tuz Gölü Basin and the Haymana-Polatlı Basin to the north (Dellaloğlu & Aksu 1984a; Görür *et al.* 1984; MTA 1989).

Another phase of brittle deformation occurred in the Neogene time (Çemen *et al.* 1999) which was characterised by right-lateral transtensional movement along the Tuz Gölü Fault Zone.

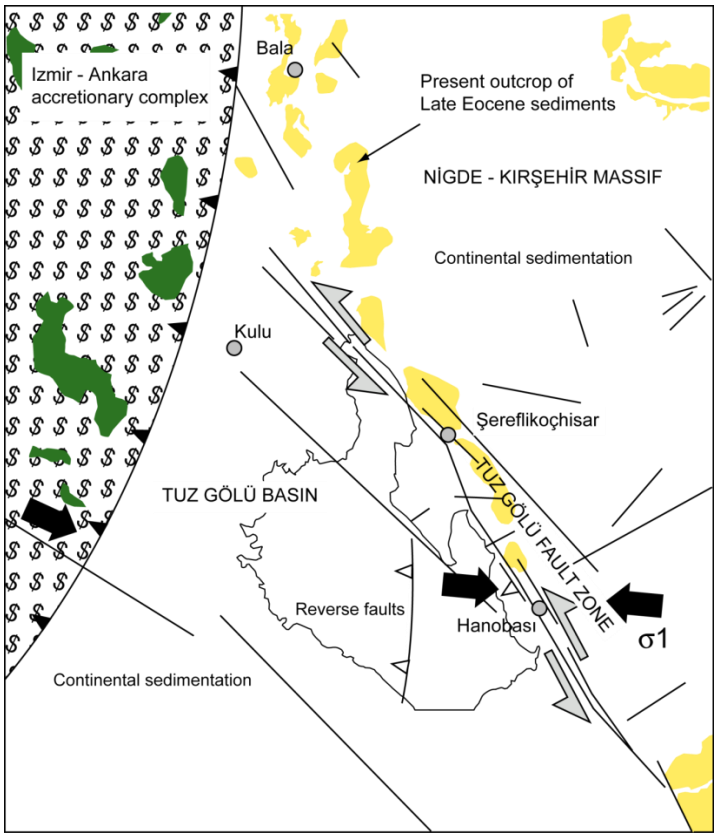

Figure 11 Non palinspastic palaeogeographic reconstruction, based on this study, of the Tuz Gölü Basin during the Late Eocene-Oligocene time. The basin underwent surface uplift and featured continental sedimentation. The Izmir-Ankara accretionary complex thrust over the northwest margin of the basin and produced compressional tectonics.

4.7 Discussion of existing models and role of new data

The nature of the basin's basement and regional tectonic setting is not fully understood. In one interpretation, the Niğde-Kırşehir Massif existed as a promontory of the Tauride-Anatolide Block to the south, with no Inner Tauride Ocean. In this scenario, the basin evolved as a post-collisional basin following Late Cretaceous closure of northern Neotethys along the İzmir-Ankara-Erzincan suture zone. The basin developed on a composite basement of the Niğde-Kırşehir Massif and an inferred accretionary prism containing blocks derived from SSZ–type oceanic crust and fragments derived from oceanic island basalts. The blocks have been metamorphosed at blueschist facies. The accretionary prism was emplaced onto the Niğde-Kırşehir Massif in post-Turonian to pre-Late Maastrichtian time (Çemen *et al*. 1999). However, one problem with this hypothesis is that the Late Cretaceous granitoids emplaced into the Niğde-Kırşehir Massif infer the existence of the Inner Tauride Ocean.

In contrast, Görür *et al*. (1984) suggested that the Inner Tauride Ocean existed between the Tauride-Anatolide Block and the Niğde-Kırşehir Massif. Basin evolution was associated with a northeast-dipping subduction zone that consumed the Inner Tauride Ocean until the Eocene time. In this model, the Tuz Gölü Basin developed as a fore-arc basin, constructed on the margin of the Niğde-Kırşehir Massif above the Inner Tauride subduction zone. One immediate problem with this model is the paucity of volcaniclastic sediments and the absence of arc-related extrusives of a suitable age.

One problem in producing a new tectonic model for the development of the basin is the absence of data on basement rocks, which severely hampers a robust interpretation. One possibility is that the basin was constructed, to the south of a north-dipping intra-oceanic arc, on the Upper Cretaceous İzmir-Ankara accretionary complex. This model proposes that the arc retreated southwards driven by slab roll-back which terminated in Turonian-Coniacian time by a trench-continent collision at the northern margin of the Niğde-Kırşehir Massif. However, an embayment of relict Neotethyan oceanic crust probably existed to the west of the Niğde-Kırşehir Massif

on which the Tuz Gölü Basin developed, where slab roll-back continued. A full discussion of this proposed model is presented in Chapter 6.

4.8 Summary and Conclusions

- Sedimentary, palaeontological and structural data discussed in this chapter shed new light on the tectono-sedimentary processes involved in the evolution of the Upper Cretaceous-Middle Eocene Tuz Gölü Basin in the context of regional convergence and continental collision in central Anatolia.
- The Tuz Gölü Basin is part of the central Anatolian Basin Complex that includes the Kırıkkale Basin, the Haymana-Polatlı Basin and the Çankırı Basin. The basin complex evolved on basements comprising the Niğde-Kırşehir Massif and Upper Cretaceous ophiolitic melange components of İzmir-Ankara accretionary complex.
- The Tuz Gölü Basin is largely covered by Neogene continental deposits, which are generally interpreted to represent post-collisional, intra-plate sedimentation. Upper Cretaceous-Lower Eocene sediments represent deposition in period of regional plate convergence. They are confined to a thin strip on the eastern basin margin south of Şereflikoçhisar, isolated outcrops near Kulu, and to the north near Bala.
- Mesozoic sediments include continental Upper Cretaceous red conglomerates (the Kartal Formation) and Maastrichtian shallow-marine, shelf-type rudist-bearing limestone (the Asmaboğazı Formation). During the Palaeocene, deposits of the Dizilitaşlar Formation included sandstone turbidites and marginal shelf-type coralgal reefs, parts of which were re-deposited as limestone blocks and debris flows onto a slope setting. The latest Palaeocene (and possibly the Middle Eocene) was characterised by thick, lenticular turbiditic pebbly sandstones, and, to the north of the basin, volcaniclastic sediments of the Yoncalı Formation.

- The Late Cretaceous-Palaeocene tectonic setting of the basin was probably influenced by extensional tectonics, which was triggered by regional exhumation of the Niğde-Kırşehir Massif to the west. Exhumation and erosion supplied volcanic and ophiolitic detritus to the eastern margin of the basin. This sediment supply is confirmed by petrographic study of sandstones, which are generally rich in volcanic lithoclasts.
- In the Eocene-Neogene time, regional compression imbricated the basin's basement, produced margin-parallel folds and reactivated older extensional faults. The Tuz Gölü Fault Zone evolved in post- middle Eocene time as a left-lateral strike-slip fault.
- Faulting in the Neogene time was characterised by right-lateral faulting with an extensional component.
- This chapter presents a new tectonic model of basin formation within regional plate convergence that occurred in three discrete steps: 1) incipient Late Cretaceous collision involving the obduction of SSZ-type ophiolites onto an inferred microcontinent, the Niğde-Kırşehir Massif; 2) a Late Cretaceous-Palaeocene period of extension or transtension, driven by exhumation of the Niğde -Kırşehir Massif ; 3) final continental collision from the Middle Eocene-Oligicene accompanied by surface uplift, extensive compressional deformation and transcurrent faulting.

Chapter 5: The Haymana-Polatlı basin

5.1 Introduction

It is widely accepted that central Anatolia comprises a tectonic collage of microcontinents, accretionary complex, ophiolites and magmatic arcs. In this area, a strand of northern Neotethys (the İzmir-Ankara-Erzincan Ocean) subducted northwards under the active Eurasian (Pontide) margin during the Late Mesozoic-Early Cenozoic time (Şengör & Yılmaz 1981; Robertson & Dixon 1984; Robinson *et al.* 1995; Okay *et al.* 2001; Koçyiğit *et al.* 2003). Subduction was associated with the genesis and emplacement of accretionary prisms, ophiolites and deep-water margin units onto the former passive margins of micro continents. This process resulted in the formation of the Izmir-Ankara-Erzincan suture zone, a major suture running approximately east-west through central Turkey which marks the collision of the Pontide continental fragment in the north and the Niğde-Kırşehir microcontinent in the south.

Associated with the suture zone is a series of Upper Cretaceous-Middle Eocene sedimentary basins that record key tectonic and sedimentary processes related to the geotectonic assembly of central Anatolia. The basins are situated to the north and west of the Niğde-Kırşehir Massif and include; 1) the Kırıkkale Basin (Norman 1972; Norman 1973a; Norman 1973b; Akyürek *et al.* 1984; Dönmez *et al.* 2008) (see Chapter 2); 2) the Çankırı Basin (Tüysüz & Dellaloğlu 1992; Koçyiğit *et al.* 1995; Erdoğan *et al.* 1996; Kaymakcı *et al.* 2009) (see Chapter 3); 3) the Tuz Gölü Basin (Arikan 1975; Dellaloğlu & Aksu 1984; Görür *et al.* 1984; Çemen *et al.* 1999; Derman *et al.* 2000; Aydemir & Ateş 2006) (see Chapter 4); and 4) the subject of this chapter, the Haymana-Polatlı Basin (Fig.5.1).

The development of the basins is an unresolved question in the Tethyan evolution of Turkey. Presently, there are two contrasting end-member tectonic models of basin development during regional plate convergence in central Anatolia. In one model, northern Neotethys comprised a single ocean basin which sutured in the Late Cretaceous. Following ocean closure, the basins developed on supra-subduction zone (SSZ)-type ophiolites and accretionary prisms which were emplaced

onto the northern margin of the Gondwana-related Tauride continent (Göncüoğlu *et al.* 1995; Boztuğ 1998; Gürer & Aldanmaz 2002).

In contrast, the other end-member model proposes that northern Neotethys was palaeogeographically complex, and included the Izmir-Ankara-Erzincan Ocean to the north and the Inner Tauride to the south. Separating the oceanic strands was the Niğde-Kırşehir Massif, a microcontinent rifted from the larger Tauride continent to the south. The basins were of accretionary forearc/syn-collisional type and developed above north-dipping subduction zones which persisted until the Middle Eocene time (Görür *et al.* 1984; Koçyiğit 1991; Görür *et al.* 1998; Robertson *et al.* 2009).

The Haymana-Polatlı Basin is a classic area of Neotethyan geology and exhibits well-exposed Upper Cretaceous-Middle Eocene stratigraphic sequences. It is situated to the northwest of the Upper Cretaceous-Middle Eocene Tuz Gölü Basin (Chapter 4) and to the west of the Niğde-Kırşehir microcontinent (Fig. 5.1). The basin is generally considered to be an accretionary-type basin because it lies to the south of the former active Pontide margin and the contemporaneous Upper Cretaceous-Middle Eocene Orhaniye Basin (Görür *et al.* 1984; Koçyiğit 1991). The basin is floored by a basement composed accretionary material represented by Upper Jurassic-Lower Cretaceous neritic limestone and the mainly Upper Cretaceous Izmir-Ankara Accretionary Complex (Ünalan *et al.* 1976; Görür *et al.* 1984; Koçyiğit *et al.* 1988; Koçyiğit 1991).

The Haymana-Polatlı Basin provides an opportunity to study Upper Cretaceous-Middle Eocene tectono-sedimentary processes related to regional convergence and enables cross-correlations and comparisons between other central Anatolian basins. This basin was chosen for study because it contains a number of features that are unique the Central Anatolian Basins: 1) it was constructed on a accretionary basement comprising the Permo-Triassic units with an Upper Jurassic-Lower Cretaceous neritic limestone cover; 2) it developed in a proximal position to the Pontide active margin to the northwest of the Niğde-Kırşehir Massif; 3) it

exhibits well exposed complete stratigraphic successions, and; 4) structurally, it suffered relatively little deformation.

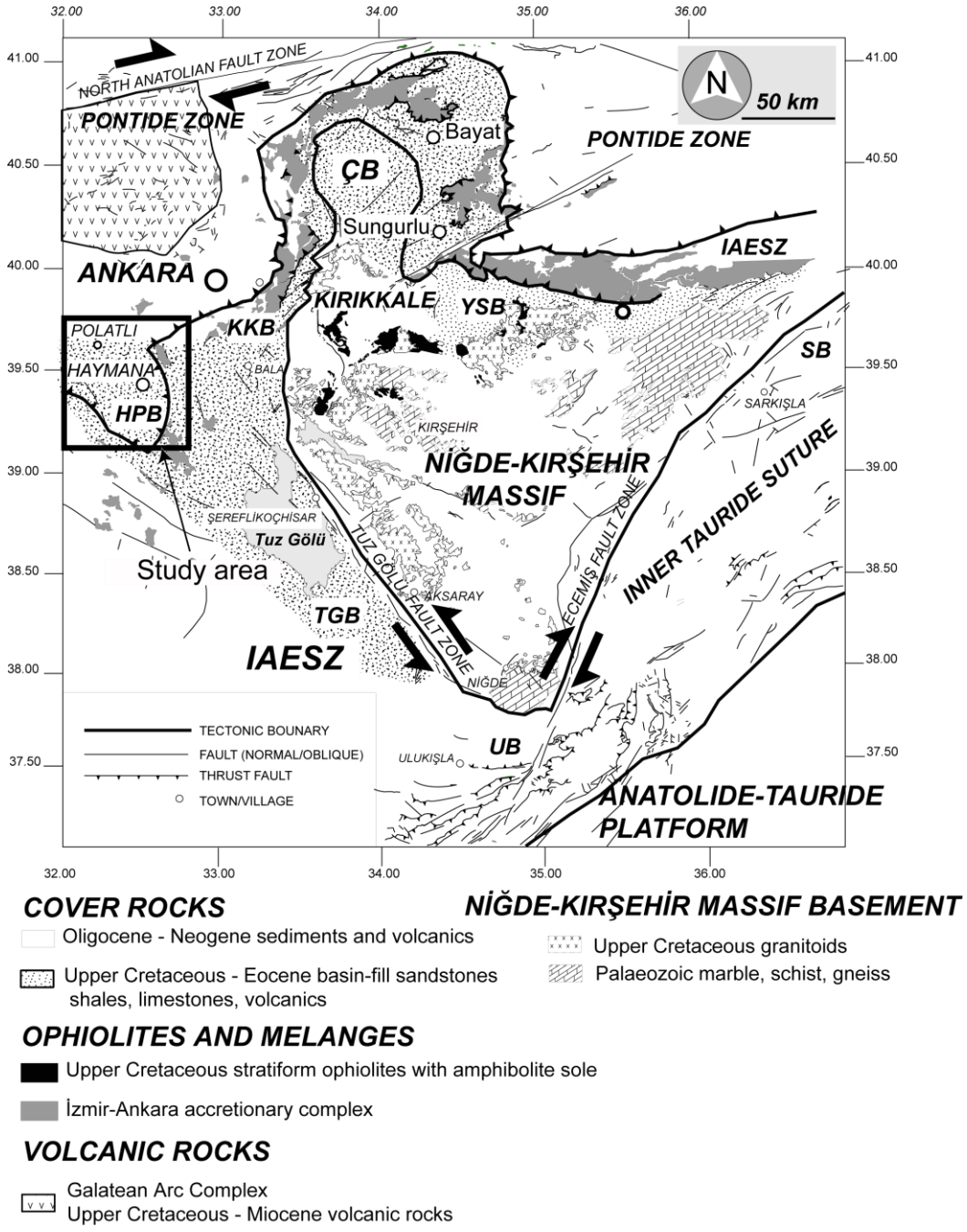

Figure 5.1 Regional map of central Anatolia indicating major basin areas and tectonic units. İzmir-Ankara-Erzincan Suture Zone (IAESZ), Tuz Gölü Basin (TGB), Kırıkkale Basin (KB), Çankırı Basin (ÇB), Ulukışla Basin (UB), Sivas Basin (SB). The area discussed in this chapter is indicated by the black box. Modified after (Clark & Robertson 2002; MTA 2002)(Clark & Robertson 2002; MTA 2002).

Post-Middle Eocene sedimentation was deposited in a continental post-collisional setting and was not included in this thesis. Previous studies have focused on local stratigraphy, sedimentology and palaeontology. However, few have considered the regional tectonic implications of the Haymana-Polatlı Basin. The aim of this chapter is to: 1) test existing stratigraphic models (e.g. Ünalan *et al.* 1976; Görür *et al.* 1984); 2) discuss structural, provenance and palaeocurrent data which, until now are largely missing from the literature; 3) test existing models of continental collision in central Anatolia, as highlighted above. Measured sections were based on the localities described by Ünalan *et al.* (1976).Each section will end with an interpretation of the new data gathered during this study. In particular this will focus on where new data have added to, confirmed, or changed previous interpretations.

5.2 Previous work

The Haymana-Polatlı basin has been the subject of numerous studies since the 1940s. Early work comprised palaeontological and stratigraphic studies (e.g. Erünal 1942; Uysal 1959). Work in the 1970s included further stratigraphic studies (Yüksel 1970; Sîrel 1975; Gökçen 1976a; Ünalan *et al.* 1976; Gökçen 1978; Görür & Derman 1978; Meriç & Görür 1979) (see Figs. 5.2a, 5.2b, 5.2c and 5.2d) and early seismic interpretations (Ünalan & Yüksel 1978). Since the 1980s, work has included regional tectonic interpretations (Görür *et al.* 1984; Koçyiğit *et al.* 1988; Koçyiğit 1991; Görür *et al.* 1998; Koçyiğit *et al.* 2003), further petroleum exploration and seismic work (Turgay & Kurtuluş 1985; Coşkun *et al.* 1990), palaeontological work (Duru & Gökçen 1985; Çetin *et al.* 1986; Meriç & Tansel 1987; Duru & Gökçen 1990; Özcan & Özkan Altıner 1997; Matsumaru 1999; Yildiz *et al.* 2001; Okan & Hoşgör 2008) and local sedimentary work (Dellaloğlu & Aksu 1984; Çetin *et al.* 1986; Çiner *et al.* 1996a; Çiner *et al.* 1996b). Recent work has focused on remote imaging using seismic, gravity and aeromagnetic data (Aydemir & Ateş 2006).

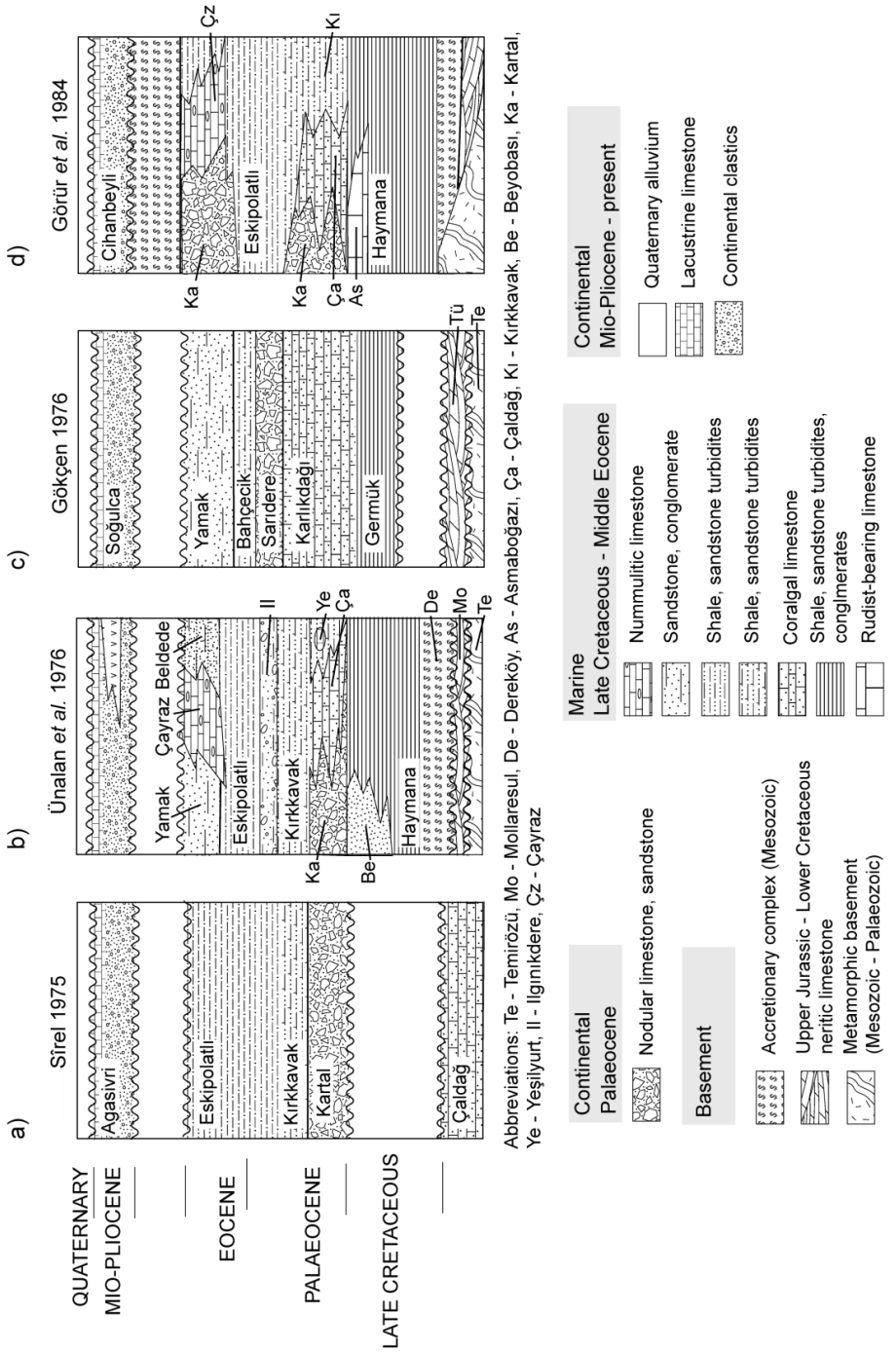

Figure 5. 2 Previous stratigraphic schemes (with formation names) of the Haymana-Polatlı Basin **(a)** an early stratigraphic interpretation (Sîrel 1975) based on the western margin of the basin **(b)** the stratigraphy of Ünalan *et al.* (1976) **(c)** the stratigraphy of Gokcen (1976) based on a study area to the south of Hayman **(d)** the stratigraphic model of Görür et al (1984) in which the basin evolved in a forearc-type tectonic setting.

This study has added the following data to previous work: 1) new, detailed lithofacies descriptions and interpretations; 2) detailed measured stratigraphic logs; 3) new palaeocurrent data; 4) structural data and interpretation; 4) a new model of continental collision in central Anatolia, a critical component

5.3 Regional geology

5.3.1 The Pontide active margin

The Haymana-Polatlı Basin is located ~70 km to the southwest of Ankara and developed on accretionary material related to the Late Cretaceous-Middle Eocene northward subduction of a branch of northern Neotethys (Görür et al. 1984) and an earlier Permo-Triassic subduction of Palaeotethys. It is bound to the north by the Galatean Arc Complex (Koçyiğit 1991; Koçyiğit et al. 2003), to the east by the Ankara Mélange and to the south by the Tuz Gölü Basin (see Chapter 4). The Pontide active margin includes the Sakarya Zone, a continental fragment which stretches from the Aegean to Iran. A major component of the Sakarya Zone is the Karakaya Complex, a Permo-Triassic subduction-accretion complex (Pickett & Robertson 1996; Okay & Tüysüz 1999). The Karakaya Complex can be divided into a lower and an upper unit. The lower part is a highly deformed and sheared sequence of metabasites intercalated with phyllite and marble and corresponds to the Nilüfer unit (Pickett & Robertson 1996; Pickett & Robertson 2004). The upper part of the Karakaya Complex is composed of several tectonostratigraphic units including: 1) arkosic sandstone; 2) greywacke with exotic limestone blocks; 3) basalts and olistostromes with Upper Permian limestone clasts (Çal unit) and; 4) black shales (Pickett & Robertson 1996; Okay & Göncüoğlu 2004; Sayıt & Göncüoğlu 2009). Interpretations of the Karakaya Complex (Pickett & Robertson 1996; 2004) suggest the development of a Triassic subduction-accretion complex related to the collision of oceanic seamounts, mid-ocean ridge type oceanic crust, pelagic sediments and continental fragments to the Eurasian active margin during the closure of

Palaeotethys. The Karakaya Complex is unconformably overlain by a Lower Jurassic to Eocene sequence comprising Lower-Middle Jurassic shallow-marine clastics (including Ammonitico Rosso horizons), Upper Jurassic-Lower Cretaceous neritic carbonates, and an Upper Cretaceous-Palaeocene volcano-sedimentary sequence.

The Central and Eastern Pontides contain magmatic arc rocks (Akıncı 1984; Robinson *et al.* 1995; Rice *et al.* 2009). Biostratigraphic ages and radiometric dating of plutonic rocks indicate that calc-alkaline magmatism was active from the Turonian to the end of the Maastrichtian in the Eastern Pontides (Okay & Şahintürk 1997; Okay *et al.* 2001). In the central Pontides, the Galatean Arc Complex, to the north of Ankara, contains a ~1500 m-thick section of Middle Campanian-Palaeocene silicic volcanics, syenodirite, trachyandesites and alkali basalts which formed in an extensional regime, and are interpreted as the result of slab roll-back processes (Koçyiğit *et al.* 2003).

5.3.2 The Ankara Mélange

The Ankara Mélange is a classic accretionary complex which trends east-west through western and central Turkey for several hundred kilometres (Norman 1984). It marks the position of the İzmir-Ankara-Erzincan suture zone and is best exposed to the south and east of Ankara. Modern interpretations of the Ankara Mélange (c.f. Bailey & MacCallien 1950; Norman 1984) recognise three tectonic units, from structurally high to low: 1) an Upper Triassic-Lower Jurassic metamorphic mélange, composed of metasedimentary and metamorphosed mafic/ultramafic rocks in a greywacke matrix, thought to correspond to the Nilüfer Unit of the Karakaya Complex (Pickett & Robertson 1996; Okay & Tüysüz 1999; Okay & Göncüoğlu 2004); 2) a Permo-Triassic limestone block mélange comprising neritic limestone, conglomerate, agglomerate, dolerite and turbidites in a shaley volcaniclastic matrix, corresponding to the Çal Unit of the Karakaya Complex (Pickett & Robertson 1996; Okay & Tüysüz 1999); 3) a mainly Upper Cretaceous

ophiolitic mélange (the Izmir-Ankara Accretionary Complex (Okay *et al.* 2006)) which features blocks and thrust sheets of serpentinised upper mantle peridotites, basalts, dykes, radiolarian chert, sandstone and limestone in a serpentinite matrix (Norman 1984; Koçyiğit 1991; Dilek & Thy 2006). Biostratigraphic studies reveal ages of Late Triassic to Mid Cretaceous (Bragin & Tekin 1996; Rojay *et al.* 2001). Radiometric dating indicates Lower Jurassic (~179±15 Ma) for a plagiogranite dyke intruding ultramafic upper mantle material (Dilek & Thy 2006). Volcanic rocks studied in the Izmir-Ankara Accretionary Complex include Mid-ocean ridge-type basalts, island arc tholeiites (see Chapter 2) and within-plate seamount-type basalts (Rojay *et al.* 2001). Most interpretations suggest the Izmir-Ankara Accretionary Complex represents Neotethyan oceanic lithosphere and pelagic sediments accreted to the Pontide margin during the northward subduction of northern Neotethys.

5.4 Stratigraphy and sedimentology

The study area comprises a 25 km x 25 km square around Polatlı in the northwest, Haymana in the centre and Bahçecik in the south. Gravity anomaly work suggests a maximum basin depth of 8 km to the east of Haymana (Aydemir & Ateş 2006). Previous stratigraphic work infers a maximum Upper Cretaceous-Middle Eocene sedimentary depth of ~5.6 km (Ünalan *et al.* 1976; Görür *et al.* 1984). The purpose of this chapter is to test previous stratigraphic schemes using new stratigraphic, sedimentary, palaeocurrent and palaeontological data gathered during this study. Sedimentary logs were measured at the localities described by Ünalan *et al.* (1976). Based on their inferred depositional environment, this chapter will present and discuss lithofacies associations for the first time in any detail (a summary of lithofacies is presented in Tables1, 2 and 3). Following lithofacies descriptions, brief interpretations discuss depositional environments and highlight how the new data adds to the understanding of basin evolution.

A new geological map, labelled with locality numbers, is presented in Fig. 5.3. The map is partly based on previous studies (Ünalan *et al.* 1976; MTA 2002) but mostly on observations during this study. Fig. 5.4 is a new stratigraphic model based on this study. The stratigraphy is constrained by new palaeontological data (N. İnan & K. Taslı pers. comm. 2009) and improves earlier models (Sîrel 1975; Gökçen 1976a; Ünalan *et al.* 1976; Görür *et al.* 1984) (Fig. 5.2).

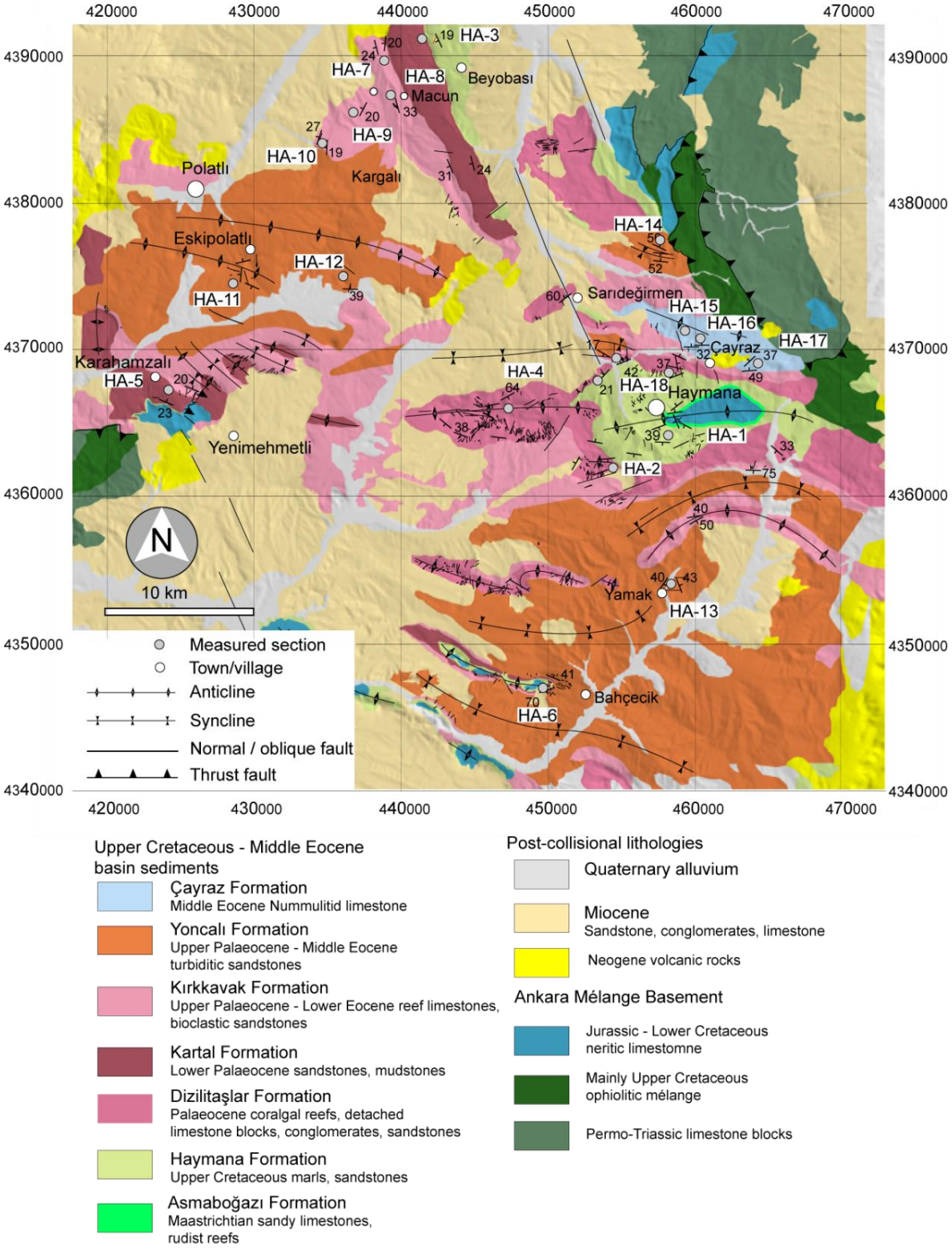

Figure 5.3 Geological map of the Haymana-Polatlı Basin, mostly based on observations during this study, partly modified after Ünalan *et al.* (1976) and MTA (2002).

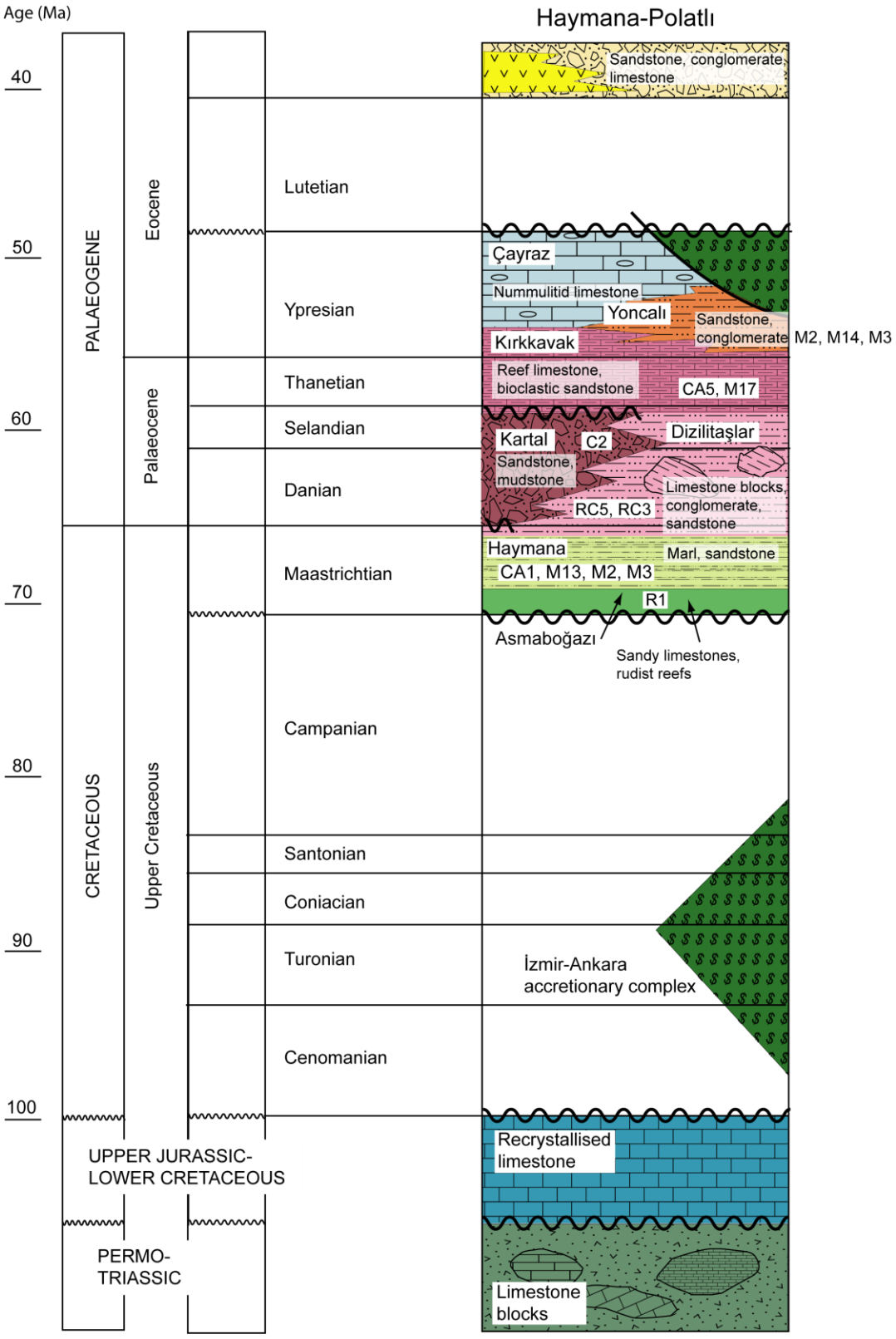

Figure 5.4 New stratigraphic scheme, as proposed by this study. Palaeontological data are after N. İnan & K. Taslı (pers. comm. 2009).

Table 1 - Summary table of siliciclastic lithofacies

Code	Lithologies	Textures	Sedimentary Structures	Bounding surfaces & bed thicknesses	Fossils and outsized clasts	Inferred depositional processes
M2	Lithoclast-rich sandstone, mudstone, siltstone.	Well sorted, medium-grained sandstone comprised of sub-angular grains. Grey mudstone.	Local flute and groove marks, syn-sedimentary slump folds. Grading is absent.	Sharp tops and bases. Beds <0.4 m thick.	Absent. Rare pebblestone deposits contain rounded pebbles of schist, marble and black chert.	Bouma-type medium-grained turbidites followed by extensive bioturbation and erosion.
M3	Clastic conglomerates. Clasts are composed of pelagic limestone, crystalline limestone, gabbro, black chert, red radiolarian chert, rare phyllite and marble.	Pebble- to cobble-sized poorly sorted clasts, mostly sub-angular. Local clast imbrication.	Local normal grading. Beds are frequently lenticular.	Commonly erosional bases; beds are frequently capped by coarse siliciclastic and bioclastic sandstones.	Bioclasts include bivalves, gastropods, brachiopods, corals. Bioclastic sandstone tops contain benthic foraminifera *Orbitoides* sp.	Debris flow.
M13	Grey siltstone.	Very fine-grained silt.	Parallel laminae. Thinning upwards packages ~1 m-thick. Local bioturbation.	Scoured bases and irregular tops. 1 – 2 cm-thick horizons.	Absent.	Dilute, low concentrations turbidity currents.
M17	Gastropod-bearing pebbly sandstone.	Well sorted, medium- to coarse-grained sandstone.	Cross-stratification, inverse and normal grading. Thin pebble horizons.	Common erosive bases; tops locally capped by conglomerate debris flows.	"Floating" pebbles, abundant gastropods, rare bivalves.	Sandy debris flows.

Table 2 - Summary of lithofacies

Code	Lithologies	Textures	Sedimentary Structures	Bounding surfaces & bed thicknesses	Fossils and outsized clasts	Inferred depositional processes
M14	Sandstone, mudstone	Very well sorted, medium grained sandstone	Parallel laminae, current ripple marks, burrowing, flute and groove casts.	Sharp tops and bases.Beds <0.4 m-thick.	Fractured benthic foraminifera, bivalve shells.	Lateral spreading of turbidity current (overbank deposit).
M18	Sandstone, mudstone, marl	Very well-sorted medium grained grey sandstone	Normal grading at base. Deformed mudstone is commonly present.	Irregular, erosive bases. Beds <0.6 m-thick.	Horizons of limestone and black chert pebbles.	Channel-fill turbidity currents.
C2	Red/grey sandstone, mudstone and conglomerate.	Well sorted fine-grained sandstone. Lenticular, clast-rich conglomerates.	Extensive development of caliche and calcareous nodules. Local normal grading.	Sharp bases and tops, often capped by rubbly limestone. Bed thicknesses 0.3 – 2.5 m.	Limestone pebbles.	Mass flow deposits on an alluvial delta plain.
R1	Carbonate conglomerates.	Poorly sorted, matrix supported clasts.	Mostly absent. Crude normal grading in bedded deposits at the southern basin margin at Bahçecik.	Lies unconformably on crystalline limestone basement. At the southern basin margin, beds are ~0.4 m-thick.	Rudist bivalves, corals, gastropods, benthic foraminifera, oncloites. Clastic pebbles at the southern basin margin.	Debris flow.

Table 3 - Summary table of carbonate lithofacies

Code	Lithologies	Textures	Sedimentary Structures	Bounding surfaces & bed thicknesses	Fossils and outsized clasts	Inferred depositional processes
CA1	Grey and pink marl, grey mudstone.	Fine-grained lime mudstone.	Extensive bioturbation.	Sharp bases and tops. Beds generally <0.3 m in thickness.	Pelagic foraminifera.	Pelagic and hemipelagic suspension fallout in intermediate to deep marine conditions.
RC5	Algal- and benthic foraminifera-rich grey/white/buff calcarenite.	Well sorted, medium-grained packstone and grainstone.	Burrowing, patchy cementation.	Sharp bases and diffuse, rubbly tops. Beds thicknesses are from 0.1 to 0.5 m, often amalgamated into ~15 m-thick packages.	Calcareous algae, large benthic foraminifera, rare bivalves.	Modified grain flow.
RC3	Detached limestone blocks.	Well sorted, medium-grained packstone and grainstone.	Absent. Brecciated block margins	No sedimentary bedding observed.	Calcareous algae, large benthic foraminifera, rare bivalves.	Mass transport in upper slope setting.
CA5	Grey/buff limestone rich in algae, coral, benthic foraminifera and macrofossils	Range of textures including moderately well sorted packstone, grainstone and encrusted coral bindstone.	Absent	Beds typically exhibit sharp tops and bases. Variable bed thicknesses, from ~0.2 m to ~2 m.	Calcareous algae, large benthic foraminifera, bivalves, coral, gastropods. Local influx of clastic pebbles.	Shelf-type bioherm deposits and reworked reef debris.
CA7	Grey/buff sandy limestone, rich in large benthic foraminifera.	Moderately well sorted sandy packstone.	Well stratified bases passing up into rubbly tops. Burrowing is locally present.	Sharp bases and coarse rubbly top. Bed thicknesses are variable from ~0.5 to ~7 m.	Abundant large benthic foraminifera. Rare bivalves.	Nummulite bank in an upper to lower open shelf.

5.4.1 Basement stratigraphy: the Ankara Mélange

5.4.1.1 Limestone basement (Jurassic-Lower Cretaceous)

The basement of the Haymana-Polatlı Basin comprises Upper Jurassic-Lower Cretaceous neritic limestone and mainly Upper Cretaceous Izmir-Ankara Accretionary Complex (Rojay *et al.* 2001). Other names given are the Türbetepe Formation (Gökçen 1976a; Gökçen 1976b; Gökçen 1978; Norman *et al.* 1980) and the Mollaresul Formation (Ünalan *et al.* 1976). The limestone basement forms topographic highs and crops out in the cores of east-west trending anticlines near Haymana, west of Bahçecik and south of Karahamzalı (Fig. 5.7a). The limestone is white/buff, structureless and locally features a Lower Cretaceous travertine coating (e.g. near Haymana at 58845:65272) (Koçyiğit 1991; Okay & Şahintürk 1997). In thin section (sample HA3.5A), the recrystallised limestone revealed Rotaliid benthic foraminifera, bryozoan and echinoderm debris (N. İnan & K. Taslı pers. comm. 2009) which were insufficient to establish a depositional age. Previous work, however, indentified benthic foraminifera which indicate an Upper Jurassic-Lower Cretaceous age (Sîrel *et al.* 1986). The date is in agreement with studies from the eastern Pontides (e.g. Robinson *et al.* 1995) who describe the limestones as thick-bedded skeletal and oncolitic grainstones that lie conformably on Middle Jurassic (Bathonian) volcaniclastic sediments. The base of the limestone basement is not exposed in this basin; however, its total thickness has been recorded as 300 m (Koçyiğit 1991) and 415 m (Ünalan *et al.* 1976).

5.4.1.2 Ophiolitic mélange basement: the İzmir-Ankara Accretionary Complex

The Izmir-Ankara Accretionary Complex crops out in the northeast and extreme west of the Haymana-Polatlı Basin study area (Fig. 5.3). In this area, the complex consists of southwest-verging thrust sheets and blocks of serpentinite, radiolarian chert and gabbro in a volcaniclastic matrix. Previous studies in this region indicate the presence of ocean island-type alkali pillow basalts to the northeast of Haymana. Biostratigraphic dating indicates a Callovian (Upper Jurassic) to Hauterivian (Lower Cretaceous) age (Rojay *et al.* 2001).

5.4.2 Asmaboğazı Formation (Upper Cretaceous)

5.4.2.1 Lithofacies R1: rudist-bearing upper slope carbonates

The Asmaboğazı Formation lies unconformably on recrystallised limestone basement. This relationship is best observed to the west of Bahçecik (50146:46905) (Log HA-2, see Fig.x) and to the southwest of Karahamzalı where the contact relationship was observed in a limestone quarry (23683:66395) (Log HA-3, Fig. 5.). At the Karahamzalı locality, the upper surface of the limestone basement is a faulted unconformity (Fig. 5.5a). The Asmaboğazı Formation consists of rudist-bearing carbonates (lithofacies R1) and is well-exposed in an anticline near Haymana, at Karahamzalı, and to the south near Bahçecik (Fig. 5.3). To the south of Haymana, the lithofacies is represented by a ~10 m-thick matrix-supported disorganised carbonate conglomerate. Clasts are angular, very poorly sorted and up to 40 cm in size. They are composed of rudist (Fig. 5.5b), gastropod and rugose coral fragments and oncolites (Fig. 5.5c). No primary bedding was observed suggestive of sediment reworking. The poor sorting, matrix support and random fabric suggest these deposits are debris flows.

To the south, near Bahçecik, lithofacies R1 is ~10 m in thickness and contains a clastic input represented by rounded pebbles of black chert, radiolarian chert, feldspar-phyric andesite (Fig. 5.5d). The sandy limestones are buff-coloured medium-bedded (~40 cm-thick) and contain and well preserved rudist; beds display crude normal grading. At the top of this sequence, grey limestone exhibits less siliciclastic material and contains non-rudist bivalve shells.

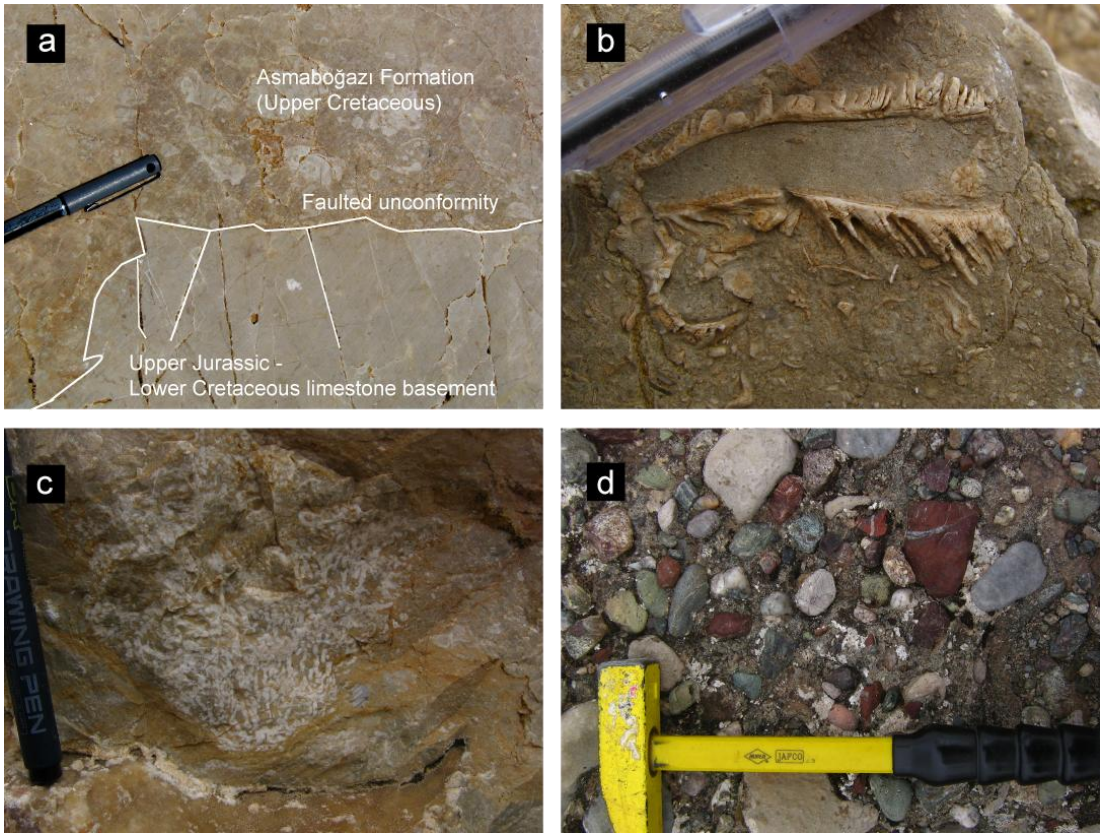

Figure 5.5 (a) Outcrop in a quarry near Karahamzalı (23683:66395) showing the unconformable relationship between the Upper Jurassic-Lower Cretaceous crystalline limestone basement and the reworked carbonates of the Upper Cretaceous Asmaboğazı Formation, **(b)** rudist in reworked carbonates of the Upper Cretaceous Asmaboğazı Formation, **(c)** an oncolite in the Upper Cretaceous Asmaboğazı Formation, **(d)** radiolarian chert and igneous pebbles.

5.4.2.2. Interpretation of the Asmaboğazı Formation

Lithofacies R1 is interpreted to represent resedimented carbonates in a lower shelf/upper slope fore reef-type setting (e.g. Wilson 1975; Selwood 1978). The presence of rudists suggests a Late Cretaceous age; comparable facies include Upper Cretaceous carbonates in the Austrian Alps (Sanders & Höfling 2000).

A key point is that the Asmaboğazı Formation unconformably covers the basement rocks throughout the basin and lies below the Haymana Formation (described below). This is in contrast to Görür *et al.* (1984) who described the formation as a marginal facies that developed stratigraphically *above* the Haymana Formation.

5.4.3 The Haymana Formation (Upper Cretaceous)

The Haymana Formation was first named by Rigo de Righi & Cortesini (1959) and is unique to the Haymana-Polatlı Basin. It comprises a ~70 m-thick basal sequence of pelagic marls (lithofacies CA1) which passes upwards into a ~1200 m-thick succession of siltstones (lithofacies M13) intercalated turbidites, siltstone and mudstone (lithofacies M2) and channelised conglomerates (lithofacies M3). The formation is particularly well-exposed in the core of an anticline near Haymana but is absent at the basin margins (Fig. 5.3). A stratigraphic log was measured to the south of Haymana and is presented in Fig. 5.6.

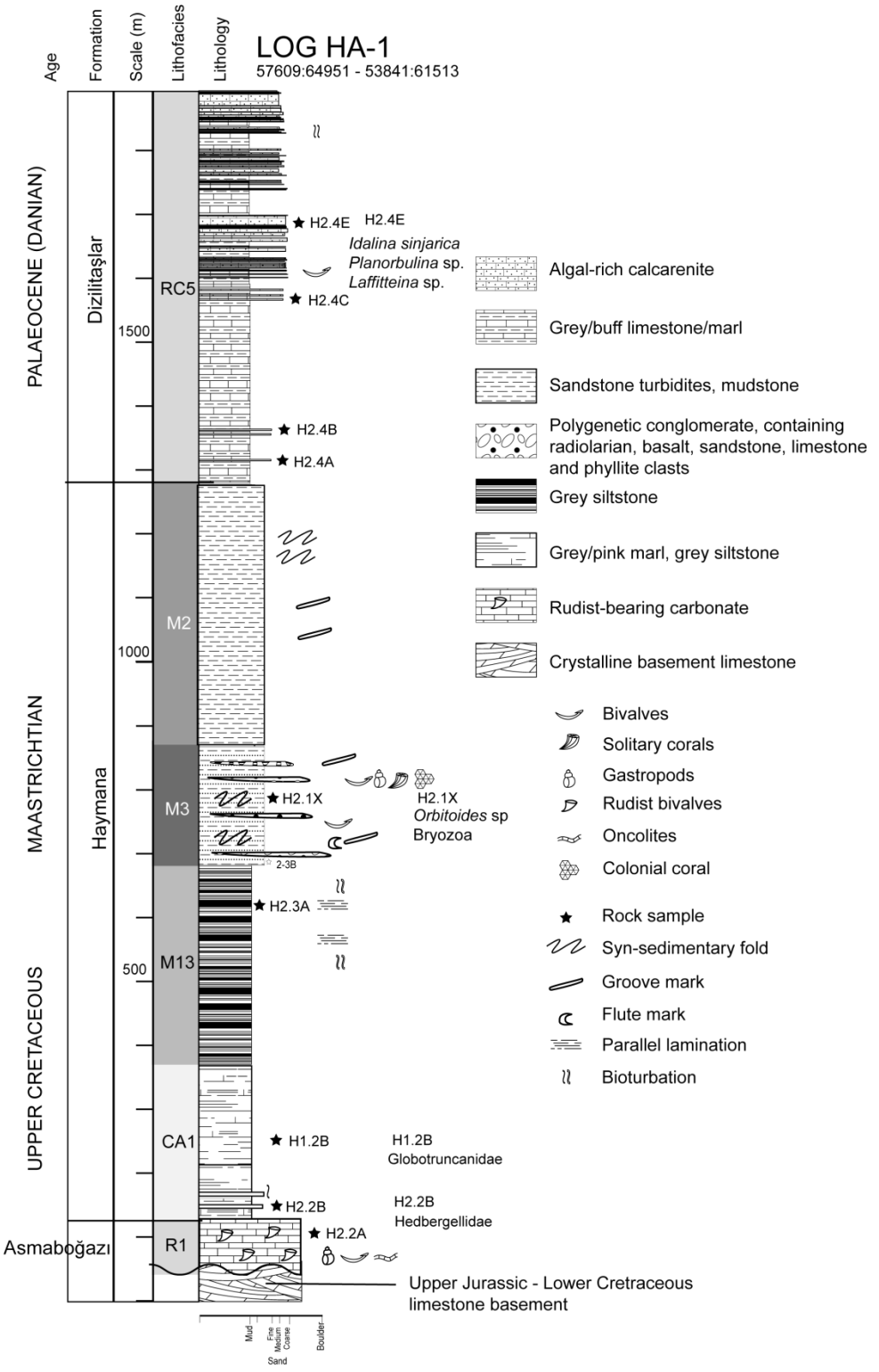

Figure 5.6 Stratigraphic log HA-1, measured on a south-dipping anticline limb to the south of Haymana. Sedimentary data are from this study, fossil data are from N. İnan & K. Taslı (pers. comm. 2009).

5.4.3.1 Lithofacies CA1: pelagic marls

The Asmaboğazı Formation grades vertically into a ~70 m-thick sequence of pelagic grey and pink marls. They are exposed to the north (58703:65561) and south (57609:64951) (Log HA-1) of Haymana. Marls are thinly-bedded, locally bioturbated and frequently intercalated with grey mudstone. Two rock samples collected during this study (HA1.1b and HA2.2b) have yielded Globotruncanid and Hedbergellid pelagic foraminifera, respectively, giving only a broad depositional age of Albian – Maastrichtian (N. İnan & K. Taslı pers. comm. 2009) and indicating intermediate to deep pelagic water depths (Hart 1980) (Fig. 5.7b and 5.7c). The depositional age is in broad agreement with previous studies (Ünalan *et al.* 1976; Görür *et al.* 1984), that dated the Haymana Formation as Maastrichtian.

5.4.3.2 Lithofacies M13: finely laminated siltstones

Above the pelagic marls come ~400 m of thinly laminated grey siltstones which represent lithofacies M13. The siltstone deposits exhibit parallel laminae which are commonly deposited in ~1 m-thick packages that thin upwards from 1 to 2 cm-thick at the base to <1 cm-thick at the top. Laminae feature scoured bases and irregular tops; bioturbation is well developed locally. Sediment transport was probably by dilute, low concentration turbidity currents (e.g. Stow *et al.* 1984).

5.4.3.3 Lithofacies M2: sandstone turbidites, mudstone and siltstone

The finely laminated siltstones grade into a ~600 m-thick package of laterally continuous sandstone beds, massive, black mudstone exhibiting conchoidal fracture

and grey siltstone (lithofacies M2). Sandstone beds are medium-grained, thinly-bedded (<0.4 m) and generally structureless; bases and tops are sharp with no indication of grading. Deposition was probably from turbidity currents (Lowe 1982; Postma 1986; Shanmugam 2000). Massive turbidites are suggestive of secondary processes which destroy primary stratification including bioturbation and erosion (Baas 2004). Rare coarse-grained deposits are represented by thin (<0.2 m) beds of pebblestone composed of rounded grains of schist, marble and black chert. Local features include slump folding, horizontal burrows and groove/flute marks. The axial planes of two syn-sedimentary folds were measured and dip at 82° to 248° (~southeast) and at 49° to 148° (~northeast). The perpendicular of slump fold axes can be used to infer the general downslope direction of palaeoslopes (Woodcock 1979) which suggests that palaeoslopes in the Haymana Formation were orientated to the northeast and southeast. Thirteen palaeocurrent measurements were recorded to the south of Haymana. Twelve grove marks indicated a flow to/from northeast and one flute mark indicated a flow from southwest to northeast. Both indicators suggest a palaeoflow approximately parallel to the implied palaeoslopes.

5.4.3.4 Lithofacies M3: conglomerates

The sandstone turbidites of lithofacies M2 are episodically interrupted by thickly bedded, lenticular deposits of matrix-rich conglomerates (e.g. 56514:62933). Clasts are randomly orientated, typically angular to sub-angular and pebble- to cobble-size, with rare boulder-sized clasts of gabbro. They are composed of marl, pelagic limestone, crystalline limestone, black chert, bioclasts and rare phyllite. Bioclasts include bivalves, gastropods, brachiopods, colonial coral fragments and well preserved solitary corals. Beds are typically capped by ~1 m-thick reworked carbonate conglomerates containing reworked clasts of pelagic limestone, which grade into bioclastic sandstone. One sample (HAY2.1X) contains the benthic foraminifera, *Orbitoides* sp. and bryozoan fragments (N. İnan & K. Taslı pers.

comm. 2009). The benthic foraminifera indicate a Late Santonian-Maastrichtian date (Fig. 5.7d).

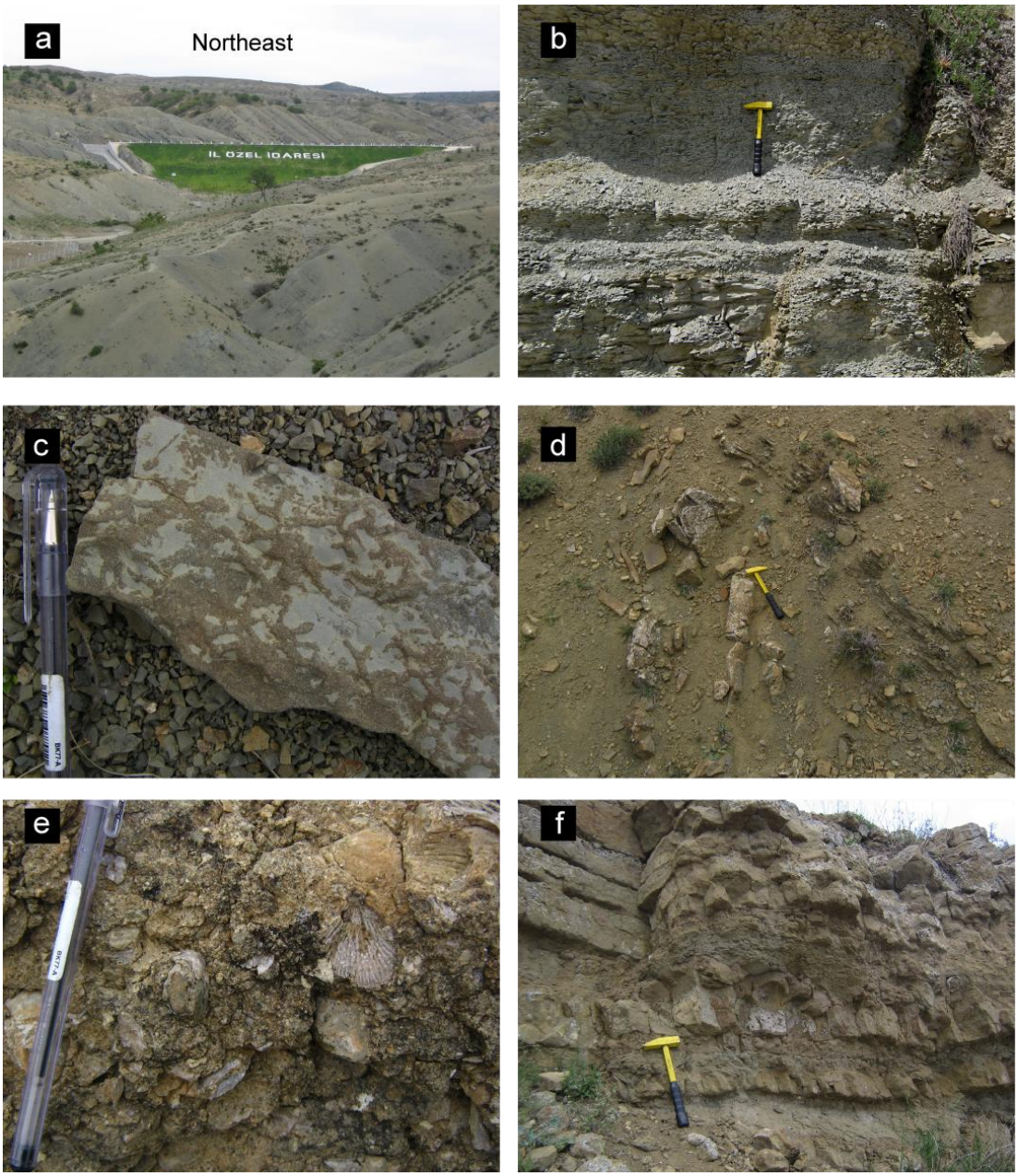

Figure 5.7 Selected field photographs of the Upper Cretaceous Haymana Formation: **(a)** field photograph, looking ~northeast, of siltstones and mudstones of lithofacies M13, **(b)** detail of lithofacies M13, showing thinly laminated siltstone, **(c)** burrowing in a siltstone of lithofaciesM2, **(d)** syn-sedimentary folding affecting sandstone turbidites of lithofacies M2, **(e)** bivalves in a conglomerate of lithofacies M3, **(f)** medium-bedded pebbly sandstone (lithofacies M3) in the north of the basin, near Beyobası (42555:91264).

Conglomerates are particularly extensive in the north of the mapping area to the north and west of Beyobası (Fig. Map). At this locality (42555:91264) conglomerates form matrix-supported beds up to ~4 m in thickness, locally forming packages up to ~9 m-thick. Clasts are moderately well sorted, sub-rounded and up to ~5 cm in size. They are composed of crystalline limestone, radiolarian chert, basalt, gabbro and serpentinite. These deposits probably represent reworked detritus from the crystalline limestone and ophiolitic mélange basin basement. Beds are generally massive; however, local grading from conglomerate at the base to pebbly sandstone at the top was observed, and well developed erosive bases are common. The conglomerates are generally intercalated with medium-bedded (0.2 to 0.3 m-thick) massive sandstone and sandy siltstone. Scattered cobbles of crystalline limestone basement were also observed.

One conglomerate bed exhibits clast imbrication; five clast measurements indicated a unidirectional flow to the southeast. Conglomerate beds thin upwards and grade into thinly-bedded marls and siltstones, which are unconformably overlain by Palaeocene marginal facies of the Kartal Formation. The observations of conglomerates throughout the Haymana Formation are suggestive of deposition from sub-aqueous debris flows (Johnson 1984). No palaeontological evidence was obtained at the Beyobası locality during this study; however, previous studies record a Maastrichtian date based on benthic foraminifera (Ünalan *et al.* 1976). On the basis of inferred depositional and lithological differences, Ünalan *et al.*(1976) considered these deposits to be distinct from the Haymana Formation to the south, and termed the sequence the Beyobası Formation (Fig. Previous strat.). However, based on deposition age, lithology and palaeocurrent data, the deposits in the northern Beyobası locality are probably proximal equivalents to the distal fine-grained material to the south near Haymana.

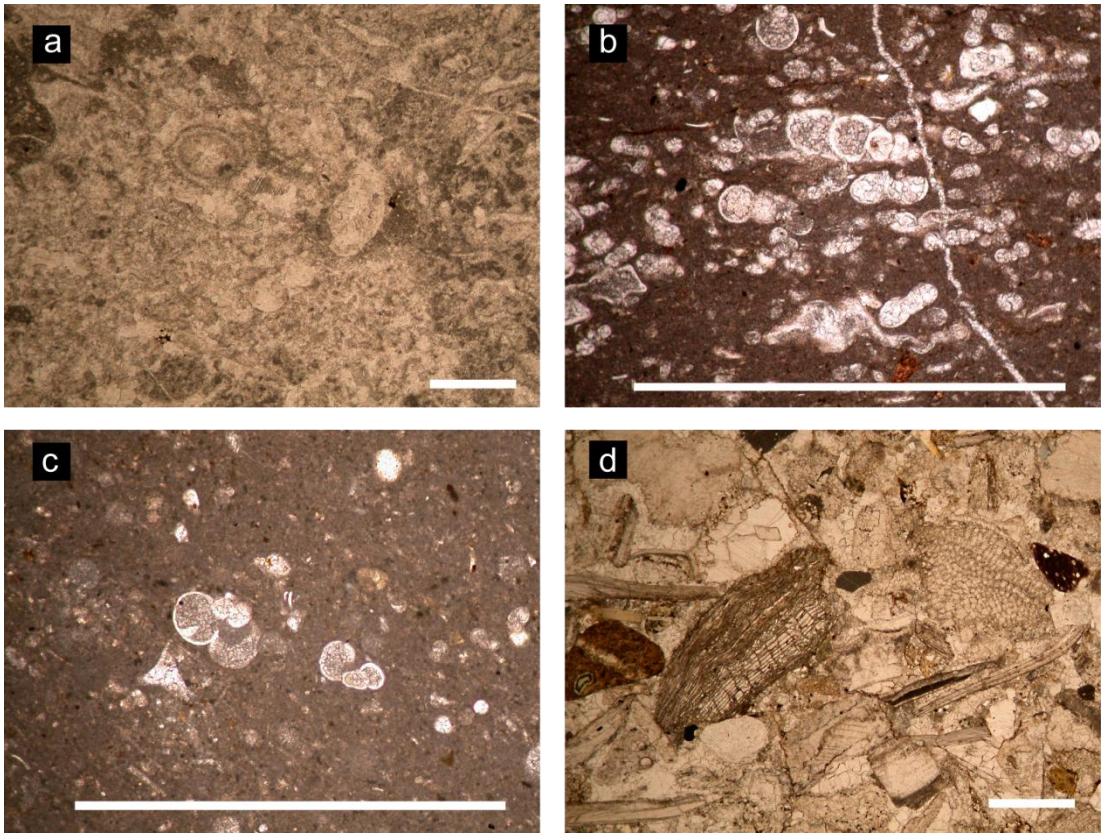

Figure 5.8 Photomicrographs (in plane-polarised light) of: **(a)** recrystallised Upper Jurassic-Lower Cretaceous basement limestone (sample HA3.5a); **(b)** Upper Cretaceous *Globotruncana*-bearing pelagic limestone of lithofacies CA1; **(c)** Upper Cretaceous Hedbergellid foraminifera in pelagic limestone of lithofacies CA1; **(d)** the Upper Cretaceous benthic foraminifera *Orbitoides* sp. in a bioclastic sandstone of lithofacies M3. Palaeontological data are from N. İnan & K. Taslı (pers. comm. 2009). All scale bars = 1 mm.

5.4.3.5 Interpretation of the Haymana Formation

The Haymana Formation records an abrupt deepening, then gradual shallowing upward sedimentary succession, from pelagic marls (lithofacies CA1) and siltstone laminations (lithofacies M13) to sandstone turbidites (lithofacies M2) and conglomeratic debris flows (lithofacies M2). This study is the first to discuss the deposits of the Haymana Formation in terms of lithofacies, and to present palaeocurrent data from south of Haymana. One previous study (Çetin *et al.* 1986) discussed palaeocurrents indicated by sandstone turbidites from north of Haymana, which indicated a flow from the northwest, in contrast to those measured during this

study, which generally show a flow to/from the northeast. New palaeontological evidence analysed during this study confirms previously published deposition dates as Late Cretaceous.

5.4.4 The Dizilitaşlar Formation: Lower Palaeocene (Danian)

The Haymana Formation grades vertically into the Dizilitaşlar Formation which is ~400 m thick and towards the Haymana-Polatlı Basin (Fig. Map) being absent at the basin margins. The formation comprises two lithofacies associated with resedimented carbonates. The most abundant lithofacies is reworked calcarenites (lithofacies RC5). Limestone blocks in a shaley matrix (lithofacies RC3) are found to the north of Haymana near Yeşilyurt (Figs. 5.3 and 5.9). The formation is also known as the Çaldağ Formation (Yüksel 1970; Ünalan *et al.* 1976; Meriç & Görür 1979; Sîrel *et al.* 1986), or the Karlıkdağ Formation (Gökçen 1976a; Gökçen 1978; Norman *et al.* 1980). However, to simplify cross-correlations between basins in central Anatolia (see Chapter 1) the Dizilitaşlar Formation is preferred as the name of the formation (Norman 1972; Norman 1973a).

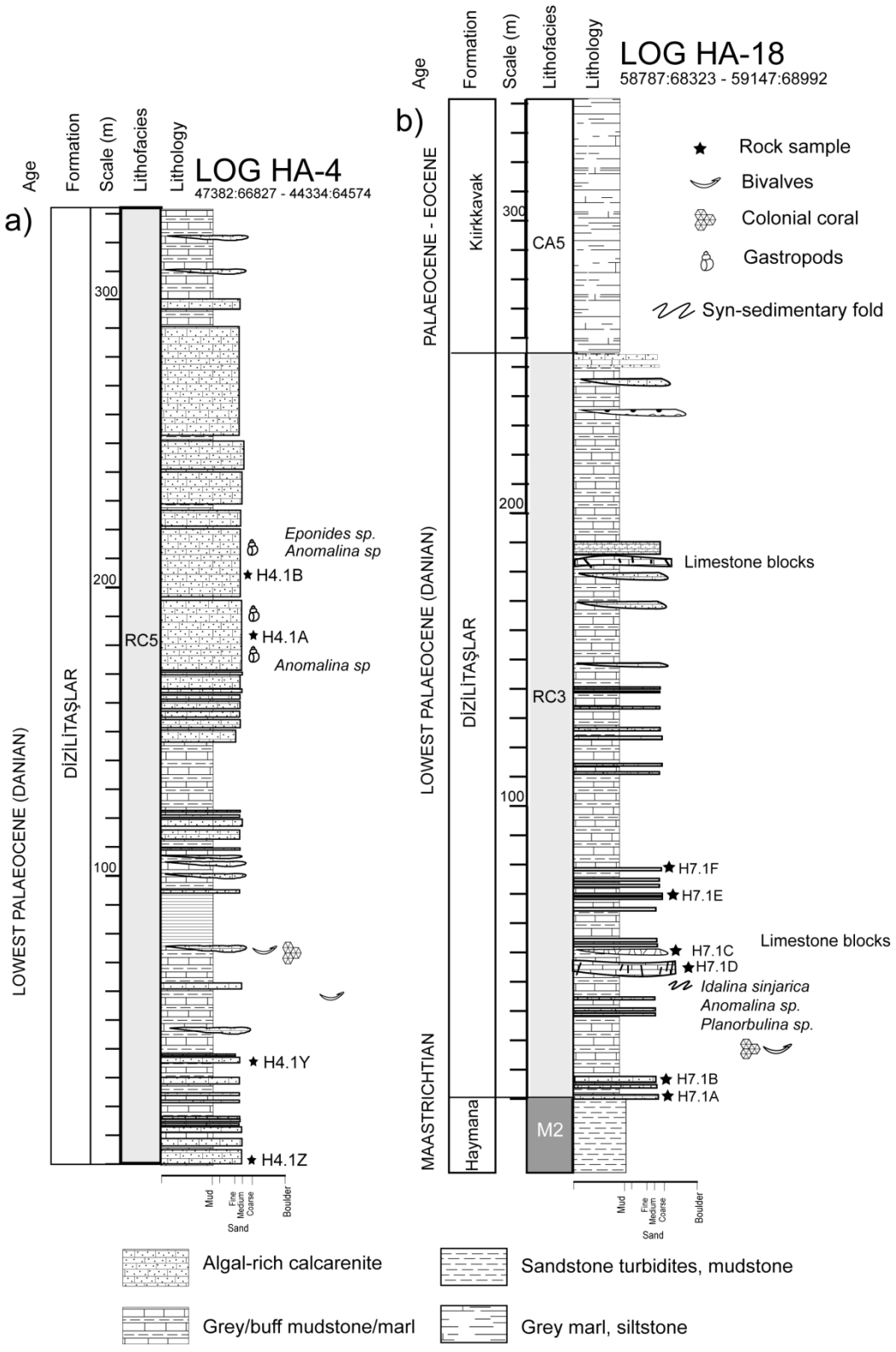

Figure 5.9 Measured stratigraphic logs of the Dizilitaşlar Formation, (a) Log HA-4, measured to the west of Haymana, shows bedded calcarenite of lithofacies RC5, (b) Log HA-18 measured to the north of Haymana shows collapsed limestone blocks of lithofacies RC3. See Fig. 5.3 for locations. Sedimentary data are from this study; fossil data are from N. İnan & K. Taslı (pers. comm. 2009).

5.4.4.1 Lithofacies RC5: reworked calcarenite

To the south of Haymana (Log HA-1) the appearance of the Dizilitaşlar Formation is marked by a series of lenticular outcrops of coarse- to medium-grained, moderately well-sorted calcarenitic deposits (lithofacies RC5). At the base of the formation, individual beds are intercalated with up to 200 m of grey mudstone. Beds are ~1.5 m-thick, orange weathered and feature bioclastic debris in a sparry calcite cement. Shelly material is frequently orientated parallel to bedding; no terrigenous material is evident. Up section, however, amalgamated pulses of calcarenitic deposits up to ~15 m-thick are typically seen. Beds 0.1 to 0.5 m-thick are interbedded with grey/yellow mudstone and marl, and frequently exhibit rubbly tops and patchy cementation (Fig.5.10a). Other sedimentary features include horizontal burrowing and rare bivalves (Fig. 5.10b, 5.10c). Deposition was probably by modified grainflow (e.g. Postma 1986).

The deposits are composed of abundant benthic foraminifera, calcareous algae and shelly fragments. Grains are abraded and rounded, well sorted and are mostly grain-supported with a micrite matrix where present; the cement is sparry calcite so that these rocks are classified as packstones or grainstones (Fig.5.11a). The following benthic foraminifera were identified in three samples*: Idalina sinjarica* Grimsdale, *Planorbulina* sp., *Laffitteina* sp. (Sample HA2.4e), *Anomalina* sp. (HA4.1a) and *Eponides* sp. (HA4.1a), which indicates an Early Palaeocene (Danian) age (N. İnan & K. Taslı pers. comm. 2009). This date confirms some previous studies in this area (Ünalan *et al.* 1976; Çetin *et al.* 1986) but contradicts the study of Meriç & Görür (1979) who reported Lower (Danian) to Middle Palaeocene (Thanetian) benthic foraminifera.

The top of the calcarentic sequence is followed by an abrupt change to brown mudstone and clastic horizons of pebblestone. Beds are laterally continuous for ~40 m and comprise moderately sorted clasts, which are composed of pelagic limestone, basalt and sandstone. Most beds grade from a base of clasts of 5 to 15 mm in size to

a coarse sandy top. Clast imbrication is locally present and one bed yielded a palaeocurrent direction from the west-northwest based on three measured clasts.

5.4.4.2 Lithofacies RC3: limestone blocks

A ~250 m-thick horizon of collapsed limestone blocks in a matrix of grey marl and mudstone is present to the north of Haymana, near Yeşilyurt (58787:68323) and near the Haymana-Polatlı Highway (59147:68992) (Log HA-18). The blocks are ~5 m-thick, exhibit brecciated margins and are composed of well lithified bioclastic limestone containing gryphea-type oyster shells and coral fragments (Fig.5.10d). No primary bedding was evident, suggesting extensive sediment reworking. Petrographic study revealed that the limestone is rich in benthic foraminifera, calcareous algae and colonial corals (Fig.5.11b). An Early Palaeocene (probably Danian) depositional date was inferred from the following benthic foraminifera: *Idalina sinjarica* Grimsdale, *Anomalina* sp. and *Planorbulina* sp. (sample HA7.1d) (N. İnan & K. Taslı pers. comm. 2009). Previous work (e.g. Meriç & Tansel 1987) give Danian dates for benthic and pelagic foraminifera in the mudstone matrix, but this study is the first to provide an age for the carbonate blocks.

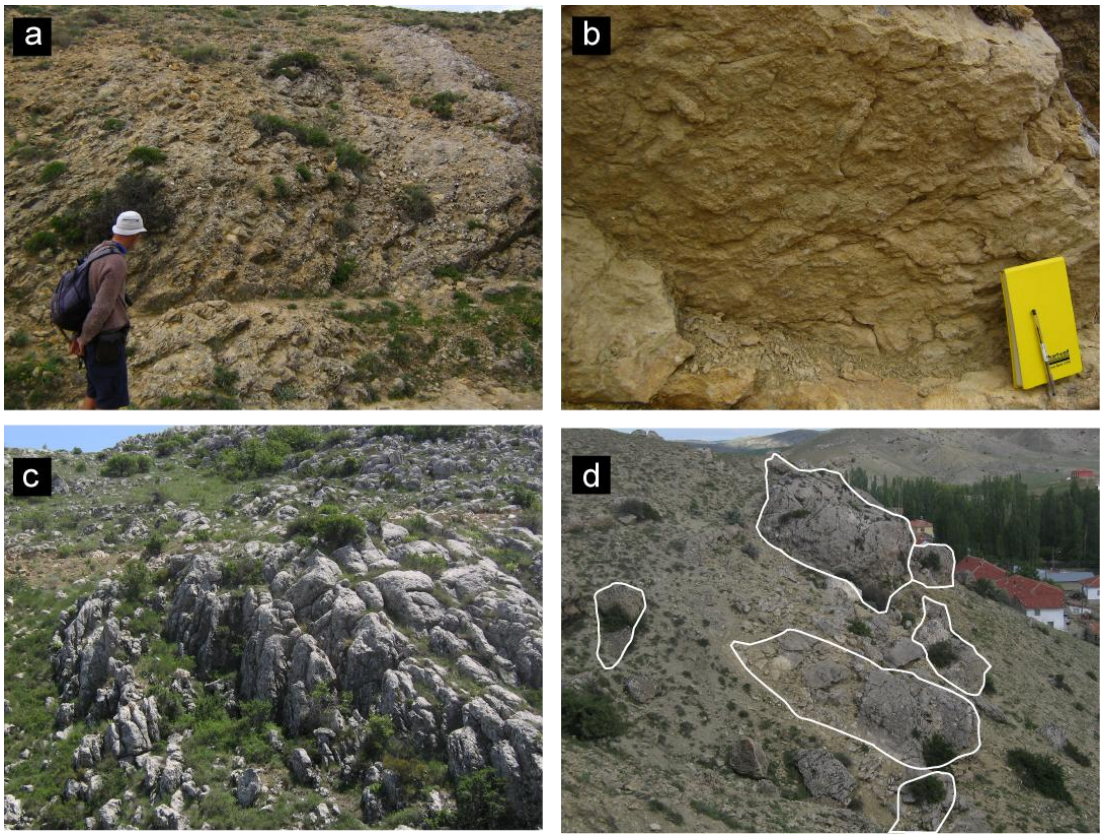

Figure 5.10 Selected photographs of the lowest Palaeocene (Danian) Dizilitaşlar Formation, **(a)** bedded, buff-coloured rubbly calcarenites of lithofacies RC5, **(b)** burrowing on base of calcarenite bed, **(c)** well-bedded grey calcarenites to the west of Haymana (see Log HA-4), **(d)** collapsed limestone blocks (outlined in white) of lithofacies RC3 near Yeşilyurt.

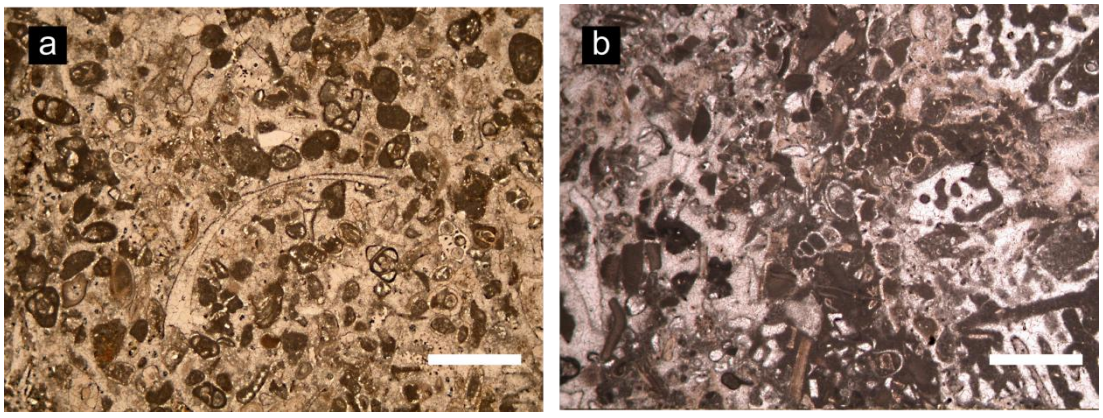

Figure 5.11 Representative photomicrographs (in plane-polarised light) of Palaeocene limestone of the Dizilitaşlar Formation: **(a)** a well-sorted bioclastic packstone (sample HA4.2e), rich in milliolid benthic foraminifera and calcareous algae, note the bivalve shell; **(b)** bioclastic grainstone containing coral, calcareous algae and benthic foraminifera. See text for discussion, fossils were identified and dated by N. İnan & K. Taslı (pers. comm. 2009). All scale bars = 1mm.

5.4.4.3 Interpretation of the Dizilitaşlar Formation

The Dizilitaşlar Formation features carbonate deposits which are characteristic of remobilised carbonates. Packstone grains include abraded benthic foraminifera, calcareous algae, coral fragments and shallow-marine macrofossils. The rounded and well sorted textures suggest sediment reworking. The presence of miliolid benthic foraminifera (*Idalina sinjarica*) suggests that the depositional environment was a low-energy shallow platform/lagoonal facies (Sartorio & Venturini 1988; Taheri *et al.* 2008). However, medium-bedded bioclastic limestones, often burrowed, with abraded, well sorted packstone grains are consistent with reworked deposits in a carbonate apron depositional setting (Flügel 2004). A possible interpretation of the Dizilitaşlar Formation is that it represents Lower Palaeocene (Danian) carbonate debris which was transported from a low-energy carbonate platform setting into a slope/upper slope setting. Sediment deposition along the flanks of carbonate platforms typically form wedge-shaped aprons parallel to the shelf/slope break (Mullins *et al.* 1984). Detached limestone blocks (lithofacies RC3) occur on the upper slope and bedded calcarenites on the lower slope (Mullins 1983) (Mullins & Cook 1986).

5.4.5 The Kartal Formation

The Dizilitaslar Formation grades laterally into marginal facies of the Kartal Formation, also referred to as the Saridere Formation (Gökçen 1976a; Gökçen 1976b; Norman *et al.* 1980). The Kartal Formation is unique to the Haymana-Polatlı Basin and is well exposed to the west, near Karahamzalı (23097:66698), to the south near Bahçecik (49864:47204) and to the north near Macun (43778:82643). The Kartal Formation is also used for similar non-marine facies in central Turkey (e.g. for Upper Cretaceous non-marine conglomerates at the eastern margin of the Tuz Gölü

Basin, see Chapter 4). However, its Palaeocene-aged deposits are unique to the Haymana-Polatlı Basin.

The formation lies unconformably on the Upper Cretaceous Haymana Formation in the north and on the Upper Cretaceous Asmaboğazı Formation in the west and south, and is unconformably overlain by the Palaeocene Kırkkavak Formation (see section 4.6). The Kartal Formation comprises red and grey sandstones, mudstones and conglomerates (lithofacies C2) and reaches a thickness of ~150 m in the west and south of the Haymana-Polatlı basin and ~800 m in the north. Its most striking feature is the development of nodular caliche horizons.

5.4.5.1 Lithofacies C2: calichified sandstone and conglomerate

At the base of the Kartal Formation, lenticular conglomeratic deposits ~1.5 m-thick are abundant. Beds contain poorly sorted, matrix-supported clasts up to 10 cm in size that display a range of angularities. Clasts are composed of radiolarian chert, black chert, basalt, limestone, phyllite, marble and gabbro. Beds are typically topped with lenses of rubbly limestone containing rare coral fragments. Up-section, lenses of red and grey fine- to medium-grained rubbly sandstone (Fig. 5.12a) are common and intercalate with red mudstone. Sandstone beds are typically featureless with the exception of "floating" limestone cobbles and abundant elongate and rounded nodular calcite concretions (Fig. 5.12b). Near the top of lithofacies C2, red marls and mudstones are abundant and intercalate with thinly-bedded (~0.4 m-thick) lenses of fine- to medium-grained red sandstone. Dating of the Kartal Formation is problematic because no fossil evidence was observed during this study; however, previous authors (Sîrel 1975; Ünalan *et al.* 1976) used marine benthic foraminifera and ostracods to date the formation as Lower Palaeocene.

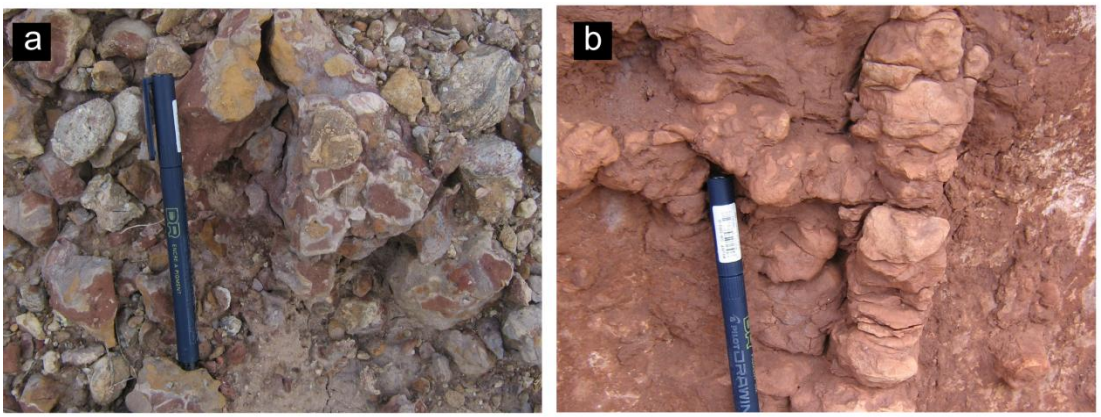

Figure 5.12 Details of the Palaeocene Kartal Formation: **(a)** rubbly red sandstone with caliche coating at the southern basin margin near Bahçecik, **(b)** well developed vertical nodule in red mudstone at the western basin margin near Karahamzalı.

5.4.5.2 Interpretation of the Kartal Formation

An interpretation of the depositional environment of this lithofacies is not straightforward. Caliche nodules frequently obscure primary depositional structures. However, given the lenticular shape of conglomerate and sandstone beds, the paucity of marine fossils and their red, oxidised colour, a mainly non-marine origin is likely. In addition, Koçyiğit (1991) noted the presence of plant debris in the Kartal formation in the Orhaniye Basin to the north and Sîrel (1975) recorded lacustrine limestone.

Comparable facies include a Devonian alluvial-deltaic plain in Alberta, Canada (Williams & Krause 1998). Caliche often forms in arid/semi-arid regions where evaporation exceeds precipitation, which is a probable palaeoenvironment during the deposition of the Kartal Formation. The sparse presence of benthic foraminifera (Ünalan *et al.* 1976; Sîrel *et al.* 1986) and ostracods suggests that parts of the Kartal Formation may have been partially submerged in shallow-marine conditions for a time. The key role played by the Kartal Formation was as a marginal equivalent to the fully marine Dizilitaşlar Formation, as inferred by (Ünalan *et al.* 1976).

5.4.6 The Kırkkavak Formation: Palaeocene-Lower Eocene

The Kırkkavak Formation was first named by Rigo de Righi & Cortesini (1959) and lies unconformably on the Kartal Formation. It features two lithofacies composed of patch reefs (lithofacies CA5) and gastropod-bearing coarse sandstone (lithofacies M17). Reef limestones are exposed at the western basin margin, east of Karahamzalı (25380:67285) (Log HA-5; Figs. 5.13 and 5.14) and southeast of Kargalı (43411:82165) (Fig. 5.3). They occur on an erosional surface which marks the top of the Lower Palaeocene Kartal formation. Lithofacies M17 is exposed in the north of the basin, west of Macun (Fig. 5.3).

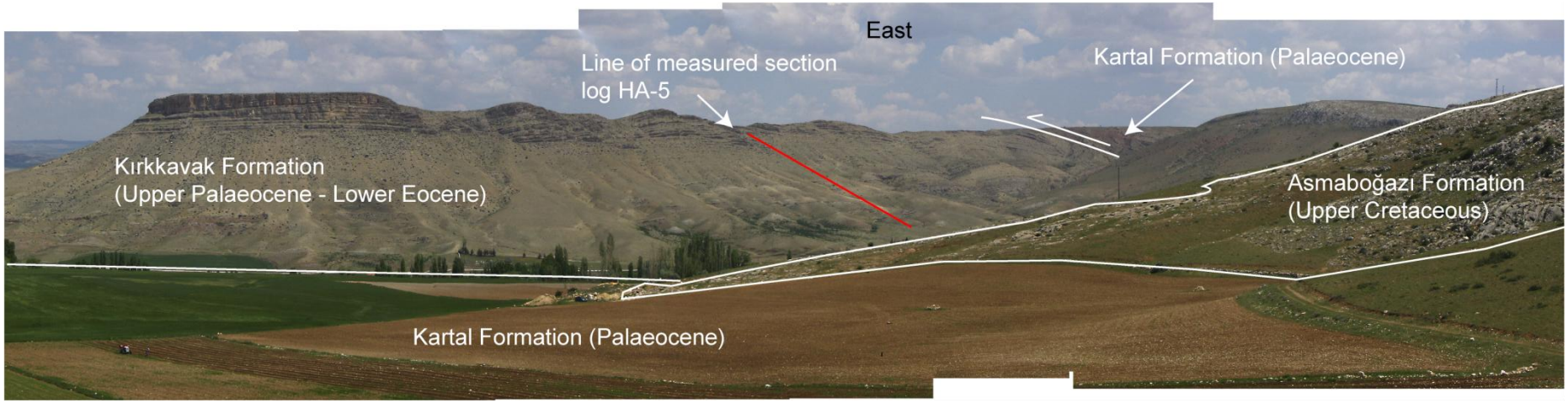

Figure 5.13 Photo-mosaic (looking east) of the sedimentary succession of the western basin margin (Karahamzalı). The Upper Cretaceous Asmaboğazı Formation (right) is unconformably overlain by red sandstone and mudstone which represents the Palaeocene Kartal Formation (foreground). Above an unconformity lies the Palaeocene – Eocene Kırkkavak Formation (background). The red line is the position of Log HA-5.

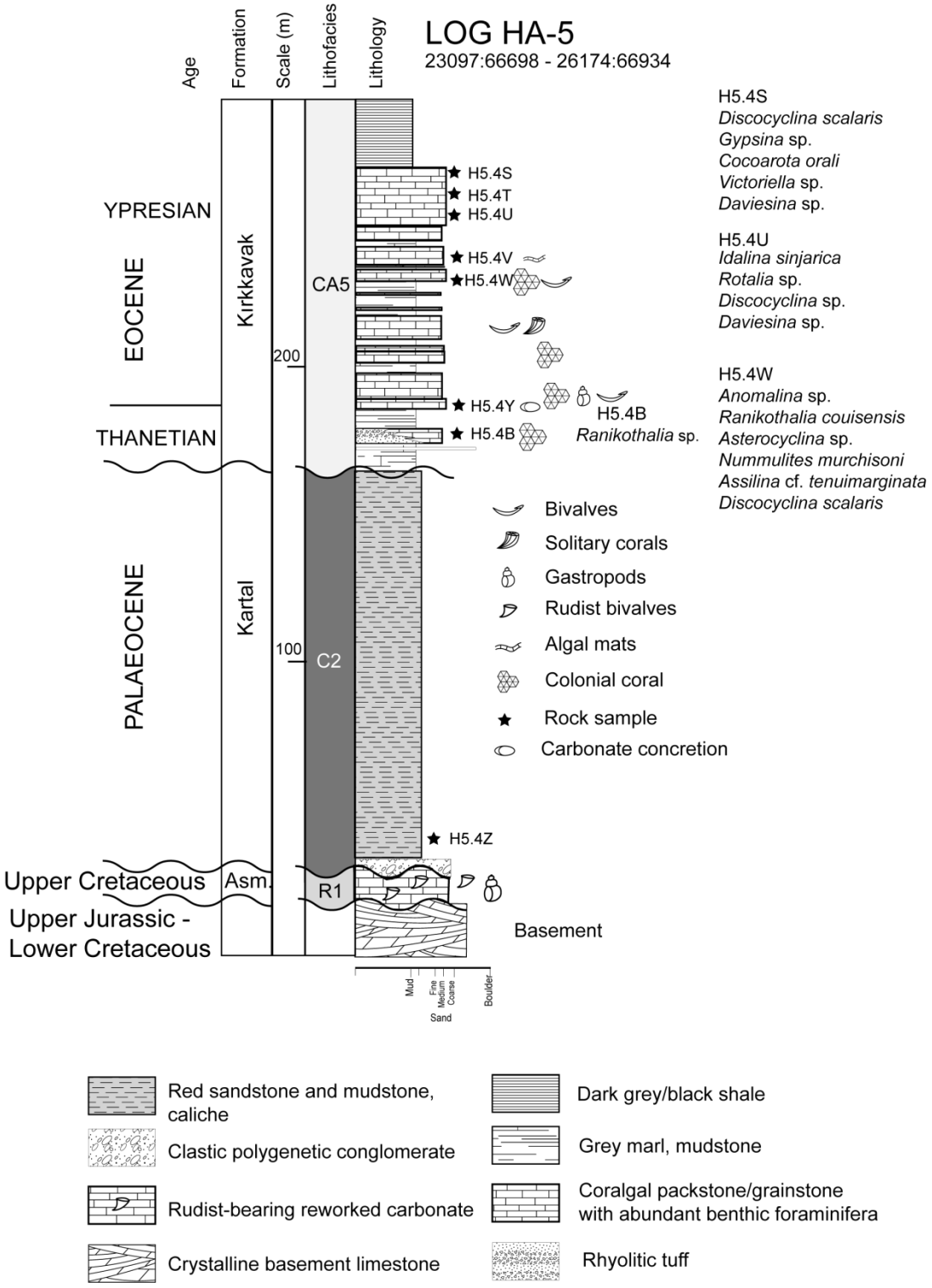

Figure 5.14 Measured log of the western basin margin near Karahamzalı showing the Palaeocene-Eocene reef limestone of the Kırkkavak Formation lying unconformably on the Palaeocene Kartal Formation; see Fig. 5.3 for location. Sedimentary data are from this study; fossil data are from N. İnan & K. Taslı (pers. comm. 2009).

5.4.6.1 Lithofacies CA5: reef limestone

At the Kargali locality (Fig.5.15a), deposition of the Kırkkavak Formation began with a 2 m-thick horizon of limestone rubble containing fragmented shelly material. Above comes a ~10 m-thick interval featuring lenses of bioclastic sandstone with mostly articulated, in situ bivalves (Fig.5.15b), gryphea-type oysters and solitary corals. This then passes into coarse sandstones containing fragmented shelly material. The sandstones then pass into a ~3 m-thick in situ bioherm constructed of oysters, oncolites, solitary corals (Fig.5.15c) and *Porites* coral (Figs.5.15d and 5.15e) that are typically encrusted in algae. The bioherm is capped by a 2 m-thick horizon of rubbly bioclastic limestone, which, in turn grades into grey mudstone.

The reef limestone to the east of Karahamzalı (25380:67285) (Log HA-5; Fig. 5.14) is ~200 m thick and best exposed in a section which spans the Palaeocene-Eocene boundary (Ünalan *et al.* (1976). The sequence begins with a ~3 m-thick deposit of rhyolitc tuff which grades horizontally into medium-bedded coarse sandstone. Above come grey marls with medium-bedded nodular sandy limestone containing reworked skeletal fragments including coral and benthic foraminifera. The sandy limestones pass upward into a ~20 m-thick succession of rubbly fine-grained limestone containing abundant pebbles of basalt, basement limestone and sandstone (Fig.5.15f). Above lie thinly-bedded limestones intercalated with ~5 m-thick horizons of grey mudstone. The limestones contain abundant well-preserved macrofossils including bivalves, solitary corals and algal encrusted *Porites* coral bindstone. These grade vertically into a ~40 m-thick sequence of medium-bedded grey/buff packstones rich in coral fragments, bivalves, benthic foraminifera and calcareous algae.

Ünalan *et al.* (1976) proposed a middle Palaeocene age on the basis of benthic foraminifera. In contrast, Sîrel (1975) indicated an Upper Palaeocene-Early Eocene age. In order to establish a deposition age for this section, four samples were selected for palaeontological study. At the base of the section (see Fig.5.14) sandy

coralgal limestone (sample HA5.4b) contains the benthic foraminifera *Ranikothalia* sp. indicating a latetst Palaeocene (Thanetian) age (N. İnan & K. Taslı pers. comm. 2009).

Up section, one sample (HA5.4w) (Fig. 5.16a) yielded benthic foraminifera *Anomalina* sp., *Ranikothalia couisensis* (d'Archiac), *Asterocyclina* sp., *Nummulites murchisoni* (Rütimeyer), *Assilina* cf. *tenuimarginata and Discocyclina scalaris* (Schlumberger).

Another sample (HA5.4u) yielded the benthic foraminifera *Idalina sinjarica* Grimsdale, *Rotalia* sp., *Discocyclina* sp. and *Daviesina* sp.

A further sample (HA5.4s) (Fig.5.16b) contained the benthic foraminifera *Discocyclina scalaris* (Schlumberger), *Gypsina* sp. ,*Cocoarota orali* İnan, *Victoriella* sp. and *Daviesina* sp. The presence of the above benthic foraminifera indicates an earliest Eocene (Ypresian) age (N. İnan & K. Taslı pers. comm. 2009), which confirms the age given by Sîrel (1975).

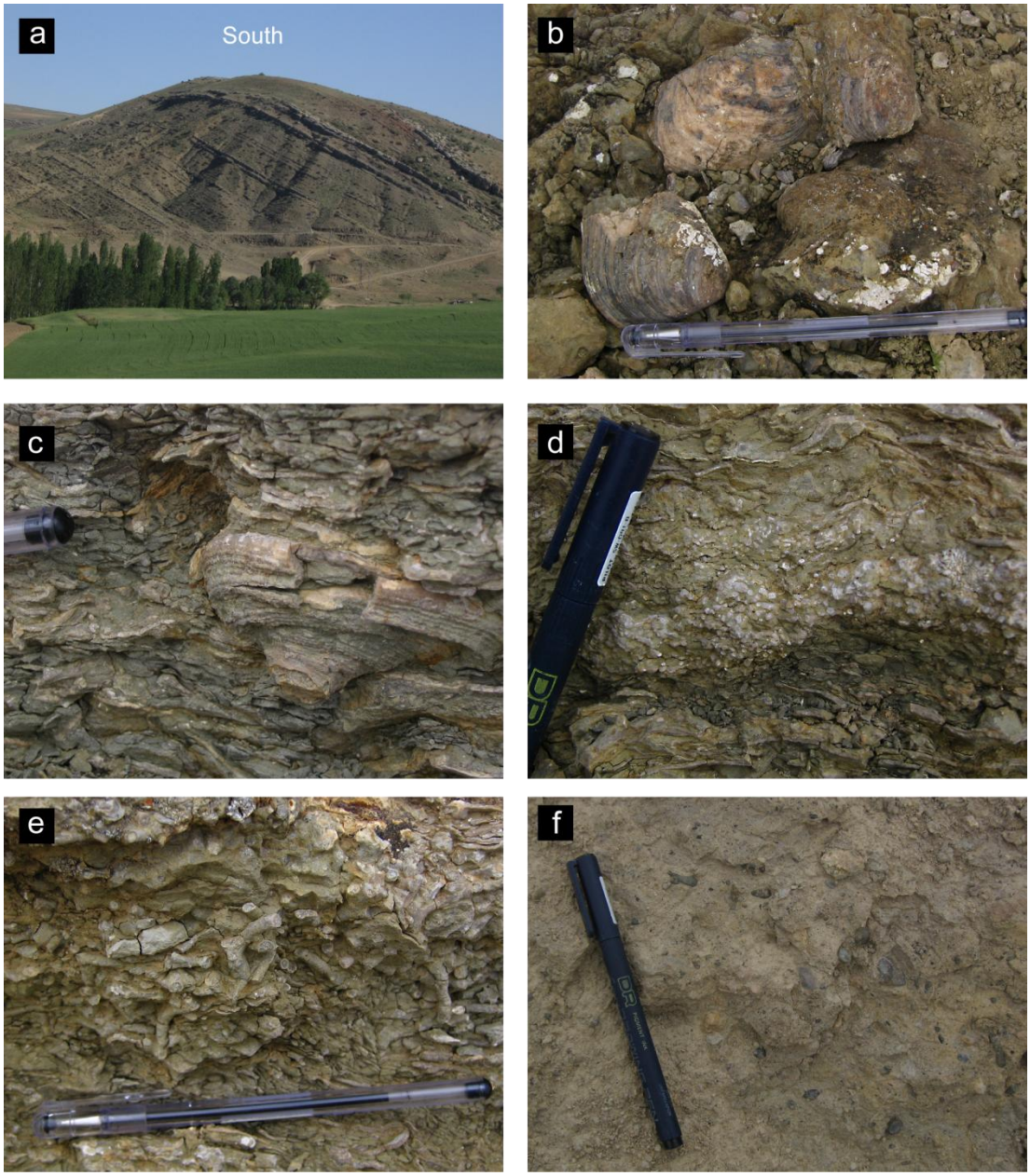

Figure 5.15 Representative field photographs of lithofacies CA5 of the Palaeocene-Eocene Kirkkavak Formation: **(a)** view, looking ~south, of a reef bioherm, **(b)** detail of bivalves, **(c)** solitary coral, preserved in life position and encrusted in algal mats (bindstone), **(d)** encrusted colonial coral, **(e)** detail of coral, **(f)** rubbly fine-grained limestone containing abundant pebbles of basalt, basement limestone and sandstone.

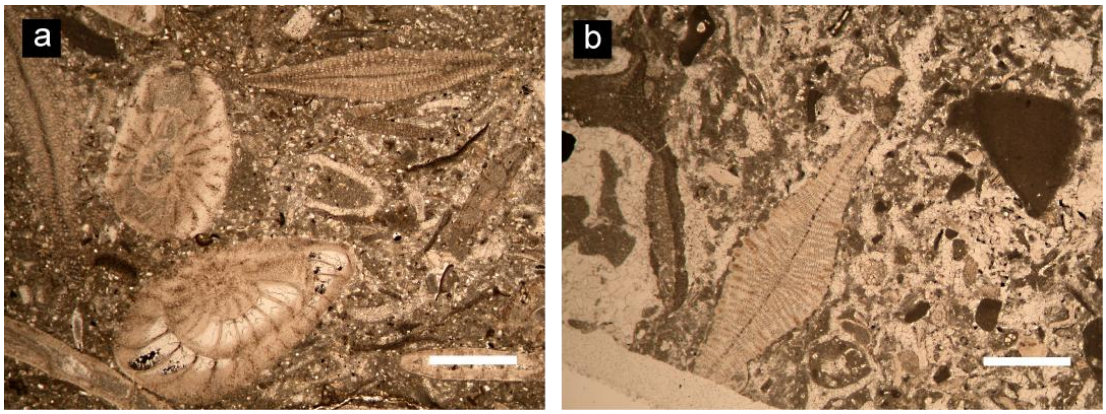

Figure 5.16 Photomicrographs of Lower Eocene bioclastic packstones from lithofacies CA5 of the Kırkkavak Formation, **(a)** sample HA5.4w, **(b)** sample HA5.4s, both images in plane-polarised light, scale bars= 1 mm.

5.4.6.2 Lithofacies M17: gastropod-bearing sandstone

In the north of the study area, to the SW of Macun (Figs. 5.3 and 5.17) another well-exposed lithofacies (M17) of the Kırkkavak Formation is notable for pebbly sandstones with vast gastropods. Four sections measured in this area (Fig. 5.18) provide new insights into the development of the Kırkkavak Formation.

The Kırkkavak Formation in this area is up to ~500 m-thick and lies unconformably on calichified mudstones of the Palaeocene Kartal Formation (Fig.5.19a). The dominant lithology of lithofacies M17 is medium-bedded, medium- to coarse-grained pebbly sandstones interbedded with grey/yellow mudstone. The sandstone beds are generally lenticular, up to ~3 m in thickness and frequently graded, both normally and inversely. Normally graded beds exhibit erosive bases containing 0.4 cm clasts of black chert, radiolarian chert and basement crystalline limestone. Discrete horizons of rounded black chert granules are commonly observed (Fig.5.19b). Inversely graded beds typically comprise two or three depositional packages consisting of pebbly sand at the base, capped by lenticular pebble- to cobble-sized conglomerates (Figs.5.19c and 5.19d). Other sedimentary features

include vertical burrowing, cross-stratification and calcareous concretions. Imbricated pebbles (n=8) indicate a palaeoflow generally from east to west.

Throughout the sections described above, gastropods, bivalves and oyster shells are abundant. Gastropods are principally of two types: the Ampullinid gastropod *Globularia* (Swainson 1840) (Fig.5.19e) and the Cerithid gastropod *Batillaria diacanthina* Cossmann 1899 (Fig.5.19f). Both types occur in warm, shallow marine or brackish watersas present in the Neotethyan realm during the Late Palaeocene to Oligocene time (Okan & Hoşgör 2008).

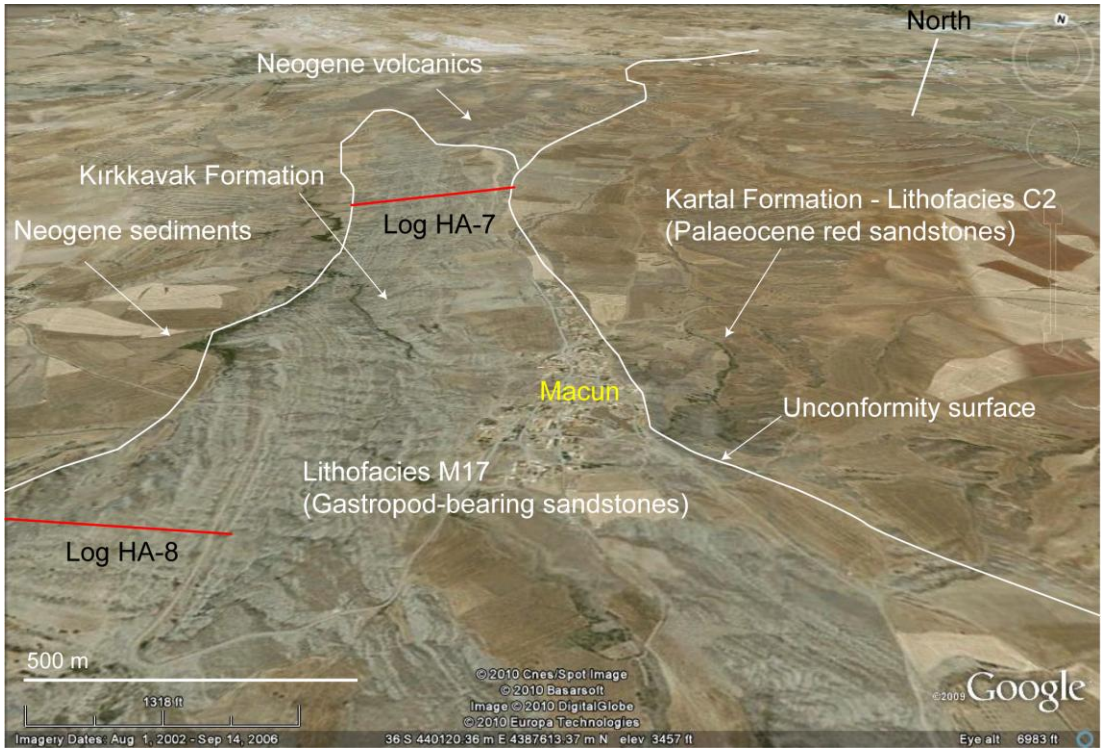

Figure 5.17 Satellite image looking ~north at the Macun area. Grey, bedded sandstones (lithofacies M17) of the Palaeocene-Eocene Kırkkavak Formation (centre) are overlying the red mudstones of the Palaeocene Kartal Formation (right). Red lines mark the positions of measured Log HA-7 (top) and Log HA-8 (left).

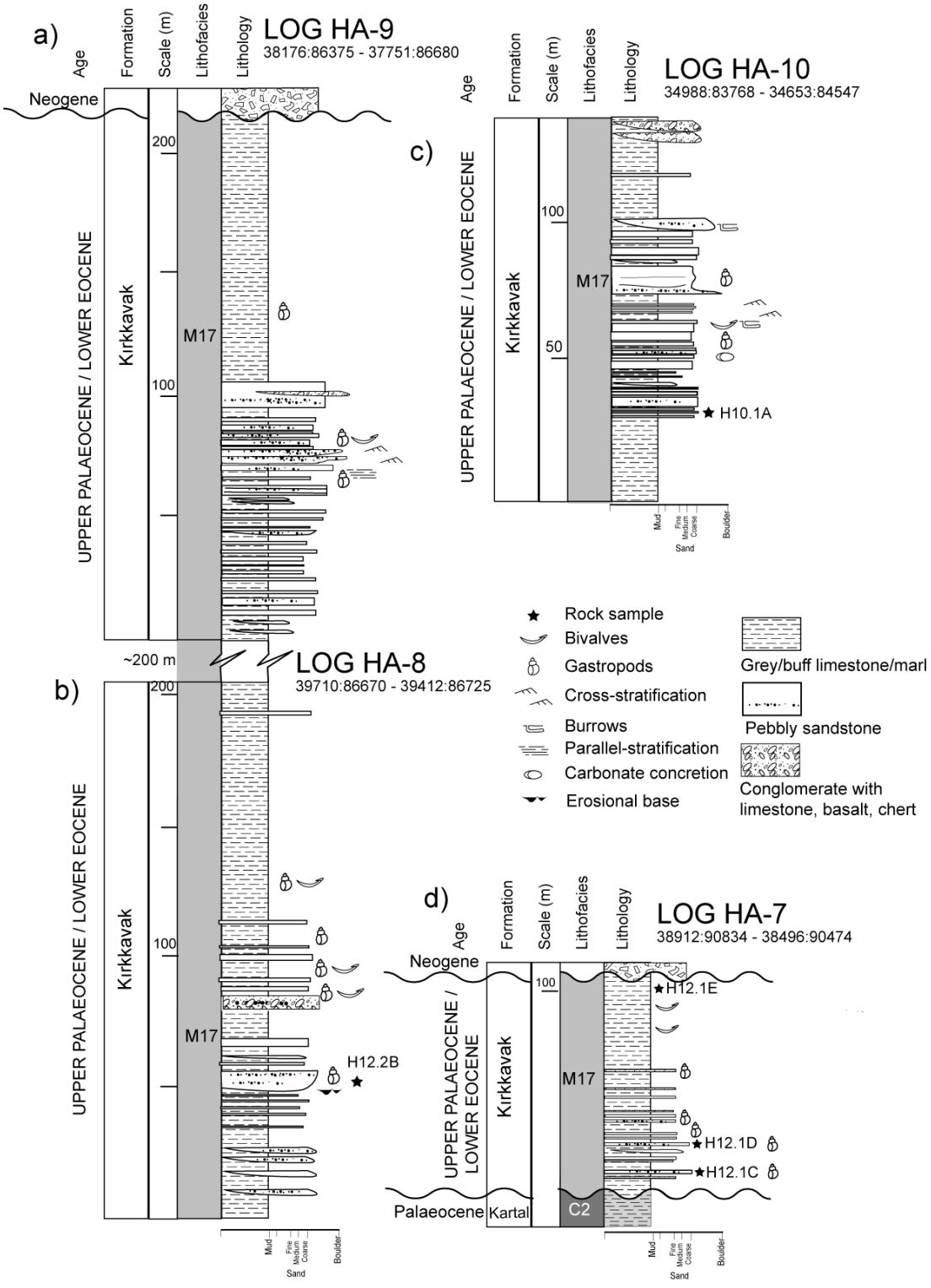

Figure 5.18 Measured logs in the gastropod-bearing pebbly sandstones (lithofacies M17) of the Kırkkavak Formation. Note the thickening and coarsening-upward bed-geometry in Log HA-8 and HA-9 and the unconformity at the base of Log HA-7. All sedimentary data were collected during this study.

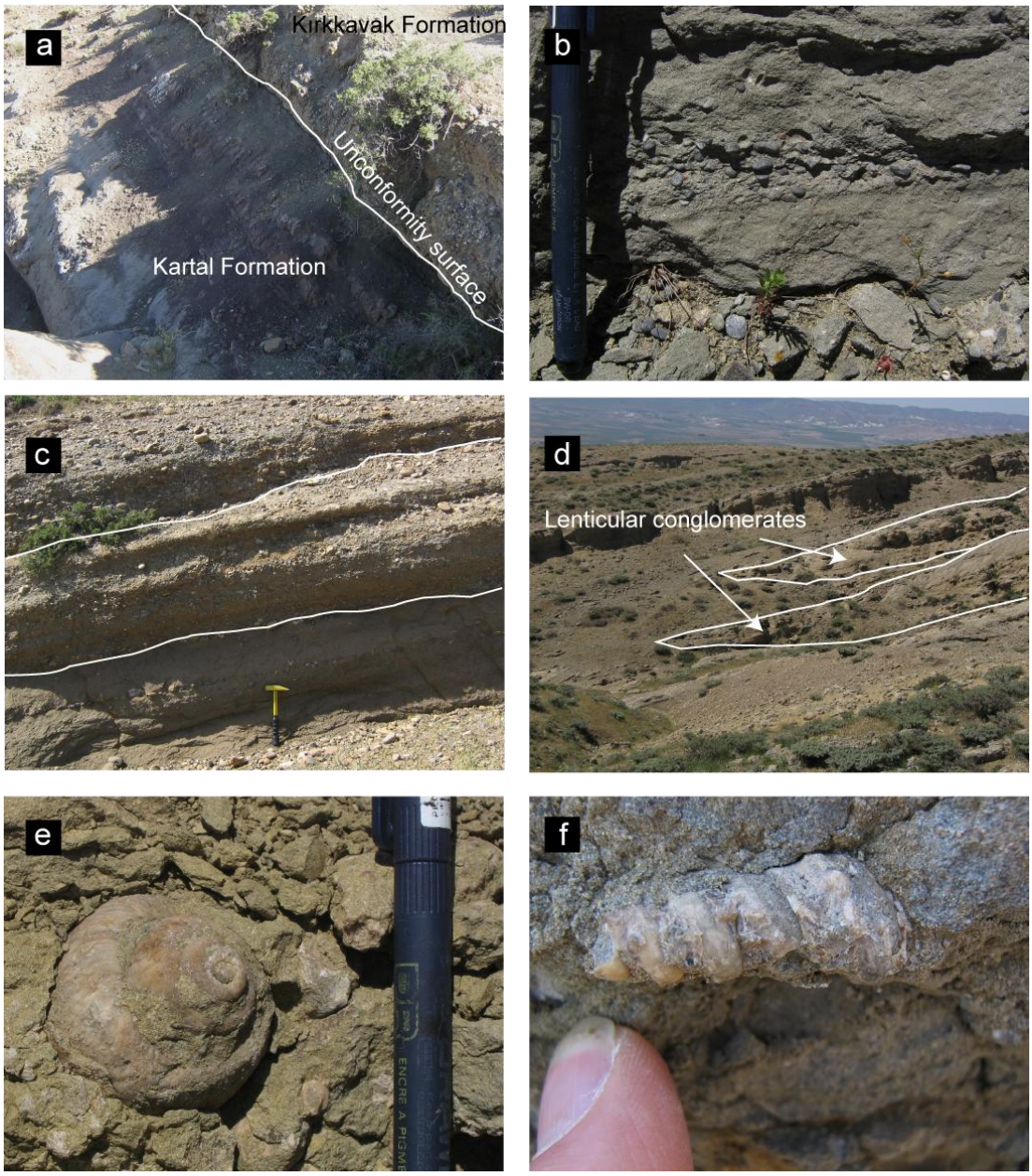

Figure 5.19 Field photographs of gastropod-bearing sandstones (lithofacies M17) of the Kırkkavak Formation: **(a)** unconformity surface representing the upper surface of the underlying Palaeocene Kartal Formation, **(b)** horizons of black chert granules, **(c)** an inversely graded bed consisting of sandstone at the base grading into conglomerates with pebble and cobble-sized clasts, **(d)** lenticular deposits of conglomerate, **(e)** an Ampullinid gastropod *Globularia* (Swainson 1840), **(f)** a Cerithid gastropod *Batillaria diacanthina* Cossmann 1899.

5.4.6.3 Interpretation of the Kırkkavak Formation

The Kırkkavak Formation has been the subject of numerous studies (Erünal 1942; Yüksel 1970; Sîrel 1975; Ünalan *et al.* 1976; Sîrel *et al.* 1986; Okan & Hoşgör 2008). This thesis adds to the existing data with new observations of large benthic foraminifera, detailed lithofacies descriptions, and the observation of an erosional surface at the base of the formation.

The general depositional setting of reef limestone (lithofacies CA5) is a shallow marine, marginal shelf-type environment following a transgressive event. There are, however, a variety of reef settings represented including reef crest bindstone and packstone representing fore-reef detritus. The control of the transgression could be basin subsidence or global sea level rise associated with the Palaeocene-Eocene thermal maximum (Kennett & Stott 1991). Onset of carbonate platform development occurred in much of the Tethyan realm at this time (Scheibner & Speijer 2008), therefore, a climatic control seems likely. Comparable facies are found, for example, in the Palaeocene - Eocene Lakadong limestone, NE India (Matsumaru & Jauhri 2003; Tewari *et al.* 2010).

Ünalan *et al.* (1976) termed lithofacies M17 as the Beldede Formation, and, based on Nummulitic benthic foraminifera, assigned a Middle Eocene age. However, this lithofacies grades laterally into the Palaeocene-Lower Eocene reef limestones of lithofacies CA5 and is interpreted here to be contemporaneous. Furthermore, no Nummulitic benthic foraminifera were observed during this study.

Ünalan *et al.* (1976) noted the presence of channelised sandstones and conglomerates and interpreted these deposits as fluvial deposits, which seems unlikely given the abundance of marine gastropods and bivalves. Instead, the following evidence from the gastropod-bearing sandstones to the north of the basin suggests a deposition in a clastic-dominated marine deltaic setting. First, lenticular pebbly sandstone beds coarsen and thicken upwards, consistent with a prograding delta-front setting (Walker 1978; Nichols 1999; Tucker 2001). Second, many

sandstone beds exhibit a horizontally stratified gravelly top, exhibiting both normal and inverse grading. This suggests deposition by debris flow; the amalgamated conglomerates could represent channel cut and fill events (Rasmussen 2000). Third, sedimentary features, including cross stratification, parallel lamination and burrowing are suggestive of a pro-delta depositional environment (Stingl 1994; Deynoux *et al.* 2005; Gani & Bhattacharya 2007). Palaeocurrent indicators imply that palaeoflow was from southeast to northwest.

5.4.7 The Yoncalı Formation: Lower-Middle Eocene

The Yoncalı Formation is mainly exposed to the northwest and southeast of the basin (Fig.5.3) and conformably overlies the Upper Palaeocene-Lower Eocene Kırkkavak Formation. It is represented by three lithofacies: 1) sheet-like sand and mud couplets (lithofacies M14); 2) lenticular sand-mud couplets (lithofacies M18); 3) clastic conglomerates (lithofacies M3). The formation is also termed the Eskipolatlı Formation in the north of the basin (Ünalan *et al.* 1976; Görür *et al.* 1984) and the Yamak Formation in the south (Gökçen & Kelling 1983; Çiner *et al.* 1996a). However, lithologies, age and depositional settings are similar making a single formation name preferable. In order to unify formation names throughout the central Anatolian basins, this study assigns the formation to the Yoncalı Formation which has been studied elsewhere in central Anatolia (e.g. Erdoğan *et al.* 1996; Kaymakcı *et al.* 2009).

Four stratigraphic logs of the Yoncalı Formation were measured: Log HA-11 south of Eskipolatlı (Fig. 5.21.1); Log HA-12, east of Eskipolatli (Fig. 5.20.b); Log HA-13 at Yamak (Fig. 5.21.b) and; Log HA-14 north of Haymana (Fig. 5.20.b). The thickness of the Yoncalı Formation is up to ~720 m, marginally more than the maximum thickness of 567 m given by Ünalan *et al.* (1976).

5.4.7.1 Lithofacies M14: sheet-like sand-mud couplets

The characteristic and most abundant lithofacies of the Yoncalı formation is represented by sand-mud couplets (lithofacies M14). Sandstone horizons are typically thinly- to medium-bedded sheet-like deposits which exhibit sharp bases and gradational tops (Fig. 5.22a). Sedimentary features include horizontal burrowing (Fig. 5.22c), parallel laminations, shale rip-up clasts, current ripple marks, subtle normal grading and load casts. These structures are consistent with T_b (plane parallel laminae), T_c (wavy ripples), T_d (upper parallel laminae) and T_e (graded muddy tops) deposits (Fig. 5.22b) of the classic Bouma (1962) turbidite model.

Sandstone is medium-grained and composed of very well-sorted grains containing abundant lithoclasts. Sandstones are interbedded with thick packages of grey shale, marl and rare thinly-bedded siltstone, reaching up to ~300 m-thick, which constitute ~90% of this lithofacies.

5.4.7.2 Lithofacies M18: lenticular sand-mud couplets

Another set of sand-mud couplets exhibit different sedimentary structures and bounding surfaces (lithofacies M18). Sandstone beds crop out to the south of Eskipolatlı (Log HA-11) (Fig. 5.21a) and at Yamak (Log HA13) (Fig. 5.21b) and are characterised by a lenticular shape and are laterally continuous for ~10 to ~40 m. Bed bounding surfaces are frequently irregular and erosive, graded bases are well developed (Fig. 5.22d) and exhibit T_a (lower, pebbly erosive bases) deposits (Bouma 1962). Other features include horizons of well-sorted, sub-rounded limestone and black chert pebbles. The sandy deposits are usually interbedded with deformed marl and mudstone.

5.4.7.3 Lithofacies M3: clastic conglomerates

Lenticular sandstone deposits of lithofacies M14 are commonly associated with the other lithofacies present in the Yoncalı Formation, which are lenticular conglomerate beds (Figs. 5.22e and 5.22f). They are abundant in Log HA-14 (Fig. 5.20b) and display a range of bed thickness and textures. Bed thicknesses range from 1 to 5 m; amalgamated depositions are common and many beds grade normally to a pebblestone or coarse sandy top. Textures range from matrix-supported to clast-supported. Clasts are generally rounded and range from pebble to boulder size and consist of red radiolarian cherts, crystalline limestone, basalt and gabbro. Clast size generally decreases towards channel margins.

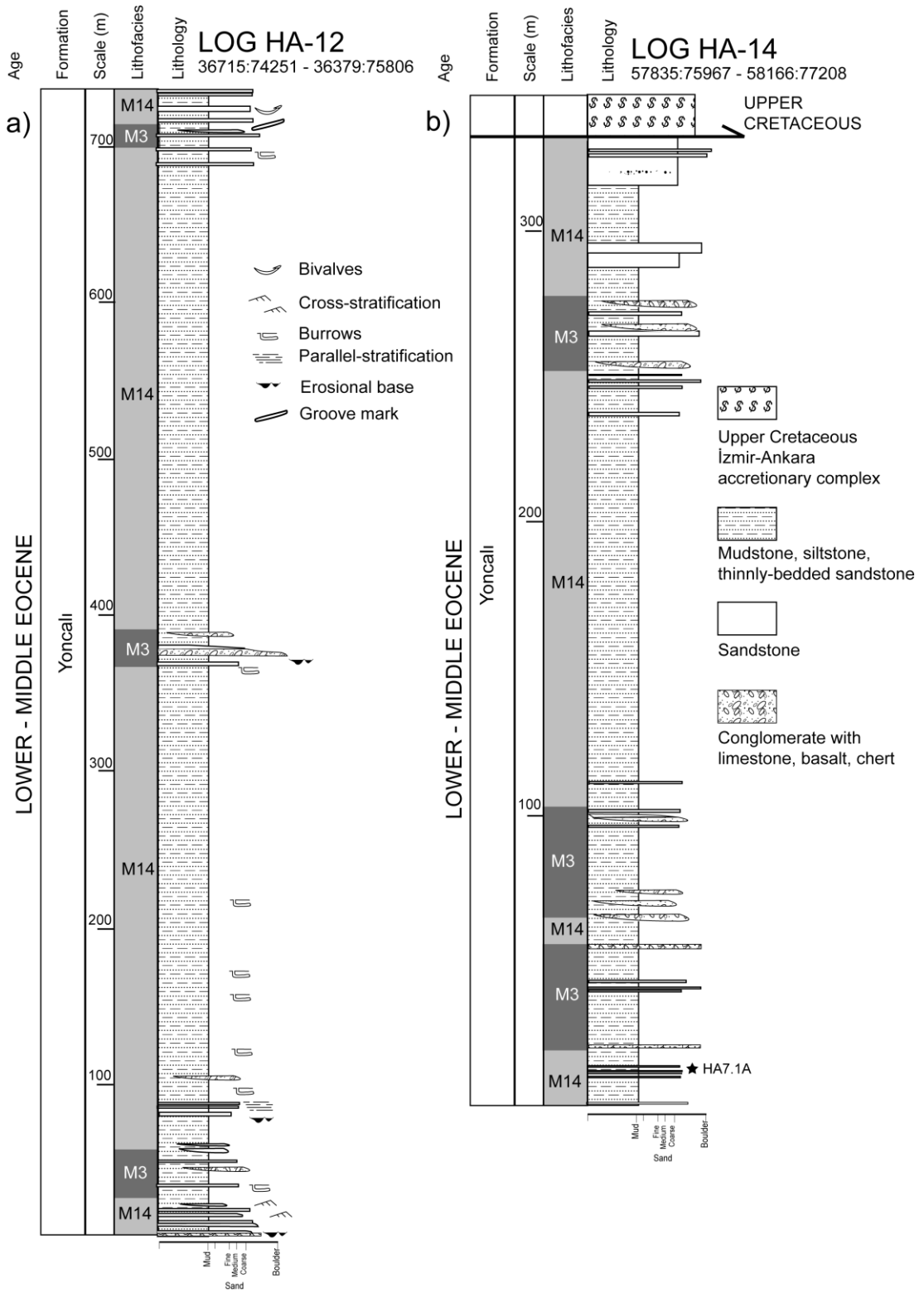

Figure 5.20 Measured stratigraphic logs: **(a)** to the east of Eskipolatlı and, **(b)** to the north of Haymana through the Lower-Middle Eocene Yoncalı Formation. These logs mostly comprise the sheet-like turbidites and mudstone of lithofacies M14. All sedimentary data are from this study.

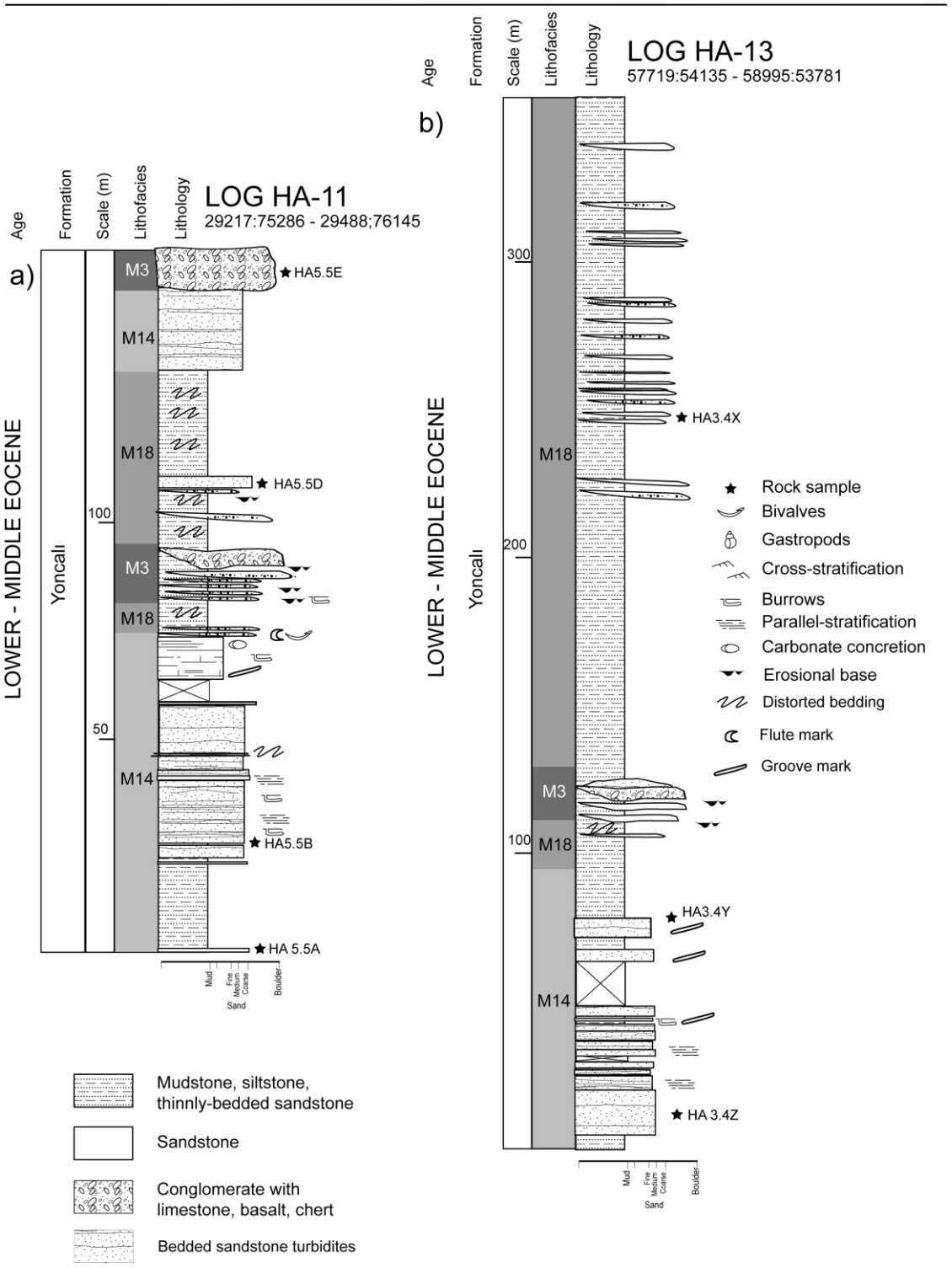

Figure 5.21 Measured stratigraphic logs: **(a)** to the south of Eskipolatlı, **(b)** at Yamak, through the Lower-Middle Eocene Yoncalı Formation. These logs focus on the lenticular sandstone beds of lithofacies M18. All sedimentary data are from this study.

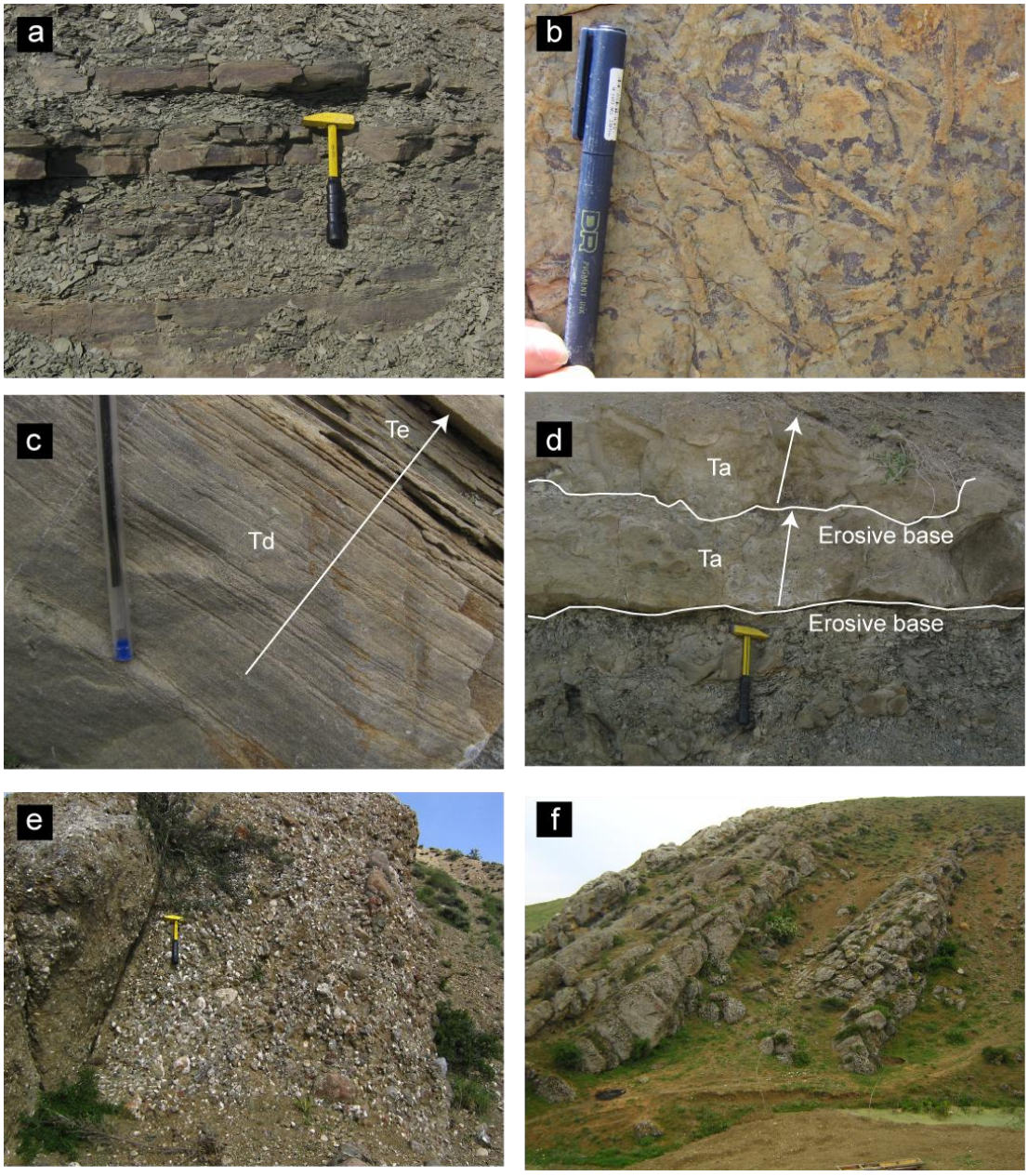

Figure 5.22 Selected field photographs of the Middle Eocene Yoncalı Formation,: **(a)** thinly- to medium-bedded sheet-like sandy turbidites of lithofacies M14, **(b)** burrowing at the base of a turbidite, **(c)** upper parallel laminae (Td) and graded muddy tops in lithofacies M14 (Te), **(d)** erosive bases (Ta) in lenticular sandy beds of lithofacies M18, **(e)** coarse conglomerates (lithofacies M3) to the north of Haymana, **(f)** lenticular conglomerate channels at Yamak (lithofacies M3).

5.4.7.4 Interpretation of the Yoncalı Formation

Previous authors (e.g. Ünalan *et al.* 1976; Görür *et al.* 1984) interpreted the Yoncalı Formation as the result of shallow to deep-marine "flysch" sedimentation by turbidity currents and used large benthic foraminifera to date the formation as Middle Eocene. Fractured Nummulitid benthic foraminifera were observed during fieldwork during this study which confirms this age.

The sand-mud couplets of lithofacies M14 are best interpreted as overbank deposits that occur when a confined turbiditic current spreads laterally (Mutti & Normark 1987). Similar facies were described in a Late Miocene forearc basin in Japan (Saito & Ito 2002). Çiner *et al.*(1996a) noted the presence of overbank turbidites in the Yamak area; however, this study extends this interpretation to include deposits in the northwest of the Haymana-Polatlı Basin.

Lenticular sandstones of lithofacies M18 are closely associated with conglomerates of lithofacies M3 and are best interpreted as channel-fill deposits from turbidity currents. Similarly, clastic conglomerates of lithofacies M3 are probably debris flow channel-fill deposits which cut into massive grey mudstones. Channels are typically ~2 m-thick and consist of basal conglomerate which grades vertically and laterally into bedded sandstone. An erosional surface marks the channel base and the centre of the channel contains several internal erosional surfaces. Fig.5.23 displays a channel to the south of Eskipolatlı which exemplifies these features.

New palaeocurrent data comprise ten measurements from flute and groove casts on sandstone beds and three imbricated clasts in the south (Yamak) flute and grove clasts indicate a palaeoflow from east-northeast to west-southwest; imbricated clasts do not show a consistent direction. These results are in agreement with those of Çiner *et al.*(1996a). In addition, twenty-one measurements were recorded from imbricated clasts in conglomerate beds in the northern (Eskipolatlı) area that indicate palaeoflow generally from east to west.

The general setting of the Yoncalı Formation has previously been described as deep marine based on the presence of pelagic microfossils in grey mudstones near Yamak (Gökçen & Kelling 1983). In addition, sandstone and conglomerate deposits are interpreted as a sand-rich submarine fan-complex (e.g. Çiner *et al.* 1996a). A lack of three-dimensional exposure hampers further interpretation of these lithofacies; however, new sedimentary data collected during this study confirm previous interpretations.

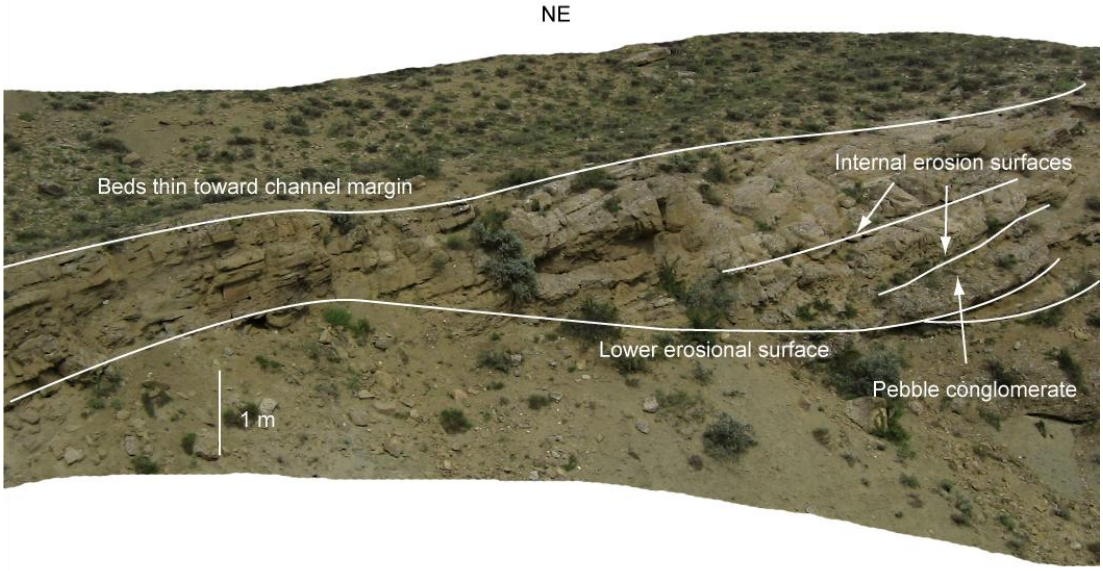

Fig.5.23 Field photograph (looking ~northeast) of a channel in the Middle Eocene Yoncalı Formation to the south of Eskipolatlı. Note the lower erosional surfaces and sandstone beds thinning toward the channel margin.

5.4.8 The Çayraz Formation: Lower-Middle Eocene

The Çayraz Formation is exposed ~5 km to the north of Haymana (Fig. 5.3) and represents the youngest sediments included in this study. The formation overlies the Kırkkavak Formation and comprises marine carbonate deposits, containing abundant large benthic foraminifera, which represent lithofacies CA7. Based on

evidence from three new stratigraphic logs measured during this study (Fig. 5.24), lithofacies CA7 features lenticular beds of sandy limestone alternating with grey/buff calcareous mudstone. Sandy limestone deposits are ~0.5 to ~7 m thick and are laterally continuous for up to ~300 m (Fig.5.25). Most deposits grade upwards from calcareous mudstone containing sparse benthic foraminifera, which is then overlain by well-stratified bioclastic sandy packstone/grainstone beds up to ~0.4 m in thickness with sharp bases and tops (Fig.5.26a). Large benthic foraminifera are commonly orientated parallel to bedding. The well stratified beds, in turn, pass upwards into grey rubbly limestone (Fig.5.26b) which is often capped by disorganised rubbly conglomerate composed of reworked clasts of bioclastic sandy limestone and rare bivalve shells. Beds thin towards the southeast and are replaced by thick (up to ~300 m) packages of grey/yellow calcareous mudstone (Fig. 5.24).

Two samples of sandy packstone yielded the following large benthic foraminifera: *Discocyclina* sp., *Nummulites atacicus* Leymerie, *Alveolina* cf. *decipiens*, *Gypsina marianensis* Hanzawa, *Asterigerina rotula* (Kaufmann), *Nummulites globulus* Leymerie, *Alveolina* cf. *pisella* , *Assilina* cf. *placentula* and *Ranikothalia* sp., *Orbitolites* sp., *Lockhartia* sp. and *Lacazina* sp. (Fig.5.26). This assemblage suggests a Lower Eocene (Ypresian) deposition (N. İnan & K. Taslı pers. comm. 2009) which is in contrast to previous studies (e.g. Ünalan *et al.* 1976) that suggested a Middle Eocene (Lutetian) age.

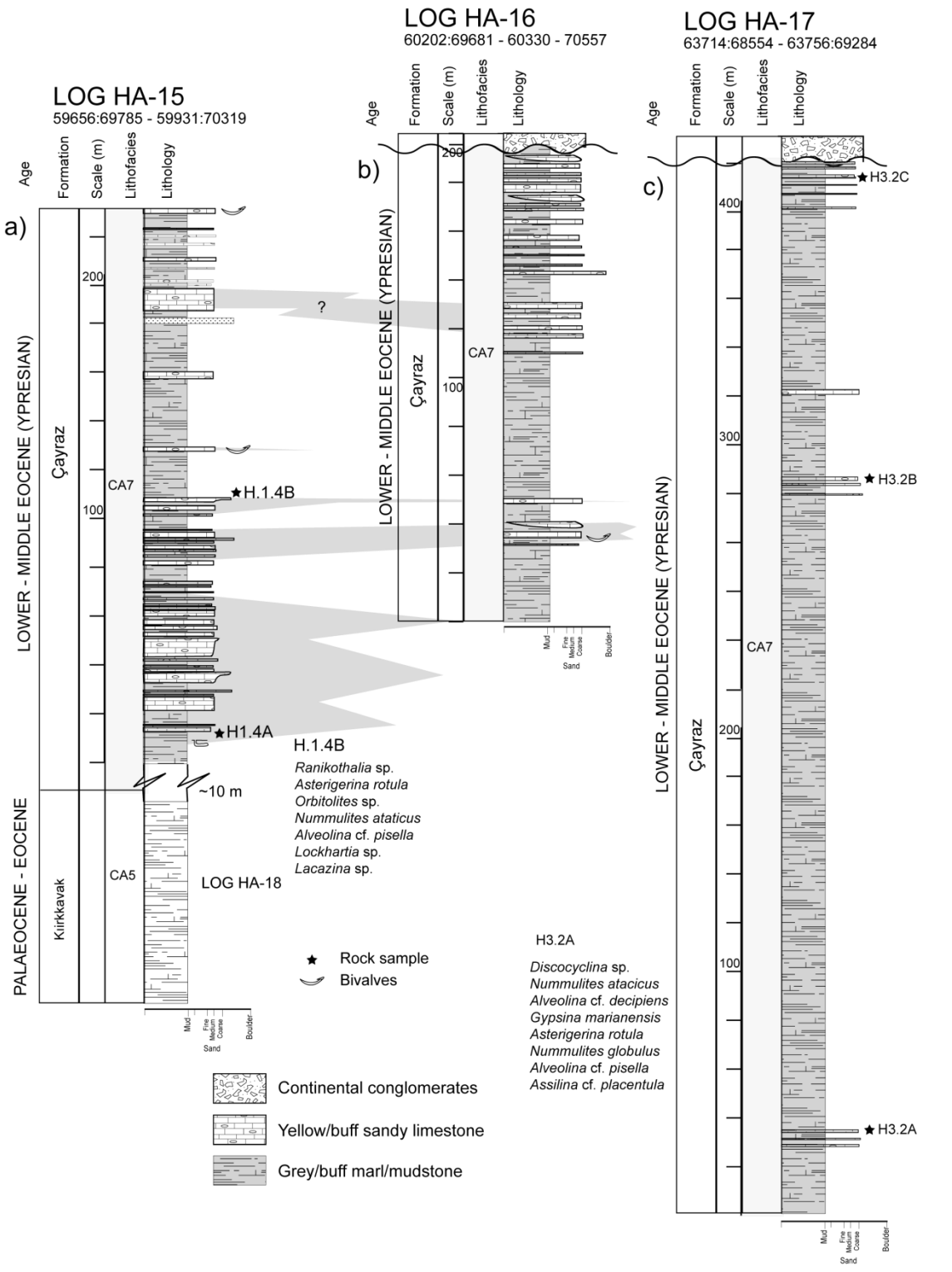

Figure 5.24 Measured logs through the Lower-Middle Eocene Çayraz Formation. Sedimentary data are from this study; fossil data are from N. İnan & K. Taslı (pers. comm. 2009).

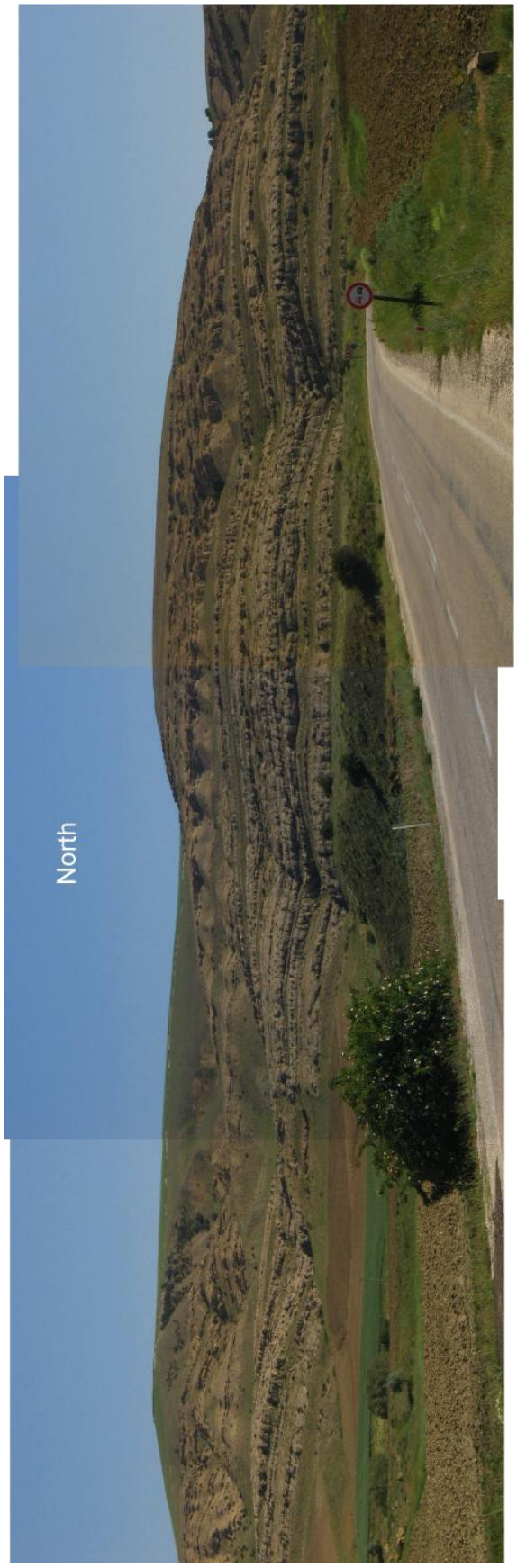

Figure 5.25 Photo-mosaic, looking north, over the benthic foraminiferal sandy limestones of the Lower-Middle Eocene Çayraz Formation.

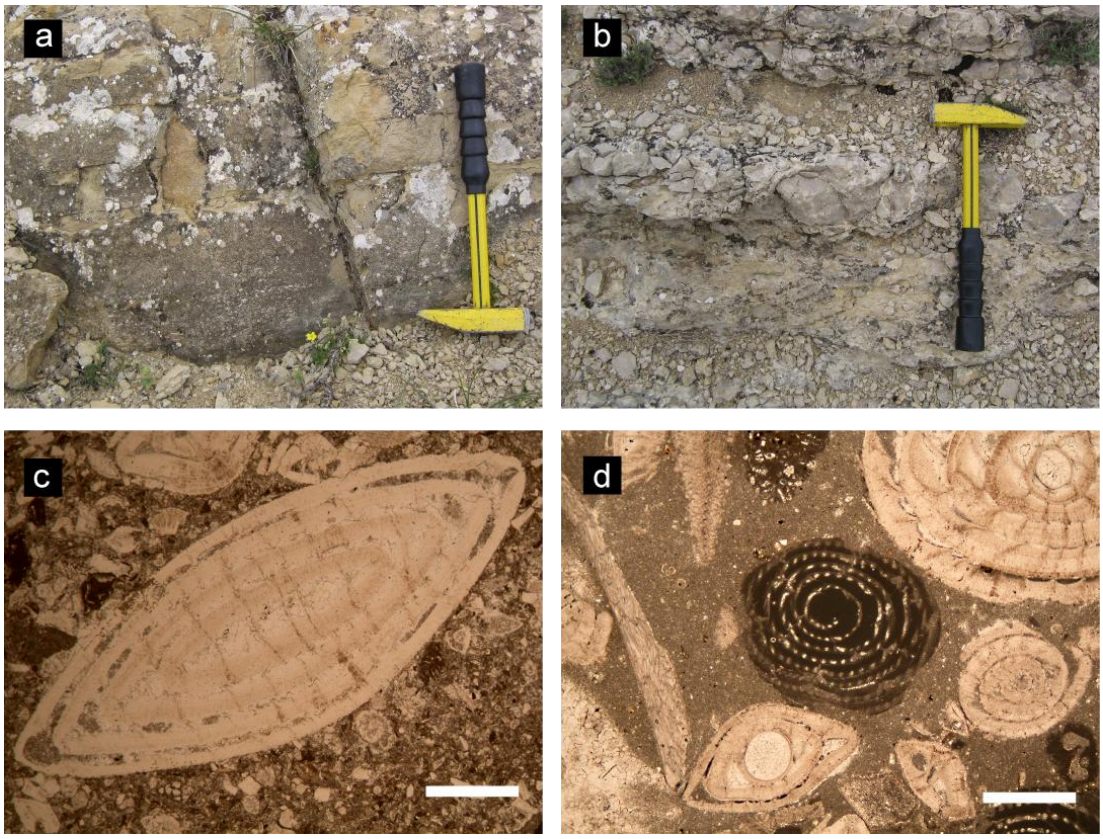

Figure 5.26 (a) Field photograph of well-stratified bioclastic sandy packstone/grainstone beds of the Lower-Middle Eocene Çayraz Formation, **(b)** grey rubbly limestone of the Çayraz Formation, **(c)** photomicrograph (in plane-polarised light) of the large benthic foraminifera *Nummulites atacicu* in sample HA1.4b, **(d)** photomicrograph (in plane-polarised light) of a diverse population of benthic foraminifera in sample HA3.2a; see text for details. Scale bars = 1mm. Fossil data are from N. İnan & K. Taslı (pers. comm. 2009).

5.4.8.1 Interpretation of lithofacies CA7

Nummulites were widespread throughout open-shelf facies in the Tethyan realm during the Palaeogene and commonly formed banks that vary in thickness from a few metres to hundreds of metres, and in lateral extent from hundreds of metres to several kilometres (Schaub 1981; Racey 2001). Nummulitic limestones often show signs of reworking by current activity. The extensive grading and rubbly tops of many nummulitic deposits in the Çayraz Formation suggests that reworking was extensive. Çiner *et al.* (1996b) proposed a Milankovitch control on the

deposition of Nummulites deposits in this area. However, given the evidence of extensive sediment reworking, and the tectonically active regional setting of the Haymana-Polatlı Basin, this interpretation should be treated with caution.

Two samples of sandy packstone yielded the following large benthic foraminifera: *Discocyclina* sp., *Nummulites atacicus* Leymerie, *Alveolina* cf. *decipiens*, *Gypsina marianensis* Hanzawa, *Asterigerina rotula* (Kaufmann), *Nummulites globulus* Leymerie, *Alveolina* cf. *pisella* , *Assilina* cf. *placentula* and *Ranikothalia* sp., *Orbitolites* sp., *Lockhartia* sp. and *Lacazina* sp. This assemblage suggests a Lower Eocene (Ypresian) deposition date (N. İnan & K. Taslı pers. comm. 2009) which is in contrast to previous studies (e.g. Ünalan *et al.* 1976) that suggested a middle Eocene (Lutetian) age.

In summary, the Çayraz Formation displays deposits that are characteristic of an open shelf setting. There is a trend from nummulite-rich carbonates and yellow mudstones in the NW (Log HA-15) to nummulite-poor grey mudstones in the SE (Log HA-17) which probably represents an upper- to lower-shelf transition. In the stratigraphic interpretation of Görür *et al.* (1984), the Çayraz Formation grades laterally into Middle Eocene continental deposits (the Kartal Formation). However, no evidence of this relationship was observed. Instead, the Çayraz Formation grades horizontally into Neogene continental sediments (Fig. 5.3).

5.4.9 Summary of Stratigraphy

New data have shed light on the stratigraphic development of the Haymana-Polatlı Basin by providing:

1) Modern lithofacies descriptions and inferred depositional settings, and;

2) A new stratigraphic model, controlled by new dating of mainly large benthic foraminifera, which improves on and highlights problems with previous stratigraphic schemes. For example, the Middle Palaeocene (Thanetian) age assigned

to the Kırkkavak Formation by Ünalan *et al.* (1976) is questionable; this study proposes a latest Palaeocene-Eocene age. In addition, the relationship of the Upper Cretaceous Asmaboğazı and Haymana formations proposed by Görür *et al.* (1984) is doubtful.

5.5 Provenance

This section discusses sandstone petrography and palaeocurrent data with the aim of inferring the provenance of the basin-fill sediments. Eight standard thin sections that were representative of sandstone from the basin were prepared and analysed under a petrographic microscope. Three hundred grains per sample were counted using the Gazzi-Dickinson method (see Appendix 1) (Gazzi 1966; Dickinson 1970). Provenance determination in complex orogenic regions involving both ophiolitic and volcanic arc material is not straightforward (e.g. Garzanti *et al.* 2000) such that traditional Dickinson-type ternary diagrams are generally unreliable, owing to a typically abundant and varied lithic grain population. In the Haymana-Polatlı Basin it is generally accepted that basin-fill sediments were derived from the Pontide active margin to the north, and the Ankara Mélange, on which the basin developed (e.g. Görür *et al.* 1984). The method employed in this study is to describe and interpret the provenance of sandstone rock types and conglomeritic clasts.

5.5.1. The Upper Cretaceous Haymana Formation

Turbidites of the Hayman Formation are medium-grained litharenites and are composed of sub-angular grains of volcanic quartz (commonly with undoluse extinction) polycrystalline quartz, micrite, red radiolarian chert, volcanic lithoclasts and plagioclase. Based on one sample (HA2.1Y, see Fig.5.27a) the Qt:F:Lt-c (where Qt = Total quartz, F = Feldspars, Lt-c = Total non-carbonate lithoclasts) ratio is

29:8:63 (Fig. 5.28). Palaeocurrents (n= 18) suggest a southwest-northeast orientated flow (Fig.5.29a).

Conglomerates to the north of the basin are composed of crystalline limestone, radiolarian chert, gabbro, basalt and serpentinite. In the basin centre, clasts of pelagic limestone, gabbro, black chert, crystalline limestone, bioclasts and rare phyllite occur. Black chert and phyllite clasts are probably derived from the Permo-Triassic Karakaya Complex to the north (e.g. Okay *et al.* 1998). The likely source of crystalline limestone, radiolarian chert, gabbro, basalt and serpentinite is the mainly Upper Cretaceous Izmir-Ankara Accretionary Complex, which forms the basin basement. Imbricated clasts (n =5) indicate a palaeoflow from northwest to southeast, perpendicular to the indicators in finer-grained sediments to the south (Fig.5.29).

5.5.2 The Lower Palaeocene Dizilitaşlar Formation

The Dizilitaşlar Formation is dominated by carbonate depositions, however rare clastic pebblestone horizons are composed of pelagic limestone, basalt and sandstone and indicate a flow (n=3) from west-northwest to east-southeast (Fig.5.29b).

5.5.3 The Palaeocene Kartal Formation

A fine-grained sandstone (sample HA5.3Z; Fig.5.27b) from the Palaeocene Kartal Formation is composed of volcanic lithoclasts, sub-rounded monocrystalline quartz, calcite and micrite (Qt:F:Lt-c ratio = 43:1:56; Fig.5.28). Volcanic lithoclasts are almost exclusively silicic in nature. At the base of the formation, conglomerates contain clasts of radiolarian chert, basalt, gabbro, limestone, black chert, phyllite and

marble. These compositions again suggest a mixed provenance from both the Izmir-Ankara Accretionary Complex and the Karakaya Complex. No palaeocurrent data were recorded due to an absence of suitable sedimentary structures.

5.5.4 The Palaeocene-Eocene Kırkkavak Formation

The Palaeocene-Eocene Kırkkavak Formation is represented by four medium-grained sandstone samples. They are generally poor in feldspars and composed of sub-angular volcanic quartz, basic and silicic volcanic lithoclasts, black chert, plagioclase, opaque oxides and rare radiolarian chert (Fig. 5.27c) (mean Qt:F:Lt-c ratio = 48:5:47; Fig. 5.28). All of the Kırkkavak Formation samples contain a relatively high abundance of fresh accessory minerals including muscovite, clinopyroxene and tourmaline, suggesting input from a volcanic source, which may have been remobilised. Pebbly sandstones and conglomerates are particularly abundant in black chert clasts which represent an increased input from the Karakaya Complex, relative to older sediments. Conglomeritic palaeocurrents (n= 8) indicate a general west to east flow (Fig.5.29c).

5.5.5 The Eocene Yoncalı Formation

Two fine-grained samples of turbiditic sandstone from the Eocene Yoncalı Formation contained basic volcanic lithoclasts, monocrystalline quartz, silicic volcanic lithoclasts with rare sedimentary lithoclasts, plagioclase and schist. Accessory minerals include opaque oxides, muscovite, chloritised clinopyroxene and calcic amphibole (Fig. 5.27d). The mean Qt:F:Lt-c ratio is 50:1:49 (Fig. 5.28). Conglomerates in the Yoncalı Formation comprise clasts of red radiolarian chert, crystalline limestone, basalt and gabbro. Flute and groove marks (n= 14) in fine-

grained sediments suggest a palaeocurrent from southeast to northwest. Imbricated clasts (n= 20) indicate a general flow from west to east (Fig. 5.29d).

In summary, sediment provenance in the Haymana-Polatlı Basin indicates a source from the Ankara Mélange basement and the Karakaya Complex to the north. Latest Palaeocene and Eocene sandstones contain relatively higher abundances of accessory minerals which could represent detritus from the Pontide Arc. This implies that the uplift and unroofing of magmatic units in the Pontide Arc had begun by the latest Palaeocene.

Palaeocurrent indicators in medium- to fine-grained turbiditic deposits are frequently perpendicular to those in pebbly sands and conglomerates. Flow parallel to an arc represents the redistribution of sediments following axial transport, typically by slump and debris flows (Dickinson & Seely 1979; Underwood & Bachman 1982). This effect has been documented in other regions including Alaska (Nilsen & Zuffa 1982) and the Nankai trough in Japan (Le Pichon *et al.* 1987). In the Haymana-Polatlı Basin, southwest – northeast longitudinal sediment transport probably occurred along palaeotopographic lows and is consistent with the southeast- and northwest-dipping palaeoslopes as inferred from the dip of slump folding (Section 5.4.3.3). New palaeocurrent data have enhanced understanding of sediment sources and pathways in the Haymana-Polatlı Basin.

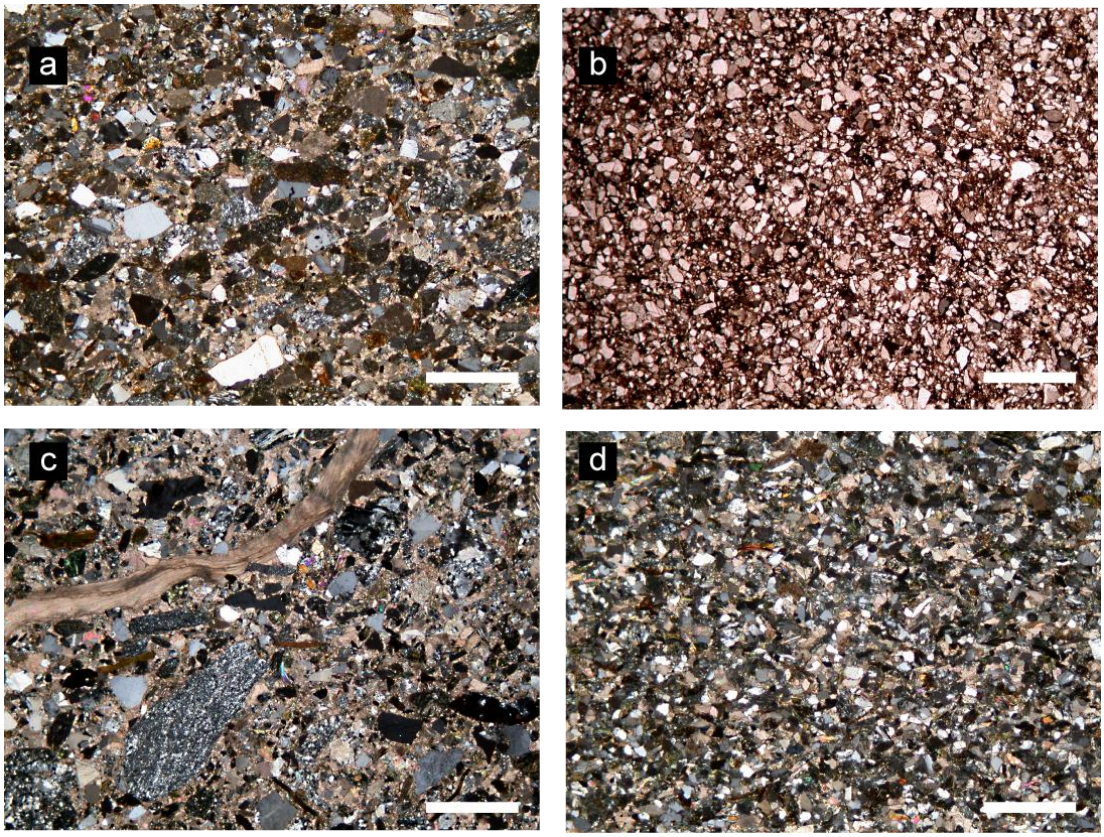

Figure 5.27 Representative photomicrographs (in crossed polars) of sandstones: **(a)** the Upper Cretaceous Haymana Formation (sample HA2.1y), **(b)** the Palaeocene Kartal Formation (sample HA5.3z), **(c)** the Upper Palaeocene-Lower Eocene Kırkkavak Formation (sample HA12.2a), **(d)** the Lower-Middle Eocene Yoncali Formation (sample HA5.5b). All scale bars = 1 mm.

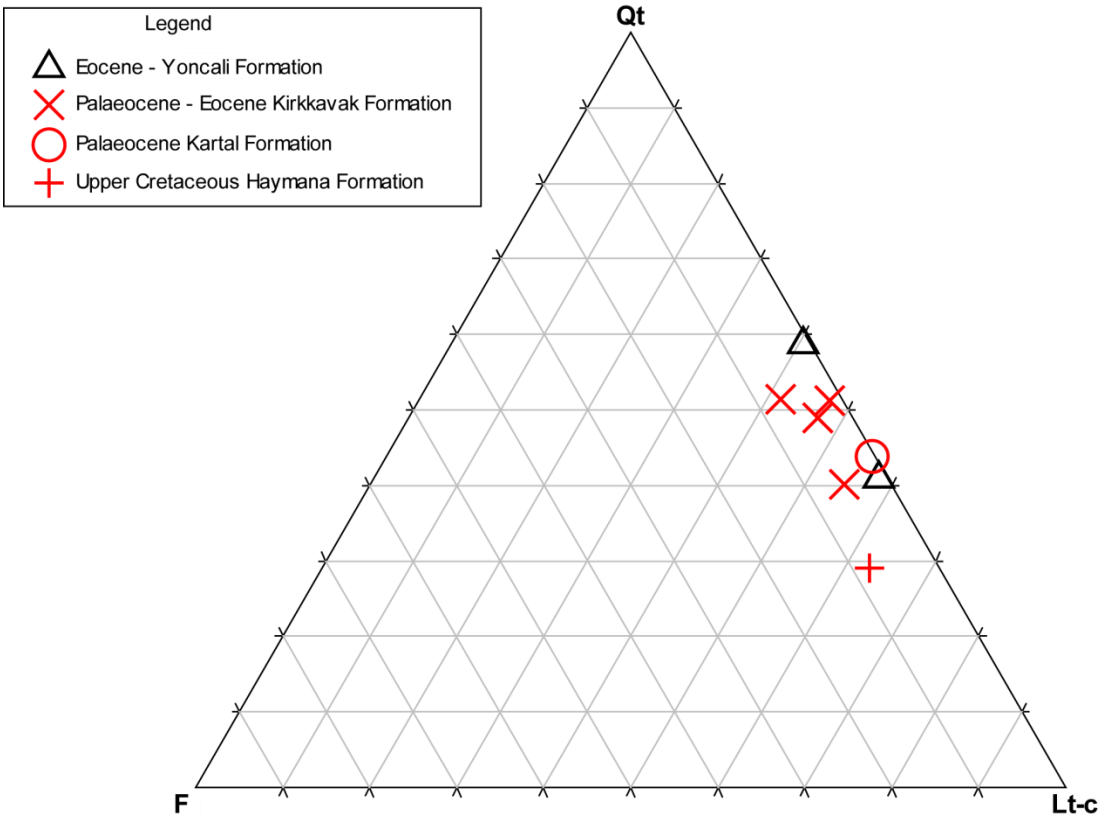

Figure 5.28 Ternary diagram of sandstone compositions counted using the Gazzi-Dickinson point counting method. Qt = total quartz, F = total feldspar, Lt-c = total lithic grains excluding carbonates.

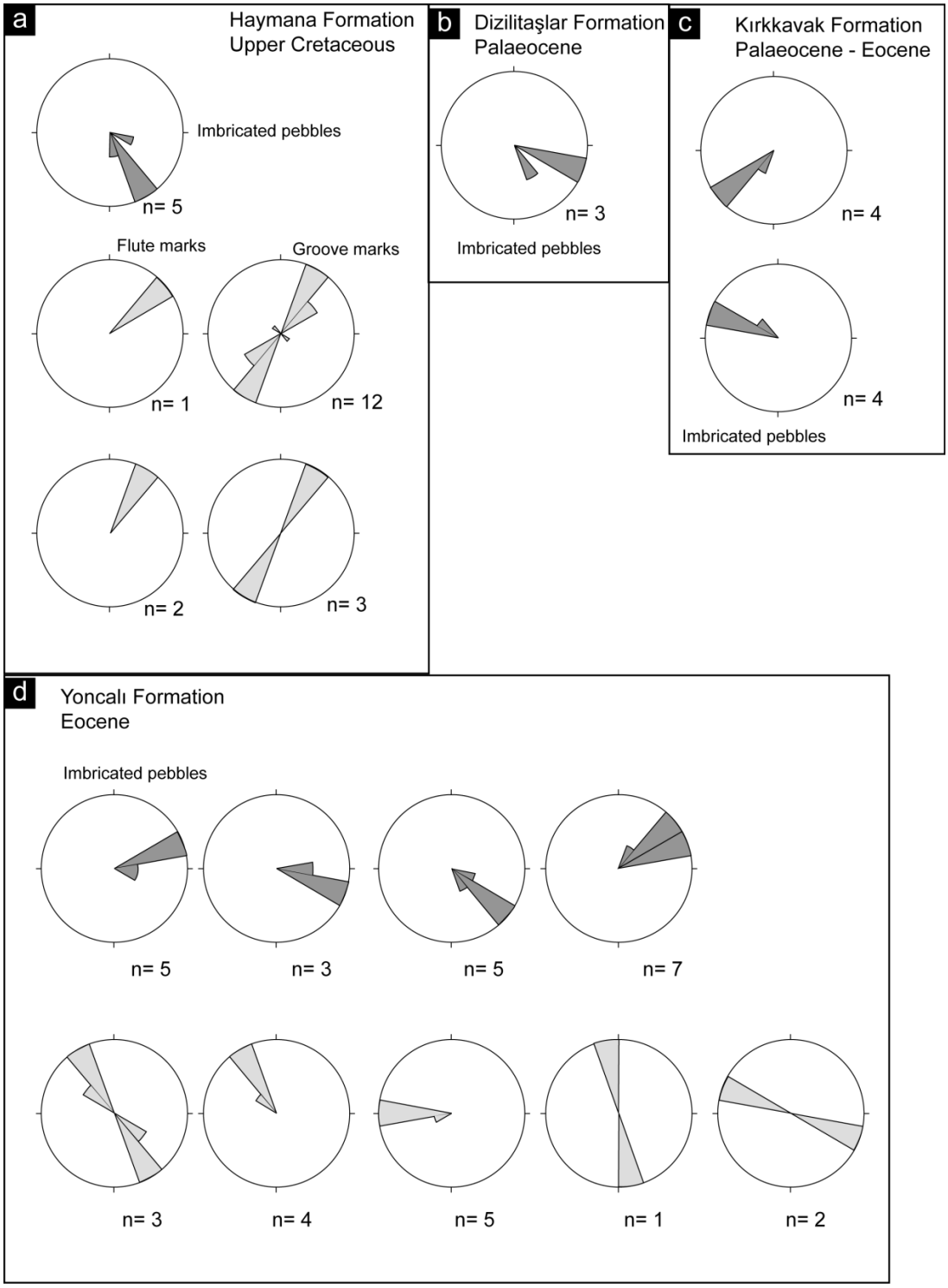

Figure 5.29 Palaeocurrent rose diagrams of formations in the Haymana-Polatlı Basin. Dark grey diagrams represent imbricated clasts in conglomerate beds. Light grey unidirectional diagrams represent flute marks. Light grey bi-directional diagrams represent groove marks.

5.6 Structural development of the Haymana-Polatlı Basin

This section aims to reconstruct the structural development of the Haymana-Polatlı Basin which was largely ignored in earlier work. Evidence comes from previous reports based on seismic profiles, and new structural data measured during this study (see Appendix 2 for methodology).

It is widely accepted that the Haymana-Polatlı Basin developed on accretionary material associated with the northward subduction of the northern branch of Neotethys under the Pontide active margin (e.g. Koçyiğit 1991). Seismic evidence (Fig.5.30a), of varying quality, points to extensional faulting (Ünalan & Yüksel 1978; Turgay & Kurtuluş 1985; Grove *et al.* 2004; Aydemir & Ateş 2006) represented by mostly northwest - southeast and normal faults forming grabens, horsts and half grabens during the basin's Upper Cretaceous development. A similar structural regime is inferred in the basement of the Upper Cretaceous-Middle Eocene Tuz Gölü Basin (Görür *et al.* 1984; Çemen *et al.* 1999) to the south (Chapter 4).

The dominant basin-scale surface structural features are mostly compressional. A series of west - east-trending folds (Fig. 5.30b) expose basement and Upper Cretaceous lithologies in anticlinal cores at Haymana and to the south at Bahçecik (Fig. 5.Map). The folds have a wavelength of ~6 km and indicate a broadly north-south compressional phase. Overlying Mio-Pliocene continental sediments are relatively undeformed, which constrains the age of folding.

The basin margin to the east (58116:77208) near Dereköy, and to the west (25667:67178) near Karahamzalı, is dissected by local, brittle thrust faulting. On the eastern margin, a slice of the Ankara Mélange is emplaced against the Eocene Yoncalı Formation (Fig.5.31a). At the western margin, the Palaeocene Kartal Formation is thrust over the Palaeocene-Eocene Kırkkavak Formation, producing an overturned footwall fold (Fig.5.31b). TectonicsFP software (Ortner *et al.* 2002) was used to calculate palaeostress tensors for this fault utilising the right dihedra method of Angelier & Mechler (1977). These new data suggest horizontal $\sigma 1$(05/209) and

σ2(02/022) and a vertical σ3 (85/134) palaeostress axes indicating west-northwest – east-southeast compression (Fig. 5.31c). The faulted slice of Ankara Mélange and the basin-fill sediments are both unconformably covered with Mio-Pliocene terrestrial sandstones, conglomerates and marls, which constrain the upper age for thrust faulting.

A further phase of brittle deformation is represented by outcrop-scale oblique- to strike-slip faults which dissect the entire basin area. This is the first study to analyse surface faulting in the Hayman-Polatlı Basin in any detail. New data represent measurements from thirtyeight fault planes, of which twenty four had reliable slickenside indicators. Of these faults, the two most abundant strike directions are east-southeast – west-northwest and east-northeast – west-southwest; the majority have a dip angle of >80° (Fig.5.32a).

In order to constrain the fault population into groups that represent distinct deformation phases, fault analysis was conducted on TectonicsFP software with the aim of reconstructing palaeostress tensors. First, the entire dataset (n=24) was analysed in terms of P-, B- and T-axes which represent an approximation of stress axes. This data treatment produced a lower hemisphere scatter plot for individual P-, B- and T-axes for each fault, along with mean values, error ellipses and R values, which give a measure of confidence.

Using the entire data set (n=24) (see Fig.5.32b for an Angelier plot), there is a large scatter of all the axes and very low confidence values (P=14%, B=29%, T=43%) indicating a heterogeneous fault population (Fig.5.32c). The data were then filtered to achieve higher confidence using a number of criteria, including age, location and the angle of fault dip. Age and location produced similar very low confidence values; however, confidence increased when using faults with a dip of >80°. A dataset of eight faults produced the following R values: P=47%, B=57%, T=88%. Mean axes vectors were P=072/02, B=076/74, T=341/06 (Fig.5.32d) which indicate a strike-slip faulting regime. The faults cut Upper Cretaceous to Middle Eocene sediments and are spatially diverse throughout the basin (Fig.5.32e).

A further increase in R was produced by filtering more of the faults leaving a smaller dataset (n=4). In this case, confidence was P=88%, B=93%, T=94%; mean axes vectors were P=079/02, B=217/86, T=164/00 (Fig.5.33a). Spatially, the faults are concentrated at the western basin margin, near Karahamzalı and cut the Upper Palaeocene – Lower Eocene Kırkkavak Formation. Using the right dihedral method of Angelier & Mechler (1977), stress tensors were calculated and gave the following results, $\sigma 1$= 082/02, $\sigma 2$= 196/85 and $\sigma 3$= 352/04, indicating a strike-slip stress regime (Fig.5.33b).

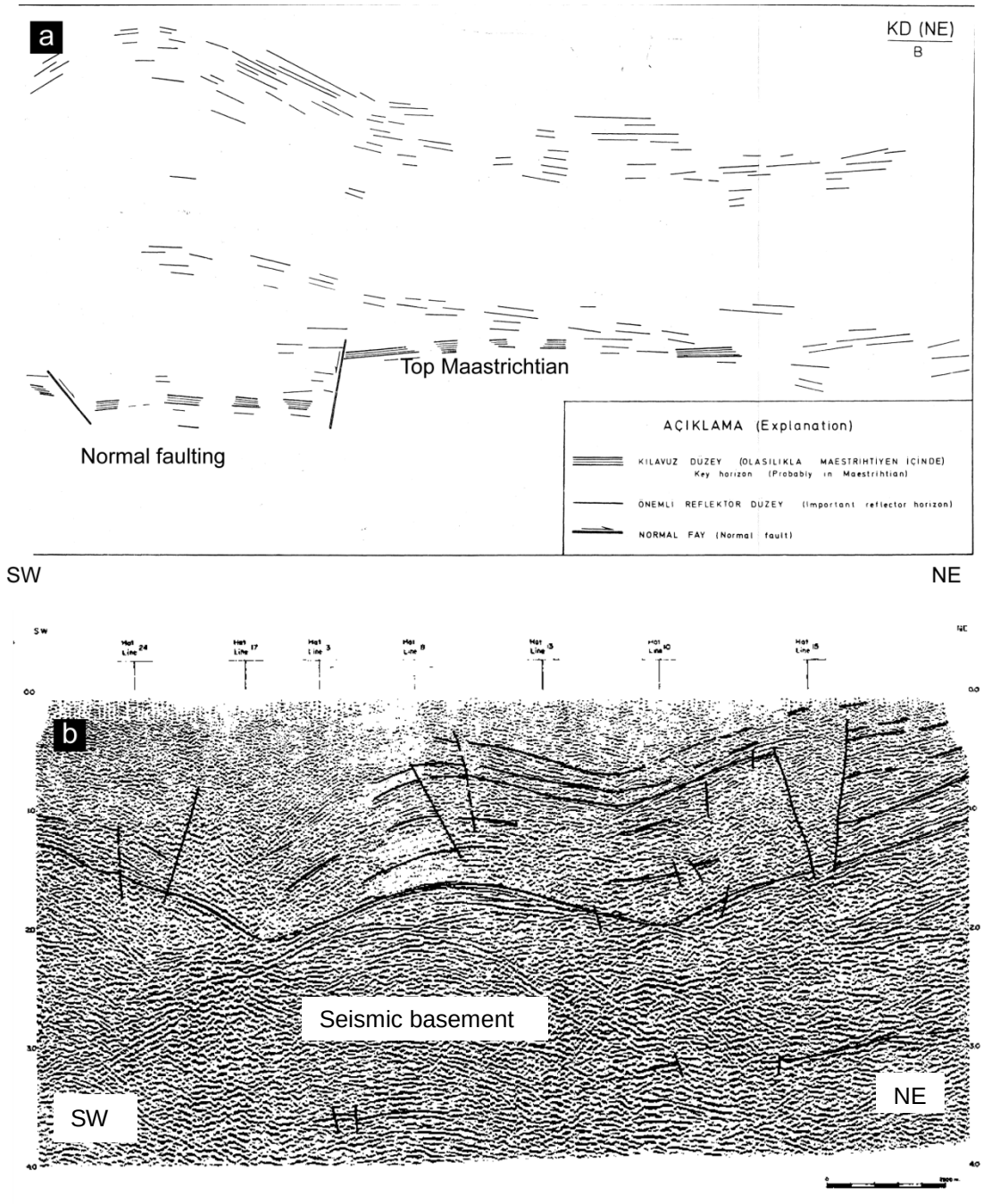

Figure 5.30 Seismic images in the Haymana-Polatlı Basin along SW-NE trending shot lines, **(a)** extensional faulting in Upper Cretaceous sediments, copied from Ünalan *et al.* (1978), **(b)** folding cut by high-angle faults, copied from Turgay & Kurtuluş((1985).

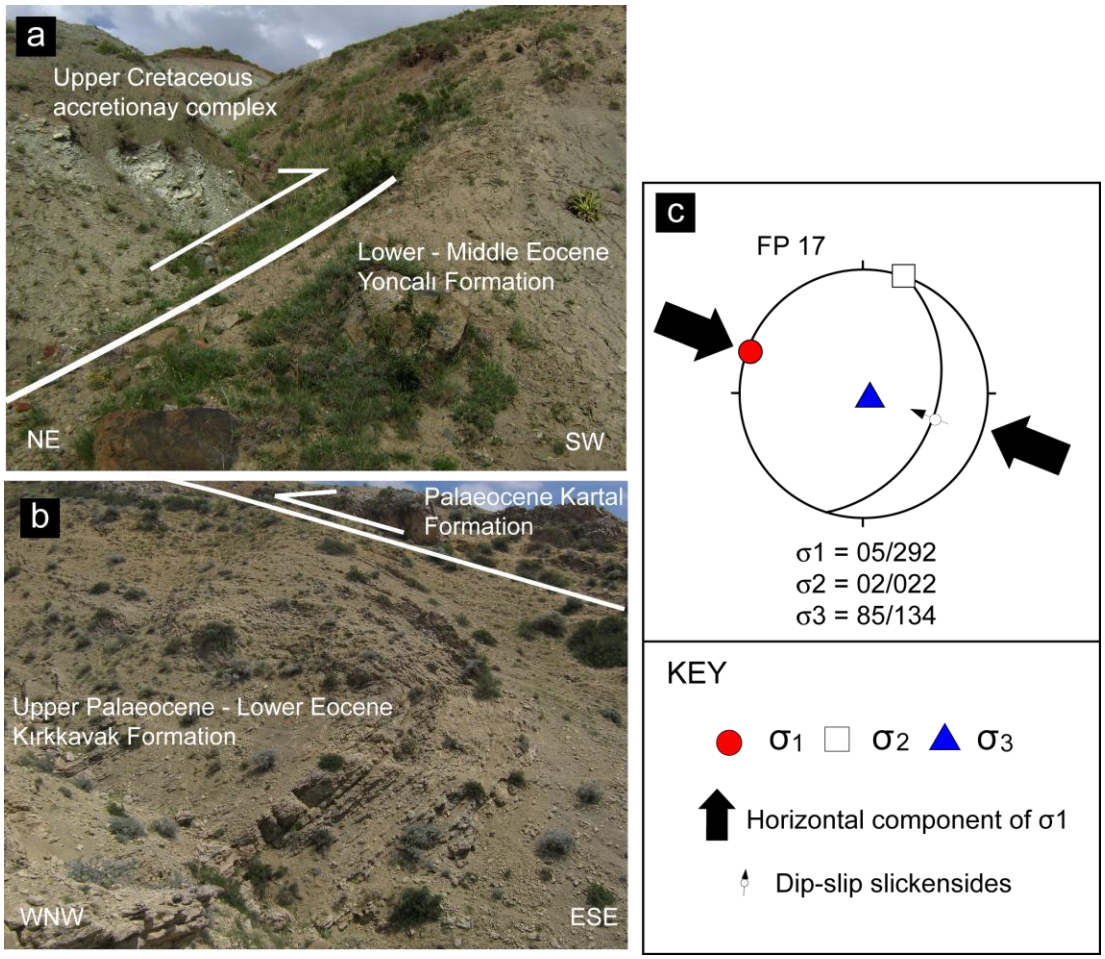

Figure 5.31 (a) field photograph, looking NW, of the Upper Cretaceous İzmir-Ankara Accretionary Complex emplaced against the Lower-Middle Eocene Yoncalı Formation, **(b)** field photograph, looking NNE, of a thrust fault emplacing the Palaeocene Kartal Formation over the Upper Palaeocene-Lower Middle Eocene Kırkkavak Formation east of Karahamzalı at the western basin margin. Note the footwall deformation, **(c)** lower hemisphere stereogram showing palaeostress tensors of the fault plane, computed on TectonicsFP software utilising the right dihedral method.

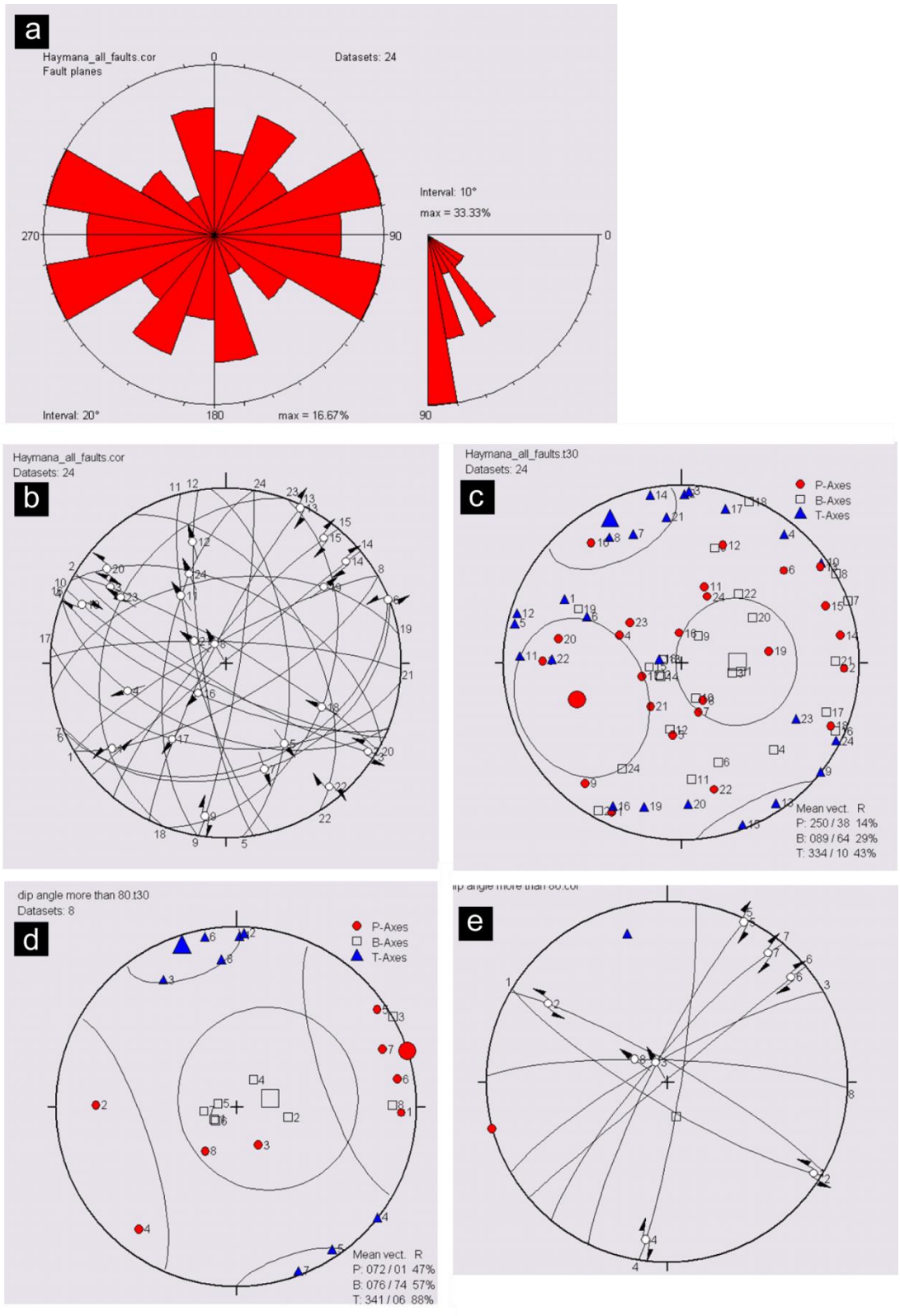

Figure 5.32 (a) Rose diagram of faults (n=24) in the Haymana-Polatlı Basin that contain slickenside indicators, **(b)** Angelier plot, **(c)** P-, T-axes plot showing the entire fault population, and associated confidence levels, of the basin, **(d)** P-T-axes plot of a subset of (n=8) faults which are characterised by a dip angle of >80°, **(e)** Angelier plot.

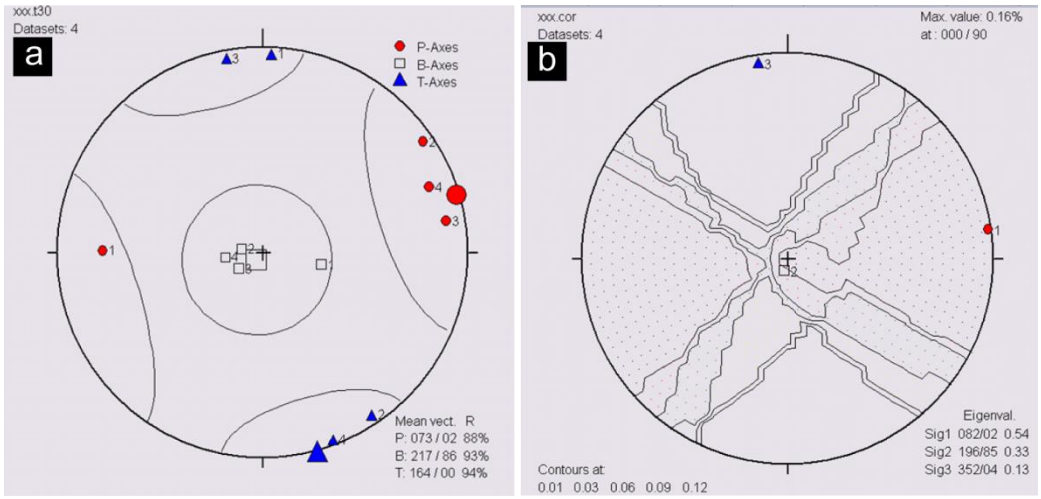

Fig.5.33 (a) P-T-axes lower hemisphere plot of mean axes vectors and confidence levels, **(b)** Palaeostress resolution using the right dihedra method.

5.6.1 Interpretation of structural development

The absence of cross-cutting relationships makes inferring the relative order of deformation phases problematic. Seismic surveys in the literature suggest that the basin developed in an extensional regime. Extensional faulting has been documented in numerous syn-convergent accretionary wedge settings (e.g. Wallis *et al.* 1993; Gutscher *et al.* 1998; Collins 2002) including the Upper Cenozoic-Mesozoic Franciscan subduction complex (Unruh *et al.* 2007), the Neogene-Quaternary Apennines (Doglioni *et al.* 1996) and the present Sunda Arc in the SW Pacific (Huchon & Le Pichon 1984; Curray 1989; Longley 1997).

Based on the presence of undeformed Mio-Pliocene sediments overlying basin-fill deposits, folding and thrust faulting probably occurred between the Middle Eocene and Mio-Pliocene time. Fold axial traces are orientated west-east and indicate north-south compression. Thrust faulting indicates compression in a west-northwest – east-southeast and northeast -southwest direction. Compressional deformation is probably related to tightening of the İzmir-Ankara-Erzincan suture zone, which is not a curvilinear feature but contains loops and Ω-shapes which are

interpreted to reflect the irregular geometry of colliding microcontinents (e.g. Kaymakcı *et al.* 2009).

Strike-slip faulting is presumably a product of the post-collisional reorganisation of central Anatolia (e.g. Kaymakcı *et al.* 2009). New data discussed in this chapter may be comparable to those of Koçyiğit & Deveci (2008) who interpreted NNE – SSW strike-slip faults (i.e. comparable to the strike-slip faults in this study) cutting Early Pliocene fluvio-lacustrine sediments to the southeast of Ankara as a result of latest Pliocene transpression. However, great care should be taken in comparing results, because Koçyiğit & Deveci (2008) did not publish their methodology in deriving palaeostress tensors; data are rather limited, and faulting may be localised rather than a regional event.

5.7 Discussion: Tectonostratigraphic evolution of the Haymana-Polatlı Basin.

New sedimentary, stratigraphic, palaeontological, palaeocurrent and structural data permit a reconstruction of the evolutionary history of the Haymana-Polatlı Basin. It is generally accepted that the basin developed on the Ankara Mélange, an imbricated accretionary complex which marks the position of the Izmir-Ankara-Erzincan Suture Zone and represents the southernmost limit of the Pontides to the north.

The geological history of the basin can be broadly represented by two tectonostratigraphic phases. The Upper Cretaceous-Middle Eocene phase was characterised by extensional faulting and subsidence followed by gradual basin in-filling. Relatively deep-water, pelagic and lower/middle slope marine environments prevailed in the basin depocentre, while the basin margins were episodically uplifted to permit continental sedimentation, and subsequently drowned by eustatic sea level rises. The post-Middle Eocene time was characterised by uplift, erosion, continental sedimentation and mostly compressional deformation.

Basement lithologies comprise: 1) the İzmir-Ankara Accretionary Complex, a mainly Cretaceous subduction-accretion complex composed of dismembered blocks and south-verging thrust sheets of Neotethyan oceanic lithosphere, within-plate seamount-type basalts, island arc tholeiites, N-MORBs and pelagic sediments. All of these were accreted to the Pontide margin during the northward subduction of northern Neotethyan oceanic lithosphere, and; 2) Upper Jurassic-Lower Cretaceous recrystallised neritic limestone which probably represents passive-margin-type sedimentary cover of a Permo-Triassic limestone block mélange.

Previous seismic studies in the Haymana-Polatlı Basin were interpreted as displaying deep extensional structures in the basin's basement which have not been accounted for in previous models of basin development. Seismic imaging in modern accretionary prisms commonly show pervasive normal faults; a good example is off the Costa Rica slope (Ranero & von Huene 2000). An extensional tectonic regime in a region of plate convergence may be brought about by several mechanisms. First, bulk thickening of the accretionary prism occurs by underplating of sediments and crustal slices at depth (Platt 1986) or by frontal off scraping at the trench axis. Either way, thickening of the accretionary prism induces uplift during subduction-accretion. In order to restore isostatic balance, gravitational collapse will trigger extensional faulting, which results in subsidence and the formation of accretionary-type sedimentary basins (Koçyiğit 1991; Rojay & Süzen 1997).

Second, chemical, petrographic and structural evidence to the northeast of the Haymana-Polatlı Basin suggests that subduction was initiated outboard of the Pontide margin and rolled back southwards, triggering the widespread genesis of supra-subduction zone (SSZ) ophiolites in a back-arc setting during the Turonian. Roll-back continued until an intra-oceanic trench collided with the northern margin of the Niğde-Kırşehir microcontinent, emplacing the SSZ-type Çiçekdağ and Sarıkaraman ophiolites (Yaliniz *et al.* 1996; Yalınız & Göncüoğlu 1998; Yılmaz & Boztuğ 1998; Yalınız & Göncüoğlu 1999; Floyd *et al.* 2000; Yalınız *et al.* 2000).

To the north of the basin evidence is less clear and is restricted to isolated Upper Cretaceous inliers exposed in the Galatean Arc Complex, a volcanic plateau to

the north of Ankara. It has been suggested that volcanism in this area started in the Late Cretaceous and persisted until the Middle Miocene (e.g. Keller *et al.* 1992). Several authors (e.g. Koçyiğit 1991; Koçyiğit *et al.* 2003) proposed that the Mid Campanian-Eocene tectonostratigraphy of the Galatean Arc Complex consists of a ~1500 m-thick sequence characterised by the following rocks: above imbricated slices of the mainly Upper Cretaceous İzmir-Ankara Accretionary Complex (referred to as the "Anatolian Complex" in Fig. 5.32) lies pinkish pelagic limestone which pass upwards into a ~1000 m-thick package of deep marine "flysch" intercalated with andesitic-basaltic lavas. It is possible that these sediments correlate with the Upper Cretaceous Haymana Formation further south. These continue into continental red clastic rocks, which grade laterally into a series of volcanic rocks, including the Saraçköy Volcanic Suite. This sequence is intruded by syenodiorites and an associated dyke swarm (Tokay *et al.* 1988).

The Saraçköy Volcanic Suite consists of basaltic and trachyandesitic volcaniclastic rocks and thin lava flows. K-Ar radiometric dating indicates hornblende cooling ages of 73.2 ± 1.2 Ma (Keller *et al.* 1992) and 76.4 ± 2.4 Ma (Koçyiğit *et al.* 2003). The volcanic sequence is unconformably overlain by Eocene Nummulitic limestones.

Chemically, the basalts and trachyandesites are alkaline to mildly alkaline and are possibly related to 'within-plate' volcanism in an extensional setting; however, both younger and older volcanic rocks display calc-alkaline affinities. The Saraçköy Volcanic Suite is, therefore, interpreted to have formed in an extensional supra-subduction zone-type setting (Koçyiğit *et al.* 2003) to the north of a southward- migrating arc (Fig.5.33).

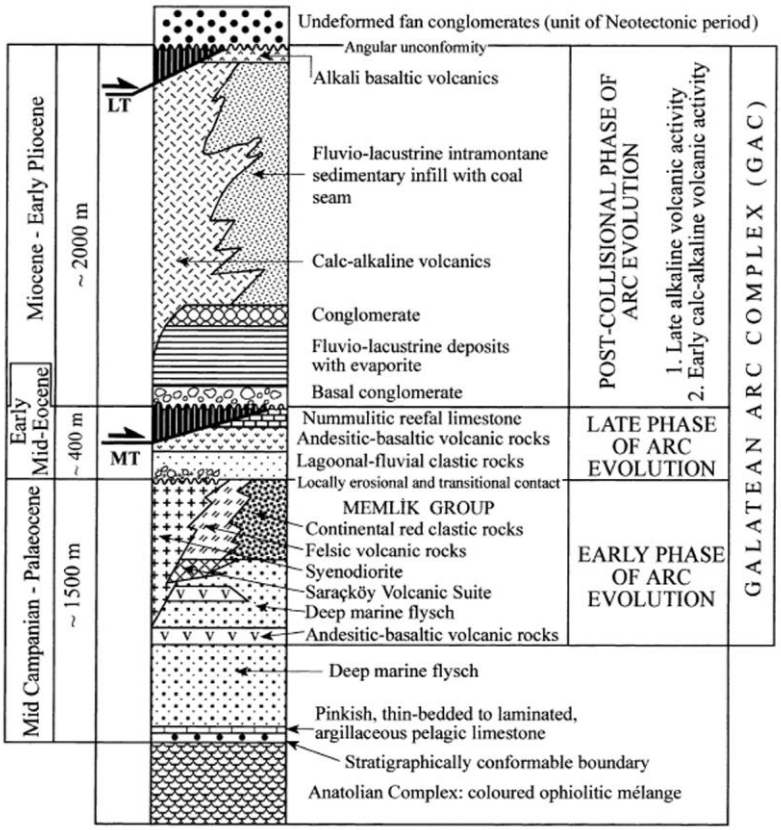

Figure 5.32 Tectonostratigraphy of the Galatean arc complex to the north of the Haymana-Polatli Basin, copied from Koçyiğit *et al.* (2003).

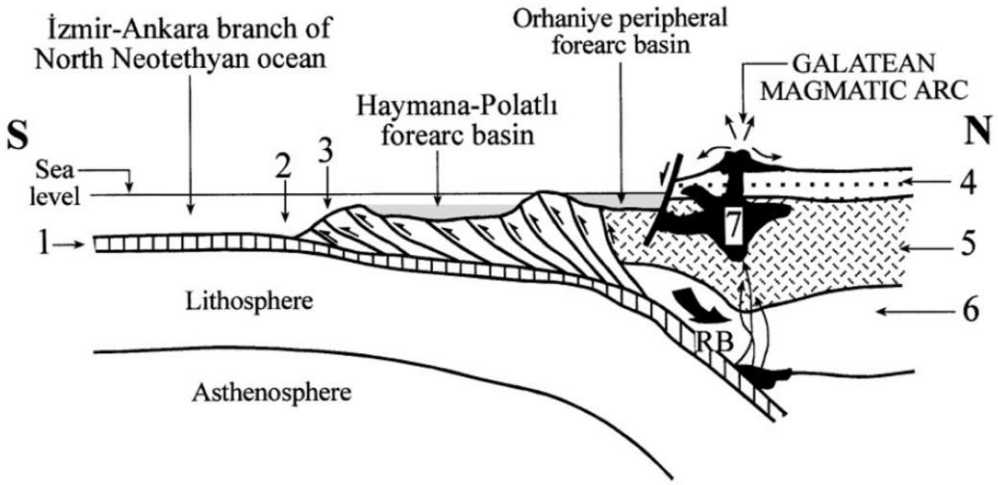

Figure 5.33 Tectonic model depicting northward subduction of northern Neotethys and the associated accretionary complex and magmatic arc during the Campanian, copied from Koçyiğit *et al.* (2003). 1 – oceanic crust, 2 – trench fill, 3 – accretionary wedge, 4 - Saraçköy Volcanic Suite, 5 – crust (arc massif), 6 – subarc mantle lithosphere, 7 – intriusion, RB – roll-back process

.

Implicit in the Upper Cretaceous stratigraphy of the Galatean Volcanic Suite (Fig.5.32) is that magmatism intruded the İzmir-Ankara Accretionary Complex. A possible analogue is in the Franciscan Complex, California, where alkali basaltic sills intrude an accretionary complex in a near trench setting (Mertz *et al.* 2001). The likely cause of alkali magmatism is thought to be either the subduction of an oceanic fracture zone or oblique collision generating an extensional tectonic setting (Mertz *et al.* 2001). However, syn-subduction alkali basalts may not necessarily be associated with extension. A younger analogue could be Cenozoic syn-subduction alkali basalts at James Ross Island in the Antarctic Peninsula (Hole *et al.* 1994). It is argued that lithospheric extension is not necessary to generate alkali basalts in a destructive plate margin setting. Instead, a possible model is that slab roll-back induced lateral replenishment of asthenosphere resulting in melting and the genesis of alkali basalt.

One possibility is that slab roll-back occurred to the north of Haymana. Slab roll-back is commonly accommodated by extension in the upper plate forearc region (Jarrard 1986) which produces lithospheric thinning and forearc basin subsidence. This process is considered to be active in many modern settings (Morley 2001; Schellart *et al.* 2006). However, the quality of seismic imaging presently available in the Haymana area is insufficient to provide further insights, and the origin of extension during the early basin development remains unresolved.

Sedimentation in the Haymana-Polatlı Basin initiated with the Asmaboğazı Formation (~10 m). This is represented by shallow-marine upper slope/shelf-type reworked carbonates comprising rudist-bearing collapsed reef debris (lithofacies R1) deposited on a faulted unconformity. Many Cretaceous carbonate platforms in the Neotethyan realm were characterised by rudist bivalves (e.g. Stössel & Bernoulli 2000) and indicate shallow-water deposition with low siliciclastic input. The Upper Cretaceous-Middle Eocene Tuz Gölü Basin to the south contains similar rudist-bearing Upper Cretaceous carbonates which indicate that carbonate platform development was regionally extensive during the Late Cretaceous.

Above comes the Upper Cretaceous Haymana Formation which is present in the basin depocentre but absent at the basin margins. The lowest part of the

formation is represented by grey and pink marls and siltstones (~70 m) (lithofacies CA1) bearing pelagic foraminifera that reflect an abrupt change to a deep-water depositional environment, in contrast to the Maastrichtian continental red conglomerates in the Tuz Gölü Basin further south. The Haymana Formation then shallows upwards through finely laminated grey siltstones (~400 m) (lithofacies M14) deposited on a lower slope by dilute turbidity currents. This sequence passes upwards into sandstone turbidites and black mudstone (~600 m) (lithofacies M2) which represent distal equivalents to the conglomerates and medium-bedded sandstones (lithofacies M3). Palaeocurrent indicators suggest a northwest-southeast conglomerate flow which changed to a southwest-northeast flow in the basin depocentre, probably indicating the pressure of local palaeotopographic lows.

During the Lower Palaeocene, red sandstones and conglomerates of the Kartal Formation (lithofacies C2) developed on the basin margins in an arid/semi-arid environment which led to the widespread formation of caliche. The Kartal Formation probably grades laterally into the contemporaneous Dizilitaşlar Formation. Lithofacies RC5 represents packstones containing reworked benthic foraminifera, calcareous algae and shelly fragments, probably deposited in an upper slope setting. A solitary palaeocurrent indicator suggests a northwest-southeast flow. Also, horizons of detached limestone blocks in a slope setting (lithofacies RC3), to the north of Haymana, suggest that a lower Palaeocene coralgal carbonate platform developed to the northwest of the basin. In contrast, Gökçen & Kelling (1983) speculated on the existence of a collapsing carbonate platform at the southern basin margin.

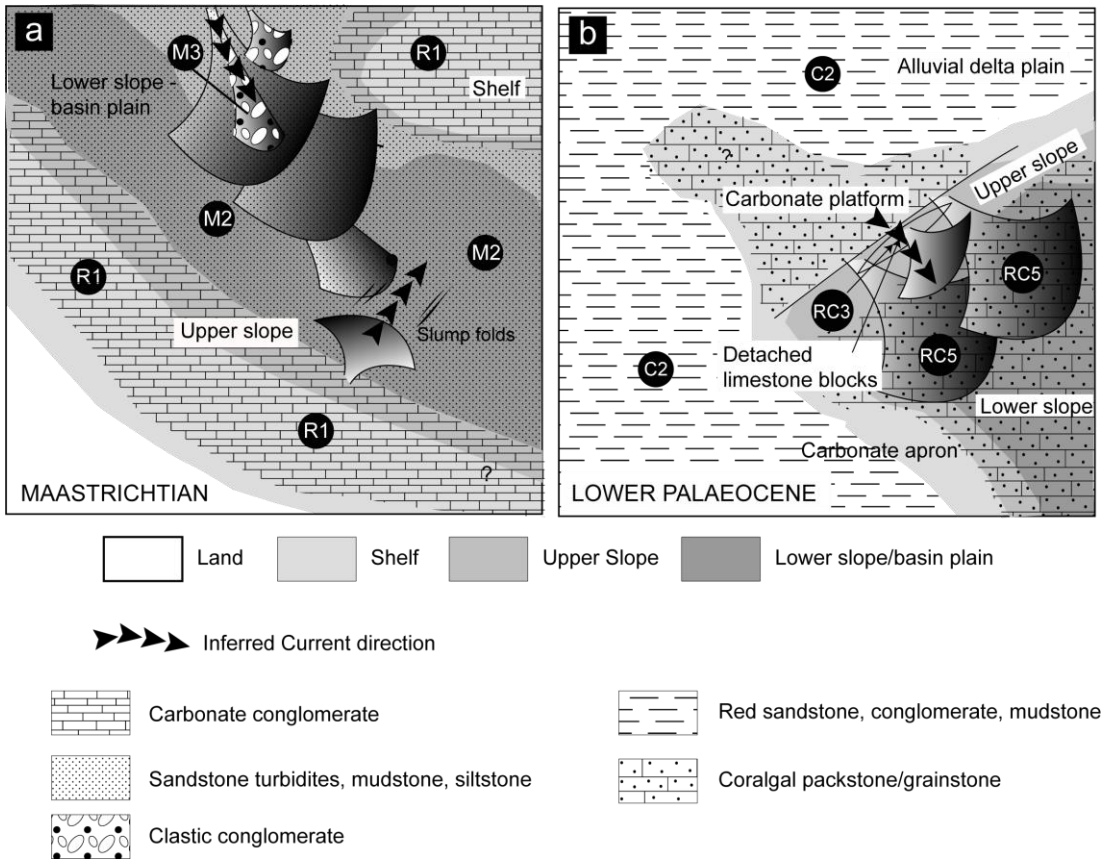

Figure 5.34 Palaeogeographic sketches of the Haymana-Polatlı Basin during **(a)** the Maastrichtian, and **(b)** the Lower Palaeocene. See text for further discussion.

In the latest Palaeocene and Lower Eocene time, shelf-type reefal facies (lithofacies CA5) of the Kırkkavak Formation developed unconformably on the Kartal Formation on the basin margins to the east and west. To the north of the basin, a shallow-marine delta system, represented by lithofacies M17, prograded to the northwest.

Middle Eocene rocks of the Haymana-Polatlı Basin characterise the final deposits of its collisional phase. The siliciclastic Yoncalı Formation is represented by three lithofacies which signal the final slope-type depositional setting. Lithofacies M3 comprises coarse clastic channelised conglomerates, lithofacies M14 contains lenticular, erosive turbidites, and lithofacies M2 comprises sheet-like overbank deposits.

The Çayraz Formation (lithofacies CA7) represents a well developed nummulite bank in an open shelf-setting at the eastern basin margin. New palaeontological dating suggests an older, Lower Eocene (Ypresian) date than previously published.

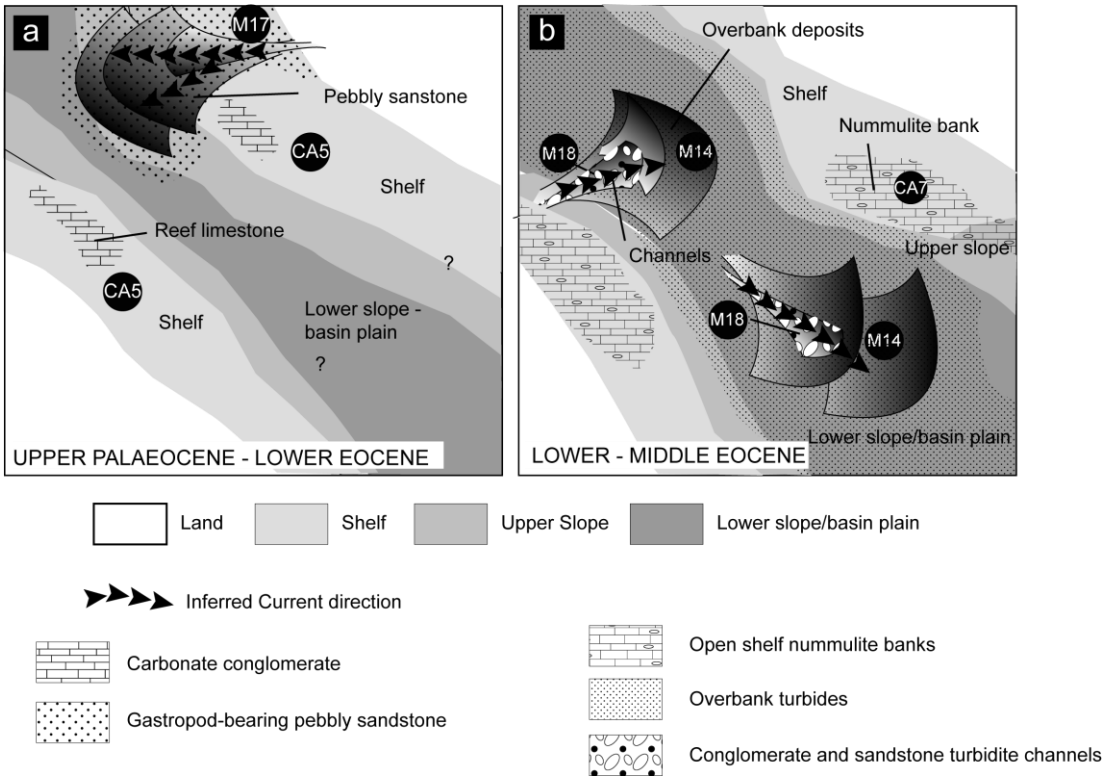

Figure 5.35 Palaeogeographic reconstructions of **(a)** the Late Palaeocene-Early Eocene time, **(b)** the Early to Middle Eocene.

The post-Middle Eocene tectonostratigraphy of the basin is characterised by uplift, erosion, continental sedimentation and poly phase, mainly compressional deformation represented by east-west trending folds and thrust faults that probably correspond to a phase of suture tightening associated with terminal continental collision in central Turkey.

5.8 Conclusions

The Upper Cretaceous-Middle Eocene Haymana-Polatlı Basin is an ideal locality to study basin formation and development in a region of plate convergence. New data gathered and interpreted during this study have improved understanding on a number of key processes including the stratigraphic, sedimentary and structural evolution of the basin.

The geodynamic setting of the basin was to the south of a southward-migrating magmatic arc, associated with subduction roll-back which was active from the Upper Cretaceous to the Middle Eocene. Subduction roll-back is a potential trigger for upper plate extension and subsidence associated with the basin's normal faulting phase.

The basin developed on a basement of accretionary material associated with the northward subduction of the northern branch of Neotethys during the Late Cretaceous-Middle Eocene time. The tectonostratigraphic history of the basin can broadly be characterised by two distinct phases: an Upper Cretaceous-Middle Eocene phase where extensional tectonics were dominant (inferred by previous seismic studies), and a post-Middle Eocene phase when compressional tectonics were active (expressed at the surface).

Sedimentary deposition was initiated on a faulted basement unconformity with reworked Upper Cretaceous neritic carbonates (Asmaboğazı Formation). An abrupt basin subsidence permitted the depth of Maastrichtian pelagic sediments, siltstones and siliciclastic turbidites (Haymana Formation). During the Palaeocene, continental facies developed at the basin margins (Kartal Formation), while reworked calcarenites and detached limestone blocks were deposited in the basin depocentre (Dizilitaşlar Formation), possibly derived from a collapsing carbonate platform to the northwest. A probable eustatic sea level rise (Kennett & Stott 1991) was associated with latest Palaeocene-lower Eocene marginal reef and delta development (Kırkkavak Formation). During the Middle Eocene, deep-marine conditions

prevailed in the basin depocentre which developed turbiditic fan-complexes (Yoncalı Formation) while nummulitic banks developed in open shelf settings (Çayraz Formation).

The post-middle Eocene time is characterised by erosion, uplift and continental sedimentation. Structural development included folding and thrust faulting which probably represent final continental collision in central Anatolia.

Chapter 6: A new model of continental collision

6.1 Introduction

The Upper Mesozoic-Lower Cenozoic geotectonic history of Central Anatolia, Turkey, represents one of the world's best examples of an ancient continental collision zone. It is generally accepted that this region comprises a tectonic collage of microcontinents, subduction-accretion complexes, ophiolites and magmatic arcs associated with the closure of the former northern Neotethyan Ocean during Upper Cretaceous-Middle Eocene time. In this region, Neotethyan ocean crust formed by rifting of a passive margin of the Gondwana supercontinent to the south during the Upper Palaeozoi- Early Mesozoic (Robertson & Dixon 1984; Şengör *et al.* 1984; Stampfli 2000; Stampfli & Borel 2002; Mackintosh & Robertson 2008) and subducted northward under the active Eurasian (Pontide) active margin during the Late Mesozoic-Early Cenozoic (Şengör & Yılmaz 1981; Görür *et al.* 1984; Koçyiğit 1991). The vestiges of Neotethyan lithosphere are recorded by the İzmir-Ankara-Erzincan suture zone (İAESZ) (Ketin 1966). The İAESZ is a major lineament that runs approximately east-west through central Turkey and delimits Eurasian tectonic units to the north and microplates associated with Gondwana to the south. It is not a curvilinear feature, but contains several loops and Ω–shapes.

Central Anatolia hosts a number of sedimentary basins (the "Central Anatolian Basins") that hold a critical record of the Upper Cretaceous-Middle Eocene tectono-sedimentary processes associated with regional plate convergence. There are two contrasting types of basin in this region. To the south and east, key localities include the Sivas Basin (Cater *et al.* 1991; Gürsoy *et al.* 1997; Dirik *et al.* 1999; Yılmaz & Yılmaz 2006) and the Ulukışla Basin (Demirtaşlı *et al.* 1984; Clark & Robertson 2002; Alpaslan *et al.* 2004; Alpaslan *et al.* 2006; Kurt *et al.* 2008). These basins are generally envisaged to have developed after Neotethyan ophiolite emplacement onto the southern Gondwana related Anatolide-Tauride Block (Clark & Robertson 2005).

Associated with the İAESZ in the north and west of central Anatolia is a series of Upper Cretaceous-Middle Eocene basins which developed on a variety of

tectonic units including: 1) the Niğde-Kırşehir Massif, an inferred microcontinent, situated between Gondwana to the south and Eurasia to the north; 2) the Eurasian (Pontide) active margin and; 3) accretionary material forming the İAESZ. The basins are ideal for study because they are well-exposed, frequently exhibit complete stratigraphic sequences, are relatively structurally undeformed and have experienced little or no metamorphism. They include the Haymana-Polatlı Basin (Uysal 1959; Yüksel 1970; Sîrel 1975; Gökçen 1976; Ünalan et al. 1976; Gökçen 1978; Ünalan & Yüksel 1978; Meriç & Görür 1979; Gökçen & Kelling 1983; Çetin et al. 1986; Sîrel et al. 1986; Coşkun et al. 1990), the Tuz Gölü Basin (Rigo de Righi & Cortesini 1959; Arikan 1975; Uğurtaş 1975; Görür & Derman 1978; Dellaloğlu & Aksu 1984a; Dellaloğlu & Aksu 1984b; Görür et al. 1984; Gürbüz & Evans 1991; Çemen et al. 1999), the Kırıkkale Basin (Norman 1972; Norman 1973a; Norman 1973b; Akyürek et al. 1984; Akyürek et al. 2001; Delibaş & Genç 2004; Dönmez et al. 2008) and the north-western margin of the Çankırı Basin (Birgili et al. 1975; Norman 1975; Tüysüz & Dellaloğlu 1992; Koçyiğit et al. 1995; Erdoğan et al. 1996; Kaymakcı et al. 2009).

Previous work in these basins has been mostly restricted to local sedimentary and stratigraphic studies, many of which were carried out in the 1970s and 1980s. Few, however, have attempted a regional synthesis. Reviews of the regional significance of the basins are given by Norman *et al.* (1980), Görür *et al.*(1998) and Gürer & Aldanmaz (2002). The basins were selected for study because each contributes a unique insight into tectono-sedimentary processes involved in regional continental collision. The Haymana -Polatlı Basin is located to the west of the Niğde-Kırşehir microcontinent and is constructed on an inferred Palaeo-Tethyan Accretionary Complex. The Tuz Gölü Basin sheds light on sedimentary deposition on the margin of a microcontinent during regional convergence. The Kırıkkale Basin presents the chance to study sedimentation on an accretionary complex which was emplaced against a microcontinent. The Çankırı Basin offers investigation into sedimentary deposits proximal to an active margin.

Based on new sedimentary, stratigraphic, structural, geochemical and palaeontological data, comprehensive tectonostratigraphic developments of each basin have been described in Chapters 2 to 5. The purpose of this chapter is to critically appraise existing models of continental collision in central Turkey, and, if necessary, propose a new one.

6.2 Existing models of continental collision

The Late Mesozoic-Early Cenozoic tectonostratigraphic evolution of the basins is an unresolved question in the Tethyan evolution of Turkey. Presently, there are two alternative end-member tectonic models of basin development during regional plate convergence in central Anatolia. In one model, northern Neotethyan comprised a single ocean basin which sutured in the Late Cretaceous. Following ocean closure, the basins developed on supra-subduction zone (SSZ)-type ophiolites and accretionary prisms which were emplaced onto the northern margin of the Gondwana-related Tauride continent (Göncüoğlu *et al.* 1995; Boztuğ 1998; Gürer & Aldanmaz 2002). In contrast, the other end-member model proposes that northern Neotethyan was palaeogeographically complex, and included the Izmir –Ankara-Erzincan Ocean to the north and the Inner Tauride to the south. Separating the oceanic strands was the Niğde-Kırşehir Massif, a microcontinent rifted from the larger Tauride continent to the south. The basins were accretionary forearc/syn-collisional type and developed above north-dipping subduction zones which persisted until the Middle Eocene time (Görür *et al.* 1984; Koçyiğit 1991; Görür *et al.* 1998; Robertson *et al.* 2009).

6.3 Regional tectonic model

This section is an attempt to establish the regional tectonic setting in which the Central Anatolian Basins evolved. There are presently two contrasting end-member tectonic models. In one end-member model, northern Neotethyan existed as a single ocean basin (the Izmir-Ankara-Erzincan Ocean) which sutured in the Late Cretaceous time following collision between the Tauride Continent to the south and the Pontide margin to the north. In this scenario, supra-subduction zone-type ophiolites and accretionary complexes were thrust southwards over the Niğde-Kırşehir Massif onto the northern margin of the Tauride continent reaching as far south as the Mersin Ophiolite on the Bolkar Dağ Platform. Basin evolution, therefore, evolved in an extensional/transtensional structural environment on over-riding accretionary complexes and ophiolites in a post-collisional setting (e.g. Göncüoğlu *et al.* 1995; Boztuğ 1998; Gürer & Aldanmaz 2002; Kaymakcı *et al.* 2009). This model makes no distinction between the Upper Cretaceous-Middle Eocene central Anatolian basins to the north and west of the Niğde-Kırşehir Massif (i.e. the Central Anatolian Basin Complex as defined by this study, comprising the Tuz Gölü, Kırıkkale, Haymana-Polatlı, and Çankırı Basins) and those to the south (e.g. the Ulukışla and Sivas Basins).

In contrast, the competing end-member model proposes that northern Neotethyan was palaeogeographically complex and consisted of two oceanic strands, the Izmir-Ankara-Erzincan Ocean to the north and the inferred Inner Tauride Ocean to the south (Görür *et al.* 1984; Görür *et al.* 1998; Robertson *et al.* 2009). Situated between the two oceanic strands was the Niğde-Kırşehir Massif, a continental fragment rifted from the larger Tauride continent to the south. In this model the central Anatolian basins evolved in accretionary forearc/syn-collisional-type settings, associated with northward subduction which persisted until the Eocene time when continental collision occurred (Görür *et al.* 1984; Koçyiğit 1991; Koçyiğit *et al.* 2003).

This study proposes a new model of basin formation in which the existence of the Inner Tauride Ocean is accepted, therefore the Niğde-Kırşehir Massif existed as a microcontinent. The inferred Inner Tauride suture is covered by the Upper Cretaceous- Middle Eocene sediments of the Ulukışla Basin, although it is exposed to the east (A. Robertson pers.comm. 2010), however, the following observations are consistent with the existence of the Inner Tauride Ocean:

1) the northern margin of the Tauride continent to the south underwent high-P/low-T metamorphism (Candan *et al.* 2005) which contrasts with the Barrovian metamorphism in the Niğde Massif, which experienced maximum metamorphic conditions of 5–6 kbar, >700°C (Whitney & Dilek 1998);

2) timing of high-grade metamorphism in the Kırşehir Massif is determined at Late Cretaceous (84.1 ± 0.8 Ma), some 50 Ma older than metamorphism in the Menderes Massif to the west (Whitney & Hamilton 2004) which makes models of a continuous Anatolide–Tauride tectonic zone, with the Niğde-Kırşehir Massif as a promontory, unlikely;

3) southward emplacement of SSZ-type ophiolites derived from the Izmir-Ankara-Erzincan onto the Tauride continent requires a thrust transport of >500 km over the Niğde-Kırşehir microcontinent, which seems an extreme distance;

4) the Niğde-Kırşehir Massif and its overlying SSZ-type ophiolitic complexes are intruded by a series of Upper Cretaceous granitoids. In particular, the tectonic setting of the Upper Cretaceous granitoid source melt is a crucial consideration. For some authors, the granitoids are syn- to post-collisional and were generated by crustal thickening following a Late Cretaceous continental collision event as the Pontide margin to the north collided with and over-rid the Anatolide-Tauride margin to the south (Boztuğ 1998; Düzgören-Aydin *et al.* 2001; Köksal *et al.* 2004; Ilbeyli 2005; Köksal *et al.* 2008). However, new stratigraphic and structural data presented in this thesis indicate that regional compression did not occur until the latest Palaeocene - Eocene time. For others workers, the granitoids relate to a northward

subduction of Inner Tauride oceanic crust under the Niğde-Kırşehir Massif (Görür *et al.* 1984; Kadıoğlu *et al.* 2006; Robertson *et al.* 2009). With the exception of the Ağacoren Intrusive Suite, on the western margin of the Niğde-Kırşehir Massif (Kadıoğlu *et al.* 1998) the granitoids form patchy exposures throughout, not an arcuate zone as might be expected from an Andean-type subduction-related magmatic arc. Further, the granitoids form three chemically distinct suites, one of which is a series of highly alkaline syenites, generally interpreted to be indicative of a post-collisional environment (Sylvester 1988). However, evidence from granitoid plutons in the Kırıkkale Basin indicates that granitoids display chemical signatures enriched in fluid-mobile elements and Large Ion Lithophile Elements (e.g. Ba, Th, K) which suggest a close association with arc magmatism and metasomatised mantle. It seems likely therefore, that granitoid emplacement was associated with a north-dipping Inner Tauride subduction zone.

The above discussion leads to the conclusion that two north-dipping subduction zones were active during the latest Cretaceous, one to north of the Niğde-Kırşehir Massif and one to the south (Fig. 6.1). This study proposes a new model to describe the tectonic setting of the Central Anatolian Basins, which is consistent with new data presented in this thesis. Following the initiation of Late Mesozoic northward subduction of northern Neotethyan oceanic lithosphere beneath the active Pontide margin, slab roll-back was initiated (Fig. 6.2a). Roll-back was associated with the formation of a southward retreating intra-oceanic subduction zone triggering the genesis of supra-subduction zone (SSZ)-type ophiolites at 90 – 85 Ma (Floyd *et al.* 2000) (Fig. 6.2b). Roll-back proceeded until the subduction trench collided with the northern margin of the Niğde-Kırşehir Massif. As a result, the ophiolitic complexes (e.g. the Çiçekdağ and Sarıkaraman ophiolites) composed of pelagic sediments, basaltic extrusive rocks, isotropic gabbro, layered gabbro and plagiogranites were thrust southwards onto the Mesozoic/Palaeozoic platform marbles and calc-silicates of the Niğde-Kırşehir Massif, terminating slab roll-back (Yaliniz *et al.* 1996; Yalınız & Göncüoğlu 1998; Yılmaz & Boztuğ 1998; Yalınız *et al.* 2000a; Yalınız *et al.* 2000b). The SSZ-basalts in the Kırıkkale Basin are assumed to be part of this process (Fig. 6.2c).

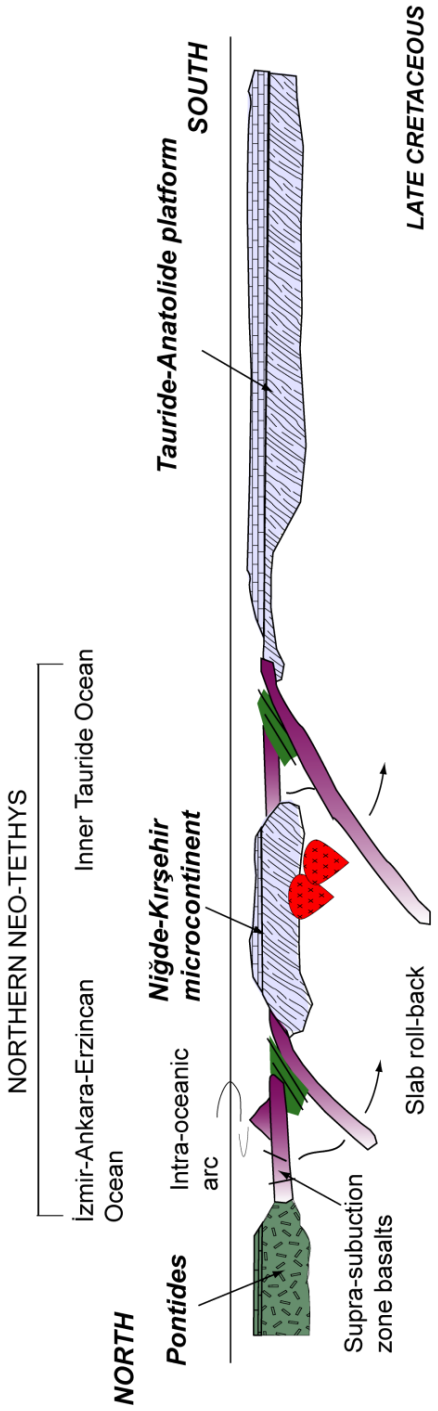

Figure 6.1 Regional cross-section through central Anatolia in the Late Cretaceous time, showing two north-dipping subduction zones. Modified after Robertson *et al.* (2009).

However, to the west of the Niğde -Kırşehir Massif, a window of Neotethyan oceanic lithosphere remained and is represented by the mid ocean-ridge basalts (MORB) in the basement of the Upper Cretaceous-Middle Eocene Kırıkkale Basin (Chapter 2). The window of Neotethyan lithosphere has important consequences for a tectonic reconstruction and relates to the westerly extent of the Inner Tauride Ocean. There is no apparent evidence of two subduction zones west of the Niğde-Kırşehir Massif (Robertson *et al.* 2009). One possibility is that the ocean terminated against a ~N-S transform fault which was situated to the immediate west of the Niğde-Kırşehir Massif.

Subduction of relict MORB continued until the Middle Eocene time under the Galatean Arc complex, situated to the north of the Haymana-Polatlı Basin (Koçyiğit *et al.* 2003). This basin was constructed on the Ankara Mélange and evolved as an accretionary forerac-type basin. The slab of relict MORB forms the basement on which the Tuz Gölü Basin evolved. These tectonic processes mark the incipient stage of Late Cretaceous continental collision in central Anatolia.

Following incipient collision, many studies suggest that a latest Cretaceous extensional phase developed in the Niğde-Kırşehir Massif. This was accompanied by the exhumation of mid-crustal rocks. Crustal extension is based on evidence from extensional shear zones in the Niğde-Kırşehir Massif at the Yozgat Batholith in the north (Isik *et al.* 2008) to the Ağacoren Granitoid in the west (Isik 2009) and the Niğde Massif to the south (Whitney & Dilek 1998).Furthermore, extension is generally accepted as triggering sedimentation in the Tuz Gölü and Haymana basins.

There are several possible explanations that take into account the extensional setting in which the basins developed. In the tectonic model of Görür *et al.* (1984), a transtensional setting was triggered by a 90° anticlockwise rotation of the Niğde-Kırşehir Massif, based on palaeomagnetic data from Sanver & Ponat (1981). However, this palaeomagnetic interpretation is now considered unreliable (see Clark & Robertson (2005)). Another possibility is as follows. After the Late Cretaceous closure of the Inner Tauride Ocean, microcontinental plates moved laterally to

accommodate continuing convergence creating zones of transtension and transpression. This effect has been documented in other suture zones including the closure of the Iapetus Ocean (Soper *et al.* 1992) and the southwest Pacific area (Hall 2002). Crustal extension or transtension is temporally and spatially associated with the intrusion of Upper Cretaceous granitoid plutons into the Niğde-Kırşehir Massif (e.g. Boztuğ & Harlavan 2008). Questions persist over the relationship between pluton emplacement and crustal extension. Specifically, whether pluton emplacement drives extension (e.g. Vanderhaeghe & Teyssier 2001) or if plutons are derived as a result of decompression and extension. Whitney *et al.* (2003) suggest a feedback mechanism for the granitoids of the Niğde-Kırşehir Massif, where extension may have been initially driven by partially molten crust, but further extension subsequently drove pluton emplacement.

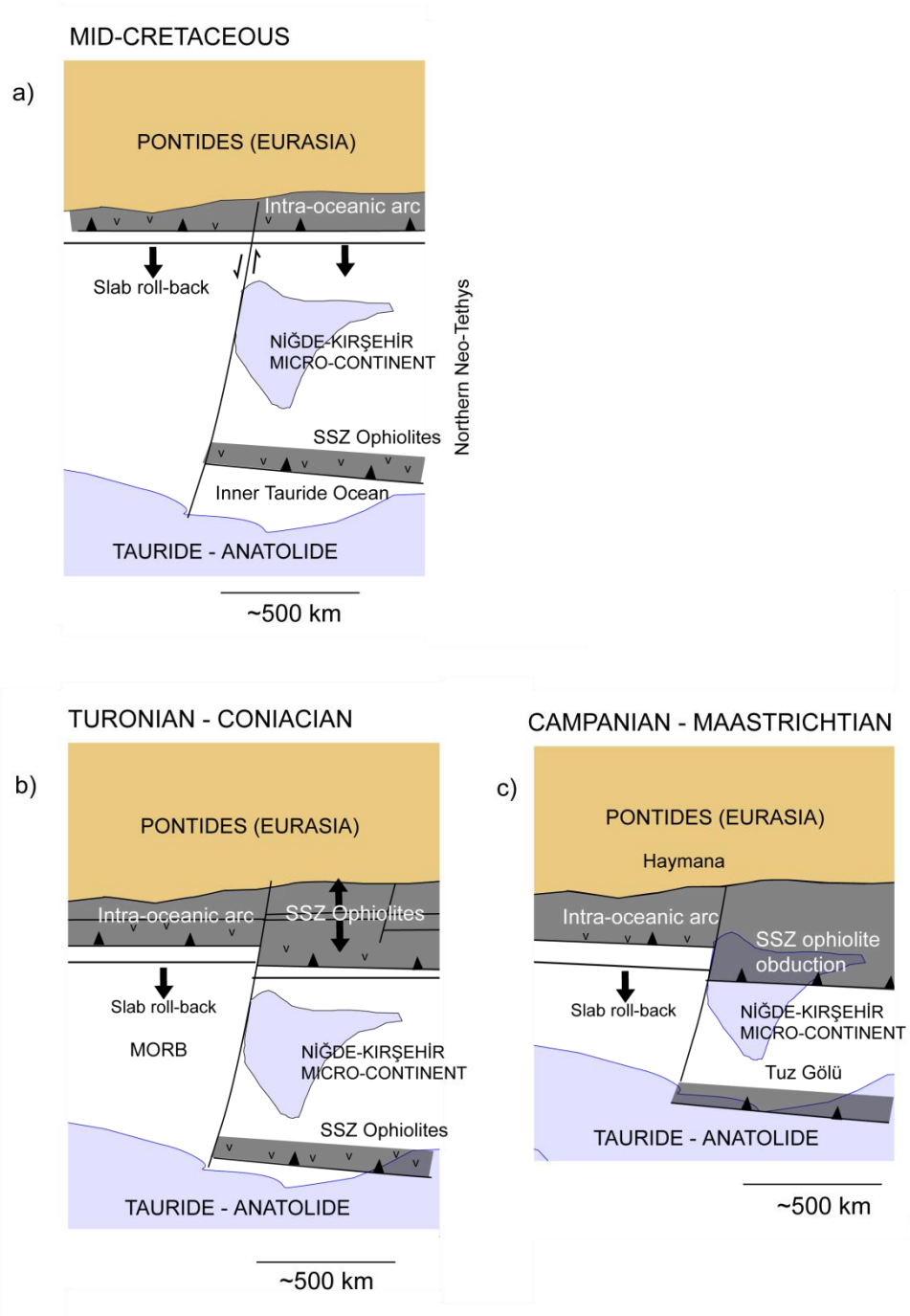

Figure 6.2 Tectonic sketches of the new model of collision proposed by this study featuring two northward-dipping subduction zones, **(a)** During the Mid-Cretaceous, intra-oceanic subduction initiated outboard of the Pontide active margin in the Izmir – Ankara – Erzincan Ocean to the north. To the south, northward subduction consumed the Inner Tauride Ocean and generated SSZ-type ophiolites, **(b)** Slab roll-back triggered the genesis of SSZ-type ophiolites to the north during the Turonian – Santonian time, **(c)** During the Campanian – Maastrichtian time, SSZ-type ophiolites obducted onto the Niğde – Kırşehir Massif. To the west of the Niğde – Kırşehir Massif, subduction continued and the Tuz Gölü Basin formed on relict MORB-type oceanic crust above a north-dipping subduction zone.

During the Palaeocene-Middle Eocene, to the west of the Niğde-Kırşehir Massif, slab roll-back and northward subduction of relict MORB oceanic crust continued under a magmatic arc. Behind the arc (i.e. to the north) calc-alkaline and alkaline magmatism in an extensional SSZ-type setting occurred (Koçyiğit *et al.* 2003). To the south of the arc, volcaniclastic sediments shed south/south-eastwards into the Tuz Gölü Basin (Bala and Kulu localities). Further regional convergence, folding, strike-slip faulting and surface uplift occurred in the Kırıkkale Basin to the north, but were delayed until Middle Eocene time in the Tuz Gölü and Haymana basins. This is consistent with the structural deformation history of the Tuz Gölü Basin. During this period, extensive thrusting and basin margin-parallel folding occurred, while extensional faults were reactivated as strike-slip faults.

In the Eocene-Oligocene time (Fig. 6.3), final continental collision eliminated the last vestiges of Neotethyan ocean crust. To the north, the Niğde-Kırşehir Massif drifted northward and indented into the Pontide margin giving the Izmir-Ankara suture zone its characteristic Ω-shape and causing intense compressional and transcurrent deformation. The rims of the northern Çankırı Basin reacted by retreating from the zone of maximum compression. Palaeomagnetic data in fine-grained sediments (Kaymakcı *et al.* 2003) suggest an anticlockwise rotation of the Çankırı Basin to the west of the Niğde-Kırşehir Massif by up to 33°, and to the east, a clockwise rotation of up to 52° and local anticlockwise rotation of 36°. the west of the indenter and northeast-southwest to the west. To the west of the Niğde-Kırşehir Massif, the Izmir-Ankara Accretionary Complex over-rid the northwest margin of the Tuz Gölü Basin (Görür *et al.* 1984). In this area, compression was aligned west-northwest – south-southeast as the Izmir-Ankara suture tightened and experienced extensive thrust faulting. This is in agreement with new palaeostress data presented in this study as compression triggered dominantly left-lateral faulting on the eastern margin of the Tuz Gölü Basin. These events correspond to a final continental collision phase which sutured central Anatolia into its present tectonic mosaic. In summary, collision in central Anatolia occurred, not as a gradual process, rather as a sequence of defined steps: 1) Late Cretaceous incipient collision as SSZ-type

ophiolites obducted onto the Niğde-Kırşehir Massif; 2) a prolonged period (Late Cretaceous-Palaeocene/Early Eocene) of microplate adjustment leading to regional extension or transtension in which the Tuz Gölü and Haymana basins started their development; 3) final continental collision occurred in the Eocene-Oligocene characterised by extensive thrusting, transcurrent faulting, surface uplift and indentation tectonics.

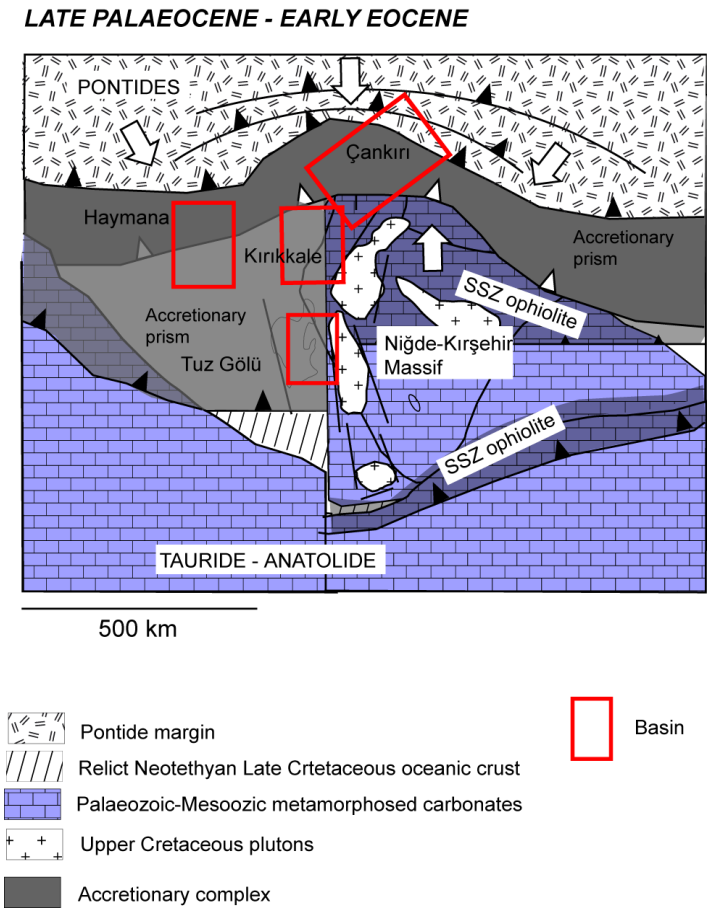

Figure 6.3 Tectonic sketch of central Anatolia during the Eocene – Oligocene time. The northern area is based on Kaymakcı *et al*. (2003). The Tuz Gölü Basin area is based on this study.

References

Ajaji, T., Weis, D., Giret, A., and Bouabdellah, M., 1998. Coeval potassic and sodic calc-alkaline series in the post-collisional Hercynian Tanncherfi intrusive complex, northeastern Morocco: geochemical, isotopic and geochronological evidence. *Lithos,* **45**, 371-393.

Akgün, F., Akay, E., and Erdoğan, B., 2002. Tertiary Terrestrial to Shallow Marine Deposition in Central Anatolia: A Palynological Approach. *Turkish Journal of Earth Sciences,* **11**, 127-160.

Akıman, O., Erler, A., Göncüoğlu, M. C., Güleç, N., Geven, A., Türel, T. K., and Kadioğlu, Y. K., 1993. Geochemical characteristics of granitoids along the western margin of the Central Anatolian Crystalline Complex and their tectonic implications. *Geological Journal,* **28**, 371-382.

Akıncı, Ö. T., 1984. The Eastern Pontide volcano-sedimentary belt and associated massive sulphide deposits. In: Robertson, A. H. F. and Dixon, J. E. (Eds.) *The Geological Evolution of the Eastern Mediterranean*. Geological Society, London, Special Publications, **17**, 415–428.

Akkuş, M. F., 1962. Geology and petroleum possibilities of the northern part of İskilip. *MTA Report No. 5084*.

Akyürek, B., Bilginer, E., Akbaş, B., Hepşen, N., Pehlivan, Ş., Sunu, O., Soysal, Y., Dağer, Z., Çatal, E., Sözeri, Z., Yıldırım, H., and Hakyemez, Y., 1984. The geology of the Ankara-Elmadağ-Kalecik region. *Jeoloji Mühendisliği Dergisi,* **20**, 31-46.

Akyürek, B., Özata, A., Toprak, S., Afşin, Ö., Çetin, N. İ., San, B. T., Aydın, A., Çıplak, R., and Yiğit, E., 2001. Kırıkkale-Kalecik (Ankara) Arasının Jeolojisi. *MTA Report No. 10407*.

Aldanmaz, E., Yaliniz, M. K., Güctekin, A., and Göncüoğlu, M. C., 2008. Geochemical characteristics of mafic lavas from the Neotethyan ophiolites in western Turkey: implications for heterogeneous source contribution during variable stages of ocean crust generation. *Geological Magazine,* **145**, 37-54.

Alpaslan, M., Boztug, D., Frei, R., Temel, A., and Kurt, M. A., 2006. Geochemical and Pb-Sr-Nd isotopic composition of the ultrapotassic volcanic rocks from the extension-related ÇamardI-UlukIsla basin, Nigde Province, Central Anatolia, Turkey. *Journal of Asian Earth Sciences,* **27**, 613-627.

Alpaslan, M., Frei, R., Boztuğ, D., Kurt, M. A., and Temel, A., 2004. Geochemical and Pb–Sr–Nd isotopic constraints for an enriched-mantle source for the late cretaceous to early tertiary volcanism in the Çamardı-Ulukışla basin Niğde province, central Anatolia, Turkey. *International Geology Revivew*, 1022–1041.

Altunkaynak, A., 2007. Collision-Driven Slab Breakoff Magmatism in Northwestern Anatolia, Turkey. *The Journal of Geology*, **115**, 63-82.

Altunsoy, M., Ozcelik, O., and Yalcin Erik, N., 2004. Organic geochemical characteristics of the bituminous Eocene units in the Corum-Suluova Basin, Central Anatolia, Turkey. *Petroleum Geoscience,* **10**, 163-171.

Andrew, T. and Robertson, A. H. F., 2002. The Beysehir-Hoyran-Hadim Nappes: genesis and emplacement of Mesozoic marginal and oceanic units of the northern Neotethys in southern Turkey. *Journal of the Geological Society,* **159**, 529-543.

Angelier, J., 1979. Determination of the mean principal directions of stresses for a given fault population. *Tectonophysics,* **56**, T17-T26.

Angelier, J. and Mechler, P., 1977. Sur une méthode graphique de recherche des contraintes principales également utilisable en tectonique et enséismologie: la methode des diédres droits. *Bull. Soc. Géol. France,* **VII**, 1309-1318.

Aqrawi, A. A. M., Thehni, G. A., Sherwani, G. H., and Kareem, B. M. A., 1998. Mid-Cretaceous rudist-bearing carbonates of the Mishrif Formation: an important reservoir sequence int he Mesopotamian Basin, Iraq. *Journal of Petroleum Geology,* **21**, 57-82.

Arikan, Y., 1975. The Geology and Petroleum prospects of the Tuzgölü basin. *Maden Tektik ve Arama Dergisi,* **85**, 17-38.

Atabey, E., 1996. The development of Nummulites Banks within the Compressional Tectonically Controlled Tertiary Basin of Gürün Autochthone, Eastern Taurus, SW Sivas (Turkey). *Turkish Journal of Earth Sciences,* **5**, 99-108.

Ateş, A., Bilim, F., and Buyuksarac, A., 2005. Curie Point Depth Investigation of Central Anatolia, Turkey. *Pure and Applied Geophysics,* **162**, 357-371.

Ayan, T., 1969. Petroleum possibilities of the Çankırı-Yerköy basins. *TPAO Report No. 469,* 101 pp.

Aydemir, A., 2008. Hydrocarbon potential of the Tuzgolu (Salt Lake) Basin, Central Anatolia, Turkey: A comparison of geophysical investigation results with the geochemical data. *Journal of Petroleum Science and Engineering,* **61**, 33-47.

---, 2009. Tectonic investigation of Central Anatolia, Turkey, using geophysical data. *Journal of Applied Geophysics,* **68**, 321-334.

Aydemir, A. and Ateş, A., 2005. Preliminary evaluation of Central Anatolian basins in Turkey using the gravity & magnetic data. *Journal of the Balkan Geophysical Society,* **8**, 7-19.

---, 2006. Structural interpretation of the Tüzgölu and Haymana Basins, Central Anatolia, Turkey, using seismic, gravity and aeromagnetic data. *Earth Planets Space,* **58**, 951-961.

---, 2008. Determination of hydrocarbon prospective areas in the Tuzgolu (Saltlake) Basin, central Anatolia, by using geophysical data. *Journal of Petroleum Science and Engineering,* **62**, 36-44.

Aydin, F., Karsli, O., and Sadiklar, M. B., 2003. Mineralogy and Chemistry of Biotites from Eastern Pontide Granitoid Rocks, NE-Turkey: Some Petrological Implications for Granitoid Magmas. *Chemie der Erde - Geochemistry,* **63**, 163-182.

Aydin, İ., Aydoğan, M. S., Oksum, E., and Koçak, A., 2006. An attempt to use aerial gamma-ray spectrometry results in petrochemical assessments of the volcanic and plutonic associations of Central Anatolia (Turkey). *Geophysical Journal International,* **167**, 1044-1052.

Aydin, N. S., Göncüoğlu, M. C., and Erler, A., 1998. Latest Cretaceous Magmatism in the Central Anatolian Crystalline Complex: Review of Field, Petrographic and Geochemical Features. *Turkish Journal of Earth Sciences,* **7**, 259-268.

Aydin, S. N. and Önen, A. P., 1999. Field, Petrographic and Geochemical Features of the Baranadağ Quartz Monzonite of the Central Anatolian Granitoids, Turkey. *Turkish Journal of Earth Sciences,* **8**, 113-123.

Ayyıldız, T., 2006. Hydrocarbon potential of the Karapinaryaylasi Formation (Paleocene–Eocene) source rock in the Tuz Gölü Basin, central Anatolia, Turkey *Petroleum Geoscience,* **12**, 41-48.

Azız, A., 1975. İskilip civarı ile güney ve güneybatısının detay jeolojisi ve petrol olanakları. *MTA Report No. 6132*.

Baas, J. H., 2004. Conditions for formation of massive turbiditic sandstones by primary depositional processes. *Sedimentary Geology,* **166**, 293-310.

Bailey, B. B. and MacCallien, W. J., 1950. The Ankara Melange and the Anatolian Thrust. *Maden Tektik ve Arama Dergisi,* **40**, 17-23.

Barbarin, B., 1999. A review of the relationships between granitoid types, their origins and their geodynamic environments. *Lithos,* **46**, 605-626.

Batchelor, R. A. and Bowden, P., 1985. Petrogenetic interpretation of granitoid rock series using multicationic parameters. *Chemical Geology,* **48**, 43-55.

Bayhan, E. and Gökçen, S. L., 1990. 'Ankara Virgasyonu' Üst Kretase - Alt Tersiyer havzalarinin petrolojik karşi-laştirilmasi. *Maden Tektik ve Arama Dergisi,* **111**, 101-110.

Beccaletto, L., Bartolini, A. C., Martini, R., Hochuli, P. A., and Kozur, H., 2005. Biostratigraphic data from the Çetmi Melange, northwest Turkey: Palaeogeographic and tectonic implications. *Palaeogeography, Palaeoclimatology, Palaeoecology,* **221**, 215-244.

Birgili, Ş., Yoldaş, R., and Ünalan, G., 1975. Preliminary report of the geology and petroleum possibilities of the Çankırı–Çorum Basin. *TPAO Report No. 1216*, 98 pp.

Bockelie, J. F., 1991. Ichnofabric Mapping and Interpretation of Jurassic Reservoir Rocks of the Norwegian North Sea. *PALAIOS,* **6**, 206-215.

Bonin, B., 2004. Do coeval mafic and felsic magmas in post-collisional to within-plate regimes necessarily imply two contrasting, mantle and crustal, sources? A review. *Lithos,* **78**, 1-24.

Bonin, B., Azzouni-Sekkal, A., Bussy, F., and Ferrag, S., 1998. Alkali-calcic and alkaline post-orogenic (PO) granite magmatism: petrologic constraints and geodynamic settings. *Lithos,* **45**, 45-70.

Bosellini, F., 1998. Diversity, composition and structure of Late Eocene shelf-edge coral associations (Nago Limestone, Northern Italy). *Facies,* **39**, 203-225.

Bouma, A. H., 1962. *Sedimentology of some flysch deposits: a graphic approach to facies interpretation.* Elvsier, Amsterdam.168 pp

Bozkurt, E., 2001. Neotectonics of Turkey - a synthesis. *Geodinamica Acta*, **14**, 3-30.

Boztuğ, D., 1998. Post–Collisional Central Anatolian Alkaline Plutonism, Turkey. *Turkish Journal of Earth Sciences,* **7**, 145-165.

---, 2000. S-I-A-type Intrusive Associations: Geodynamic Significance of Synchronism Between Metamorphism and Magmatism in Central Anatolia, Turkey. In: Bozkurt, E., Winchester, J. A., and Piper, J. D. A. (Eds.) *Tectonics and Magmatism in Turkey and the Surrounding Area*. Geological Society, London, Special Publications, **173**, 441-458

Boztuğ, D. and Arehart, G. B., 2007. Oxygen and sulfur isotope geochemistry revealing a significant crustal signature in the genesis of the post-collisional granitoids in central Anatolia, Turkey. *Journal of Asian Earth Sciences,* **30**, 403-416.

Boztuğ, D., Arehart, G. B., Platevoet, B., Harlavan, Y., and Bonin, B., 2007a. High-K, calc-alkaline I-type granitoids from the composite Yozgat batholith generated in a post-collisional setting following continent-oceanic island arc collision in central Anatolia, Turkey. *Mineralogy and Petrology,* **91**, 191–223.

Boztuğ, D. and Harlavan, Y., 2008. K–Ar ages of granitoids unravel the stages of Neo-Tethyan convergence in the eastern Pontides and central Anatolia, Turkey. *International Journal of Earth Sciences,* **97**, 585-599.

Boztuğ, D. and Jonckheere, R. C., 2007. Apatite fission track data from central Anatolian granitoids (Turkey): Constraints on Neo-Tethyan closure. *Tectonics,* **26**.

Boztuğ, D., Jonckheere, R. C., Heizler, M., Ratschbacher, L., Harlavan, Y., and Tichomirova, M., 2009a. Timing of post-obduction granitoids from intrusion

through cooling to exhumation in central Anatolia, Turkey. *Tectonophysics,* **473**, 223-233.

---, 2009b. Timing of post-obduction granitoids from intrusion through cooling to exhumation in central Anatolia, Turkey. *Tectonophysics,* **473**, 223-233.

Boztuğ, D., Temiz, H., Jonckheere, R. C., and Ratschbacher, L., 2008. Punctuated Exhumation and Foreland Basin Formation and Infilling in (Circum)–Central Anatolia (Turkey) Associated with the Neo-Tethyan Closure. *Turkish Journal of Earth Sciences,* **17**, 673-684.

Boztuğ, D., Tichomirowa, M., and Bombach, K., 2007b. 207Pb-206Pb single-zircon evaporation ages of some granitoid rocks reveal continent-oceanic island arc collision during the Cretaceous geodynamic evolution of the central Anatolian crust, Turkey. *Journal of Asian Earth Sciences,* **31**, 71-86.

Bragin, N. and Tekin, U. K., 1996. Age of radiolarian-chert blocks from the Senonian Ophiolitic Mélange (Ankara, Turkey). *Island Arc,* **5**, 114-122.

Bullard, E. C., Everett, J. E., and Smith, A. G., 1965. Fit of continents around the Atlantic. In: Blackett, P. M. S., Bullard, E. C., and Rucorn, S. A. (Eds.) *A symposium on continental drift*. Philosophical Transactions of the Royal Society of London, Series A, **258**, 41-75

Burke, K., 1988. Tectonic evolution of the Caribbean. *Annual review of earth and planetary sciences,* **16**, 201-230.

Burke, K., Dewey, J. F., and Kidd, W. S. F., 1976. Precambrian palaeomagnetic results compatible with contemporary operation of the Wilson cycle. *Tectonophysics,* **33**, 287-299.

Byerlee, J., 1978. Friction of rocks. *Pure and Applied Geophysics,* **116**, 615-626.

Candan, O., Çetinkaplan, M., Oberhänsli, R., Rimmelé, G., and Akal, C., 2005. Alpine high-P/low-T metamorphism of the Afyon Zone and implications for the metamorphic evolution of Western Anatolia, Turkey. *Lithos,* **84**, 102-124.

Cater, J. M. L., Hanna, S. S., Ries, A. C., and Turner, P., 1991. Tertiary evolution of the Sivas Basin, central Turkey. *Tectonophysics,* **195**, 29-46.

Çemen, I., Göncüoğlu, M. C., and Dirik, K., 1999. Structural Evolution of the Tuzgölü Basin in Central Anatolia, Turkey. *Journal of Geology,* **107**, 693-706.

Çetin, H., Demirel, I. H., and Gökçen, S. L., 1986. Haymana (Sw Ankara) doğusu ve batısındaki Üst Kretase-Alt Tersiyer istifinin sedimantolojik ve sedimanter petrolojik incelenmesi. *Bulletin of the Geological Society of Turkey,* **29**, 21-33.

Chappell, B. W., 1984. Source rocks of I- and S-type granites in the Lachlan Fold Belt, southeastern Australia. *Philosophical Transactions of the Royal Society of London. Series A, Mathematical and Physical Sciences,* **310**, 693-707.

---, 1999. Aluminium saturation in I- and S-type granites and the characterization of fractionated haplogranites. *Lithos,* **46**, 535-551.

Chappell, B. W. and White, A. J. R., 1974. Two contrasting granite types. *Pacific Geology,* **8**, 173-174.

Charlton, T. R., 2000. Tertiary evolution of the Eastern Indonesia Collision Complex. *Journal of Asian Earth Sciences,* **18**, 603-631.

Chen, F., Siebel, W., Satir, M., Terzioğlu, M., and Saka, K., 2002. Geochronology of the Karadere basement (NW Turkey) and implications for the geological evolution of the Istanbul zone. *International Journal of Earth Sciences,* **91**, 469-481.

Çiner, A., Deynoux, M., and Kosun, E., 1996a. Cyclicity in the Middle Eocene Tamak turbidite complex of the Haymana basin, Central Anatolia, Turkey. *International Journal of Earth Sciences (Geol Rundsch),* **85**, 669 - 682.

---, 1996b. Cyclicity in the Midle Eocene Yamak turbidite complex of the Hayman basin, Central Anatolia, Turkey. *International Journal of Earth Sciences (Geol Rundsch)*, **85**, 669-682.

Çiner, A., Deynoux, M., Ricou, S., and Kosun, E., 1996c. Cyclicity in the Middle Eocene Çayraz Carbonate Formation, Haymana Basin, Central Anatolia, Turkey. *Palaeogeography, Palaeoclimatology, Palaeoecology*, **121**, 313-329.

Clark, M. and Robertson, A. H. F., 2002. The role of the Early Tertiary Ulukışla Basin, southern Turkey, in suturing of the Mesozoic Tethys ocean. *Journal of the Geological Society*, **159**, 673-690.

---, 2005. Uppermost Cretaceous-Lower Tertiary UlukIsla Basin, south-central Turkey: sedimentary evolution of part of a unified basin complex within an evolving Neotethyan suture zone. *Sedimentary Geology*, **173**, 15-51.

Clemens, J. D., 2003. S-type granitic magmas--petrogenetic issues, models and evidence. *Earth-Science Reviews*, **61**, 1-18.

Çoban, H., 2007. Basalt magma genesis and fractionation in collision- and extension-related provinces: A comparison between eastern, central and western Anatolia. *Earth-Science Reviews*, **80**, 219-238.

Collins, W. J., 2002. Hot orogens, tectonic switching, and creation of continental crust. *Geology*, **30**, 535-538.

Collins, W. J. and Richards, S. W., 2008. Geodynamic significance of S-type granites in circum-Pacific orogens. *Geology*, **36**, 559-562.

Collinson, J. D., 1986. Alluvial sediments. In: Reading, H. G. (Eds.) *Sedimentary environments and facies*. Blackwell Scientific Publications, Oxford

Collinson, J. D. and Thompson, D. B., 1989. *Sedimentary structures*. Unwin Hyman Ltd, London

Cook, H. E., McDaniel, E., Mountjoy, E. W., and Pray, L. C., 1972. Allochthonous carbonate debris flows at Devonian bank ('reef') margins Alberta, Canada. *Bull. Can. Pet. Geol*, **20**, 439-497.

Corrigan, D., Pehrsson, S., Wodicka, N., and de Kemp, E., 2009. The Palaeoproterozoic Trans-Hudson Orogen: a prototype of modern accretionary processes. *Geological Society, London, Special Publications*, **327**, 457-479.

Coskun, B., 2004. Aksaray and Ecemis Faults–Diapiric Salt Relationships: relevance to the hydrocarbon exploration in the Tuz Golu (Salt Lake) Basin, Central Anatolia, Turkey. *Energy Sources*, **26**, 1005-1022.

Coşkun, B., Özdemir, A., and Işık, V., 1990. Oil possibilities of the region between Hayman - Mandıra - Dereköy Towns. *TAPG Bulletin*, **2/1**, 135-143.

Curray, J. R., 1989. The Sunda Arc: A model for oblique plate convergence. *Netherlands Journal of Sea Research*, **24**, 131-140.

Davis, G. H. and Reynolds, S. J., 1996. *Structural geology of rocks and regions*. John Wiley and sons, New York.776 pp

de La Roche, H., Leterrier, J., Grandclaude, P., and Marchal, M., 1980. A classification of volcanic and plutonic rocks using the R1-R2 diagram and major element analyses. Its relationships with current nomenclature. *Chemical Geology*, **29**, 183-210.

Debon, F. and Le Fort, P., 1982. A chemical-mineralogical classification of common plutonic rocks and associations. *Transactions of the Royal Society of Edinburgh: Earth Sciences*, **73**, 135-149.

Defant, M. J. and Drummond, M. S., 1990. Derivation of some modern arc magmas by melting of young subducted lithosphere. *Nature*, **347**, 662-665.

Delibaş, O. and Genç, Y., 2004. Origin and Formation Processes of Iron, Copper-Molybdenum and Lead Mineralisations of Karacaali (Kırıkkale) Magmatic Complex. *Türkiye Jeoloji Kurumu Bülteni*, **47**, 47-60.

Dellaloğlu, A. and Aksu, R., 1984a. Haymana - Tuz Gölü Kaya Stratigrfi Birimleri. *TPAO Report No. 2006*.

---, 1984b. Kulu-Şereflikoçhisar- Aksaray dolayinin jeolojisi ve petrol olanaklari. *TPAO rep. no. 2020.*

Dellaloğlu, A., Tüysüz, O., Kaya, O. H., and Harput, B., 1992. Kalecik (Ankara)-Eldivan-Yapraklı (Çankırı)-İskilip (Çorum) ve Devrez Çayı arasindaki alanın jeolojisi ve petrol olanakları. *TPAO Report No. 3194*.

Demirtaşlı, E., Turhan, N., Bilgin, A. Z., and Selim, M., 1984. Geology of the Bolkar Mountains. In: Tekili, O. and Göncüoğlu, M. (Eds.) *Geology of the Taurus Belt, Proc. Internat. Symp.* Mineral Research and Exploration Institute of Turkey (MTA), Ankara, Turkey, 125-141

DePaolo, D. J., 1981. Trace element and isotopic effects of combined wallrock assimilation and fractional crystallization. *Earth and Planetary Science Letters*, **53**, 189-202.

Dercourt, J., Zonenschain, L. P., Ricou, L. E., Kazmin, V. G., Le Pichon, X., Knipper, A. L., Grandjacquet, C., Sbortshikov, I. M., Geyssant, J., Lepvrier, C., Pechersky, D. H., Boulin, J., Sibvet, J.-C., Savostin, L. A., Sorokhtin, O., Westphal, M., Bazhenov, M. L., Lauer, J. P., and Biju-Duval, B., 1986. Geological evolution of the Tethys belt from the Atlantic to the Pamirs since the Lias. *Tectonophysics*, **123**, 214-315.

Derman, A. S. and Engin, M. A., 2007. Tuzgölü (Koçhisar-Aksaray) Fay Zonunun Yeraltı ve Yerüstü Verileri Yardımıyla Karakterinin Belirlenmesi ve Basen Evrimine Katkısı *60th Geological Congress of Turkey*, Ankara.

Derman, A. S., Rojay, B., Güney, H., and Yıldız, M., 2000. New sedimentological data on the evolution of Şereflikoçhisar-Aksaray fault zone. In: Haymana-Tuzgölü-Ulukışla Basins Workshop. *TAPG Special Publication*, **5**, 47-70.

Dewey, J. F. and Şengör, A. M. C., 1979. Aegean and the surrounding regions: Complex multiplate and continuum tectonics in a convergent zone. *Geological Society of America Bulletin*, **90**, 84-92.

Deynoux, M., Çiner, A., Monod, O., KarabIyIkoglu, M., Manatschal, G., and Tuzcu, S., 2005. Facies architecture and depositional evolution of alluvial fan to fan-delta complexes in the tectonically active Miocene Köprüçay Basin, Isparta Angle, Turkey. *Sedimentary Geology*, **173**, 315-343.

Dickinson, W. R., 1970. Interpreting detrital modes of graywacke and arkose. *Journal of Sedimentary Petrology*, **40**, 695-707.

---, 1985. Interpreting provenance relations from detrital modes of sandstones. In: Zuffa, G. G. (Eds.) *Provenance of arenites*. Reidel, Dordrect333-361

Dickinson, W. R., Beard, L. S., Brakenridge, G. R., Erjavec, J. L., Ferguson, R. C., Inman, K. F., Knepp, R. A., Lindberg, F. A., and Ryberg, P. T., 1983. Provenance of North American Phanerozoic sandstones in relation to tectonic setting. *Geological Society of America Bulletin*, **94**, 222-235.

Dickinson, W. R. and Seely, D. R., 1979. Structure and Stratigraphy of Forearc Regions. *AAPG Bulletin*, **63**, 2-31.

Dickinson, W. R. and Suczek, C. A., 1979. Plate tectonics and Sandstone Compositions. *The American Association of Petroleum Geologists Bulletin*, **63**, 2164-2182.

Dilek, Y., 2006. Collision tectonics of the Mediterranean region: Causes and consequences. In: Dilek, Y. and Pavlides, S. (Eds.) *Postcollisional tectonics and magmatism in the Mediterranean region and Asia*. Geological Society of America Special Paper, **409**, 1-13

Dilek, Y. and Thy, P., 2006. Age and petrogenesis of palgiogranite intrusions in the Ankara mélange, central Turkey. *Island Arc*, **15**, 44-57.

Dirik, K., 2001. Neotectonic evolution of the northwestward arched segment of the Central Anatolian Fault Zone, Central Anatolia, Turkey. *Geodinamica Acta*, **14**, 147-158.

Dırık, K. and Göncüoğlu, M. C., 1996. Neotectonic Characteristics of central Anatolia. *International Geology Review*, **38**, 807-817.

Dirik, K., Göncüoğlu, M. C., and Kozlu, H., 1999. Stratigraphy and pre-Miocene tectonic evolution of the southwestern part of the Sivas Basin, Central Anatolia, Turkey. *Geological Journal*, **34**, 303-319.

Doglioni, C., Harabaglia, G., Martinelli, F., Mongelli, F., and Zito, G., 1996. A geodynamic model of the Southern Apennines. *Terra Nova*, **8**, 540-547.

Dominguez, S., Lallemand, S. E., Malavieille, J., and von Huene, R., 1998. Upper plate deformation associated with seamount subduction. *Tectonophysics*, **293**, 207-224.

Dönmez, M., Akçay, A. E., Kara, H., Yergök, A. F., and Esentürk, K., 2008. *Türkiye jeoloji haritalari No.90 Kırşehir - İ30 Paftasi, 1:100 000*. Maden Tektik ve Arama Genel Müdürlüğü (General Directorate of Mineral Research and Exploration), Ankarapp

Drummond, M. S. and Defant, M. J., 1990. A Model for Trondhjemite-Tonalite-Dacite Genesis and Crustal Growth via Slab Melting: Archaen to Moderm Comparisons. *Journal of Geophysical Research*, **95**, 21503-21521.

Duru, M. and Gökçen, N., 1985. Polatı (GB Ankara) güneyi Alt Paleojen'in beşyeni türü kapsayan ostrakod faunası ve stratigrafik yorumu. *Bulletin of the Geological Society of Turkey*, **28**, 147 - 157.

---, 1990. Polatlı (GB Ankara) Güneyi Monsiyen-Küiziyen Istifinin ostrakod biyostratigrafisi ve ortamsal yorumu. *Maden Tektik ve Arama Dergisi*, **110**
165-174.

Düzgören-Aydin, N. S., Malpas, J., Göncüoğlu, M. C., and Erler, A., 2001. A Review of Magmatism in Central Anatolia during the Mesozoic Post-Collisional Period. *International Geology Review*, **43**, 695-710.

Erdoğan, B., Akay, E., and Sirin Ugur, M., 1996. Geology of the Yozgat Region and Evolution of the Collisional Cankiri Basin *International Geology Review*, **38**, 788-806

Ergün, M. and Sari, C., 1982. Methods of data analysis in gravity and magnetics and the interpretation of Ankara - Polatlı region. *Bulletin of the Geological Society of Turkey*, **25**, 137-142.

Erkan, Y., 1981. Result of the studies on the metamorphism of the Central Anatolian Massif. In: Akkök, R., Oygur, V., and Terlemez, I. (Eds.) *Proceedings of Symposium on Geology of Central Anatolia*. Türkiye Jeoloji Kurumu, Ankara

Erler, A. and Göncüoğlu, M. C., 1996. Geologic and Tectonic Setting of the Yozgat Batholith, Northern Central Anatolian Crystalline Complex, Turkey. *International Geology Review*, **38**, 714-726.

Erünal, L., 1942. Sivrihisar-Polatlı mıntakasının Paleosen faunası. *Maden Tektik ve Arama Dergisi*, **26**, 126-133.

Fayon, A. K. and Whitney, D. L., 2007. Interpretation of tectonic versus magmatic processes for resetting apatite fission track ages in the Niğde Massif, Turkey. *Tectonophysics*, **434**, 1-13.

Fayon, A. K., Whitney, D. L., Teyssier, C., Garver, J. I., and Dilek, Y., 2001. Effects of plate convergence obliquity on timing and mechanisms of exhumation of a mid-crustal terrain, the Central Anatolian Crystalline Complex. *Earth and Planetary Science Letters*, **192**, 191-205.

Fitton, J. G., Saunders, A. D., Hardarson, B. S., and Norry, M. S., 1998. Volcanic rocks of the southeastern Greenland margin. In: Saunders, A. D., Larsen, H. C., and Wise, S. W. (Eds.) *Proceedings of the Ocean Drilling Program, Scientific Results, 152*. Ocean Drilling Program, TX, 331-350

Floyd, P. A., Göncüoğlu, M. C., Winchester, J. A., and Yaliniz, M. K., 2000. Geochemical Character and Tectonic Environment of Neotethyan Ophiolitic Fragments and

Metabasites in the Central Anatolian Crystalline Complex, Turkey. In: Bozkurt, E., Winchester, J. A., and Piper, J. D. A. (Eds.) *Tectonics and Magmatism in Turkey and the Surrounding Area*. Geological Society, London, Special Publications, **173**, 183-202

Floyd, P. A., Göncüoğlu, M. C., Yalınız, M. K., and Parlak, O., 1998a. Geochemical overview and relations of metabasites from the Central Anatolian Crystalline Complex*Proceedings of the Third International Turkish Geology Symposium, METU-Ankara, Abstracts*.

Floyd, P. A., Yaliniz, M. K., and Göncüoğlu, M. C., 1998b. Geochemistry and petrogenesis of intrusive and extrusive ophiolitic plagiogranites, Central Anatolian Crystalline Complex, Turkey. *Lithos*, **42**, 225-241.

Flügel, E., 2004. *Microfacies Analyses of Limestones*. Berlin-Heidelberg, New York.976 pp

Förster, H.-J., Tischendorf, G., and Trumbull, R. B., 1997. An evaluation of the Rb vs. (Y + Nb) discrimination diagram to infer tectonic setting of silicic igneous rocks. *Lithos*, **40**, 261-293.

Frost, B. R., Barnes, C. G., Collins, W. J., Arculus, R. J., Ellis, D. J., and Frost, C. D., 2001. A Geochemical Classification for Granitic Rocks. *Journal of Petrology*, **42**, 2033-2048.

Gani, M. R. and Bhattacharya, J. P., 2007. Basic Building Blocks and Process Variability of a Cretaceous Delta: Internal Facies Architecture Reveals a More Dynamic Interaction of River, Wave, and Tidal Processes Than Is Indicated by External Shape. *Journal of Sedimentary Research*, **77**, 284-302.

Garfunkel, Z., 2004. Origin of the Eastern Mediterranean basin: a reevaluation. *Tectonophysics*, **391**, 11-34.

Garzanti, E., Ando, S., and Scutella, M., 2000. Actualistic Ophiolite Provenance: The Cyprus Case. *The Journal of Geology*, **108**, 199-218.

Gautier, P., Bozkurt, E., Bosse, V., Hallot, E., and Dirik, K., 2008. Coeval extensional shearing and lateral underflow during Late Cretaceous core complex development in the Niğde Massif, Central Anatolia, Turkey. *Tectonics*, **27**.

Gazzi, P., 1966. Le Arenarie del Flysch Sopracretaceo dell'Appennino Modenese: Correlazioni con il Flysch di Monghidoro. *Mineralogica e Petrografica Acta*, **12**, 69-97.

Genç, S. and Yılmaz, Y., 1997. An Example of Post-collisional Magmatism in Northwestern Anatolia: the Kızderbent Volcanics (Armutlu peninsula, Turkey). *Turkish Journal of Earth Sciences*, **6**, 33-42.

Genç, Y. and Yürür, M. T., Coeval extension and compression in Late Mesozoic-Recent thin-skinned extensional tectonics in central Anatolia, Turkey. *Journal of Structural Geology*, **32**, 623-640.

---, 2010. Coeval extension and compression in Late Mesozoic-Recent thin-skinned extensional tectonics in central Anatolia, Turkey. *Journal of Structural Geology*, **32**, 623-640.

Gill, R. C. O., Aparicio, A., El Azzouzi, M., Hernandez, J., Thirlwall, M. F., Bourgois, J., and Marriner, G. F., 2004. Depleted arc volcanism in the Alboran Sea and shoshonitic volcanism in Morocco: geochemical and isotopic constraints on Neogene tectonic processes. *Lithos*, **78**, 363-388.

Gökçen, S. L., 1976a. Sedimentology and provenance of resedimented deposits in part of the Haymana basin (Central Anatolia) 1: Regional framework, stratigraphy and tectonics. *Yerbilimleri*, **2**, 161-200.

---, 1976b. Sedimentology and provenance of resedimented deposits in part of the Haymana basin (Central Anatolia) 2: Sedimetary features and palaeocurrents. *Yerbilimleri*, **2**, 201-235.

---, 1978. Haymana (GB Ankara) güneyindeki tortul istifin sedimenter petrolojik incelenmesi. *Maden Tektik ve Arama Dergisi*, **89**, 99-117.

Gökçen, S. L. and Kelling, G., 1983. The Palaeogene Yamak sand-rich submarine-fan complex, Haymana Basin, Turkey. *Sedimentary Geology*, **34**, 219-243.

Gökten, E. and Floyd, P. A., 2007. Stratigraphy and geochemistry of pillow basalts within the ophiolitic mélange of the Izmir–Ankara–Erzincan suture zone: implications for the geotectonic character of the northern branch of Neotethys. *International Journal of Earth Sciences*, **96**, 725-741.

Göncüoğlu, M. C., 1986. Geochronological data from the southernmost part of the Central Anatolian Massif. *Maden Tektik ve Arama Dergisi*, **105-106**, 111-124.

Göncüoğlu, M. C., Dirik, K., Olgun, E., Kuscu, I., and Kozlu, H., 1995. Evolution of central Kizilmark Basin: A prototype of Tertiary basins in central Anatolia: 8th meeting, Eur. Union of Geosci. *TERRA Abstracts*, 192.

Göncüoğlu, M. C., Erler, A., Toprak, V., Olgun, E., Yalınız, M. K., and Kuşcu, I., 1991. Geology of the western part of the Central Anatolian Massif. *Türkiye Petrolleri Anonim Ortaklığı Rapor No. 2909*.

Göncüoğlu, M. C. and Türeli, T. K., 1994. Alpine Collisional-Type Granitoids from western Central Anatolian Crystalline Complex, Turkey. *Journal of Kocaeli University, Earth Science Section*, **1**, 39-46.

Goncuoglu, M. C., Turhan, N., Senturk, K., Ozcan, A., Uysal, S., and Yaliniz, M. K., 2000. A Geotraverse Across Northwestern Turkey: Tectonic Units of the Central Sakarya Region and their Tectonic Evolution. In: Bozkurt, E., Winchester, J. A., and Piper, J. D. A. (Eds.) *Tectonics and Magmatism in Turkey and the Surrounding Area*. Geological Society, London, Special Publications, **173**, 139-161

Göncüoğlu, M. C., Yalınız, K. M., and Tekin, U. K., 2006. Geochemistry, tectono-magmatic discrimination and radiolarian ages of basic extrusives from the İzmir-Ankara suture belt (NW Turkey): time constraints for the Neotethyan evolution. *Ofioliti*, **31**, 25-38.

Görür, N. and Derman, S., 1978. Tuz Gölü-Haymana havzasının stratigrafik ve tektonik analizi. *Unpublished TPAO Report, No.1514*.

Görür, N., Oktay, F. Y., Seymen, I., and Sengör, A. M. C., 1984. Palaeotectonic evolution of the Tuzgölü basin complex, Central Turkey: sedimentary record of a Neo-Tethyan closure. In: Dixon, J. E. and Robertson, A. H. F. (Eds.) *The Geological Evolution of the Eastern Mediterranean*. Geological Society, London, Special Publications, **17**, 467-482

Görür, N. and Tüysüz, O., 2001. Cretaceous to Miocene palaeogeographic evolution of Turkey: implications for hydrocarbon potential. *Journal of Petroleum Geology*, **24**, 119-146.

Görür, N., Tüysüz, O., and Sengör, A. M. C., 1998. Tectonic Evolution of the Central Anatolian basins. *International Geology Review*, **40**, 831-850.

Gradstein, F. M., Ogg, J. G., Smith, A. G., and AL, E., 2004. *A Geologic Time Scale*. Cambridge University Press, pp

Green, T. H., 1995. Significance of Nb/Ta as an indicator of geochemical processes in the crust-mantle system. *Chemical Geology*, **120**, 347-359.

Grove, K. W., Silverman, D. R., Rasmussen, D. R., Penfield, G. T., Gurnet, W. R., and Grateral, V., 2004. Geophysical evaluation and exploration potential of the Haymana - Polatli and Cankiri Basins, central Anatolia, Turkey.*AAPG Regional International Conference*, Istanbul, Turkey.

Güleç, N., 1991. Crust-mantle interaction in western Turkey: implications from Sr and Nd isotope geochemistry of Tertiary and Quaternary volcanics. *Geological Magazine*, **128**, 417-435.

---, 1994. Rb-Sr isotope data from the Ağaçören granitoid (East of Tuz Gölü): Geochronological and genetical implications. *Turkish Journal of Earth Sciences*, **3**.

Gürbüz, C. and Evans, J. R., 1991. A seismic refraction study of the western Tuz Gölü basin, central Turkey. *Geophysical Journal International*, **106**, 239-251.

Gürer, Ö. F. and Aldanmaz, E., 2002. Origin of the Upper Cretaceous—Tertiary sedimentary basins within the Tauride—Anatolide platform in Turkey. *Geological Magazine*, **139**, 191-197.

Gurnis, M., 1988. Large-scale mantle convection and the aggregation and dispersal of supercontinents. *Nature*, **332**, 695-699.

Gürsoy, H., Piper, J. D. A., Tatar, O., and Temiz, H., 1997. A palaeomagnetic study of the Sivas Basin, central Turkey: Crustal deformation during lateral extrusion of the Anatolian Block. *Tectonophysics*, **271**, 89-105.

Gutscher, M.-A., Kukowski, N., Malavieille, J., and Lallemand, S., 1998. Material transfer in accretionary wedges from analysis of a systematic series of analog experiments. *Journal of Structural Geology*, **20**, 407-416.

Hall, R., 2002. Cenozoic geological and plate tectonic evolution of SE Asia and the SW Pacific: computer-based reconstructions, model and animations. *Journal of Asian Earth Sciences*, **20**, 353-431.

Harris, N. B. W., Kelley, S., and Okay, A. I., 1994. Post-collision magmatism and tectonics in northwest Anatolia. *Contributions to Mineralogy and Petrology*, **117**, 241-252.

Hart, M. B., 1980. A water depth model for the evolution of the planktonic Foraminiferida. *Nature*, **286**, 252-254.

Hinschberger, F., Malod, J.-A., Réhault, J.-P., Villeneuve, M., Royer, J.-Y., and Burhanuddin, S., 2005. Late Cenozoic geodynamic evolution of eastern Indonesia. *Tectonophysics*, **404**, 91-118.

Hiscott, R. N., Colella, A., Pezard, P., Lovell, M. A., and Malinverno, A., 1993. Basin plain turbidite succession of the Oligocene Izu-Bonin intraoceanic forearc basin. *Marine and Petroleum Geology*, **10**, 450-466.

Hiscott, R. N. and James, N. P., 1985. Carbonate debris flows, Cow Head Group, western Newfoundland. *Journal of Sedimentary Petrology*, **55**, 735-745.

Hole, M. J., Saunders, A. D., Rogers, G., and Sykes, M. A., 1994. The relationship between alkaline magmatism, lithospheric extension and slab window formation along continental destructive plate margins. In: Smellie, J. L. (Eds.) *Volcanism Associated with Extension at Consuming Plate Margins*. Geological Society, London, Special Publications, **81**, 265-285

Homberg, C., Lacombe, O., Angelier, J., and Bergerat, F., 1999. New constraints for indentation mechanisms in arcuate belts from the Jura Mountains, France. *Geology*, 827-830.

Hoy, R. G. and Ridgway, K. D., 1997. Structural and sedimentological development of footwall growth synclines along an intraforeland uplift, east-central Bighorn Mountains, Wyoming. *Geological Society of America Bulletin*, **109**, 915-935.

Huchon, P. and Le Pichon, X., 1984. Sunda Strait and Central Sumatra fault. *Geology*, **12**, 668-672.

Huw Davies, J. and von Blanckenburg, F., 1995. Slab breakoff: A model of lithosphere detachment and its test in the magmatism and deformation of collisional orogens. *Earth and Planetary Science Letters*, **129**, 85-102.

Ilbeyli, N., 2005. Mineralogical–geochemical constraints on intrusives in central Anatolia, Turkey: tectono-magmatic evolution and characteristics of mantle source. *Geological Magazine*, **142**, 187-207.

Ilbeyli, N., Pearce, J. A., Meighan, I. G., and Fallick, A. E., 2009. Contemporaneous Late Cretaceous Calc-alkaline and Alkaline Magmatism in Central Anatolia, Turkey: O Isotope Constraints on Petrogenesis. *Turkish Journal of Earth Sciences,* **18**, 529-547.

Ilbeyli, N., Pearce, J. A., Thirlwall, M. F., and Mitchell, J. G., 2004. Petrogenesis of collision-related plutonics in Central Anatolia, Turkey. *Lithos,* **72**, 163-182.

Inan, N., Tasli, K., and Inan, S., 2005. Laffitteina from the Maastrichtian-Paleocene shallow marine carbonate successions of the Eastern Pontides (NE Turkey): biozonation and microfacies. *Journal of Asian Earth Sciences,* **25**, 367-378.

Ingersoll, R. V., 1982. Initiation and evolution of the Great Valley forearc basin of northern and central California, U.S.A. In: Leggett, J. K. (Eds.) *Geological Society, London, Special Publications*, **10**, 459-467

Ingersoll, R. V., Bullard, T. F., Ford, R. L., Grimm, J. P., Pickle, J. D., and Sares, S. W., 1984. The effect of grain size on detrital modes: a test of the Gazzi-Dickinson point-counting method. *Journal of Sedimentary Petrology,* **54**, 103-116.

Irvine, T. N. and Baragar, W. R. A., 1971. A guide to the chemical classification of the common volcanic rocks. *Canadian Journal of Earth Sciences*, **8**, 523-548.

Isik, V., 2009. The ductile shear zone in granitoid of the Central Anatolian Crystalline Complex, Turkey: Implications for the origins of the Tuzgölü basin during the Late Cretaceous extensional deformation. *Journal of Asian Earth Sciences,* **34** 507-521.

Isik, V., Lo, C.-H., Göncüoğlu, M. C., and Demirel, S., 2008. 39Ar/40Ar Ages from the Yozgat Batholith: Preliminary Data on the Timing of Late Cretaceous Extension in the Central Anatolian Crystalline Complex, Turkey. *The Journal of Geology,* **116**, 510-526.

İşseven, T. and Tüysüz, O., 2006. Palaeomagnetically defined rotations of fault-bounded continental blocks in the North Anatolian Shear Zone, North Central Anatolia. *Journal of Asian Earth Sciences,* **28**, 469-479.

Jaffey, N. and Robertson, A. H. F., 2001. New sedimentological and structural data from the Ecemis Fault Zone, southern Turkey: implications for its timing and offset and the Cenozoic tectonic escape of Anatolia. *Journal of the Geological Society,* **158**, 367-378.

Jakes , P. and White, A. J. R., 1972. Major and Trace Element Abundances in Volcanic Rocks of Orogenic Areas. *Geological Society of America Bulletin,* **83**, 29-40.

Jarrard, R. D., 1986. Causes of compression and extension behind trenches. *Tectonophysics,* **132**, 89-102.

Johnson, A. M., 1984. Debris flow. In: Brunsden, D. and Prior, D. B. (Eds.) *Slope Instability*. Wily, Chichester257-361

Kadıoğlu, Y. K., Ateş, A., and Güleç, N., 1998. Structural interpretation of gabbroic rocks in Ağaçören Granitoid, central Turkey: field observations and aeromagnetic data. *Geological Magazine,* **135**, 245-254.

Kadıoğlu, Y. K., Dilek, Y., and Foland, K. A., 2006. Slab break-off and syncollisional origin of the Late Cretaceous magmatism in the Central Anatolian crystalline complex, Turkey *Postcollisional tectonics and magmatism in the Mediterranean region and Asia*. Geological Society of America Special Paper, **409**, 381-415

Kadıoğlu, Y. K., Dilek, Y., Güleç, N., and Foland, K. A., 2003. Tectonomagmatic Evolution of Bimodal Plutons in the Central Anatolian Crystalline Complex, Turkey. *The Journal of Geology,* **111**, 671-690.

Karadenizli, L., Seyitoğlu, G., Saraç, G., Kazancı, N., Şen, Ş., Hakymez, Y., and Savaşçı, D., 2003. Çankırı-Çorum Havzası Batı Kenarının Erken-Orta Miyosen Paleocoğrafik Evrimi. *Maden Tektik ve Arama Dergisi,* **126**, 69-86.

Karig, D. E., 1982. Initiation of subduction zones: implications for arc evolution and ophiolite development. In: Leggett, J. K. (Eds.) *Trench-Forearc Geology:*

Sedimentation and Tectonics on Modern and Ancient Active Plate Margins. Geological Society, London, Special Publications, **10**, 563-576

Kavak, K., Poisson, A., and Guezou, J., 1997. Tectonostratigraphy of the Southern Sivas Tertiary Basin (Central Turkey) and Comparison with Landsat MSS Imagery. *International Geology Review,* **39**, 353 - 364.

Kaymakcı, N., 2000. *Tectono-stratigraphical evolution of the Çankiri Basin (Central Anatolia, Turkey),* Utrecht University, The Netherlands.248 pp

Kaymakcı, N., Duermeijer, C. E., Langereis, C. O. R., White, S. H., and Van Dijk, P. M., 2003a. Palaeomagnetic evolution of the Çankiri Basin (central Anatolia, Turkey): implications for oroclinal bending due to indentation. *Geological Magazine,* **140**, 343-355.

Kaymakcı, N., Ozcelik, Y., White, S. H., and Van Dijk, P. M., 2009. Tectono-stratigraphy of the Cankiri Basin: Late Cretaceous to early Miocene evolution of the Neotethyan Suture Zone in Turkey. *Geological Society, London, Special Publications,* **311**, 67-106.

Kaymakcı, N., White, S. H., and Van Dijk, P. M., 2000. Palaeostress Inversion in a Multiphase Deformed Area: Kinematic and Structural Evolution of the Cankiri Basin (Central Turkey), Part 1 - Northern Area. In: Bozkurt, E., Winchester, J. A., and Piper, J. D. A. (Eds.) *Tectonics and Magmatism in Turkey and the Surrounding Area*. Geological Society, London, Special Publications, **173**, 295-323

Kaymakcı, N., White, S. H., and Vandijk, P. M., 2003b. Kinematic and structural development of the Çankiri Basin (Central Anatolia, Turkey): a paleostress inversion study. *Tectonophysics,* **364**, 85-113.

Kazancı, N., Sen, S., Seyitoglu, G., de Bonis, L., Bouvrain, G., Araz, H., Varol, B., and Karadenizli, L., 1999. Geology of a new Late Miocene mammal locality in central Anatolia, Turkey. *Comptes Rendus de l'Académie des Sciences - Series IIA - Earth and Planetary Science,* **329**, 503-510.

Kazancı, N. and Varol, B., 1990. Development of a mass flow-dominated fan-delta complex and associated carbonate reefs within a transgressive Paleocene succession, central Anatolia, Turkey. *Sedimentary Geology,* **68**, 261-278.

Kazmin, V. G. and Tikhonova, N. F., 2006. Evolution of early mesozoic back-arc basins in the Black Sea-Caucasus segment of a Tethyan active margin. In: Robertson, A. H. F. and Mountrakis, M. (Eds.) *Tectonic development of the Eastern Mediterranean Region*. Geological Society, London, Special Publications, **260**, 179-200

Keller, J., Jung, D., Eckhardt, F.-J., and Kreuzer, H., 1992. Radiometric ages and chemical characterization of the Galatean andesite massif, Pontus, Turkey. *Acta vulcanologica,* **2**, 267-276.

Kennett, J. P. and Stott, L. D., 1991. Abrupt deep sea warming, paleoceanographic changes and benthic extinctions at the end of the Palaeocene. *Nature,* **353**, 225-229.

Keskin, M., Genç, S. C., and Tüysüz, O., 2008. Petrology and geochemistry of post-collisional Middle Eocene volcanic units in North-Central Turkey: Evidence for magma generation by slab breakoff following the closure of the Northern Neotethys Ocean. *Lithos,* **104**, 267-305.

Ketin, İ., 1966. Anadolu'nun tektonik birlikleri. *Maden Tektik ve Arama Dergisi,* **66**, 20-34.

Kimura, J.-I., Yoshida, T., and Iizumi, S., 2002. Origin of Low-K Intermediate Lavas at Nekoma Volcano, NE Honshu Arc, Japan: Geochemical Constraints for Lower-Crustal Melts. *Journal of Petrology,* **43**, 631-661.

King, P. L., White, A. J. R., Chappell, B. W., and Allen, C. M., 1997a. Characterization and Origin of Aluminous A-type Granites from the Lachlan Fold Belt, Southeastern Australia. *Journal of Petrology,* **38**, 371–391.

---, 1997b. Characterization and Origin of Aluminous A-type Granites from the Lachlan Fold Belt, Southeastern Australia. *J. Petrology,* **38**, 371-391.

Kocak, K., IsIk, F., Arslan, M., and Zedef, V., 2005. Petrological and source region characteristics of ophiolitic hornblende gabbros from the Aksaray and Kayseri regions, central Anatolian crystalline complex, Turkey. *Journal of Asian Earth Sciences,* **25**, 883-891.

Koçyiğit, A., 1991. An example of an accretionary forearc basin from northern central Anatolia and its implications for the history of subduction of Neo-Tethys in Turkey. *Geological Society of America Bulletin,* **103**, 22-36.

Koçyiğit, A. and Beyhan, A., 1998. A new intracontinental transcurrent structure: the Central Anatolian Fault Zone, Turkey. *Tectonophysics,* **284**, 317-336.

Koçyiğit, A. and Deveci, S., 2008. Ankara Orogenic Phase, Its Age and Transition From Thrusting-dominated Palaeotectonic Period to the Strike-slip Neotectonic Period, Ankara (Turkey). *Turkish Journal of Earth Sciences,* **17**, 433-459.

Koçyiğit, A., Özkan, S., and Rojay, F. B., 1988. Examples from the forearc basin remnants at the active margin of northern Neo-Tethys; development and emplacement ages of the Anatolian nappe, Turkey. *Middle East Technical University Journal of Pure and Applied Sciences,* **21**, 183-210.

Koçyiğit, A., Türkmenoğlu, A., Beyhan, A., Kaymakcı, N., and Akyol, E., 1995. Post-collisonal tectonics of Eskişehir–Ankara–Çankırı segment of İzmir–Ankara–Erzincan Suture Zone. *Turkish Association of Petroleum Geologists Bulletin,* **6**, 69-87.

Koçyiğit, A., Winchester, J. A., Bozkurt, E., and Holland, G., 2003. Saraçköy Volcanic Suite: Implications for the subuction phase of arc evolution in the Galatean Arc Complex, Ankara, Turkey. *Geological Journal,* **38**, 1-14.

Köksal, S., Göncüoğlu, M. C., Floyd, P. A., and 2001. Extrusive members of Postcollisional A-Type Magmatism in Central Anatolia: Karahidir Volcanics, Idis Dagi-Avanos Area, Turkey. *International Geology Review,* **43**, 683-694.

Köksal, S., Göncüoğlu, M. C., Toksoy-Köksal, F., Möller, A., and Kemnitz, H., 2008. Zircon typologies and internal structures as petrogenetic indicators in contrasting granitoid types from central Anatolia, Turkey. *Mineralogy and Petrology*.

Köksal, S., Romer, R. L., Göncüoğlu, M. C., Toksoy-Köksal, F., and 2004. Timing of post-collisional H-type to A-type granitic magmatism: U–Pb titanite ages from the Alpine central Anatolian granitoids (Turkey). *International Journal of Earth Sciences,* **93**, 974-989.

Kulm, L. D., Thornburg, T. M., Schrader, H. J., and Resig, J. M., 1982. Cenozoic structure, stratigraphy and tectonics of the central Peru forearc. In: Leggett, J. K. (Eds.) *Geological Society, London, Special Publications*, **10**, 151-169

Kuno, H., 1966. Lateral variation of basalt magma types across continental margins and island arcs. *Bulletin of Volcanology,* **29**, 195-222.

Kurt, M. A., Alpaslan, M., Göncüoğlu, M. C., and Temel, A., 2008. Geochemistry of late stage medium to high-K calc-alkaline and shoshonitic dykes in the Ulukişla Basin (Central Anatolia, Turkey): Petrogenesis and tectonic setting *Geochemistry International,* **46**, 1145-1163.

Kuşcu, I., Gençalioglu Kuscu, G., Meinert, L. D., and Floyd, P. A., 2002. Tectonic setting and petrogenesis of the Çelebi granitoid, (KIrIkkale-Turkey) and comparison with world skarn granitoids. *Journal of Geochemical Exploration,* **76**, 175-194.

Le Bas, M. J., Maitre, R. W. L., Streckeisen, A., and Zanettin, B., 1986. A chemical classification of volcanic rocks based on the total alkali-silica diagram. *Journal of Petrology,* **27**, 745-750.

Le Fort, P., 1986. Metamorphism and magmatism during the Himalayan collision. In: M.P., C. and A.C., R. (Eds.) *Collision Tectonics*. Geological Society Special Publication, London**19**, 159 - 172

Le Maitre, R. W., 1989. *A Classification of Igneous Rocks and Glossary of Terms. Recommendations of the IUGS Commission on the Systematics of Igneous Rocks. .* Blackwell, Oxfordpp

Le Pichon, X., Iiyama, T., Chamley, H., Charvet, J., Faure, M., Fujimoto, H., Furuta, T., Ida, Y., Kagami, H., Lallemant, S., Leggett, J., Murata, A., Okada, H., Rangin, C., Renard, V., Taira, A., and Tokuyama, H., 1987. Nankai Trough and the fossil Shikoku Ridge: results of Box 6 Kaiko survey. *Earth and Planetary Science Letters,* **83**, 186-198.

Legros, F., 2002. Can Dispersive Pressure Cause Inverse Grading in Grain Flows? *Journal of Sedimentary Research,* **72**, 166-170.

Lei, J. and Zhao, D., 2007. Teleseismic evidence for a break-off subducting slab under Eastern Turkey. *Earth and Planetary Science Letters,* **257**, 14-28.

Lloyd, M. J., Nichols, G. J., and Friend, P. F., 1998. Oligo-Miocene alluvial-fan evolution at the southern Pyrenean thrust front, Spain. *Journal of Sedimentary Research,* **68**, 869-878.

Loiselle, M. C. and Wones, D. R., 1979. *Geological Society of America Abstract Program,* **11**, 468.

Longley, I. M., 1997. The tectonostratigraphic evolution of SE Asia. In: Fraser, A. J., Matthews, S. J., and Murphy, R. W. (Eds.) *Petroleum Geology of Southeast Asia*. Geological Society, London, Special Publications, **126**, 311-339

Lowe, D. R., 1982. Sedimentary gravity flows II: Depositional models with special reference to the deposits of high-density turbidity currents. *Journal of Sedimentary Petrology,* **52**, 279-297.

Lünel, A. T., 1985. An approach to the naming, origin and age of Baranadağ monzonite of the Kırşehir intrusive suite. *METU Journal of Pure and Applied Sciences*, **18**, 385-404.

Mackintosh, P. W., 2008. Unpublished PhD thesis.Tectonic-sedimentary evolution of the northern margin of Gondwana during Late Palaeozoic – Early Cenozoic time in the Eastern Mediterranean region: evidence from the Central Taurus Mountains, Turkey., University of Edinburgh, UK

Mackintosh, P. W. and Robertson, A. H. F., 2009. Structural and sedimentary evidence from the northern margin of the Tauride platform in south central Turkey used to test alternative models of Tethys during Early Mesozoic time. *Tectonophysics,* **473**, 149-172.

Major, J. J., 1998. Pebble orientation on large, experimental debris-flow deposits. *Sedimentary Geology,* **117**, 151-164.

Maniar, P. D. and Piccoli, P. M., 1989. Tectonic discrimination of granitoids. *Geological Society of America Bulletin,* **101**, 635-643.

Mantovani, E., Viti, M., Babbucci, D., Tamburelli, C., and Albarello, D., 2006. Geodynamic connection between the indentation of Arabia and the Neogene tectonics of the central eastern Mediterranean region. In: Dilek, Y. and Pavlides, S. (Eds.) *Postcollisional tectonics and magmatism in the Mediterranean region and Asia*. Geological Society of America Special Paper, **409**, 15-41

Marr, J. G., Harff, P. A., Shanmugam, G., and Parker, G., 2001. Experiments on subaqueous sandy gravity flows: The role of clay and water content in flow dynamics and depositional structures. *Geological Society of America Bulletin,* **113**, 1377-1386.

Matsumaru, K., 1999. Multiple fission in Alveolina oblonga d'Orbigny in Turkey. *Revue de Micropaléontologie,* **42**, 245-251.

Matsumaru, K. and Jauhri, A. K., 2003. Lakadongia, a New Orbitoidal Foraminiferal Genus from the Thanetian (Paleocene) of Meghalaya, NE India. *Micropaleontology*, **49**, 277-291.

Mattern, F., 2005. Ancient sand-rich submarine fans: depositional systems, models, identification, and analysis. *Earth-Science Reviews,* **70**, 167-202.

McNaught, M. A. and Mitra, G., 1993. A kinematic model for the origin of footwall synclines. *Journal of Structural Geology*, **15**, 805-808.

McPherson, J. G., Shanmugam, G., and Moiola, R. J., 1987. Fan-deltas and braid deltas: Varieties of coarse-grained deltas. *Geological Society of America Bulletin,* **99**, 331-340.

Meijers, M. J. M., Kaymakcı, N., Langereis, C. G., Stephenson, R. A., and van Hinsbergen, D. J. J., 2009. Timing and Formation of the Central Pontides Orocline: Relations with the Indentation of the Kırşehir Block and the Opening of the Black Sea Basins*62nd Geological Kurultai of Turkey*, MTA - Ankara.

Meriç, E., Ersoy, S., and Görmüs, M., 2001. Palaeogeographical distribution of the species of Loftusia (Foraminiferida) in the Tethyan Ocean during the Maastrichtian (Late Cretaceous). *Cretaceous Research,* **22**, 353-364.

Meriç, E. and Görür, N., 1979. Haymana - Polatlı Havzasındaki Çaldağ Kireçtaşının yaş konağı. *Maden Tektik ve Arama Dergisi*, **93**, 137-141.

Meriç, E. and Tansel, I., 1987. Stratigraphical distribution of Laffitteina bibensis zone in the Haymana Basin (central Anatolia). *Bulletin of the Faculty of Engineering, Cum. Uni. Serie A - Earthsciences,* **4**, 87-93.

Mertz, D. F., Weinrich, A. J., Sharp, W. D., and Renne, P. R., 2001. Alkaline Intrusions in a Near-Trench Setting, Franciscan Complex, California: Constraints from Geochemistry, Petrology, and 40AR/39AR Chronology. *American Journal of Science*, **301**, 877-911.

Meschede, M., 1986. A method of discriminating between different types of mid-ocean ridge basalts and continental tholeiites with the Nb---1bZr---1bY diagram. *Chemical Geology*, **56**, 207-218.

Meschede, M. and Frisch, W., 1998. A plate-tectonic model for the Mesozoic and Early Cenozoic history of the Caribbean plate. *Tectonophysics*, **296**, 269-291.

Meschede, M., Zweigel, P., and Kiefer, E., 1999. Subsidence and extension at a convergent plate margin: evidence for subduction erosion off Costa Rica. *Terra Nova,* **11**, 112-117.

Middlemost, E. A. K., 1994. Naming materials in the magma/igneous rock system. *Earth-Science Reviews*, **37**, 215-224.

Middleton, G. V., 1970. Experimental studies related to problems of flysch sedimentation. In: Lajoie, J. (Eds.) *Flysch Sedimentology in North America*. Geological Association of Canada, Special Paper, **7**, 253-272

Miller, K. G., Kominz, M. A., Browning, J. V., Wright, J. D., Mountain, G. S., Katz, M. E., Sugarman, P. J., Cramer, B. S., Christie-Blick, N., and Pekar, S. F., 2005. The Phanerozoic Record of Global Sea-Level Change. *Science,* **310**, 1293-1298.

Milsom, J., 2001. Subduction in eastern Indonesia: how many slabs? *Tectonophysics*, **338**, 167-178.

Mo, X., Zhao, Z., Deng, J., Flower, M., Yu, X., Luo, Z., Li, Y., Zhou, S., Dong, G., Zhu, D., and Wang, L., 2006. Petrology and geochemistry of postcollisional volcanic rocks from the Tibetan plateau: Implications for lithosphere heterogeneity and collision-induced asthenospheric mantle flow. In: Dilek, Y. and Pavlides, S. (Eds.) *Postcollisional tectonics and magmatism in the Mediterranean region and Asia*. Geological Society of America Special Paper, **409**, 507-530

Moix, P., Beccaletto, L., Kozur, H. W., Hochard, C., Rosselet, F., and Stampfli, G. M., 2008. A new classification of the Turkish terranes and sutures and its implication for the palaeotectonic history of the region. *Tectonophysics*, **451**, 7-39.

Monstad, S., 2000. Carbonate sedimentation on inactive fan-delta lobes: response to sea-level changes, Sant Llorenç del Munt fan-delta complex, NE Spain. *Sedimentary Geology*, **138**, 99-124.

Morley, C. K., 2001. Combined escape tectonics and subduction rollback-back arc extension: a model for the evolution of Tertiary rift basins in Thailand, Malaysia and Laos. *Journal of the Geological Society*, **158**, 461-474.

MTA, 1989. *Türkiye Jeoloji Haritaları Serisi: Aksaray - H17 Paftası. 1:100 000*. Maden Tektik ve Arama Genel Müdürlüğü (General Directorate of Mineral Research and Exploration), Ankara.1 pp

---, 2002. *1:500 000 scale geological maps of Turkey*. Maden Tektik ve Arama Genel Müdürlüğü (General Directorate of Mineral Research and Exploration), Ankara.1 pp

Mulder, T. and Alexander, J., 2001. The physical character of subaqueous sedimentary density flows and their deposits. *Sedimentology*, **48**, 269-299.

Mullins, H. T. and Cook, H. E., 1986. Carbonate apron models: Alternatives to the submarine fan model for paleoenvironmental analysis and hydrocarbon exploration. *Sedimentary Geology*, **48**, 37-79.

Mullins, H. T., Heath, K. C., Buren, H. M., and Newton, C. R., 1984. Anatomy of a modern open-ocean carbonate slope: northern Little Bahama Bank. *Sedimentology*, **31**, 141-168.

Mutti, E. and Normark, W. R., 1987. Comparing examples of modern and ancient turbidite systems: problems and concepts. In: Leggett, J. K. and Zuffa, G. G. (Eds.) *Deep water clastic deposits: models and case stories*. Graham and Thotman, London1-38

Nemec, W., Porebski, R. J., and Steel, R. J., 1980. Texture and structure of resedimented conglomerates: examples from Książ Formation (Famennian—Tournaisian), southwestern Poland. *Sedimentology*, **27**, 519-538.

Nemec, W. and Steel, R. J., 1984. Alluvial and coastal conglomerates: their significant features and some comments on gravelly mass-flow deposits. In: Koster, E. H. and Steel, R. J. (Eds.) *Sedimentology of Gravels and Conglomerates*. Can. Soc. Petrol. Geol. Memoir, **10**, 1-31

Nichols, G., 1999. *Sedimentology and Stratigraphy*. Blackwell Science Ltd, Cambridgepp

Nilsen, T. H. and Zuffa, G. G., 1982. The Chugach Terrane, a Cretaceous trench-fill deposit, southern Alaska. In: Leggett, J. K. (Eds.) *Trench-Forearc Geology: Sedimentation and Tectonics on Modern and Ancient Active Plate Margins*. Geological Society, London, Special Publications, **10**, 213-227

Norman, T. N., 1972. Ankara Yahşıhan bölgesinde Üst Kretase-Alt Tersiyer istifinin stratigrafisi. *Bulletin of the Geological Society of Turkey*, **15**, 180-276.

---, 1973a. Ankara Yahşıhan bölgesinde Üst Kretase-Alt Tersiyer sadimentasyonu. *Bulletin of the Geological Society of Turkey*, **16**, 41-66.

---, 1973b. Ankara Yahşıhan bölgesinin Eosen'den sonraki tektonik gelişmesi. *Bulletin of the Geological Society of Turkey*, **16**, 67-81.

---, 1975a. Çankırı - Çorum - Yozgat bölgesinde Alt Tersiyer yaşta sedimenüerde Paleo-akıntılar ve denizaltı heyelanları. *Türkiye Jeoloji Bülteni*, **18**, 108-110.

---, 1975b. Kuzey Kızılırmak Havzasının ERTS-Â Uydusu Tarafından Çekilmiş Görüntülerinde Bazı Yeni Tektonik Gözlemler ve Bunların Yorumlanması. *Türkiye Jeoloji Bülteni*, **18**, 47-52.

---, 1984. The role of the Ankara Mélange in the development of Anatolia. In: Robertson, A. H. F. and Dixon, J. E. (Eds.) *The Geological Evolution of the Eastern Mediterranean*. Geological Society, London, Special Publications, **17**, 441-447

Norman, T. N., Gökçen, S. L., and Şenalp, M., 1980. Sedimentation pattern in Central Anatolia at the Cretaceous-Tertiary boundary. *Cretaceous Research,* **1**, 61-84.

Ocakoğlu, F. and Çiner, A., 1997. Characteristics and evolution of sedimentary fill in a fault controlled basin: a Lutetian example from northern Çankırı basin. *Yerbilimleri*, 89-108.

Okan, Y., 1981. A new fusuiinid genus (Erkina) from the Elmadağ region, Ankara - Turkey. *Bulletin of the Geological Society of Turkey,* **24**, 67-74.

Okan, Y. and Hoşgör, I., 2008. The Ampullinid Gastropod Globularia (Swainson 1840) from the Late Thanetian–Early Ilerdian Kırkkavak Formation (Polatlı-Ankara) of the Tethyan Realm. *Turkish Journal of Earth Sciences,* **17**, 785-801.

Okan, Y. and Hoşgör, İ., 2009. Early Eocene (middle-late Cuisian) Molluscs Assemblage from the Harpactocarcinid Beds, in the Yoncalı Formation of the Çankırı Basin, Central Anatolia, and Implications for Tethys Paleogeography. *Türkiye Jeoloji Bülteni,* **52**, 1-30.

Okay, A. I. and Göncüoğlu, M. C., 2004. The Karakaya Complex: A Review of Data and Concepts. *Turkish Journal of Earth Sciences*, **13**, 75-95.

Okay, A. I., Harris, N. B. W., and Kelley, S. P., 1998. Exhumation of blueschists along a Tethyan suture in northwest Turkey. *Tectonophysics*, **285**, 275-299.

Okay, A. I. and Şahintürk, Ö., 1997. Geology of the Eastern Pontides. In: Robinson, A. G. (Eds.) *Regional and petroleum geology of the Black Sea and surrounding region:* . AAPG Memoir, **68**, 291-311

Okay, A. I. and Satir, M., 2006. Geochronology of Eocene plutonism and metamorphism in northwest Turkey: evidence for a possible magmatic arc. *Geodinamica Acta*, **19**, 251-266

Okay, A. I., Satir, M., and Siebel, W., 2006. Pre-Alpide Palaeozoic and Mesozoic orogenic events in the Eastern Mediterranean region. In: Gee, D. G. and Stephenson, R. A. (Eds.) *European Lithosphere Dynamics*. Geological Society, London, Memoirs, **32**, 389-405

Okay, A. I., Tansel, I., and Tuysuz, O., 2001. Obduction, subduction and collision as reflected in the Upper Cretaceous-Lower Eocene sedimentary record of western Turkey. *Geological Magazine*, **138**, 117-142.

Okay, A. I. and Tüysüz, O., 1999. Tethyan sutures of Northern Turkey. In: Durand, B., Jolivet, L., Horvárth, F., and Séranne, M. (Eds.) *The Mediterranean Basins: Tertiary Extension within the Alpine Orogen*. Geological Society, London, Special Publications, **156**, 475-515

Ortner, H., Reiter, F., and Acs, P., 2002. Easy handling of tectonic data: the programs TectonicVB for Mac and TectonicsFP for Windows(TM). *Computers & Geosciences*, **28**, 1193-1200.

Otlu, N. and Boztuğ, D., 1998. The Coexistence of the Silica Oversaturated (ALKOS) and Undersaturated Alkaline (ALKUS) Rocks in the Kortundag and Baranadag Plutons from the Central Anatolian Alkaline Plutonism, E Kaman/NW Kırsehir, Turkey. *Turkish Journal of Earth Sciences*, **7**, 241–257.

Özcan, E. and Özkan-Altiner, S., 1999. The genera Lepidorbitoides and Orbitoides: evolution and stratigraphic significance in some Anatolian basins. *Geological Journal*, **34**, 275-286.

Özcan, E. and Özkan Altıner, S., 1997. Late Campanian - Maastrichtian evolution of orbitoidal foraminifera in Hayman Basin succession (Ankara, Central Turkey). *Revue Palébiol., Genève*, **16**, 271-290.

Özer, S., 1988. The paleontology and biogeography of the pironaean (Rudist) species from the Central-East-Southeast Anatolia and Kocaeli Peninsula. *Türkiye Jeoloji Bülteni,* **31**, 47-58.

Özkan-Altiner, S. and Özcan, E., 1999. Upper Cretaceous planktonic foraminiferal biostratigraphy from NW Turkey: calibration of the stratigraphic ranges of larger benthonic foraminifera. *Geological Journal*, **34**, 287-301.

Özsayin, E. and Dirik, K., 2007. Quaternary Activity of the Cihanbeyli and Yeniceoba Fault Zones: İnönü-Eskişehir Fault System, Central Anatolia. *Turkish Journal of Earth Sciences*, **16**, 471-492.

Parlak, O. and Robertson, A. H. F., 2004. The ophiolite-related Mersin Melange, southern Turkey: its role in the tectonic-sedimentary setting of Tethys in the Eastern Mediterranean region. *Geological Magazine*, **141**, 257-286.

Pearce, J. A., 1982. Trace element characteristics of lavas from destructive plate boundaries. In: Thorpe, R. S. (Eds.) *Andesites*. Wiley, New York525-548

Pearce, J. A. and Cann, J. R., 1973. Tectonic setting of basic volcanic rocks determined using trace element analyses. *Earth and Planetary Science Letters*, **19**, 290-300.

Pearce, J. A., Harris, N. B. W., and Twindle, A. G., 1984a. Trace Element Discrimination Diagrams for the Tectonic Interpretation of Granitic Rocks. *Journal of Petrology*, **25**, 956-983.

Pearce, J. A., Lippard, S. J., and Roberts, S., 1984b. Characteristics and tectonic significance of supra-subduction zone ophiolites. In: Kokelaar, B. P. and Howells, M. F. (Eds.) *Marginal Basin Geology: Volcanic and Associated Sedimentary and Tectonic Processes in Modern and Ancient arginal Basins*. Geological Society, London, Special Publications, **16**, 77-94

Pearce, J. A. and Norry, M. J., 1979. Petrogenic implications of Ti, Zr, Y and Nb variations in volcanic rocks. *Contributions to Mineralogy and Petrology*, **69**, 33-47.

Peccerillo, A. and Taylor, S. R., 1976. Geochemistry of eocene calc-alkaline volcanic rocks from the Kastamonu area, Northern Turkey *Contributions to Mineralogy and Petrology*, **58**, 63-81.

Pettijohn, F. J., Potter, P. E., and Siever, R., 1987. *Sand and sandstone*. Springer-Verlag, New Yorkpp

Pickering, K. T., Hiscott, R. N., and Hein, F. J., 1989. *Deep marine environments, clastic sedimentation and tectonics*. Unwin Hyman London.416 pp

Pickett, E. A. and Robertson, A. H. F., 1996. Formation of the Late Palaeozoic-Early Mesozoic Karakaya Complex and related ophiolites in NW Turkey by Palaeotethyan subduction-accretion. *Journal of the Geological Society, London*, **153**, 995-1009.

---, 2004. Significance of the Volcanogenic Nilüfer Unit and Related Components of the Triassic Karakaya Complex for Tethyan Subduction/Accretion Processes in NW Turkey. *Turkish Journal of Earth Sciences*, **13**, 97-143.

Piedilato, S. and Prosser, G., 2005. Thrust sequences and evolution of the external sector of a fold and thrust belt: An example from the Southern Apennines (Italy). *Journal of Geodynamics*, **39**, 386–402.

Piper, J. D. A., Tatar, O., and Gürsoy, H., 1997. Deformational behaviour of continental lithosphere deduced from block rotations across the North Anatolian fault zone in Turkey. *Earth and Planetary Science Letters*, **150**, 191-203.

Platt, J. P., 1986. Dynamics of orogenic wedges and the uplift of high-pressure metamorphic rocks. *GSA Bulletin*, **97**, 1037-1053.

Platzman, E. S., Tapirdamaz, C., and Sanver, M., 1998. Neogene anticlockwise rotation of central Anatolia (Turkey): preliminary palaeomagnetic and geochronological results. *Tectonophysics*, **299**, 175-189.

Postma, G., 1986. Classification for sediment gravity-flow deposits based on flow conditions during sedimentation. *Geology*, **14**, 291-294.

Racey, A., 1995. Lithostratigraphy and Larger Foraminiferal (Nummulitid) Biostratigraphy of the Tertiary of Northern Oman. *Micropaleontology*, **41**, 1-123.

---, 2001. A Review of Eocene Nummilite Accumulations: Strcuture, formation and reservoir potential. *Journal of Petroleum Geology,* **24**, 79-100.

Ranero, C. R. and von Huene, R., 2000. Subduction erosion along the Middle America convergent margin. *Nature,* **404**, 748-752.

Rasmussen, H., 2000. Nearshore and alluvial facies in the Sant Llorenç del Munt depositional system: recognition and development. *Sedimentary Geology,* **138**, 71-98.

Rice, S. P., Robertson, A. H. F., and Ustaömer, T., 2006. Late Cretaceous-Early Cenozoic tectonic evolution of the Eurasian active margin in the Central and Eastern Pontides, northern Turkey. In: Robertson, A. H. F. and D, M. (Eds.) *Tectonic Development of the Eastern Mediterranean Region*. Geological Society, London, Special Publications.,

Rice, S. P., Robertson, A. H. F., Ustaömer, T., İnan, N., and Taslı, K., 2009. Late Cretaceous - Early Eocene tectonic development of the Tethyan suture zone in the Erzincan area, Eastern Pontides, Turkey. *Geological Magazine,* **146**, 567-590.

Ricou, L. E., Marcoux, J., and Whitechurch, H., 1984. The Mesozoic organization of the Taurides: one or several ocean basins? In: Robertson, A. H. F. and Dixon, J. E. (Eds.) *The Geological Evolution of the Eastern Mediterranean.* . Geological Society, London, Special Publications, **17**, 349-359

Rigo de Righi, M. and Cortesini, A., 1959. Regional studies of the Central Anatolian basin, Progress Report. *Unpubl. Petro Isleri rep.,* **no. 11**.

Robertson, A. H. F., 1990. Late Cretaceous oceanic crust and Early Tertiary foreland basin development, Euboea, Eastern Greece. *Terra Nova,* **2**, 333-339.

---, 2002. Overview of the genesis and emplacement of Mesozoic ophiolites in the Eastern Mediterranean Tethyan region. *Lithos,* **65**, 1-67.

---, 2004. Development of concepts concerning the genesis and emplacement of Tethyan ophiolites in the Eastern Mediterranean and Oman regions. *Earth-Science Reviews,* **66**, 331-387.

---, 2006. Contrasting modes of ophiolite emplacement in the Eastern Mediterranean region. *Geological Society, London, Memoirs,* **32**, 235-261.

Robertson, A. H. F. and Dixon, J. E., 1984. Introduction: aspects of the geological evolution of the eastern Mediterranean. In: Robertson, A. H. F. and Dixon, J. E. (Eds.) *The Geological Evolution of the Eastern Mediterranean.* Geological Society, London, Special Publications, **17**, 1-74

Robertson, A. H. F., Dixon, J. E., Brown, S., Collins, A., Morris, A., Pickett, E., Sharp, I., and Ustaomer, T., 1996. Alternative tectonic models for the Late Palaeozoic-Early Tertiary development of Tethys in the Eastern Mediterranean region. In: Morris, A. and Tarling, D. H. (Eds.) *Geological Society, London, Special Publications*, **105**, 239-263

Robertson, A. H. F., Parlak, O., and Ustaömerr, T., 2009. Melange genesis and ophiolite emplacement related to subduction of the northern margin of the Tauride-Anatolide continent, central and western Turkey. In: Van Hinsbergen, D. J. J., Edwards, M. A., and Govers, R. (Eds.) *Collision and collapse at the Africa-Arabia-Eurasia Subduction Zone*. Geological Society, London, Special Publications, **311**, 9-66

Robinson, A. G., Banks, C. J., Rutherford, M. M., and Hirst, J. P. P., 1995. Stratigraphic and structural development of the Eastern Pontides, Turkey. *Journal of the Geological Society,* **152**, 861-872.

Roger, H., 1990. Sedimentology and tectonic implications of Cretaceous fan-delta conglomerates, Queen Charlotte Islands, Canada. *Sedimentology,* **37**, 83-103.

Rojay, B. and Süzen, M. L., 1997a. Tectonostratigraphic evolution of an arc-trench basin on accretionary ophiolitic melange prism, Central Anatolia, Turkey. *Turkish Association of Petroleum Geologist Bulletin,* **9**, 1-12.

---, 1997b. Tectonostratigraphic evolution of the Cretaceous dynamic basins on accretionary melange prism, SW of Ankara Region. *TPJD Bülteni,* **9**, 1-12.

Rojay, B., Yaliniz, K. M., and Altiner, D., 2001. Tectonic Implications of Some Cretaceous Pillow Basalts from the North Anatolian Ophiolitic Mélange (Central Anatolia-Turkey) to the Evolution of Neotethys. *Turkish Journal of Earth Sciences,* **10**, 93-102.

Şahbaz, A. and Köksoy, M., 1985. Stratigraphic and tectonic study of the Palaeogene sedimentary sequence of the Paşadağ (N of Tuzgölü). *Yerbilimleri,* **12**, 1-17.

Saito, T. and Ito, M., 2002. Deposition of sheet-like turbidite packets and migration of channel-overbank systems on a sandy submarine fan: an example from the Late Miocene-Early Pliocene forearc basin, Boso Peninsula, Japan. *Sedimentary Geology,* **149**, 265-277.

Sanders, D. and Höfling, R., 2000. Carbonate deposition in mixed siliciclastic-carbonate environments on top of an orogenic wedge (Late Cretaceous, Northern Calcareous Alps, Austria). *Sedimentary Geology,* **137**, 127-146.

Sanver, M. and Ponat, E., 1981. Kırşehir ve dolayarina ilişkin paleomanyetik bulgular, Kırşehir Masfinin rotasyonu *Istanbul Yerbilimleri,* **2**, 231-238.

Sarı, B. and Özer, S., 2009. Upper Cretaceous rudist biostratigraphy of the Bey DaglarI Carbonate Platform, Western Taurides, SW Turkey. *Geobios,* **42**, 359-380.

Sartorio, D. and Venturini, S., 1988. *Southern Tethys Biofacies*. Agip S.p.A., Milan.235 pp

Saunders, A. D., Norry, M. J., and Tarney, J., 1988. Origin of MORB and chemically depleted mantle reservoirs: Trace element constraints. *Journal of Petrology,* **29 Special Lithosphere Issue**, 415-445.

Sayıt, K. and Göncüoğlu, M. C., 2009. Geochemistry of mafic rocks of the Karakaya complex, Turkey: evidence for plume-involvement in the Palaeotethyan extensional regime during the Middle and Late Triassic. *International Journal of Earth Sciences (Geol Rundsch),* **98**, 367-385.

Schaub, H., 1981. Nummulites et Assilines de la Tethys Paleogene, Taxonomie, phylogenese et biostratigraphie. *Abhandlengen Schweize Palaontologie Geologie,* **104-106**, 1-236.

Scheibner, C. and Speijer, R. P., 2008. Late Paleocene-early Eocene Tethyan carbonate platform evolution -- A response to long- and short-term paleoclimatic change. *Earth-Science Reviews,* **90**, 71-102.

Schellart, W. P., Lister, G. S., and Toy, V. G., 2006. A Late Cretaceous and Cenozoic reconstruction of the Southwest Pacific region: Tectonics controlled by subduction and slab rollback processes. *Earth-Science Reviews,* **76**, 191-233.

Seghedia, I., Downesb, H., Szakacsa, A., Masonc, P. R. D., Thirlwalld, M. F., Rosue, E., Pecskayf, Z., Martong, E., and Panaiotuh, C., 2004. Neogene–Quaternary magmatism and geodynamics in the Carpathian–Pannonian region: a synthesis. *Lithos,* **72**, 117–146.

Selwood, B. W., 1978. Shallow-marine carbonate environments. In: Reading, H. G. (Eds.) *Sedimentary Environments and Facies*. Elvesier, 557

Şenalp, M., 1979. Turbidites, olistostrome and olistoliths of Eocene age in the Sungurlu region of the Çankırı-Çorum basin. *Maden Tektik ve Arama Dergisi,* **73**, 27-55.

---, 1981. Sedimentological Studies of the Continental Formations Around the Region of Çankırı-Çorum Basin. *Türkiye Jeoloji Kurumu Bülteni,* **V. 24 65-74,**, 65-74.

Şengör, A. M. C., 1979. The North Anatolian transform fault: its age, offset and tectonic significance. *Journal of the Geological Society,* **136**, 269-282.

---, 2003. The repeated redisvovery of mélanges and its implications for the possibility and the role objective evidence in the scientific enterprise. In: Dilek, Y. and Newcomb, S. (Eds.) *Ophiolite Concept and the Evolution of Geological Thought*. Geological Society of America Special Paper, **373**, 385-447

Şengör, A. M. C., Satir, M., and Akkök, R., 1984a. Timing of tectonic events in the Menderes Massif, western Turkey: implications for tectonic evolution and evidence for Pan-African basement in Turkey. *Tectonics,* **3**, 693-707.

Şengör, A. M. C. and Yılmaz, Y., 1981. Tethyan evolution of Turkey: A plate tectonic approach. *Tectonophysics,* **75**, 181-241.

Şengör, A. M. C., Yılmaz, Y., and Sungurlu, O., 1984b. Tectonics of the Mediterranean Cimmerides: nature and evolution of the western termination of Palaeo-Tethys. In: Robertson, A. H. F. and Dixon, J. E. (Eds.) *The Geological Evolution of the Eastern Mediterranean*. Geological Society, London, Special Publications, **17**, 77-112

Şengün, M., 2006. A critical review of the Anatolian geology: a dialectic to sutures and evolution of the Anatolian Tethys and Neotethys. *Mineral Res. Expl. Bull,* **133**, 1-29.

Serkan, M., Kayseri, M. S., and Akgün, F., 2008. Palaeoecology of Coal-Bearing Eocene Sediments in Central Anatolia (Turkey) Based on Quantitative Palynological Data. *Turkish Journal of Earth Sciences,* **17**, 317–360.

Seyitoğlu, G., Kazancı, N., Karadenizli, L., Şen, Ş., Varol, B., and Karabıyıkoğlu, T., 2000. Rockfall avalanche deposits associated with normal faulting in the NW of Çankırı basin: implications for the postcollisional tectonic evolution of the Neo-Tethyan suture zone. *Terra Nova,* **12**, 245-251.

Seymen, I., 1981. Stratigraphy and metamorphism of the Kırşehir Massif around Kaman (Kırşehir - Turkey). *Bulletin of the Geological Society of Turkey,* **24**, 7-14.

Shand, S. J., 1951. *Eruptive Rocks*. J.Wiley, New Yorkpp

Shanmugam, G., 2000. 50 years of the turbidite paradigm (1950s--1990s): deep-water processes and facies models--a critical perspective. *Marine and Petroleum Geology,* **17**, 285-342.

Sinclair, H. D., Sayer, Z. R., and Tucker, M. E., 1998. Carbonate sedimentation during early foreland basin subsidence: the Eocene succession of the French Alps. In: Wright, V. R. and Burchette, T. R. (Eds.) *Geological Society, London, Special Publications*, **149**, 205-227

Sîrel, E., 1975. Polatlı (GB Ankara) güneyinin stratigrafisi. *Bulletin of the Geological Society of Turkey,* **18**, 181-192.

Sîrel, E., Dağer, Z., and Sözeri, B., 1986. Some biostratigraphic and palaeogeographic observations on the Cretaceous/Tertiary boundary in the Haymana - Polatlı Region (central Turkey). In: Walliser, O. (Eds.) *Lecture Notes in Earth Sciences*. Springer-Verlag, Berlin**8**,

Sohn, Y. K., 2000. Depositional processes of submarine debris flows in the Miocene fan deltas, Pohang Basin, SE Korea with special reference to flow transformation. *Journal of Sedimentary Research,* **70**, 491-503.

Soja, C. M., 1996. Island-arc carbonates: characterization and recognition in the ancient geologic record. *Earth-Science Reviews,* **41**, 31-65.

Soper, N. J., Strachan, R. A., Holdsworth, R. E., Gayer, R. A., and Greiling, R. O., 1992. Sinistral transpression and the Silurian closure of Iapetus. *Journal of the Geological Society,* **149**, 871-880.

Spence, G. H. and Tucker, M. E., 1997. Genesis of limestone megabreccias and their significance in carbonate sequence stratigraphic models: a review. *Sedimentary Geology,* **112**, 163-193.

Sperner, B., Ratschbacher, L., and Ott, R., 1993. Fault-striae analysis: A turbo pascal program package for graphical presentation and reduced stress tensor calculation. *Computers & Geosciences*, **19**, 1361-1388.

Stampfli, G. M., 2000. Tethyan oceans. In: Bozkurt, E., Winchester, J. A., and Piper, J. D. A. (Eds.) *Tectonics and Magmatism in Turkey and the Surrounding Area*. Geological Society, London, Special Publications, **173**, 1-23

Stampfli, G. M. and Borel, G. D., 2002. A plate tectonic model for the Paleozoic and Mesozoic constrained by dynamic plate boundaries and restored synthetic oceanic isochrons. *Earth and Planetary Science Letters*, **196**, 17-33.

Stampfli, G. M., Mosar, J., Faure, P., Pilleveut, A., and Vannay, J. C., 2001. Permo-Mesozoic evolution of the western Tethys realm: the Neotethys East Mediterranean basin connection. In: Ziegler, P., Cavazza, W., Robertson, A. H. F., and Crasquin-Soleau, S. (Eds.) *Peri-Tethys Memoir no. 5 Peri-Tethyan Rift/Wrench Basins and Passive Margins. Memoirs du Museum National D'Histoire Naturelle*, 51-108

Steel, R. J., 1974. New Red Sandstone floodplain and piedmont sedimentation in the Hebridean province. *Journal of Sedimentary Petrology*, **44**, 336-357.

Stingl, K., 1994. Depositional environment and sedimentary of the basinal sediments in the Eibiswalder Bucht (Radl Formation and Lower Eibiswald Beds), Miocene Western Styrian Basin, Austria. *Geologische Rundschau*, **83**, 811-821.

Storti, F. and Salvini, F., 1996. Progressive Rollover Fault-Propagation Folding: A Possible Kinematic Mechanism to Generate Regional-Scale Folds in Shallow Foreland Belts. *AAPG Bulletin*, **80**, 174-193.

Stössel, I. and Bernoulli, D., 2000. Rudist lithosome development on the Maiella Carbonate Platform margin. In: Insalco, E., Skelton, P. W., and Palmer, T. J. (Eds.) *Carbonate Platform Systems: Components and Interactions*. Geological Society, London, Special Publications, **178**, 177-190

Stow, D. A. V., 1986. Deep Clastic Seas. In: Reading, H. G. (Eds.) *Sedimentary environments and facies*. Blackwell Scientific Publications, Oxford

Stow, D. A. V., Alam, M., and Piper, D. J. W., 1984a. Sedimentology of the Halifax Formation, Nova Scotia: Lower Palaeozoic fine-grained turbidites. In: Stow, D. A. V. and Piper, D. J. W. (Eds.) *Geological Society, London, Special Publications*, **15**, 127-144

---, 1984b. Sedimentology of the Halifax Formation, Nova Scotia: Lower Palaeozoic fine-grained turbidites. *Journal of the Geological Society*.

Suppe, J., 1985. *Principles of Stuctural Geology*, pp

Sylvester, P. J., 1988. Post-collisional alkaline granites. *Journal of Geology*, **97**, 261-280.

Teixell, A., Arboleya, M. L., and Julivert, A., 2003. Tectonic shortening and topography in the central High Atlas (Morocco). *Tectonics*, **22**.

Tekin, E., Ayyildiz, T., Gündogan, I., and Orti, F., 2007. Modern halolites (halite oolites) in the Tuz Gölü, Turkey. *Sedimentary Geology*, **195**, 101-112.

Temizel, I. and Arslan, M., 2008. Petrology and geochemistry of Tertiary volcanic rocks from the Ikizce (Ordu) area, NE Turkey: Implications for the evolution of the eastern Pontide paleo-magmatic arc. *Journal of Asian Earth Sciences*, **31**, 439-463.

ten Veen, J. H. and Kleinspehn, K. L., 2003. Incipient continental collision and plate-boundary curvature: Late Pliocene-Holocene transtensional Hellenic forearc, Crete, Greece. *Journal of the Geological Society*, **160**, 161-181.

Tewari, V. C., Kumar, K., Lokho, K., and Siddaiah, N. S., 2010. Lakadong limestone: Paleocene–Eocene boundary carbonate sedimentation in Meghalaya, northeastern India. *Current Science*, **98**, 88-95.

TGO, 1961. Orta Anadolu'da Tuz Gölü baseninin bölgesel jeolojisi ve yapılan petrol aramaları*T.C. Petrol İsleri Gn. Mud. dergisi*.

Thatcher, W., Foulger, G. R., Julian, B. R., Svarc, J., Quilty, E., and Bawden, G. W., 1999. Present-Day Deformation Across the Basin and Range Province, Western United States. *Science*, **283**, 1714-1718.

Thompson, G., 1991. Metamorphic and hydrothermal processes:basalt-seawater interactions. In: Floyd, P. A. (Eds.) *Oceanic basalts*. Blackie, Glasgow148-73

Tokatlı, K., Demirel, I. H., and Karayiğit, A. I., 2006. Burial history and thermal maturity assessment of Upper Cretaceous-Lower Tertiary formations in the Çankırı Basin, Turkey. *International Journal of Coal Geology*, **66**, 35-52.

Tokay, M., Lünel, T., and Koçyiğit, A., 1988. Geology and petrology of the Gökdere stock of the Orhaniye syenite. *METU Journal of Pure and Applied Sciences*, **21**, 1-38.

Tokel, S., 1977. Doğu Karadeniz Bölgesinde Eosen yaşlı kalk-alkalen andezitler ve jeotektonizma. *Türkiye Jeoloji Bülteni*, **20**, 49-54.

Trop, J. M., 2008. Latest Cretaceous forearc basin development along an accretionary convegent margin: South-central Alaska. *GSA Bulletin*, **120**, 207-224.

Tucker, M. E., 2001. *Sedimentary petrology*. Blackwell Science, Oxfordpp

Turgay, M. I. and Kurtuluş, C., 1985. Seismic Reflection studies in Polatlı Region, Turkey. *Maden Tektik ve Arama Dergisi*, **104**, 130-139.

Turner, F. J., 1953. Nature and dynamic interpretation of deformation lamellae in calcite of three marbles. *American Journal of Science*, **251**, 276-298.

Tüysüz, O. and Dellaloğlu, A. A., 1992. Tectonic units and geologic evolution of the Çankırı–Çorum Basin*9th Turkish Petroleum Congress. Proceedings*.

Tüysüz, O., Dellaloğlu, A. A., and Terzioğlu, N., 1995. A magmatic belt within the Neo-Tethyan suture zone and its role in the tectonic evolution of northern Turkey. *Tectonophysics*, **243**, 173-191.

Uğurtaş, G., 1975. Geophysical interpretation of part of the Tuz Gölü Basin. *Maden Tektik ve Arama Dergisi*, **85**, 38-45.

Ünalan, G. and Yüksel, V., 1978. Eski bir graben Örneği: Haymana - Polatlı Havzası. *Bulletin of the Geological Society of Turkey*, **21**, 165-169.

Ünalan, G., Yüksel, V., Tekeli, T., Gönenç, O., Seyîrt, Z., and Hüseyin, S., 1976. The stratigraphy and paleogeographical evolution of the Upper Cretaceous-Lower Tertiary sediments in the Haymana-Polatlı region (SW of Ankara). *Bulletin of the Geological Society of Turkey*, **19**, 159-176.

Underhill, J. R., 1989. Late Cenozoic deformation of the Hellenide foreland, western Greece. *Geological Society of America Bulletin*, **101**, 613-634.

Underwood, M. B. and Bachman, S. B., 1982. Sedimentary facies associations within subduction complexes. In: Leggett, J. K. (Eds.) *Trench-Forearc Geology: Sedimentation and Tectonics on Modern and Ancient Active Plate Margins*. Geological Society, London, Special Publications, **10**, 537-550

Unruh, J. R., Dumitru, T. A., and Sawyer, T. L., 2007. Coupling of early Tertiary extension in the Great Valley forearc basin with blueschist exhumation in the underlying Franciscan accretionary wedge at Mount Diablo, California. *Geological Society of America Bulletin*, **119**, 1347-1367.

Ustaömer, P., Ustaömer, T., Gerdes, A., and Zulauf, G., Detrital zircon ages from a Lower Ordovician quartzite of the İstanbul exotic terrane (NW Turkey): evidence for Amazonian affinity. *International Journal of Earth Sciences*.

Ustaömer, P. A., Ustaömer, T., Collins, A. S., and Reischpeitsch, J., 2009. Lutetian arc-type magmatism along the southern Eurasian margin: New U-Pb LA-ICPMS and whole-rock geochemical data from Marmara Island, NW Turkey *Mineralogy and Petrology*, **96**, 177-196.

Uysal, H., 1959. Bolu-Merkeşler Bölgesinin Jeolojisi ve Linyit Imkânları. *Maden Tektik ve Arama Dergisi*, **52** 107-116

Valladares, M. I., 1995. Siliciclastic-carbonate slope apron in an immature tensional margin (Upper Precambrian-Lower Cambrian), Central Iberian Zone, Salamanca, Spain. *Sedimentary Geology,* **94**, 165-186.

Van Weering, T. C. E., Nielsen, T., Kenyon, N. H., Akentieva, K., and Kuijpers, A. H., 1998. Large submarine slides on the NE Faeroe continental margin. *Geological Society, London, Special Publications,* **129**, 5-17.

Vanderhaeghe, O. and Teyssier, C., 2001. Partial melting and flow of orogens. *Tectonophysics,* **342**, 451-472.

Vannucchi, P., Galeotti, S., Clift, P. D., Ranero, C. s. R., and von Huene, R., 2004. Long-term subduction-erosion along the Guatemalan margin of the Middle America Trench. *Geology,* **32**, 617-620.

von Huene, R., Ranero, C. R., and Vannucchi, P., 2004. Generic model of subduction erosion. *Geology,* **32**, 913-916.

Walker, R. G., 1978a. Deep-Water Sandstone Facies and Ancient Submarine Fans: Models for Exploration for Stratigraphic Traps. *AAPG Bulletin,* **62**, 932-966.

---, 1978b. Deepwater sandstone facies and ancient submarine fans: models for exploration for stratigraphic traps. *AAPG Bulletin,* **62**, 932-966.

Walker, R. G. and Cant, D. J., 1986. Sandy fluvial systems. In: Walker, R. G. (Eds.) *Facies Models*. Geoligical Association of Canada Ontario71-103

Wallis, S. R., Platt, J. P., and Knott, S. D., 1993. Recognition of syn-convergence extension in accretionary wedges with examples from the Calbrian Arc and the Eastern Alps. *American Journal of Science,* **293**, 463-495.

Wetzel, A., 1984. Bioturbation in deep-sea fine-grained sediments: influence of sediment texture, turbidite frequency and rates of environmental change. *Geological Society, London, Special Publications,* **15**, 595-608.

Whalen, J. B., Currie, K. L., and Chappell, B. W., 1987. A-type granites: geochemical characteristics, discrimination and petrogenesis. *Contributions to Mineralogy and Petrology,* **95**, 406-419.

Whitney, D. L. and Dilek, Y., 1997. Core complex development in central Anatolia, Turkey. *Geology,* **25**, 1023-1026.

---, 1998. Metamorphism during Alpine Crustal Thickening and Extension in Central Anatolia, Turkey: the Niğde Metamorphic Core Complex. *Journal of Petrology,* **39**, 1385-1403.

---, 2001. Metamorphic and Tectonic Evolution of the Hırkadağ Block, Central Anatolian Crystalline Complex. *Turkish Journal of Earth Sciences,* **10**, 1-15.

Whitney, D. L. and Hamilton, M. A., 2004. Timing of high-grade metamorphism in central Turkey and the assembly of Anatolia. *Journal of the Geological Society, London,* **161**, 823-828.

Whitney, D. L., Teyssier, C., Dilek, Y., Fayon, A. K., and 2001. Metamorphism of the Central Anatolian Crystalline Complex, Turkey: influence of orogen-normal collision vs. wrench dominated tectonics on P-T-t paths. *Journal of metamorphic geology,* **19**, 411-432.

Whitney, D. L., Teyssier, C., Fayon, A. K., Hamilton, M. A., and Heizler, M., 2003. Tectonic controls on metamorphism, partial melting, and intrusion: timing and duration of regional metamorphism and magmatism in the Niğde Massif, Turkey. *Tectonophysics,* **376**, 37-60.

Whitney, D. L., Umhoefer, P. J., Teyssier, C., and Fayon, A. K., 2008. Yo-yo Tectonics of the Niğde Massif During Wrenching in Central Anatolia. *Turkish Journal of Earth Sciences,* **17**, 209-217.

Wilcox, R. E., Harding, T. P., and Seely, R., 1973. Basic wrench tectonics. *AAPG Bulletin,* **57**, 74-96.

Williams, C. A. and Krause, F. F., 1998. Pedogenic-phreatic carbonates on a Middle Devonian (Givetian) terrigenous alluvial-deltaic plain, Gilwood Member (Watt Mountain Formation), northcentral Alberta, Canada. *Sedimentology,* **45**, 1105-1124.

Wilson, J. L., 1975a. *Carbonate facies in geologic history*. Springer Verlag, New York.439 pp

---, 1975b. *Carbonate Facies in Geologic Time*. Springer-Verlag, New York.471 pp

Wilson, J. T., 1966. Did the Atlantic Close and then Re-Open? *Nature,* **211**, 676-681.

Winchester, J. A. and Floyd, P. A., 1977. Geochemical discrimination of different magma series and their differentiation products using immobile elements. *Chemical Geology,* **20**, 325-343.

Woodcock, N. H., 1979. The use of slump structures as palaeoslope orientation estimators. *Sedimentology,* **26**, 83-99.

Yalınız, K. M., Aydin, İ., Göncüoğlu, M. C., and Parlak, O., 1999. Terlemez quartz monzonite of Central Anatolia (Aksaray-Sarıkaraman): age, petrogenesis and geotectonic implications for ophiolite emplacement. *Geological Journal,* **34**, 233-242.

Yalınız, K. M., Floyd, P. A., and Göncüoğlu, M. C., 2000a. Geochemistry of Volcanic Rocks from the Çiçekdaĝ, Ophiolite, Central Anatolia, Turkey, and Their Inferred Tectonic Setting within the Northern Branch of the Neotethyan Ocean. In: Bozkurt, E., Winchester, J. A., and Piper, J. D. A. (Eds.) *Tectonics and Magmatism in Turkey and the Surrounding Area*. Geological Society, London, Special Publications, **173**, 203-218

Yaliniz, M. K., Floyd, P. A., Göncüoğlu, M. C., and 1996. Supra-subduction zone ophiolites of Central Anatolia; geochemical evidence from the Sarikaraman Ophiolite, Aksaray, Turkey. *Mineralogical Magazine,* **60**, 697-710.

Yalınız, M. K. and Göncüoğlu, M. C., 1998. General geological characteristics and distribution of the Central Anatolian ophiolites. *Yerbilimleri,* **20**, 19-30.

---, 1999. Clinopyroxene Compositions of the Isotropic Gabbros From the Sarıkaraman Ophiolite: New Evidence on Supra-Subduction Zone Type Magma Genesis in Central Anatolia. *Turkish Journal of Earth Sciences,* **8**, 103-111.

Yalınız, M. K., Göncüoğlu, M. C., and Özkan-Altiner, S., 2000b. Formation and emplacement ages of the SSZ-type Neotethyan ophiolites in Central Anatolia, Turkey: palaeotectonic implications. *Geological Journal,* **35**, 53-68.

Yildiz, A., Ayyildiz, T., and Sonel, N., 2001. Tüzgölu Havzası kuzeybatısı (Karahoca - Mangaldağ - Yeşilyurt - Sarıhalit bölgesi) Üst Maastrihtiyen-Paleosen biyostratigrafisi

ve paleoekolojisi. *Yerbilimleri,* **23** 33-52.

Yıldız, A., Ayyıldız, T., and Sonel, N.

Yildiz, A., Karahasan, G., Demircan, H., and Toker, V., 2000. Lower Maastrichtian-Palaeocene biostratigraphy and palaeocology in southeast Kalecik (Ankara). *Yerbilimleri,* **22**, 247-259.

Yilmaz - Sahin, S., 2005. Transition from arc- to post-collision extensional setting revealed by K-Ar dating and petrology: an example from the granitoids of the Eastern Pontide Igneous Terrane, Araklı-Trabzon, NE Turkey. *Geological Journal,* **40**, 425-440.

Yılmaz, A. and Yılmaz, H., 2006. Characteristic features and structural evolution of a post collisional basin: The Sivas Basin, Central Anatolia, Turkey. *Journal of Asian Earth Sciences,* **27**, 164-176.

Yılmaz, S. and Boztuğ, D., 1998. Petrogenesis of the Çiçekdağ Igneous Complex, N of Kırşehir, Central Anatolia Turkey. *Turkish Journal of Earth Sciences,* **7**, 185-199.

Yılmaz, Y. and Clift, P. D., 1990. Allochthonous Terranes in the Tethyan Middle East: Anatolia and the Surrounding Regions [and Discussion]. *Philosophical Transactions of the Royal Society of London. Series A, Mathematical and Physical Sciences*, **331**, 611-624.

Yüksel, S., 1970. Étude geologique de la region d'Haymana (Turquie Centrale), L'Universite de Nancy.PhD Thesis 178

Yurtmen, S. and Rowbotham, G., 2002. Geochemistry, mineralogy and petrogenesis of the northeast Niğde volcanics, central Anatolia, Turkey. *Geological Journal*, **37**, 189-202.

Zweigel, P., 1998. Arcuate accretionary wedge formation at convex plate margin corners: results of sandbox analogue experiments. *Journal of Structural Geology*, **20**, 1597-1609.

Appendix 1: Whole rock geochemistry

Whole rock chemical analysis was carried out by X-Ray Fluorescence at the school of GeoSciences, University of Edinburgh. Techniques were used as described by Fitton *et al.* (1998).

Approximately 50 g of rock was crushed, and any alteration or veining was removed. The sample was then ground to a fine-grained uniform powder in a tungsten carbide grinding mill for ~2 minutes. Powder was then dried in an oven overnight.

For major element analysis, measured quantities of lithium flux were added to previously ignited powder samples. These were fused at 1100°C then pressed into glass discs. The samples were analysed using standard procedures on the Edinburgh University Panalytical PW2404 wavelength-dispersive sequential X-Ray spectrometer.

For trace elements, powder was pressed into pellets after mixing the powder with a binding agent, and compressing to 8 tons using a hydraulic press. These were analysed using the same spectrometer as described above.

This appendix now presents tabulated data from selected igneous rocks from the Kırıkkale Basin (Tables 1-3) and the Çankırı Basin (Tables 4-5).

Table 1. Whole rock major oxide (wt. %) and trace element (ppm) abundances determined by X-Ray Fluorescence of samples from basin basement and İzmir-Ankara Accretionary complex in the Kırıkkale Basin.

	Basin Basement				**İzmir-Ankara Accretionary Complex**								
Locality	KK2/10A →				KK31.1 →					KK6.10 →			
Field no.	KK2/10A	KK2/10B	KK2/10C	KK2/10D	KKYY1	KKYY2	KKYY23	KKYY4	KKYY5	KKMB1	KKMB2	KKMB3	KKMB4
Lab no.	SN6	SN7	SN24	SN25	Nairn-119	Nairn-120	Nairn-121	Nairn-122	Nairn-123	SN14	SN15	SN16	SN17
Major oxides (wt %)													
SiO_2	49.74	48.61	49.25	49.30	45.81	45.62	45.53	45.21	45.07	56.69	51.71	51.56	52.7
Al_2O_3	14.64	13.90	14.35	14.31	14.54	14.41	14.13	14.01	14.11	14.12	14.85	14.78	14.54
$Fe2O_3$	11.97	12.87	12.49	12.70	10.55	10.43	10.36	10.72	10.61	10.82	12.5	12.71	11.96
MgO	6.83	6.71	6.86	6.88	6.31	6.39	6.40	6.72	6.43	3.68	5.02	5.09	4.6
CaO	7.18	6.92	7.11	7.10	8.54	8.77	9.18	9.72	9.16	2.96	3.5	3.5	3.39
Na_2O	3.62	4.32	3.76	3.77	2.69	2.64	2.58	2.53	2.53	5.83	5.48	5.46	5.61
K_2O	0.29	0.17	0.21	0.20	3.53	3.53	3.43	3.24	3.43	0.03	0.03	0.03	0.03
TiO_2	1.88	1.93	1.92	1.94	0.66	0.66	0.66	0.67	0.66	1.76	1.68	1.7	1.70
MnO	0.25	0.23	0.24	0.24	0.18	0.18	0.18	0.19	0.19	0.18	0.23	0.24	0.22
P_2O_5	0.18	0.19	0.18	0.19	0.71	0.68	0.68	0.65	0.68	0.19	0.15	0.15	0.16
LOI	3.15	3.71	3.36	3.38	6.06	6.17	6.10	6.49	6.49	3.32	4.58	4.5	4.12
Total	99.72	99.56	99.74	100.0	99.57	99.48	99.23	100.16	99.36	99.59	99.73	99.72	99.03
Trace elements (ppm)													
Zn	127.3	120.7	122	125.1	138.4	135.6	133.5	138.8	135.6	119.5	308.6	310	255.1
Cu	6.3	5.8	5.7	6.9	140.6	136.3	136.1	133.3	131.9	6.5	7.7	8.8	7.8
Ni	42.1	37.9	39.5	40.5	29.7	28.5	27.6	31.8	29.3	3.2	13.7	15.4	12.1
Cr	56.6	30.3	40	38.5	10.3	10.1	6.4	12.3	10.3	-	-	-	-
V	377.2	393.5	384.6	391.1	260.4	255.3	253.5	268.1	259.4	234.8	403.4	407.9	359
Ba	37.9	36.8	40.9	39	1306.7	1312.7	1317.0	1235.4	1262.0	8.8	5.4	6.6	9.1
Sc	51.6	49.1	50.3	48.2	17.6	18.5	18.9	19.2	19.1	33.9	38.5	38.6	37.2
La	3.1	2.5	0.6	0	42.3	39.8	41.5	40.3	41.0	2.8	2.3	2	1.8
Ce	11.6	12.1	11.9	15.5	63.5	62.1	61.2	60.3	59.7	21.7	14.7	13.8	15.1
Nd	6.4	7.2	6.6	8.6	23.1	25.0	25.2	24.5	25.2	15.5	11.1	10.5	13.4
U	0.6	0.3	0.7	0.7	3.4	3.5	3.4	3.2	3.3	0	0.2	0.2	0.3
Th	0	0.5	0.6	0.6	8.0	7.7	7.5	7.7	7.6	0.2	0.1	0.4	-
Pb	9.8	9.2	8.6	10.1	13.7	12.7	12.8	12.9	12.7	0.9	1.2	1.3	1.2
Nb	5.8	6.2	5.8	6	5.8	5.5	5.6	5.4	5.4	3.5	2.8	2.8	2.9
Zr	110.4	117.2	114.9	115.4	56.9	56.1	56.3	55.8	55.1	128.8	98.3	99.1	107.1
Y	34.2	34.1	34.4	35.5	25.4	25.2	25.2	24.8	24.6	46.6	37.8	38.1	40.5
Sr	186.6	163.7	177.4	176.6	533.1	519.8	517.1	504.1	504.8	29.8	27.8	28.2	28.9
Rb	4.2	2.3	3.1	3	51.4	51.2	50.0	49.2	49.0	0.4	0.1	0.2	-

Table 2. Whole rock major oxide (wt%) and trace element (ppm) abundances determined by X-Ray Fluorescence of samples from Dyke and Kırıkkale Massif.

	Dyke	**Kırıkkale**	**Massif**							
Locality	KK10/31	KK3/14C	KK3/14C2	KK3/141	KK3/142	KK3/14A	KK3/14B	KK3/14C	KK3/14D	
Field no.	KK10/31	KK3/14C1	Nairn-133	Nairn-115	Nairn-116	SN-10	SN-11	SN12	SN-13	
Lab no.	Nairn-130	Nairn-132								
SiO_2	59.57	46.98	47.06	48.52	48.02	50.44	50.20	47.28	48.41	
Al_2O_3	16.39	14.23	14.19	14.98	14.87	15.34	15.22	14.32	15.19	
$Fe2O_3$	8.46	13.31	13.32	13.24	13.23	12.77	12.81	13.23	13.20	
MgO	3.04	5.05	5.02	6.27	6.28	5.17	5.43	5.04	6.17	
CaO	6.90	5.69	5.70	4.28	4.27	4.72	3.56	5.70	3.45	
Na_2O	3.68	4.64	4.61	5.20	5.13	5.12	5.27	4.78	4.82	
K_2O	0.20	0.03	0.04	0.04	0.05	0.04	0.04	0.03	0.04	
TiO_2	0.67	1.92	1.92	1.86	1.85	1.82	1.83	1.93	2.02	
MnO	0.12	0.23	0.23	0.25	0.25	0.19	0.21	0.23	0.25	
P_2O_5	0.09	0.34	0.34	0.24	0.24	0.25	0.24	0.35	0.35	
LOI	0.40	6.23	6.19	4.66	4.78	5.55	4.96	6.35	5.98	
Total	99.52	98.65	98.61	99.54	98.96	101.42	99.76	99.23	99.87	
Zn	38.5	104.2	104.2	100.9	100.8	98.0	107.1	101.4	130.8	
Cu	4.2	26.9	28.9	34.8	34.0	37.7	40.0	29.2	39.8	
Ni	-	5.0	4.8	3.2	3.4	7.3	8.3	10.8	9.9	
Cr	-	-	-	-	-	-	-	-	-	
V	169.4	345.2	347.2	343.6	340.4	334.8	365.5	347.1	366.1	
Ba	24.0	29.5	32.5	23.4	26.3	8.1	15.4	10.7	7.6	
Sc	41.6	43.7	43.9	43.9	43.4	45.9	46.2	48.5	48.0	
La	0.3	-	-	-0.2	-0.6	-	0.1	-	-	
Ce	2.8	8.0	9.0	8.8	6.4	8.2	6.0	6.7	10.5	
Nd	4.8	6.9	6.4	5.5	5.7	6.8	5.2	7.1	5.5	
U	0.4	0.6	-	0.2	-	-	0.1	-	-	
Th	-0.3	0.2	0.4	0.2	-	-	-	0.3	0.2	
Pb	6.9	0.9	0.7	0.7	1.0	1.4	1.2	0.6	1.5	
Nb	0.4	1.0	1.0	1.0	1.0	0.8	0.9	1.1	0.9	
Zr	27.1	45.9	46.1	39.5	39.1	37.1	38.6	45.2	43.1	
Y	21.7	25.6	25.5	24.4	24.3	23.3	23.1	25.4	24.8	
Sr	164.5	44.2	44.2	56.9	57.2	83.7	63.7	44.1	45.0	
Rb	3.9	0.7	0.6	0.7	0.7	0.7	0.6	0.3	0.6	

Table 3. Whole rock major oxide (wt. %) and trace elements (ppm) abundances determined by X-Ray Fluorescence of samples from granitoid plutons.

	Granite				**Quartz Monzonite**						
Locality	KKBG10 →				KK18/48A →				KK30/1 →		
Field no.	KKBG10	KKBG11	KKBGA2	KKBGA1	KK18/48A	KK18/48B	KK18/48C	KK18/48D	KK30/1	KK30/2	KK30/3
Lab no.	Nairn-134	Nairn-135	SN1	SN2	SN20	SN21	SN22	SN23	Nairn-105	Nairn-106	Nairn-107
Major oxides (wt %)											
SiO_2	75.04	75.05	75.51	75.33	63.81	64.19	63.83	64.04	64.62	65.32	65.5
Al_2O_3	12.67	12.72	12.84	12.75	15.92	16.01	16.02	16.18	16.49	16.53	16.44
$Fe2O_3$	1.32	1.28	1.27	1.31	4.54	4.48	4.46	4.42	3.2	3.02	3.21
MgO	0.96	0.96	0.94	0.95	1.49	1.44	1.42	1.41	0.76	0.62	0.68
CaO	3.5	3.48	3.53	3.51	3.71	3.65	3.65	3.67	2.73	2.62	2.64
Na_2O	3.36	3.43	3.46	3.51	3.50	3.47	3.55	3.56	3.82	3.75	3.73
K_2O	0.348	0.351	0.34	0.34	4.36	4.50	4.41	4.45	5.618	5.685	5.718
TiO_2	0.381	0.359	0.37	0.38	0.50	0.49	0.47	0.48	0.3	0.295	0.301
MnO	0.05	0.047	0.04	0.04	0.08	0.08	0.07	0.08	0.086	0.07	0.089
P_2O_5	0.069	0.07	0.07	0.07	0.17	0.17	0.16	0.16	0.119	0.109	0.111
LOI	0.88	0.81	0.90	0.92	0.81	0.81	0.81	0.83	0.47	0.58	0.57
Total	98.578	98.557	99.27	99.12	98.88	99.28	98.85	99.27	98.213	98.599	98.989
Trace elements (ppm)											
Zn	172.3	173.2	195	196.8	43.3	42.9	43.8	39.5	35.8	31.3	34.8
Cu	27.5	26.3	27.2	27.2	6.7	7	7.1	6.1	6.6	5.5	5.7
Ni	-	-	-	-	1.7	0.9	2.2	0.2	-	-	-
Cr	-	-	-	-	-	-	-	-	-	-	-
V	41.8	45.4	44.3	45.8	90.6	85.5	87.7	80.7	42.2	41.2	42.3
Ba	85.6	83	86.4	81.6	1761.3	1837.7	1799.3	1703.3	837.4	822.1	833.1
Sc	21.1	22.5	21.7	22.8	9.8	9.9	10.1	9.6	6.4	6.5	5.9
La	8.1	8.7	10.4	9.7	32.5	32.5	29.8	29.5	47.8	62.2	59.2
Ce	23.7	22.7	25.2	24.4	64.3	60.1	59.6	57.4	80.7	92.8	93
Nd	9.2	9.4	9.4	10	23.2	21	22	19.4	24.6	26.2	27.5
U	1.8	1.9	1.8	2.2	5.5	5.1	5.4	5.2	7.6	7.8	8
Th	4.6	4.7	4.8	4.8	29.6	28.9	28.8	28.3	46.3	54	55.4
Pb	18.4	19.9	19	20.4	34.1	33.9	33.6	33.4	28.2	26.9	29.4
Nb	3.9	4.1	3.8	4.1	13.4	12.7	12.5	12.4	22.6	22.4	22.3
Zr	51.4	48.6	50.8	50.2	164	157.7	153.7	155.9	205.4	216.2	231
Y	23.9	25.2	24.2	25.4	28.9	27.7	27.4	26.8	26.7	28.2	28
Sr	141.5	140.3	143.3	142.6	384.9	386.1	387.9	380.6	428.7	428.3	429
Rb	8.8	8.7	8.6	8.7	90.5	92.7	91.5	89.9	234.6	236.1	239.6

Table 4. Whole rock major oxide (wt%) and trace element (ppm) abundances, determined by X-Ray Fluorescence, of samples from Bayat feldspar-phyric trachy basalts and basaltic trachy-andesites.

	Bayat feldspar-phyric trachy basalts and basaltic trachy-andesites													
Locality	BAY3/ 6			BAY1/1			BAY1/1D						BAY11E	
Lab no.	Nairn-101	Nairn-102	Nairn-103	Nairn-104	Nairn-108	Nairn-109	Nairn-110	Nairn-111	Nairn-112	Nairn-113	Nairn-114	Nairn 127	Nairn-128	Nairn-129	Nairn-131
Major oxides (wt %)															
SiO_2	51.54	51.43	52.92	54.48	55.57	55.66	55.31	52.71	52.47	52.76	52.8	53.94	52.56	50.67	50.72
Al_2O_3	16.45	16.39	17.33	18.34	18.49	18.68	18.85	19.01	18.7	19.19	19.11	18.49	18.51	19.26	19.02
$Fe2O_3$	8.03	7.99	7.82	5.92	6.04	5.92	5.94	6.52	6.76	6.48	6.43	6.36	6.43	9.99	9.87
MgO	5.54	5.54	5.28	2.31	2.34	2.23	2.35	1.55	1.84	1.43	1.42	2.03	1.94	2.47	2.45
CaO	8.7	8.73	8.48	6.62	6.76	6.68	7.12	7.87	8.06	7.87	7.87	7.69	7.72	8.76	8.7
Na_2O	2.69	2.7	2.95	3.7	3.65	3.67	3.67	3.71	3.68	3.75	3.74	3.63	3.55	3.38	3.27
K_2O	2.49	2.46	2.63	3.39	3.59	3.62	3.45	3.95	3.84	4.0	4.00	3.81	3.79	2.35	2.40
TiO_2	0.95	0.94	0.95	0.85	0.87	0.87	0.85	0.89	0.90	0.90	0.90	0.87	0.87	0.99	0.984
MnO	0.10	0.10	0.09	0.09	0.09	0.09	0.09	0.12	0.12	0.12	0.12	0.12	0.11	0.12	0.12
P_2O_5	0.43	0.43	0.45	0.45	0.47	0.46	0.45	0.46	0.44	0.44	0.45	0.43	0.43	0.34	0.35
LOI	2.34	2.54	2.44	1.6	1.16	1.14	1.21	2.25	2.22	2.18	2.24	1.63	1.78	0.96	0.89
Total	99.26	99.25	101.33	97.74	99.03	99.01	99.23	99.02	99.04	99.13	99.08	99.00	97.69	99.30	98.77
Trace elements (ppm)															
Zn	80.7	81	-	61.7	62.7	63.3	62.5	62.9	60.9	65.8	66.3	61.1	57.5	81	75.8
Cu	127	126.9	-	83.3	81.2	82.1	80.9	100	98.9	101.9	102.5	95.7	97.4	110.8	102
Ni	55.1	55.6	-	8.1	9.5	7.3	7.7	9.5	9.9	9	9.5	8.8	9.6	11.6	12.8
Cr	170.8	169.8	-	-	-	-	-	-	-	-	-	-	-	-	-
V	264	266.6	-	170.6	171.8	169.8	168.2	196.3	199.2	200.5	196.2	190.9	193.9	290	284
Ba	674.8	674.8	-	633.9	636.2	651.9	631.9	650.9	644.5	650.9	648.3	623.5	631.9	547.8	549.3
Sc	26.4	27.3	-	15.9	15.5	14.7	15.4	17.6	18	19	17.4	16.9	17.1	26.2	25.1
La	22.3	23.3	21.6	29	30.4	30.7	29.3	28.4	26.9	29.6	28.3	27	28.7	16.6	16.3
Ce	44.8	44.2	46.7	58.2	59.7	59.7	56.5	56	56.7	59.6	57.8	52.1	56.2	33.7	37.5
Nd	22.2	22.2	22.4	25.8	26.9	25.8	24.8	25	24.7	24.6	25.3	24.2	24.4	19.5	19.5
U	2.4	2.3	2.5	3.6	3.7	3.6	3.4	3.2	3.4	3.6	3.2	3.3	3.6	0.9	0.9
Th	7.4	7.5	7.7	11.6	11.9	11.7	11.4	10.7	10.4	10.5	10.5	10.5	10.2	2.6	3.1
Pb	11.2	11.3	12.2	17.4	17.2	17.4	16.9	14.7	14.3	17.4	17.8	11.4	11.2	9.8	10.2
Nb	9.8	9.7	-	10.8	11.1	11.1	10.4	10	10.1	10.1	10	9.6	9.9	3.9	4.1
Zr	153.8	152.4	-	189	194.1	193.8	183.8	179.8	176.2	180.9	181.2	172.8	174.8	80.3	84.2
Y	24.4	24.2	-	22.7	23.4	22.9	22.6	22.5	22.7	22.8	22.7	22.8	22.8	24	24
Sr	623.8	630.1	-	746.3	739	749.6	779.3	768.5	763.6	767.9	763	762.5	774	832.4	824.1
Rb	39	38.5	-	82.8	82.7	81.9	76.5	108.1	106.1	108.9	108.8	104.4	105.4	45.4	47.6

Table 5. Whole rock major oxide (wt%) and trace element (ppm) abundances, determined by X-Ray Fluorescence, of samples from Sungurlu hornblende-phyric andesites

	Sungurlu hornblende-phyric andesites		
Locality	SU10		
Field no.	SU1A	SU1B	SU1C
Lab no.	SN-3	SN-4	SN-5
Major oxides (wt %)			
SiO_2	60.41	60.59	61.08
Al_2O_3	16.41	16.38	16.61
$Fe2O_3$	4.64	4.59	4.57
MgO	2.75	2.63	2.67
CaO	5.16	5.03	5.08
Na_2O	4.28	4.31	4.38
K_2O	1.42	1.41	1.42
TiO_2	0.49	0.49	0.48
MnO	0.08	0.08	0.08
P_2O_5	0.13	0.13	0.126
LOI	3.64	3.15	3.02
Total	99.41	98.78	99.53
Trace elements (ppm)			
Zn	56.9	54.8	55.3
Cu	30	30	30.1
Ni	35.3	34.8	34.6
Cr	9.9	9.7	8
V	111.3	111.2	109.5
Ba	462.6	456.6	461.5
Sc	15.2	16	14.8
La	13	12.1	11.6
Ce	28	26.8	27.9
Nd	10.4	9.4	10.2
U	1.1	0.9	1
Th	2	2	1.9
Pb	9.8	9.3	9.7
Nb	4.1	4.2	3.9
Zr	99.6	99.8	99.7
Y	16.2	16.2	16
Sr	377.9	372	381.4
Rb	32.8	32.6	32.7

Appendix 2: Sandstone Provenance

Modern petrographers often use optical methods to determine the composition and infer the provenance of ancient sandstones. Typically 200 – 500 per slide points are counted; grains are then assigned to classes which are plotted against each other, usually on ternary diagrams. Over time, ternary diagrams have developed and aim to distinguish sedimentary detritus from different tectonic settings (Dickinson & Suczek 1979; Dickinson *et al.* 1983; Dickinson 1985). There are two principal techniques, the **QFR** (Quartz-Feldspar-Rock fragment) and the **QFL** (Quartz-Feldspar-Lithic clast), also known as the Gazzi-Dickinson method (Gazzi 1966; Dickinson 1970), see Ingersoll *et al.* (1984) for a review. The principal difference between the two methods is the treatment of coarse, polymineralic grains. In the QFR method, a coarse polymineralic grain is assigned to 'R' (rock fragment). However, as sedimentary detritus reduces in grain size with increasing transport distance, a coarse polymineralic grain reduces into its constituent parts. Thus, sandstone composition is driven by grain size. In the QFL method, a sand-sized grain in a coarse polymineralic grain is assigned to its own class, rather than 'rock fragment'. In this way, sandstone composition is independent of grain size. Point counting in this study used the Gazzi-Dickinson method. This study utilised the QFL method, matrix (where present) was not counted.

Provenance determination in complex orogenic regions involving both ophiolitic and volcanic arc material, however, is not straightforward (e.g. Garzanti *et al.* 2000) such that traditional Dickinson-type ternary diagrams are generally unreliable, due to a typically abundant and varied lithic-grain population. Therefore, the method employed in this study is to describe and interpret the provenance of sandstone rock types using careful petrographic descriptions and interpretations.

Table 1: Sandstone provenance data derived from point counting using the Gazzi-Dickinson QFL method, see text for discussion. Qm – Monocrystalline quartz, Qp – Polycrystalline quartz, F – Feldspar, Ls – Sedimentary lithoclasts, Lm – Metamorphic lithoclasts, Lv – Volcanic lithoclasts, CPX – Clinopyroxene.

Sample No.	Basin	Qm	Qp	F	Ls	Lm	Lv	Oxides	CPX	Hornblende	Micas	Bioclast	Carbonate grains	Total:
KK13/36C	Kırıkkale	28	6	79	17	0	135	0	2	33	0	0	0	300
KK13/36G	Kırıkkale	18	0	95	2		65	22	0	98	0	0	0	300
KK13/36A	Kırıkkale	16	0	168	8	0	52	12	42	0	2	0	0	300
KK13/36H	Kırıkkale	33	0	166	2	0	34	7	48	0	10	0	0	300
KK9/29G	Kırıkkale	33	3	186	9	0	35	4	5	15	10	0	0	300
KK7/24F	Kırıkkale	31	1	150	9	0	32	17	36	0	22	0	2	300
KK7/24G	Kırıkkale	33	0	165	3	0	34	7	50	0	8	0	0	300
KK13/36J	Kırıkkale	13	0	15	0	1	116	8	1	0	0	37	109	300
KK12/34C	Kırıkkale	34	10	5	19	0	123	0	0	0	0	11	98	300
kk7/24b	Kırıkkale	10	0	16	0	0	133	0	0	0	0	23	118	300
KK7/25A	Kırıkkale	34	0	19	16	0	134	7	0	0	0	19	71	300
KK6/21A	Kırıkkale	12	16	5	25	5	218	3	10	0	0	0	6	300
KK4.17B	Kırıkkale	81	73	7	0	0	139	0	0	0	0	0	0	300
KK4/17A	Kırıkkale	96	56	5	0	0	143	0	0	0	0	0	0	300
KK8/26D	Kırıkkale	204	7	8	76	0	2	1	0	0	0	0	2	300
KK8/28A	Kırıkkale	85	23	7	131	0	50	3	0	0	0	0	1	300
SK6.6D	Tuz Gölü	146	2	14	6	2	111	1	1	0	0	0	17	300
SK7.7C	Tuz Gölü	122	5	11	31	3	104	0	0	0	0	6	18	300
SK4.1A	Tuz Gölü	183	40	26	4	0	40	0	0	0	0	0	7	300
SK4.1E	Tuz Gölü	98	4	8	60	2	113	9	0	0	0	3	3	300
SK5.4A	Tuz Gölü	78	2	7	28	2	114	44	11	0	0	0	14	300
SK4.2D	Tuz Gölü	170	2	2	3	2	113	6	1	0	0	0	1	300
SK5.5C	Tuz Gölü	154	3	11	2	4	115	8	3	0	0	0	0	300
SK6.6E	Tuz Gölü	191	6	6	1	4	79	3	4	0	0	1	5	300
HAY12.1D	Haymana	102	7	9	11	7	87	38	7	0	10	0	22	300
HAY12.2A	Haymana	130	8	4	9	4	114	0	8	0	5	4	14	300
HAY5.5B	Haymana	151	4	2	11	3	93	9	9	0	18	0	0	300
HAY2.1Y	Haymana	77	7	23	34	6	142	5	1	0	1	0	4	300
HAY5.5D	Haymana	112	4	3	10	7	148	7	1	0	2	4	2	300
HAY11.1D	Haymana	135	11	20	13	5	100	1	1	0	2	0	12	300
HAY5.3Z	Haymana	118	12	1	21	3	142	0	0	0	0	0	3	300
HAY12.3A	Haymana	87	20	14	61	1	83	20	2	0	4	2	6	300
KULU15.2D	Haymana	34	1	85	1	1	144	5	17	0	5	0	7	300
BAL1.1.	Haymana	55	31	29	20	13	122	4	0	0	2	2	22	300
SU2.4C	Çankırı	67	4	68	18	2	129	2	0	0	0	2	8	300
SU14.21A	Çankırı	58	18	7	54	21	127	4	2	0	0	0	9	300
SU6.9A	Çankırı	51	23	2	108	4	103	3	2	0	0	0	5	301
SU5.8B	Çankırı	140	11	51	61	0	33	2	2	0	0	0	0	300
SU1.1B	Çankırı	48	35	10	162	0	40	0	1	0	0	0	4	300
UG-B	Çankırı	75	5	21	138	0	42	4	3	0	0	0	12	300
BAY2.2A	Çankırı	58	42	2	79	9	83	5	4	0	1	11	6	300
BAY4.1B	Çankırı	52	80	1	75	24	65	0	1	0	0	2	0	300
BAY3.10A	Çankırı	16	0	173	5	0	40	0	11	0	55	0	0	300
BAY YY	Çankırı	10	0	114	0	0	142	4	29	0	1	0	0	300
BAYZZ	Çankırı	21	0	124	0	0	61	13	77	0	2	2	0	300

Appendix 3: Palaeocurrents

Palaeocurrent indicators

Palaeocurrent indicators are evidence of direction of flow at the time of sedimentary deposition. They are commonly used in facies analysis and palaeogeographic reconstructions. Two groups of palaeocurrent indicators are distinguished in this study: 1) Unidirectional indicators (flute casts and clast imbrication) and; 2) flow axis indicators (groove casts). Flute casts are scours generated by vortices in a turbulent flow. Clast imbrication forms when gravel clasts are orientated into a stable position with one of the longer clasts axes dipping upstream. Groove casts are elongate scours on bed bases caused by particle indentation parallel to the palaeoflow.

Data treatment

In the field, flute and groove casts were treated as lineaments therefore azimuth and plunge were recorded, along with bed azimuth and dip angle. Imbricated clasts were treated as planes, therefore, dip azimuth and angle were recorded. To produce palaeocurrent rose diagrams, beds with a dip angle of >10° were rotated to the horizontal on a lower hemisphere stereonet. The resultant rotation axis, comprising a dip angle and an azimuth (parallel to strike) were used to rotate the palaeocurrent indicators to their true bearing. Data for each palaeocurrent are presented in Table x, negative plunge values plot in the upper hemisphere. Poles to the planes representing imbricated clasts plot in the lower hemisphere and thus represent downstream palaeocurrent azimuths.

Haymana – Polatlı Basin

Bedding		Indicator				Axis of rotation		
Azimuth	Dip	Azimuth	Plunge	Type	Formation	Azimuth	Angle	Palaeocurrent azimuth
218	31	224	29	Grooves	Haymana	308	31	43
218	31	216	30	Grooves	Haymana	308	31	36
201	25	213	23	Grooves	Haymana	291	25	32
201	25	217	20	Grooves	Haymana	291	25	36
201	25	220	18	Grooves	Haymana	291	25	39
180	31	131	14	Grooves	Haymana	270	31	312
205	32	215	28	Grooves	Haymana	295	32	34
205	32	42	-25	Flute	Haymana	295	32	40
180	36	226	18	Grooves	Haymana	270	36	44
180	36	211	24	Grooves	Haymana	270	36	28
180	36	221	20	Grooves	Haymana	270	36	39
182	37	229	18	Grooves	Haymana	272	37	47
182	37	226	19	Grooves	Haymana	272	37	44
188	30	205	25	Grooves	Haymana	278	30	23
188	30	210	23	Grooves	Haymana	278	30	28
188	30	204	25	Grooves	Haymana	278	30	23
190	31	25	-26	Flute	Haymana	280	31	24
190	31	31	-23	Flute	Haymana	280	31	29
131	39	157	60	Imbrication	Yoncalı	221	39	157
131	39	168	45	Imbrication	Yoncalı	221	39	168
131	39	122	61	Imbrication	Yoncalı	221	39	122
122	56	155	35	Grooves	Yoncalı	212	56	329
131	42	135	40	Flute	Yoncalı	221	42	314
131	42	158	30	Flute	Yoncalı	221	42	334
131	42	156	29	Flute	Yoncalı	221	42	333
131	42	151	26	Flute	Yoncalı	221	42	330
23	75	270	19	Flute	Yoncalı	113	75	268
23	75	267	20	Flute	Yoncalı	113	75	257
23	75	260	21	Flute	Yoncalı	113	75	262
23	75	264	22	Flute	Yoncalı	113	75	263
23	75	260	21	Flute	Yoncalı	113	75	262
200	86	20	46	Imbrication	Yoncalı	290	86	
1	58	318	37	Imbrication	Yoncalı	91	58	44
1	58	298	49	Imbrication	Yoncalı	91	58	62
1	58	319	27	Imbrication	Yoncalı	91	58	29
1	58	307	49	Imbrication	Yoncalı	91	58	63
1	58	321	41	Imbrication	Yoncalı	91	58	50
1	58	328	38	Imbrication	Yoncalı	91	58	41
1	58	300	48	Imbrication	Yoncalı	91	58	61
2	43	15	45	Imbrication	Yoncalı	92	43	264
2	43	14	20	Imbrication	Yoncalı	92	43	351
17	40	351	59	Imbrication	Dizilitaşlar	107	40	142

Haymana – Polatlı Basin continued

Bedding		Indicator				Axis of rotation		
Azimuth	Dip	Azimuth	Plunge	Type	Formation	Azimuth	Angle	Palaeocurrent azimuth
17	40	345	43	Imbrication	Dizilitaşlar	107	40	103
127	41	160	26	Grooves	Yoncalı	217	41	336
127	41	132	39	Grooves	Yoncalı	217	41	310
318	22	311	48	Imbrication	Yoncalı	68	22	115
318	22	317	27	Imbrication	Yoncalı	68	22	88
318	22	321	30	Imbrication	Yoncalı	68	22	107
210	85	125	5	Grooves	Yoncalı	300	-95	115
285	27	120	18	Imbrication	Yoncalı	15	27	292
285	27	118	11	Imbrication	Yoncalı	15	27	289
285	27	159	7	Imbrication	Yoncalı	15	27	296
285	27	158	21	Imbrication	Yoncalı	15	27	310
222	27	246	37	Imbrication	Yoncalı	312	27	105
222	27	253	26	Imbrication	Yoncalı	312	27	150
222	27	261	20	Imbrication	Yoncalı	312	27	173
222	27	271	27	Imbrication	Yoncalı	312	27	154
222	27	263	29	Imbrication	Yoncalı	312	27	145
255	24	36	51	Imbrication	Yoncalı	345	24	224
255	24	39	60	Imbrication	Yoncalı	345	24	224
255	24	18	50	Imbrication	Yoncalı	345	24	210
255	24	30	41	Imbrication	Yoncalı	345	24	223
1	39	335	79	Imbrication	Yoncalı	91	39	144
1	39	331	58	Imbrication	Yoncalı	91	39	120
1	39	337	59	Imbrication	Yoncalı	91	39	130
1	39	344	50	Imbrication	Yoncalı	91	39	127
1	39	334	47	Imbrication	Yoncalı	91	39	104
353	20	309	25	Imbrication	Yoncalı	83	20	78
353	20	310	23	Imbrication	Yoncalı	83	20	73
353	20	293	44	Imbrication	Yoncalı	83	20	91
353	20	309	37	Imbrication	Yoncalı	83	20	101
353	20	319	19	Imbrication	Yoncalı	83	20	62
353	20	342	16	Grooves	Yoncalı	83	20	162

Kirikkale Basin

Bedding		Indicator				Axis of rotation		
Azimuth	Dip	Azimuth	Plunge	Type	Formation	Azimuth	Angle	**Palaeocurrent azimuth**
232	64	222	39	Imbrication	Dizilitaşlar	322	64	246
232	64	236	43	Imbrication	Dizilitaşlar	322	64	225
232	64	233	39	Imbrication	Dizilitaşlar	322	64	231
232	64	209	23	Imbrication	Dizilitaşlar	322	64	245
275	47*	180	-3	Flute	Dizilitaşlar	5	-133	191
263	39*	194	6	Groove	Dizilitaşlar	353	-141	153
332	40	36	56	Groove	Dizilitaşlar	62	40	7
30	86	170	-48	Flute	Dizilitaşlar	120	86	181
30	86	176	-52	Flute	Dizilitaşlar	120	86	187
258	49*	184	3	Groove	Dizilitaşlar	348	-131	155
151	54*	280	-24	Flute	Samanlık	241	-126	197
309	58	190	19	Flute	Samanlık	39	58	187
309	58	174	29	Flute	Samanlık	39	58	169
283	56	163	-19	Flute	Samanlık	13	56	160
265	85	170	-5	Flute	Samanlık	355	85	170
283	42*	175	2	Flute	Samanlık	13	-138	205
283	42*	179	4	Flute	Samanlık	13	-138	201
283	42*	181	5	Flute	Samanlık	13	-138	199
306	45*	197	-10	Flute	Samanlık	36	-135	237
270	72*	164	-13	Flute	Samanlık	0	-108	198
120	53	91	61	Imbrication	Güvendik	210	53	220
120	53	87	60	Imbrication	Güvendik	210	53	215
120	53	94	57	Imbrication	Güvendik	210	53	213
120	53	92	62	Imbrication	Güvendik	210	53	223
91	64	18	38	Imbrication	Güvendik	181	64	134
91	64	26	45	Imbrication	Güvendik	181	64	143
91	64	20	35	Imbrication	Güvendik	181	64	131

*Denotes overturned bedding

Çankırı Basin

Bedding		Indicator				Axis of rotation		
Azimuth	Dip	Azimuth	Plunge	Type	Formation	Azimuth	Angle	Palaeocurrent azimuth
BAYAT								
223	41	268	25	Imbrication	Yoncalı	313	41	184
230	40	228	39	Flutes	Yoncalı	320	40	228
230	40	231	39	Flutes	Yoncalı	320	40	231
230	40	223	37	Flutes	Yoncalı	320	40	224
230	40	238	35	Flutes	Yoncalı	320	40	237
152	60	181	47	Imbrication	Yoncalı	242	60	99
152	60	193	50	Imbrication	Yoncalı	242	60	90
152	60	210	43	Imbrication	Yoncalı	242	60	100
152	60	211	47	Imbrication	Yoncalı	242	60	95
264	52	221	60	Imbrication	Yoncalı	354	52	354
264	52	230	70	Imbrication	Yoncalı	354	52	16
264	52	229	51	Imbrication	Yoncalı	354	52	341
UĞURLUDAĞ								
169	80	2	62	Imbrication	Yoncalı	259	80	7
183	85	274	-1	flute	Yoncalı	271	-95	270
183	85	266	7	flute	Yoncalı	271	-95	278
183	85	279	-8	flute	Yoncalı	271	-95	262
183	85	270	3	groove	Yoncalı	271	-95	274
183	85	265	6	groove	Yoncalı	271	-95	278
183	85	271	2	groove	Yoncalı	271	-95	273
123	41	206	3	groove	Yoncalı	213	41	26
123	41	176	22	groove	Yoncalı	213	41	351
SUNGURLU								
307	35	335	48	Imbrication	Yoncalı	37	35	193
307	35	325	42	Imbrication	Yoncalı	37	35	192
307	35	329	53	Imbrication	Yoncalı	37	35	176
167	41	123	19	Imbrication	Yoncalı	257	41	194
48	50	63	42	Imbrication	Yoncalı	138	50	360
62	37	168	55	Imbrication	Yoncalı	152	37	6
160	66	220	22	groove	Yoncalı	250	66	217
275	35	341	43	Imbrication	Yoncalı	5	55	220
290	44	339	37	Imbrication	Yoncalı	20	44	231
280	53	320	41	Imbrication	Yoncalı	10	53	226
10	27	21	41	Imbrication	Yoncalı	100	27	218
10	27	39	45	Imbrication	Yoncalı	100	27	246
10	27	18	40	Imbrication	Yoncalı	100	27	212

Tuz Gölü Basin

Bedding		Indicator				Axis of rotation		
Azimuth	Dip	Azimuth	Plunge	Type	Formation	Azimuth	Angle	Palaeocurrent azimuth
TUZ GOLU								
320	50	340	50	Imbrication	Dizilitaşlar	50	50	237
297	33	341	43	Imbrication	Dizilitaşlar	27	33	205
307	40	338	62	Imbrication	Dizilitaşlar	37	40	186
327	31	321	63	Imbrication	Dizilitaşlar	57	31	137
329	41	331	63	Imbrication	Dizilitaşlar	59	41	154
345	45	345	88	Imbrication	Dizilitaşlar	75	45	165
BALA								
97	47	156	16	Flute	Yoncalı	107	47	132
97	47	155	16	Groove	Yoncalı	107	47	131
138	28*	76	10	Flute	Yoncalı	228	-152	19
70	64	163	-2	Flute	Yoncalı	160	64	163
70	64	176	-11	Flute	Yoncalı	160	64	177
70	64	178	-13	Flute	Yoncalı	160	64	180
294	49*	326	27	Flute	Yoncalı	24	-135	85
292	36*	311	28	Groove	Yoncalı	22	-154	95
296	31	270	58	Imbrication	Yoncalı	26	31	72
296	31	270	70	Imbrication	Yoncalı	26	31	79
296	31	281	58	Imbrication	Yoncalı	26	31	89
296	31	280	60	Imbrication	Yoncalı	26	31	88

*Denotes overturned bedding

Appendix 4: Fault data

Introduction

Outcrop-scale fault surfaces were measured in the field along with the trend, plunge and sense of slickenside indicators where present. These data were analysed using TectonicsFP software (Ortner *et al.* 2002) with the aim of analysing palaeostress tensors and quantitatively reconstructing brittle basin deformation.

Data Processing

After input of raw fault data, datafiles were corrected so that all striae lay perfectly on their respective fault planes (i.e. misfit angle = 0°). To achieve this, fault-striae are rotated along a great circle, which is defined by the striae and the pole of the fault plane. This operation is necessary before further processing of the data files. Fault data with a misfit angle of >10° were rejected. Fault-striae data are represented graphically in an equal area, lower hemisphere stereonet known as the "Angelier plot" (Angelier 1979), which displays fault planes as great circles and the relative slip of the hanging wall as an arrow on the great circle.

Data Treatment

Fault data sets in each basin were analysed in terms of P-, B- and T-axes (Turner 1953). Concentrations of the P (pressure)- and the T (tension)-axes are interpreted as the orientation of $\sigma 1$ and $\sigma 3$, respectively and thus represent an approximation of stress axes. The angle between the shear plane and the P-axis is 45 °. The T-axis is perpendicular to the P-axis, and B is normal to both P and T (Sperner *et al.* 1993). The "P-T" function in TectonicsFP software includes an estimation of probability that individual fault planes belong to a common fault population which were active in the same stress field. The P-T function produces a lower hemisphere scatter plot for individual P-, B- and T-axes for each fault, along with mean values, error ellipses and R values, which give a measure of probability.

The requirement for reconstructing palaeostress tensors is a homogenous dataset. Heterogeneous data sets are represented by a wide scatter of P-, B- and T-axes and low confidence values. Data can be filtered to achieve higher confidence using a number of criteria, including age, location and the angle of fault dip into homogenous fault populations which represent phases of brittle deformation.

This method can be used for analysing palaeostress data, however, mechanical rock properties should be considered. The assumption of the P-T method is an Andersonian isotropic rock mass, which is usually not present in nature because of anisotropic features including bedding, foliation and pre-existing fractures (i.e. non-Andersonian conditions) (Sperner *et al.* 1993). Realistic data treatment should consider variations in cohesion and friction coefficients which lead to variations in the theta angle (i.e. the angle between the fault plane and $\sigma 1$). Experimental theta angles of between 0 – 40 ° are usually determined in experimental work; 30° is assumed to be a reasonable approximation of natural cases (e.g. Byerlee 1978) and is therefore assumed in this study. Other variations, e.g. cohesion and friction coefficients, are beyond the scope of this thesis.

An alternative technique to visualise palaeostress is the Right Dihedra method (Angelier & Mechler 1977). This graphical method is based on the assumption that the orientation of the maximum principal stress axis is constrained to the P- quadrant, while the orientation of the minimum principal stress axis is constrained to the T- quadrant associated with a chosen fault. The spatial orientation of the P- and T- quadrants is defined by the orientation of the fault plane and slip direction on it.

Table 1. Fault plane and slickenside movement in the Haymana- Polatlı Basin

FAULT PLANE		INDICATOR LINEAMENT			
Dip direction	Dip angle	Azimuth	Plunge	Sense	Formation
150	72	233.13	20.2	4	Asmaboğazı
211	80	121.98	5.4	4	Asmaboğazı
30	82	303.35	22.56	4	Haymana
179	53				Dizilitaşlar
201	56	254.07	41.7	2	Dizilitaşlar
85	61	144.06	42.85	2	Dizilitaşlar
157	40	68.57	1.32	4	Dizilitaşlar
159	36	159.99	36	2	Dizilitaşlar
330	80	329.9	89	2	Asmaboğazı
99	84	187.6	13.05	3	Asmaboğazı
205	78	292.27	12.65	3	Asmaboğazı
255	76	326.49	51.86	2	Dizilitaşlar
250	69				Dizilitaşlar
320	79				Haymana
186	80				Kartal
261	79	344.82	28.97	3	Kırkkavak
97	47				Kırkkavak
301	48				Kırkkavak
296	82	25.68	2.26	3	Kırkkavak
320	89	49.8	11.28	3	Kırkkavak
319	84				Kırkkavak
130	62				Kırkkavak
310	80	38.12	10.54	3	Kırkkavak
278	76				Kırkkavak
202	72	222.87	70.83	2	Kırkkavak
186	50	215.31	46.1	2	Kırkkavak
110	40	114.63	86	1	Kırkkavak
351	50	52.03	30	2	Kartal
28	55	308.67	14.82	2	Dizilitaşlar
2	80	304.97	72.05	2	Dizilitaşlar
58	50	140.21	9.18	3	Dizilitaşlar
109	78				Kırkkavak
290	31	302.09	30.44	2	Haymana
97	79				Haymana
47	79				Kırkkavak
190	60				Dizilitaşlar
56	63				Dizilitaşlar
279	62	337.6	44.42	2	Yoncalı

Sense – 1 up; 2 down; 3 right; 4 left. (movement of hangingwall).

Table 2. Fault plane and slickenside movement in the Kırıkkale Basin

FAULT PLANE		INDICATOR LINEAMENT			
Dip direction	Dip angle	Azimuth	Plunge	Sense	Formation
160	78	248	7	3	Dizilitaşlar
163	85	251	20	3	Dizilitaşlar
135	86				Dizilitaşlar
103	86	14	15	3	Kırıkkale Massif
13	86				İncik
22	82				Incik
232	70				Çayraz
227	73				Çayraz
321	88	50	16	3	Ankara Melange
182	85	227	78	3	Dizilitaşlar
351	80				Dizilitaşlar
291	69				Dizilitaşlar
323	40				Çayraz
227	78	317	1	3	Ankara Melange
152	82	240	12	3	Dizilitaşlar
168	78	256	6	3	Ankara Melange
282	88	11	23	3	Dizilitaşlar
151	43	92	32	2	Dizilitaşlar
273	83				Ilıcıpınar
80	42	71	41	2	Dizilitaşlar
80	41	77	42	2	Dizilitaşlar
72	41				Dizilitaşlar
227	45				Dizilitaşlar
322	23				Samanlık
328	51				Samanlık
320	45				Dizilitaşlar

Sense – 1 up; 2 down; 3 right; 4 left. (movement of hangingwall).

Table 3. Fault plane and slickenside movement in the Çankırı Basin

	FAULT PLANE		INDICATOR LINEAMENT			
	Dip direction	Dip angle	Azimuth	Plunge	Sense	Formation
Bayat	209	87	123	4	3	Yoncalı
	1	63	80	8	3	Yoncalı
Uğurludağ	113	85	18	4	4	Yoncalı
	255	83	341	16	4	Yoncalı
	68	77				Yoncalı
Sungurlu	20	57	294	5	4	Yoncalı
	18	58	288	1	4	Yoncalı
	353	38	264	1	4	Yoncalı
	47	61	128	7	3	Yoncalı
	357	89	89	1	3	Yoncalı
	290	77				Yoncalı
	90	89				Yoncalı
	349	43				Yoncalı
	282	81				Yoncalı
	245	68				Yoncalı
	312	38	7	24	3	Yoncalı
	351	29				Yoncalı
	97	70	13	16	4	Yoncalı
	69	82	340	6	4	Incik
	52	77	322	4	4	Incik
	182	89	92	3	4	Incik
	319	73	43	18	3	Yoncalı
	235	62	310	12	3	Yoncalı
	217	73	297	27	3	Yoncalı
	95	61				Yoncalı
	185	30	185	30	1	Yoncalı
	280	88				Yoncalı
	23	71				Yoncalı
	327	52	45	14	3	Incik
	275	69				Incik
	138	89	230	27	2	Çayraz
	237	65	320	20	3	Çayraz
	171	70				Çayraz
	129	74				Ankara Melange
	107	44				Ankara Melange
	145	50				Ankara Melange
	80	70				Ankara Melange
	110	74	22	1	4	Ankara Melange
	357	63	76	21	4	Ankara Melange
	263	80				Ankara Melange

Sense – 1 up; 2 down; 3 right; 4 left. (movement of hangingwall).

Table 4. Fault plane and slickenside movement in the Tuz Gölü Basin

	FAULT PLANE		INDICATOR LINEAMENT			
	Dip direction	Dip angle	Azimuth	Plunge	Sense	Formation
Tuz Golu	220	58	308	3	3	Asmaboğazı
	31	79	302	1	4	Asmaboğazı
	41	42	329.13	15.65	4	Dizilitaşlar
	41	42	96.02	27.3	0	Dizilitaşlar
	220	75	130.5	1.87	4	Dizilitaşlar
	220	75	131.12	4.17	4	Dizilitaşlar
	226	51	229.06	50.96	2	Dizilitaşlar
	161	81	71.54	3.39	4	Dizilitaşlar
	161	81	147.39	80.74	2	Dizilitaşlar
	279	45	3.99	4.99	3	Dizilitaşlar
	187	43	162	159.05	2	Dizilitaşlar
	178	71	82	88.6	4	Asmaboğazı
	357	70	83.9	8.45	3	Asmaboğazı
	42	77	312.85	3.67	4	Dizilitaşlar
	42	77	41.99	77	2	Dizilitaşlar
	5	67				Dizilitaşlar
	270	63				Dizilitaşlar
	97	65				Dizilitaşlar
	141	75				Dizilitaşlar
	193	70	103.2	0.56	4	Dizilitaşlar
	135	65	223.34	3.56	3	Dizilitaşlar
	143	67				Dizilitaşlar
	140	79	140	79	2	Dizilitaşlar
	66	60	336.37	0.64	4	Dizilitaşlar
	19	67				Dizilitaşlar
	253	90	163.04	1.07	4	Dizilitaşlar
	277	50				Dizilitaşlar
	249	88				Dizilitaşlar
Bala	56	88	326	1	3	Yoncalı
	53	89	147	2	4	Yoncalı

Sense – 1 up; 2 down; 3 right; 4 left. (movement of hangingwall).